Undrained Shear Strength of Ultra-Soft Soils Admixed with Lime

by

Asad A. Khedheyer Al-Alwan

A thesis submitted in fulfilment of the requirements for the degree of

Doctor of Philosophy

School of Engineering

College of Science and Engineering

University of Glasgow

January 2019

Abstract

This thesis describes the results of a study on the undrained shear strength (C_u) of ultra-soft clay soils in admixtures of calcium hydroxide (slaked-lime). The pozzolanic gains in strength over time, over periods as long as one year were recorded. The undrained shear strengths were measured primarily using penetration tests: a Tinius Olsen desk-top compression machine was modified to conduct these constant-rate of strain tests, using circular disc penetrometers.

Measured bearing resistances were interpreted in terms of undrained shear strengths: data from the literature, as well as some finite element analyses, were employed to establish the necessary depth-dependent correlations. The strength testing programme was supplemented by triaxial compression and vane shear tests.

The parametric study of the factors affecting the strength of lime-admixed clay slurries included soil type, water content, lime content, curing time, and curing temperature. The results show how the rate of strength gain is affected by soil mineralogy. The greatest strength gains can only occur if sufficient clay fractions are present to utilize any unbound additive and conversely sufficient additive is present. For clays, samples prepared at the same water content/ liquid limit ratio ($W = w \ / w_{LL}$) produced approximately the same undrained shear strength after one year of curing.

Tests were also conducted on remoulded samples: as expected, these admixed soils have high sensitivity. However, remoulding is not achieved without the expenditure of considerable work. Moreover, the remoulded strengths remain some orders of magnitude higher than their untreated counterparts.

Diffusion of additive from the admixture into surrounding water was observed; this was manifest in softening of the near-surface material and over a period of one year extended to depths of the order of 10 cm depending on lime content.

Curing temperature has a significant effect on the rate of strength development. Lower curing temperatures retard strength development while higher temperatures have the opposite effect. The Arrhenius model for the rates of chemical reactions describes this temperature dependent phenomenon very satisfactorily.

Finite element studies, including small-strain Lagrangian and coupled Eulerian-Lagrangian large-displacement formulations (incorporated within ABAQUS) were conducted to investigate whether penetrometer data interpretation required consideration of the finite size of the test chamber. These numerical results tended to confirm the experimental finding that

penetrometer disk diameters up to 30 mm were sufficiently small to be unaffected by constraints imposed by the test chambers.

In addition, oedometer testing was carried out on both intact and remoulded samples. The former revealed the existence of reasonably well-defined "yield stresses", which were found to correlate well with the corresponding undrained shear strengths. The compression and swell indices were found to be largely dependent on soil type and correspondingly unaffected by lime content.

Table of Contents

List of Tables

List of Figures

Acknowledgments

In the name of God, the Most Gracious, the Most Merciful. Praise to God who gave me continual good health and opportunity to finish this project. I gratefully acknowledge the Iraqi Ministry of Higher Education and Scientific Research MOHESR for sponsoring this project which was carried out in the School of Engineering at the University of Glasgow.

I would like to express my gratitude to my supervisor Dr. Trevor Davies, Senior Lecturer of Civil Engineering, for his sincere encouragement and thoughtful guidance. His explanations of issues related to this project during our meetings created a comprehensive understanding atmosphere.

I acknowledge Professor Simon J. Wheeler, Cormack Professor of Civil Engineering, for his valuable suggestions and clear explanations of experimental procedures during our meetings.

I would like to thank Dr. Zahur Ullah (former post-doctoral researcher) and Karol Lewandowski (current PhD student) in Computational Engineering at the University of Glasgow for their stimulating suggestions and discussions about the ABAQUS software.

My sincere and special thanks go to the tireless laboratory technician **Mr. Tim Montgomery** for his help with many technical issues in the experimental programme. Also, I thank all staff members of the Civil Engineering Department and the workshop for their technical help. I would like to also to thank Mrs. Elaine McNamara, Miss Barbara Grant and Mrs. Karen Docherty for their administrative assistance.

I pray for the soul of my mother who passed away back home while I was too far away to attend her funeral. Very special thanks to my family. I am grateful to my father, brothers, and sisters for all the sacrifices that they have made on my behalf. I am indebted to my beloved wife Anfal for her sacrifices and for her cheerful and tireless support. To my beloved son and daughters Al-Fadhel, Fatma, and Afnan, I would like to express my thanks for being such a bundle of joy and happiness. I know it is hard for them, at this age, to imagine their contribution to my doctoral work, but in fact, it is their brilliance that inspired me all the time.

Special thanks also to the community friends Babul-Hawaij Sangat group who were available for help whenever I asked them.

Author's Declaration

I declare that this thesis is a record of the original work carried out by myself under the supervision of Dr Trevor Davies in the School of Engineering at the University of Glasgow, United Kingdom, during the period of October 2014 to September 2018. The copyright of this thesis therefore belongs to the author under the terms of the United Kingdom Copyright acts. Due acknowledgement must always be made of the use of any material contained in, or derived from, this thesis. The thesis has not been presented elsewhere in consideration for a higher degree.

List of Symbols

A_f	Skempton's pore water pressure parameter
A	Cross-sectional area
B	Skempton's pore water pressure parameter
c'	Soil cohesion intercept
CEL	Coupled Eulerian-Lagrangian
C_u	Undrained shear strength
C_c^*	Intrinsic compression index
C_c	Compression index
C_s	Swelling index
CB	Calcium base bentonite
C	Lime content (%)
$C_{u,0}$	Undrained shear strength at the reference shear strain rate of $\dot{\gamma}_0$
C_{ur}	Remoulded undrained shear strength
c_v	Coefficient of consolidation
d, D	Penetrometer diameter
D_f	Depth of penetrometer/ foundation
D_o	Initial sample diameter
d_d	Diffusion depth
d_{do}	Diffusion depth after one day of curing
E_a	Apparent activation energy (J/mol)
e	Void ratio
e_{100}^*	Intrinsic void ratio at vertical effective stress of 100 kPa
e_{1000}^*	Intrinsic void ratio at vertical effective stress of 1000 kPa
e_{10}^*	Intrinsic void ratio at vertical effective stress of 10 kPa
G	Shear modulus
G_s	Specific gravity of soil solids
G	Grangemouth clay
H	Height of the vane
h	Height of sample
I_B	Brittleness index

I_L	Liquidity index
I_P	Plasticity index
Iv	Void index
K	Rate constant (Arrhenius model), in Chapter 5
K	Kelvin unit of temperature
k	Vane blades constant
K1	Kaolin (1) clay
K2	Kaolin (2) clay
m_s	Soil mass
m_c	Lime mass
N_c	Bearing capacity factor
N_q	Bearing capacity factor
Nɣ	Bearing capacity factor
P	Axial load
P_c	Cell pressure
ΔP_c	Cell pressure increase
q_{net}	Net bearing pressure
q_o	in situ total vertical pressure
q_{ult}	Total bearing pressure
q_{peak}	Peak deviator stress
$q_{ultimate}$	Ultimate deviator stress
R	Universal gas constant (8.3144 J/K mol)
$S.D.$	Standard deviation
SW	Sodium base bentonite
S_t	Strength sensitivity
$S_б$	Stress sensitivity
S_i	Initial stress sensitivity
S_r	Degree of saturation
T	Torque (vane test)
T	Absolute temperature (˚K)
T_o	Reference temperature
t_e	Equivalent time

t	Time
t_f	Time to failure (triaxial)
t_{100}	Notional consolidation time
τ_f	Ultimate shearing resistance
U-U	Unconsolidated-undrained triaxial compression test
u	Pore water pressure
Δu_f	Excess pore water pressure at failure
Δu	Pore water pressure increase
V	Normalized penetration velocity
v	Penetration velocity
W	Water content ratio, w/w_{LL}
w	Water content
w_{LL}	Water content at liquid limit
w_{PL}	Water content at plastic limit
$\bar{X}$	Mean value
z	Penetration depth
σ_1	Major principal stress
σ_3	Minor principal stress
δ_{rem}	Remoulded strength ratio
α	Friction ratio
γ	Unit weight of soil
σ_n	Normal (total) stress
$\emptyset'$	Angle of shearing resistance
σ_{vy}'	Vertical yield (effective) stress
ε	Axial strain
θ_{net}	Net rotation angle (vane)
θ_{shaft}	Shaft rotation angle
θ_t	Total rotation angle

Chapter 1 INTRODUCTION

1.1 Background

This research study grew out of an oil industry-funded research project into stabilization of highly fluid ocean sediments. There are many such applications. For example, land reclamation can involve huge volumes of dredged submarine sediments (Federico et al., 2015). Similarly, large quantities of very soft clayey soils are dredged annually, for the maintenance of navigation channels, and dumped in enclosures. The lack of dumping sites and the high construction costs of such facilities are serious concerns (Kang et al., 2015). Offshore pipelines, which transport hydrocarbons from production wells to processing facilities, present similar geotechnical problems. The protection of these pipelines from external disturbance (e.g., trawling gear) and internal disruption (i.e., buckling due to thermal stresses (Brown, 1969; Charlton and Rouainia, 2017)) could be achieved more economically if the mechanics of ultra-soft soils and their stabilization by means of additives were better understood.

The treatment of soil with chemical additives is commonly adopted to improve their mechanical properties. Portland cement is one such additive, and several papers have been published on its effects on ultra-soft soils. For example, strength gains due to cement treatment is discussed by Horpibulsuk et al. (2004b), Sasanian and Newson (2014), Kang et al. (2015). Compressibility characteristics is explored in papers such as Horpibulsuk et al. (2004a), (Miura et al., 2001)), Federico et al. (2015), and Xiao et al. (2014).

Calcium hydroxide (slaked-lime) is another commonly used additive for soil stabilization. When lime is used, the absence of a primary hydration reaction leads to a different microstructure than that produced by cement treatment (Chew et al., 2004). Lime forms high-strength products in a secondary pozzolanic reaction. Comparatively few studies have focused on the impact of lime treatment on the mechanical properties of ultra-soft soils. Although chemical bonding must enhance the shear strength of soils, evidently high-water content has an adverse effect which inhibits the shear strength gain (Quang et al., 2012). However, it has been argued that a high-water content soil may perform better in the long term, than a soil with a low water content, because movement of solutes is easier in the

former case (Locat et al., 1990). There are many other facets of admixed soil behaviour which remain relatively unexplored in ultra-soft soils.

Slaked lime could be used in place of the Portland cement currently employed in the production of lightweight treated soil (LWTD) from dredged soils for backfilling (Otani et al., 2002; Satoh et al., 2001). Portland cement has a number of disadvantages: its rapid setting creates difficulties in pumping the soil over long distances (Seng and Tanaka, 2011). In addition, the use of Portland cement has undesirable environmental consequences.

1.2 Research objectives

The over-arching aim of this study is to investigate the effect of lime on the mechanical properties of ultra-soft soils. By mechanical properties, we mean the undrained shear strength (principally) and compressibility.

The objectives of the project can be summarised as follows:

- To devise apparatus and techniques for curing lime-admixed soils for periods of up to one year, and at elevated/cold temperatures, and subsequently to measure their mechanical properties.
- To model numerically the penetration test using Finite Element methods, in order to interpret the experimental test data.
- To investigate the influence of strain rate on penetration test strength data, and to identify the optimum rates.
- To establish the correlation between measured penetrometer resistance and soil undrained shear strength.
- To conduct a wide-ranging parametric study of the effect of water content, lime content, curing time, and curing temperatures on the undrained shear strength of a variety of clayey soils, in the ultra-soft (high water content) state.
- To investigate experimentally the remoulded undrained shear strength of these lime admixed soils.
- To investigate the one-dimensional consolidation behaviour of these soils in both intact and remoulded conditions.

1.3 Novel Contribution

The principal novel element of the thesis is the exploration of the effect of slaked lime on the strength of clayey soils at very high water contents. This wide-ranging study has provided insights into the effects of water content, lime content, soil mineralogy, duration and temperature which have not been quantified before.

1.4 Thesis Layout

The thesis is set out as follows:

Chapter 2 is a literature review. The first part contains a discussion on the mechanical properties of the lime-admixed soils. The undrained shear strength is discussed, and various measurement methods are described. Penetration tests are presented in depth. Finally, the compressibility of structured soils is discussed in this chapter.

Chapter 3 describes the tests and laboratory apparatus used in this study: penetration tests; vane shear tests; triaxial compression; pH tests, etc. Apparatus calibration is also documented here. The curing equipment and techniques are described in detail. There follows a report on the strength data obtained from vane shear and triaxial tests. The chapter concludes with results obtained from a study on strain-rate effects in penetration testing.

Chapter 4 contains results of the Finite Element modelling of the penetration test, using small and large displacement ABAQUS analysis. The results, in conjunction with published data, are used in the following chapter to interpret the penetration resistance in terms of undrained shear strength.

Chapter 5 presents the results of a wide-ranging parametric study on intact and remoulded lime-admixed ultra-soft soils and encompasses: water content, lime content, soil type, curing time, and curing temperatures.

Chapter 6 presents the results of one-dimensional consolidation tests on intact and remoulded lime admixed soils.

Finally, **Chapter 7** draws together the principal conclusions of this study and offers some suggestions for future work.

Chapter 2 LITERATURE REVIEW

2.1 Introduction

The first part of the chapter (Section 2.2) deals with stabilization of soil with lime. A description of the chemical reactions associated with lime treatment (2.2.2) is followed by a review of the factors affecting the resulting improved properties of lime admixed soils (2.2.3). A general review of clay shear strength is presented in Section (2.3) focusing on the undrained condition of loading. A review of some common methods used to measure the undrained shear strength of clay (2.4) is followed by longer discussion of penetration tests using circular disc penetrometers (2.5). Empirical descriptions of undrained shear strength of admixed soils are briefly reviewed in section (2.6). Finally, clay compressibility is reviewed in section 2.7, with a focus on the difference in response between structured and de-structured states.

2.2 Chemical Stabilization of Soil

2.2.1 General

Stabilization of soil with chemicals involves shallow or deep mixing, with the objective of improving the soils' mechanical engineering characteristics. Portland cement, lime, and latent hydraulic or pozzolanic material are among the materials used for this purpose. They react with water to form reaction products of high strength. Quick lime (CaO) reacts with water to form calcium hydroxide ($Ca(OH)_2$) which then forms high strength materials in a secondary reaction with pozzolanic material in the soil. Latent hydraulic materials (such as granulated blast furnace slag) need calcium hydroxide to activate the reaction while pozzolanic material (such as fly ash and silica gel) require calcium hydroxide to sustain the reaction (Janz and Johansson, 2002; Vichan et al., 2013). Table 2-1 below summarizes the strength-enhancing reactions of different types of binders.

Table 2-1: Strength-enhancing reactions (Janz and Johansson, 2002)

Binder	Reaction	Coreagents	Time scale
Cement	Hydraulic	Water	Days
Lime	Puzzolanic[1)]	Water + puzzolanic soil or puzzolanic additive	Months
Granulated blast furnace slag	Latent hydraulic	Water + $Ca(OH)_2$ from e.g. cement or lime	Weeks
Fly ash[2)] and silica fume	Puzzolanic	Water + $Ca(OH)_2$ from e.g. cement or lime	Months

1) An initial hydraulic reaction forms $Ca(OH)_2$, which then participates in a pozzolanic reaction. The strength gain is due to the products of the secondary pozzolanic reaction.

2) Fly ash from power and heating plants fuelled with pulverized coal.

2.2.2 Lime stabilization

2.2.2.1 Introduction

The addition of lime to soils to improve their properties for construction purposes is over 5000 years old. (Bell, 1996) reported that stabilized earth roads were used in ancient Mesopotamia and Egypt, and that the Greeks and Romans used soil-lime mixtures in road improvement. Such methods were also used in China, Tibet, and India. It was, however, in the USA during the 1940's that lime–soil admixtures were first subjected to testing using soil mechanics techniques.

The lime used for soil stabilization is produced from limestone (which is mainly calcium carbonate) after crushing and heating to about 1000 ^{o}C. The main product of this process is calcium oxide "quicklime" or "burnt lime" CaO (Janz and Johansson, 2002).

$$CaCO_3 + \text{Heat} \rightarrow CaO + CO_2$$

Burnt lime can be added directly as a stabilizer to the soil or it can be used in another form after being slaked (hydrated) with water. When quick lime is mixed with water it produces slaked lime $Ca(OH)_2$ (Janz and Johansson, 2002)

$$CaO + H_2O \rightarrow Ca(OH)_2$$

and the latter is the most often used, partly because quick lime is corrosive. Slaked lime does not set and, therefore, no purely mechanical strength gain is obtained from the addition

of slaked lime to soil. The strength gain is obtained from an ion exchange reaction and/or a secondary pozzolanic reaction between the lime and soil minerals (Janz and Johansson, 2002).

2.2.2.2 Ion exchange reaction of soil treated with lime

Clay particles carry a negative charge due to isomorphous substitution and dis-continuity of crystal structure (Das, 1985; Mitchell, 1976). To balance the negative charge, the clay particles attract positively charged ions from salts in their pore water. These are referred to as exchangeable ions. Cation replacement can take place depending on the availability of various types of cations in the pore fluid. Cations themselves are different in their power to exchange (Das, 1985; Mitchell, 1976). Some are more strongly attracted than others according to the lythotropic series in terms of their affinity for attraction as follows: $Li^+ < Na^+ < H^+ < K^+ < NH_4^+ < Mg^{2+} < Ca^{2+} < Al^{3+}$ (Das, 1984). In other words, any cation will tend to replace any other to the left of it in this series and monovalent cations are replaced by multivalent cations (Das, 1985; Rao and Rajasekaran, 1996). This process is illustrated by Figure 2-1: on the negatively charged faces of soil particles the currently attracted positive $2K^+$ cations tend to exchange with Ca^{++} cation from lime.

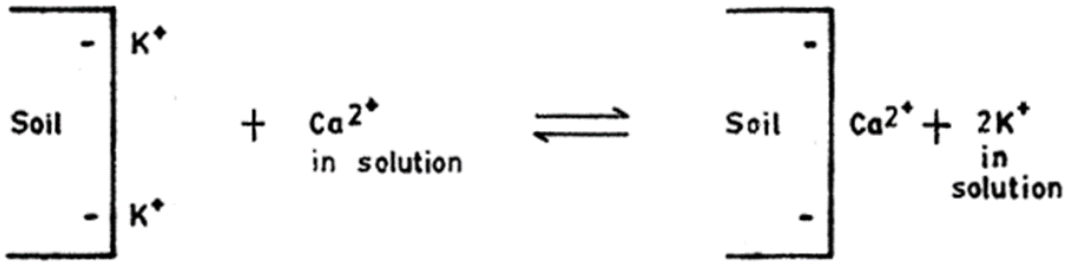

Figure 2-1: An example of cation exchange due to lime treatment (Loganathan, 1987).

The reaction of lime and soil can be described as a series of chemical reactions. Four types of reaction can be distinguished in this process. First is the ion exchange. Second is the flocculation of particles. Third is the lime carbonation and the fourth is the pozzolanic reaction (Eades and Grim, 1960; Locat et al., 1990). Clay particles are surrounded by a diffuse hydrous double layer. Directly after addition of lime to the soil and dissolution of lime in water, an alkaline medium (with pH>12) is induced. This medium provides OH^- ions and Ca^{++} cations. The double layer is modified by the ion exchange of calcium which alters the density of the electrical charge around the clay particles and attracts them closer to each other to form flocs (flocculation). Depending on the crystallographic nature of clay minerals, a partial destruction in the bonds of clay minerals leads to cation exchange with

the Ca^{++} forming bridges between clay mineral particles which leads to flocculation of clay particles making new aggregations (assemblies). These new assemblies are responsible for the rapid change in soil consistency, texture, and increased shear strength (Al-Mukhtar et al., 2010; Al-Mukhtar et al., 2014; Bell, 1996)

2.2.2.3 Pozzolanic reaction and strength development in lime-admixed soil

Some of the aluminous and siliceous minerals contained in clayey and silty soils possess pozzolanic properties, that is, they can, under certain conditions, react with $Ca(OH)_2$ to form strength-enhancing reaction products (Janz and Johansson, 2002). In the long term, as long as there is a high level of alkalinity (pH>12), the reaction results in the dissolution of both silica (SiO_2) and alumina (Al_2O_3) from the soil. The available Ca^{++} ions unite with the dissolved alumina and silica (SiO_4^{n-}) fractions in the pozzolanic reaction forming Calcium Aluminium Hydrates (CAH), Calcium Silicate Hydrate (CSH), or Calcium Silicate Aluminium Hydrate (CSAH) (Pakbaz and Farzi, 2015) that can vary in composition depending on the pozzolanic minerals in the soil.

$Ca(OH)_2$ + pozzolana + $H_2O \rightarrow$CASH (CSH)

These are the resulting compounds of the pozzolanic reaction that is initiated at the edge sites of the clay plates. These cementitious gels crystallise with time (Metelková et al., 2012), resulting in significant increases in shear strength (Boardman et al., 2001).

According to Boardman et al. (2001), no significant pozzolanic activity (and certainly no crystallisation of reaction products) appears to take place until after 7 days of curing.

2.2.2.4 Micro-structure changes

The micro-structure of a clay deposit is the structural arrangement of microscopic sized clay particles, or groups of particles. During deposition, clay particles usually form flocculated honeycombed, or even dispersed structures by the action of Van der Waal forces (Smith, 1990), which affects compressibility, permeability and shear strength. The formation of new minerals due to the pozzolanic reaction fills the pore spaces and reduces the permeability (Locat et al., 1996). A similar observation was made by Sakr et al. (2008) for natural organic soft clay after two months of curing. However, Tran et al. (2014) found an increase in hydraulic conductivity of lime-admixed plastic silty clay after short-term curing. Metelková et al. (2012) concluded after a long-term observation of pore space of clayey silt (using

mercury intrusion porosimetry) that the initial macro-porosity (pore radius r>0.025μm) increases while the initial meso-porosity (pore radius r<0.025 μm) is unaffected. With time, however, the meso-porosity increases as shown in Figure 2-2(a) and the macro-porosity decreases (Figure 2-2(b)) due to the formation of new minerals.

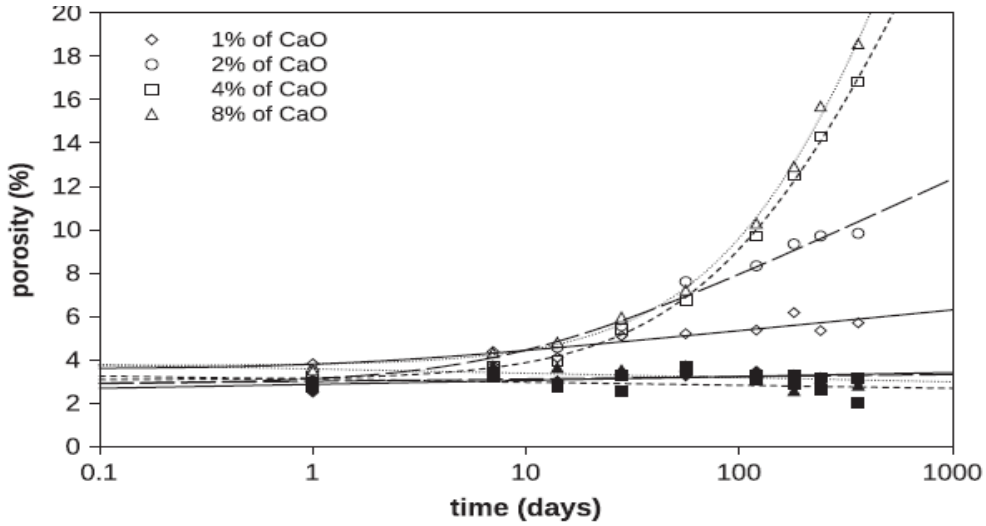

(a)

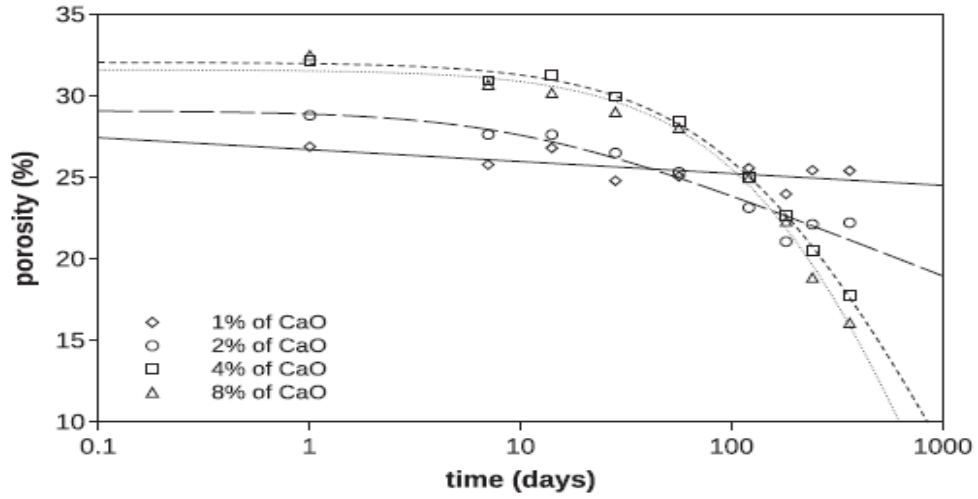

(b)

Figure 2-2: Development of (a) meso-porosity (empty black markers) and porosity of coarse pores (full black markers); and (b) macro-porosity of Horky clayey silt after lime treatment (Metelková et al., 2012).

A significant change in permeability over time could, in principle, result in a change of coefficient of consolidation which, in turn, has implications for determining appropriate loading strain rates for undrained tests.

The flocculation/agglomeration of clay particles after lime treatment modifies the size distribution of the soil aggregation by reducing the percentage of fine matter (Osula, 1991; Osula, 1996). The pozzolanic reaction then leads to the development of the CASH cementitious gel (Osula, 1991) that stays localized at the agglomerate periphery (Lemaire

et al., 2013). Due to the morphology and extension of this gel, it provides continuity throughout the soil matrix and connects adjoining agglomerates via many contact points; at the millimetre scale, the distribution of this gel forms a network of cells resembling a honeycomb structure (Lemaire et al., 2013). This microstructure provides the material with greater mechanical strength. Over time, such a microstructural organization is only slightly modified or does not evolve to any noticeable extent (Lemaire et al., 2013).

2.2.3 Strength and compressibility of lime-admixed soils

2.2.3.1 Clay mineralogy

The complex nature of soils has resulted in disagreements over whether chemical reactions take place sequentially or concurrently (Boardman et al., 2001). A brief discussion is given here for completeness. Clay minerals are complex aluminium silicates composed of two basic units: silica tetrahedra (T) and alumina octahedra (O) as shown in Figure 2-3. Each tetrahedral unit consists of four oxygen atoms surrounding a silicon atom (Das, 2002). The combination of tetrahedral silica units gives a silica sheet (Figure 2-3). Three oxygen atoms at the base of each tetrahedron are shared by the neighbouring tetrahedra. The octahedral units consist of six hydroxyls surrounding an aluminium atom as shown in Figure 2-4, and the combination of the octahedral aluminium hydroxyl units gives an octahedral sheet, also called a gibbsite sheet, Figure 2-3. (Das, 2002).

Clay minerals differ in their reactions to lime. While smectite (such as montmorillonite) is highly reactive, illite is less reactive, while kaolinite, is the least reactive (Al-Mukhtar et al., 2014; Bell, 1996). This difference is linked to differences in cation exchange capacity and strength of mineralogical structure. Smectites have soft structures with large TOT layers (i.e., one octahedral sheet between two tetrahedral sheets as shown in Figure 2-4.). Because the bonding by van der Waals' forces between the tops of silica sheets is weak and there is a net negative charge deficiency in the octahedral sheet, water and exchangeable ions can enter and separate the layers (Das, 1985). Illite also has 2:1 structure similar to montmorillonite (TOT) but the interlayers are bonded together with a potassium atom which makes the cation exchange more difficult (Das, 2002). Kaolinite, on the other hand, theoretically has very little cation exchange capacity (CEC), defined as the quantity of cations available for exchange at a given pH and traditionally expressed in milliequivalents (meq)/100 g of calcined clay. The cation exchange capacity for kaolinite is only 3-15 (meq)/100 g while it is 70-150 (meq)/100 g for montmorillonite (Bergaya et al., 2006). Also, the kaolinite has one tetrahedral layer and one octahedral layer (TO) which is not so

easily opened (Bergaya et al., 2006). Consequently, the changes in the smectite physico-chemical properties due to lime treatment are likely to be more extreme. This can also explain the observations made by Diamond and Kinter (1966) that initial adsorption of calcium hydroxide by kaolinite is completed within about ten minutes at room temperature, and that further removal of lime from solution does not take place for several hours while the chemical reaction with montmorillonite occurs relatively soon after initial uptake.

The practical consequences of these differences (in CEC) is that strength gains in different soils take place at different rates and may well differ in magnitude.

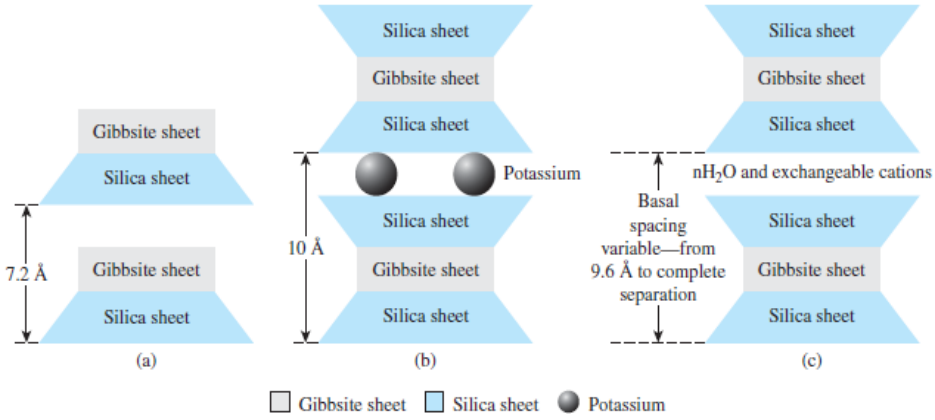

Figure 2-3: Diagram of the structures of (a) kaolinite (b) illite (c) montmorillonite (Das, 2002)

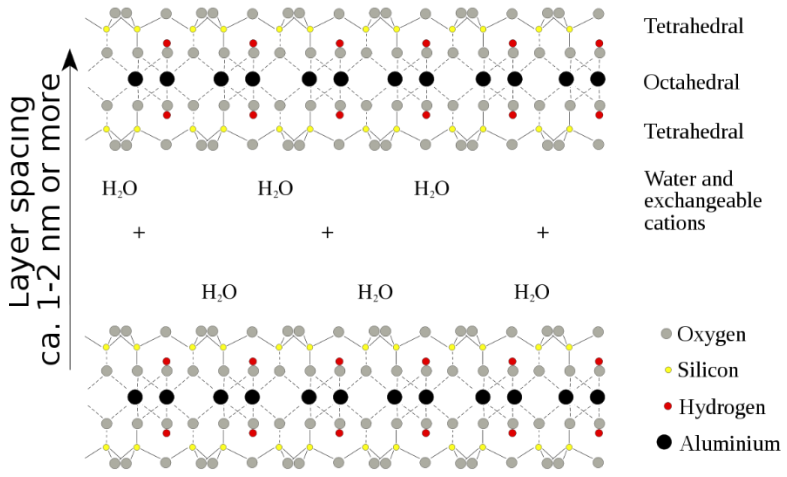

Figure 2-4: Structure of montmorillonite

2.2.3.2 Lime content

The minimum effective quantity of lime must be sufficient to build up a load-bearing skeleton. Otherwise, no stabilization will occur (Janz and Johansson, 2002). The main

controlling factors in lime treatment are: the pH value and the free calcium (Locat et al., 1996). The pH evolution can be used to monitor and evaluate the development of the pozzolanic reaction with time (Al-Mukhtar et al., 2010). Soil should contain enough pozzolanic minerals to react with the lime. Otherwise, adding more lime will not yield any additional strength gain.

Although very small lime dosages cause short term changes in the mechanical properties of clays due to cation exchange, these changes can be lost by subsequent changes in pore water chemistry due to diffusion or leaching of lime (Diamond and Kinter, 1966). However, Le Runigo et al. (2009) demonstrated that long-term water circulation in lime-treated compacted silt did not seem to have a significant impact on either soil fabric or permeability.

When lime is added to a clay soil, it must first satisfy the affinity of the soil for lime: that is, ions are adsorbed by the clay minerals and are not available for pozzolanic reactions until this affinity is satisfied. The amount of hydrated lime required to bring about physical changes in soil properties to an optimum limit is called the lime fixation point (or initial lime consumption) (Eades and Grim, 1960). Usually lime contents of 3-8% by dry weight of treated soil are typical for soil improvement (Eades and Grim, 1960; Eades and Grim, 1966; Pakbaz and Farzi, 2015; Sakr et al., 2008; Zukri, 2013). Lower percentages (below 3%) are usually associated with short-term changes in soil properties such as flocculation (Bell, 1996; Locat et al., 1996). Eades and Grim (1966) proposed that the fixation point should be defined as the percentage of added lime required to produce a soil pH of 12.4 one hour after treatment. This is based on the philosophy that the pH of the pore fluid will reach the value of a saturated solution of $Ca(OH)_2$ only once ion exchange is complete. However Bell (1996) defined the fixation point as the lime percentage by weight which does not bring about further changes in the plastic limit. Interestingly, some observed soils appear never to reach the pH of a saturated lime solution. The reasons for this are complex and may be simply measurement error (Eades & Grim 1966).

Over time, the free lime concentration falls (as the reaction proceeds) which eventually leads to pH decrease (Metelková et al., 2012). Figure 2-5 shows the results of long term observation of pH values of loess treated with lime, and the decrease in pH over that time.

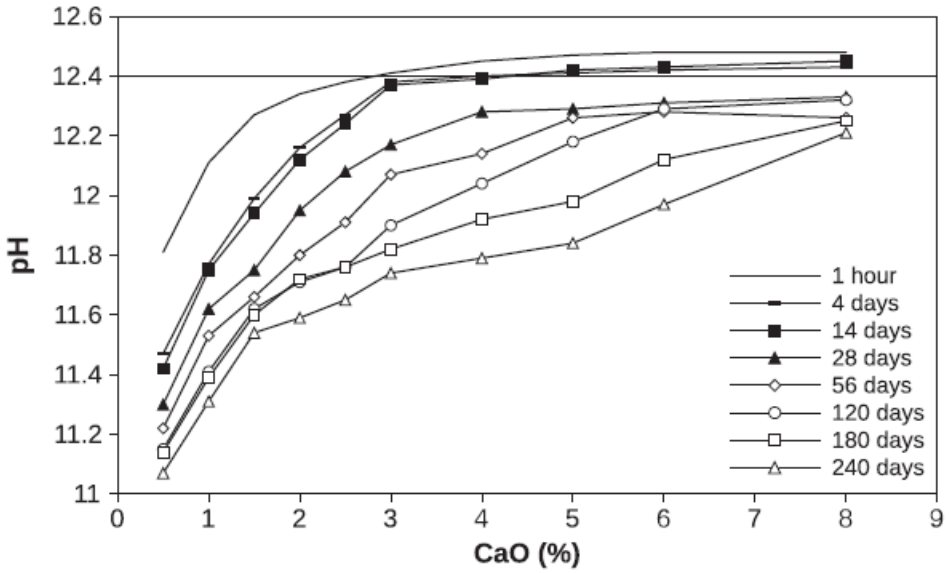

Figure 2-5: The pH of lime-treated loess soils over time (Metelková et al., 2012)

2.2.3.3 Water content

For saturated insensitive (or remoulded) soils, an increase in water content has an adverse effect on undrained strength. A commonly quoted observation is that while the undrained shear strength of clays of different plasticity indices ranges 0.36-1.27 (London, Horten, Shellhaven, and Gosport clays) is approximately 170 kPa at the plastic limit, it falls to about 1.7 kPa at the liquid limit (Wroth and Wood, 1978).

It is plausible that initially high water content also adversely affects chemical bonding (Quang et al., 2012). As the water content of clay increases, the spacing between clusters as well as that between particles increases. This might be countered by increasing the additive concentration (Miura et al., 2001), in soils of high water content.

2.2.3.4 Curing time

A schematic model describing the physico-chemical process, taking into account water content, is presented in Figure 2-6. It illustrates how the reaction products are disseminated within the soil matrix, creating bridges (or coating) between (or on) soil particles which primarily enhances particle bonding. It has been argued that a high water content soil may perform better than a soil with a low water content, because movement of solutes is easier within the porous space (Locat et al., 1990).

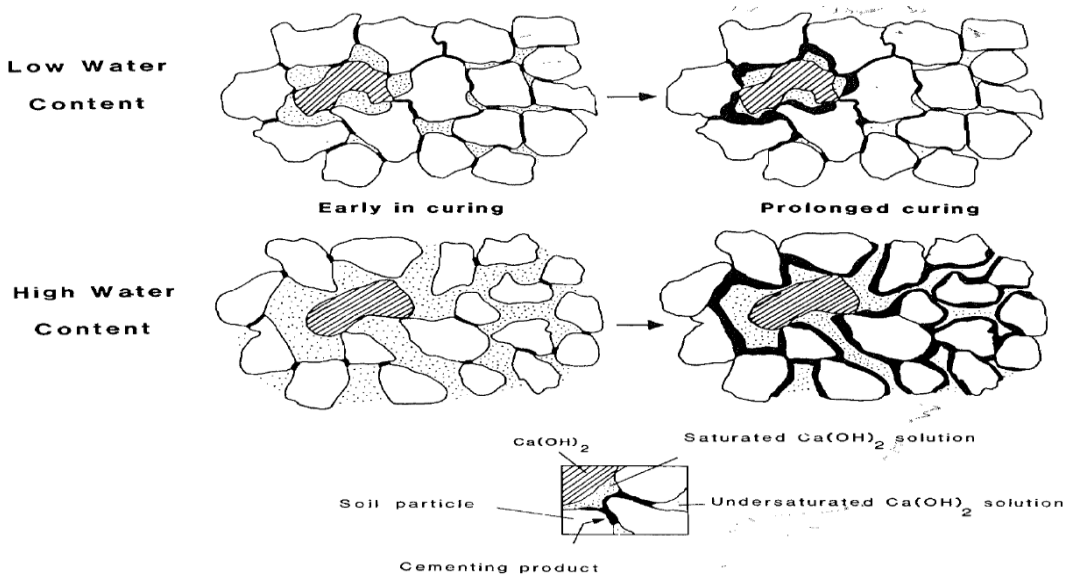

Figure 2-6: Physical conceptual model of lime stabilization of sensitive clays (Locat et al., 1990).

Locat et al. (1990) described the evolution of strength due to lime treatment as shown in Figure 2-7. For a high water content (HWC) lime-treated clayey soil, the time frame can be divided into three phases. During phase I, very little mechanical improvement occurs despite active chemical reactions. During phase II, significant increase in strength occurs due to bonding formation as a result of the pozzolanic reaction. In the final phase, the strength gain eases and stops. This happens because of the completion of the pozzolanic reaction; obstacles to diffusion of solutes within the soil, etc. (Locat et al., 1990).

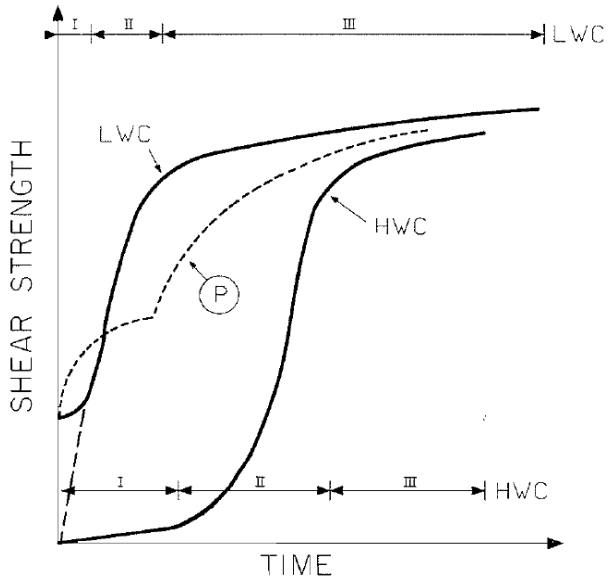

Figure 2-7: Shear strength development over time for high water content (HWC) and low water content (LWC) lime-stabilized clayey soils (P refers to the model of Perret (1977) for silty soils) (Locat et al., 1990).

Janz and Johansson (2002) reported that although Portland cement treatment can quickly yield high strengths, lime can give higher final strengths (Figure 2-8), judging by the weight of the reaction products. However, the weight of the reaction products is not a sufficient proof of improvement because this depend on how well the soil particles are bound together by the products and how effectively they fill the voids. Locat et al. (1990) suggest that high water content soils can be successfully stabilized with lime if enough time is given for the soil to build significant bonding.

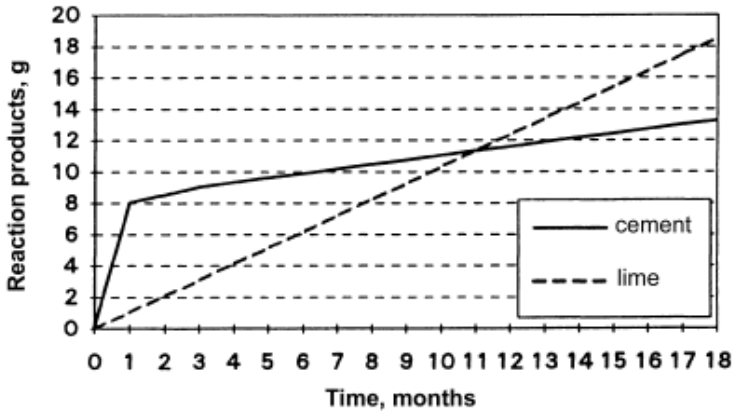

Figure 2-8: Schematic plot of weight of pozzolanic reaction products formed by10 g stabilizer per 100 g dry solids in the presence of an excess of pozzolanic minerals (Janz and Johansson, 2002).

2.2.3.5 Curing temperature

The pozzolanic reaction is strongly temperature dependent; significantly improved strength can be developed with relatively small increases in temperature (Baghdadi, 1982). Conversely, a low temperature results in slow strength gain (Janz and Johansson, 2002).If the temperature falls below around ~4°C, pozzolanic reactions are retarded and may cease at lower temperatures. In fact, pozzolanic reactions may remain dormant during periods of low temperatures but regain reaction potential when temperatures increase (Bell, 1996). For a curing period of seven days, Bell (1996) noticed a substantial increase in unconfined compression strength of tills and laminated clays cured at 40 °C compared to those cured at 20°C as shown in Figure 2-9. Also, Bell (1996) noted that the rate of strength gain is higher at higher curing temperatures. However, the study did not show if this increased rate of strength gain is maintained over longer periods.

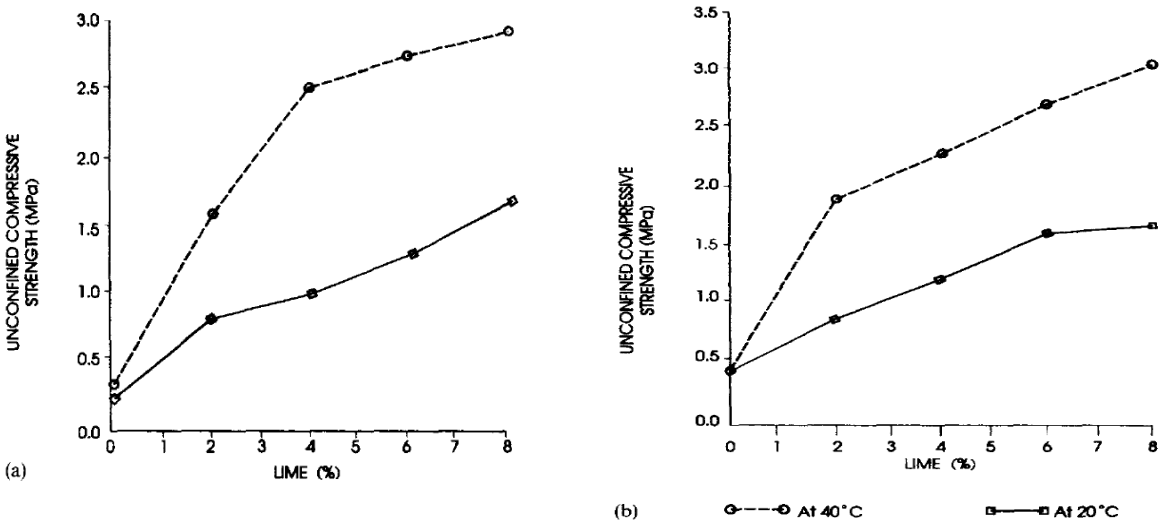

Figure 2-9: The influence of temperature on the unconfined compressive strength of (a) Tees Laminated Clay and (b) Upper Boulder Clay, admixed with lime and cured for 7 days (Bell, 1996).

Thompson (1970) reported that laboratory curing of samples at 120°F for 48 hours produced unconfined compressive strengths approximately equivalent to those obtained from samples cured for 30 days at 70°F and recommended that minimum design requirements be based on those results. Al-Mukhtar et al. (2014) showed that increasing curing temperature to 50°C accelerates lime consumption (Figure 2-10). For example, a kaolinite consumed 95% of a 10% dosage in 30 days at 50 °C, which was not matched after 6 months at 20°C. The increases in lime consumption with temperature may be assumed to follow an Arrhenius law (Al-Mukhtar et al., 2014). The Arrhenius model can be expressed in the form (Marzano et al., 2008):

$$\mathbf{K = A.\exp(-\frac{E_a}{RT})} \qquad \textbf{2-1}$$

where *K* is the rate constant, T is the absolute temperature (K), R is the universal gas constant (8.3144 J/K mol) and E_a (J/mol) is the apparent activation energy. The apparent activation energy is a measure of how sensitive the reaction is to temperature changes. A plot of ln *K* versus *1/T* produces a straight line whose slope is $-E_a/R$. For any given curing temperature (*T*) maintained for time t, an equivalent curing time (t_e) can be calculated for the temperature (T_o) as follows (Eq.2-2):

$$t_e = t.\exp[-\frac{E_a}{R}(\frac{1}{T}-\frac{1}{T_o})] \qquad \textbf{2-2}$$

The ratio t_e/t is the shift factor (a_T) by which results at temperature T should be shifted along the x-axis (time) in order to replicate the results obtained at the reference temperature. In

other words, the equivalent time t_e represents the time required at the reference temperature T_o to obtain the same results as that obtained at an elevated temperature T in time t. The chemical activation energy Ea has been shown (Al-Mukhtar et al., 2014) to be different for different mineralogies. Similar results have been obtained by Diamond and Kinter (1966).

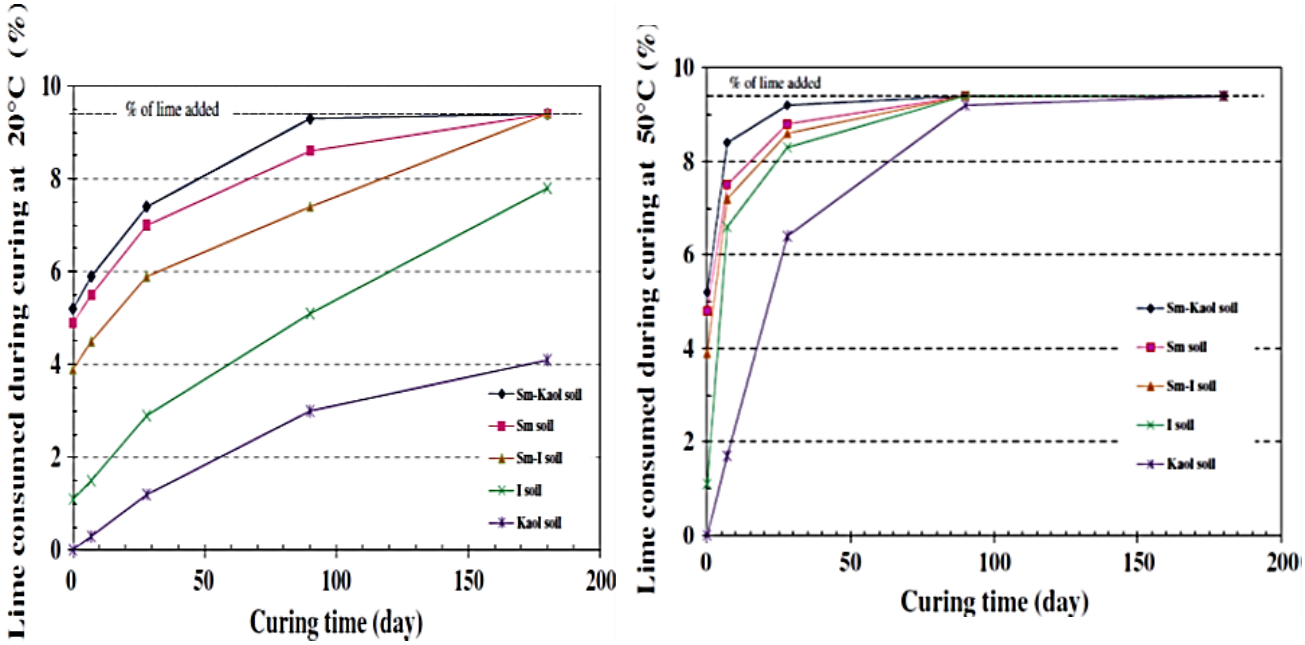

Figure 2-10: Lime consumption for clayey soils at (a) 20 °C and (b) 50 °C (Al-Mukhtar et al., 2014).

2.2.3.6 Organic content

Organic particles can be adsorbed on the surface of soil particles. This impedes both the formation of chemical reaction products and the interaction between soil particles and these products. Black humic acid in organic matter has a strong chemical affinity to calcium. Hence where calcium is present in solution, humic acid may react with calcium and form insoluble calcium humic acid. On the other hand, fluvic acid in organic matter tends to combine with mineral particles containing aluminium, which may induce the decomposition of a layered crystal lattice (Chen and Wang, 2006). Consequently, organic matter tends to inhibit reactions with binders.

Nevertheless, (Sakr et al., 2008) found that sandy mud of high organic content (14%) could be successfully treated with 3% lime, although the best results were obtained at 7% lime. (Quang et al., 2012) found that organic clays needed an extra 2% lime to compensate for the negative effects of organics. Kang et al. (2017) found that humic acid has a negative effect on strength development in cement-treated clay.

2.3 Undrained Shear strength of Clay

The shear strength of soil can be defined as its peak resistance of soil to shearing (τ_f) along a plane of rupture. The failure envelope is normally expressed as a function of the effective stress (σ_n') applied normal to the plane of rupture as (Das, 1985):

$$\tau_f = f(\sigma_n') \qquad \textbf{2-3}$$

The failure envelope is typically curved as shown in Figure 2-11, with the slope of the envelope $\emptyset'$ decreasing with increasing normal effective stress (Lee et al., 1983). For practical purposes, the envelope is normally idealized by a straight-line over the effective stress range of interest. The linear relationship may give a non-zero "cohesion" (c') parameter, even though, the failure envelope passes through the origin. This does not imply that the material has real cohesion (Lee et al., 1983).

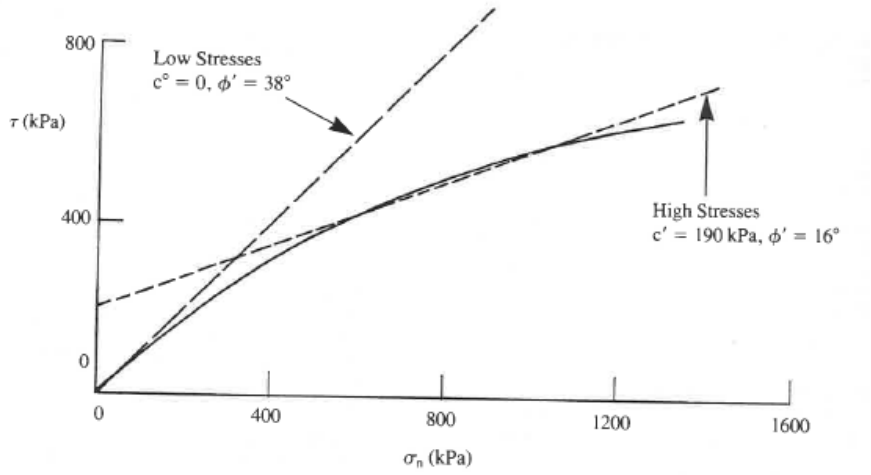

Figure 2-11: A typical failure (peak strength) envelope for soils (Lee et al., 1983)

However, for naturally cemented soils, and soils treated with additives, a significant part of the shear resistance can arise from the bonding (cohesion) between the soil particles or particle aggregations (Burland, 1990; Cotecchia and Chandler, 2000; Gens and Nova, 1993; Horpibulsuk et al., 2003). Of course, other definitions of shear strength (i.e. residual, constant volume) are commonly employed.

Under undrained conditions, the effective stress path to failure may be determined by measurement of the pore water pressures: the path's invariance with respect to total stresses elevates its end point (i.e. the failure condition) to, very nearly, a material property C_u. (Atkinson, 1993). It follows, under the insitu stress conditions pertaining to laboratory

penetration tests (where the effective stresses are low), that the undrained shear strength of additive-treated soils will be little different from the cohesion parameter c' (related to bonding strength). The difficult issues of the precise definition of a distinct failure stress state in soft materials will not be entered into here.

In analysis, undrained shear strength can be characterised by the Tresca (maximum shear stress) model (Atkinson, 1993) (Figure 2-12):

$$(\sigma_1 - \sigma_3) - 2C_u = 0 \qquad \textbf{2-4}$$

where σ_1 and σ_3 are the major and minor principal stresses, respectively.

Shown also in Figure 2-12 is the Von Mises (maximum distortional stress criterion) model.

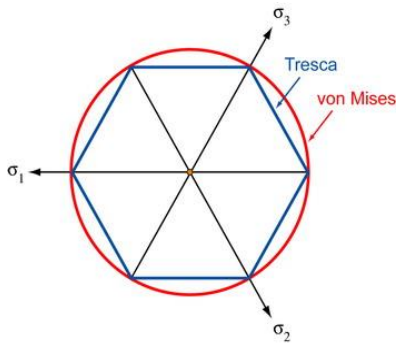

Figure 2-12: Tresca and Von Mises yield surface in principal stress space

2.4 Laboratory Measurement of Undrained Shear Strength

2.4.1 Introduction

Measurements of shear strength can be conducted by intrusive tests (such as vane shear and penetrometer tests) or element tests (such as triaxial and shear tests). Element tests such as triaxial tests are better controlled and are suitable for most soils from which it is possible to prepare undisturbed specimens (Head, 1988b). However, intrusive tests have certain advantages: they can be used to test soils of very low strength and, also, they offer advantages of ease of operation and convenience.

2.4.2 Triaxial compression test

The unconsolidated undrained triaxial test (U-U test) is the method of choice for short-term loading (Smith, 1990). This type of triaxial test was chosen to simulate the short-term

loading of soil to evaluate the shear strength gain developed due to lime-admixing bonding. The consolidated-undrained triaxial test (C-U test) was avoided to prevent the bonding damage that can occur during the consolidation phase. The cylindrical soil sample is subjected to constant cell pressure while axial load is increased at a constant rate of strain until failure (Smith, 1990). Depending on soil type, the rate of axial straining should be low enough to allow for pore water pressure equalization. The undrained shear strength is, by definition, half of the deviatoric stress at failure (Head, 1988b).

2.4.3 Miniature vane shear test

2.4.3.1 General

The vane shear test is a direct method of shear strength measurement of clay on a predetermined cylindrical failure surface. The undrained shear strength of the soil is calculated by measuring the torque developed by the shear resistance on the failure surface. The vane test can be used to measure the intact (undisturbed) as well as remoulded undrained strength. Its main advantage is its simplicity in both performance and interpretation. It is suitable for soft and sensitive clays of low shear strength that would be unsuitable for testing by other methods because of sample disturbance. This test was used by many other researchers to evaluate the undrained shear strength of soft admixed soils (e.g. Kang et al., 2015; Boardman et al., 2001; Sasanian and Newson, 2014; Locat et al., 1990).

However, Bjerrum (1972) showed that the vane shear test overestimated the undrained shear strength in some cases and underestimated it in others. O'Malley and Wright (1987) have shown that vane tests produce higher undrained strength results than U-U tests and the difference increases with decreasing soil water content and some correction is necessary. Others (Kang et al., 2015; Kogure et al., 1988) have reported similar findings. Chung and Randolph (2004) also reported discrepancies, of up to 20% between the shear strengths measured by hand vane with those measured by penetration tests, which was attributed to strain softening effects and soil anisotropy.

2.4.3.2 Measurement and interpretation of vane strength

The disturbance of soil around the vane (see Figure 2-13 below) decreases the measured resistance due to remoulding, which has been found to be linearly related to the ratio of the vane perimeter to thickness ratio (Chandler, 1988; Roy and Leblanc, 1988). On the other

hand, local displacement of soil particles together with a corresponding increase in pore pressures can result in an increase in the effective stresses, with dissipation of the excess pore water pressure as shown in Figure 2-14 below. If enough time is allowed for pore pressure dissipation, the measured undrained strength Cu increase can exceed by up to 20% the true undisturbed strength C_{uo} of highly sensitive soils (Chandler, 1988; Roy and Leblanc, 1988). Increases in undrained shear strength (compared with the standard test of 1min rest period) if a rest period is allowed between the insertion and the rotation of the vane. The increase in strength becomes greater as the rest period becomes longer. This is attributable to the dissipation of the pore water pressure set up by the vane insertion, resulting in the increase in the effective stresses. Partial consolidation of soil around the tip of the vane shaft was also found to affect the measured strengths for low vane to shaft diameter ratios (<1.5). Based on the results obtained by (Low and Randolph, 2010), a minimum vane to shaft ratio of three is recommended.

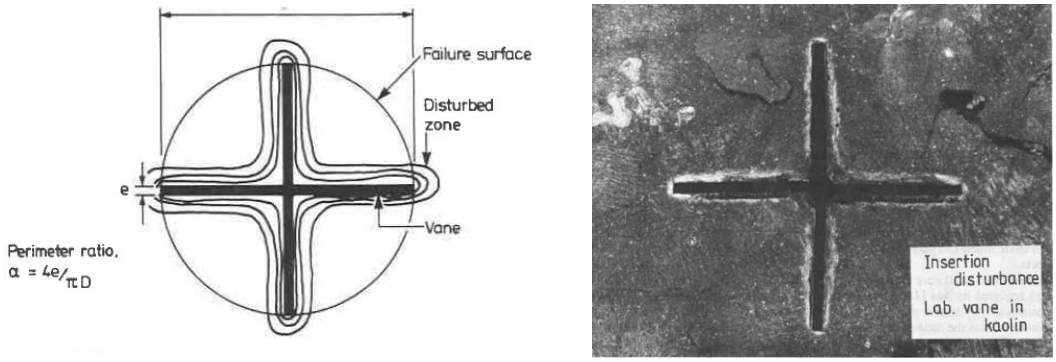

Figure 2-13: Vane insertion disturbance (white area) around laboratory vane in kaolin (Chandler, 1988)

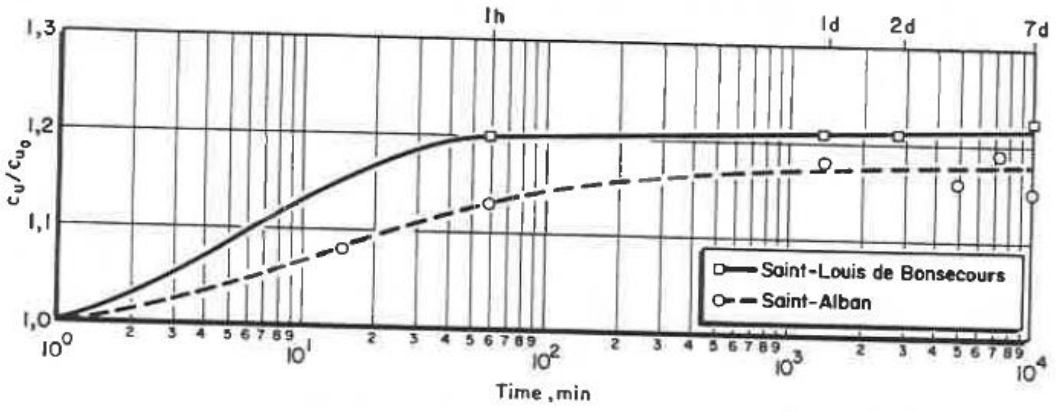

Figure 2-14: Effect of consolidation on undrained shear strength (Roy and Leblanc, 1988)

Some other factors which require consideration are:

- **Viscous strain rate effects and drainage conditions:** these two effects are in conflict (Chandler, 1988). This is reflected in the differences between the British (BS, 1990a) and ASTM (2005) standards which advocate rotational speeds of 12-16 deg./min and 60-90 deg./min. respectively. It can be seen in Figure 2-15 that measured undrained shear strengths increase significantly at rotational speeds less than 0.2 deg./sec (12 deg/min). However, higher rates of rotation have little effect. This suggest that viscous effects are less important than drainage. The results of Schlue et al. (2010) show a higher influence of increasing strain rates on the residual undrained shear strength than the peak undrained shear strength for organic harbour mud.

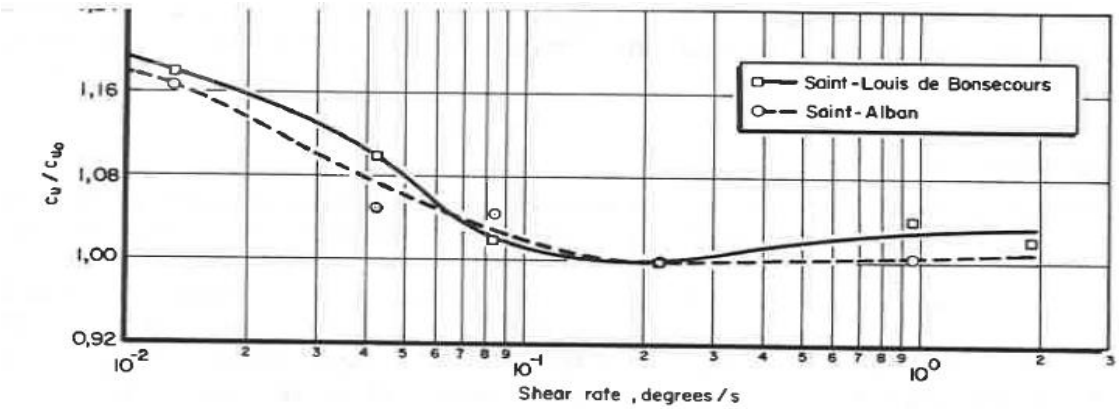

Figure 2-15: Shear rate effect on the undrained shear strength of Canadian clays (Roy and Leblanc, 1988)

- **Variation in stress mobilization around the vane:** The assumption of a uniform shearing stress distribution over the cylindrical failure surface is inaccurate (Silvestri and Aubertin (1988), Kogure et al. (1988), Chandler (1988)). A typical shear stress distribution is shown in Figure 2-16. For a brittle soil, the implication is that the measured undrained shear strength may be significantly less than the peak value. DeAlencar et al. (1988) have confirmed this expectation using finite element analysis. The stress distribution is also vane size dependent which further complicates matters.

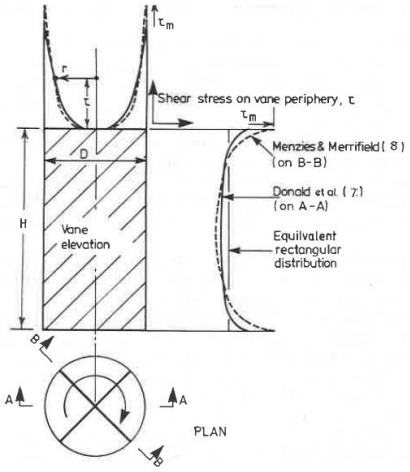

Figure 2-16: Shear stress distribution on cylindrical surface described by the rotating vane (Chandler, 1988)

- **The geometrical shape of the failure mode:** The failure surface is commonly assumed to be perfectly cylindrical. However, the actual shape can be quite different depending on the stage of shearing and soil micro-structure. It has been found that the failure geometry resembles a rounded square at the point of peak global resistance, as shown in Figure 2-17 below (Chandler, 1988). Similar conclusions have been made by Gylland et al. (2012) and Veneman and Edil (1988) who also suggested that the actual shear failure surface shape is soil type dependent.

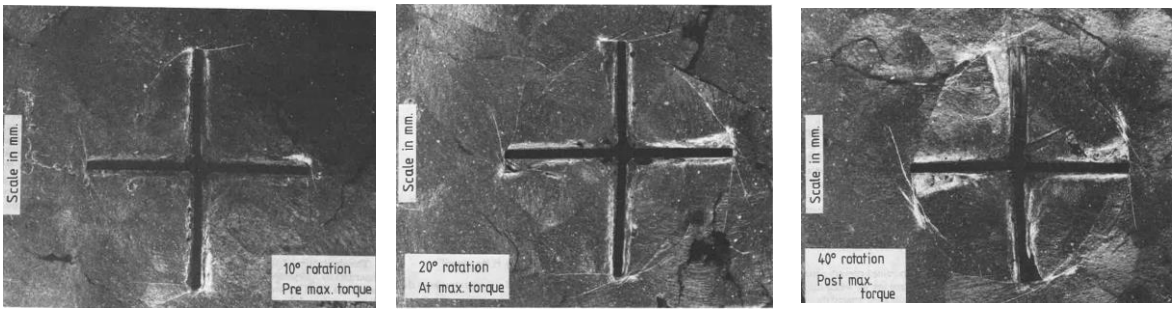

(a) (b) (c)

Figure 2-17: Vane shear structure in kaolin (a) pre-peak shear (b) at peak shear, and (c) post-peak shear (Chandler, 1988)

However, the results obtained by Roy and Leblanc (1988) for sensitive structured soft clay suggests that the failure surfaces is indeed cylindrical but with a diameter which is approximately 5% larger than that the vane.

2.5 Penetration Tests

2.5.1 Introduction

A small cylindrical probe with a flat pressure-sensitive tip was used first by Ladanyi (1968) and Ladanyi and Eden (1969) as a laboratory tool to determine the undrained shear strength of sensitive clays. A field cylindrical bar (or T-bar) was introduced by Stewart and Randolph (1994) and has since been adopted by the offshore industry for deep site investigations in soft clay. Later, an axisymmetric ball head was suggested to reduce the potential for the load cell to be subjected to bending moments arising from non-symmetric resistance along the T-bar. A circular plate is an obvious extension of this idea, although may also be more prone to induced bending moments than the spherical ball at high soil resistance in stiff layers. The major difference compared to the cone is that the T-bar, ball and circular plate penetrometers are 'full-flow' devices, with projected areas typically ten times that of the cone shaft (Einav and Randolph, 2005). Some penetrometers are shown in Figure 2.17 below.

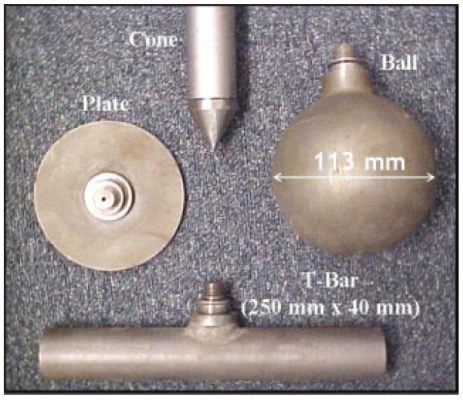

Figure 2-18: Full-Flow penetrometers (Einav and Randolph, 2005)

2.5.2 Interpretation of penetration test results

2.5.2.1 Theoretical background

For all penetration devices, the undrained shear strength, C_u, can be evaluated as:

$$C_u = \frac{q_{net}}{N} = \frac{q_{ult} - q_o}{N} \qquad \textbf{2-5}$$

in which q_{ult} is the bearing pressure of the soil, q_o is the in situ vertical total pressure, q_{net} is the net bearing pressure and N is a penetration resistance factor.

In this study a circular disc penetrometer will be employed: the theoretical background to determining N is discussed in the following section. In the soil mechanics context, bearing resistance is an outgrowth of the Prandtl (1921) plastic theory of indentation. The Terzaghi (1943) bearing resistance equation is the well-known:

$$q_{ult} = c' N_c + q_o N_q + 0.5 B \gamma N_\gamma \quad \textbf{2-6}$$

where c' is the cohesion intercept, γ is the unit weight of soil, q_o is the surcharge pressure, and B is the footing width. N_c, N_q, and N_γ are bearing capacity factors and are dependent only on $\emptyset'$. In terms of total stresses, this equation becomes:

$$q_{ult} = C_u N_c + q_o \quad \textbf{2-7}$$

which is of the same form as equation 2-5. The undrained shear strength C_u of clays, using the bearing capacity equation of foundations, can thus be determined from:

$$C_u = q_{net} / N_c \quad \textbf{2-8}$$

where N_c is a bearing capacity factor and C_u is the undrained shear strength.

2.5.2.2 Bearing capacity of surface circular foundations

Levin (1955) presented an upper-bound solution (namely, $N_c = 5.84$) for the problem of the indentation of a smooth circular punch on a half-space of a perfectly plastic (Tresca) material. Shield (1955) found a lower bound solution ($N_c = 5.69$) using the slip-line method which was confirmed by Tani and Craig (1995). Eason and Shield (1960) extended the same method to perfectly rough footings to obtain $N_c = 6.05$. Both values were confirmed by Houlsby and Wroth (1984) and Martin (2004). Pressure distributions under the foundation for both of these cases is given in Figure 2-19.

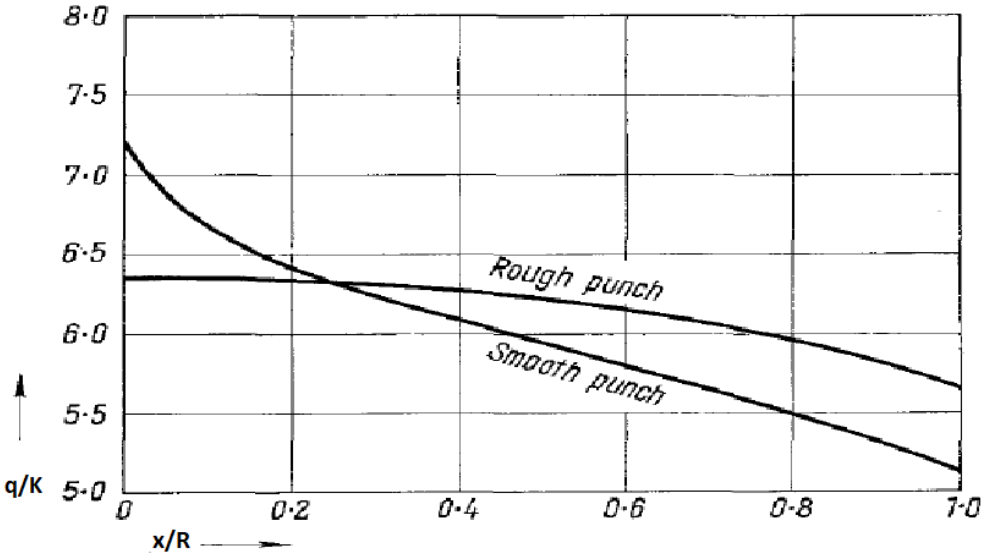

Figure 2-19: Contact pressure (q) distribution under a circular punch resting on an incompressible material (Eason and Shield, 1960)

Taiebat and Carter (2008) examined the rough foundation problem for a Tresca material using the Finite Element Method and obtained the result of N_c=5.87. Similar results were obtained by Tapper et al. (2014). Osman and Bolton (2005) developed a kinematically admissible mechanism for a smooth circular footing to obtain a value of N_c= 5.86.

2.5.2.3 Bearing capacity of deep circular foundations

It is difficult to extend the classical methodds of analysis to problems where the indenter is embedded in the substrate. The following review encompases a wide range of solutions, mostly obtained by numerical modelling.

The solutions presented in Table 2-2, solve the problem of solid cylindrical indenters with smooth (or rough) side walls at different depths in soil. These solutions must yield upper bounds because backflow into the penetrometer cavity is prevented.

Table 2-2: Summary of bearing capacity solutions for solid cylindrical footings

Problem Category	Author	Foundation	Interface Condition	Approach	Depths	Remarks
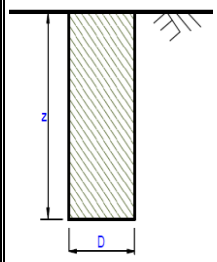	(Martin and Randolph, 2001)	Rigid deep circular caisson	Rough base with Rough or smooth sides	UB and LB solutions of stress characteristics	0<z/D <2.0	Alternative independent upper bound mechanism & lower stress field
	(Houlsby and Martin, 2003)	Deep Conical footing	Rough base with Rough or smooth sides	method of characteristics to obtain LR bound solution	z/D < 2.5	Compares well with some semi-empirical solutions of deep footings
	(Hu et al., 1999)	Rigid deep shaft footing	Smooth or rough foundation	Small Strain FE (Tresca)	z/D < 5.0	Both smooth and rough base results coincide when z/D>1. When z/D>2. Nc=9.9
	(Hu et al., 1999)	Rigid deep shaft footing	Rough base with Smooth Sides	Large Displ. FE (Tresca)	z/D < 5.0	LD FE using Re-meshing and Interpolation Technique with Small Strain (RITSS). When z/D>4, Nc=12.7
	(Gourvenec and Mana, 2011)	Rigid deep shaft footing	Rough base with smooth sides	Small Strain FE (Tresca)	z/D<1.0	Agrees well with the solution of (Martin and Randolph, 2001).
	(Edwards et al., 2005)	Rigid deep shaft footing	Rough base with smooth or rough sides	Small Strain FE . Tresca soil	z/D<4.0	Results are similar to those of (Hu et al., 1999) but Nc keeps increasing after z/D>2.
	(Nguyen and Merifield, 2012)	Rigid deep shaft footing	Rough Base with smooth sides	3D Small strain FE. Tresca soil	z/D<5.0	Results coincides with (Salgado et al., 2004) UB solution with increasing Nc values with increasing depth
	(Benmebarek et al., 2017)	Rigid deep foundation	Smooth or rough sides and base	Small Strain FE	z/D<5.0	Results coincide with (Salgado et al., 2004) UB solution and

The second group of solutions (Table 2-3) refer to problems of circular rigid plates buried at different depths. These solutions too provide upper bounds because although they admit a local rotational mechanism, the soil above the disc has shear strength.

Table 2-3: Summary of bearing capacity solutions for buried circular footings

Problem Category	Author	Foundation	Interface Condition	Approach	Depth	Remarks
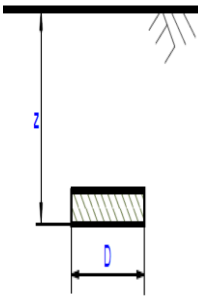	(Salgado et al., 2004)	Rigid plate embedded in soil	Rough base	UB & LB limit analysis with linear 3D FE	z/D<5	Difference < 6% in UB and LB results at surface level but increases to 22% at z/D=5
	(Martin and Randolph, 2001)	Rigid plate embedded inside soil	Smooth and rough bases	UB and LB solutions of stress characteristic	Deeply buried	Rough: Nc(LB)=Nc(UB)=13.1 Smooth: NC(LB)=NC(UB)=12.4
	(Hossain and Randolph, 2009b)	Deep penetration of spudcan	Smooth and rough bases	Small strain & large displ. FE	0<z/D<3	Nc increasing depending on Cu/γD until Nc(rough)=13.1 and Nc(smooth)=12
	(Hu et al., 2001)	Rigid plate pre-embeded in soil	Smooth and rough bases N.C. soil Cu=0.9z, kPa	Small strain FE	z/D<3	Well bracketed by the bound solutions of (Martin and Randolph, 2001) for circular plate
	(Hu et al., 2001)	Rigid plate pre-embeded in soil	Smooth and rough bases N.C.soil (Cu=0.9Z , kPa)	Large Displ. FE	0<z/D<4	LD FE using Re-meshing and Interpolation Technique with Small Strain (RITSS). No effect of plate roughness Nc=11.7

The last group (Table 2-4), presents solutions for the bearing resistance of soils due to spudcan and plate penetration, which are more relevant to disc penetration. The small strain FE solution of Hossain and Randolph (2009b) suggests that N_c increases with depth up to a constant N_c=10 for z/D>1.5. However, a large displacement FE analysis by Hossain and Randolph (2009b), which allows a soil backflow mechanism during penetration, indicates a continuous increase in bearing resistance beyond z/D>1.5. Although no further information is given for penetration beyond z/D=3, the experimental data reported by Khoa and Jostad (2016) shown in Figure 2-21(a) suggests that the penetration resistance of spudcan models reaches an asymptotic value of Nc=11 beyond penetration depths of z/D>2.0. This result agrees with their solution of smooth base spudcan penetration using a coupled Eulerian-Lagrangian (CEL) technique. However, for rough base spudcans, their analysis indicates a rapid increase of N_c above 12 to which does not seem credible.

Table 2-4: Summary of bearing capacity solutions for deep circular footings

Problem Category	Author	Foundation	Interface Condition	Approach	Depth	Remarks
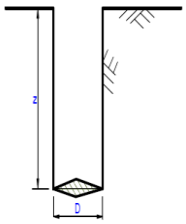	(Hossain and Randolph, 2009b)	Rigid deep spudcan foundation	Smooth or rough base	Small strain FE (Tresca)	z/D<3.0	Nc=10 for z/D>1.5 for rough base and Nc=9.0 for z/D>1.25 for smooth base
	(Hossain and Randolph, 2009b)	Rigid spudcan foundation	Smooth or rough base	Large displ. FE. Tresca soil	z/D<3.0	LD FE using Re-meshing and Interpolation Technique with Small Strain (RITSS). Nc increasing with depth
	Khoa and Jostad (2016)	Rigid spudcan foundation	Smooth or rough base	Large displ. FE (Modified Mohr coulomb)	z/D<3.0	LD FE using Coupled Eulerian-Lagrangian (CEL) technique. Good agreement with experimental data
	Hui et al. (2013)	Rigid spudcan foundation	Rough base resting on N.C. soil	LD FE (Tresca)	z/D<3	LD FE using Coupled Eulerian-Lagrangian (CEL) technique Results are slightly higher than those obtained by (RITSS) but both converge at Nc=11
	(Tho et al., 2012)	Rigid spudcan foundation	Rough base resting on N.C. soil	LD FE (Tresca)	z/D<10	LD FE using Coupled Eulerian-Lagrangian (CEL) technique Results are in agreement with those obtained by (RITSS) but reach an asymptote Nc=12

Some solutions, as can be seen from Figure 2-20 bracket the true result between close upper and lower bounds such as that of Martin and Randolph (2001).

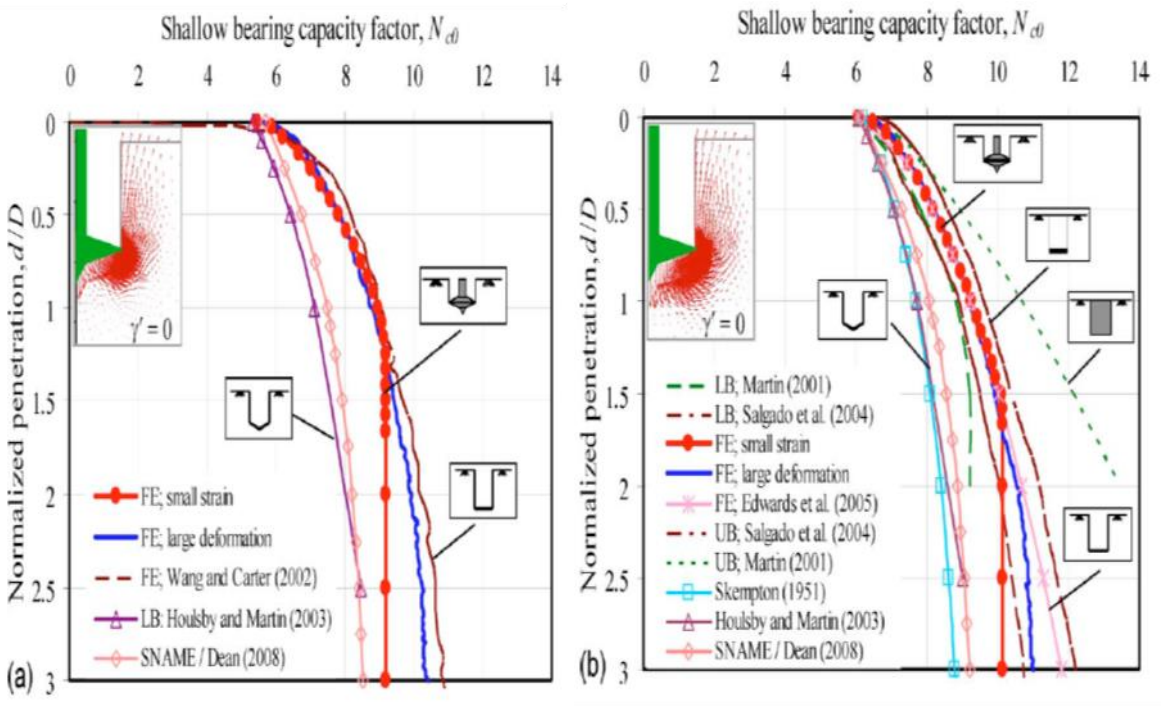

(a) (b)

Figure 2-20: Bearing capacity factors for circular spudcan foundations on weightless homogeneous soil: (a) smooth base; (b) rough base (Hossain and Randolph, 2009b)

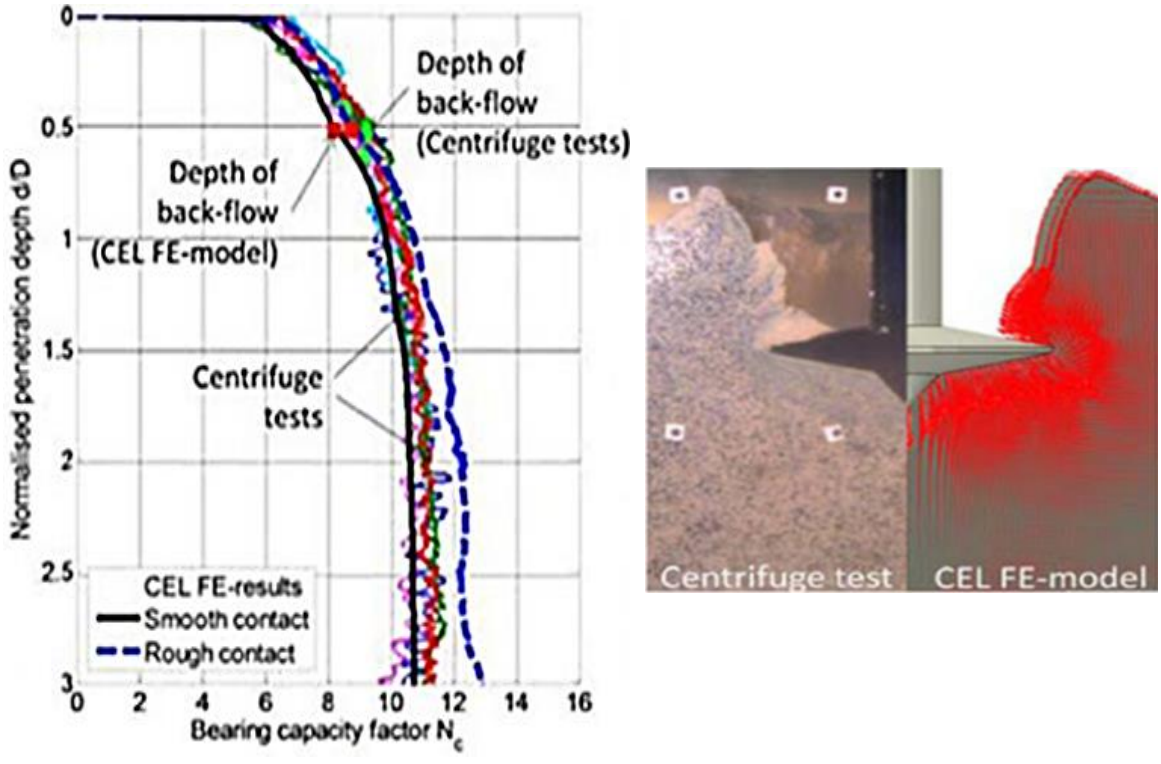

(a) (b)

Figure 2-21: Spudcan penetration modelling: (a) Bearing capacity factors and (b) failure mechanism at onset of soil back-flow (after Khoa and Jostad (2016))

Figure 2-22 illustrates captured digital images of spudcan models at various penetration depths during centrifuge tests conducted by Hossain and Hu (2005). The soil surface heaves

up, during initial penetration (Figure 2-22-a), and a cavity is formed above the spudcan. When penetration is deeper, soil starts to fill into the cavity. Figure 2-23 shows the corresponding displacement vectors using the images captured during the same test.

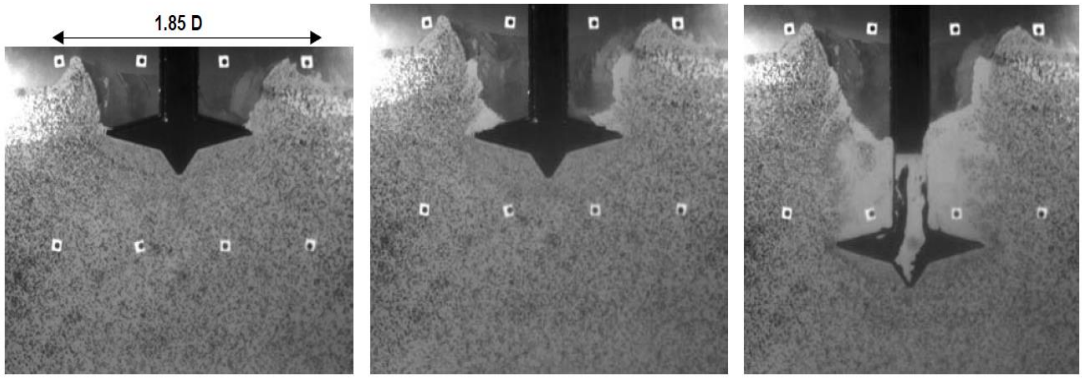

Figure 2-22: Captured digital images of spudcan model images in uniform clay (Hossain and Hu, 2005)

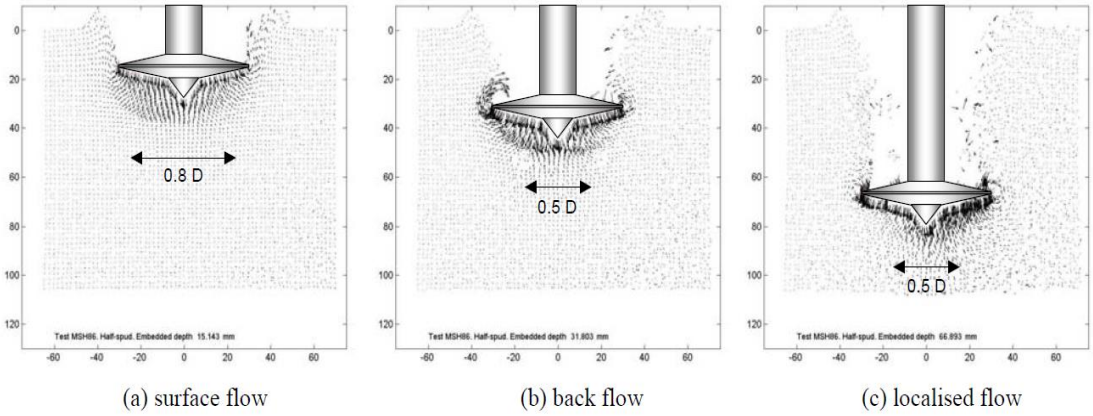

Figure 2-23: Soil flow mechanisms in uniform clay (Hossain and Hu, 2005)

2.5.3 Factors affecting penetration tests

2.5.3.1 Strain rate effects

Penetration resistance in clay increases with reduced penetrometer velocity (v) due to consolidation around the penetrometer (Chung et al., 2006; DeJong et al., 2011; Ganesan and Bolton, 2013; Lehane et al., 2009; Mahmoodzadeh et al., 2011). At slow velocities, there is time for pore pressure developed during shearing to dissipate (Chung et al., 2006). At higher velocities, the soil response becomes increasingly undrained. However, if penetrometer velocities are too high, viscous (and even dynamic) resistances may become significant (Lehane et al., 2009).

Figure 2-24(a) shows the results of T-bar penetration tests at various velocities. Penetration resistance result (q_{T-bar}) are normalized ($\frac{q_{T-bar}}{q_{T-bar,ref}}$) with respect to penetration resistance at a reference velocity of v =1.0mm/sec, ($q_{T-bar,ref}$). It can be seen that when the velocity is reduced to 0.01 mm/sec, the penetration resistance is about 2.5 times greater than that measured at 1 mm/sec. This can be attributed to consolidation around the penetrometer tip at lower velocities. The degree of consolidation during continuous penetration may be characterized by a normalised non-dimensional velocity V, defined as (Finnie and Randolph, 1994):

$$\mathbf{V} = \frac{\mathbf{v}.\mathbf{d}}{\mathbf{c_v}} \qquad \textbf{2-9}$$

where v is the penetration velocity, d is the diameter of the penetrometer and c_v is the coefficient of consolidation of the soil. The same results are normalized with respect to the non-dimensional velocity V in Figure 2-24(b). Table 2-5 shows the range of the normalized velocities to attain drained and undrained penetration conditions using different penetrometers as obtained by different authors. Drained conditions arise in the velocity range of 0.01-0.1 and fully undrained conditions are attained at normalized velocities in the range of 20-100. Differences in interpretation of drained/undrained conditions, as well as difficulties in determining c_v can account for differences between authors in identifying the critical normalized velocities (Jaeger et al., 2010; Mahmoodzadeh and Randolph, 2014).

To account for different penetrometer shapes, Chung et al. (2006) suggest the use of a normalized velocity: $V' = vd_e/c_v$, where d_e is the diameter of a disk with the same area as the penetrometer.

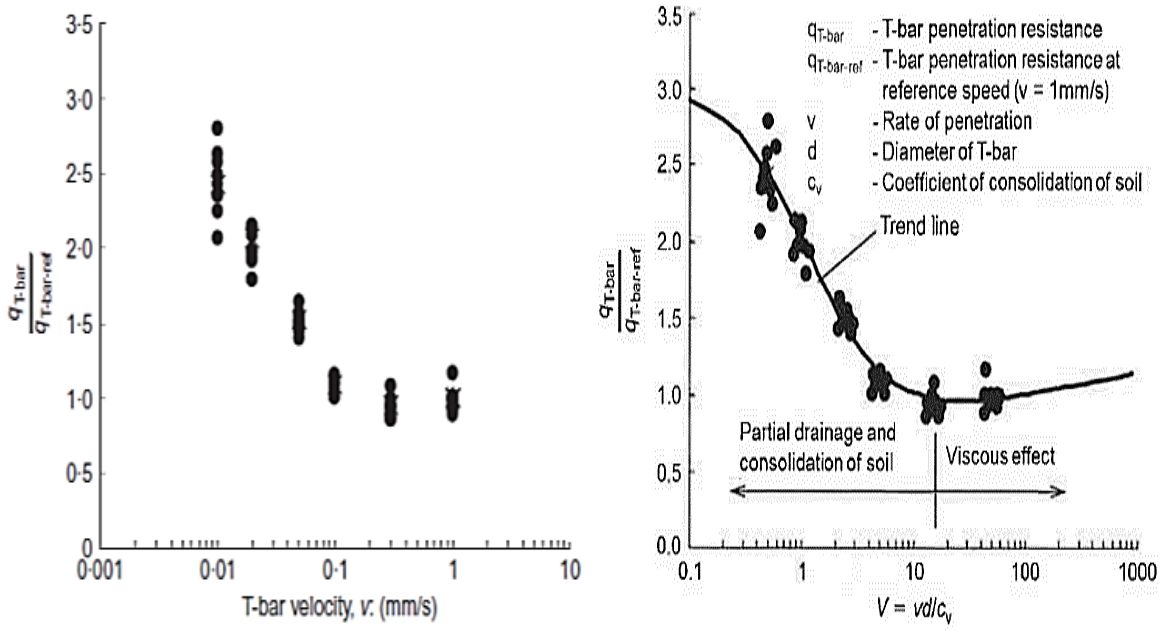

(a) (b)

Figure 2-24: Normalised T-bar resistance variation with: (a) T-bar velocity; (b) normalised velocity (after Lehane et al. (2009) and Ganesan and Bolton (2013))

Table 2-5: Normalized velocities ranges for drained and undrained penetration conditions.

Author	Penetrometer	V=vd / C_v		Soil	C_v measurement
		Drained	Undrained		
(Finnie and Randolph, 1994)	T-bar	V<0.01	V>30-100		
Mahmoodzadeh et al. (2011)	Piezoball	V<0.10	V>50	Carbonate muddy marine silt.	Rowe cell
(Schneider et al., 2007)	Piezocone	V<0.04	V>100	N.C and O.C kaolin and silica flour + Bentonite	Rowe cell
(Jaeger et al., 2010)	CPT	V=0.01	V>20	75% sand+25% kaolin	Vertic. consolid.
Chung et al. (2006)	T-bar & ball		300	Natural soil	Vertical consolidation in centrifuge
Ganesan and Bolton (2013)	T-bar		V>50	High plasticity marine clay.	Oedometer test
Kim et al. (2008)	Flat and cone tipped	V≈0.05	V>10	Sand + kaolin mix.	Isotropic and 1D consolidation

Due to viscosity, soils exhibit different measured undrained shear strengths if sheared at different strain rates (Einav and Randolph, 2006; Einav and Randolph, 2005). The shear strength at a strain rate of $\dot{\gamma}$ can be expressed as (Dayal and Allen, 1975; Peck, 1966):

$$C_u = C_{u,0}\left(1 + \mu \log \frac{\dot{\gamma}}{\dot{\gamma}_0}\right) \quad \text{2-10}$$

where $C_{u,0}$ is the shear strength at the reference shear strain rate of $\dot{\gamma}_0$. Typical values of the coefficient μ are in the range of 0.1–0.2 (or 10–20% change in shear strength per log cycle) (Casacrande and Wilson, 1951; Graham et al., 1983).

Yafrate and DeJong (2007) propose that bearing resistance should follow a similar relationship:

$$\frac{q}{q_0} = 1 + \mu \log\left(\frac{(v/d)}{(v/d)_0}\right) \qquad \textbf{2-11}$$

However, some researchers believe that viscosity is a function of strain rate and not a constant (Pinkert and Klar, 2012; Robinson and Brown, 2013). More complex correlations have been proposed by Lehane et al. (2009) to account for both consolidation and viscous effects which can be seen schematically in Figure 2-25 below.

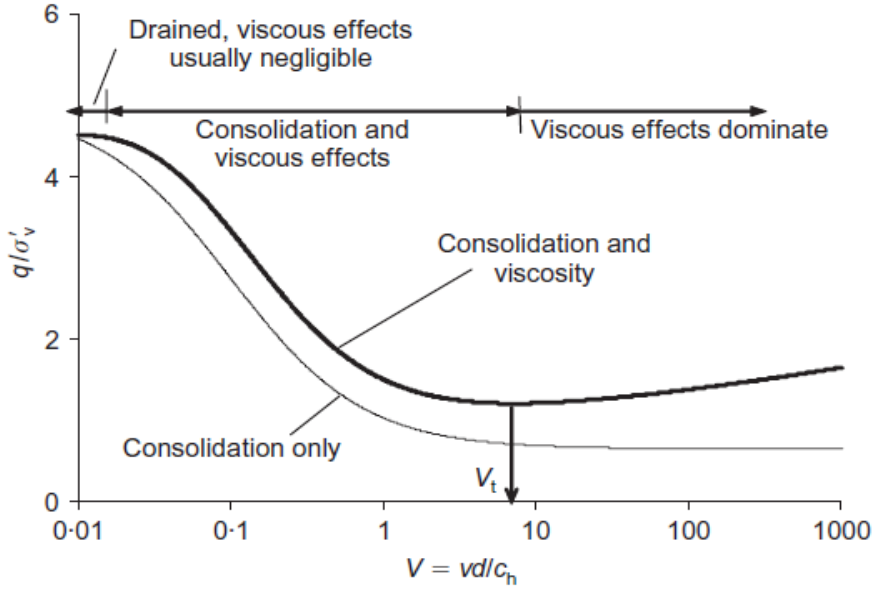

Figure 2-25: Strain rate effect on penetration resistance q normalized by vertical effective stress б'v (Lehane et al., 2009)

2.5.3.2 Strain softening effects

The strength measurement of strain-softening materials, such as soil admixtures, raises many difficulties. Certainly, the difficulties are magnified in intrusive testing if the material is both highly sensitive and brittle. For the soils tested in this study, there is evidence (mainly based on the work required to remould these soils) that the measured strengths reflect peak (intact) strengths. For natural soils, this question has attracted the attention of, for example: Einav and Randolph (2005), Pinkert and Klar (2012), Ladanyi (1968), Randolph and Andersen (2006), Ganesan and Bolton (2013), and Yafrate et al. (2009). Strain-softening constitutive models have been used in many numerical solutions (Ansari et al., 2014; Pinkert and Klar, 2012; Pinkert and Klar, 2013; Randolph et al., 2008; Tian et al., 2014; Wang et

al., 2010; Zheng et al., 2016; Zhou and Randolph, 2007; Zhou and Randolph, 2009a, b; Zhou et al., 2016).

A particularly interesting study by Zhou and Randolph (2009b) numerically simulates deep steady penetration resistance of ball penetrometers in sensitive clays. The shear strength of the surrounding soil reduces with continuous development of plastic shear strain using an exponential decay function (Einav and Randolph, 2005) as:

$$C_{us} = C_{u,i}(\delta_{rem} + (1 - \delta_{rem})e^{-3\xi/\xi_{95}}) \qquad 2\text{-}12$$

where C_{us} and $C_{u,i}$ are the softened and initial strengths respectively, δ_{rem} is the inverse of the sensitivity (S_t), and ξ is the cumulative plastic shear strain, with ξ_{95} being the cumulative plastic shear strain required to achieve 95% (since $e^{-3}\approx0.05$) remoulding which might be taken around 10-50 (1000-5000%). Pinkert and Klar (2012) suggested the following relation for ξ_{95} for T-bar penetrometers:

$$\xi_{95} = 50 - \frac{40}{1 + (S_t/10)^{-3}} \qquad 2\text{-}13$$

The effect of varying the soil ductility (that increases with increasing ξ_{95}), is shown in Figure 2-26(a). Reducing soil ductility tends to decrease penetration resistance from the ideal (fully ductile soil). Also shown in Figure 2-26(b), is the effect of increasing the soil sensitivity on penetration resistance. Increasing soil sensitivity (by reducing δ_{rem}) reduces the penetration resistance from the ideal insensitive case (where $\delta_{rem} = 1/S_t = 1$). Decreasing the friction ratio between the penetrometer and the soil α was also shown (Figure 2-26(b)) to reduce the penetration resistance. Significant oscillations of about 0.25D periodicity can be seen in these solutions, which is a real material phenomenon (Zhou and Randolph, 2007), arise due to the periodic shear bands evolving ahead of the advancing penetrometer (Zhou and Randolph, 2009b).

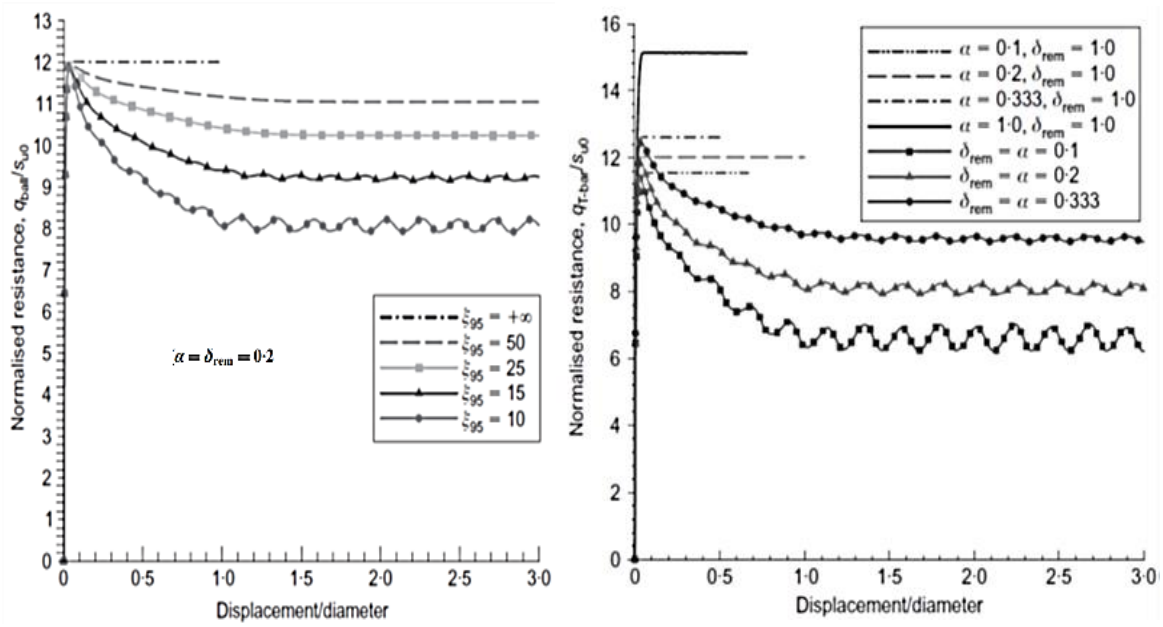

(a) (b)

Figure 2-26: Resistance-displacement response of ball penetrometer in rate-dependent, strain-softening clay (a) effect of soil ductility on the penetration resistance; and (b) effect of soil sensitivity (Zhou and Randolph, 2009b)

Hossain and Randolph (2009a) also numerically simulate the bearing capacity of spudcan foundations in non-homogeneous sensitive clay. Figure 2-27 shows the effect of strain-softening and strength sensitivity parameters on the bearing capacity N_c factor with depth as compared to non-softening soil. In Figure 2-27(a), as the ductility of the soil increases (with increasing ξ_{95}), the response approaches that of the non-softening soil. By reducing soil ductility, there is a significant reduction in N_c with depth, up to depth ratio of about z/D=1.0 compared to the non-softening soil The effects of soil sensitivity (described by the remoulded strength ratio, δ_{rem}) and spudcan base roughness α, is shown in Figure 2-27(b). Increasing soil sensitivity (by decreasing δ_{rem}) tends to reduce the soil resistance to spudcan penetration.

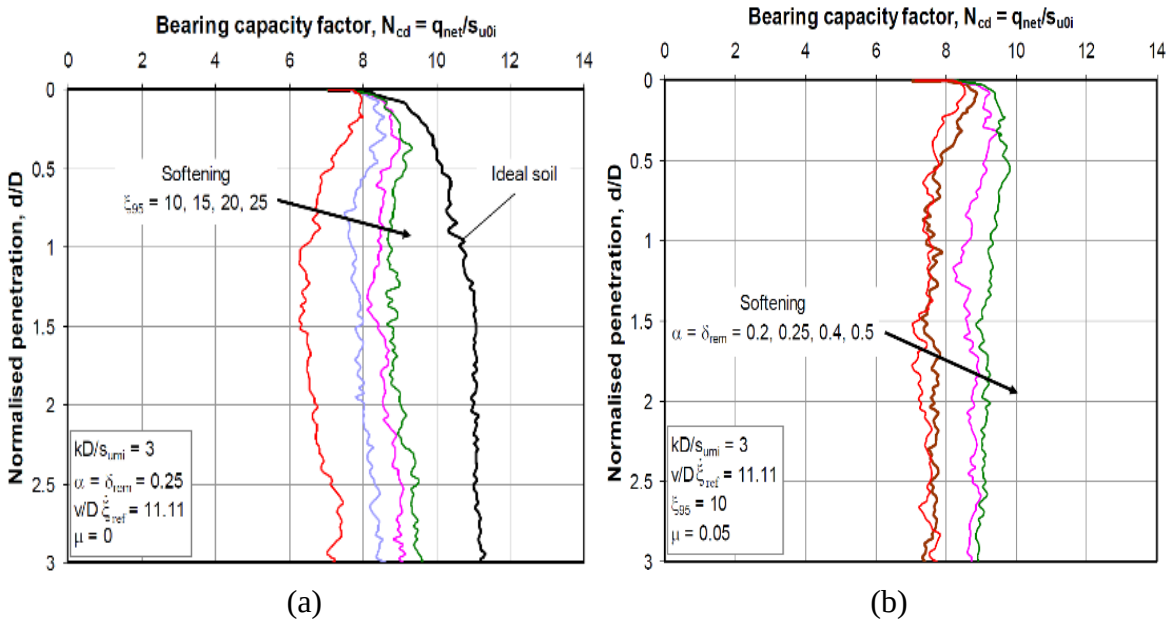

Figure 2-27: Effect of (a) strain-softening and (b) strength sensitivity on the penetration resistance factor N_c of a spudcan in non-homogeneous clay (Hossain, 2008; Hossain and Randolph, 2009a)

Given sufficient data on the strain-softening characteristics of a soil (itself a major undertaking) it is possible in principle to improve the interpretation of penetrometer data, in order to (for example) extract peak strength values. In practice, this seems scarcely possible as a practical proposition.

2.5.4 Empirical relationships for undrained shear strength

The effectiveness of chemical (lime) stabilization can be quite difficult to predict. The gain in shear strength (C_u), at a given time, will be a function of many variables (Locat et al., 1990):

$$C_u = f(C_{ui}, A, A_w, W_{w0}, c, t_a, t) \qquad \textbf{2-14}$$

where C_{ui} (kPa) is the undrained shear strength immediately after treatment; A is a mineralogical parameter that includes mineralogy, grain size, specific surface area, and cation exchange capacity; A_w is a parameter related to the initial pore-water chemistry; W_{w0}(%) is the moulding water content, c (%) is the additive concentration; and t_a and t (days) the time of mellowing, and curing, respectively. The mellowing time corresponds to the time between lime mixing and moulding and curing time is the elapsed time since moulding. These considerations explain why, in the field of soil treatment, usually only empirical approaches are known. Sasanian and Newson (2014), for example, suggested that, for cement admixed clays, the undrained shear strength can be satisfactorily modelled by

the following polynomial function using a parameter β that correlates between clay activity, cement/water ratio (c/w), and the undrained shear strength. However this relationship might be only applicable in a limited range of cement contents may give an overestimate of strength gains of some natural soils (Sasanian and Newson, 2014). Locat et al. (1990) suggested that the resulting undrained shear strength of lime admixed soils at high water content with constant lime concentration as a function of water content (w) is changing according to the following power-law relationship:

$$C_u = a.w^b \quad \text{2-15}$$

where a and b are constants that are themselves functions of soil nature, curing time, and lime concentration. This empirical approach would have merit if the form of the functions a and b were relatively simple which seems to be unlikely.

2.6 Remoulded and Intact Shear Strength

The effects of structure are understood most readily through a comparison of the stress-void ratio states which are possible for structured soils with those that are possible for destructured soils. After destruction of a soil's structure, the resulting shear strength has been variously called the remoulded, residual, or ultimate strength. However, the specific term to be used depends upon the way that the soil structure has been destroyed. Soils that have their natural structure modified by manipulation (i.e., by kneading) are called remoulded soils (ASTM Standard Terminology Relating to Soil, Rock, and Contained Fluids D 653-97).

The sensitivity of soil (S_t) was defined by Terzaghi as the ratio between the peak undrained shear strength in the undisturbed condition (C_u) to the residual undrained shear strength of the soil after remoulding (C_{ur}) (Skemption and Northey, 1952). It serves as a criterion for examining the development of the microstructure bonding or inter-particle forces between individual soil particles or their aggregates (Bobei and Locks, 2013). Based on comprehensive laboratory and field reported data, in which S_t for many natural clays increases exponentially with liquidity index (I_L) as shown in Figure 2-28, Wood (1990) suggested the relationship:

$$S_t = \exp(k.I_L) \quad \text{2-16}$$

where the factor k ranges between 1 and 3 although a value of 2 is suggested by the "best fit". (Sahdi et al. (2014)).

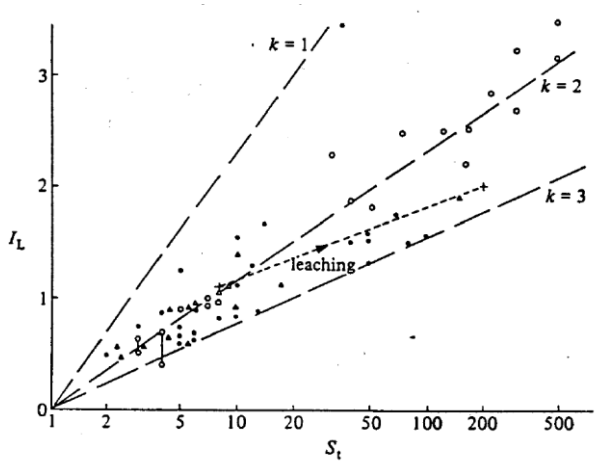

Figure 2-28: Interrelationship between sensitivity and liquidity index (Wood, 1990)

For soils of high liquidity indices (in the range 1.5 to 6), Locat and Demers (1988) proposed the power law:

$$C_u = (1.167/I_L)^{2.44} \qquad \textbf{2-17}$$

Similar relations but with different coefficients have been suggested by other researchers (e.g. (Boukpeti et al., 2009; Leroueil et al., 1983; Sahdi et al., 2014))

2.7 Compression of Structured Clays

2.7.1 Intrinsic properties

Clayey soils can be encountered or produced in four different states of structure (Leroueil et al., 1985), namely: (a) the intact state, as occurs in natural deposits; (b) the destructured state, observed when an initially intact clay is submitted to volumetric or shear deformations of such magnitude that the original clay structure is broken, which occurs for example in an oedometer test or beneath under an embankment when the vertical effective stress exceeds the preconsolidation pressure; (c) the remoulded state, obtained when sufficient mechanical energy is imparted to a clay mass to reduce its strength to a minimum, and; (d) the re-sedimented state from slurry (Leroueil et al., 1985).

(Burland, 1990) added a fifth state of soil, termed the reconstituted state, which is when clay has been thoroughly mixed at a water content equal to or greater than the liquid limit (W_{LL}). The mechanical properties of soil in this state are called intrinsic properties. They are usually are denoted by the symbol * attached to the relevant mathematical symbols. For example, Cc* is the intrinsic compressibility (Burland, 1990). Figure 2-29 shows the one-dimensional intrinsic compression curves for some reconstituted clays. Although some of them have approximately the same liquid limit (W_{LL}), the void ratios at their liquid limits states e_{LL} are less similar because of differences in their specific gravities. This led (Burland, 1990) to claim that e_{LL} is a more fundamental parameter than w_{LL}. Burland (1990) suggested a normalization of the one-dimensional compression results with respect to the parameters e^*_{100} and e^*_{1000} which are the void ratios at vertical effective stresses of 100 kPa and 1000 kPa respectively.

The normalizing parameter chosen was defined as the void index I_V such that:

$$I_v = \frac{e - e^*_{100}}{e^*_{100} - e^*_{1000}} = \frac{e - e^*_{100}}{C_c^*} \qquad \textbf{2-18}$$

where Cc*= e^*_{100} - e^*_{1000} and is called the intrinsic compression index.

Figure 2-29 (b) is the normalization of three of the intrinsic curves on Figure 2-29(a). The unique curve is termed the intrinsic compression line (ICL). However, Cerato and Lutenegger (2004) have argued that the intrinsic parameter I_V is not a true intrinsic soil property since the reconstituted consolidation behaviour is dependent on sample preparation. Nevertheless, other researchers agree that the void index is a powerful tool for correlating the compression curves of various reconstituted clays over a wide range of initial water contents from 0.7~2.0 times their liquid limits (Hong et al., 2010; Hong et al., 2012; Zeng et al., 2015). Recently, Chu et al. (2017) report that the void index (I_v) and the normalized curves are more suitable for evaluating the compression behaviour of pure clays (irrespective of their mineralogy) than sand‑clay mixtures, which need a different unified framework. A similar index , I'_v has been proposed by Tremblay et al. (2001) but founded on the stress range of 10-100 kPa.

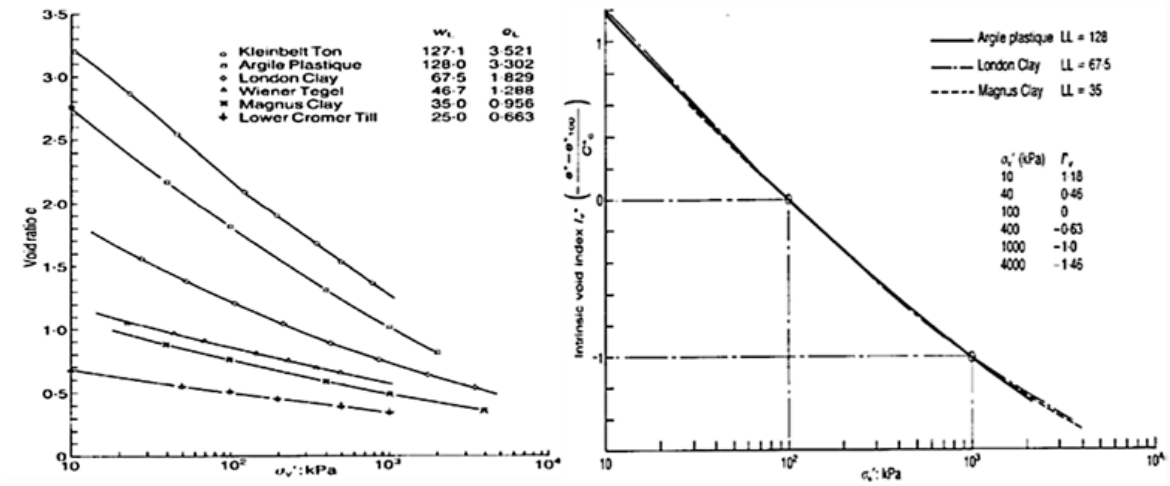

(a) (b)

Figure 2-29: One dimensional compression curves for reconstituted clays (Burland, 1990)

2.7.2 Naturally structured soil

Following (Mitchell, 1976), the term ‘structure’ means the combination of ‘fabric’ (arrangement of particles) and interparticle ‘bonding’. The term `soil structure' is used here to mean the arrangement and bonding of the soil constituents. To avoid the inference that they must have any particular origin, soils which show them will be described as ‘structured’. It encompasses all features of a soil that cause its mechanical behaviour to be different from that of the material with the same mineralogy at a selected reference state (reconstituted state). Soils from which they have been removed by strain or remoulding, or in which they have never existed, will be described respectively as ‘destructured’ or ‘non structured’ (Hong et al., 2012; Leroueil et al., 1985; Leroueil and Vaughan, 1990).The removal of soil structure is usually a progressive process (Liu and Carter, 2000) (Liu et al., 2003). The structured soils can be conceptualized as binary medium materials consisting of bonded blocks and weakened bands (Shen, 2004, 2006; Liu and Shen, 2005). During loading process, the brittle bonded blocks are gradually broken and transformed to weakened bands behaving elastoplastically, so the two components bear the loads collectively (Liu et al., 2013).

Although, there is no agreed terminology by which the effects of soil bonding may be described (Leroueil and Vaughan, 1990), when bonds are developed between grains, they affect the behaviour of such kind of soils in various ways. For instance, soils acquire tensile strength, and since bonds are often fragile in nature, they also develop a collapsible structure that may give rise to unexpected instabilities (Nova et al., 2003). In their review of soils

with bonding, Leroueil and Vaughan (1990) have shown that the patterns of behaviour observed in all cemented soils, clays, silts, sands, and weak rocks are similar even though the cementation may result from different causes. Therefore, artificially cemented soils may be expected to show many of the characteristics of naturally cemented materials (Huang and Airey, 1998)

Cementation involves the bonding together of soil particles by the precipitation of material in the pore spaces. The cementing material may be derived by partial intrastratal solution of grains or may be introduced into the pore spaces from an extraneous source by circulating waters (Bell, 2007). Natural cementation like repeated wetting and drying of clay soils can bring about aggregation of soil particles and cementation by compounds of Ca, Mg, Al and Fe (Sridharan and Allam, 1982). The role of the induced cementation is to weld the fabric (Horpibulsuk et al., 2003). In the case of soft clays, the role of cementing agents here is to strengthen the fabric at the intercluster spacing: that is, to weld the fabric at these sites (Horpibulsuk et al., 2003). If a cementing agent is admixed with such a system, the strength increases over time as the clay reduces to the non-particulate state as a result of cementation (Horpibulsuk et al., 2003).

Owing to the effect of structure, natural (undisturbed) clays have a compression curve lying above that of the reconstituted state in the space of e–log $б_v$' (Burland, 1990; Federico et al., 2015; Leroueil and Vaughan, 1990).

As illustrated schematically in Figure 2-30 (a), it has long been recognised that the soil structure of natural clays remain strongly resistant to deformation until the vertical effective stress reaches a threshold value (Butterfield, 1979). Leonards and others have used the term 'quasi preconsolidation pressure' to describe this critical pressure (point Y of Figure 2-30(a)). Burland (1990) recommended that the term '*yield stress*' or more precisely '*vertical yield stress'* should be used and be denoted by $б_{vy}$'. The term 'overconsolidation ratio' should be reserved for describing a known stress history. The ratio of yield stress to the effective overburden pressure ($б_{vy}$'/$б_{vo}$') could be termed the 'yield stress ratio'. As in the example of one-dimensional compression curves given in Figure 2-30, the compressive response can be sub-divided into two states: the pre-yield (intact) state, which arises in natural deposits for vertical stresses below the yield stress and is characterised by reversible deformation; and the post yield state of behaviour which causes elasto-plastic deformation. Leroueil et al. (1979) have termed the post-yield disruption of the clay structure as 'destructuration'. Structure is not removed immediately by primary yield: this requires

substantial post-yield strain. Post yield behaviour involves a gradual loss of structure with further strain. In this respect it differs from yield due to overconsolidation (Leroueil and Vaughan, 1990). On loading, the difference between the void ratios of natural clays and reconstituted clays at the same stress level increases up to the consolidation yield stress, but decreases thereafter (Hong et al., 2012; Xiao and Lee, 2014). Substantial further strain may be required to establish similar fabric and particle packing (Leroueil and Vaughan, 1990). (Wood, 1990) argues that undisturbed and disturbed compression curves intersect at a water content equal to the plastic limit (I_L=0); at this liquidity, sensitivity is in general close to unity (Skemption and Northey, 1952).

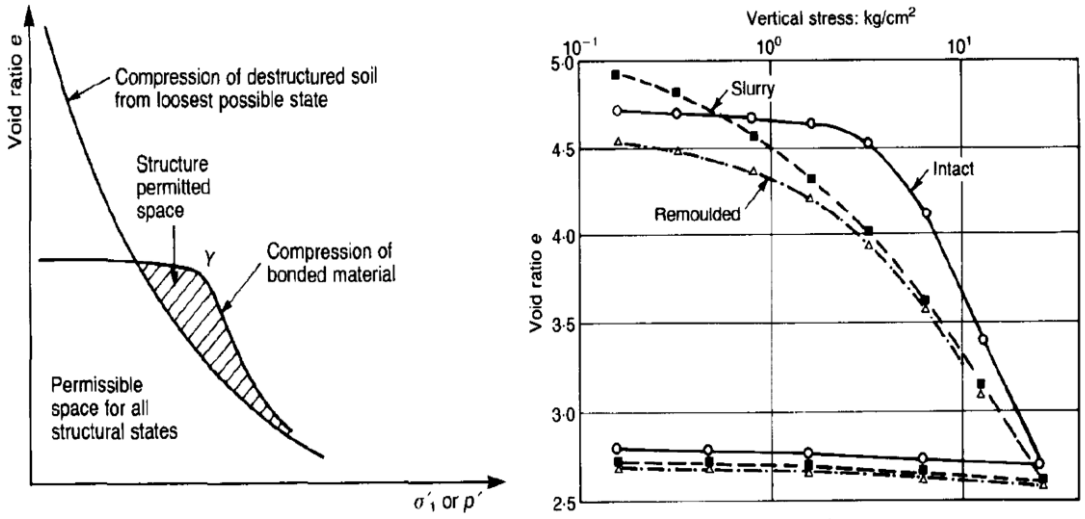

(a) (b)

Figure 2-30: (a) The comparison of structured and destructured compression in the oedometer teat; and (b) Oedometer tests on undisturbed and remoulded samples of residual soil from Java (Leroueil and Vaughan (1990)

(Cotecchia and Chandler, 2000) suggested that sensitivity is related to void index I_v as shown in Figure 2-31. The compression curves are all quasi-parallel, with the curve for reconstituted clays (S_t =1) lying to the left. The compression curves for which S_t >1 lie to the right, the distance increasing with sensitivity.

A parameter called the "stress sensitivity" S_{σ} can be defined as the ratio of the vertical effective stress on the virgin compression curve (of a natural structured clay) to the vertical effective stress at the same void ratio on the compression curve for the reconstituted soil ($S_{\sigma}=\sigma'_{vy}/\sigma^*_e$) (Cotecchia and Chandler, 2000) demonstrate that this parameter is approximately equal to the strength sensitivity S_t. If this is true in general, then either stress sensitivity or strength sensitivity could be used as a measure of clay structure.

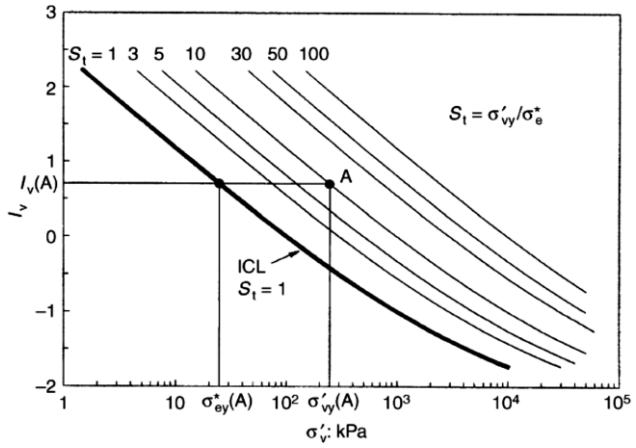

Figure 2-31: Sedimentation compression curves in the idealized sensitivity framework (Cotecchia and Chandler, 2000)

The yield stress $б_{vy}$' is defined as the maximum point of curvature observed in one dimensional consolidation tests on undisturbed soils. More than one graphical procedure has been proposed as alternatives to the commonly used method suggested by Casagrande (1936) to determine this parameter. For example, one-dimensional compression test results may be drawn on a bi-logarithmic scale (Hong et al., 2012; Sridharan et al., 1991).

2.7.3 Artificially structured clays

Artificial cementation can be performed in different techniques and/or chemical agents such as s electroosmotic chemical treatment (ECT) (Ou et al., 2015), microbially induced calcite precipitation (MICP) (Cheng and Cord-Ruwisch, 2012; Cheng et al., 2013), or lime and cement treatment. In lime treatment, the siliceous and aluminous constituents can chemically react with lime in the presence of water to form cementitious compounds.(Barnes, 2000). Cementation increases peak strength initial stiffeness and brittleness. Also gives some tensile strength (Leroueil and Vaughan, 1990) (Horpibulsuk and Liu, 2015)

Tremblay et al. (2001) pointed out, for lime or cement treated clay soils, at the same binder content that oedometer compression curves converge to a single compression line. Its slope is a function of binder content and curing time, but not water content. This observation was confirmed by (Lorenzo and Bergado, 2004) for cement-admixed soft plastic Bangkok clay at different water contents as can be seen in Figure 2-32. Similar conclusions have been drawn by Horpibulsuk et al. (2004a).

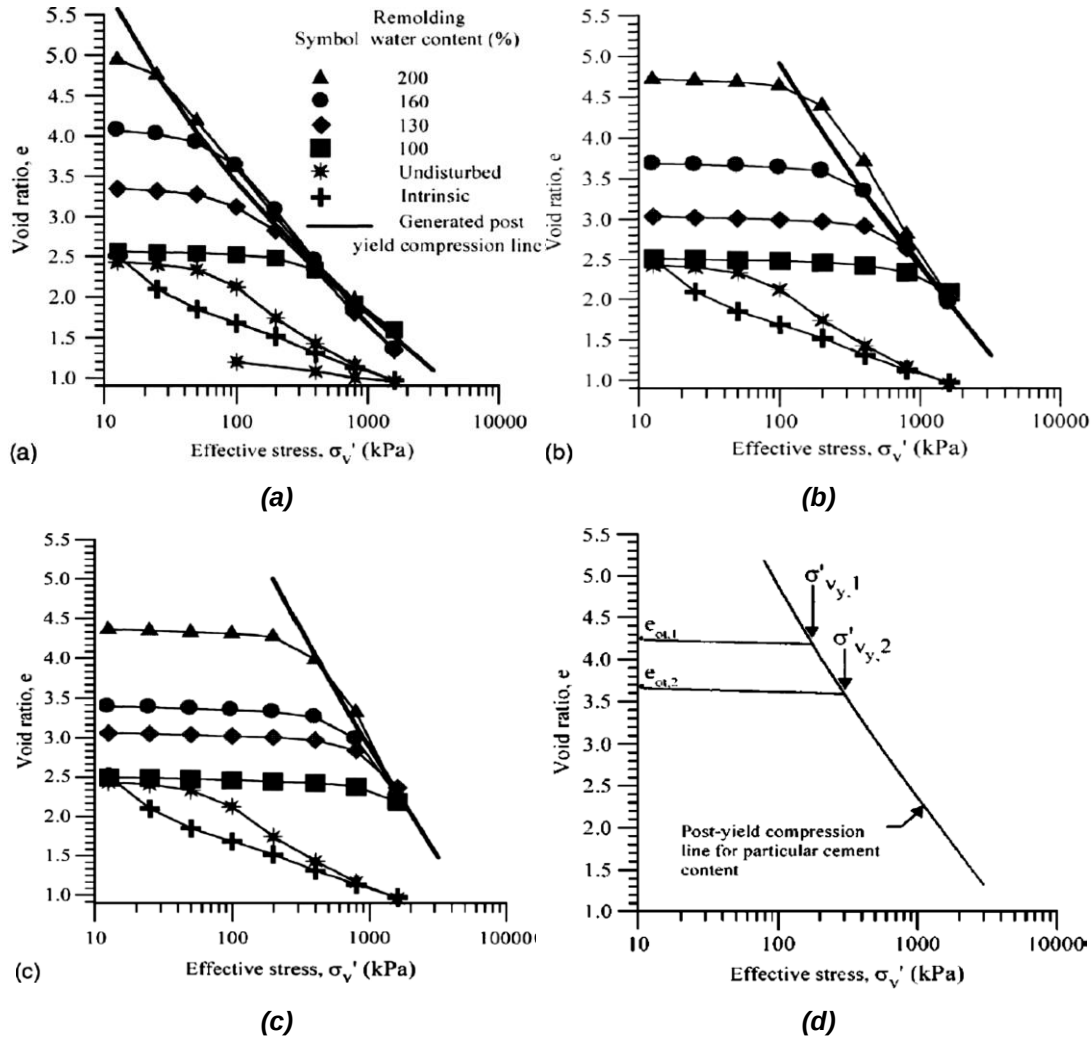

Figure 2-32: One-dimensional compression curves: (a) 5%, (b) 10%, (c) 15% cement contents, and (d) schematic diagram of one-dimensional compression curve of cement-admixed soft clay. After Lorenzo & Bergado (2004)

The vertical yield stress is found to be directly related to the undrained strength of soil. For example, (Hassan and Ravaska, 2009) have found that the vertical yield stress of three different clays dosed with Portland cement at water contents near to their liquid limits and cured for 28 days can be correlated with undrained shear strength by the equation:

$$C_{\mathrm{u}} = 0.42 * 6'\mathrm{vy} \qquad \textbf{2-17}$$

Other researchers (Federico et al. (2015) and Horpibulsuk et al. (2004b)) have found correlation coefficents of 0.45 ~ 0.79 for artificially cemented soils. On the other hand, (Burland, 1990) reported a correlation coefficient of approximately 0.3 for naturally structured normally consolidated soils.

Chapter 3 LABORATORY APPARATUS & TECHNIQUES

This chapter describes the experimental procedures followed during the course of this study, including soil sample preparation and the testing techniques. It begins with a description of how the soils were prepared, treated with slaked lime, and cured. The various tests conducted on these specimens, and the interpretation of the data, are described.

3.1 Sample Preparation

3.1.1 Soils

A range of soils was tested in the experimental programme. In particular, a local natural Grangemouth soil in addition to commercially available kaolin and bentonite mineral compounds were employed. These soils are depicted in Figure 3-1:

Figure 3-1: Soils used in the experimental programme

Speswhite kaolin (China clay)

Speswhite kaolin clay (China clay) is a commercially produced material supplied by IMERYS Kaolin Co. for industrial as well as research purposes. The material consists mainly of hydrated aluminosilicate minerals of the chemical form, $Al_2Si_2O_5(OH)_4$. It is a highly refined powder of ultrafine particle size and high brightness. It consists, according to x-ray fluorescence (XRF) tests conducted by the producer, of kaolinite of at least 38% Al_2O_3 and 47% SiO_2. Two slightly different batches of kaolin supplied by IMERYS Kaolin Co. were used in this research denoted by **K1** and **K2** respectively. Their properties are summarized in Table 3-1. From the particle size distributions given in Figure 3-2, it can be

seen that the clay fractions in K1 is about 75% while it is about 68% in K2. However, as given in Table 3-1, the liquid limit of K1 is 66% and it is 67.5% for K2.

Bentonite CB

Bentonites (from the smectite family) are hydrated aluminosilicate minerals, comprised chiefly of montmorillonite. When bentonite is mixed with water, water molecules enter between the clay plates, forcing them apart. These clays can absorb and adsorb extremely high volumes of water (high W_{LL}, W_{PL}).

Bentonite CB (also known as Fuller's Earth referring to naturally occurring material that has a high absorptive capacity (Hosterman and Patterson, 1992)) is a natural non-activated calcium bentonite, named after the dominant element, calcium (Ca). It is supplied by RS Minerals Ltd as a powder for use in pelletizing applications, fertilisers, seed coatings and effluent treatment. This soil is milled by the supplier to give a consistent fine powder. Chemical analysis results, mineralogy, and other properties are shown in Table 3-2. Its physical properties are summarised in Table 3-1 while its particle size distribution is shown in Figure 3-2. As can be seen in Figure 3-2, the clay fractions is about 58% which indicates that it is not a pure bentonite clay although according to the plasticity chart it is a clay of high plasticity.

SW Bentonex-Kaolin mix (SW-K)

Bentonex SW (sodium bentonite) is a high-quality Argentinian natural sodium bentonite, milled to a consistent fine powder, supplied by RS Minerals Ltd and used in the manufacture of cosmetics and other specialist applications. Chemical analysis results and mineralogy are shown in Table 3-2.

A mix of 60% of kaolin K1 and 40% of Bentonex SW was used as an artificial soil type. This mix ratio was chosen to produce a liquid limit equal to that of the CB bentonite clay, i.e., 1.22. The relationship between the mix ratio and liquid limit is illustrated in Figure 3-3. The physical properties of the mix are summarized in Table 3-1, while its particle size distribution is given in Figure 3-2.

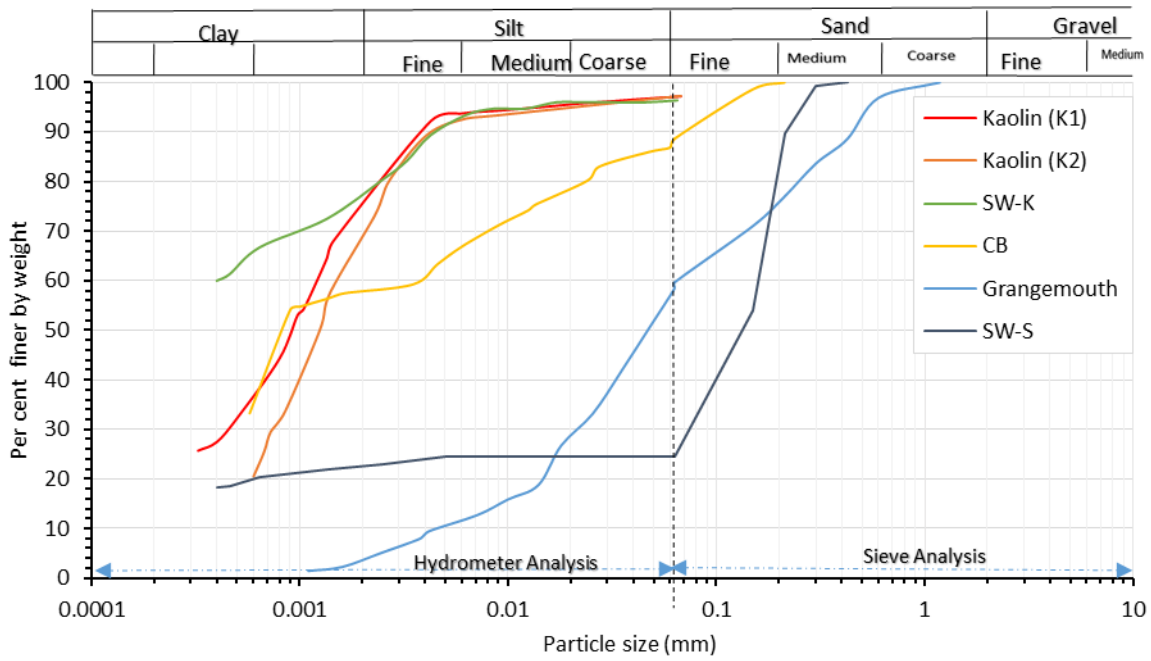

Figure 3-2: Particle size distributions[1] of the soils used in the experimental programme.

Table 3-1: Physical properties of the soils used in the experimental programme.

Soil type	Speswhite kaolin	Speswhite Kaolin	Calcium base bentonite	Sodium base bentonite-kaolin	Sodium base bentonite-sand mix	Natural Grangemouth soil
Symbol	K1	K2	CB	SW-K	SW-S	G
Specific gravity G_s	2.67	2.6	2.77	2.69	2.71	2.72
Liquid limit W_{LL}[2] (%)	66	67.5	122	122	67.5	44
Plastic limit W_{PL}[3] (%)	34.3	34.7	39.7	31	24.4	22.9
Plasticity index I_P (%)	33.2	31.3	82.3	91	43.1	20.6
Loss on ignition (L.O.I) %	10.91	10.74	2.65	1.8 (for SW only)	1.8 (only for SW only)	7[4]

[1] Particle size distribution tests conducted in accordance with BS 1924: Part1, as described in BS 1377: part2 (1990) and BS 812-103.1: 1985

[2] The liquid limit tests were conducted using the fall cone apparatus following BS 1377:Part 2 (1990)

[3] The plastic limit tests were conducted following BS 1377: Part 2 (1990).

[4] The chemical test using Hydrogen Peroxide according to BS 1377: part 3 (1990) indicated only 3% organic content in Grangemouth soil.

Table 3-2: Chemical constituents of bentonite (RS Minerals Ltd.)

Property	Compound	Bentonite CB	Bentonite SW
Chemical compounds %	SiO_2	60.7	60.61
	Al_2O_3	18.31	18.42
	Fe_2O_3	3.95	4.79
	MgO	3.32	2.78
	K_2O	3.14	<0.45
	CaO	2.85	2.07
	Na_2O	1.56	3.2
	TiO_2	0.49	0.47
	Mn_3O_4	0.08	<0.06
	L.O.I.	6.05	6.34
Minerology %	Montmorillonite	88	88
	Gypsum	5	5
	Feldspars	5	5
	Quartz	2	<2

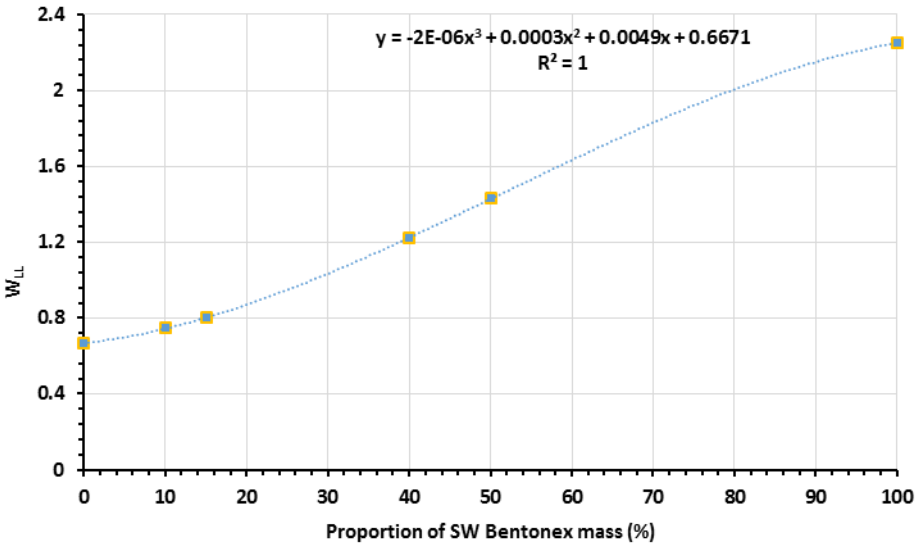

Figure 3-3: Effect of addition of SW Bentonex to kaolin on the liquid limit of the resulting mix

SW Bentonex-Sand mix (SW-S)

A mix of 75.6% of uniform fine sand (S) and 24.4% of SW Bentonex was used as a second artificial soil type. This mix ratio produced a soil with a liquid limit equal to that of the kaolin clay K2, i.e. 67.5%. The effect of mix ratio on the liquid limit is illustrated in Figure 3-4. The particle size distribution of the resulting SW-S mix is shown in Figure 3-2.

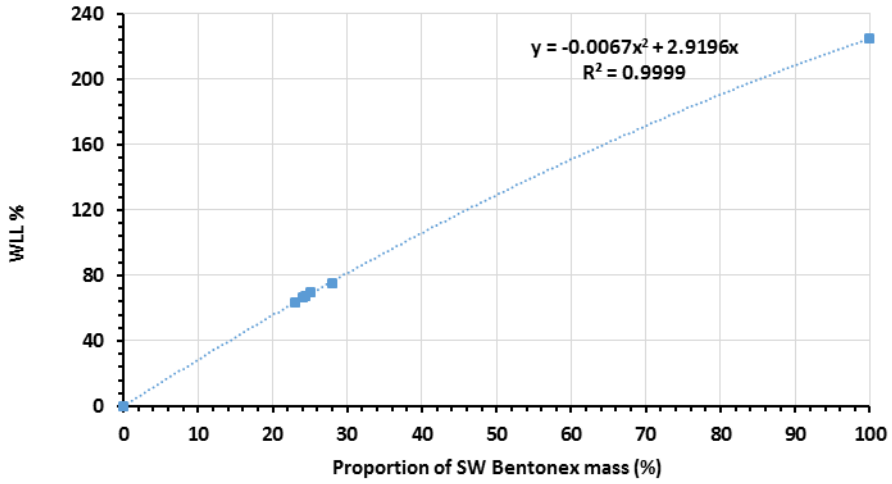

Figure 3-4: Effect of the addition of SW Bentonex to fine sand on the liquid limit of the resulting mix

Grangemouth soil

The Grangemouth soil samples were recovered from stores held by the Soil Mechanics laboratory of the University of Glasgow. Grangemouth lies on the southern shores of the River Forth and at the mouth of the River Carron, situated between the Scottish Highlands to the North, and the Southern Uplands.

Boring records at Grangemouth revealed the stratigraphy shown in Figure 3-5 which consists of an upper thin peat layer overlaying in some areas the extensive Carse[5] clay recorded in a major part of the area. Another sub-Carse peat layer occurs below the Carse clay in certain locations at high altitudes. This is followed by a gravel layer in most districts of the Forth valley. Beneath the gravel layer, thick deposits of a layered late glacial marine clay of varying thickness rests on a boulder clay or till overlying the bedrock (Sissons, 1970) as shown in the diagrammatic section of the area in Figure 3-5.

The samples had been extracted from 10 meters below ground level using Laval sampler, which is capable of yielding high quality samples (Clayton et al., 1992; Clayton et al., 1995). The samples had been well waxed and stored carefully.

The natural water content of the samples was 35%. After removing the wax, the samples were broken in to small pieces, as shown in Figure 3-6, and oven dried at 60 °C, to avoid modifying the organic content. After drying, sea shells were removed from the soil and then

5 In Scottish geography, a Carse is an area of fertile, low-lying (typically alluvial) land occupying certain Scottish river valleys, such as that of the River Forth.

the soil was machine grinded to fine particles. The physical properties of this soil are given in Table 3-1. The particle size distribution curve (Figure 3-2) shows that the Grangemouth soil is a sandy silt with less than 5% clay.

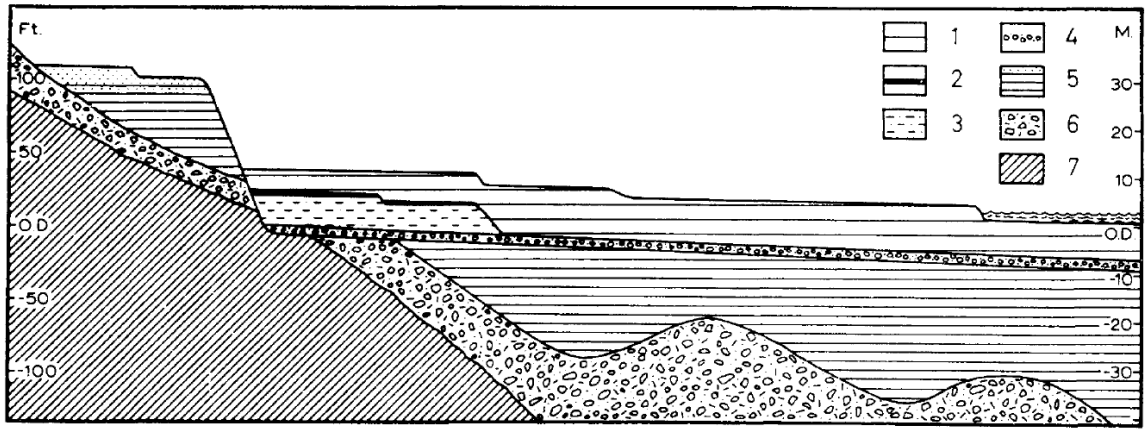

Figure 3-5: Diagrammatic section of drift deposits and related morphological features in the Grangemouth area. 1, Carse clay. 2, Peat. 3, Buried beach deposits. 4, Buried gravel layer.5, Late Glacial marine deposits. 6, Till. 7, Bedrock (Sissons, 1970).

Figure 3-6: Grangemouth soil before and after de-waxing and cutting.

3.1.2 Water content

For dredged soil and sea-bed sediments, Skempton (1969) reported that mean water contents in the top 250mm of the sea bed are typically 1.5 times their liquid limit, as shown in Figure 3-7 below. The clays deposited in tidal flats have water contents close to their liquid limits. Similar results has been reported by Kristinof and Marketos (2016) and Morin and Dawe (1987) but much higher liquidity indices have also been observed by Hong et al. (2010) Hong et al. (2010), Bo et al. (2016).

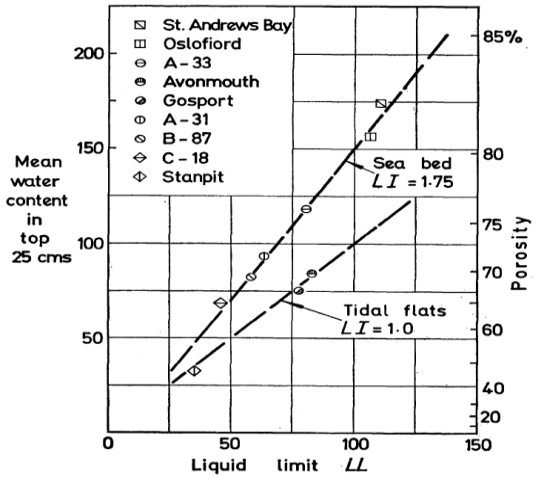

Figure 3-7: Depositional water contents of clays on the sea bed and intertidal flats (Skempton, 1969)

In this thesis, water content w_w has generally been normalized with respect to the water content at the liquid limit, thus yielding the normalized water content.

$$W = \frac{w}{W_{LL}} \qquad \textbf{3-1}$$

The normalized water contents employed in the tests on each soil are listed below.

Table 3-3: Normalized water contents used in the experimental test programme.

Soil	$W=w/W_{LL}$
K1	**1.8** and **2.2**
K2	**1.8, 2.0,** and **2.2**
CB	**1.8** and **2.2**
SW- K	**1.8** and **2.2**
SW-S	**1.8** and **2.0**
G	**1.4** and **1.6**

3.1.3 Slaked lime dosing rates

The lime used in the experimental programme was a calcium hydrated lime, [$Ca(OH)_2$], manufactured by ACROS ORGANICS Co. and supplied by Fisher Scientific Co. This is a high-quality product with no less than 95% active material. In appearance, it is a fine white powder.

To avoid carbonation of the lime, small batches of 2.5 kg, contained in a sealed bag inside a plastic jar, were ordered when required. After first opening, the lime was stored in vacuumed plastic bags to prevent carbon dioxide from the atmosphere reacting with the lime. The lime content of lime-admixed soil c (%) is defined as the ratio of dry weight of slaked lime m_c to dry weight of soil m_s :

$$\mathbf{C} = \frac{\mathbf{m_c}}{\mathbf{m_s}} \times \mathbf{100}\ (\%) \qquad \textbf{3-2}$$

The lime content required to bring about significant physical changes in soil properties is called the lime fixation point (Eades and Grim, 1960). Usually lime contents of 3-8% are typical for soil improvement (Eades and Grim, 1960; Eades and Grim, 1966; Pakbaz and Farzi, 2015) but these pertain to soil in a plastic state. Certainly, lower percentages than these can cause short-term changes in soil properties such as flocculation (Locat et al., 1996) and may produce substantial strength gains in soft soils (Balasubramaniam et al., 1989; Bell, 1996; Locat et al., 1990). Eades and Grim (1966) define *the fixation point* as the lime content which raises the pH of the soil above 12.40 an hour after treatment.

The method suggested by Eades and Grim (1966), which is referred to by BS1924 (BS, 1990b) as the Initial Consumption of Lime (ICL) method, was adopted to determine the fixation point. For each soil type, six oven dried 20gm soil samples (passing sieve 0.425mm) were mixed in separate bottles (Figure 3-8) with 1, 2, 3, 4, 5, and 6% lime respectively and 100 mL of CO_2-free distilled water was then added to each bottle and thoroughly hand-shaken. The bottles were then placed in a shaking machine for 15 minutes. After a further 45 minutes, the pH of each suspension was determined using a pH meter (Section 3.2.5). A saturated solution of the calcium hydroxide was also prepared, by mixing 5 gm lime with 100 mL of distilled water. The mixture was shaken in the shaking machine for 60 minutes and then left for 24 hours before pH testing. The results of the ICL tests are shown in Figure 3-9.

Figure 3-8: Mixing bottles used for Initial Consumption of Lime (ICL) tests.

Noting that the threshold is a pH of 12.4, the results show that the fixation point of kaolin clays is less than 1%. However, for the other soils, using 1% lime is probably insufficient to bring about significant changes in their strength properties.

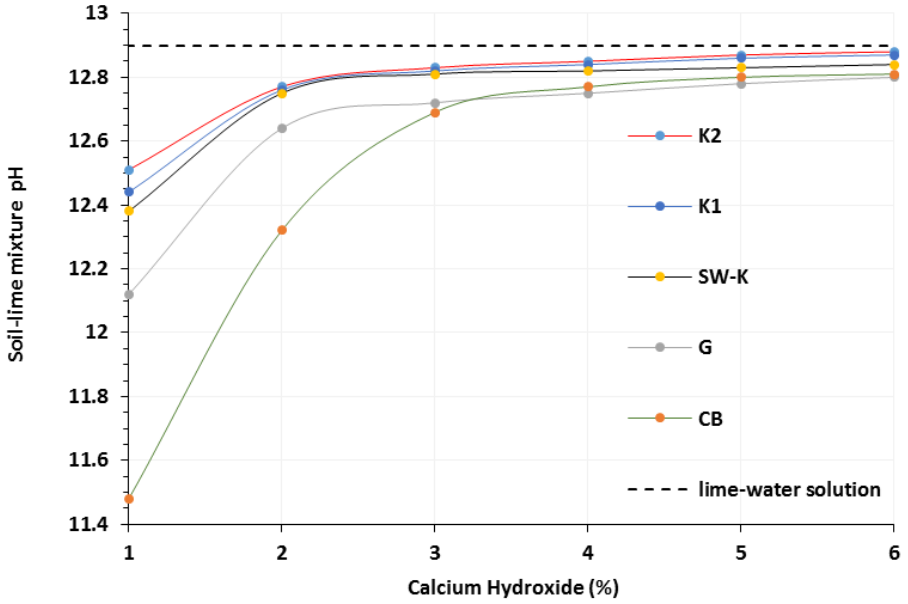

Figure 3-9: Initial lime consumption (ICL) test results.

Based on these results and customary practice, the following dosage rates were employed in the investigation:

Table 3-4: Lime dosing rates used in the experimental programme.

	K1	K2	CB	SW-K	SW-S	G
Lime content C (%)	1 , 5	1, 3, 5	3 , 5	3 , 5	3 , 5	3 , 5

At an early stage in this research, it was discovered that carbonation of slaked lime could occur if the slaked lime was exposed to air. This become apparent when some systematic discrepancies were noted between the soil strengths measured in repeated tests. In fact, this

problem had been reported in the literature by Janz and Johansson (2002) who refer to a loss in lime activity in excess of 70% after uncovering lime for more than 5 weeks. Thereafter, the lime was kept in sealed bags to avoid carbonation (ASTM, 2004) and the air was extruded using vacuum. The contaminated data were discarded.

3.1.4 Mixing of soil samples

To obtain homogeneous mixes of soil slurry, the motor driven Winkworth mixer shown in Figure 3-10 was used, coupled to a vacuum pump. The closed mixer inhibited water loss during mixing while the vacuum prompted the release of air voids. The mixer capacity is 10 litres.

Each soil batch was first oven-dried before mixing to reduce any variation in water content. Carefully measured masses of dry soil and water, usually sufficient for six test samples, were prepared each time. The dry soil was placed in the mixer drum and water in excess of the soil liquid limit water content was added. Sixty minutes of continuous mixing coupled with vacuum was applied to the soil which by observation proved to be sufficient to produce de-aired slurries of high homogeneity. The mixing process was sometimes stopped in order to return any soil pushed out of reach of the mixer blades back into the mix. After this first round of mixing, the lime dose was mixed with water to form a thick solution and then added to the slurry in the mixer. It was found by trial and error (testing samples' water contents) that twenty minutes of mixing in this second round was sufficient to produce homogeneous lime-treated admixtures. Longer mixing times could have been employed but this increased the risk of adversely affecting the bonding of the soil particles.

Figure 3-10: The Winkworth soil mixer.

3.1.5 Sampling

Immediately after mixing, the admixtures were poured into cylindrical curing moulds. The moulds were manufactured from clear Perspex acrylic tubes of 100mm inner diameter, 150mm inner depth, and 5mm wall thickness. These moulds were used to cure soils for both penetration tests and vane shear tests. Consolidation test samples were also cured in the same moulds, but a plastic bag was used to line the inside of these moulds. A 3mm thick and 97mm diameter plastic disc placed inside the bag facilitated the removal, without distortion, of the sample. To minimize entrapment of air voids, the soils were poured slowly in four lifts, punctuated by light tapping of the mould. The moulds were filled to a depth of at least 130mm.

A different type of mould was used for the triaxial test samples (summit moulds). These cylindrical split moulds were 50 mm in diameter and 105 mm in height. A similar technique (using three lifts) was employed to fill these moulds.

3.1.6 Curing

3.1.6.1 Curing technique

To cure soil samples for long-term curing periods without moisture loss, two different techniques were employed: the first method was by *flooding* the samples with water to prevent evaporation. This method was used with the kaolin (K2) samples only. Curing samples in this way leads to softening of their upper layers and the extent of the softened

zone increased with time. A better method of curing was employed subsequently, by *sealing* the samples under Perspex lids using silicone grease. This method was also used for the triaxial test samples. The effectiveness of this technique in water content preservation is discussed in section 3.2.6. Wax sealing was considered as an alternative, but the method offered no advantages and some disadvantages, such as local disturbance and additional labour during sealing and recovery.

3.1.6.2 Curing temperatures

Tests were conducted on specimens cured at three different temperatures: normal (20℃), low (5℃), and high (38℃), as described below:

A. ***Normal curing temperature:***

   The most comprehensive series of tests were carried out for soils cured at room temperature (20 ±1°C), in the temperature-controlled Soil Mechanics Research Laboratory. Further, the thermal mass of the water baths (Figure 3-11) in which the samples were stored tended to shield them from any short-term fluctuation in temperature.

Figure 3-11: Samples at room temperature and immersed in water baths

B. ***Low curing temperature:***

In the offshore environment, the ambient temperature may approach 4°C. Strength tests on specimens cured at low temperature (5 ± 0.5°C) were carried out on two soils: kaolin (K2) and the SW-K mix, while strain-rate tests were carried out on the kaolin (K1) soil. The parameters are summarized in Table 3-5 below. These soils were cured in a domestic refrigerator as shown in Figure 3-12. The raw materials (water + solids) were pre-cooled in this refrigerator for at least 24 hours prior to mixing. The temperature was monitored regularly using a thermometer immersed in

a water-filled glass cylinder. Again, the thermal mass of the samples and raw materials tended to damp any short-term fluctuations in temperature.

Table 3-5: Soils and lime contents: low temperature programme.

Soil Type	K2 (W=1.8)	K2 (W=2.2)	SW-K (W=1.8)	K1 (W=1.8)
Lime Content C (%)	1	1	3	1
	5	5	5	5

Figure 3-12: Curing specimens at low temperature.

C. ***High curing temperature:***

These tests, which were conducted on samples cured in warm water baths, were carried out to investigate thermal acceleration of the curing process. The temperature used for the accelerated curing was 38ºC (ASTM, 2003) and was maintained throughout the curing period. For lime-treated soil samples, ASTM (2004) states that temperatures of up to 40°C is appropriate for accelerated curing: these temperatures should not produce pozzolanic reactive products that significantly differ from those expected during field curing.

The parameters investigated in this part of the programme are summarized in the Table 3-6 below. Curing times of up to 100 days were explored.

Table 3-6: Scope of the high curing temperature programme.

Soil type	K2 (W=1.8)	SW-K (W=1.8)
Lime Content C (%)	1	3
	5	5

Two hot-water baths were used to cure the specimens as shown in Figs. 3.13-3.14. The first bath has plan dimensions of 300mm x 340mm and a depth of 200mm, while the second bath has plan dimensions of 195mm x 325mm and is 195mm deep. They are similar to the water baths described by (ASTM, 2003) for accelerated concrete curing.

The baths were equipped with thermostatically-controlled electrical heaters. The samples were seated on a steel mesh that separated them from the underlying heater. The first bath was normally used for short-term curing (<30 days) and could comfortably hold four moulds. The second was reserved for long-term (100 days) curing and held two moulds. To eliminate thermal bridges, the baths were encased in 50 mm thick thermal insulation boards. A beneficial side-effect was a reduction in evaporation. Regular monitoring of the baths' temperatures showed that the insulation significantly decreased temperature fluctuations.

Figure 3-13: Water baths used for accelerated curing

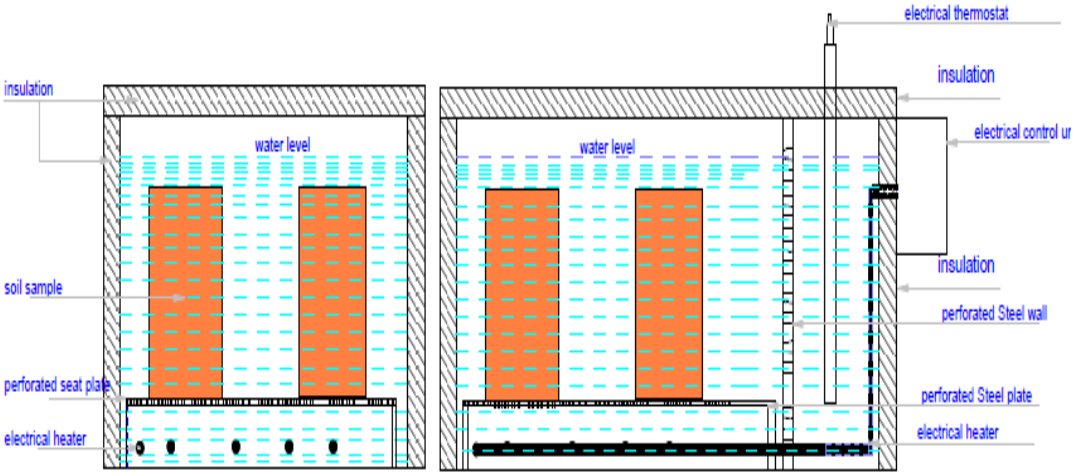

Figure 3-14: A diagram of accelerated curing water baths.

3.1.6.3 Curing Schedules

Samples were prepared in batches: each batch produced samples to be cured for 1, 3, 10, 30, 100, and 365 days. In addition, samples were cured for 100 and 365 days for consolidation testing. In general, only samples cured for 365 days were strong enough to be tested in the triaxial chamber without noticeable disturbance.

All moulds were identified by number and a comprehensive mix and test schedule was devised to ensure that the test programme could be completed efficiently.

3.1.7 Remoulding of soil samples

Although remoulded soil strength is not a primary focus of this work, some insight into the character of post-peak strength is necessary in order to interpret strength data. Moreover, from practical point of view, it is important to establish whether these soils exhibit similar characteristics to natural "quick clays". Quick clays are characterized by high sensitivity, defined as the ratio of undisturbed to remoulded strength. However, another characteristic, namely toughness (the ability to absorb energy and plastically deform without fracturing) is also important in practice. Quantitative measurements of toughness could be deduced from the triaxial tests data presented in this thesis. We simply note that this evidence, together with the qualitative experience of the considerable physical work required to remould these soils, suggests that lime-treated slurry admixtures are not prone to the types of catastrophic failure witnessed in natural quick clays. This lend some confidence in the utility of these soils for construction purposes.

For that purpose, soil samples were hand remoulded, after being transferred into plastic bag (as shown in Figure 3-15) and kneaded for about 30-60 minutes. The considerable physical work that this entailed (the extent to which it is felt that it became easier to remould the samples) provided qualitative evidence that the cured soils were far from brittle, even if they exhibited substantial softening. The remoulded samples were then returned to the moulds for strength testing.

Figure 3-15: Hand remoulding of soil samples

3.2 Laboratory Testing Techniques

3.2.1 Triaxial tests

Standard constant rate of strain U-U triaxial compression tests were employed wherein the lime-treated samples were loaded to failure. The procedure is described by Bishop and Henkel (1962) and is similar to the quick undrained test but with measurement of pore water pressure during the shearing. The triaxial tests were conducted in two stages: a saturation stage followed by a sufficiently slow shearing stage, to allow for pore water pressure equalization. Failure was taken to correspond to the maximum principal stress difference attained or its value at 15 % axial strain, whichever was obtained first (ASTM 2007, BS 1990). For these soils, failure invariably occurred before 15% axial strain was reached.

3.2.1.1 Triaxial compression system set-up

The general layout of the equipment used in the triaxial compression tests is shown in Figure 3-16. Also, Figure 3-17 shows a schematic diagram of the setup and its control. During the saturation phase, the cell pressure is admitted through opening valve d while keeping valves a and b closed. The back pressure is then admitted to the specimen by opening valve a.

Throughout the shearing stage, drainage from the sample was prevented. Pore water pressure measurements were obtained from the transducer connected to the cell base at valve c.

Triaxial cell: The triaxial cell (VJ Tech.) has a maximum working pressure capacity of 2000 kPa. A base pedestal of 50mm diameter was used to match the soil samples.

Axial Loading Device: The axial loading device was a Wykeham-Farrance screw jack driven by an electric motor through a geared transmission, with capacity and control to provide a wide range of prescribed strain rates. Motor-driven gears provide a very effective means of applying strain-controlled loads (Ehrgott, 1971)**.**

Data acquisition system: Output from the transducers (i.e., displacement, load, pressure and volume gauge transducers) were brought to a wall-mounted analogue/digital data acquisition converter/logger (Datascan type 7220 MSL) before being transferred to a PC. Input and output data were processed using the software "Triax 5.1.7" developed by Toll (2010). The software can control advanced multi-stages traiaxial tests. The software accepts manual calibration of measurement transducers and provides graphical representation of the output data. Output data can be presented in tables or graphical forms and/or transferred to Excel or MATLAB spreadsheets.

Figure 3-16: Triaxial compression apparatus

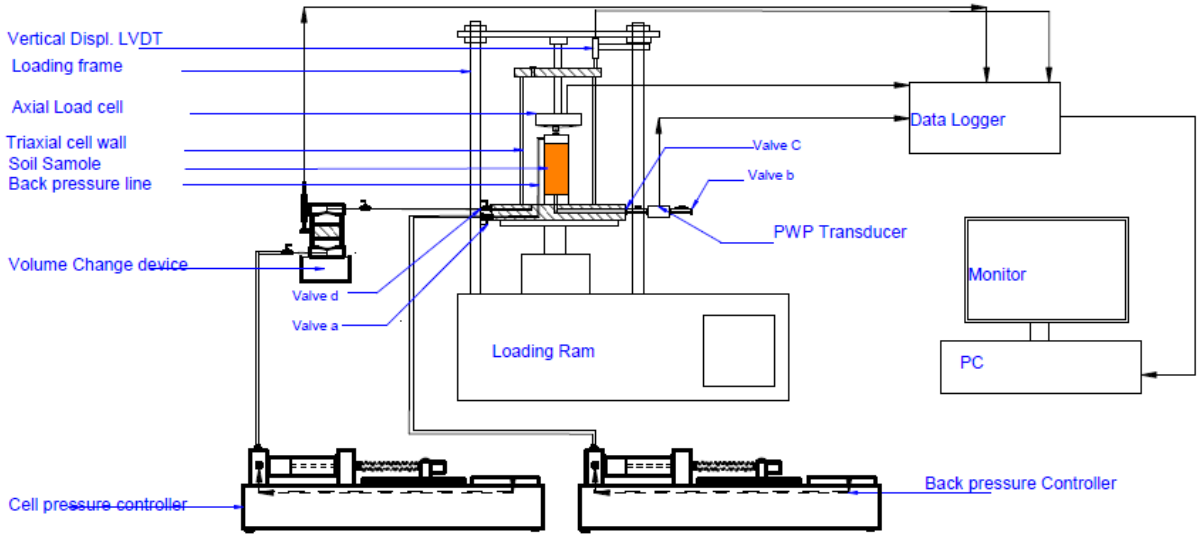

Figure 3-17: Triaxial compression test set-up.

3.2.1.2 Pressure/ volume controllers and measurement devices

Automated water pressure/volume controllers (AWPC): Two automated water pressure/volume controllers (AWPC) manufactured by GDS Instruments Ltd., were used to control the cell and back pressures (Figure 3-17). The AWPC responsible for applying the back pressure was used during the saturation phase of the tests while the other one

responsible for cell pressure control was used throughout the test from the saturation phase up to the end of shearing phase.

Figure 3-18 shows a schematic diagram of the GDS AWPC used. A pressure transducer fitted inside the steel pressure cylinder measures the fluid (water) pressure inside the cylinder and reports it to the control panel of the device. The control system maintains the target pressure by triggering a compression piston inside the cylinder through the rotation and movement of a stepper motor and a spindle shaft (Hasan, 2016). The water pressure controllers can also be used to measure volume change; the change of water volume inside the piston is deduced from the number of steps of the stepper motor.

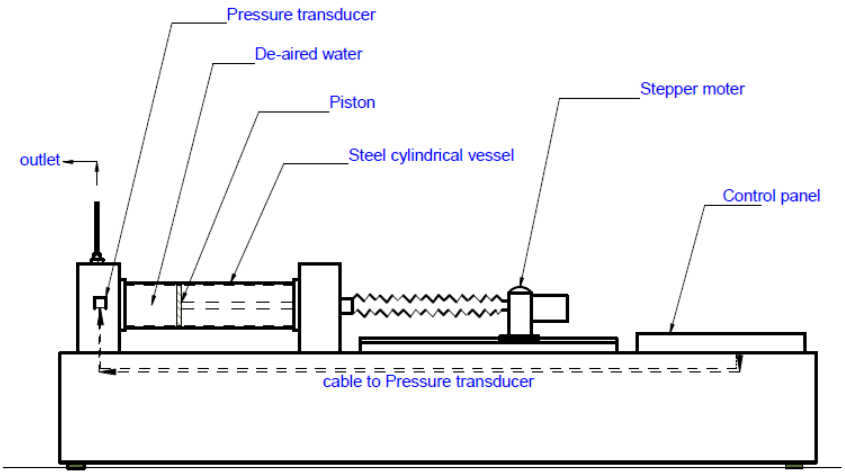

Figure 3-18: Schematic diagram of the GDS automated water pressure/volume controller (AWPC).

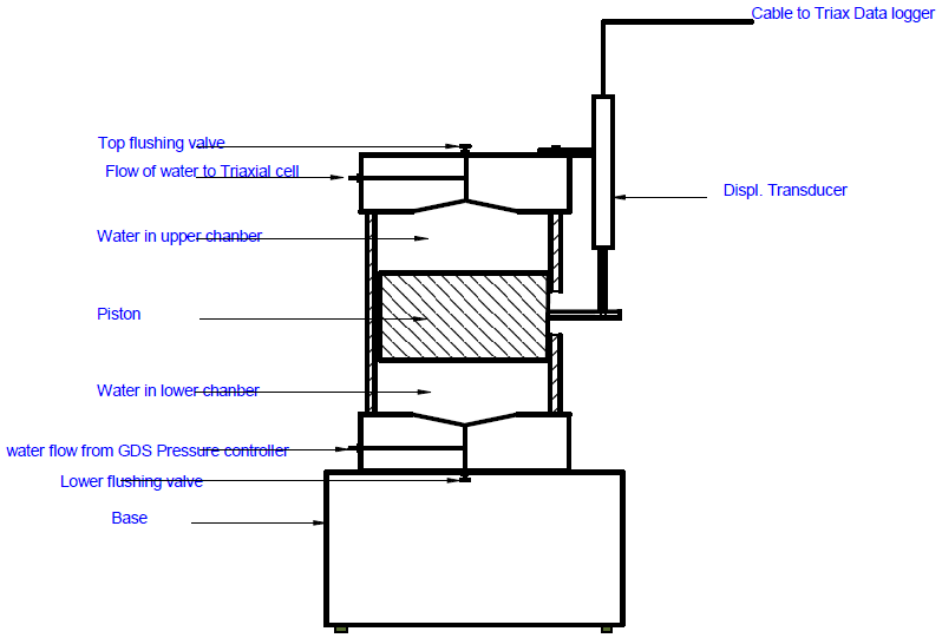

Figure 3-19: Schematic diagram of the volume change transducer (VCT)

3.2.1.3 Calibration of transducers

Volume change transducer (VCT): To ensure that the samples did not increase in volume during the saturation phase, their volumes were monitored by monitoring the volume of the cell water. This process was achieved by connecting the GDS AWPC to a separate volume change transducer before connecting it to the triaxial cell. Any change in specimen volume (ΔV) caused a change in the volume of the cell water that was compensated by the GDS AWPC. Figure 3-19 shows a schematic diagram of the volume change transducer manufactured by VJ Tech. Ltd., based on an Imperial College design (Hasan, 2016). The pressure was supplied from the GDS AWPC to the lower chamber of the VCT, which acted on a piston that transmitted the pressure to the upper chamber which was connected to the triaxial cell. The upward and downward movements of the piston was detected by the linear variable differential transformer (LVDT) displacement transducer connected to the piston. To convert piston translation to water volume change, a calibration exercise (following Hasan (2016) was adopted to calibrate the VCT against the volume change readings of the GDS AWPC using the set-up shown in Figure 3-20. The calibration results are shown in Figure 3-21.

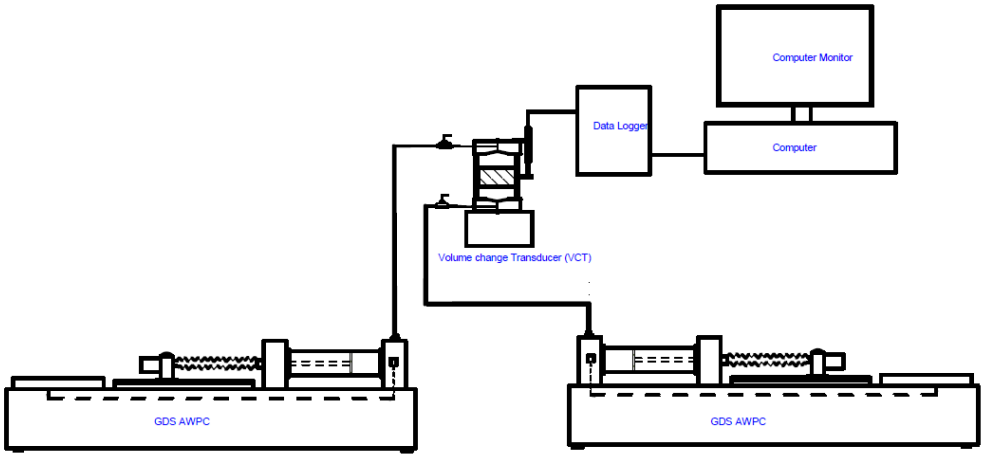

Figure 3-20: Calibration of volume change transducer (VCT) through use of GDS AWPC

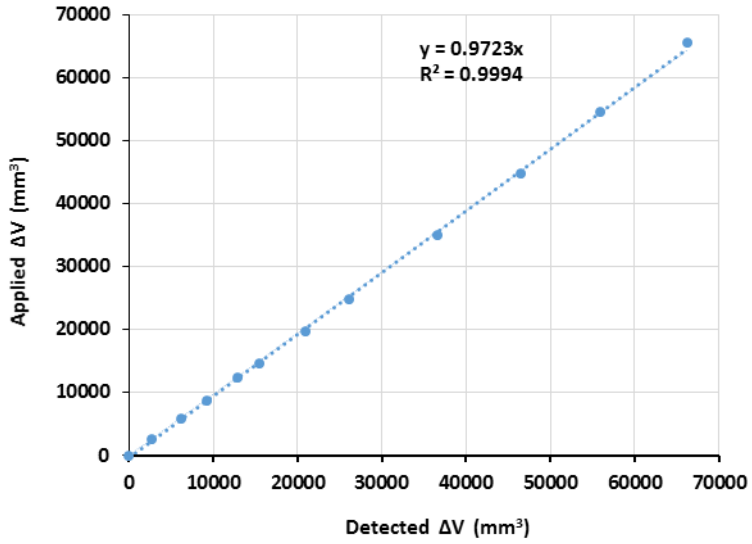

Figure 3-21: Volume Change Transducer (VCT) calibration

Load cell: A 1.0 kN submersible load cell with ±0.1 N accuracy (VJ Tech.) was used to measure the axial load applied on the specimens. To calibrate the load cell, the triaxial cell cover (including the integrated load cell) was placed upside down and loaded with static weights. The weights were applied in increments of 0.5 N up to 10N and thereafter in increments of 5N up to 120 N. The results are shown in Figure 3.22.

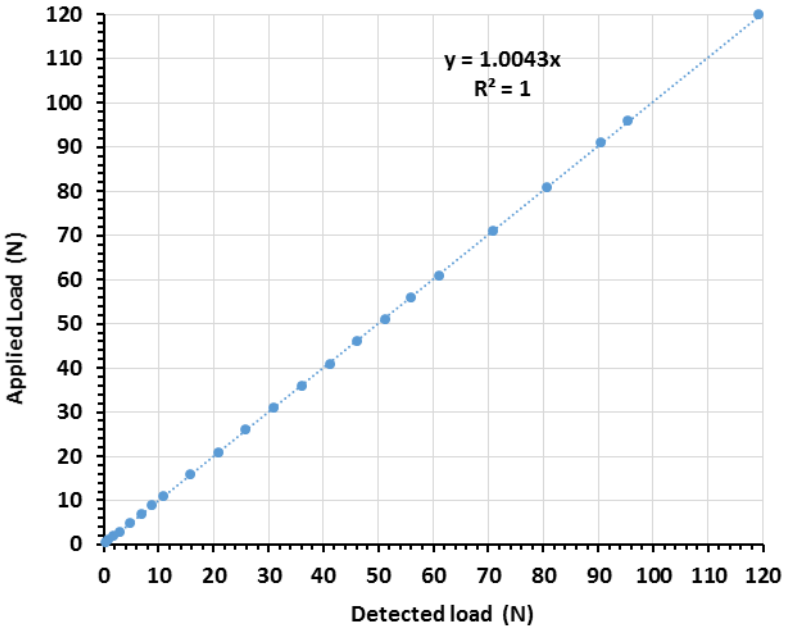

Figure 3-22: Triaxial test load cell calibration check

Axial displacement transducer: To monitor the axial strain in soil specimens, an exterior LVDT displacement transducer with a resolution of ±0.001mm attached to the top cover of the triaxial cell was used to measure the displacement of the loading ram. The calibration of the axial displacement transducer was conducted manually by applying displacements

starting from 0.50 mm up to 27 mm using a standard slip gauge (gauge block) kit. The calibration results are shown in Figure 3-23.

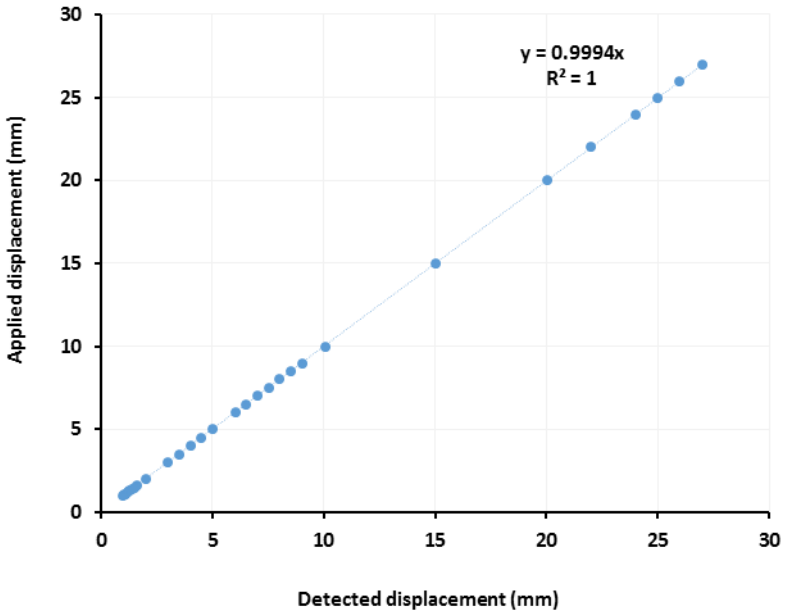

Figure 3-23: Axial displacement transducer calibration

Pore water pressure transducer: To measure the pore water pressures, a 10 bar capacity VJ Tech pressure transducer was used by connecting it to the base of the specimen through the loading pedestal. The transducer was calibrated using an automated water pressure/volume controller (AWPC). The calibration results are shown in Figure 3-24.

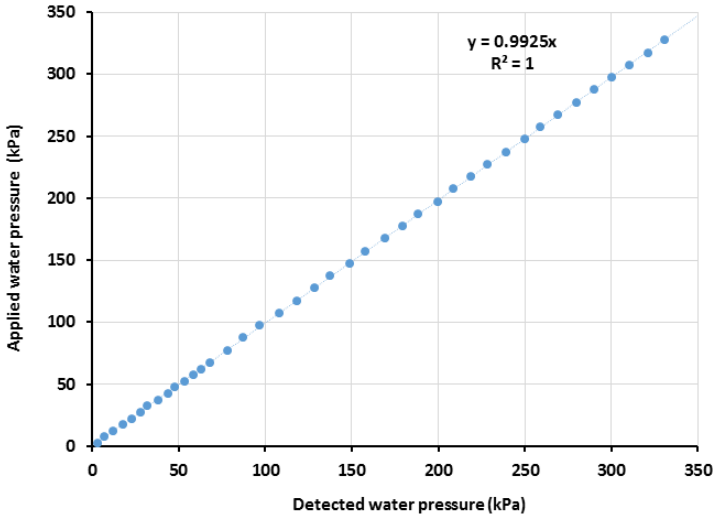

Figure 3-24: Pore water pressure transducer calibration.

3.2.1.4 Triaxial compression test samples

Attempts to extrude samples from their moulds following the procedure suggested by the manufacturer of the moulds were unsuccessful. Instead, the samples were extruded by

cutting off the plastic bases using a hand saw and then pushing the stainless-steel base out of the mould by hand as shown in Figure 3-25. The samples' dimensions were measured prior to testing to ensure no change occurred during extrusion. Specimens' masses were also recorded prior to testing for unit weight calculations.

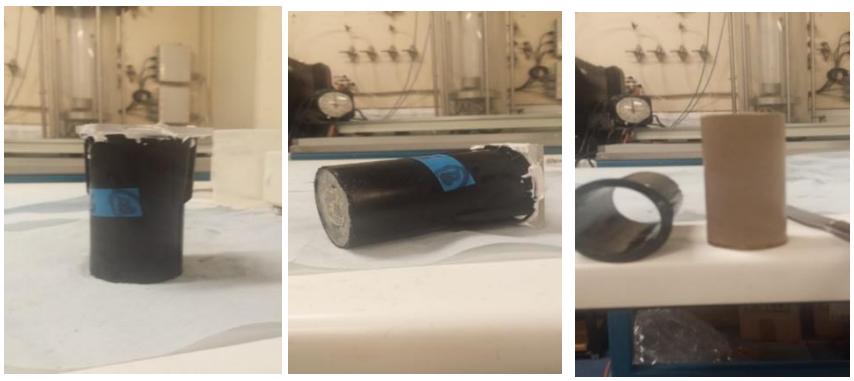

Figure 3-25: Triaxial test sample extrusion from the curing mould.

3.2.1.5 Sample Saturation

Sample saturation by the application of back pressure is normal practice for triaxial tests (Head, 1988c). Here, it is assumed that the initial degree of saturation of specimens is high enough to allow the application of the increments of cell and back pressures successively, not simultaneously. However, as a precaution, the relatively low increment of 25 kPa was chosen for successive saturation cycles. At the beginning of each increment, the cell pressure was increased by 25 kPa while keeping the back pressure closed off from the sample. The increase in cell pressure causes the pore water pressure to increase and then stabilize. For soft soils, the value of Skempton's pore water pressure parameter, B at 100% saturation is close to 1.0, and a B value of 0.97 is obtained at 98% saturation. For stiff soils, lower values of B arise and accordingly the B value of 0.97 was adopted as an acceptable target. If B values less than 0.97 were obtained, then the saturation process was continued by maintaining the cell pressure and increasing the back pressure. The back pressure was maintained at a value of 5 kPa below the cell pressure. As the back pressure pushed water into the sample, the pore water pressure increased up to a steady state. It was assumed that the volume of the sample remained constant during this process and hence, no corrections for changes in sample dimensions were employed.

Saturation time differed for different soils: while kaolin (K2) samples took around 3 days to reach saturation, SW-K and SW-S took a longer time (about 7 days). These responses reflect differences in these soils permeability.

3.2.1.6 Strain rates

For triaxial samples (L/D = 2) and drainage from one end, the time required to failure t_f based on pore water equalization is given by the relationship (Head, 1988b)*:*

$$t_f = 0.508\ t_{100} \qquad \textbf{3-3}$$

where t_{100} is the "notional consolidation time". This parameter can be determined from isotropic consolidation test results. For this purpose, a series of isotropic consolidation tests were conducted on remoulded samples of kaolin (K2), CB bentonite, and SW-K mix at a cell pressure of 40 kPa. In each case, W=1.8 and C=5%. The resulting consolidation curves are shown in Figure 3-26 below.

The initial straight-line portion of each consolidation curve is extrapolated to intersect the horizontal line representing the end of consolidation: the corresponding time is t_{100}. For the SW-K soil, t_f = 65hrs. The loading rate was calculated based on the assumption that the failure of lime-treated soils occur at axial strains not exceeding 5% (D 5102–04)(ASTM, 2004). Consequently, for SW-K soils, a strain rate corresponding to 0.0013 mm/min was determined. In practice, the limitation of the apparatus required use of 0.00122 mm/minute, but the difference is trivial. The same velocity was used for SW-S soil, and twice this velocity for other soils.

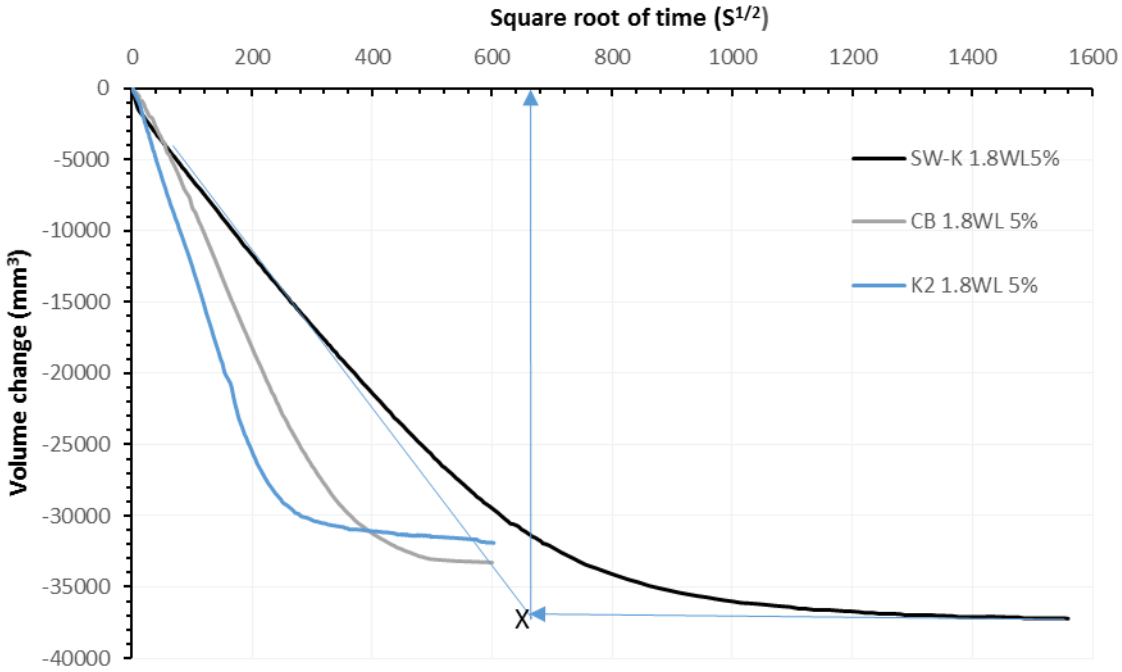

Figure 3-26: Isotropic consolidation of remoulded soil samples.

3.2.1.7 Deviator stress correction

A. Correction for barrel effect (area correction)

Under undrained conditions, the sample diameter must increase under axial compression and this ought to be accounted for in calculation of stresses (Head, 1988b). The simplest assumption is that the sample deforms as a right circular cylinder (ASTM, 2007). This method is commonly used in soil mechanics where only axial deflection is measured (Ehrgott, 1971). The deviator stress, can then be written as:

$$\sigma_1 - \sigma_3 = \frac{P.h}{V} \qquad \textbf{3-4}$$

where P is the axial load, h is the height of the specimen during the loading, and V is the volume of the sample.

For the standard 100 mm specimen height and assuming no volume change during shearing, the deviator stress is (ASTM, 2007):

$$\sigma_1 - \sigma_3 = \frac{100\ P}{\mathrm{A}}\ (1 - \varepsilon) \qquad \textbf{3-5}$$

where A is the original cross-sectional area of the sample and ε is the axial strain. More sophisticated correction are possible (Omar and Sadrekarimi, 2014), but for relatively low axial strains are hardly warranted. The simplest form of area correction has been adopted because the peak resistance to shearing happens at low strain levels (~3%).

B. Rubber membrane correction

The rubber membrane enclosing triaxial specimens has a restraining effect which gives rise to greater shear resistance. This can be particularly significant for residual shear strengths after strain-softening (Omar and Sadrekarimi, 2014). Two types of correction are commonly employed depending on whether the material is plastic or brittle (Head, 1988b).

In plastic soil, because the failure mode is barrel shaped, the correction depends on the axial strain in the sample, the elastic modulus of the membrane material, and the diameter of the sample (Raghunandan et al., 2014). (Henkel and Gilbert, 1952), based on shell theory, derived the rubber membrane correction:

$$C_{\mathrm{M}} = \frac{4000\mathrm{M}.\ \varepsilon(1 - \varepsilon)}{D_o} \qquad \textbf{3-6}$$

where C_M is the rubber membrane correction (kPa), ε is the axial strain during shearing, D_o is the initial diameter of the specimen (mm), and M is the compression modulus of the membrane material (*N* per mm width).

Here, the compression modulus of the membrane material is assumed to be equal to its extension modulus following Henkel and Gilbert (1952). To determine its value, a 25mm cylindrical strip of the 50mm diameter rubber membrane was cut out and a load hanger was used to apply incremental tensile loads. The set-up, following (Henkel and Gilbert, 1952), (Head, 1988b), and (ASTM, 2007) is shown in Figure 3-27.

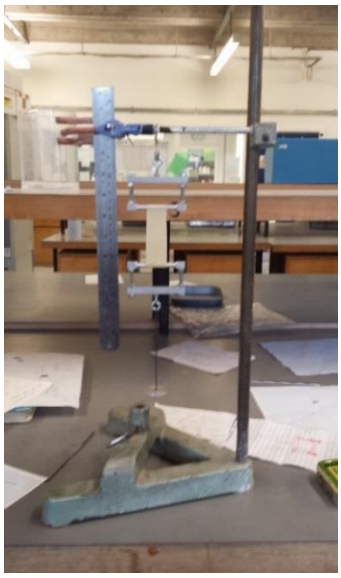

Figure 3-27: Determination of the extension membrane modulus

The load-extension results for the rubber membrane are plotted in Figure 3-28. For example, the load giving 5% strain (or x=3.933mm) is 0.85N. The membrane extension secant modulus M is then calculated to be 0.34 N/mm.

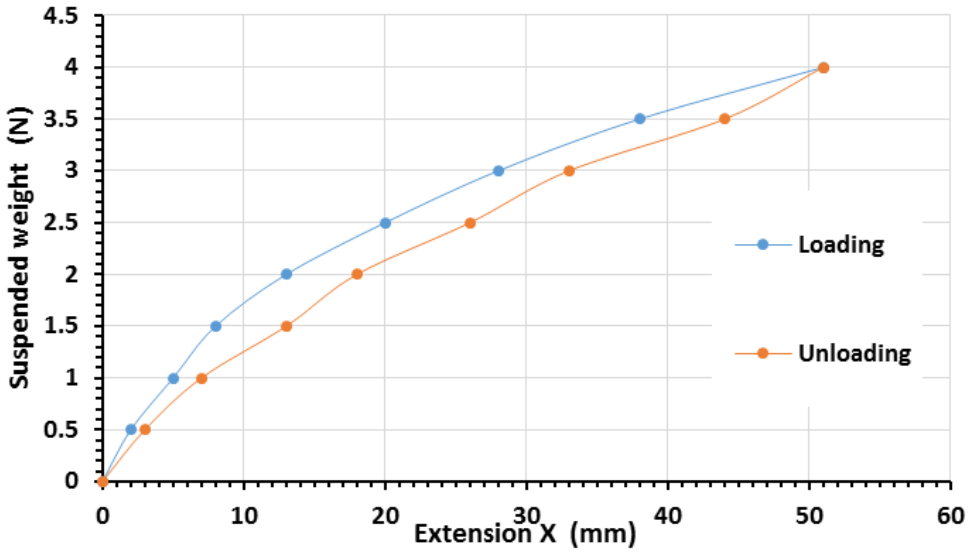

Figure 3-28: Rubber membrane load test

The rubber membrane correction for each strain level calculated using equation 3-6 is shown in Figure 3-29.

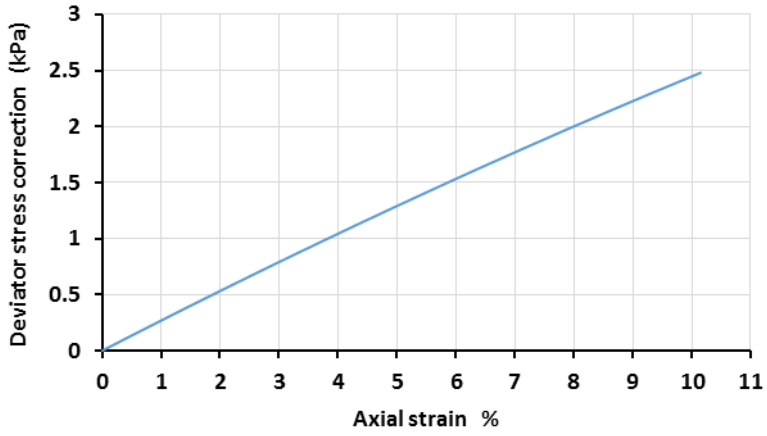

Figure 3-29: Rubber membrane correction for triaxial compression.

For brittle soil, the rubber membrane correction depends on the strain at which a slip plane first develops (Head, 1988b). This assumes that a classical inclined slip-plane develops but this was rarely observed: several samples developed brittle fracture modes of failure (akin to concrete/rock failure) as depicted in Figure 3-30.Therefore, it was assumed that for all samples, the failure type was barrel shaped and the correction due to this type of failure was applied.

Figure 3-30: CB Bentonite specimen at failure in triaxial compression.

3.2.2 Vane Shear Test

A miniature vane apparatus was used to obtain independent measurements of the undrained shear strength of the lime-admixed soils.

3.2.2.1 Apparatus

The Wykeham-Farrance self-contained desk-top vane apparatus consists of a steel frame and stand as shown in Figure 3-31(a). The vane assembly consists of four rectangular bladed vanes of height H=19mm which sweep out a diameter D=12.7mm (H/D = 1.5), as illustrated in Figure 3-31(b) and Figure 3-32. The torque is applied to the vane by a torque spring. Although the device has an electrical motor, it operates at a single speed of 15°/min. Because this is substantially less than the D4648 (ASTM, 2005) standard of 60 to 90°/min, it was decided to use hand rotation by applying a rotation rate of approximately 60° /min. Similar rotation rates were adopted by other researchers for soft soils (Low and Randolph, 2010). The tests start 1 minute after vane insertion in the soil to a depth of 80 mm.

(a)

(b)

Figure 3-31: (a) Wykeham-Farrance vane apparatus and (b) springs, vane, and vane shaft.

The applied torque *T* is proportional to the spring rotation angle Θ_t which corresponds to the peak shear resistance. To account for shaft shearing resistance, a plain steel shaft with same diameter was then inserted to the same depth as the vane. The net rotation angle Θ_{net} is

$$\theta_{net} = \theta_t - \theta_{shaft} \qquad \textbf{3-7}$$

where θ_{shaft} is the rotation angle generated by the shearing resistance of the plain shaft. The readings of the rotation angles were recorded manually to the nearest 0.5 degree.

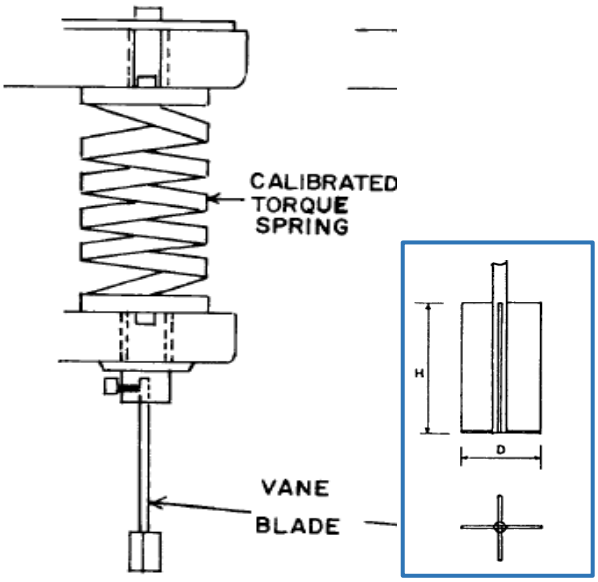

Figure 3-32: Vane assembly

3.2.2.2 Spring Calibration

A set of four springs of different stiffnesses was available to allow for a wide range of soil strengths. However, only the two softest springs No.1 and No.2 (Figure 3-31(b)) were suitable for this study. The springs were supplied with a calibration certificate from Wykeham Farrance Co. These calibrations were checked, following D4648 (ASTM, 2005). For this purpose, a circular Perspex pulley (102mm diameter and 20 mm thickness) was fabricated and attached to the vane shaft. With the shaft horizontal, static loads hung from the pulley imposed torques and the corresponding angles of rotation were readily measured. The calibration confirmed those provided by Wykeham Farrance Co. (Figure 3-33-a)

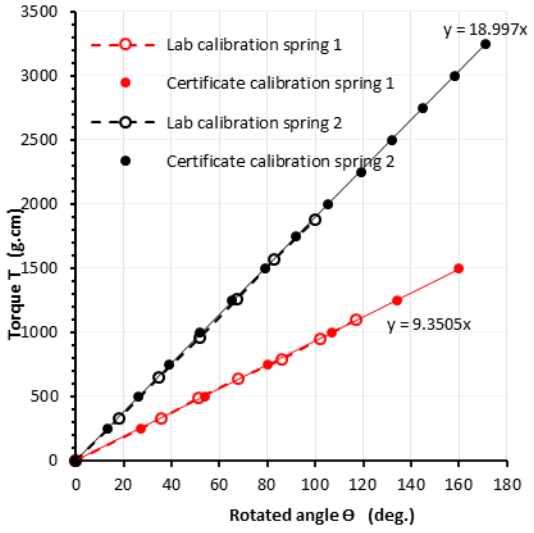

(a) Calibration results

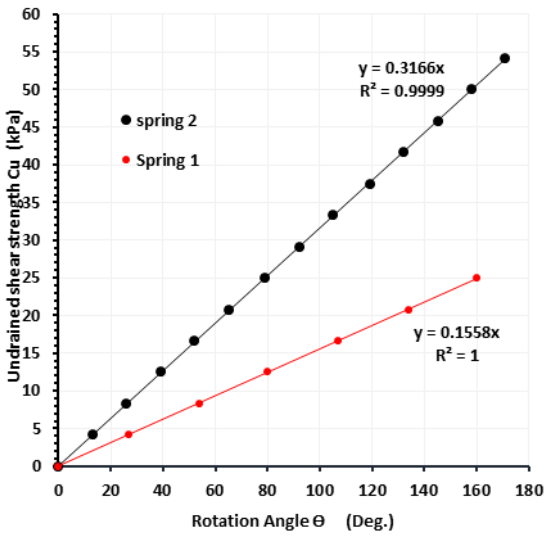

(b) Shear strength, calculated for 12.7x19 mm vane

Figure 3-33: (a) Vane spring calibration and (b) Undrained shear strength

3.2.2.3 Shear strength

Following BS 1377: Part 7-1990 and D4648 (ASTM, 2005), the simplified assumption was adopted, in that the parameter k (the integral of the product of area and lever arm) is:

$$k = \pi D^2 (\frac{H}{2} + \frac{D}{6}) \quad \textbf{3-8}$$

where D is the diameter of the vane (12.7 mm) and H is the height of the vane (19 mm). The average undrained shear strength, C_u is (ASTM, 2005):

$$C_u = \frac{T}{k} \quad \textbf{3-9}$$

where T is the measured torque. Noting that $k = 5886$ mm^3, and adopting the calibration curves of Figure 3-33(a), the undrained shear strength can be determined from the (net) rotation using Figure 3-33(b).

3.2.3 Penetration tests

Strength tests using steel circular disc penetrometers were used extensively in this study. The test provided rapid determinations of the shear strength of undisturbed and remoulded soils.

3.2.3.1 Apparatus

Three flat circular steel penetrometers of diameters 10, 20, and 30 mm and of 2 mm thickness and attached concentrically to a 5mm diameter, long steel shaft (as shown in Figure 3-34) were fabricated to conduct the strain-controlled penetration tests. Most of the tests were conducted using the small, desk top strain-controlled Tinius Olsen H1KS machine shown in Figure 3-36. The machine has a velocity range up to 1000 mm/min and has a 250 N capacity load cell. Because the machine was not designed for this kind of testing, some modifications were made to conduct the penetration tests. A 15mm thick circular Perspex base of 130mm diameter, shown in Figure 3-35 was fixed to the moving arm of the machine as shown in Figure 3-36 to hold the mould during testing. The penetrometer was held constant by the load cell while the mould moved upwards at the prescribed velocity as shown in Figure 3-37. Figure 3-38 shows the apparatus in operation. The mould was prevented from lateral translation by seating it inside a 5 mm deep circular depression in the base.

To conduct the penetration tests, it was necessary first to use the command language of the software running the machine to develop procedures for prescribed velocities, penetration depths, and outputs and to recall them when conducting the tests. The apparatus has a data logger which facilitates subsequent data processing and a controller which facilitates the conduct of the tests.

Figure 3-34: Penetrometer shaft and steel disc penetrometers.

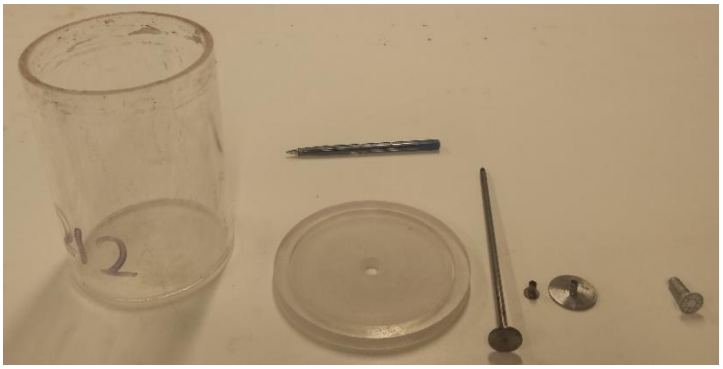

Figure 3-35: Circular Perspex loading base .

(a) (b)

Figure 3-36: Tinius Olsen machine: (a) before modification and (b) after modification

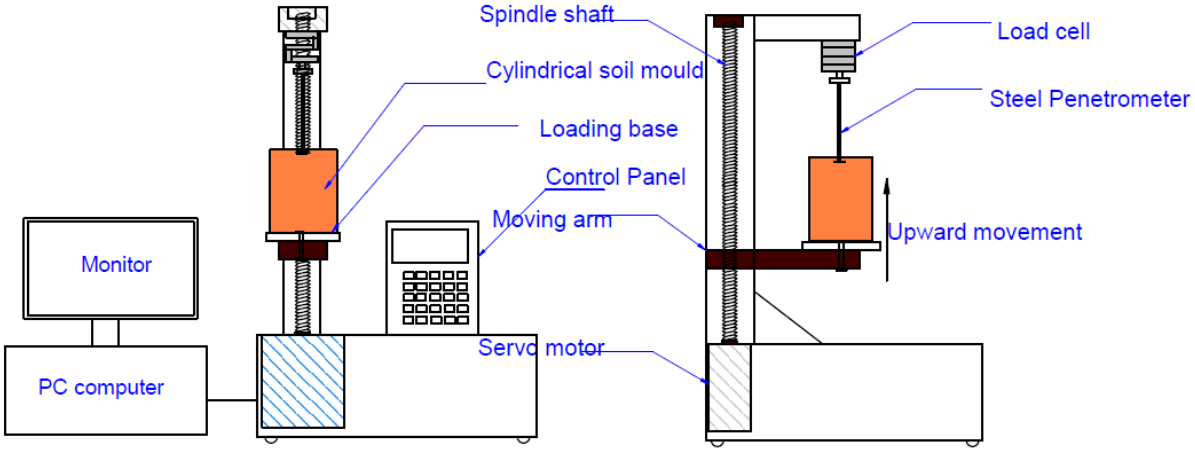

Figure 3-37: Layout of the penetration machine

Figure 3-38: Penetration test apparatus

3.2.3.2 Force and displacement measurement calibration

Load-cell calibration data was entered in to the software by the manufacturer. This was checked by loading the cell externally as shown in Figure 3-39. Loads were increased with in increments of 5 N up to 130 N, and the corresponding measured loads were recorded. The results, shown in Figure 3-40 reveal that the manufacturer's calibration is extremely accurate.

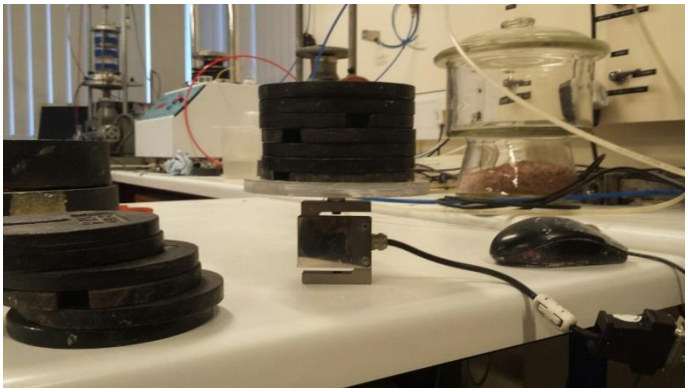

Figure 3-39: Load cell calibration of Tinius Olsen machine.

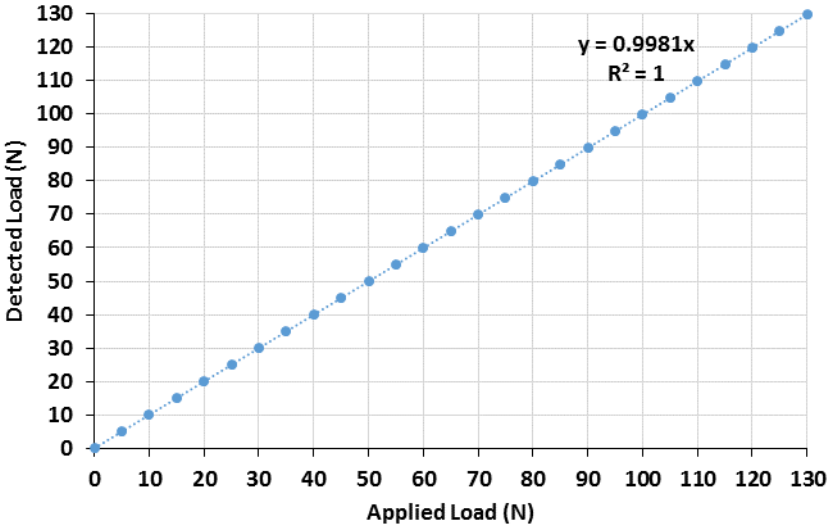

Figure 3-40: Calibration of Tinius Olsen load cell

The displacement mechanism of the Tinius Olsen machine is by rotation of a spindle shaft, shown in Figure 3-41, by a servo motor. Servo motors have high accuracy and resolution owing to the sensor-fixed encoder.

Figure 3-41: The spindle shaft of the Tinius Olsen apparatus.

The accuracy of the prescribed displacements was checked by using a scale attached to the side of the machine, as shown in Figure 3-42. The results of this calibration are shown in Figure 3-43. The accuracy is excellent throughout the range of 0-120 mm.

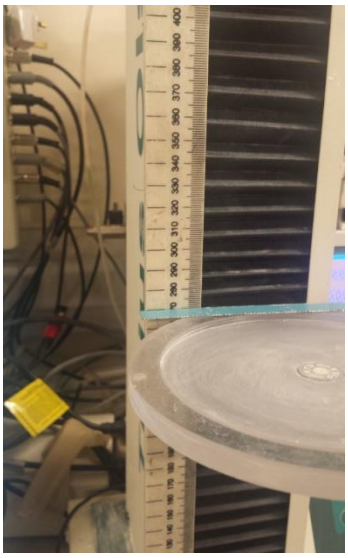

Figure 3-42: Calibration of the prescribed displacement.

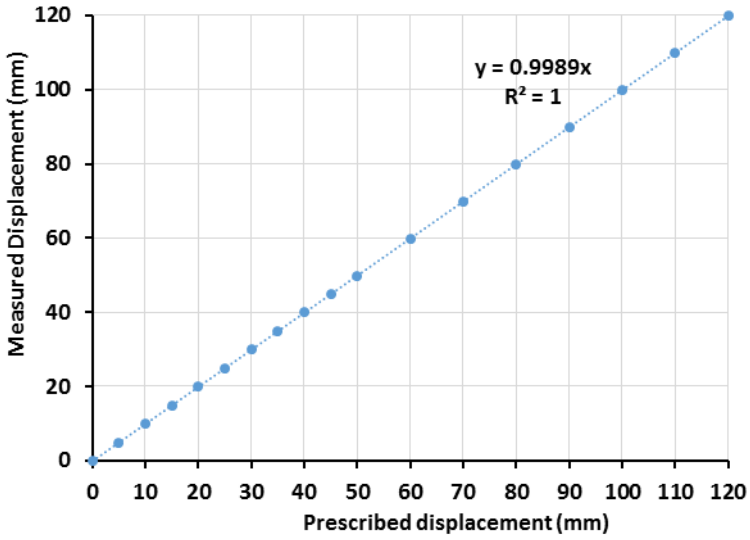

Figure 3-43: Displacement measurement calibration of the Tinius Olsen machine.

Penetration velocities were checked using a digital timer. A displacement of 120mm was first prescribed, and penetration trials with different velocities were conducted. The real velocity was calculated then based on the elapsed time. The results of the velocity calibrations are shown in Figure 3-44. The results indicate a high consistency between the prescribed and measured velocities.

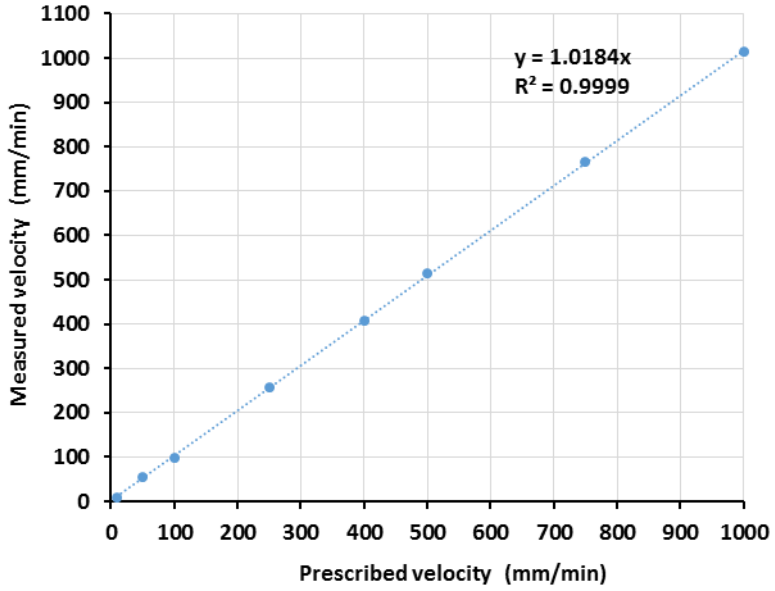

Figure 3-44: Velocity calibration of the Tinius Olsen apparatus

3.2.3.3 Test procedure

The mould was raised until the top surface of the soil approached the disc penetrometer, as shown in Figure 3-38. The load and the displacement readings were zeroed, and the test was launched. The penetration was halted at a depth of 110 mm, some 20 mm above the rigid base of the mould. The resulting load-displacement data (Figure 3-45) was then exported to a PC for analysis. Only one test was conducted per soil sample, because repeat tests might be affected by strain softening.

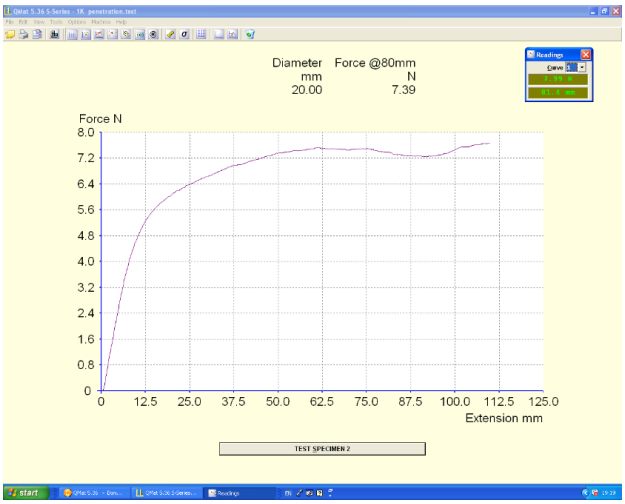

Figure 3-45: Load-displacement curve obtained from penetration test.

3.2.3.4 Penetration test interpretation

As the penetrometer advances, a cavity is formed above the disc as shown in Figure 3-46. The soil resistance is measured by the load cell as a tip resisting force F. The resulting ultimate bearing pressure (resistance) q_{ult} at the tip of the penetrometer is equal to the force F divided by the disc area. To this pressure should be added any surcharge (soil and/or water) which bears down on the upper face of the disc, over its reduced area. In principle, this could amount to a pressure (over the gross area of a 20 mm disc) of 1.3 kN/m^2 or a force of 0.4 N. For comparison purposes, a very weak soil (say, C_u=1 kN/m^2) the bearing pressure will be about 10 kN/m^2 and the bearing resistance is 3 N.

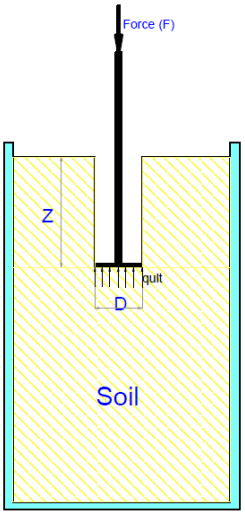

Figure 3-46: Force equilibrium of the penetrometer

For the smaller diameter penetrometers, there is a greater risk that cavity closure will inhibit penetration by means of shaft friction. For smaller diameter (10 mm) penetrometers, it can be shown that the ratio of the shaft friction force P_s to the disc bearing force P_B may approach α (the adhesion factor, in pile bearing capacity analysis). Although the parameter α is likely to be <<1.0 here, it is desirable to use larger diameter penetrometers, where shaft friction is proportionately less. Thus, only in extreme circumstances, have the results to be corrected for infilling of the cavity.

To calculate the net bearing resistance q_{net}, the ultimate bearing resistance needs to be corrected for the overburden pressure due to the ambient stress field. Thus, the net bearing pressure is:

$$q_{net} = q_{ult} - \gamma\, z \qquad \textbf{3-10}$$

from which the undrained shear strength can be inferred:

$$C_u = {}^{q_{net}}/_{N_c} \qquad \textbf{3-11}$$

where N_c is the bearing capacity factor. The usual caveat regarding the meaning of "undrained shear strength" is assumed.

3.2.3.5 Penetrometer size effect

The effect of changes in penetrometer diameter was investigated to establish the significance, if any, of the finite dimensions of the mould. Samples of kaolin clay (K1) soil at a water content of 1.8 times its liquid limit ($\gamma = 13.7\ kN/m^3$) and treated with 5% lime were cured for 30 days. Using 10, 20, and 30mm disc diameters, repeated penetration tests were conducted. The raw results are shown in Figure 3-47(a) and show that good repeatability is obtained. When normalized, it can be seen (Figure 3-47b) that the results for the three disc diameters are indistinguishable. Therefore, at least up to D=30 mm, penetration resistance is not affected by proximity of the cylinder mould walls. The figure also indicates the dependency of the bearing capacity on the depth ratio z/D. As the depth ratio increases beyond z/D = 2, the net bearing pressure continues to slowly increase in the case of the 10 mm diameter penetrometer in contradiction to the suggestion that a steady state bearing resistance is eventually reached (Hu and Randolph, 1999; Ladanyi and Eden, 1969). It is likely that the greater than expected resistance reflects a combination of cavity closure, which inhibits the back-flow mechanism, and the shear resistance of the shaft.

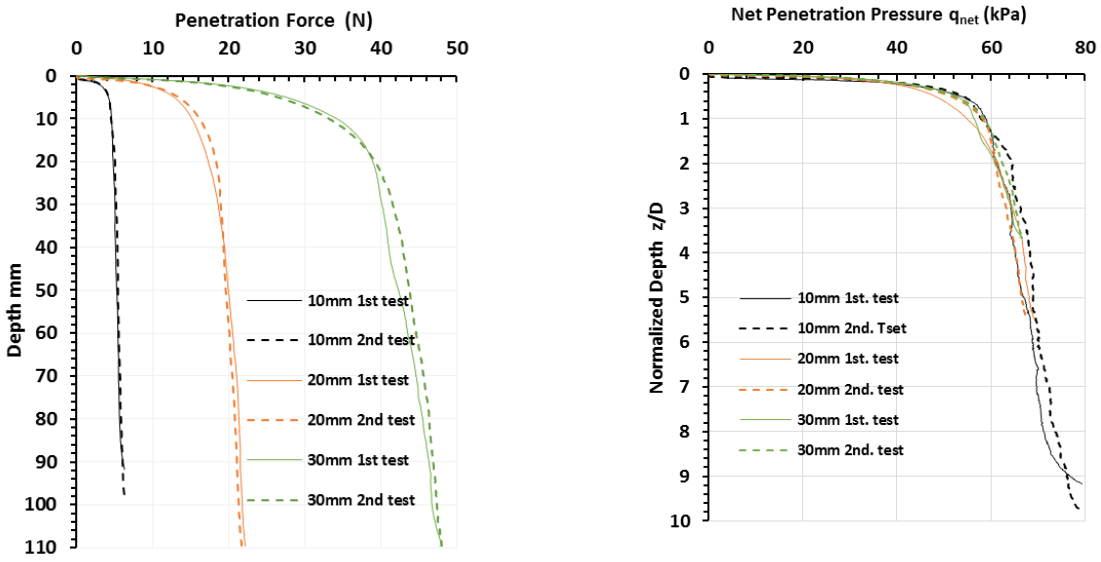

(a) Raw results

(b) Normalized results

Figure 3-47: Penetration test results for kaolin clay (K1) at 1.8W_{LL} treated with 5% lime and cured for 30 days: (a) force-displacement response and (b) the same results after normalization.

Remoulded soil specimens were also tested, giving the results shown in Figure 3-48. These results are in qualitative agreement with those obtained for the intact specimens. Normalizing the net penetration pressures curves in Figure 3-47(b) and Figure 3-48(b) with their corresponding maximum penetration pressure at z/D=5 and re-plotting them as shown in Figure 3-49 indicates approximately the same response of different sized penetrometers with respect to the normalized depth z/D, irrespective of the specimens' conditions (intact/remoulded). Although, remoulding results in a significant loss of strength (S_t>3), the strength of the remoulded soil remains several orders of magnitude higher than the untreated soil.

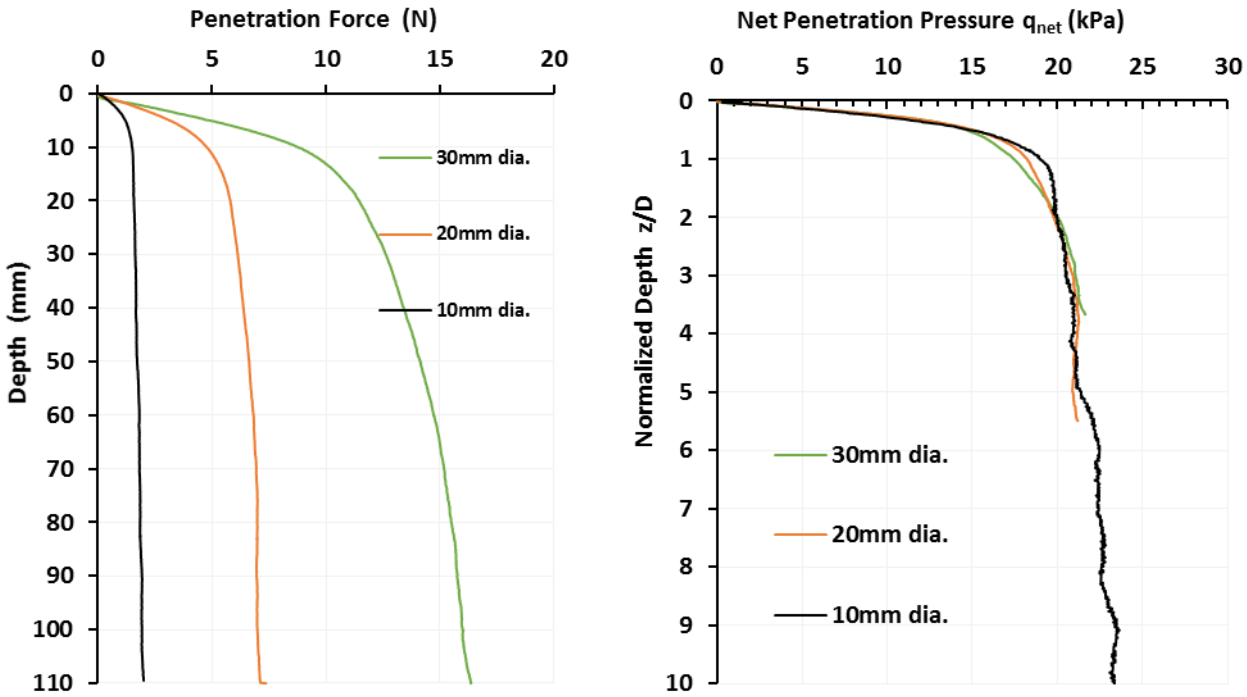

(a) Raw results (b) Normalized results

Figure 3-48: Penetration test results for remoulded kaolin clay (K1) at 1.8W_{LL} treated with 5% lime and cured for 30 days: (a) force-displacement response and (b) the same results after normalization.

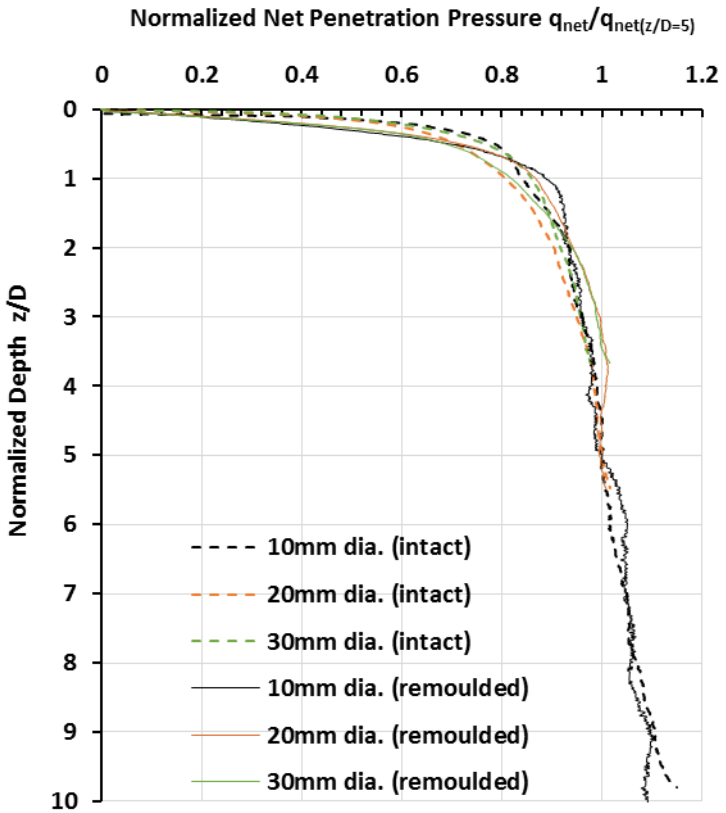

Figure 3-49: A comparison of normalized penetration test results for intact and remoulded kaolin clay (K1) at 1.8W_{LL} treated with 5% lime and cured for 30 days using different size penetrometers.

The decision was made to use the 20 mm diameter penetrometer in all subsequent tests. The 20 mm disc is less affected by shaft friction than the smaller disc, but still allows exploration of high z/D values.

The calculated shear strength of the soil from these tests is shown in Figure 3-50. These results were obtained using the N_c values discussed in Chapter Four based on the numerical solutions obtained by (Hossain and Randolph, 2009b).

In none of these tests was it possible to determine consistent values of undrained shear strength, above a normalized depth z/D of 0.5, or thereabouts. This depth corresponds to approximately 10 mm for the 20 mm diameter penetrometer. The reason of this is unclear: a non-level surface certainly plays a part. Softening in this zone is also likely.

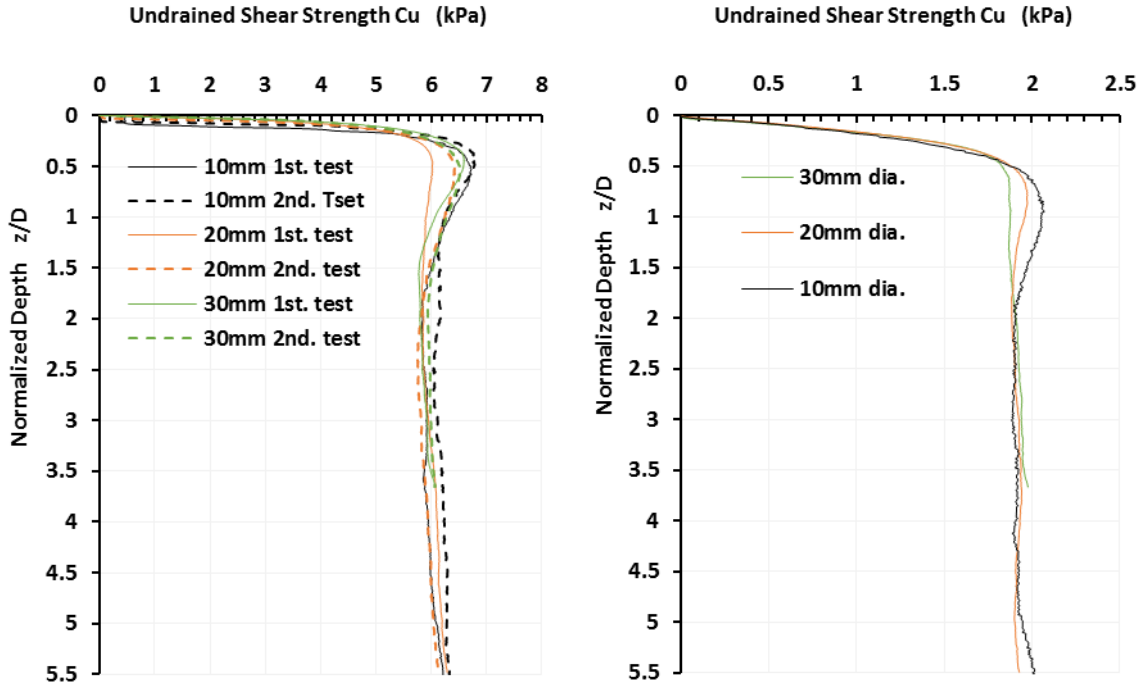

(a) Intact soil (b) soil Remoulded

Figure 3-50: Undrained shear strength: (a) intact soil, and (b) remoulded soil

The results are summarized in Table 3-7. For each penetration test, the mean value of the undrained shear strength was calculated for $1 \leq z/D \leq 5.5$. The standard deviation (S.D.) and the coefficient of variation (C.O.V.) were calculated for this mean undrained shear strength value. For the repeated penetration tests, the average value of undrained shear strength of the mean values from each single test were calculated. The standard deviation of this averaged value was calculated using the form:

$$S.D. = \sqrt{\frac{\sum_{i=1}^{n}(x_i - \bar{X})^2}{n}} \quad \text{3-12}$$

where x_i is the mean C_u value from a single test, $\bar{X}$ is the average C_u value of these repeated tests, and n is the number of repeated tests.

These results also demonstrated the repeatability of the tests for all disc diameters, with less than 5% difference between repeated tests. The shear strengths calculated using the 30mm penetrometer yielded slightly lower (2-3% lower) values compared with the 10 and 20mm disc diameters. Presumably this reflects the influence of the boundary condition at the side walls of the mould and thus different wall roughnesses might yield different results. Upward plastic flow of soil during the penetration process is apparent in Figure 3-51.

Table 3-7: Penetration test results for kaolin clay at 1.8W_{LL} treated with 5% lime

Dia. (mm)	1st test (intact soil)			2nd test (intact soil)			Averaging the two tests		
	Cu (kPa)	S.D.	C.O.V (%)	Cu (kPa)	S.D.	C.O.V (%)	Cu_{av} (kPa)	St. deviation	C.O.V (%)
10	6.02	0.12	1.94	6.23	0.10	1.58	6.12	0.11	1.76
20	6.01	0.14	2.31	5.93	0.12	2.06	5.97	0.04	0.68
30	6.02	0.08	1.25	5.88	0.08	1.31	5.95	0.07	1.19

Remoulded soil			
Dia. (mm)	Cu (kPa)	S.D.	C.O.V (%)
10	1.93	0.04	2.16
20	1.91	0.02	0.87
30	1.92	0.03	1.57

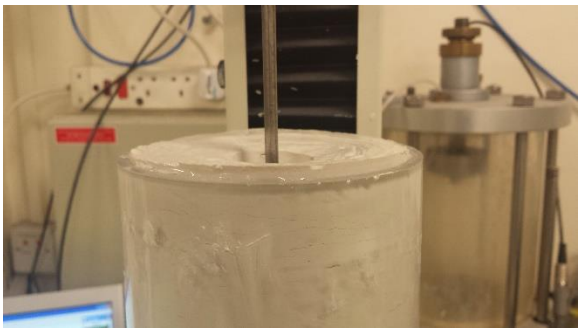

Figure 3-51: Penetration test in progress using a 30mm diameter disc [kaolin (K1) clay]

3.2.3.6 Effect of penetration velocity

To study the effect of strain rate, a series of penetration tests was conducted on kaolin clay (K1) at 1.8 times its liquid limit and treated with 1% and 5% lime. The samples were cured for curing periods of 3, 10, 30, and 100 days, and at two different curing temperatures 5°C and 20°C. The penetration tests were conducted at velocities of 10, 50, 250, and 1000

mm/min. To ensure the repeatability of the experiments, the tests were repeated. Some representative results from these penetration tests are shown in Figure 3-52.

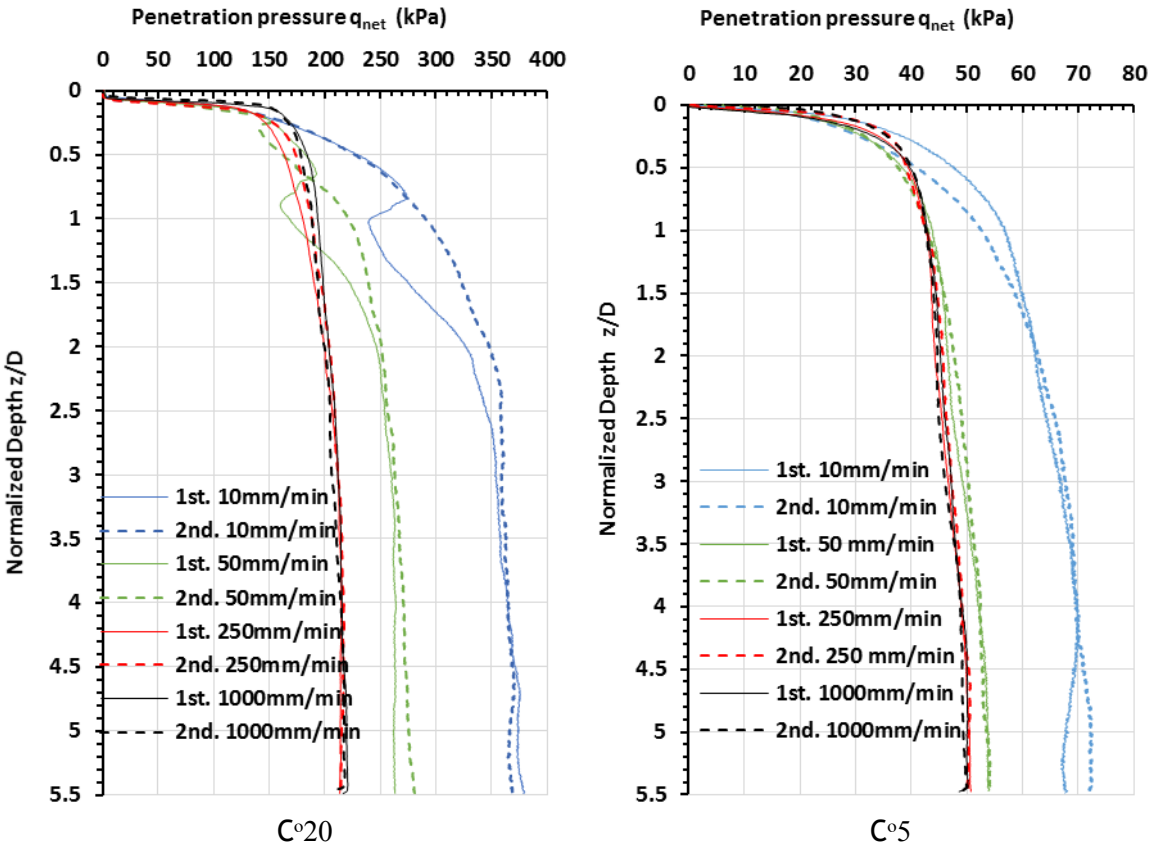

Figure 3-52 Penetration tests results for kaolin (K1) at 1.8W_{LL}, 5% lime after 100 days curing: (a) at 20°C and (b) at 5°C.

The results show that penetration resistances at low velocities are high but decrease with increased velocity. The high penetration resistance may be attributed to consolidation around the penetrometer which induces greater frictional resistance in the soil. At very high velocities, greater resistance to shearing might be expected due to viscous (and ultimately, dynamic) effects but there is little evidence of this in these results.

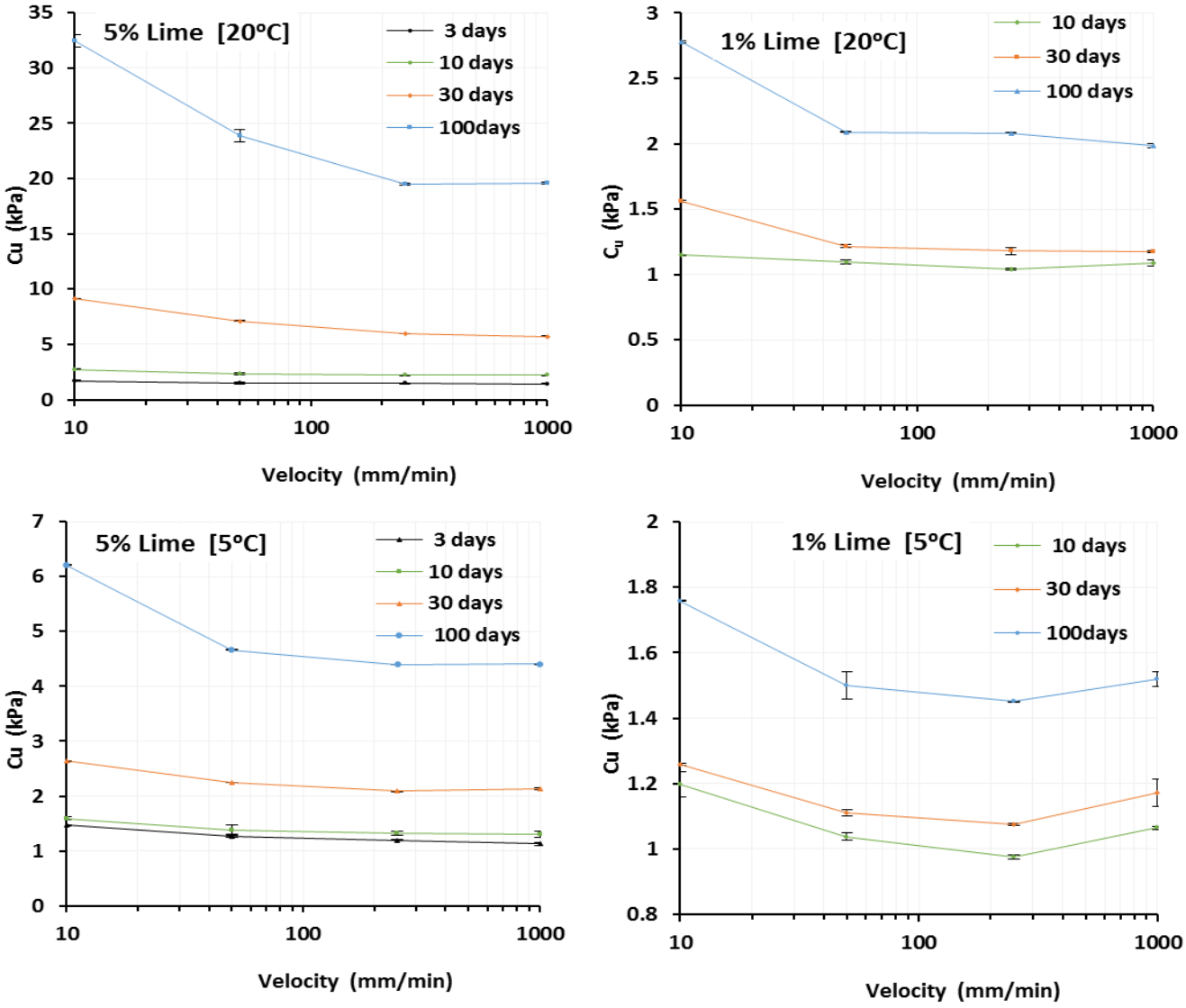

Figure 3-53: Effect of penetration velocity on the undrained shear strength of lime-admixed kaolin clay (K1) at 1.8W_{LL} at different temperatures, 5°C and 20°C

Figure 3-53 shows the undrained shear strengths C_u obtained from the penetration tests at different velocities for kaolin clay K1 at 1.8W_{LL} admixed with 1% and 5% lime and cured for 3, 10, 30, and 100 days at normal and cold curing temperature. The results suggest that partially drained behaviour occurs at velocities of 10mm/min. and that fully undrained conditions are realized at approximately at 250mm/min. Figure 3-54 shows the same results after normalization of the shear strength with respect to the corresponding strengths at a penetration velocity of 250 mm/min. The difference in measured shear strength for low and high velocities is proportionately greater for longer curing periods. An increase in the rate of consolidation be attributed to an increase of the soil inter-aggregates pores (Tran et al., 2014) and the increase in the mesoporosity of the soil (Metelková et al., 2012) due to the pozzolanic reaction and the accompanying mineralogical changes in the clay, giving rise to an increase in hydraulic conductivity. Beyond a velocity of 250mm/min, the undrained shear strength tends to increase due to the viscous nature of soil at high strain rates.

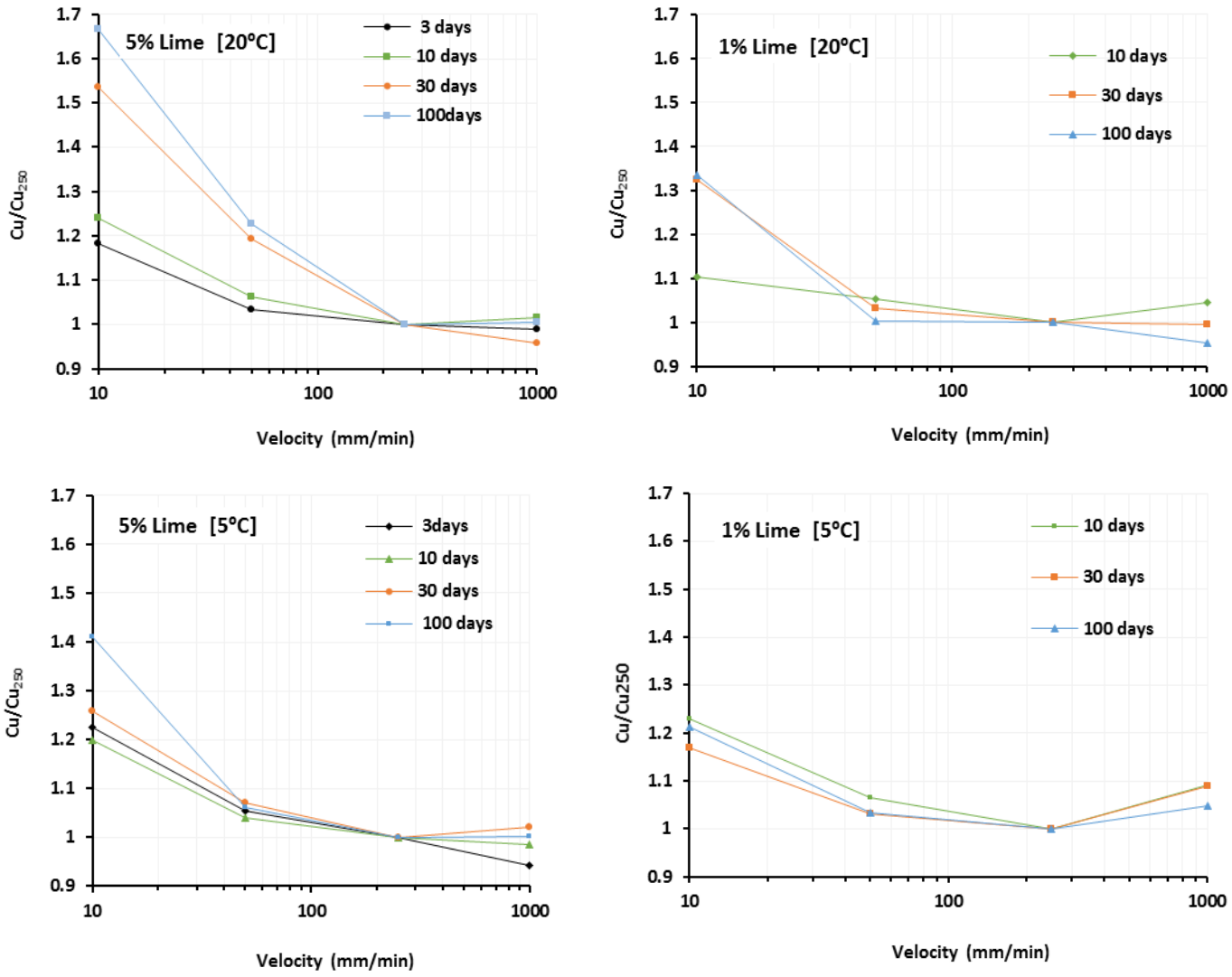

Figure 3-54: Normalized undrained shear strength at different velocities, for lime admixed kaolin clay (K1) at 1.8 W_{LL} at 20°C and 5°C

Based on these results, the optimum penetration velocity to conduct penetration tests in which fully undrained conditions are achieved can be taken to be 250 mm/min. Although several factors affect optimum penetration velocity, this value appears to be sufficiently high to avoid testing in partially undrained conditions. The effect of decreasing curing temperatures, which retards the pozzolanic reaction, appears to have little effect.

To investigate the effect of penetrometer diameter on strain rates, penetration tests using 10 mm and 20mm diameter penetrometers were conducted on remoulded samples of K1 clay at 1.8 times its liquid limit as shown in Figure 3-55. The results indicate that (for lime contents of 5%) for the 20 mm diameter penetrometer, the undrained condition is achieved at 250mm/min while for the 10mm diameter penetrometer, slightly higher velocities are required to attain fully undrained conditions. This is consistent with the normalisation proposed by Finnie & Randolph (1994). For the kaolin (K1) soil treated with only 1% lime,

it was found that 250mm/min seems to be the optimum penetration velocity to attain fully undrained conditions for both the 10mm and 20mm penetrometer diameters. Selection of the "optimum" strain rate is a somewhat subjective process, masked by experimental error.

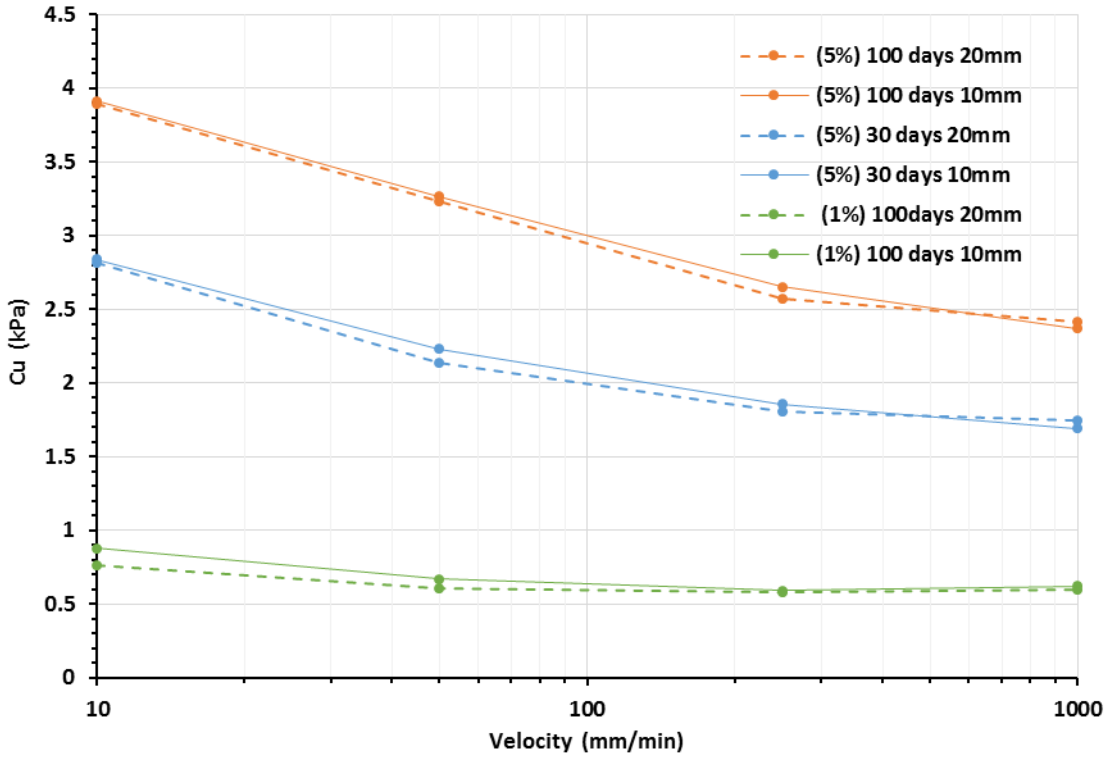

Figure 3-55: Effect of penetration velocity on the undrained shear strength of remoulded lime admixed kaolin (K1) at 1.8W_{LL} using 10mm and 20 mm penetrometers.

3.2.4 Consolidation tests

The compressibility of the lime treated clay was investigated using standard oedometer testing techniques in general accordance with BS1377-5 (BSI 1990c). The consolidometer ring had an inner diameter of 76 mm and a height of 20mm. Two fixed ring oedometer consolidation cells, as shown in Figure 3-56, were used in the experiments.

Figure 3-56: Consolidometer cell.

3.2.4.1 Sample preparation

Intact soil specimens cured for 100 and 365 days, were tested. The specimens were trimmed using a piano wire saw; inserted into the consolidometer ring and trimmed again. Remoulded soil specimens were introduced into the mould using a spatula. Care was taken to avoid air pockets. The upper face of the sample was then trimmed and levelled using a sharp metallic scraper. Whatman filter papers were placed between the specimen and each of the porous discs, as recommended by the British Standard.

For remoulded specimens and intact specimens of very low strength such as kaolin admixed with 1% lime and Grangemouth soil, directly after seating the specimen with the ring inside the cell , water was added to the cell to a level just below the top of the ring. It was necessary to add water at this stage to the very soft soils or otherwise water could be observed to drain from them. The upper Whatman paper was then placed, followed by the saturated upper porous disc. Water was then added to the level of the porous disc and the loading cap was then seated above the porous and disc. For stronger intact specimens, inundation was delayed until the seating pressure was applied.

3.2.4.2 Loading of samples

These soft soil specimens required careful handling. Very small loadings were applied initially to prevent soil squeezing out through the gap between the ring and the upper porous disc. The weight of the porous disc and the loading cap were measured under water and found to apply a stress of 0.445 kPa. The test proper however was started on the application of the first load (0.5N) which imposed a further stress increment of 1.32 kPa (or 1.77 kPa cumulatively). Loads were added systematically according to the British Standard by doubling the existing loads from the previous loading increment, with loading increments of 24 hrs. Unloading was conducted in a series of decrements to allow for swelling in about half the number of loading stages. An unloading increment duration of 12 hrs was found to be suitable for all soils tested. Table 3-8 shows the loading and unloading sequence adopted for the oedometer tests.

Table 3-8: Loading-unloading sequence used for oedometer tests.

Load (N)	Cap	0.5	1	2	5	10	20	40	80	160	320	620
Pressure(kPa)	0.45	1.77	3.1	5.74	13.7	26.9	53.4	106.3	212.1	423.7	847	1640.5
Loading	●	●	●	●	●	●	●	●	●	●	●	●
Unloading					●	●		●		●		●

The Wykeham-Farrance loading frames used for these consolidation tests are shown in Figure 3-57. Micrometre dial gauges of 5mm travel graduated in 0.002 mm divisions (readable to 0.001mm) were used to measure vertical deformation, as shown in Figure 3-57.

Figure 3-57: Wykeham-Farrance oedometer test loading frames.

3.2.5 Soil pH tests

The Thermo Scientific Orion 5 Star pH meter shown in Figure 3-58 was used to take the pH measurements of the lime-admixed soils after curing periods of 1, 3, 10, 30, 100, and 365 days. To measure the pH of soils, ASTM D 4972 – 01 recommends use of a specimen of 10 gm of air dried soil sample mixed with 10 mL of distilled water. BS ISO 10390:2005 and BS 7755-3.2: 1995 standards recommend use of a soil suspension of 5 mL of air dried soil after mixing with 5 times its volume of water, left for 2 hours before taking the pH measurements. A similar procedure is suggested by (Head, 1988a), namely mixing 30 gm of dried soil with 75 mL of CO_2-free distilled water. However, drying lime admixed soil may change pH due to carbonation. Consequently, a different procedure is adopted here wherein, without drying, the samples were brought to a water content of 250% by addition of the appropriate volume of distilled water. After stirring for a few minutes, the beaker containing the mixture was covered and left for two hours before testing.

Before each use of the pH meter, the device was calibrated, at pH 7 and at two other pH buffer solutions at pH 10 and pH 4.0 (Eckert and Sims, 1995). These buffer solutions were supplied by ACROS ORGANICS. After calibration, the pH meter's electrode was rinsed with distilled water and immersed in the soil sample. Digital readings were taken twice, when they reached the equilibrium, separated by a brief stirring of the sample (Head, 1988a).

Figure 3-58: Thermo Scientific Orion 5 Star pH meter.

3.2.6 Water content and saturation following long-term curing

The water content, degree of saturation, and bulk unit weight of samples cured for 100 and 365 days were measured for the entire range of soils at room temperature. These data provided the initial conditions for the water content measurements for consolidation tests after their extraction from their moulds. The results of these measurements are outlined below:

Table 3-9 to Table 3-13 summarise the raw data obtained for water content w, saturation degree S_r, and unit weight γ. Examination of the repeated test data shows that a high degree of repeatability has been achieved in most, if not all, cases. This lend confidence to the reliability of the curing technique, to produce consistent results.

The mean values of these data are plotted in Figure 3-59 to Figure 3-63 below. In general, these results show a slight decrease of water content with increasing curing time. For example, for kaolin, (Figure 3-59(a)) with $w=2.2W_{LL}$ admixed with 1% lime, the water content decreases from 1.45 to 1.43 after 365 days of curing. Similar reductions occur for all other water contents and lime contents. In percentage terms, the water content loss due to long-term curing is less than 2%. For other soils, the percentage water content loss (up to 365 days) is never greater than 3%. For example CB clay at $2.2W_{LL}$ admixed with 3% lime (Figure 3-60(a)) suffers a decrease in water content from 2.6 to 2.54; a fall 0f 2.7%.

The reduction in water content may be attributable to the chemical reaction of water with lime and the pozzolanic clay minerals during the curing process. The fall in water content is reflected in saturation levels based on measurements of unit weight. Although the measurements of unit weight, founded on the weight of the oedometer samples, are less reliable than the water content data, the saturation values are consistent with the reduction in water content without shrinkage. In about two-thirds of cases, the final saturation level (i.e. after one year) exceeded 98%, while the rest with few exceptions exceeded 97%. The question whether significant suctions developed due to the loss of full saturation can be answered in the negative by observing that the (unsoftened) strength of samples cured using "flooding" curing technique are essentially identical to the strengths obtained using sealing technique.

For completeness, the unit weights are also plotted in Figure 3-59(c) to Figure 3-63(c). It is worth noting that the lowest of these (for near-saturated soil) is just 11.9 kN/m^3.

Table 3-9: Effect of long-term curing on water content, degree of saturation, and unit weight [kaolin K2, T=20ºC]

W=w/W_{LL}	Lime (%)	Time (days)	Water content w						Degree of Saturation S_r (%)						Unit weight γ (kN/m^3)					
			1st	2nd	3rd	x̄	S.D.	COV	1st	2nd	3rd	x̄	S.D.	COV	1st	2nd	3rd	x̄	S.D.	COV
1.8	1	0	1.194	1.191	1.188	1.191	0.00	0.19												
		100	1.184	1.193	1.184	1.189	0.00	0.38	98.8	97.9		98.4	0.49	0.49	13.54	13.42		13.48	0.06	0.45
		365	1.184	1.195	1.166	1.182	0.01	1.01	96.8	99.2	99.4	98.5	1.20	1.22	13.33	13.55	13.60	13.49	0.12	0.89
	3	0	1.172	1.170	1.165	1.169	0.00	0.25												
		100	1.161	1.166		1.164	0.00	0.20	97.4	96.9		97.2	0.25	0.26	13.45	13.38		13.42	0.03	0.25
		365	1.155	1.144	1.144	1.148	0.01	0.46	97.1	96.7	98.1	97.3	0.58	0.60	13.45	13.44	13.53	13.47	0.04	0.31
	5	0	1.145	1.147	1.144	1.145	0.00	0.11												
		100	1.142	1.134		1.138	0.00	0.35	97.1	98.4		97.7	0.63	0.64	13.60	13.68		13.64	0.04	0.29
		365	1.130	1.135	1.123	1.129	0.01	0.45	96.9	98.2	98.9	98.0	0.81	0.83	13.51	13.63	13.81	13.65	0.12	0.88
2	1	0	1.330	1.326	1.330	1.329	0.00	0.14												
		100	1.319	1.315		1.317	0.00	0.17	99.5	99.5		99.5	0.02	0.02	13.30	13.28		13.29	0.01	0.06
		365	1.323	1.290	1.328	1.314	0.02	1.31	98.7	98.3	100.0	99.0	0.73	0.74	13.28	13.15	13.38	13.27	0.09	0.68
	3	0	1.303	1.320		1.312	0.01	0.65												
		100	1.300	1.29		1.295	0.01	0.39	98.5			98.5			13.26			13.26	0.00	0.00
		365	1.280	1.307		1.293	0.01	1.04	96.9	99.0		97.9	1.04	1.07	13.33	13.05		13.19	0.14	1.05
	5	0	1.271	1.280	1.270	1.274	0.00	0.35												
		100	1.247	1.277	1.265	1.263	0.01	0.98	98.2	98.3		98.3	0.04	0.04	13.24	13.35		13.29	0.06	0.42
		365	1.260	1.260	1.260	1.260	0.00	0.02	98.2	97.5	98.9	98.2	0.57	0.58	13.30	13.24	13.36	13.30	0.05	0.39
2.2	1	0	1.445	1.451	1.455	1.450	0.00	0.28												
		100	1.435	1.450		1.442	0.01	0.54	100.0	99.9		100.0	0.04	0.04	13.17	13.09		13.13	0.04	0.30
		365	1.444	1.384	1.454	1.427	0.03	2.16	99.9	98.8	98.6	99.1	0.55	0.56	13.10	13.11	12.95	13.05	0.07	0.56
	3	0	1.422	1.426		1.424	0.00	0.14												
		100	1.417	1.410		1.414	0.00	0.26	97.3	97.8		97.6	0.22	0.22	12.88	12.93		12.90	0.02	0.19
		365	1.409			1.409			97.2			97.2			12.88			12.88	0.00	0.00
	5	0	1.397	1.416		1.407	0.01	0.68												
		100	1.382	1.422		1.402	0.02	1.44	99.4	99.4		99.4	0.02	0.02	13.17	13.08		13.12	0.04	0.31
		365	1.371	1.387		1.379	0.01	0.57	98.5	97.0		97.7	0.72	0.73	13.09	12.94		13.02	0.08	0.59

Table 3-10: Effect of long-term curing on water content, degree of saturation, and unit weight [Calcium Bentonite CB, T=20ºC]

W=w/W_{LL}	C (%)	Time (days)	Water content w						Degree of Saturation S_r (%)						Unit weight γ (kN/m^3)					
			1st	2nd	3rd	x̄	S.D.	COV	1st	2nd	3rd	x̄	S.D.	COV	1st	2nd	3rd	x̄	S.D.	COV
1.8	3	0	2.14	2.14	2.13	2.14	0.01	0.27												
		100	2.14	2.14		2.14	0.00	0.05	99.38	99.21		99.30	0.08	0.09	12.25	12.23		12.24	0.01	0.06
		365	2.12	2.10	2.10	2.11	0.01	0.44	99.55	99.21	98.78	99.18	0.31	0.32	12.29	12.28	12.23	12.26	0.03	0.22
	5	0	2.09	2.09	2.10	2.09	0.00	0.11												
		100	2.09			2.09			99.17			99.17		0.00	12.28			12.28		
		365	2.03	2.05	2.04	2.04	0.01	0.55	99.00	98.61	98.42	98.68	0.24	0.25	12.32	12.26	12.27	12.28	0.02	0.20
2.2	3	0	2.61	2.60		2.61	0.00	0.15												
		100	2.58			2.58			100.00			100.00			12.02			12.02		
		365	2.54			2.54			99.90			99.90			11.96			11.96		
	5	0	2.55	2.54		2.55	0.01	0.27												
		100	2.54	2.53		2.53			98.24	98.07		98.15			11.79	11.77		11.78		
		365	2.45	2.44	2.52	2.47	0.03	1.32	98.77	98.06		98.41	0.35	0.36	11.86	11.83	11.90	11.86	0.03	0.24

Table 3-11: Effect of long-term curing on water content, degree of saturation, and unit weight [SW-K mix, T=20ºC]

W=w/W_{LL}	C (%)	Time (days)	Water content w							Degree of Saturation S_r (%)							Unit weight γ (kN/m^3)						
			1st	2nd	3rd	4th	x̄	S.D.	COV	1st	2nd	3rd	4th	x̄	S.D.	COV	1st	2nd	3rd	4th	x̄	S.D.	COV
1.8	3%	0	2.13	2.13			2.13	0.00	0.02														
		100	2.12				2.12			97.26	98.34			97.80			12.00	12.11			12.05	0.05	0.45
		365	2.11	2.12			2.11	0.00	0.21	97.10	98.49			97.79	0.69	0.71	11.99	12.13			12.06	0.07	0.57
1.8	5%	0	2.10	2.09	2.09		2.09	0.00	0.21														
		100	2.08	2.09			2.09	0.01	0.30	97.13	96.88			97.01	0.13	0.13	11.98	12.02			12.00	0.02	0.15
		365	2.06	2.07	2.07	2.09	2.07	0.01	0.54	97.74	99.29	95.42	94.85	96.82	1.79	1.85	12.10	12.28	11.87	11.80	12.01	0.19	1.58
2.2	5%	0	2.55	2.54	2.55		2.55	0.00	0.18														
		100	2.55	2.54			2.54	0.01	0.24	99.78	99.23			99.51	0.00	0.00	11.90	11.83			11.86	0.03	0.29
		365	2.51	2.53	2.51	2.47	2.51	0.02	0.83	99.37	99.11	99.67	97.99	99.04	0.64	0.64	11.88	11.84	11.90	11.77	11.85	0.05	0.43

Table 3-12: Effect of long-term curing on water content, degree of saturation, and unit weight [SW-S mix, T=20ºC]

W=w/W_{LL}	C (%)	Time (days)	Water content w						Degree of Saturation S_r (%)					Unit weight γ (kN/m^3)				
			1st	2nd	3rd	x̄	S.D.	COV	1st	2nd	x̄	S.D.	COV	1st	2nd	x̄	S.D.	COV
1.8	5%	1	1.143	1.142		1.143	0.00	0.04										
		3	1.142	1.141		1.142	0.00	0.04										
		10	1.142	1.140		1.141	0.00	0.08										
		30	1.141	1.142		1.142	0.00	0.04										
		100	1.140	1.135	1.145	1.140	0.00	0.19	97.75	97.72	97.73	0.01	0.01	13.67	13.68	13.68	0.01	0.04
		365	1.136	1.142	1.132	1.136	0.00	0.28	97.60	98.12	97.86	0.26	0.27	13.67	13.71	13.69	0.02	0.16
2.0	5%	1	1.182	1.183		1.183	0.00	0.04										
		3	1.181	1.183		1.182	0.00	0.08										
		10	1.182	1.181		1.182	0.00	0.02										
		30	1.180	1.181		1.181	0.00	0.04										
		100	1.171	1.185	1.170	1.175	0.01	0.56	96.95	97.81	97.38	0.43	0.44	13.51	13.56	13.53	0.03	0.21
		365	1.165	1.176		1.171	0.01	0.45	97.98	97.62	97.80	0.18	0.18	13.61	13.59	13.60	0.01	0.07
2.0	3%	1	1.220	1.220		1.220	0.00	0.00										
		3	1.220	1.220		1.220	0.00	0.00										
		10	1.219	1.218		1.219	0.00	0.07										
		30	1.218	1.219		1.219	0.00	0.05										
		100	1.220	1.217	1.218	1.218	0.00	0.12	97.89		97.89			13.48		13.48		
		365	1.218	1.218	1.217	1.218	0.00	0.00	97.96		97.96			13.49		13.49		

Table 3-13: Effect of long-term curing on water content, degree of saturation, and unit weight [G, T=20ºC]

W=w/W_{LL}	C (%)	Time (days)	Water content w							Degree of Saturation S_r (%)						Unit weight γ (kN/m^3)					
			1st	2nd	3rd	4th	x̄	S.D.	COV	1st	2nd	3rd	x̄	S.D.	COV	1st	2nd	3rd	x̄	S.D.	COV
1.4	5	0	0.579	0.578			0.579	0.00	0.09												
		100	0.575	0.575			0.575	0.00	0.02	99.0	98.5		98.7	0.24	0.24	16.29	16.24		16.27	0.02	0.14
		365	0.566	0.562	0.563	0.602	0.573	0.02	2.94	98.7	98.3	96.6	98.5	0.92	0.93	16.33	16.32	16.13	16.32	0.09	0.54
	3	0	0.585	0.590			0.588	0.00	0.43												
		100	0.584	0.583			0.583	0.00	0.11	100.0	99.0		99.5	0.49	0.50	16.13	16.23		16.18	0.05	0.31
		365	0.578	0.566	0.590		0.578	0.01	1.70	99.5			99.5			16.38			16.38		
1.6	5	0	0.585	0.590			0.588	0.00	0.43												
		100	0.622	0.623			0.622	0.00	0.13	98.1	99.3		98.7	0.60	0.61	15.89	16.00		15.94	0.06	0.35
		365	0.622	0.618	0.609	0.624	0.620	0.01	0.92	98.8	98.4		98.6	0.22	0.23	15.96	15.95		15.95	0.01	0.04
	3	0	0.639	0.631			0.635	0.00	0.61												
		100	0.633				0.633			99.2			99.2			15.91			15.92		
		365		0.629			0.629														

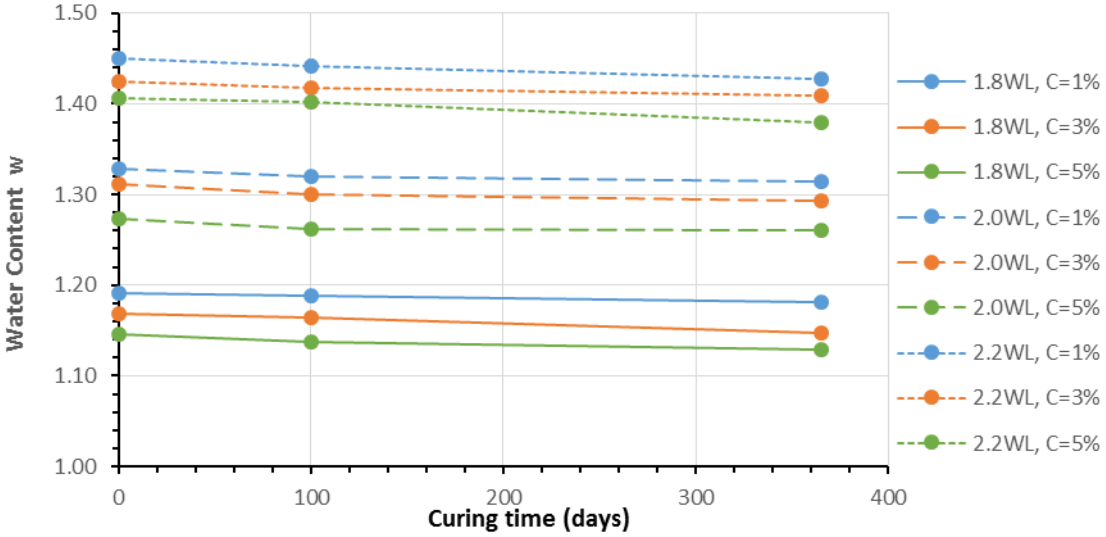

(a)

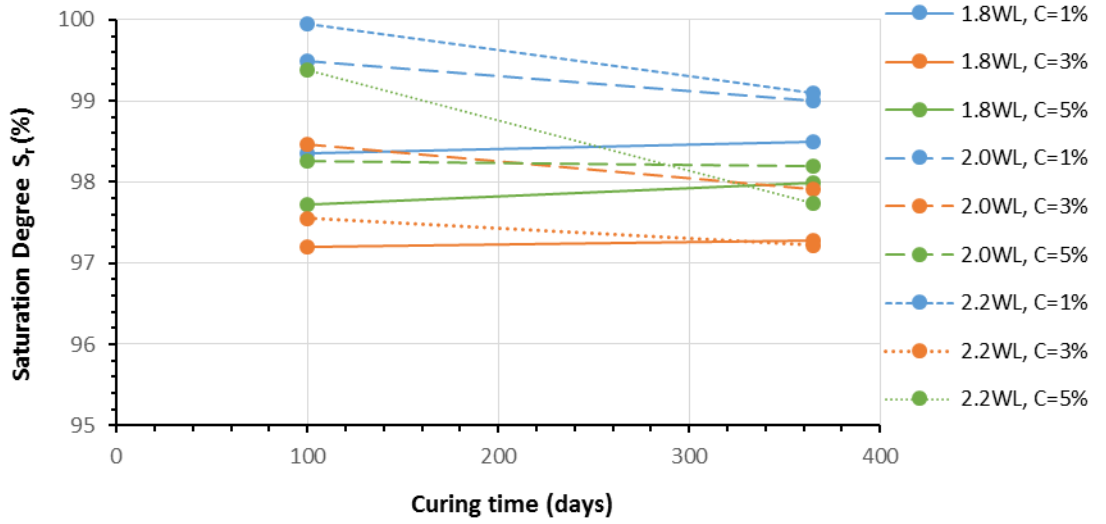

(b)

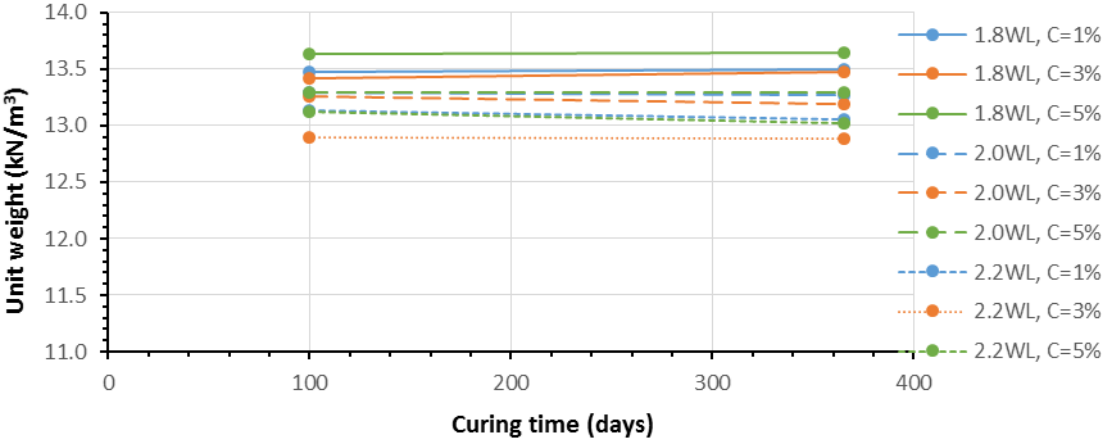

(c)

Figure 3-59: Effect of long-term curing on: (a) water content, (b) degree of saturation, and (c) unit weight [kaolin K2, T=20ºC]

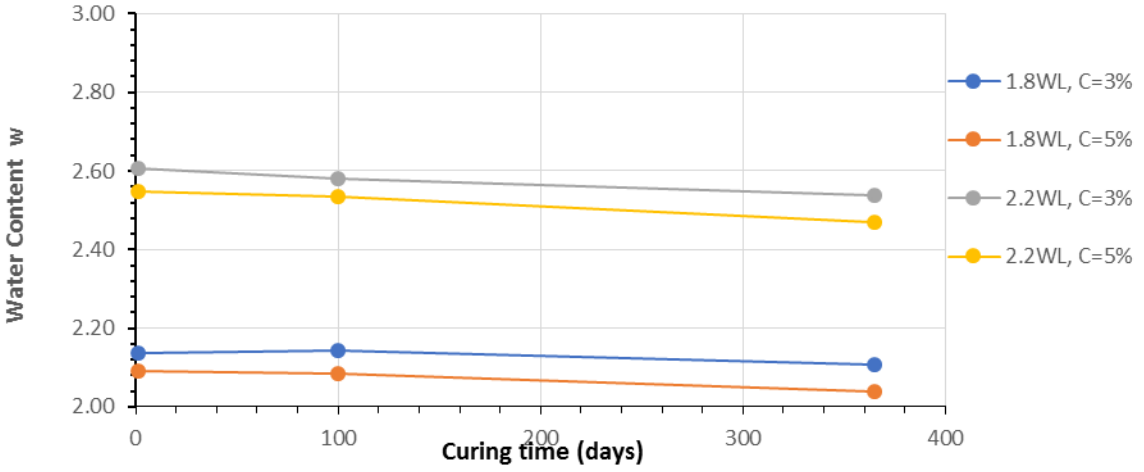

(a)

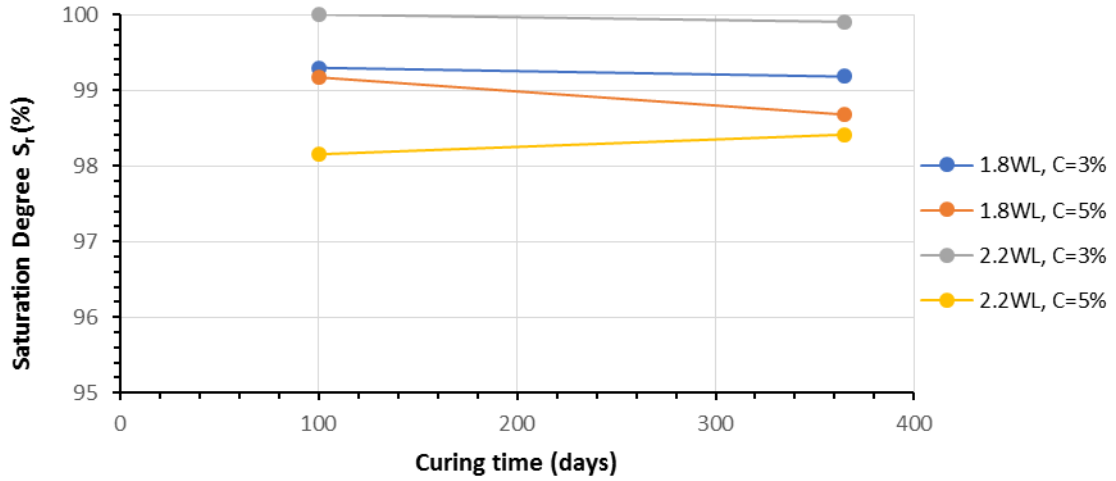

(b)

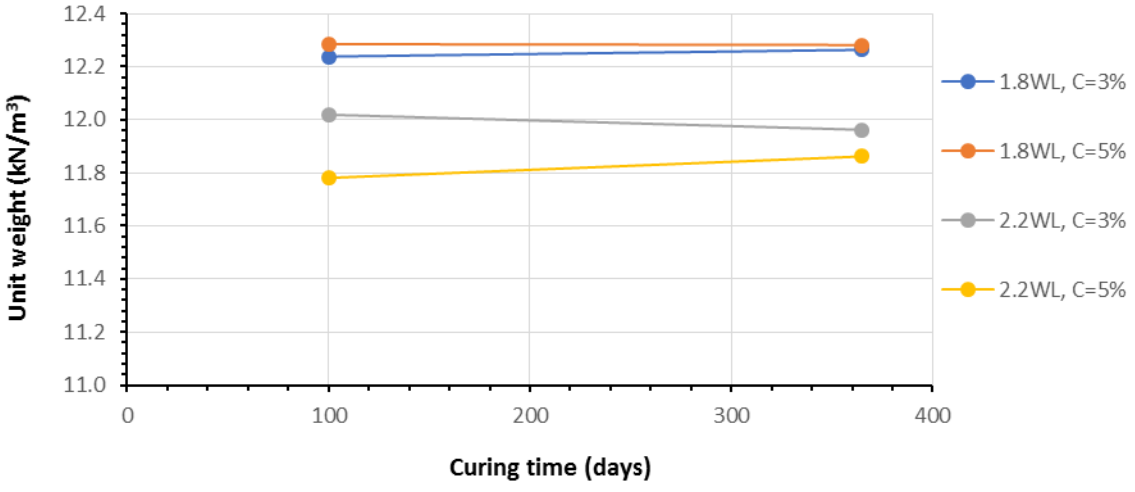

(c)

Figure 3-60: Effect of long-term curing on: (a) water content, (b) degree of saturation, and (c) unit weight [Calcium Bentonite CB, T=20ºC].

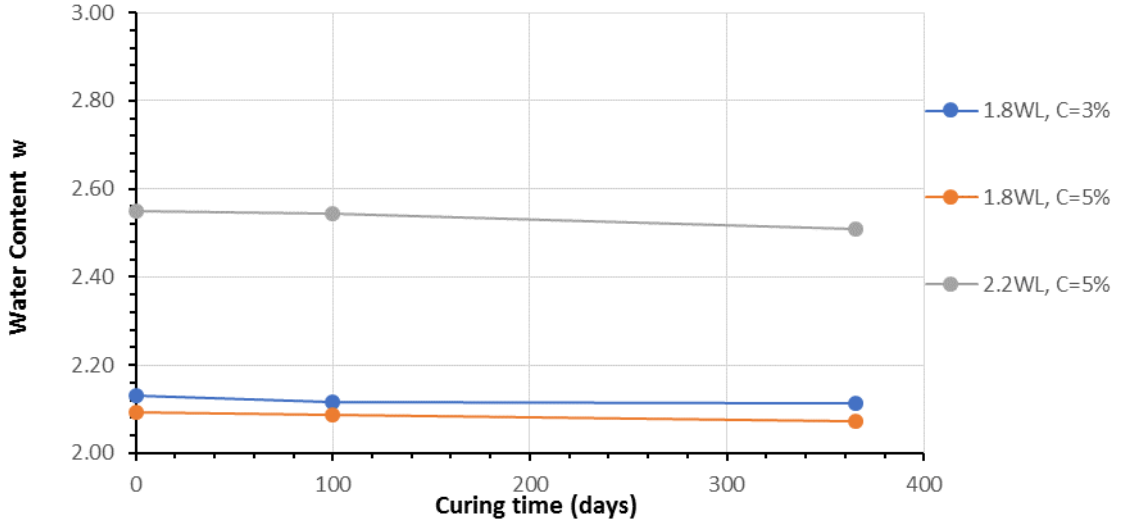

(a)

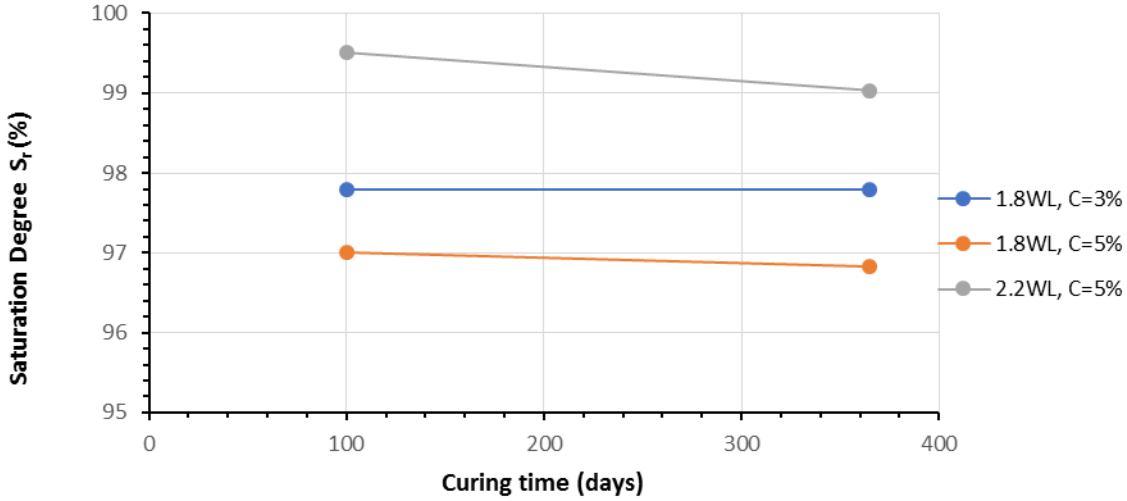

(b)

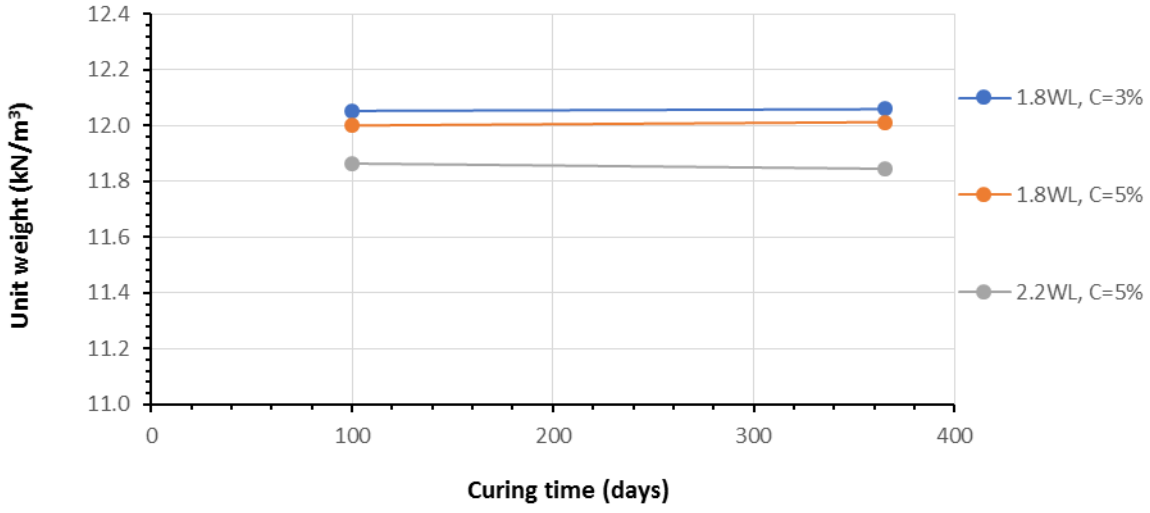

(c)

Figure 3-61: Effect of long-term curing on: (a) water content, (b) degree of saturation, and (c) unit weight [SW-K mix, T=20ºC].

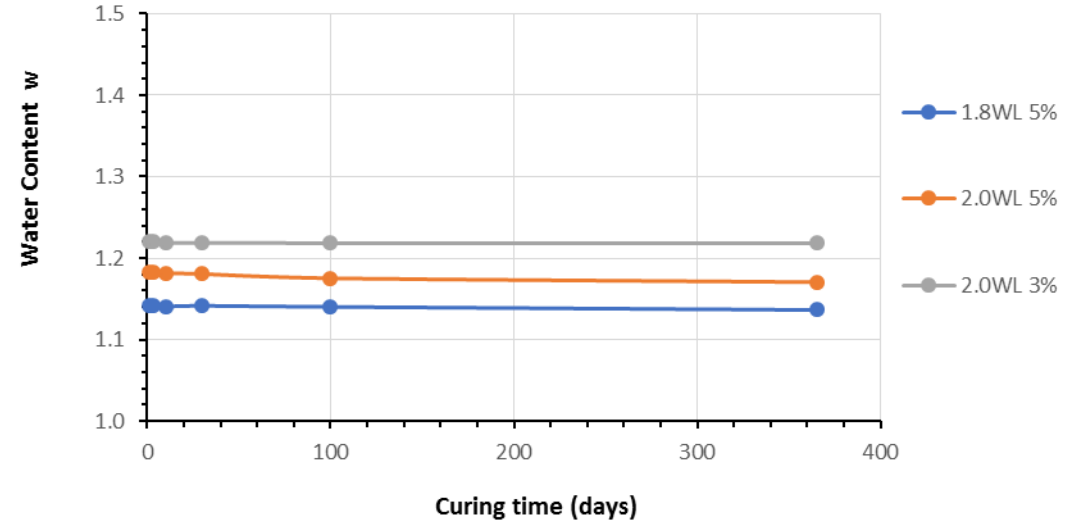

(a)

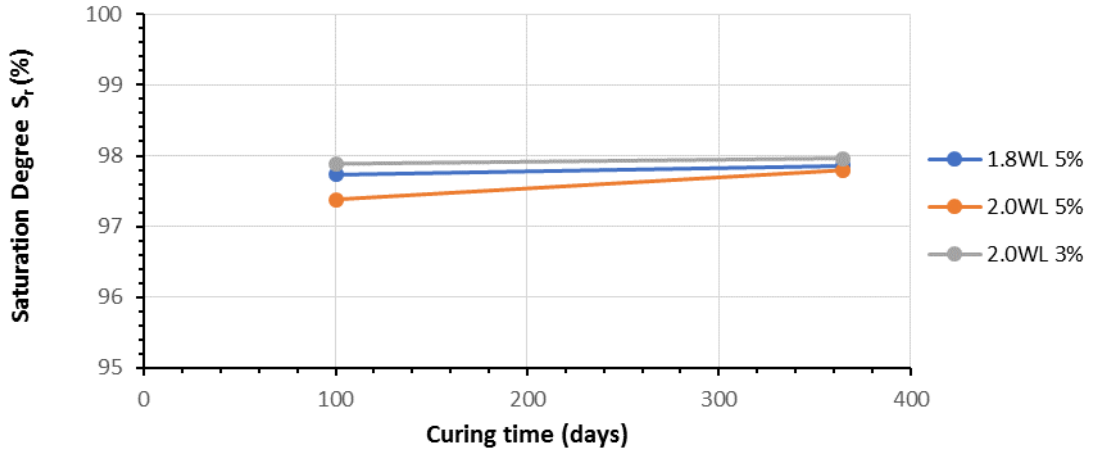

(b)

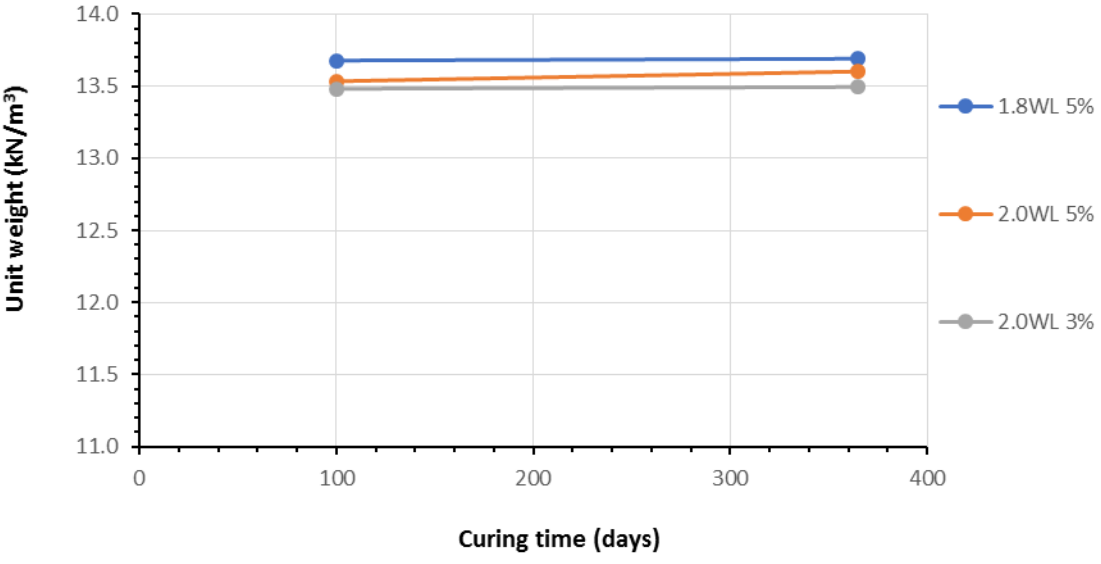

(c)

Figure 3-62: Effect of long-term curing on: (a) water content, (b) degree of saturation, and (c) unit weight [SW-S mix, T=20ºC].

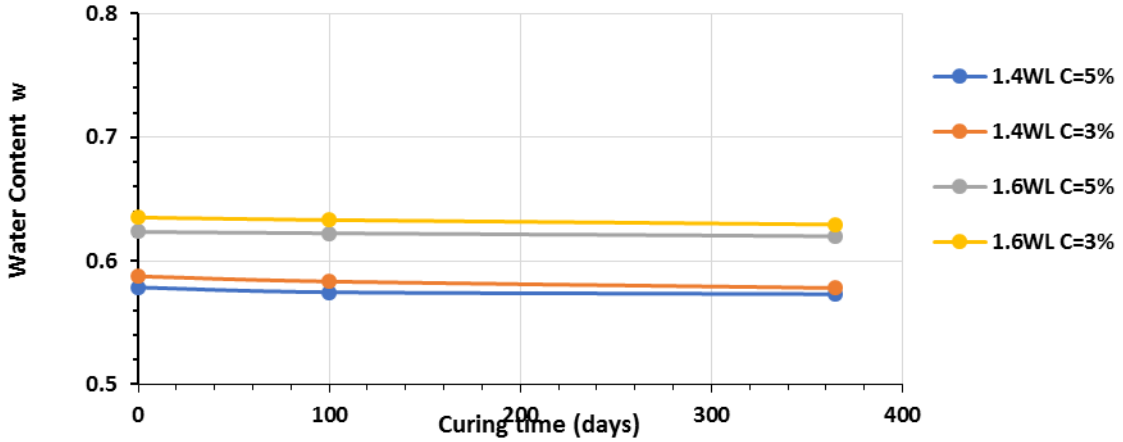

(a)

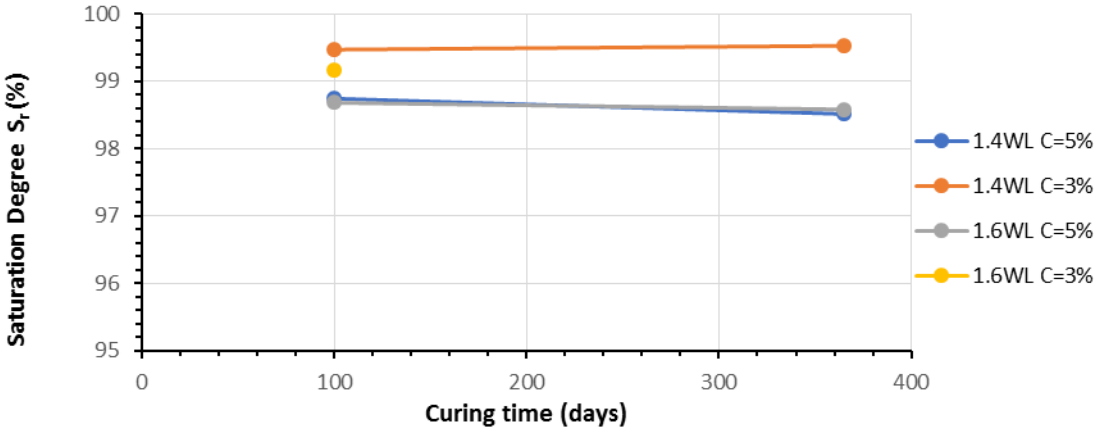

(b)

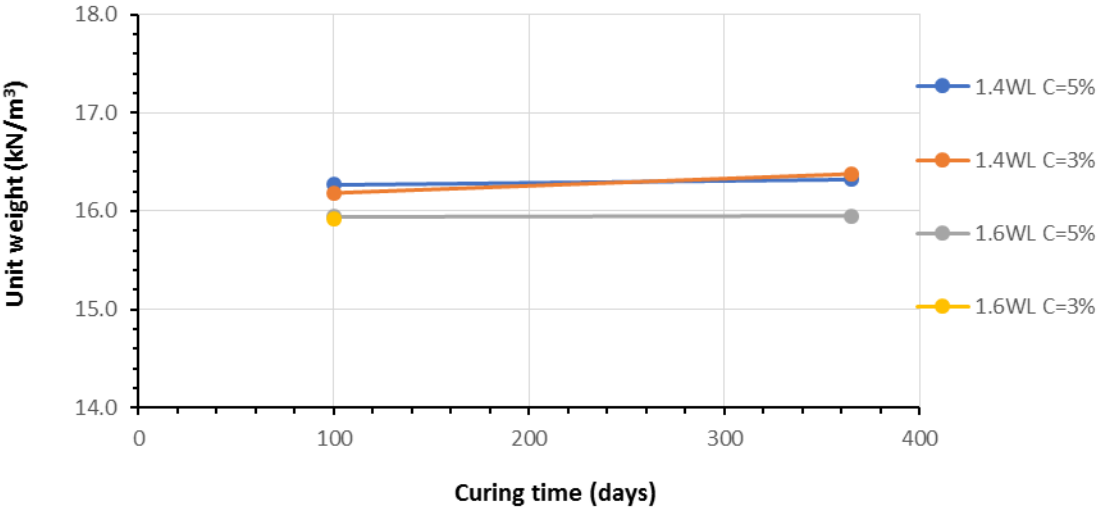

(c)

Figure 3-63: Effect of long-term curing on: (a) water content, (b) degree of saturation, and (c) unit weight [G soil, T=20ºC].

A more limited set of water content data is available for long-term curing at other temperatures. Table 3-14 and Table 3-15 show the change in water contents of kaolin (K2) and SW-K clay specimens respectively cured at 5ºC, 20ºC, and 38ºC. As before, the data for repeated tests demonstrate that the experimental technique yields very consistent results.

Table 3-14: Effect of long-term curing on water content of kaolin (K2) at 5ºC, 20ºC, and 38ºC.

w/W_{LL}	Lime (%)	Temp. (°C)	Time (days)	Water content w					
				1st	2nd	3rd	$\bar{x}$	S.D.	COV
1.8	5	20° C	0	1.145	1.147	1.144	1.145	0.00	0.11
			100	1.142	1.134		1.138	0.00	0.35
			365	1.130	1.135	1.123	1.129	0.01	0.45
		38° C	0	1.145	1.146		1.146	0.00	0.04
			30	1.1401	1.138		1.139	0.00	0.09
			100	1.136			1.136		
		5° C	0	1.146	1.145		1.146	0.00	0.04
			30		1.143		1.143		
			100		1.14		1.140		
			365	1.132	1.133		1.133	0.00	0.04
1.8	1	20	0	1.194	1.191	1.188	1.191	0.00	0.19
			100	1.184	1.193		1.189	0.00	0.38
			365	1.184	1.195	1.166	1.182	0.01	1.01
		38	0	1.192	1.193		1.193	0.00	0.04
			30	1.191			1.191	0.00	0.00
			100	1.185	1.188		1.187	0.00	0.13
		5	0	1.192	1.193		1.193	0.00	0.04
			100	1.189			1.189		
			365	1.183	1.182		1.183		

Table 3-15: Effect of long-term curing on water content of SW-K clay mix at 5ºC, 20ºC, and 38ºC.

w/W_{LL}	Lime (%)	Temp (°C)	Time (days)	Water content w						
				1st	2nd	3rd	4th	$\bar{x}$	S.D.	COV
1.8	3%	20	0	2.13	2.13			2.13	0.00	0.02
			100	2.12				2.12		
			365	2.11	2.12			2.11	0.00	0.21
		38	0	2.125	2.13			1.63	0.00	0.12
			30	2.118	2.121			2.12	0.00	
			100	2.111	2.115			2.11	0.00	0.09
1.8	5%	20	0	2.10	2.10	2.09		2.10	0.01	0.25
			100	2.08	2.09			2.09	0.01	0.30
			365	2.06	2.07	2.07	2.09	2.07	0.01	0.54
		5	0	2.1	2.101			2.10	0.00	0.02
			30	2.09	2.1			2.10	0.01	0.24
			100	2.085	2.093			2.09	0.00	0.19
			365	2.08				2.08		

Mean water contents $\bar{x}$ obtained from Table 3-14 and Table 3-15 are plotted in Figure 3-64 and Figure 3-65 respectively. These results reveal a consistent trend: curing at higher temperatures results in a higher loss of water content (and vice-versa), for the same curing period. This observation is consistent with the accelerated rate of chemical reaction at higher

temperatures; as can be verified by replotting the data using Arrhenius scaling. It is particularly noteworthy that the data for the cold temperature curing, for which the test cells were not submerged in water baths, follow precisely the same trend. Assuming that the volume of the samples cannot increase during the curing, then the percentage fall in saturation cannot be greater than the percentage decrease in water content, typically 2%.

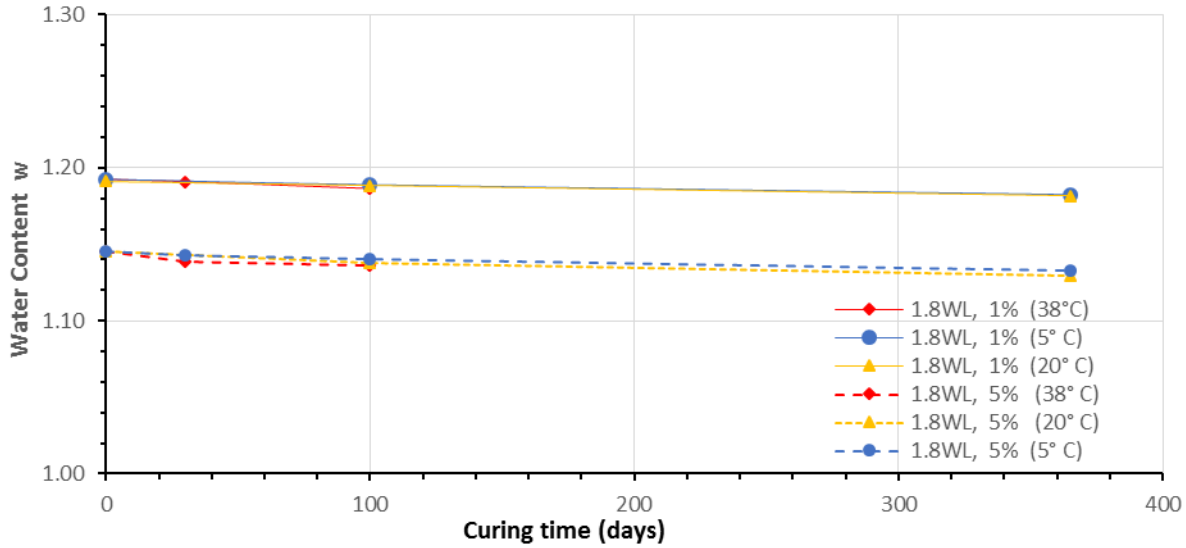

Figure 3-64: Effect of long-term curing on water content of kaolin (K2) at 5ºC, 20ºC, and 38ºC.

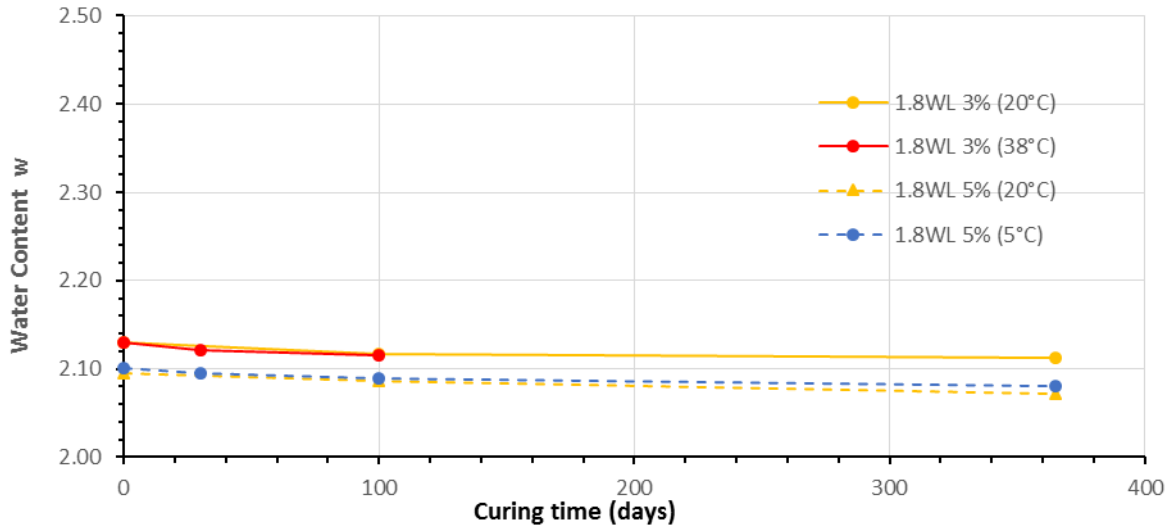

Figure 3-65: Effect of long-term curing on water content of SW-K clay mix at 5ºC, 20ºC, and 38ºC.

3.2.7 Summary of the experimental programme

The main objective of the experimental programme was to explore the development of the undrained shear strength of ultra-soft lime admixed soils. To reach this goal, the experimental programme was planned in the following steps:

1. Several soil types were used to study the effect of minerology on the lime treatment. In addition, two soils were produced by mixing SW Bentonex with kaolin and fine sand. Mix ratios were selected in these two cases to produce soils at liquid limits equal to the liquid limits of other soils used. A local natural soil was also used in the programme.
2. Curing of specimens under a wide range of conditions/temperatures was undertaken to investigate the effect of these parameters on the development of undrained shear strength over time.
3. Penetration test using disc penetrometers was the principal test used to measure the undrained shear strength of soil:
    - Preliminary tests were conducted on intact and remoulded lime-admixed specimens to select the proper disc diameter.
    - Systematic repeated tests were planned to produce, cure and test, specimens at different lime and water contents using different strain rates to select the optimum test speed to achieve fully undrained conditions. Specimens cured for different times and at three different curing temperatures were investigated.
    - Systematic repeated tests were planned to produce, cure, and test specimens at different lime contents, water contents, and curing times for five different soils to determine their intact undrained shear strength.
    - To better understand the nature of these soils, penetration tests were also conducted after hand remoulding of the cured samples to evaluate their strength sensitivity due to remoulding.
4. A series of repeated unconsolidated-undrained triaxial compression tests was conducted on intact specimens of the same soils (lime admixed and cured for 365 days) to compare their undrained shear strengths with the undrained shear strength from penetration tests. Also, the U-U test results gave some insight to the behaviour of lime admixed soils in terms of pore water pressure development, brittleness, and shear band development.

5. Specimens were produced and cured for use in miniature vane shear tests to measure the undrained shear strength for comparison with triaxial tests results.
6. To monitor the progress of the pozzolanic reaction, pH tests were conducted to monitor the pH level in the treated soil with time. Also, pH measurements were used to determine the initial consumption of lime in different soils.
7. Finally, to study the compressibility of lime admixed soils at high water contents, a series of one-dimensional consolidation tests were conducted. Repeated intact and remoulded lime-admixed soil specimens cured for 100 and 365 days were used. The rationale for this experimental programme was to measure the vertical yield stress due to lime treatment and correlate it with the undrained shear strength of these soils. It also aimed to quantify the consequences of remoulding on the consolidation behaviour of these soils.

To summarize, Table 3-16 outlines the main tests conducted in this programme. Some other supplementary tests (referred to elsewhere in this chapter) are not tabulated here:

Table 3-16: Summary of the main tests conducted

Test	Test Description	Soil	Curing period (days)	Curing temperature (°C)	Soil condition
Penetration	Circular plate penetrometer with constant rate of straining	K1 , K2, CB, SW-K, SW-S, G	1, 3, 10, 30, 100, and 365	5 2o 38	Intact and remoulded
Triaxial Compression	U-U test with pore water pressure measurements	K2, CB, SW-K, SW-S	365	20	Intact
Vane shear	Using a hand-rotated miniature vane of depth/diameter (2:1.5)	K1, K2, CB, SW-K, SW-S, G	365	5 20 38	Intact and remoulded
Consolidation	One dimensional consolidation tests using a fixed ring oedometer cells	K1, K2, CB, SW-K, SW-S, G	100 and 365	20	Intact and remoulded
pH	Using Electronic pH meter calibrated with 4, 7, and 10 PH buffers	K1, K2, CB, SW-K, SW-S, G	1, 3, 10, 30, 100, and 365	20	Remoulded

3.3 Triaxial Compression Test Results

This section summaries the results of 24 U-U triaxial tests conducted on 365-day lime-admixed soils. The samples water contents, void ratios, unit weights, and degrees of saturation after curing are given in Table 3-17. The calculations are based on specimens' dimensions and weights after extrusion. These results demonstrate not only a very high degree of repeatability, but also that the sealing procedure was effective. Also shown in Table 3-17 are the bulk unit weights of these soils obtained from oedometer ring specimens' γ_o tabulated in section 3.2.6. The results are highly comparable and the differences can be accounted for by measurements tolerances.

Table 3-17: 365 days cured triaxial samples properties.

soil type	w/w_{LL}	Lime (%)	Sample No.	γ (kN/m^3)	w†	e_o	S_r	$\gamma_{av.}$ (kN/m^3)	γ_o (kN/m^3)
K2	1.8	3	1st	13.34	1.15	3.11	0.96	13.34	13.47
K2	1.8	5	1st	13.49	1.13	3.03	0.97	13.52	13.65
K2	1.8	5	2nd	13.55	1.13	3.01	0.98		
K2	2.2	5	1st	13.12	1.38	3.62	0.99	13.11	13.02
K2	2.2	5	2nd	13.09	1.38	3.63	0.99		
K2	2	5	1st	13.22	1.26	3.36	0.98	13.23	13.30
K2	2	5	2nd	13.24	1.26	3.35	0.98		
CB	1.8	3	1st	12.21	2.11	5.92	0.99	12.22	12.26
CB	1.8	3	2nd	12.23	2.11	5.91	0.99		
CB	1.8	5	1st	12.29	2.04	5.72	0.99	12.28	12.28
CB	1.8	5	2nd	12.26	2.04	5.74	0.99		
CB	2.2	3	1st	11.78	2.54	7.10	0.99	11.77	11.96
CB	2.2	3	2nd	11.75	2.54	7.07	0.99		
CB	2.2	5	1st	11.86	2.47	6.95	0.98	11.84	11.86
CB	2.2	5	2nd	11.82	2.47	6.98	0.98		
SW-S	1.8	5	1st	13.70	1.14	3.15	0.98	13.75	13.69
SW-S	1.8	5	2nd	13.80	1.14	3.12	0.99		
SW-S	2	3	1st	13.45	1.22	3.38	0.98	13.45	13.49
SW-K	1.8	5	1st	11.94	2.07	5.79	0.96	11.93	12.01
SW-K	1.8	5	2nd	11.92	2.07	5.80	0.96		
SW-K	1.8	3	1st	11.99	2.11	5.84	0.97	11.98	12.06
SW-K	1.8	3	2nd	11.96	2.11	5.86	0.97		
SW-K	2.2	5	1st	11.82	2.52	6.86	0.99	11.81	11.85
SW-K	2.2	5	2nd	11.80	2.52	6.87	0.99		

† Water contents are taken equal to these tabulated in section 3.2.6 for similar specimens cured in same conditions

The triaxial tests results are shown in Figure 3-66 to Figure 3-69. For a given soil, it is clear that peak (failure) deviatoric stress increases with increasing lime content and decreasing water content.

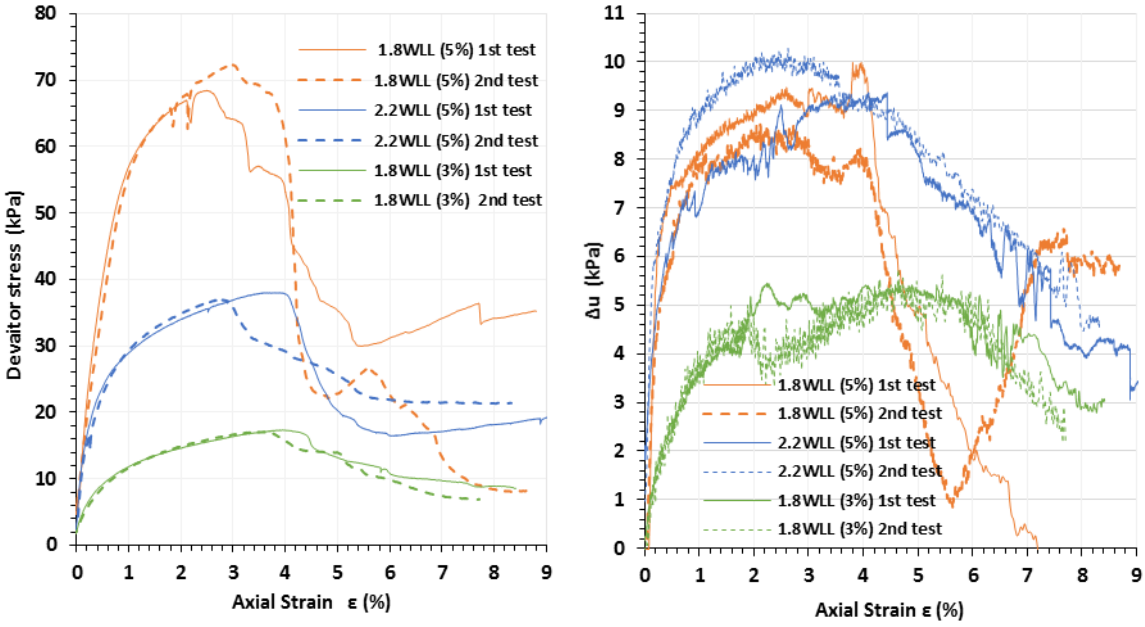

(a) strain relationship-Stress (b) Excess p.w.p. development

Figure 3-66: U-U triaxial tests results for lime admixed SW-K soils cured for 365 days, a: strain-stress curves and b: excess pore water pressure.

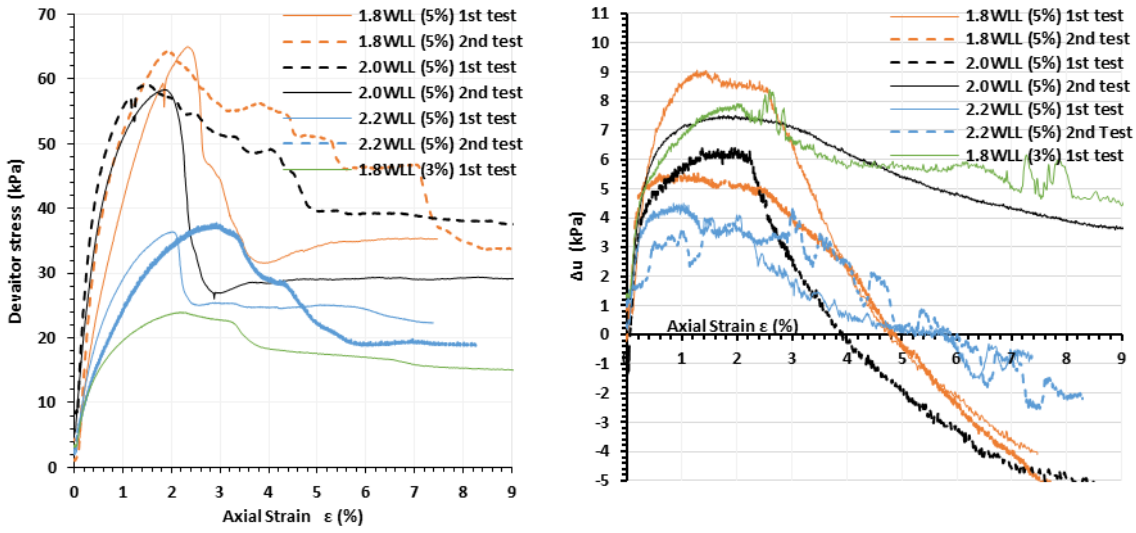

a) strain relationship-Stress b) Excess p.w.p. development

Figure 3-67: U-U triaxial tests results for lime admixed K2 soils cured for 365 days, a: strain-stress curves and b: excess pore water pressure.

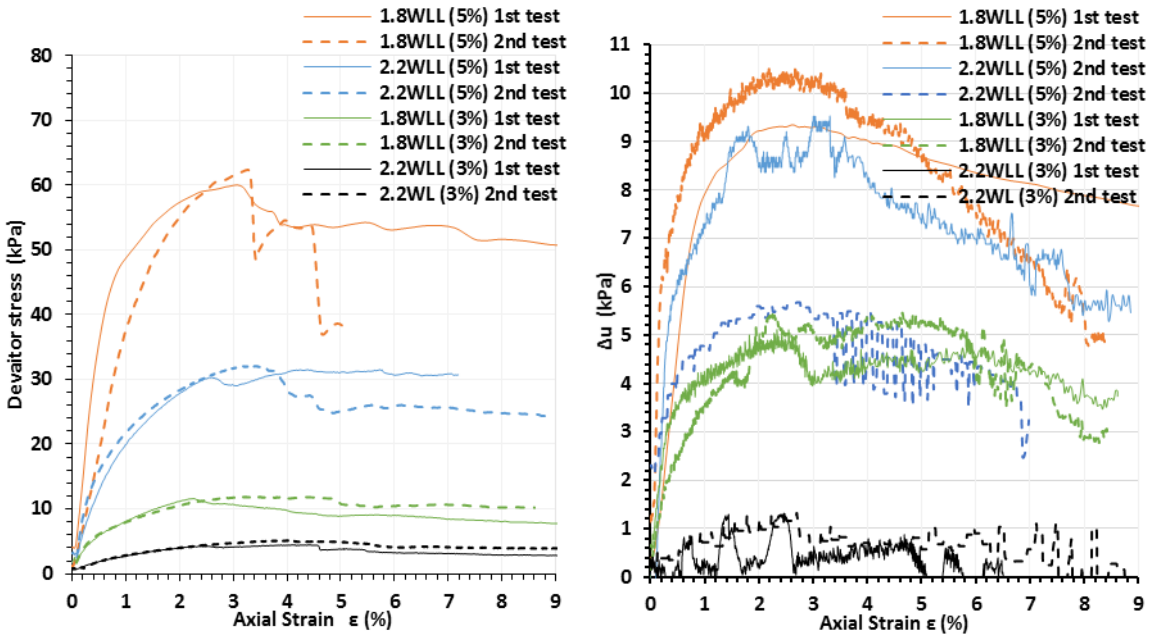

a) strain relationship-Stress b) Excess p.w.p. development

Figure 3-68: U-U triaxial tests results for lime admixed CB bentonite soils cured for 365 days, a: strain-stress curves and b: excess pore water pressure.

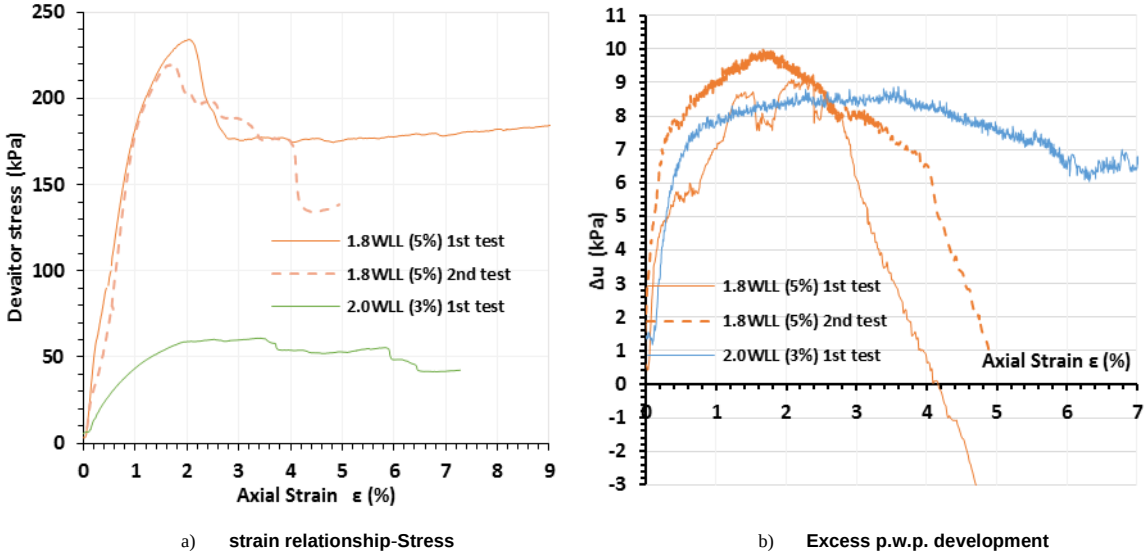

a) strain relationship-Stress b) Excess p.w.p. development

Figure 3-69: U-U triaxial tests results for lime admixed SW-S soils cured for 365 days, a: strain-stress curves and b: excess pore water pressure.

Figure 3-66(b) to Figure 3-69(b) show the measured excess pore water pressure during shearing. For all the cases studied, positive excess pore developed initially during shearing, and reached values as high as 10 kPa. The deviator stress reaches a peak at a rather small axial strain and then decreases with further strain. The pore pressure continues to increase even after the deviator stress has peaked. This type of behaviour is similar to the behaviour of sensitive normally consolidated clay under undrained triaxial loading (Lambe and Whitman, 1979). Large pore water pressures are induced during undrained shear as the open metastable skeleton fractures. The response differs depending on soil type, lime content and

water content. For kaolin clay K2 and the SW-S soil (which have the same liquid limit) both treated with 5% lime, the pore water pressure falls after reaching the peak resistance and becomes negative in the post-peak zone. For these soils, with 3% lime content, the pore water pressure also drops but does not become negative. A similar response occurs in CB bentonite and the SW-K mix. The maximum pore water pressure for soils treated with 3% lime was lower than those treated with 5% lime

Table 3-18 below summarises the results of the U-U triaxial compression tests conducted on lime treated soils, cured for 365 days. It can be seen that there is no significant increase in the deviator stress at failure with increasing cell pressure. The relation between peak deviator stress ($\sigma_1 - \sigma_3$) and the excess pore water pressure at failure Δu_f can be represented by Skempton's pore water pressure parameter at failure ($A_f = \Delta u_f/(\sigma_1 - \sigma_3)$) taking B=1 (as shown in Table 3-9). The range of A_f for 3% lime admixed specimens is 0.2-0.4 while for 5% lime admixed specimens is 0.1-0.27 which is in the range given by (Skempton, 1954) for lightly overconsolidated clays.

The brittleness of these soils increases with increasing lime content as can be seen for SW-K soils (Figure 3-65) and the K2 soils (Figure 3-67). Increasing water content, on the other hand, tends to reduce the brittleness. Similar observations were recorded by (Balasubramaniam et al., 1999) and (Pakbaz and Alipour, 2012) for chemically admixed soft clays. In all cases, the axial strain to attain peak resistance decreases with increasing the lime contents; these are always lower than 4%.

Soil brittleness can be described by the *Brittleness Index* parameter I_B defined as a function of the magnitude of the peak and "ultimate" deviatoric stresses (Bishop, 1967; Bishop, 1971)

$$I_B = \frac{q_{peak} - q_{ultimate}}{q_{peak}} = 1 - \frac{q_{ultimate}}{q_{peak}} \qquad \textbf{3-13}$$

in which q_{peak} and $q_{ultimate}$ are respectively, the peak and ultimate deviatoric stresses. As the index approaches zero, failure becomes increasingly ductile.

A similar expression is also used to describe the brittleness index defining I_B as the ratio of the difference between the magnitude of peak and ultimate compressive strengths to that of ultimate strength (Consoli et al., 1998; Maher and Ho, 1993), also termed the "brittle

component" by Fang and Harrison (2001) which can be greater than 1.0 with increasing brittleness:

$$I_B = \frac{q_{peak} - q_{ultimate}}{q_{ultimate}} = \frac{q_{peak}}{q_{ultimate}} - 1 \qquad 3\text{-}14$$

Brittleness indices and sensitivities express virtually the same thing.

Brittleness indices values for the triaxial tests calculated using Equation 3-13 (Bishop, 1967; Bishop, 1971) are shown in Table 3-18. Although there is some scatter in the I_B values, increasing lime content and decreasing water content tends to increase brittleness. Comparing different soil types, the highest I_B values were obtained in the case of kaolin (K2) and SW-K soil mix.

Proper characterisation of brittle failure also requires data on the work (absorbed strain-energy) required to reach the "ultimate" deviatoric stress state (e.g., Maher and Ho, 1993) Quantative measurements of toughness have not been pursued in this work, although toughness is evidently a very important consideration in practice. The qualitative evidence from this study suggests that lime-admixed soils exhibit considerable toughness. This was noticed from the physical work expended on kneading these admixed soils after curing to gradually reaching the fully remoulded state compared with the behaviour of quick soils such as some Norwegian soils described elsewhere (Wood, 1990).

Figure 3-70 illustrates some observed failure patterns for 365-day cured lime-admixed soil specimens from U-U triaxial compression tests. All these specimens developed distinct shear bands at failure. However, the modes of the developed shear bands do differ depending on soil type and lime content. For CB and SW-K specimens admixed with 5% lime, an axial split fracture mode of failure can be seen irrespective to water content. At lower lime contents (3%) inclined shear fracture planes can be seen. For kaolin (K2) specimens, inclined slip planes are also developed, albeit the slip plane is steeper at a higher lime dosing rate (5%). It seems that these failure patterns are not related to the soils' brittleness in that samples of different brittleness indices I_B show similar failure patterns. For example, CB and SW-K specimens at lime content of 5% show vertical split failure planes although their brittleness indices are about 0.2 and 0.5 respectively (on a brittleness scale from 0 to 1.0). The only common property of these two plastic soils is their high liquid limit. Kaolin (K2) specimens, on the other hand, have inclined slip planes of failure even at high lime content (5%). Although the normalized water content ($W=w/W_{LL}$) of kaolin

samples is same as these for CB and SW-K specimens, kaolin water content is far less than the water contents of these soils. These results indicate that high lime content soils with very high water contents are prone to show axial split fracture. This type of fracture is similar to the behaviour of cylindrical rock specimens during uniaxial loading (e.g. Heap et al. (2015)).

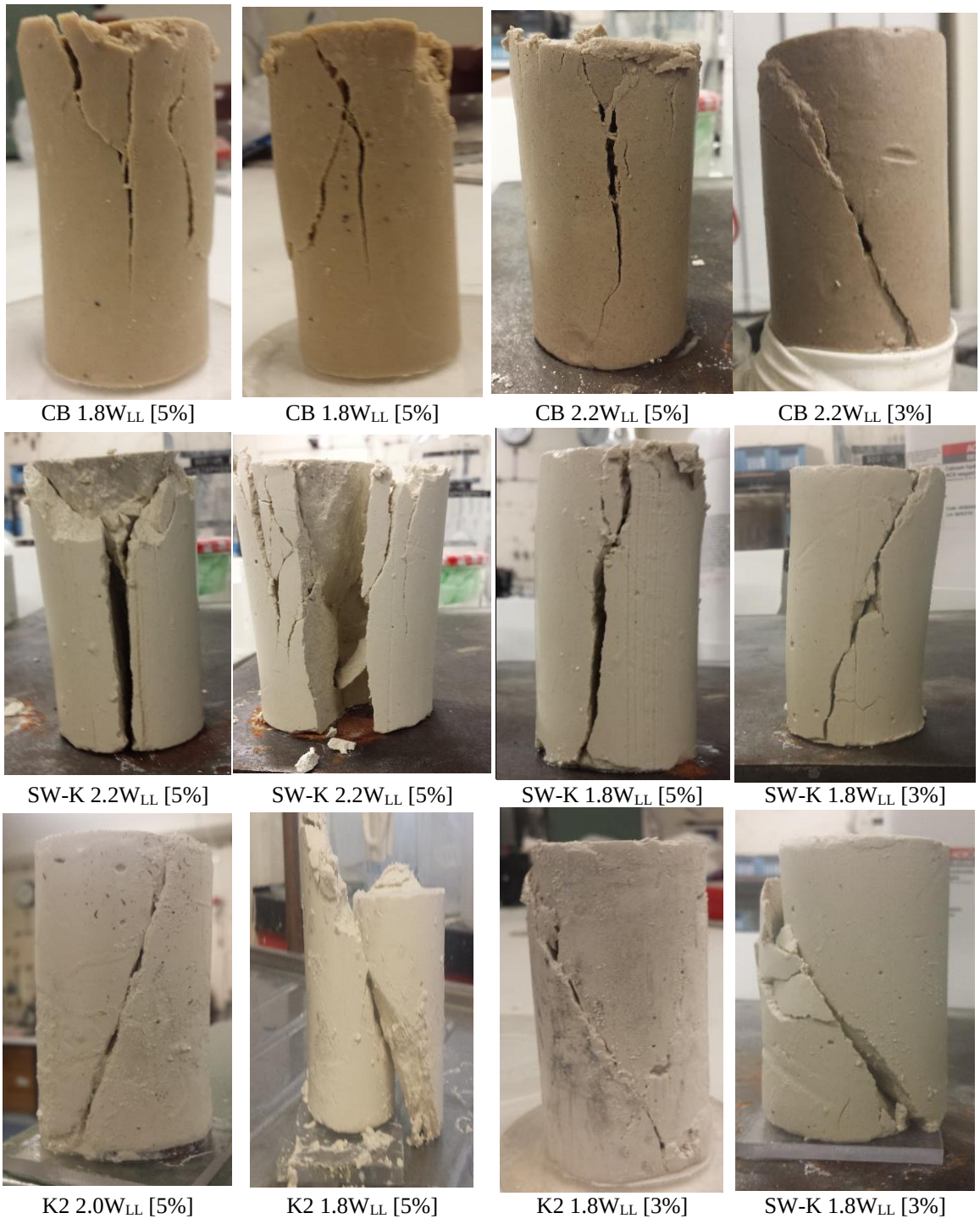

Figure 3-70: Failure patterns in triaxial compression tests of different lime-admixed clay slurries cured for 365 days

Table 3-18: U-U triaxial compression test results of 365 days cured specimens

soil type	W=w/W_{LL}	Lime C (%)	Test No.	w	e	S_r	σ_3 (kPa)	$\epsilon_{failure}$ %	$\Delta u_{failure}$ (kPa)	$\sigma_1 - \sigma_3$ (kPa)	A_f	I_B	C_u (kPa)	$C_u$av. (kPa)
K2	1.8	3	1st	1.15	3.11	0.96	325	1.5	7.5	22.1	0.34	0.4	11.1	11.1
K2	1.8	5	1st	1.13	3.03	0.97	425	2.4	8.7	65.0	0.13	0.5	32.5	32.3
K2	1.8	5	2nd	1.13	3.01	0.98	400	2.0	6.6	64.3	0.08	0.5	32.2	
K2	2.2	5	1st	1.38	3.62	0.99	250	2.0	4.1	36.4	0.11	0.4	18.2	18.4
K2	2.2	5	2nd	1.38	3.63	0.99	375	3.7	4.2	37.1	0.11	0.5	18.6	
K2	2	5	1st	1.26	3.36	0.98	500	1.9	7.7	58.4	0.11	0.5	29.2	29.4
K2	2	5	2nd	1.26	3.35	0.98	475	1.5	10.0	59.3	0.12	0.4	29.7	
CB	1.8	3	1st	2.11	5.92	0.99	250	3.5	4.1	11.9	0.34	0.1	6.0	5.9
CB	1.8	3	2nd	2.11	5.91	0.99	150	2.3	5.0	11.7	0.43	0.3	5.8	
CB	1.8	5	1st	2.04	5.72	0.99	200	3.1	9.7	60.0	0.16	0.2	30.0	30.5
CB	1.8	5	2nd	2.04	5.74	0.99	250	3.3	10.4	62.1	0.17	0.2	31.1	
CB	2.2	3	1st	2.54	7.10	0.99	150	3.0	1.0	5.1	0.20	0.3	2.6	2.7
CB	2.2	3	2nd	2.54	7.07	0.99	325	3.8	0.8	5.6	0.18	0.3	2.8	
CB	2.2	5	1st	2.47	6.95	0.98	200	2.5	5.6	30.3	0.18	0.1	15.2	15.6
CB	2.2	5	2nd	2.47	6.98	0.98	500	3.2	9.3	32.0	0.29	0.2	16.0	
SW-S	1.8	5	1st	1.14	3.15	0.98	375	2.3	9.1	233.7	0.14	0.2	116.9	113.2
SW-S	1.8	5	2nd	1.14	3.12	0.99	350	1.8	9.8	219.2	0.04	0.2	109.6	
SW-S	2	3	1st	1.22	3.38	0.98	350	2.5	8.4	60.3	0.04	0.3	30.2	30.2
SW-K	1.8	5	1st	2.07	5.79	0.96	250	2.5	9.5	68.5	0.14	0.6	34.3	35.2
SW-K	1.8	5	2nd	2.07	5.80	0.96	275	3.0	8.4	72.5	0.12	0.7	36.3	
SW-K	1.8	3	1st	2.11	5.84	0.97	325	4.1	5.1	17.3	0.30	0.5	8.6	8.6
SW-K	1.8	3	2nd	2.11	5.86	0.97	300	3.3	4.6	17.0	0.27	0.6	8.5	
SW-K	2.2	5	1st	2.52	6.86	0.99	300	3.5	9.2	37.9	0.24	0.5	19.0	18.7
SW-K	2.2	5	2nd	2.52	6.87	0.99	450	2.8	9.8	36.9	0.27	0.4	18.5	

3.4 Vane Test Results

Some of the vane test results are shown in Table 3-19 below. These results correspond to the same cases tested in triaxial compression. These tests were repeated to evaluate test repeatability. The standard deviations and the coefficients of variation of the net rotation angles are shown in the table. The maximum C.O.V. of 5% indicates good repeatability.

Table 3-19: Vane shear test results.

soil type	W	Lime %	spring No.	1st test			2nd test			3rd test			Θ_{net} average	S.D.	C.O.V %	C_u (kPa)
				Θ_t	Θ_{shaft}	Θ_{net}	Θ_t	Θ_{shaft}	Θ_{net}	Θ_t	Θ_{shaft}	Θ_{net}				
K2	1.8	5	2	153	37	116	157	40	117	162	40	122	118.3	2.6	2.2	37.5
K2	2.0	5	1	240	54	186	234	40	194	230	37	193	191	3.6	1.9	29.8
K2	2.2	5	1	178	22	156	185	38	147	172	20	152	151.7	3.7	2.4	23.6
K2	1.8	3	1	92	19	73	83	14	69	93	17	76	53	2.9	5.4	8.3
SW-S	1.8	5	2	310	75	235	300	73	227				231	4.0	1.7	73.2
SW-S	2.0	3	1	210	33	177	216	35	181				179	2.0	1.1	27.9
K2	1.8	5	2	187	40	147	200	40	160				153.5	6.5	4.2	48.6
CB	1.8	5	1	295	58	237	285	57	228				232.5	4.5	1.9	36.9
CB	1.8	3	1	87	18	69	89	20	69	79	15	64	67.3	2.4	3.5	10.5
CB	2.2	5	1	175	36	139	165	32	133				136	3.0	2.2	21.2
CB	2.2	3	1	42	8	34	41	8	33				33.5	0.5	1.5	5.2
SW-K	2.2	5	1	160	33	127	165	34	131	175	36	139	132.3	5.0	3.8	20.6
SW-K	1.8	5	2	145	39	106	141	34	107	136	33	103	105.3	1.7	1.6	33.4
SW-K	1.8	3	1	93	18	75	95	19	76	90	17	73	74.7	1.5	1.7	11.6

Figure 3-71 shows the correlation between vane shaft resistance and the total resistance obtained during vane tests on intact and remoulded soils. The shaft resistance is about 20% of the total resistance. This high relative resistance is attributed to the deep insertion (50 mm) of the vane shaft into the soil, which indicates the importance of taking shaft resistance into consideration.

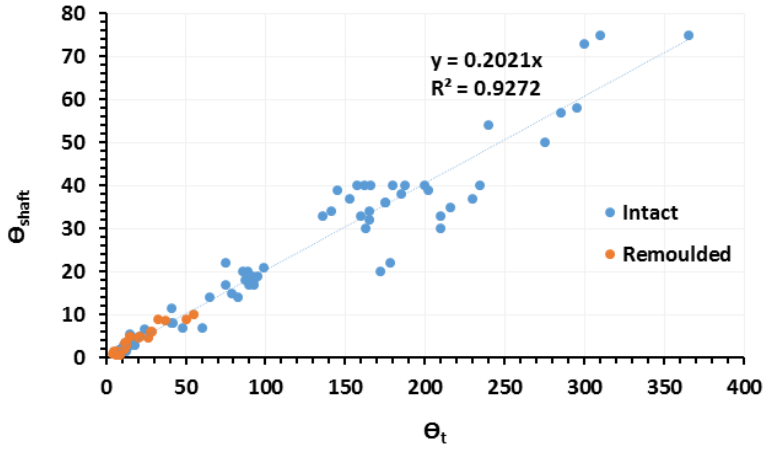

Figure 3-71: Correlation between vane shaft resistance and total resistance

Table 3-20 shows a comparison between the undrained shear strength results obtained from the triaxial compression tests and those obtained from the vane shear tests. In Figure 3-72, a straight-line correlation is shown. The correlation is quite good, particularly for stronger soils: the observed scatter underlines the uncertainties which arises from the cumulative effect of the numerous sources of experimental errors

Table 3-20: Undrained shear strength of 365 day lime admixed soils: U-U triaxial tests & vane shear tests.

Soil	$W = w_w/W_{LL}$	Lime C (%)	C_u Triax. (kPa)	C_u vane (kPa)
K2	1.8	5	32.3	37.5
K2	2.0	5	29.4	29.8
K2	2.2	5	18.4	23.6
K2	1.8	3	11.1	8.3
SW-S	2.0	3	30.1	27.9
CB	1.8	5	30.5	36.9
CB	1.8	3	5.9	10.5
CB	2.2	5	15.6	21.2
CB	2.2	3	5.9	5.2
SW-K	2.2	5	18.7	20.6
SW-K	1.8	5	35.2	33.4
SW-K	1.8	3	8.6	11.6

The trend line does suggest a bias in the data: measured vane strengths are 9% higher than triaxial measured strengths on this line. However, there are insufficient data here to support a definitive conclusion, or that a linear correlation is appropriate. (Bjerrum, 1972) showed that the vane test overestimated the undrained shear strength in some cases and underestimated it in other cases. Silvestri and Ewane (2017) have shown that vane shear tests results are higher for cement-treated clay slurries than those obtained from U-U tests

by a ratio of 1.6-2.0. O'Malley and Wright (1987) have also shown that vane tests produce higher undrained strength results than UU tests and the difference increases with decreasing soil water content (Figure 3-73) and some correction is necessary. (Kang et al., 2015) proposed such a correction factor for cement admixed soils. Kayser et al. (2011) multiplied triaxial strengths by a factor of 1.6 to 1.8 to account for the rate difference between vane and triaxial tests. Others, including La Rochelle et al.(1974), Flaate (1966), Kimura and Saitoh (1983), Schmertmann (1975), Roy and Leblanc (1988), Chandler (1988), Gylland et al. (2012) have discussed the factors that limit the accuracy of vane tests.

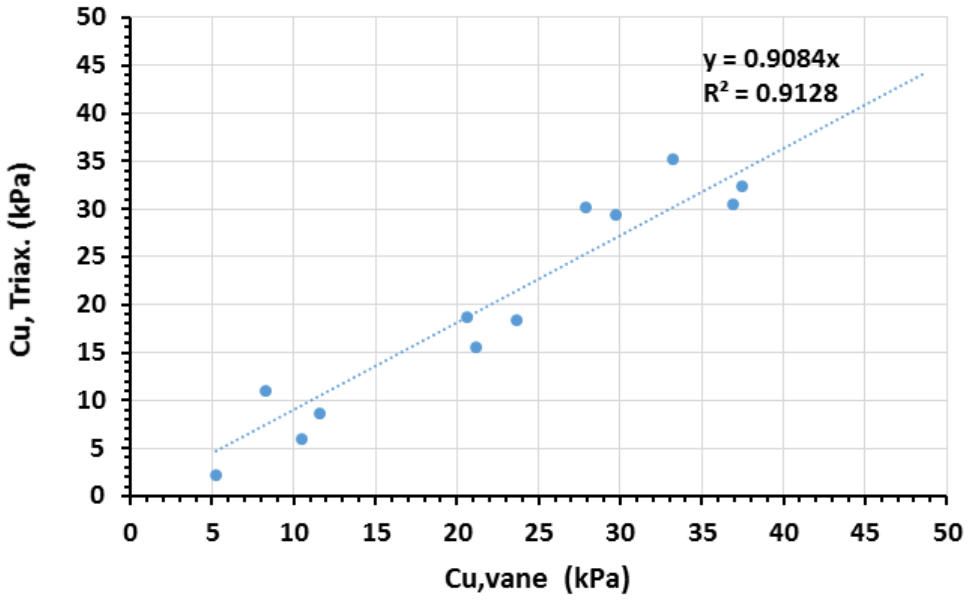

Figure 3-72: Correlation between vane and UU triaxial undrained shear strength

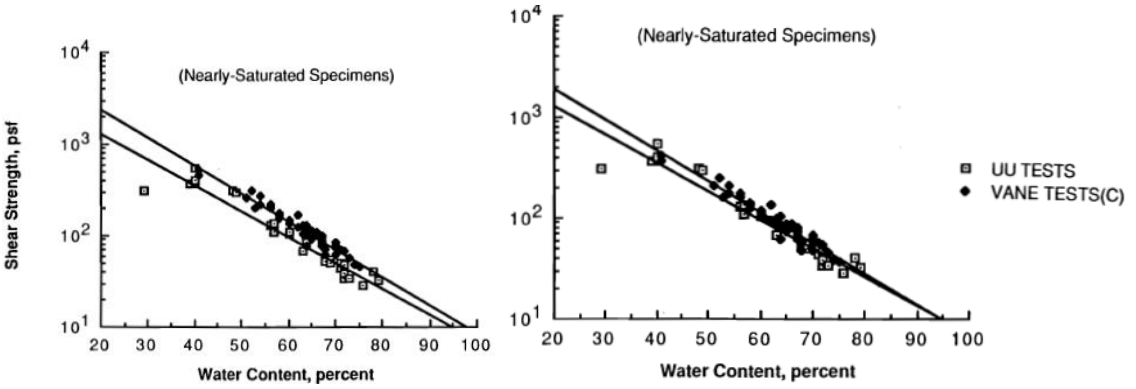

Figure 3-73: Variation in undrained shear strength with water content from laboratory vane and unconsolidated-undrained tests on nearly-saturated specimens: a) before, and, b) after correction (O'Malley and Wright (1987))

3.5 Conclusions

1) For disc penetrometers up to about 30 mm diameter, penetration resistance is not significantly affected by the proximity of the 100 mm diameter cylindrical mould walls. The 20 mm disc penetrometer offers the best compromise between conflicting constraints and is adopted for all future tests.
2) The optimal penetration velocity for the 20mm penetrometer is of the order of 250 mm/min.
3) The peak (failure) deviatoric stress obtained from UU triaxial compression test increases with increasing lime content and decreasing water content.
4) Peak deviatoric stress is reached (in UU tests) at relatively low strains, and the deviatoric stress reduces thereafter. However, no sudden collapse occurs.
5) In UU triaxial tests, positive pore pressures develop (pre-peak) during shearing but fall away under post-peak shearing. Skempton's pore pressure parameter A_f ranges between 0.1-0.4, which is comparable to the values obtained for lightly overconsolidated clays.
6) The brittleness (sensitivity) of the lime admixed soils increases with increasing lime content and decreasing water content.
7) The data suggests that the vane test yields undrained shear strengths which are marginally higher than those obtained from the triaxial test, but further work is needed to arrive at a definitive conclusion.

Chapter 4 NUMERICAL MODELLING OF PENETRATION TESTS

4.1 Introduction

One of the main objectives of this chapter is to establish, using the Finite Element method, whether the finite size of the test cells used in the experimental programme has any significant effect on the bearing resistance of the disc penetrometers. A second objective is to establish a formula for the variation of the bearing capacity factor N_C as a function of embedment depth. All analyses were carried out using the well-known ABAQUS program (Simulia, 2014b).

The geometry of the problem is depicted in Figure 4-1. The rigid disc penetrometer (of diameter D) is embedded at a depth Z in a soil sample of height H = 130mm, and subjected to mean vertical pressure, q. The cell's (internal) diameter is D_C = 100 mm. A cavity is assumed to exist above the penetrometer.

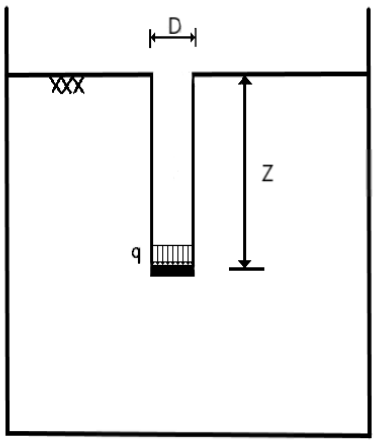

Figure 4-1: Geometry of the Problem

Although the geometry of the problem is axi-symmetric, it does not necessarily follow that deformation of the (real) soil sample, nor the failure mechanism, will be axisymmetric. However, for computational convenience, no attempt has been made here to seed the numerical model to simulate this behaviour and, in most of the analyses reported here, the axisymmetric assumption has been adopted. Moreover, there appears to be no evidence in the literature to suggest that the symmetric classical plasticity solutions of failure (of Prandtl

(1920), (Hill, 1951), Levin (1955), etc., cited by (Chen, 1975)) can be improved upon by considering non-symmetric modes of failure.

4.2 Material Properties

The elastic/perfectly-plastic Tresca material model was used to model the soil (total stress analysis). Except where noted otherwise, the parameters employed were as follows:

E = 4 MPa, (Young's modulus); k = 10 kPa (shear strength); ν = 0.49 (Poisson's ratio); ρ= 1800 kg/m^3 (mass density)

These values are broadly representative of a soft clay soil although, for the purposes of this study, this is not a critical consideration. While the stiffness/strength ratio of 400 is not unreasonable for such soils, a different stiffness would only affect the magnitude of the deformations; not the collapse load. A value of Poisson's ratio reasonably close to 0.5 was used to simulate the zero volume change condition, although this risks numerical difficulties. In hindsight, given that the soil is not in an overly constrained configuration, it seems plausible that a significantly lower value could have been adopted without compromising the results. The mass density is relevant only in the context of inertial forces: at this scale, gravitational forces are negligible.

The Tresca yield criterion, in principal stress space, is depicted in Figure 4-2. In the π-plane (the plane normal to the hydrostatic axis, i.e., the deviatoric plane) it appears as a regular hexagon.

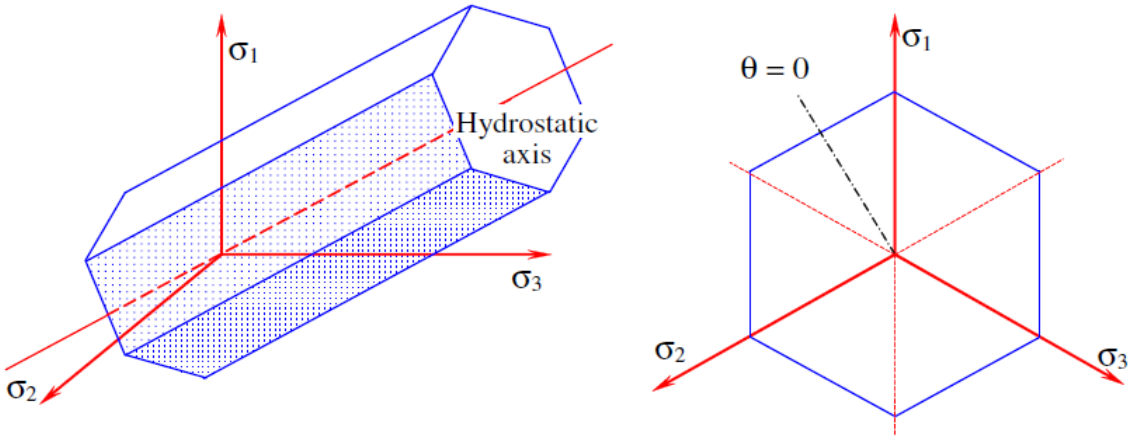

Figure 4-2: Tresca failure criterion in principal stress space (Taiebat and Carter, 2008)

The Tresca criterion posits that yield takes place when the maximum shear stress reaches a critical value, k. Thus, if (say) σ_1 and σ_3 are the major and minor principal stresses, respectively, then the Tresca yield function F_T takes the simple form:

$$F_T = \sigma_1 - \sigma_3 - 2k = 0 \qquad \textbf{4-1}$$

where k is the material parameter (here, the undrained shear strength).

If an associated flow rule is assumed, then a difficulty immediately arises at the corners, where the outward normal and therefore the plastic flow direction is undefined. Experience has shown that numerical solutions are disproportionately affected by this local problem (Sloan and Booker, 1986). This can be attributed to the fact that that a significant region of stress-space outside the yield surface is not in one-to-one correspondence with that surface and hence iteration back towards it requires careful management.

Several simplified methods have been advanced to deal with this problem (Taiebat and Carter, 2008). One approach is to use a non-associated flow rule, using the Von Mises criterion (maximum distortional stress criterion) as the plastic potential. The von Mises criterion F_M can be defined in terms of principal stresses as:

$$F_M = (\sigma_1 - \sigma_2)^2 + (\sigma_2 - \sigma_3)^2 + (\sigma_3 - \sigma_1)^2 - 2\sigma_y^2 = 0 \qquad \textbf{4-2}$$

where σ_y is the "equivalent stress". This criterion assumes the shape of a circle in the π-plane and can be made coincident with the Tresca criterion at specific points by an appropriate choice of the equivalent stress, σ_y. For example, at the vertices, $\sigma_y = 2k$, whereas at the mid-sides, $\sigma_y = \sqrt{3}\,k$. Evidently, this approach eliminates the corner problem, but numerical experimentation is needed to justify this approximation.

Local rounding of the yield surface in the vicinity of the vertices (Figure 4-3b) appears to offer a better approximation but can be criticised on the grounds that it is an empirical solution. In this approach, the Tresca criterion is assumed to apply provided that the absolute value of the Lode angle θ [$0 \leq \theta \leq 30^\circ$] is less than some (arbitrary) threshold value θ_T (Sloan and Booker, 1986). At larger angles, a circular yield surface is assumed. To avoid numerical ill-conditioning problems, a threshold value of $\theta_T = 25^\circ$ has been suggested (Abbo and Sloan, 1995).

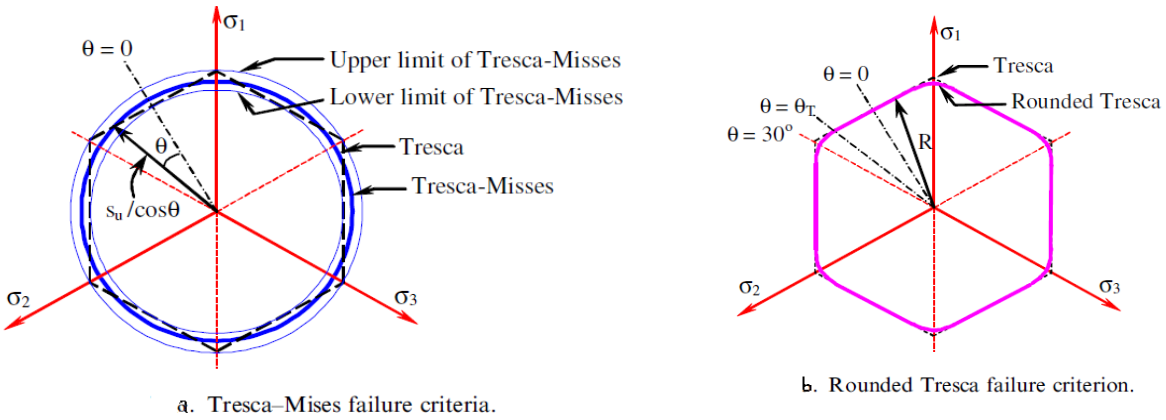

Figure 4-3: Eliminating the Tresca "corner problem" (Taiebat and Carter, 2008)

Figure 4-4 below, after (Taiebat and Carter, 2008), demonstrates the effectiveness of these material modelling assumptions. The benchmark shown here is the classic problem of a rough circular disc foundation, subjected to vertical pressure. The exact result (corresponding to $N_c = 6.05$) is captured using the rounded Tresca model, with $\theta_T = 25^\circ$. The results are not quite so good if the threshold angle θ_T is set very close to 30˚, nor if the combined Tresca-Mises model is employed. Nevertheless, for most practical purposes, all of these results can be judged to be satisfactory.

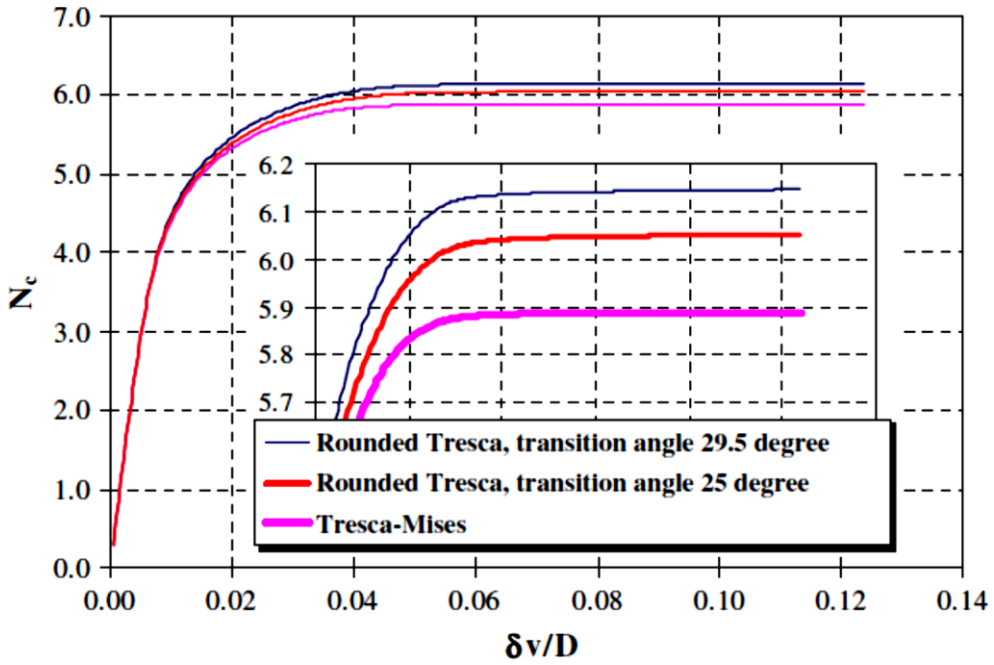

Figure 4-4: Normalized pressure-settlement response of rough rigid disc, (Taiebat and Carter, 2008)

From a theoretical point of view, the most convincing solution is to adopt an analytical approach (e.g., Clausen et al. (2006)), as implemented by Andersen and Clausen (2009); Tapper et al. (2014), which fixes the unique stress paths which follow finite stress excursions beyond yield. This capability exceeds that required to meet our current

objectives and accordingly, the Tresca-Mises model described above, and implemented in ABAQUS is employed hereafter. We note, as exemplified in the preceding figure, that this approach tends to under-predict bearing capacity, (Mana et al., 2011; Taiebat and Carter, 2008; Tapper et al., 2014).

4.3 Small-Displacement Finite Element Analysis

The assumed boundary conditions are shown in Fig. 4.5 for a typical problem [D = 20 mm, Z = 40mm]. In case (a), the cell walls are assumed to be smooth (zero shear stress), while in case (b) the cell walls are fully rough (zero vertical displacement). The base of the cell is assumed to be fully rough in both cases. The boundary conditions on the axis of symmetry (zero radial displacement; zero shear) are applied automatically.

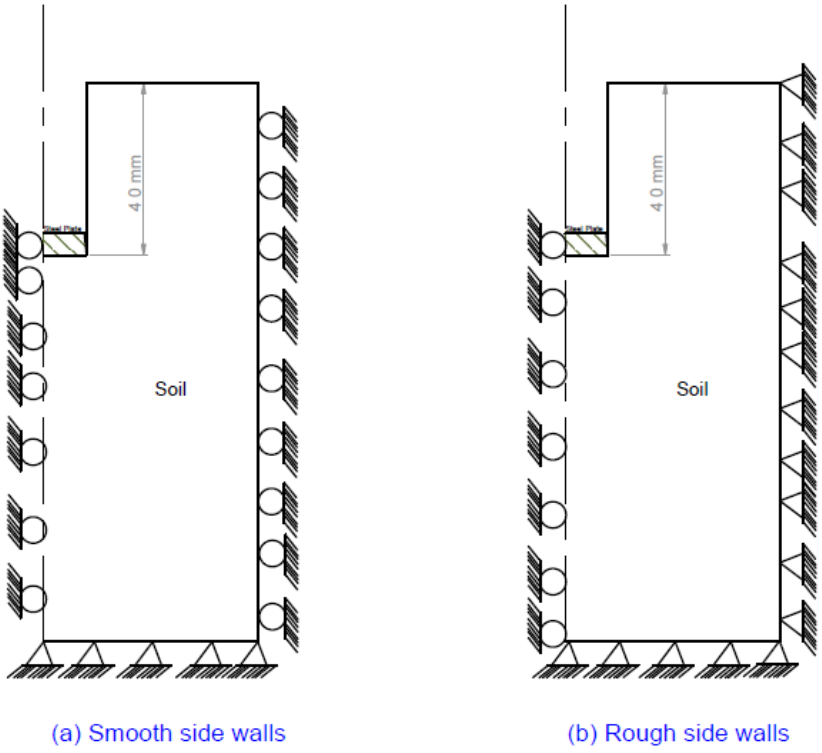

Figure 4-5: Boundary conditions for, (a), smooth cell walls, and, (b), rough cell walls.

The penetrometer is idealized as a thin rough elastic disc ($E_S = 10\ GPa,\ \nu = 0.3\ ,\ t = 5\ mm$). Following (Brown, 1969), this combination of parameters ensures that the disc is effectively rigid: the relative flexural rigidity is proportional to $(E_S/E)(t/D)^3$. The cavity is assumed to be traction free.

4.3.1 Mesh discretisation

Although in general, higher-order finite elements (e.g., linear strain elements) are more efficient than lower-order (e.g., constant strain elements), there are circumstances where lower-order elements can be used to advantage. The intended application is a case in point. As confirmed by exploratory numerical trials, second-order triangular elements (using both full and reduced-integration) develop volumetric locking due to the incompressiblity constraint (Simulia, 2014c). On the other hand, the first-order (3-noded) triangular element, with reduced integration, was found to perform satisfactorily.

(Gourvenec and Mana, 2011) and (Tapper et al., 2014) provide some useful guidance on optimizing the discretisation scheme, and full use of the ABAQUS Adaptive Re-Meshing (ARM) facility was made to obtain accurate results. ARM aims to optimize the mesh by preferentially reducing element sizes in those regions where the stress gradients are highest (Hu et al., 1999).

Figure 4-6 illustrates the roles of ABAQUS and the user in the ARM process: the iterative re-meshing performed by ABAQUS is controlled in part by user-defined rules. Each successive analysis solves the same problem but uses a different mesh. Once the ARM process is complete, the results obtained for each of these meshes can then be accessed.

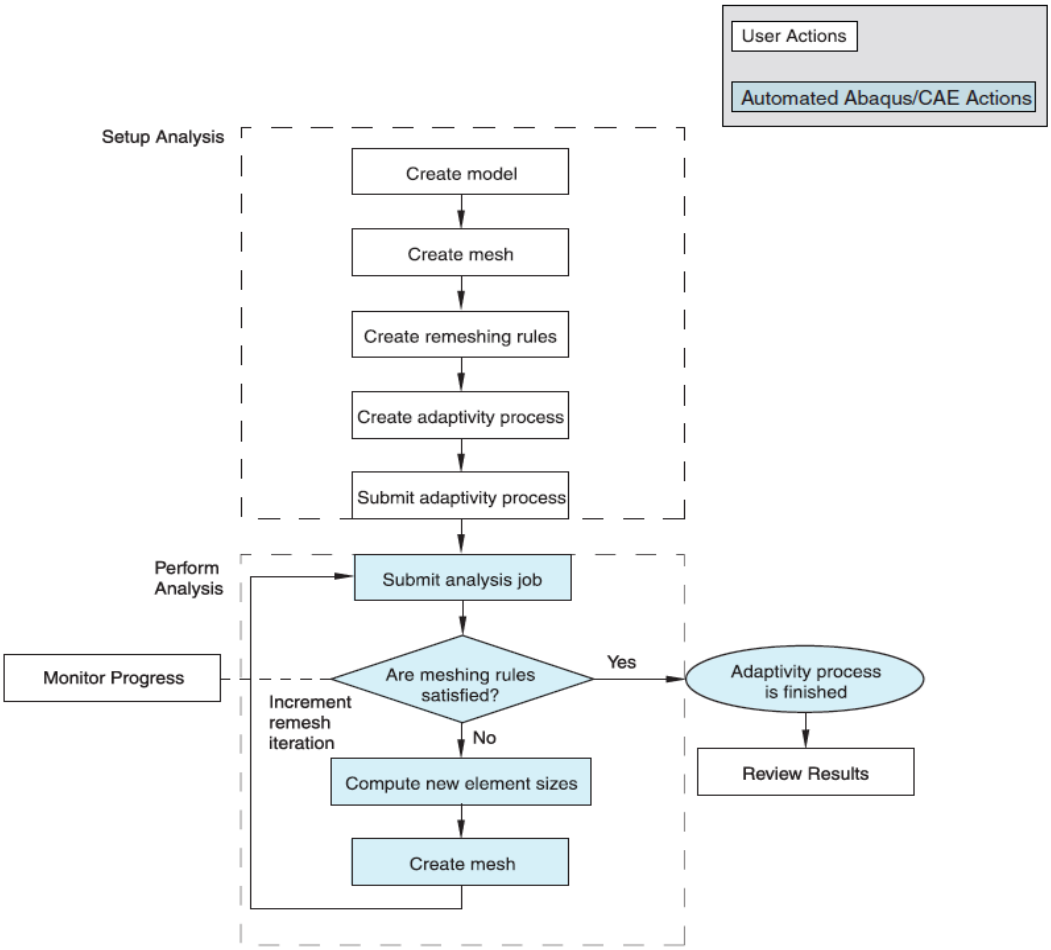

Figure 4-6: The ABAQUS adaptive re-meshing process (Simulia, 2014a)

ABAQUS allows users to select several parameters to define the re-meshing rules. After some experimentation, default values were adopted except where noted otherwise. To initiate the analyses, grid-like meshes with elements of side length of 2 mm were specified. The re-meshing rule permitted the generation of elements with sizes in the range between 0.01mm and 5 mm. The maximum number of mesh iterations was set at ten (10) but sufficient convergence was normally achieved in fewer iterations, as illustrated below.

4.3.2 Convergence studies

Figure 4-7 shows the successive mesh refinements which are generated by the ARM process. The first of these is the user-generated grid pattern. As can be seen, the element density increases towards the disc and that configuration changes very little after the fourth or fifth iteration. In retrospect, it appears that the restriction on maximum element size (of 5 mm) could have been relaxed, although this would not have significantly reduced the run times.

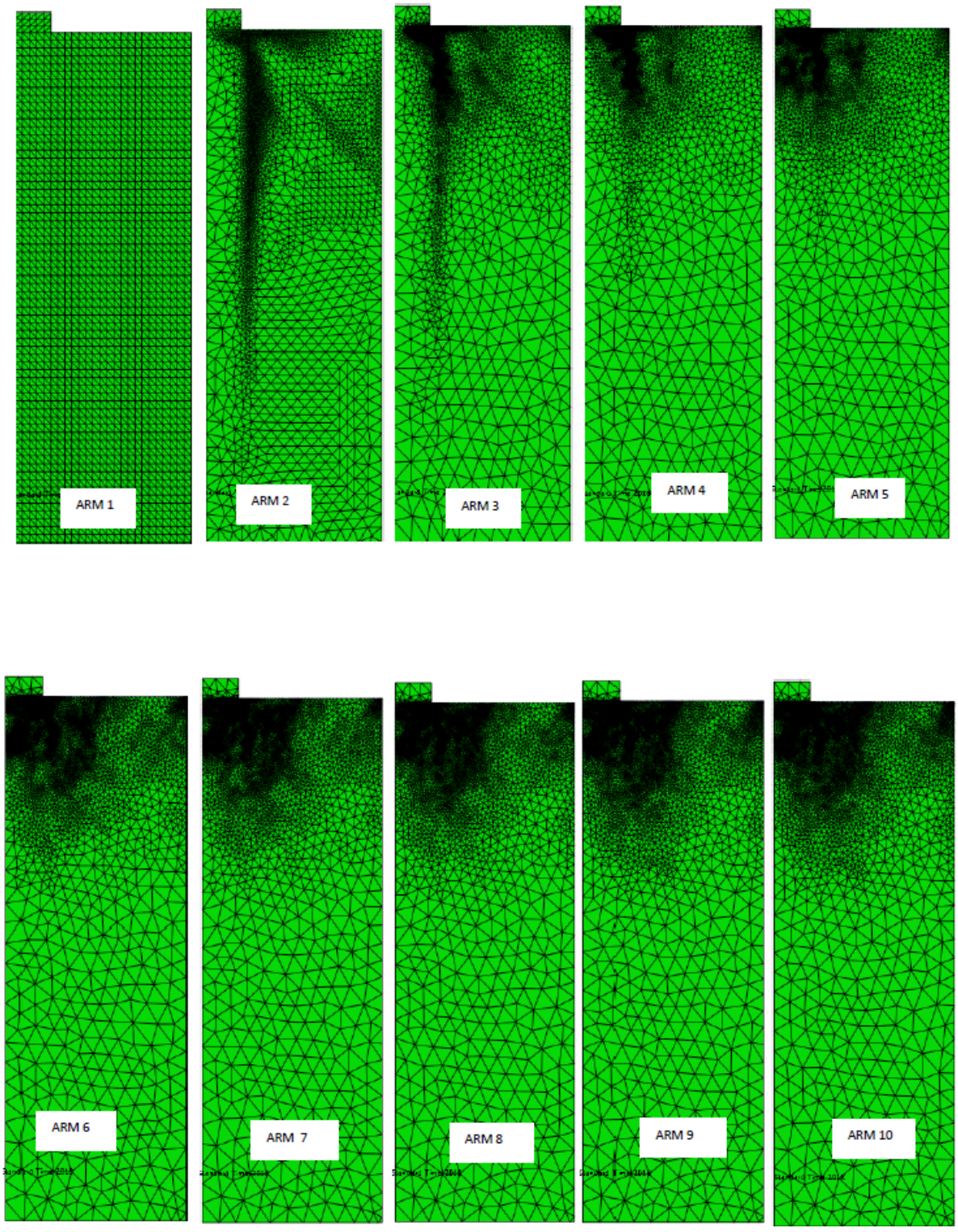

Figure 4-7: Adaptive mesh refinement (20mm disc on surface)

Figure 4-8 illustrates how element numbers increase during the ARM process. Eventually, some 40,000 elements are generated and consequently demand substantial computing resources – typically half an hour on a desktop PC [Intel Core i7 4.2GHz, single processor], as recorded in Figure 4-9. In Figure 4-8, one can see a reduction in element numbers (for the 10 mm disc) between the 7th and 10th iterations, although the reasons why this occurred

are not known. In general, a steep rise in element numbers is observed only over the first six iterations, which parallels the increasing accuracy.

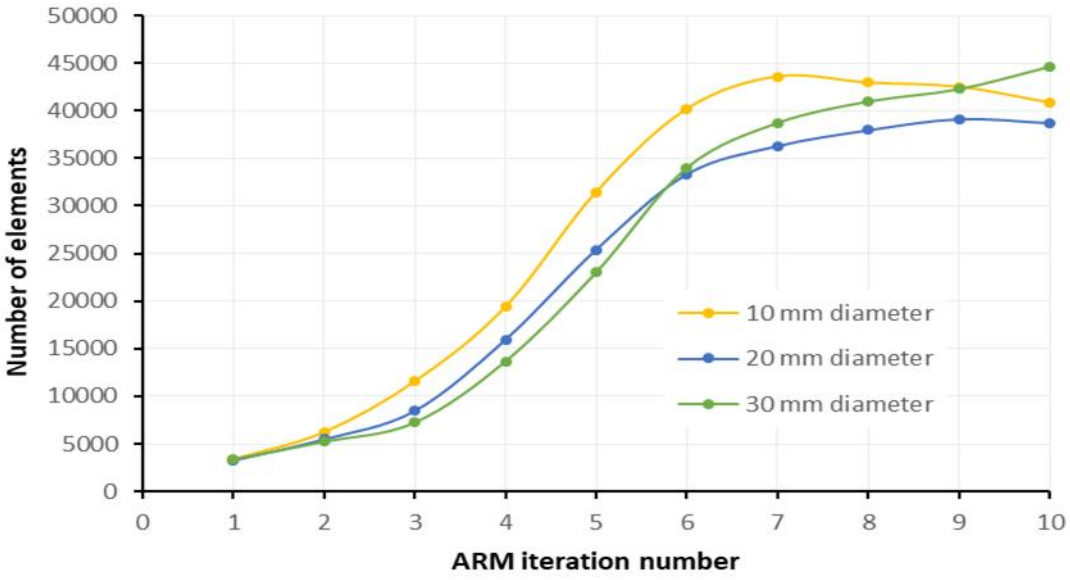

Figure 4-8: Number of finite elements generated by the ARM process.

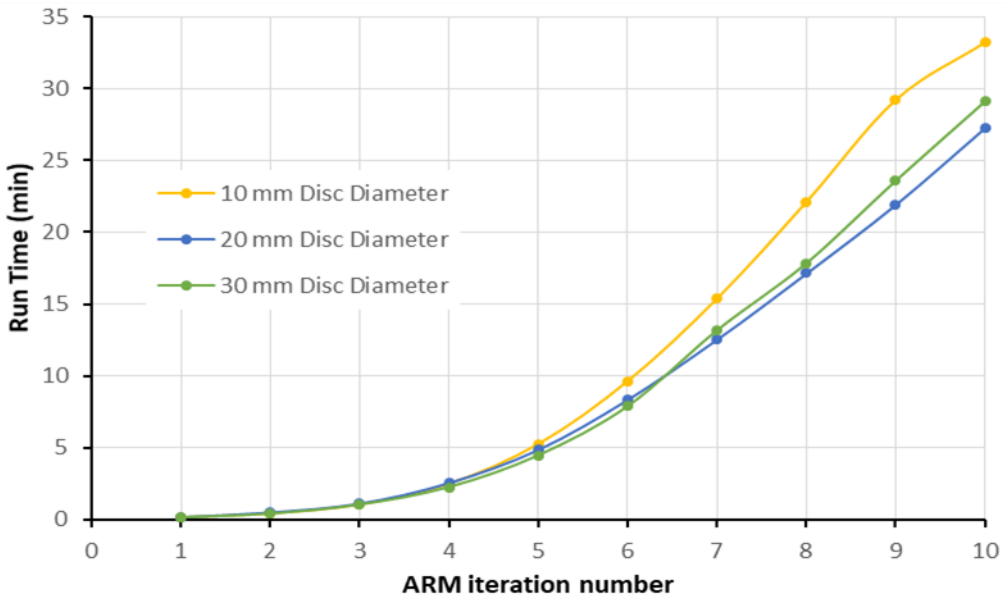

Figure 4-9: Run times: ABAQUS simulation with adaptive mesh refinement (ARM)

The convergence test results for 10 mm, 20mm and 30 mm diameter discs positioned at the surface of a rough-walled test cell are shown in Figure 4-10 to Figure 4-12, respectively. These figures show the normalized pressure-displacement relationships for the discs up to collapse. It can be seen that excellent convergence is attained in every case after six or seven iterations.

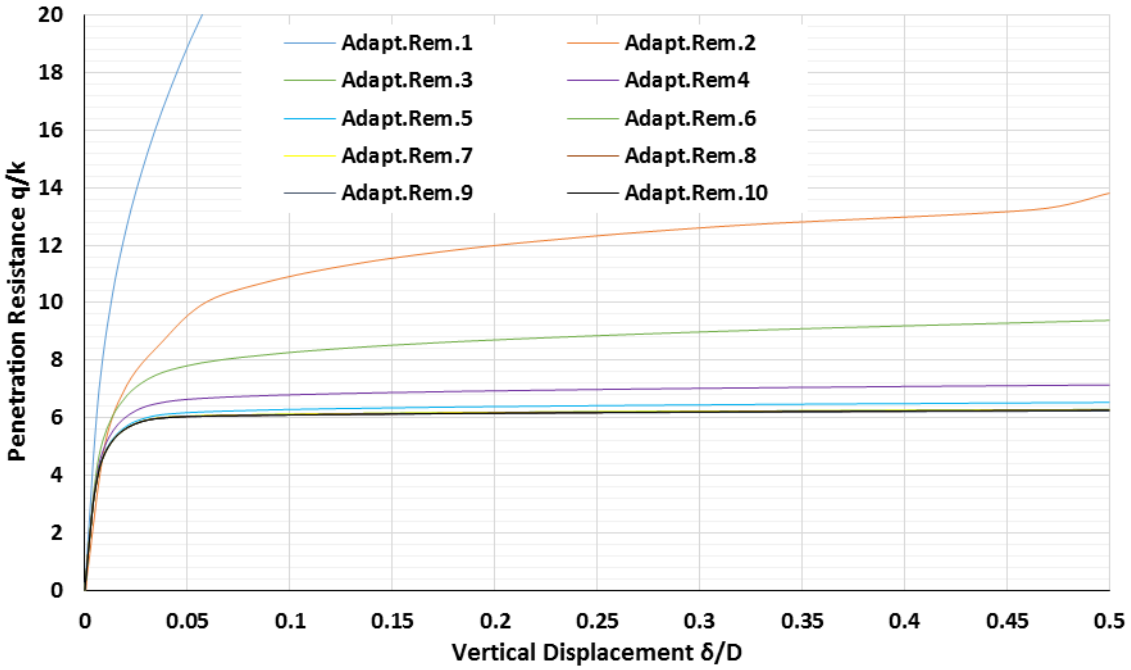

Figure 4-10*:* Convergence using Adaptive Re-Meshing (10 mm disc)

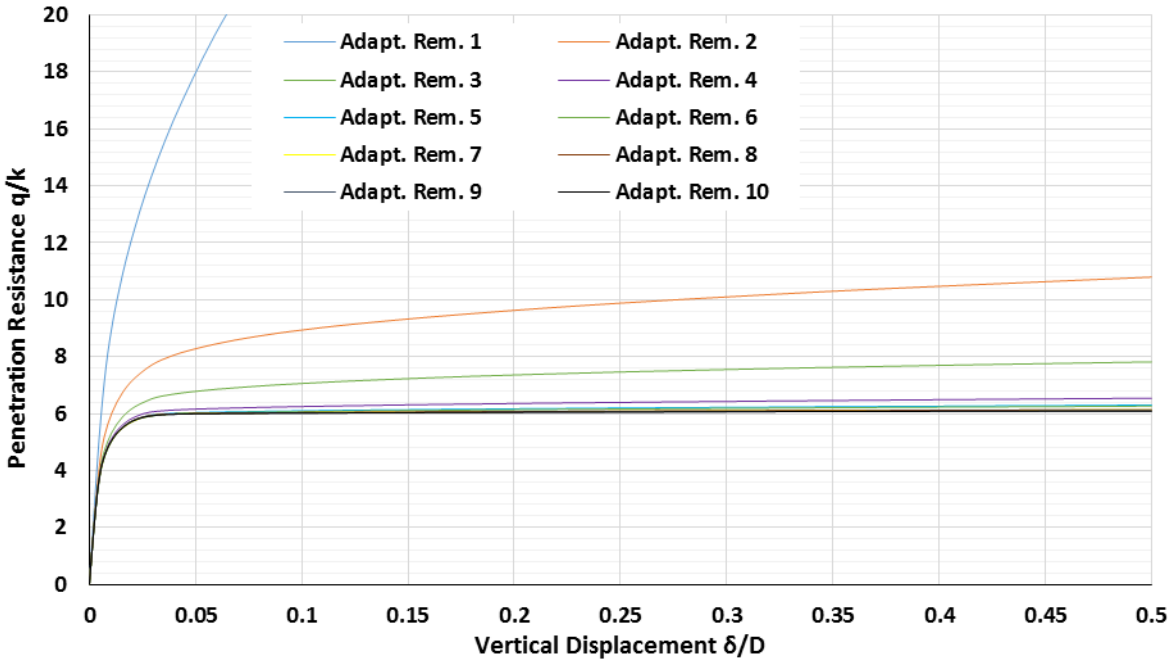

Figure 4-11*:* Convergence using Adaptive Re-Meshing (20 mm disc)

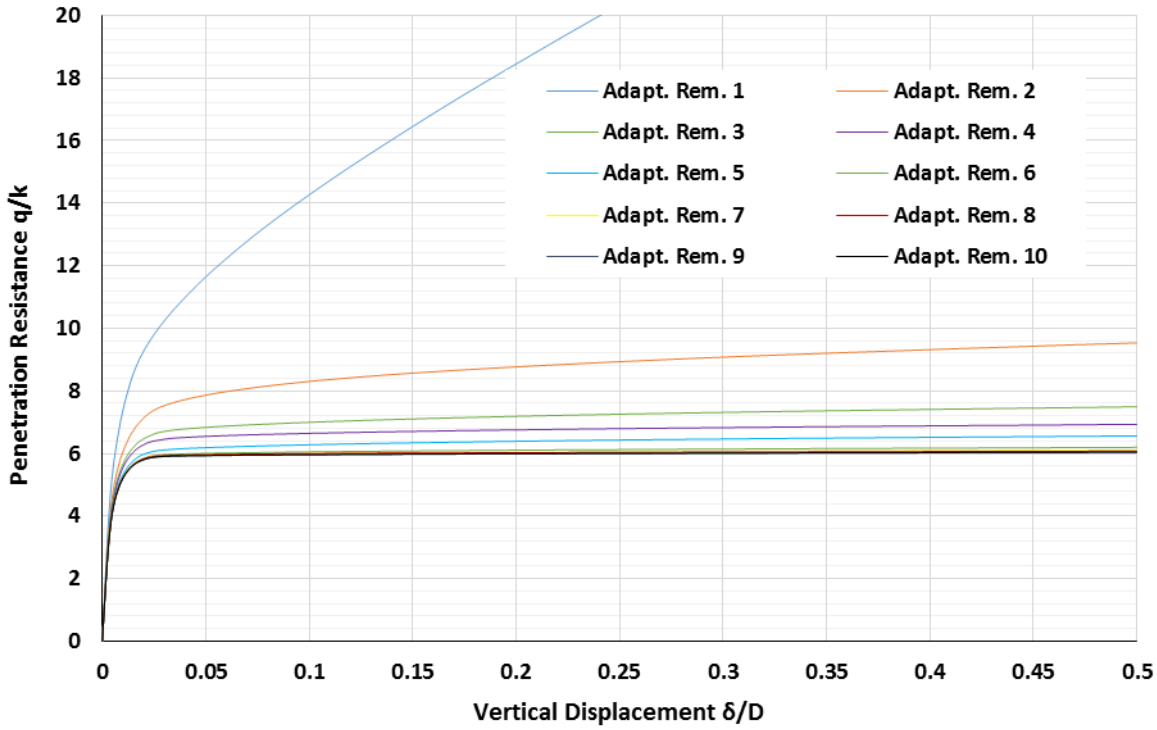

Figure 4-12: Convergence using Adaptive Re-Meshing (30 mm disc)

The bearing capacity factors N_c obtained from these data are plotted in Figure 4-13.

The theoretical value of N_C for these conditions is 6.05, and this is captured very well from the analyses of the 20mm and 30mm discs, but the value obtained from the analysis of the 10mm disc is some 3% higher than this. This is probably linked to the observation that there is a reduction in the number of elements between the 7^{th} and 10^{th} iterations, mentioned earlier. These results are promising given that deviations from the exact result can be expected due to the assumed material model (Tresca/Mises) and the small-displacement assumption.

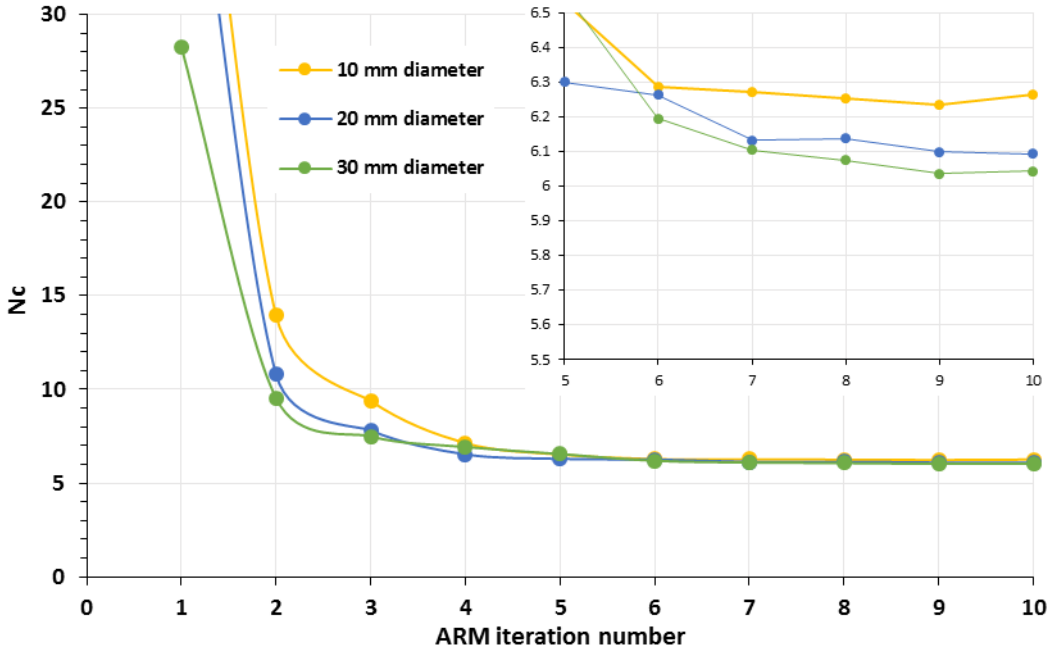

Figure 4-13: Convergence of bearing capacity factor NC for surface discs

4.3.3 Numerical results

To simulate the disc penetration process, using the small-displacement FE approach, various initial embedment depths were assumed. Penetration by discs of various diameters in the range 10-50mm were considered. Figure 4-14 illustrates some of the cases examined for a 20 mm disc penetrometer. Both rough and smooth side-wall conditions were considered, as noted earlier.

Figure 4-14: Geometric modelling of penetration by 20mm disc

The pressure-displacement curves obtained from this parametric study are shown in Figure 4-15 to Figure 4-19, for both the rough side-wall and the smooth side-wall conditions.

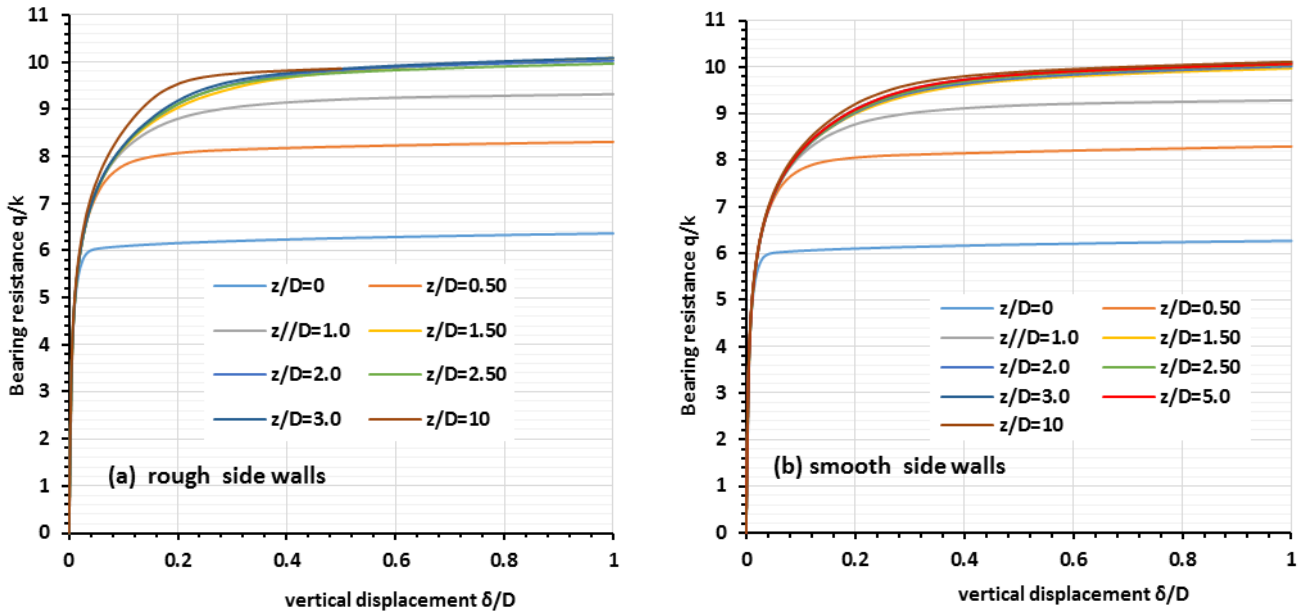

(a) (b)

Figure 4-15: Bearing resistance of 10 mm disc penetrometers: (a) rough side walls, (b) smooth side walls

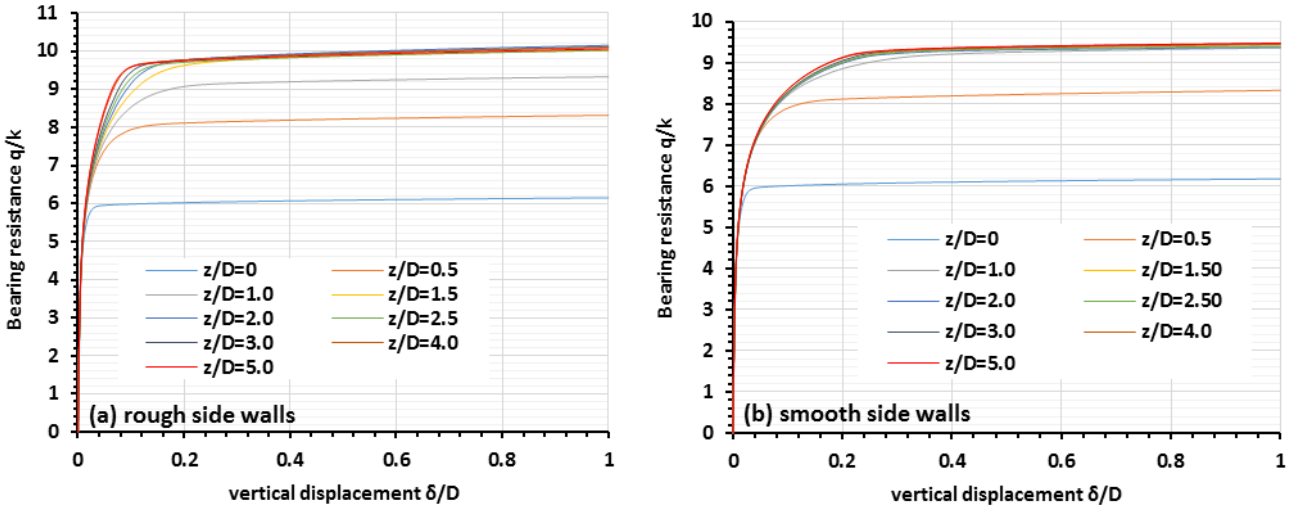

(a) (b)

Figure 4-16: Bearing resistance of 20 mm disc penetrometers: (a) rough side walls, (b) smooth side walls

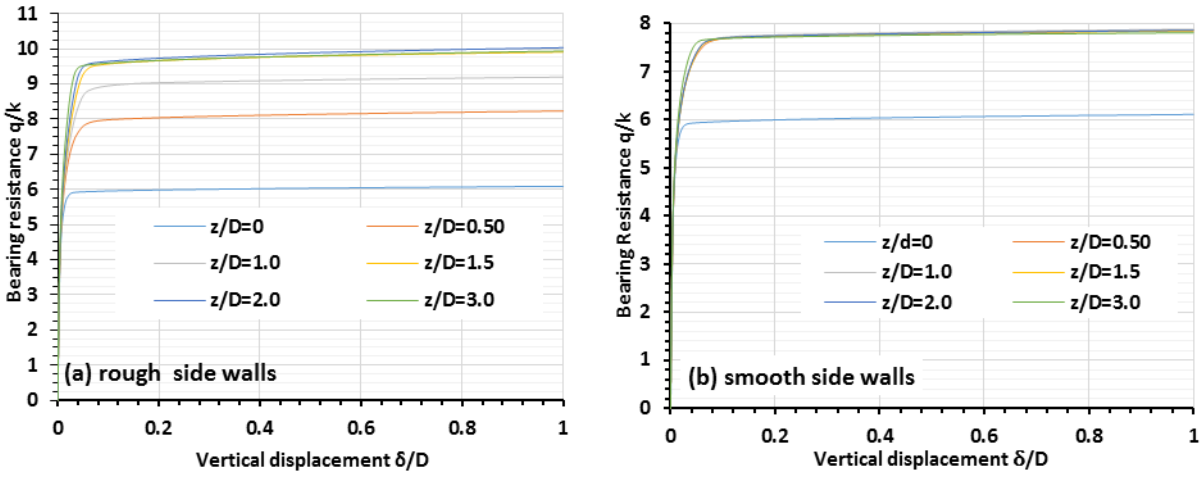

(a) (b)

Figure 4-17: Bearing resistance of 30 mm disc penetrometers :(a) rough side walls, (b) smooth side wall

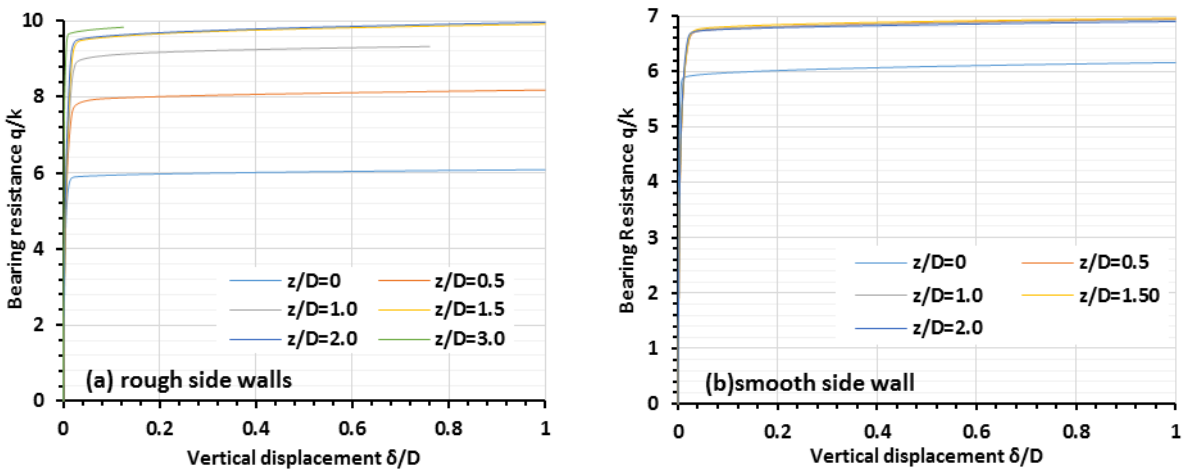

(a) (b)

Figure 4-18: Bearing resistance of 40 mm disc penetrometers: (a) rough side walls, (b) smooth side walls

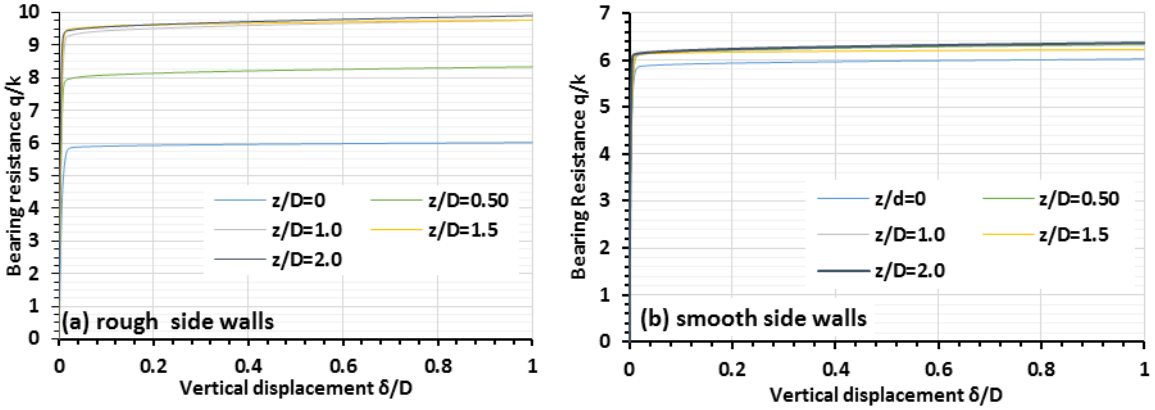

(a) (b)

Figure 4-19: Bearing resistance of 50 mm disc penetrometers: (a) rough side walls, (b) smooth side walls

The collapse pressure is evident in every case, from which the bearing capacity factors N_C can be readily inferred. In general, relatively larger displacements are needed to develop failure conditions in the more deeply embedded penetrometers. These displacements depend in part on the assumed value for the soil's Young's modulus of elasticity: lower soil stiffness value would place the validity of the small-strain assumption in doubt.

The bearing capacity factors for each case are plotted in Figure 4-20. For rough-sided cells, bearing failure appears to transition from a surface mechanism (general shear failure) to a deep mechanism (localized shear failure) at a depth ratio Z/D of about 1.5. At this depth, the bearing capacity factor approaches its maximum value of ten (approximately). For these cells, there appears to be no significant difference between the bearing capacities of the different discs. This suggests that for discs up to 50mm in diameter, the finite diameter of the test cells has very little effect on the computed bearing capacity. This result may be attributable to fact that the diameter of the rotational failure mechanism is of the order of the disc radius and is therefore largely unimpeded by the cell walls.

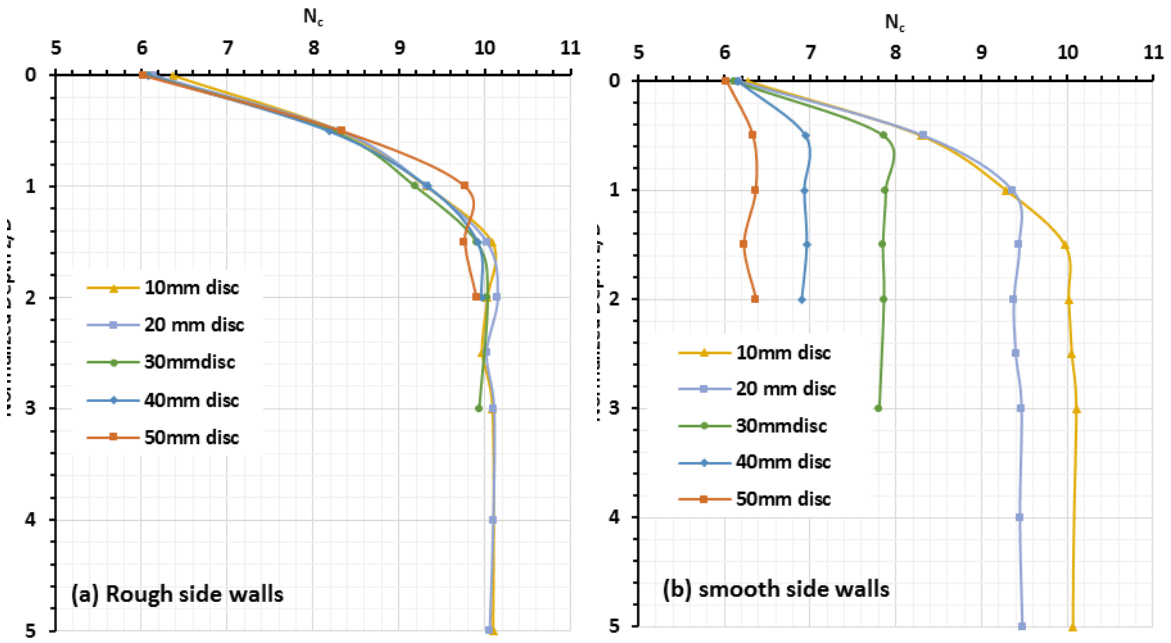

(a) (b)

Figure 4-20: Bearing capacity of disk penetrometers: (a) rough side walls, (b) smooth side walls

A quite different picture emerges for smooth-walled cells. For these cells, the effect of disc diameter can be quite profound. For the 10mm disc, the results for both smooth-walled and rough-walled cells are practically identical: N_C reaches a maximum value of ca 10.1 in both cases. For the 20 mm disc, the difference between the two cases is no more than 5%. Given that the "real" boundary condition (for an infinitely extended soil, or equivalently a cell of

infinite extent) will lie somewhere between these two extremes, it can be concluded that for this case too, the effect of the test cell diameter is negligible.

For larger disk diameters, this argument becomes more difficult to hold as the difference between the bearing capacities in smooth-walled and rough-walled cells continues to widen. Evidently, if the "real" boundary condition is more closely aligned with the "rough-wall" assumption, then larger diameter discs (D > 20mm) should still produce results in accord with those obtained for an infinitely extended soil. Given that the experimental data for 30mm diameter discs does not support the numerical prediction of (practically) constant bearing resistance with depth (as shown in Fig. 3.47), it can be inferred that the rough-walled assumption is more nearly correct than the alternative. Hence, it can be concluded that the finite test cell is an accurate model of an infinitely extended soil for disc diameters up to at least 20 mm, but that it may yield increasingly conservative estimates of bearing capacity for greater disc diameters.

The flow patterns for a typical case (D = 20 mm, Z = 100 mm), for both rough-walled and smooth-walled cells, are illustrated in Figure 4-21. In both cases, the local rotational failure mechanism can be clearly seen, and the soil tends to flow into the cavity above the disc. For this disc diameter, the centre of the mechanism is located far from the cell walls and therefore the rotational restraint of the wall itself does not play a significant role.

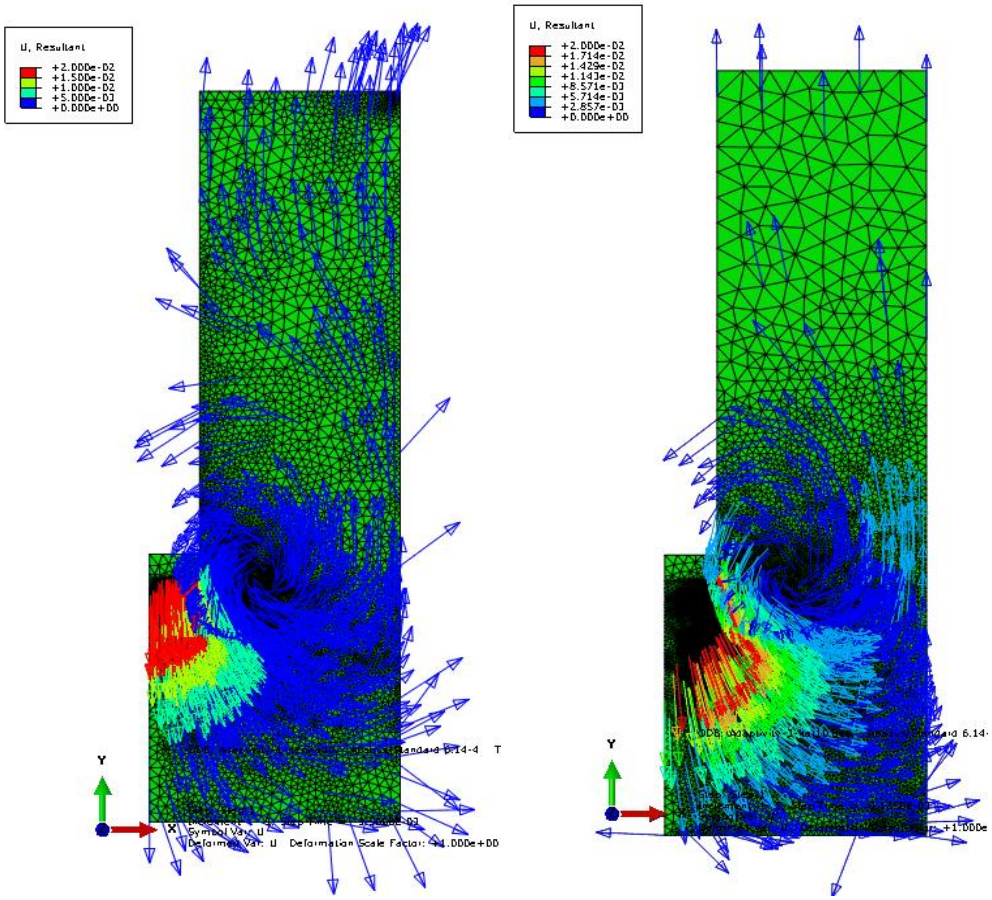

(a) Rough-walled cell (b) Smooth-walled cell

Figure 4-21: Displacement field for: (a) rough-walled cell, (b) smooth-walled cell

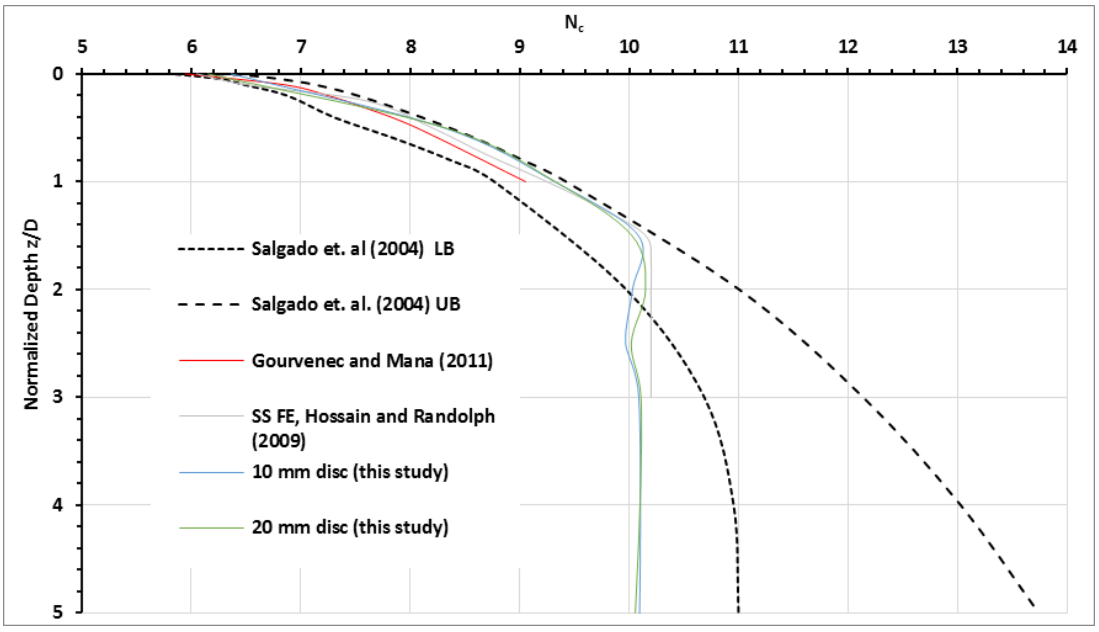

Figure 4-22: Comparison between bearing capacity factor N_c and some published data

Figure 4-22 is a comparison between the bearing capacity data obtained for disc diameters of 10mm and 20mm, and the results obtained by some other researches for the bearing capacity factor N_c for circular footings. The results of (Gourvenec and Mana, 2011) are in

good agreement with the current results although their work focusses on a cylindrical drum with smooth sides. However, the results presented are only applicable for embedment ratios less than unity. More convincingly, the results are in good agreement with the results of Hossain and Randolph (2009b) who used a small-displacement FE approach. They too found that for embedment ratios greater than 1.5, the soil resistance is constant. This echoes the conclusions of Hossain and Randolph (2009b) for small strain FE analysis of soil resistance to spudcan penetration. This result is different, however, from that suggested by the plasticity solution of (Salgado et al., 2004) in which the Nc values are bracketed by upper and lower bound solutions which increase with depth. Perhaps this may be explained by differences in geometry between these studies.

4.3.4 Effect of a rigid base

As the disc penetrometer approaches the cell base, the bearing capacity inevitably rises. The key objective here is to determine the magnitude of that increase as a function of the separation distance z' between the disc and the base. The results of a series of analyses are depicted in Figure 4-23. The cell walls were assumed to be rough and a disc diameter of 20mm was considered. The separation distance is normalized with respect to the disc diameter, although cell diameter may also be relevant for large disc diameters.

The results show that the base proximity effect (on bearing capacity) can be neglected provided that $z'/D > 0.5$. The proximity effect can be detected at much greater separations by examining the displacements prior to collapse, although this is not a relevant consideration in this work. The bearing capacity data are re-plotted in Figure 4-24 for clarity.

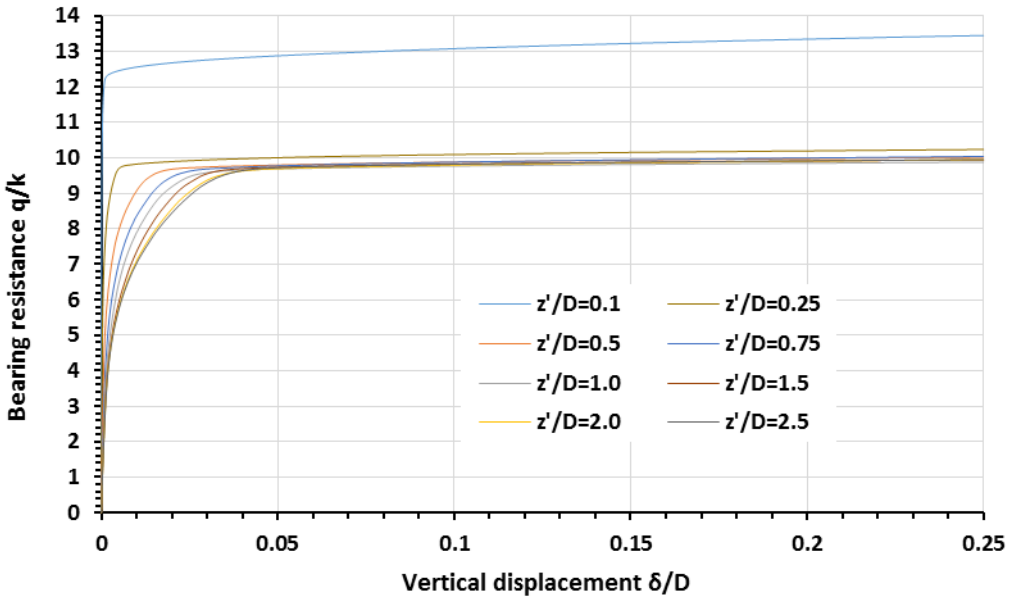

Figure 4-23: Effect of a rigid base on the bearing resistance of a disc penetrometer (D = 20mm)

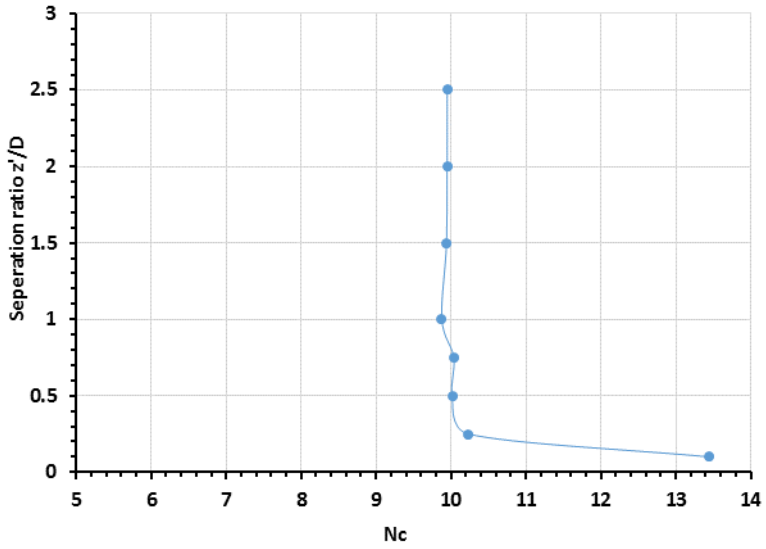

Figure 4-24: Bearing capacity factor N_C for a 20mm disk overlying a rigid base.

4.4 Large Displacement Finite Element Analysis

4.4.1 Introduction

Due to the significant geometric distortion that occurs in penetration problems, it may be worthwhile exploring whether more advanced finite element formulations, than those which are based on small-strain assumptions, can yield more robust solutions. There is an extensive literature on these advanced methods and the following review is not intended to be comprehensive.

In such analyses, the position of material points can be described by means of either a Lagrangian or an Eulerian reference frame, as illustrated in Figure 4-25. In the Lagrangian approach, the reference frame moves together with the material, while in the Eulerian approach, the reference frame is stationary, and the material flows relative to it. In the finite element context, flow causes a Lagrangian mesh to become distorted.

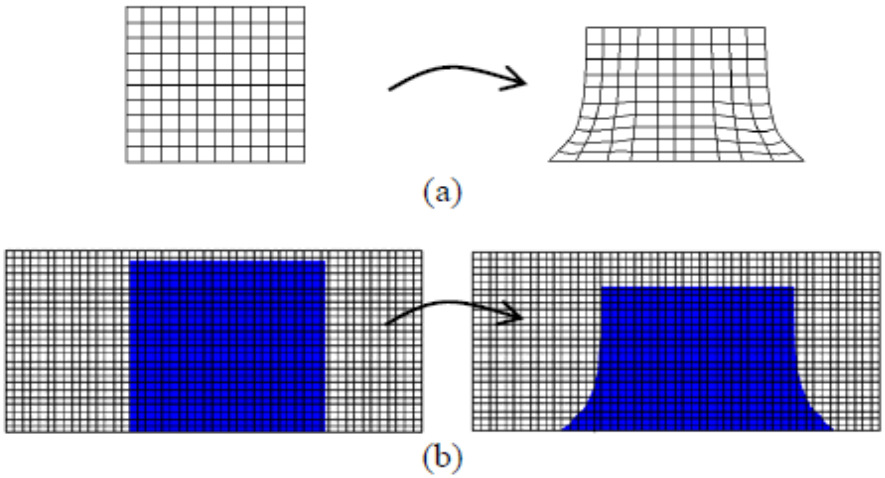

Figure 4-25: Material deformation viewed from (a) Lagrangian and, (b) Eulerian perspectives (Fallah et al., 2016).

The Arbitrary Lagrangian-Eulerian (ALE) technique aims to reduce mesh distortion by re-meshing the domain as the deformation proceeds. The field values are interpolated and transferred from the old mesh to a new mesh. The number of elements and their connectivity do not change during the re-meshing process. Instead the nodes are moved to new position. The ALE technique is often used in conjunction with an explicit solution scheme (Tho et al., 2012). Applications of the ALE technique to simulate the cone penetration process can be found in, for example, (Sheng et al., 2013) and (Konkol and Bałachowski, 2017).

The re-meshing and interpolation with small strain (RITSS) technique is described by Hu and Randolph (1998). Like the ALE technique, the mesh is updated at intervals. However, new elements may also be introduced during this process. Applications of the RITSS technique to simulate the penetration into soil can be found in several papers , e.g.,(Hossain et al., 2005); (Liu et al., 2005); (Hossain and Randolph, 2009b); (Hossain and Randolph, 2010); (Wang et al., 2010); (CHATTERJEE et al., 2012); (Chatterjee et al., 2014); (Han et al., 2016); (Tian et al., 2014).

The coupled Eulerian-Lagrangian (CEL) technique offers a compromise between a full Lagrangian implementation and the elementary Eulerian formulation: it enjoys a good

reputation despite sacrificing some of the rigour (and complexity) of the Eulerian perspective. Excessive mesh distortions are avoided but problems may arise at the boundaries if these become discontinuous. In the geotechnical field, many penetration studies have been conducted using the CEL approach, e.g., (Pichler et al., 2012), (Zhao and Liu, 2017), (Hui et al., 2013), (Li et al., 2018), (Hawlader et al., 2015), (Grabe and Wu, 2016), (Zheng et al., 2013), (Zheng et al., 2016), (Fallah et al., 2016), (Tho et al., 2012), (Qiu et al., 2011), (Qiu and Grabe, 2012), (Hamann et al., 2015), (Ko et al., 2017), (Hu et al., 2014).

For example, (Qiu and Henke, 2011) used the CEL method to simulate the installation of spudcan foundations and validated their results against analytical solutions and centrifuge model data. (Tho et al., 2012) and Khoa and Jostad (2016) similarly demonstrated the ability of the CEL method to model spudcan penetration. Zheng et al. (2013) found excellent agreement between the results obtained using the CEL and RITSS approaches in a similar application. However, Hui et al. (2013) reported some slight discrepancies between the two methods.

In a CEL analysis, bodies that undergo large deformations are meshed with Eulerian elements, while stiffer bodies in the model are meshed with more efficient Lagrangian elements. As with the case of the ALE technique, a standard large deformation explicit Lagrangian finite-element analysis is conducted in the first step. However, in contrast to the ALE technique, there is no requirement to obtain a new improved mesh since the original mesh is always the frame of reference. In the second step, which is an Eulerian step, advection is performed where the solution variables (such as stress, strain, etc.) are mapped from the deformed mesh back to the original mesh. This formulation is termed Lagrange plus-remap. Increased efficiency is possible by excluding the Eulerian step in those elements which have suffered little distortion (Tho et al., 2012). The process is repeated for the next increment.

4.4.2 Numerical discretisation

ABAQUS offers a three-dimensional CEL analysis capability, which was employed here with linear hexahedral elements, with reduced integration (element type: EC3D8R). For convenience, a one-quarter sector of the cylinder was analysed, by imposing the necessary symmetry conditions on the faces of the quadrant. A thin void layer (20mm thick) was prescribed above the soil surface, or otherwise material might flow out of the discretised

zone and be lost to the simulation (Simulia, 2014d). The penetration of the disc into the soil is displacement-controlled, at constant velocity. A typical discretisation is shown in Figure 4-26. The same material parameters for the soil are assumed as for the small-displacement analyses. In addition, the circular penetrometer is modelled as a discrete rigid body of 2mm thick and a mass density ρ_S = 8000 kg/m^3.

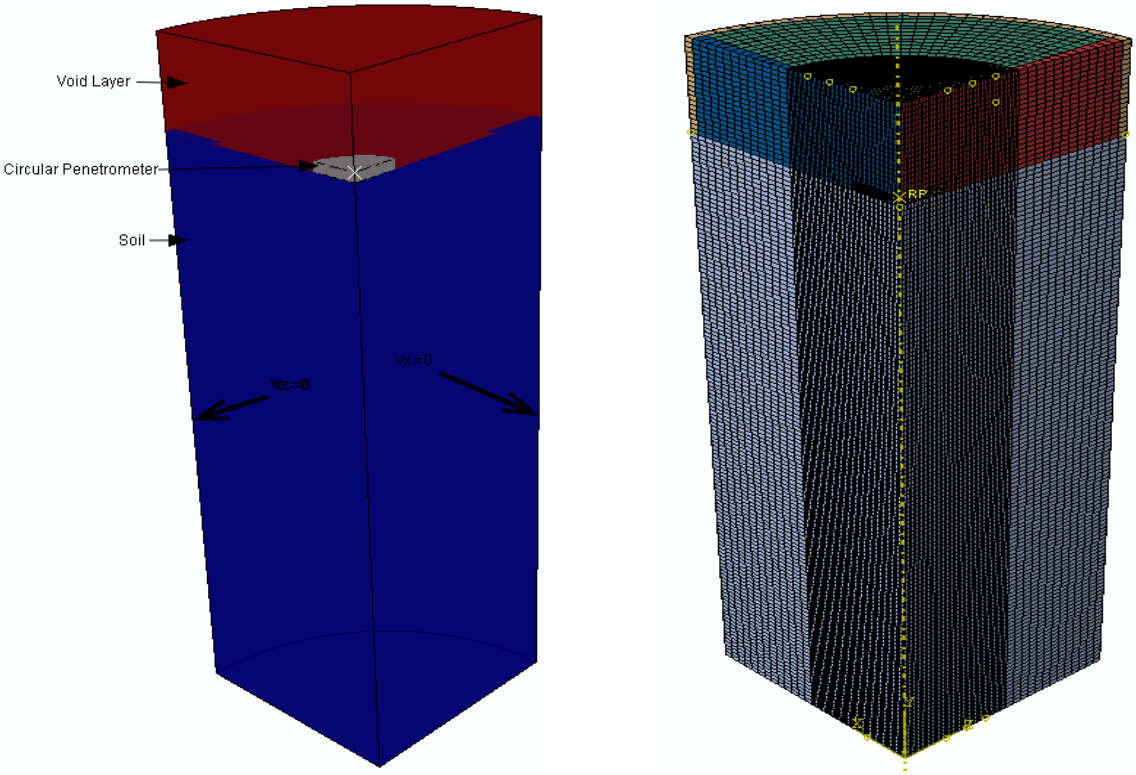

Figure 4-26: CEL Finite Element model: (a) materials, and, (b) discretisation.

The frictional contact between the soil and the penetrometer was modelled using the general contact algorithm, which uses the penalty contact method, and specifying a (total stress) Coulomb friction law together with a limiting shear stress (τ_{max}) along the penetrometer–soil interface. The Coulomb friction coefficient (i.e., the ratio of shear stress to normal stress at the interface) was set to a high value of μ_c=50, in order to allow the value of τ_{max} to govern failure (Kim and Hossain, 2015; Kim et al., 2015; Ma et al., 2014). The maximum shear stress on the penetrometer–soil interface, mobilised along the contact interface was limited to (Kim and Hossain, 2015; Kim et al., 2015; Ma et al., 2014)

$$\tau_{max} = \alpha . C_u \qquad \textbf{4-3}$$

in which α is the limiting shear stress ratio, ranging from 0 to 1, and C_u is the undrained soil strength. A roughness factor of α = 1.0 was adopted which limited the shear stress to 10 kPa before sliding between the disc and the soil occurs. However, other researchers have

assumed a smooth interface between spudcan and soil in simulations using the CEL technique (Li et al., 2018; Tho et al., 2012). This simplification may have been adopted because other numerical studies e.g., (Hu et al., 2001), (Martin and Randolph, 2001) have found only a 5% difference in N_c values between fully smooth and fully rough circular plate penetrometers. Also, (Qiu and Henke, 2011) found that penetration resistance based on the smooth interface assumption was closer to centrifuge test results.

4.4.3 Numerical results

Table 4-1 below lists the discretisation strategies which were used to explore mesh convergence. Meshes 1- 3 employ uniform sized elements, while Meshes 4 & 5 offer greater efficiency by employing a range of element sizes, within the range shown. In these tests, a penetration velocity of 10 mm/sec was adopted: discussion of this parameter is deferred to a later section.

Table 4-1: Mesh convergence: discretisation strategies

Mesh No.	1	2	3	4	5
Meshing strategy	uniform	uniform	uniform	biased	biased
Element size (mm)	2	1	0.5	0.1 – 2.0	0.1 – 2.0
Number of elements	50,000	100,000	200,000	170,000	250,000

The results of these analyses are shown in Figure 4-27. The oscillations in the data is an undesirable feature of the results, but appears to be a characteristic of CEL analyses, as observed by (Tho et al., 2012), (Qiu et al., 2011) and (Zheng et al., 2013). As expected, the results converge with increasing numbers of elements and the "biased" (non-uniform) meshes clearly outperform the uniform meshes. Mesh 5, shown in Figure 4-26b was adopted for the subsequent work.

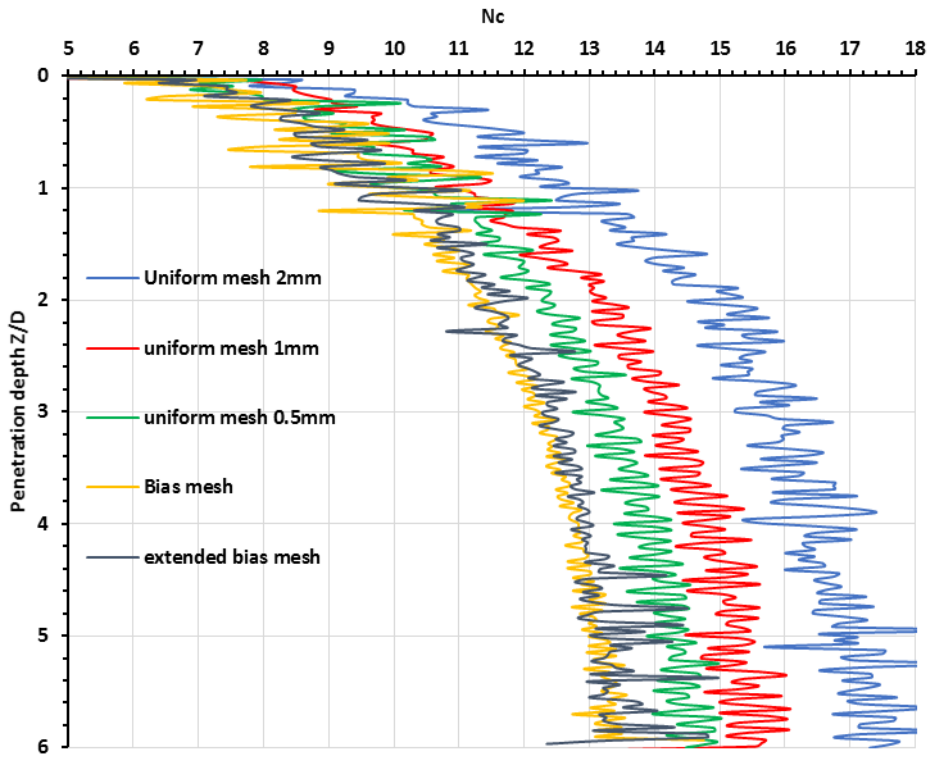

Figure 4-27: Bearing Capacity: mesh discretisation convergence study

The CEL technique incorporates the equations of motion and is therefore capable of determining whether inertial (dynamic) effects are significant in practice, where penetration velocities of the order of 5 mm/s may be employed. In addition, rate-dependent constitutive relationships could also be examined although that lies outside the scope of the present investigation.

In ABAQUS, this dynamic capability is implemented using an explicit solver, but this is not unconditionally stable: stability is guaranteed only if the time increment is less than the critical time step Δt_{crit}, which is the time taken for a signal to traverse the smallest element. In other words, the critical time step size is:

$$\Delta t_{crit} = \frac{L_e}{C_d} \qquad \textbf{4-4}$$

where L_e is the element length and C_d is the wave speed. For an ideal incompressible solid material, the compressive wave speed (p-wave) is infinite, and a rigorous analysis of such cases requires special treatment. The shear wave speed (s-wave) is approximately 31 m/s (= √ (G/ρ). Thus, for elements of 1 mm in length, Δt_{crit} = 32 μs. Thus, in principle, to capture the shearing response for a 20s penetration time (corresponding to a penetration rate of 5mm/s) requires 600, 000 time steps. The computational costs of such analyses exceed

the resources available so here we adopt a heuristic approach based on the examination of the results of convergence studies.

It is important to note that the computational time, for the present problem, is inversely proportional to the penetration rate, v. Although typical penetration rates are of the order of 5mm/s, analyses have been conducted for penetration rates of 1 – 100 mm/s, as shown in Figure 4-28. From this figure, we conclude that, (a), the results are better behaved (oscillate less) at low penetration rates, (b), dynamic effects are minimal at the lower penetration rates (convergence is observed), and, (c), bearing resistance continues to increase significantly beyond normalized embedment depths of 1.5 (in contrast to the small-strain results.).

The second conclusion confirms the presumption that the penetration test can be assumed to quasi-static. In turn, further analyses can be conducted at the low penetration rates (1 mm/s), taking advantage of the better-behaved results, albeit at the expense of substantial computing time. In some cases, run-times of three days were recorded.

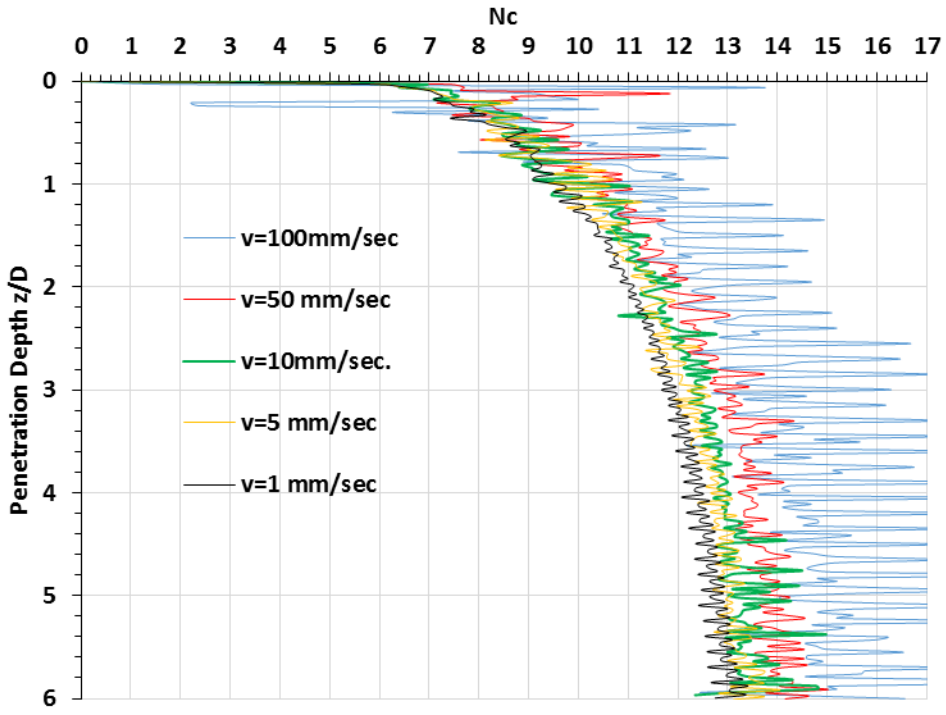

Figure 4-28: Bearing capacity: penetration velocity convergence study

Figure 4-29 compares the resulting normalized penetration resistance curve obtained from the CEL technique with other published solutions. The resulting N_c values for depths z/D>1.5 are higher than those obtained by (Khoa and Jostad, 2016) for smooth spudcans but are lower than those obtained for rough spudcans. The CEL results are bracketed by the upper and lower bound solutions of (Salgado et al., 2004) for pre-embedded plates, albeit

that these bounds are widely separated. At z/D=6, the resulting Nc is 13.2 which is close to the Nc=13.11 suggested by (Martin and Randolph, 2001) from plasticity solutions for deeply buried circular plates. The figure also shows the results obtained by Hossain and Randolph (2009b), using the RITSS technique, for spudcan penetration into a uniform clay. Their data indicates that the bearing capacity approaches a constant value of approximately 11.0 as suggested by Hu and Randolph (1999) and Hu et al. (2001) for deep plate penetration, whereas the CEL data indicates that the bearing capacity continues to increase with depth. This is in accord with the results of (Hui et al., 2013)) and (Hu et al., 2014) who similarly reported that CEL penetration resistances consistently exceeded those computed using RITSS. However, the RITSS results appear to be more plausible, because penetration resistance must reach some maximum within a few diameters of ground level, as the "deep" mechanism of failure is developed.

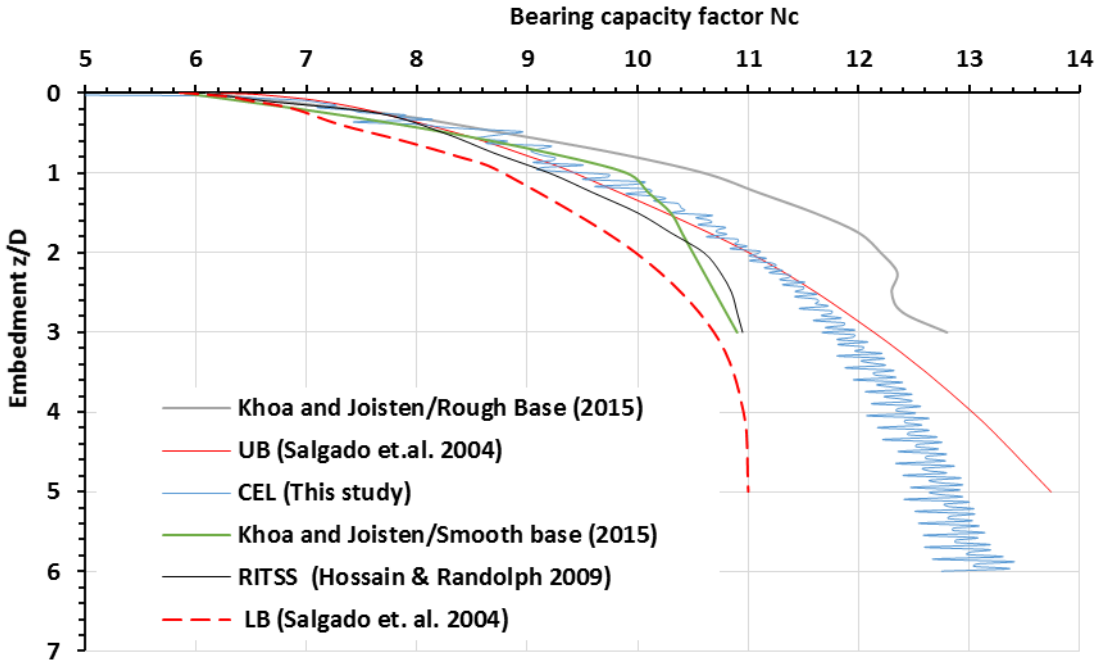

Figure 4-29: Comparison between CEL prediction and published data.

Figure 4-30 shows the displacement fields of the soil during the penetration test simulation using CEL technique. It can be seen that during the initial disc penetration, the soil at the penetrometer edge flows upwards to the surface and the soil beneath the central part of the penetrometer is forced downwards to the lower layer, the soil surface heaves up and a cavity starts forming above the disc level with the progress of the penetrometer. This behaviour

persists down to a depth ratio z/D≈1.5. With further penetration, however, the soil begins to flow back gradually onto the top of the penetrometer while the top part of the initial cavity stays open. At this transitional phase, failure has occurred through a combination of general shear (at the edge of the disc) and partial punching shear.

At a depth ratio z/D=1.5, the transition occurs between a shallow bearing capacity failure mechanism and a deep punching mechanism. At this depth ratio, the small strain finite element (SSFE) simulation stopped showing a change in Nc with depth as shown in Figure 4-20(a). In this context, the CEL technique is required account for the progressive accumulation of the soil during the back flow as the disc progresses deeper into the soil. This behaviour could not be proved experimentally since it needs special arrangement and techniques to capture the deep flow mechanism of soil around the penetrometer (Hossain and Randolph, 2010).

Comparing the displacement fields obtained from small strain and large displacement finite element approaches investigated here as shown in Figure 4-21(a) and

Figure 4-30 respectively for a depth ratio z/D=5 indicates that the CEL technique has a good ability to simulate the deep penetration mechanism. Soil back-flow if any is localised without affecting the soil surface profile. This type of plastic flow has been termed *flow failure* (Hossain and Hu, 2005; Hossain and Randolph, 2010; Qiu and Henke, 2011).

In neither the physical tests nor the numerical modelling was there any observation of cavity wall failure or cavity closure. Cavity failure is certainly a scale dependent (Hossain et al., 2005) and cavity depths of 120mm are far too small (except for extremely weak soils) to permit such failure.

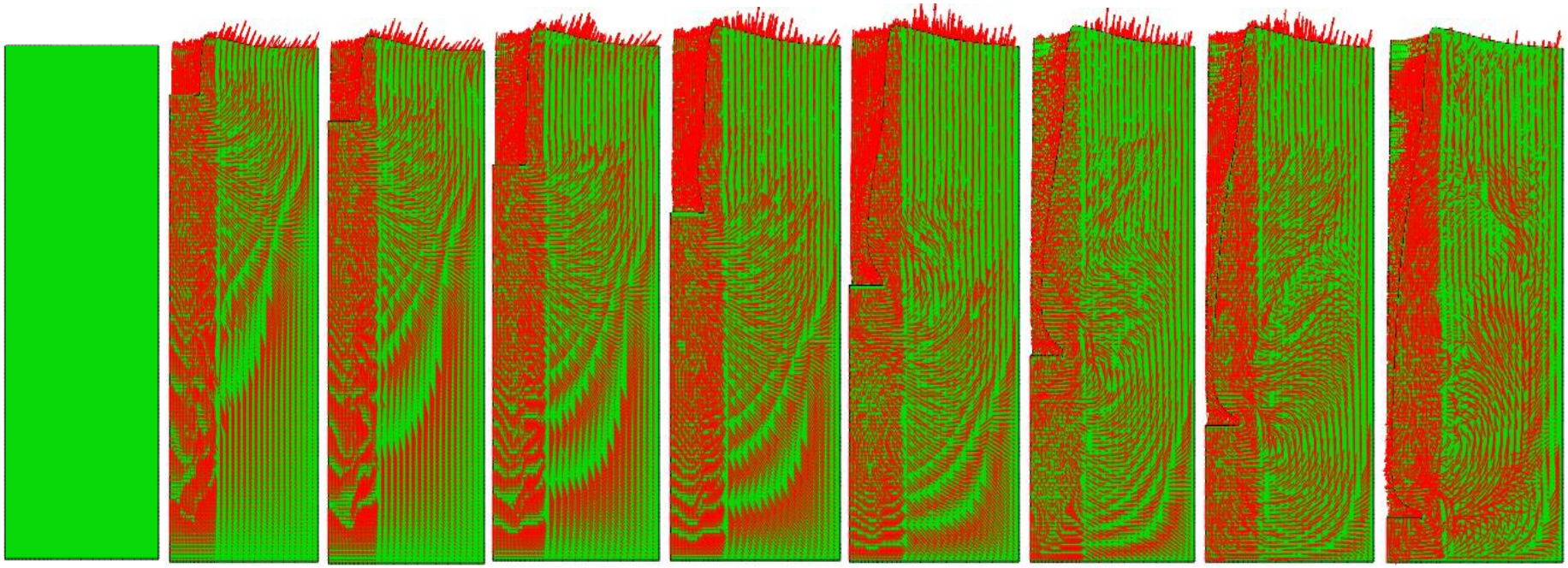

z/D=0 z/D=0.75 z/D=1.0 z/D=1.55 z/D=2 z/D=3 z/D=4 z/D=5 z/D=6

Figure 4-30: Displacement fields due to progressive penetration of 20 mm disc into soil

4.5 A Closed-Form Equation for Bearing Capacity

To interpret the bearing resistance data obtained from the experimental programme, the effect of depth on the bearing capacity factor N_c must be known. For that purpose, it is useful to express N_c in closed-form. The equation:

$$N_c = A - Be^{-M\left(\frac{Z}{D}\right)^N} \quad \text{4-5}$$

can be used to fit a wide range of experimental and theoretical results. The constant A is the value of N_c for deeply embedded penetrometers. The corresponding value of N_c for penetrometers resting on the surface is the difference A – B. The parameters M & N determine how rapidly the bearing capacity transitions from the "surface" value to the deep value.

Table 4-2 list the parameters deduced from some selected publications (and this work); the bearing capacity data and their corresponding empirical equations are plotted in Figure 4-31. It can be observed that the empirical equations fit the data extremely well: in fact, reasonable results can be obtained by taking N equal to unity in all cases (and making compensatory changes to M). For example, Model 1 (with M = N = 1) fits the data within 2%.

Table 4-2: Empirical constants for the bearing capacity factor Nc

Model	Technique	Source	A	B	A - B	M	N	Remark
1	RITSS	(Hossain and Randolph, 2009b)	11.0	4.9	6.1	1.06	1.10	Extrapolated after z/D=3.0 to N_c=11.0
2	Plasticity solution	(Salgado et al., 2004)	12.5	6.5	6.0	0.65	0.95	Average of UB and LB solutions
3	SS FE	This study	10.1	4.0	6.1	1.61	1.06	
4	CEL	This study	13.5	7.5	6.0	0.63	0.82	

While there is universal agreement on the "surface" value of N_c, there remains wider disagreement on the "deep" value, and consequently on the rate of increase with depth. However, on physical grounds, it seems unreasonable for the "deep" value to be more than twice the "surface" value.

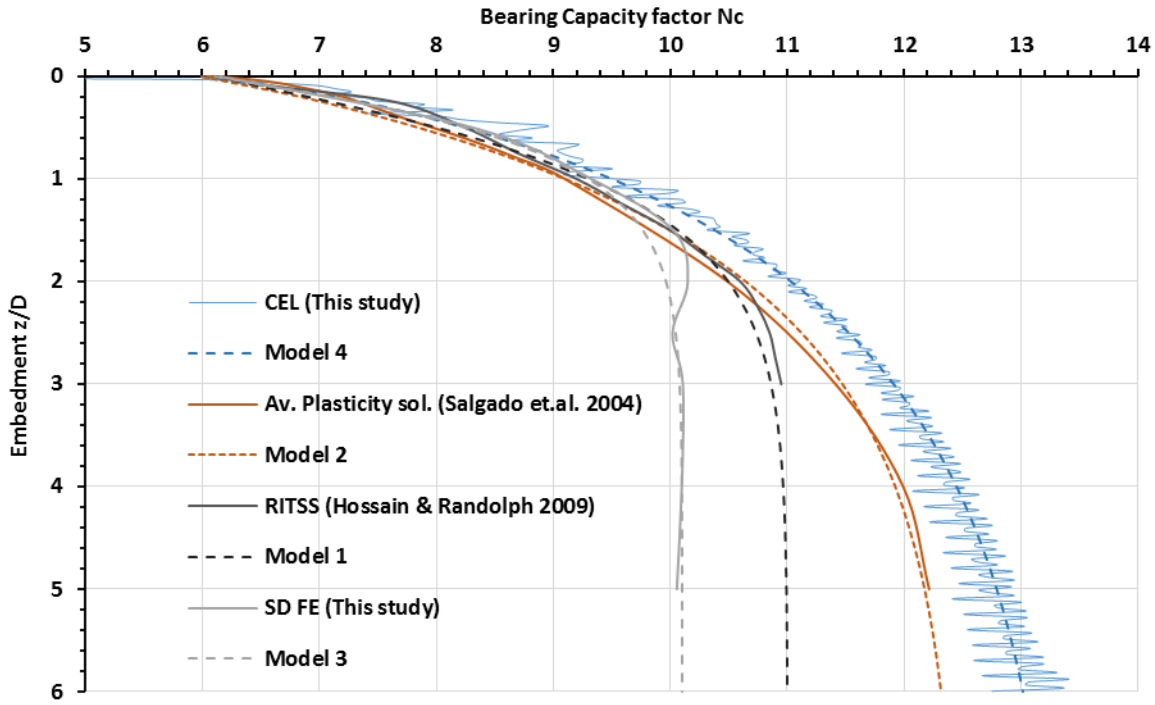

Figure 4-31: Curve-fitting of the bearing capacity factor N_c

If the numerical/theoretical predictions of N_c are correct, then their use to interpret bearing capacity data should yield constant values of undrained shear strength (with depth) in the sample cells. In other words, the recorded bearing pressure distributions (with depth) should mirror the variation of N_C with depth. These should also be in agreement with direct measurements of undrained shear strength (e.g., from triaxial tests).

The data in Figure 4-32 are the values of undrained shear strength interpreted from penetration tests on 365-day samples. Inspection of these figures reveal that Models 2 & 4 (those with the largest "deep" values of N_C) consistently predict a decrease in strength with depth, which is implausible. There is relatively little evidence here to choose between Models 1 & 3, other than the directly measured values of undrained shear strength, from UU triaxial tests, tend to be closer to the predictions of Model 1. The UU data plotted here are the corresponding resulting peak undrained shear strength averaged from duplicated triaxial compression tests on specimens cured for the same periods as shown in chapter 3. Finally, the evidence (discussed earlier) that Model 3 tends to under-predict N_C values tends to reinforce the view that Model 1 lies closest to the truth.

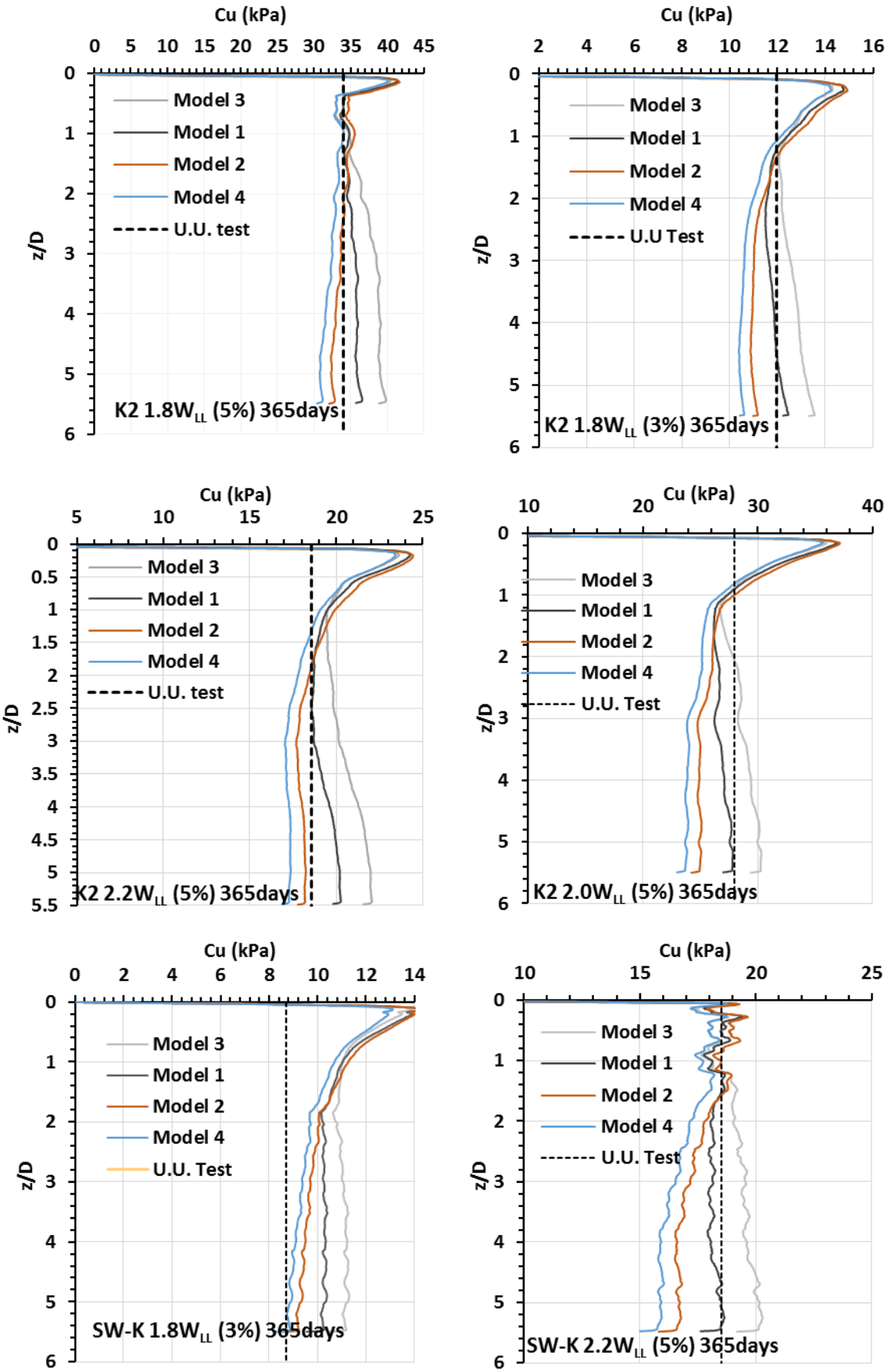

Figure 4-32: Back calculation of undrained shear strength Cu from penetration tests.

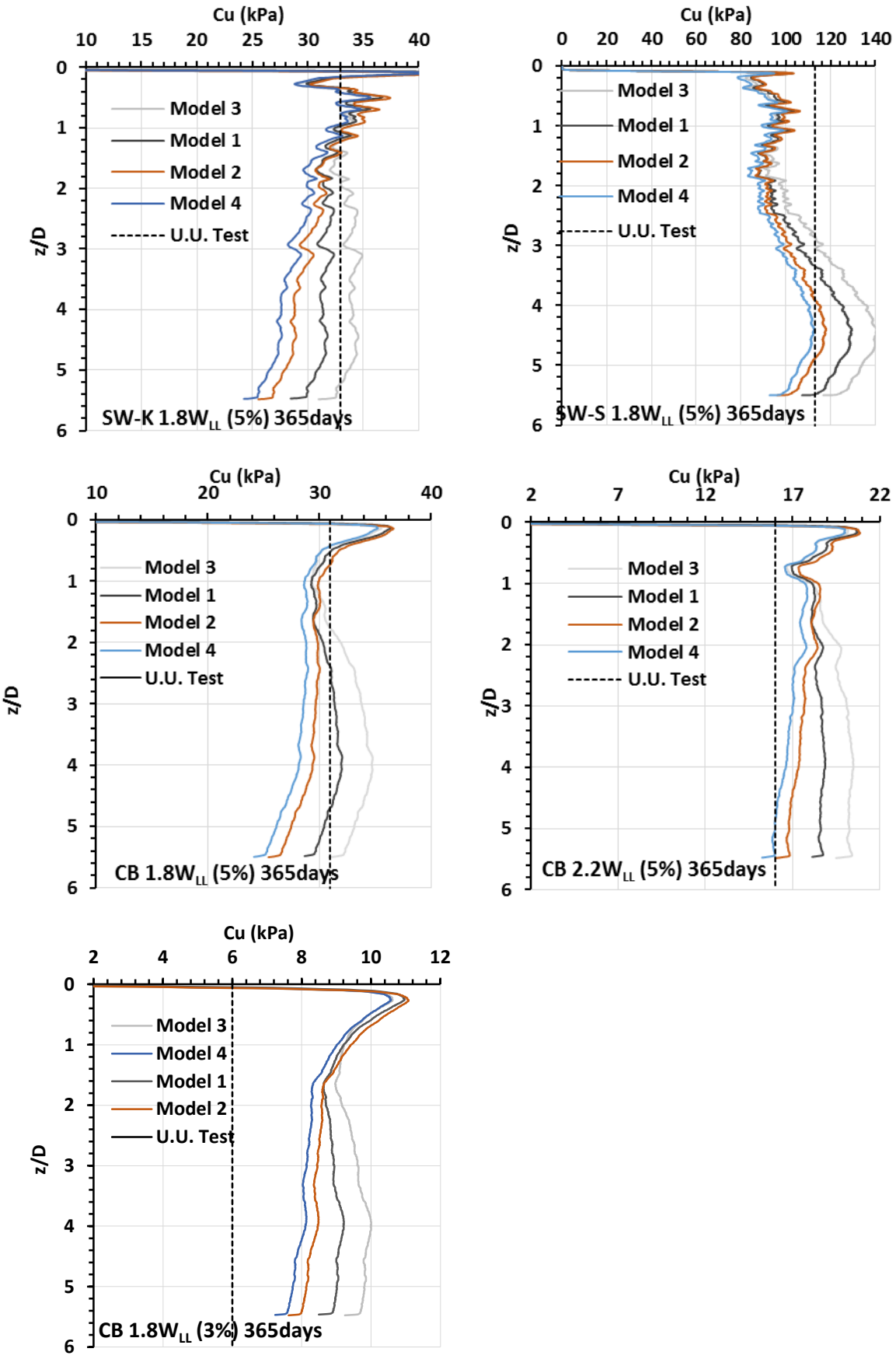

Figure 4-32: (continued) Back calculation of undrained shear strength Cu from penetration tests.

To compare the results of each model with the UU test results, the back-calculated depth-averaged undrained shear strengths (using Eq. 3-11, Eq. 4-5, Eq. 5-4, and Eq.5-5) from the penetration results are compared with the corresponding triaxial strengths in Figure 4-33. Model 1 offers the most consistent results: the strength values differ by less than 1% on average.

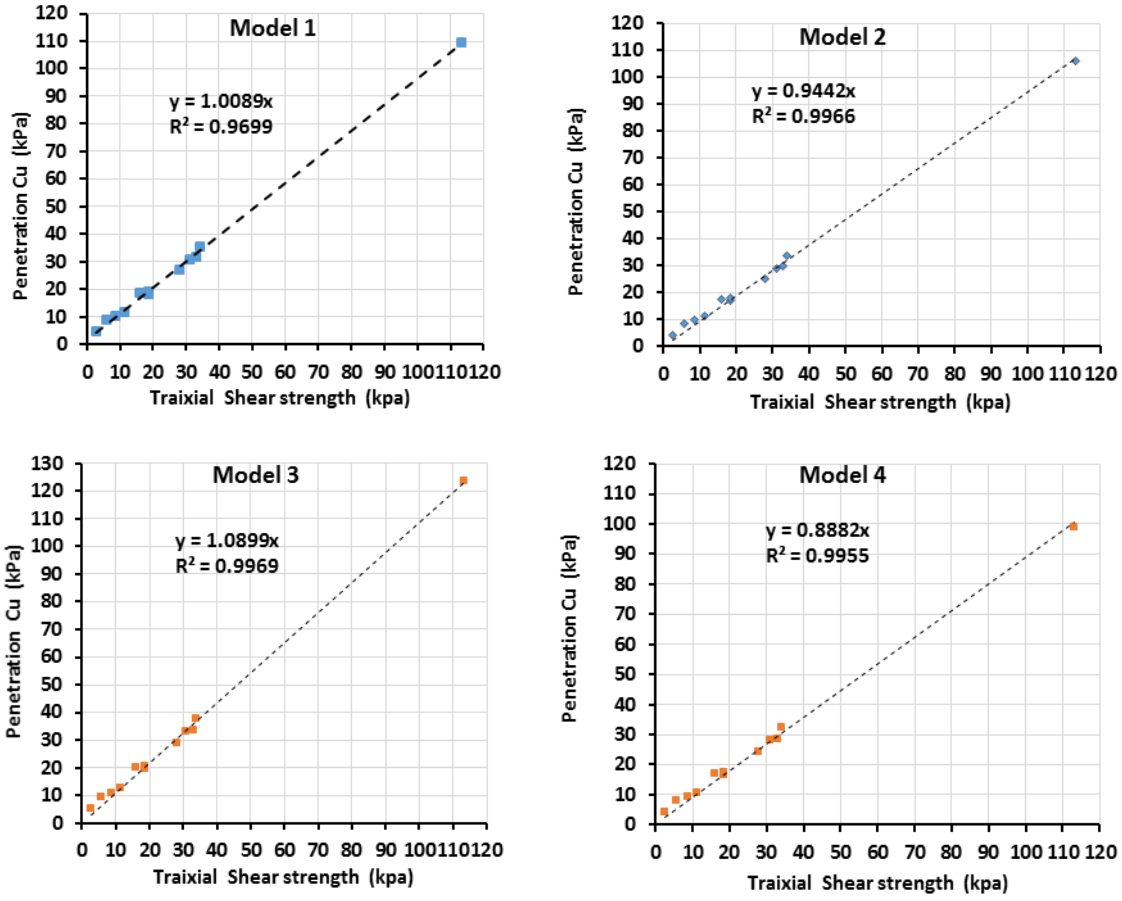

Figure 4-33: Correlation between undrained shear strength from penetration tests and triaxial tests.

It can be seen that in most cases, the correlation between triaxial strengths and penetrometer strengths is reasonable. However, closer inspection of Figure 4-33 shows that triaxial strengths are consistently less than penetromter strengths, for strengths below 10kPa. It may be that these soils are more prone to sample disturbance during triaxial test preparation.

In the above, we make the tacit assumption that these soils have a unique undrained shear strength. However, these lime-treated soils will exhibit similar post-yield behaviour to sensitive clays (Ladanyi and Eden, 1969); that is, strength degradation will occur during remoulding of the soil around the penetrometer (Khoa and Jostad, 2016). This expectation is reinforced by an examination of the stress fields which develop during penetration, shown in Figure 4-34.

The red zones in Figure 4-34 depict the extent of the yielded area: the wide expanse of the yielded zone suggests that extensive volumes of soil around the penetrometer undergo significant accumulated plastic strain, and consequent softening. Thus, in any analysis which does not explicitly account for strain softening, the bearing resistance can only be interpreted in terms of some average soil strength rather than peak strength.

Strain softening has not been taken into account in this work: this would require data on strength degradation (e.g., from a ring shear apparatus) to serve as parameters within a more sophisticated constitutive model than has been employed here. It seems likely that the localisation associated with strain-softening would also give rise to more sharply defined flow mechanisms. This issue has been discussed by Randolph et al. (2008) in the context of penetrometer tests in natural soils.

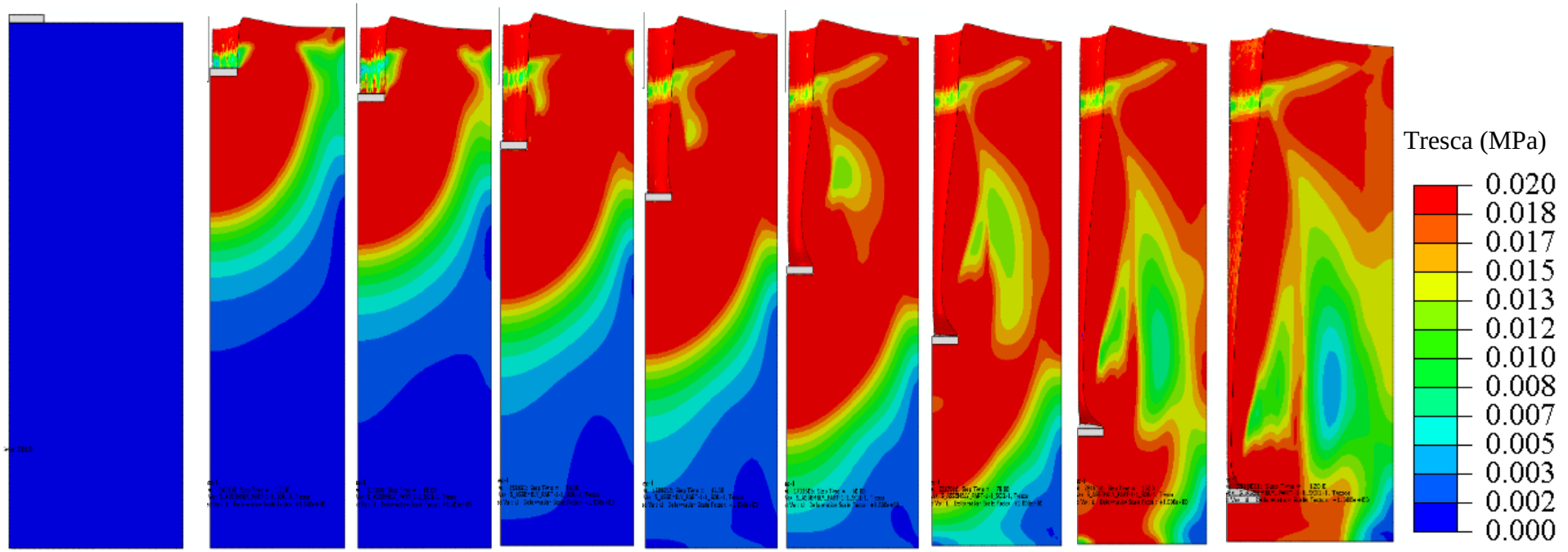

Figure 4-34: Stress fields due to progressive penetration of 20mm disc into soil.

4.6 Conclusions

The main conclusions to be drawn from this chapter are that:

- Penetrometers with diameters of up to 30mm can be employed in 100mm diameter cells without any significant boundary effect (on bearing capacity),

- Similarly, the effect of a rigid base beneath the penetrometer becomes significant only when the gap is less than half the penetrometer diameter.

- In principle, the large-strain finite element method (CEL) provides a more rigorous method for simulating continuous penetration, rather than the snapshot approach using a small-strain technique. However, the results obtained here, for bearing capacity, appear to be inferior to those obtained using the small-strain technique. Further investigation, using a more powerful platform, may be worth pursuing in the future.

- From these (and other published) numerical simulations, as well as an examination of the experimental data conducted here, a closed-form equation for the bearing capacity factor N_C for a disc penetrometer of diameter D, and embedded at a depth Z was derived, namely:

  - $$N_c = A - Be^{-M\left(\frac{Z}{D}\right)^N}$$

  where the parameters A, D, M, N are taken to be: 11.0, 4.9, 1.06, 1.10, respectively. This equation is used in all subsequent work, to determine undrained shear strength from penetrometer bearing capacity data.

- It is noted that in a strain-softening material, measures of undrained shear strength obtained by penetrometer testing will not yield the peak strength.

Chapter 5 PENETRATION TEST RESULTS

5.1 Introduction

This chapter summarizes the results of a comprehensive series of penetration tests conducted on both intact and remoulded admixed soils to determine their undrained shear strengths. Drawing on the results of Chapter Three, a 20 mm diameter disc penetrometer was employed, and the tests were conducted at a penetration velocity of 250 mm/min. The tests were repeated in order to assess their repeatability. Over 800 tests results are reported here. For brevity, only the mean undrained shear strength (C_u) for each test is given here: the full strength-depth profiles are relegated to Appendices A to G. To better understand the role of lime in the chemical reaction with clay minerals during curing of the admixtures, pH measurements were taken for these soils at various stages.

5.2 Undrained Shear Strength

The values of undrained shear strength (C_u) reported in this chapter (and Appendices A-G) were obtained from measured bearing pressures q, according to the following equations (from Chapter 3):

$$C_u(z) = q_{net}/N_c \qquad 5\text{-}1$$

where

$$q_{net} = q - \gamma\, z \qquad 5\text{-}2$$

and,

$$N_c = A - Be^{-M\left(\frac{Z}{D}\right)^N} \qquad 5\text{-}3$$

where: $A = 11.0$, $B = 4.9$, $M = 1.06$, and $N = 1.1$.

The depth-averaged value of the undrained shear strength over the range $z_1 \leq z \leq z_2$ is:

$$C_u = \frac{1}{L}\int_{z_1}^{z_2} C_u(z).dz \qquad 5\text{-}4$$

where $L = z_2 - z_1$

For the "*sealed*" (S) specimens, the limits are taken to be:

$$z_1 = D \quad , z_2 = h - D$$

where h is the height of the soil specimen.

For the "*flooded*" (F) specimens, the limit z_1 is commonly taken to be 2D except for samples cured for the longest periods. In these cases, if visual inspection of the penetration resistance data reveals that softening extends below 2D from the surface, then a higher value of z_1 is selected.

Given that the penetration resistance data is recorded at equal depth intervals (Δz=0.125mm), the above integral can be replaced by summation:

$$C_u = \frac{1}{N}\sum_{i=1}^{N} C_u^i \qquad 5\text{-}5$$

where N computations of the undrained shear strength C_u^i are carried out over the range $z_1 \leq z \leq z_2$. Typically, N > 800.

The distribution of the discrete data C_u^i can be analysed to determine their standard deviations. These will be the results of measurements errors; sample inhomogeneity; errors in N_c approximation; departures from the assumed test boundary conditions; etc.

The standard deviation data (and the corresponding COVs) for each test are recorded in the appendices. The median COV for all tests is ca 4% which demonstrates that it is possible to identify an (unique) undrained shear strength for each soil with good precision.

5.3 Repeatability of Tests

In most cases, the penetration tests were repeated on duplicate samples; sometimes more than once. The arithmetic mean of the test results was assumed to be the population mean, and the standard deviations and coefficient of variation were computed on that basis. Thus, for a set of two tests, the standard deviation is equal to one half of the difference between the two test results. For brevity, these data are tabulated in the appendices, from which we draw the following conclusions:

Excluding just 1% of the data as outliers, the median COV is 3.4% and the mean COV is 4.4%. The largest COVs were generally associated with low values of C_u. This evidence of good repeatability lends confidence to the interpretation of the influence of factors such as dosage rates, water content, temperature, etc. on the undrained shear strength of these soils.

In general, comparable standard deviations and COV's were obtained for remoulded soils despite the fact that hand remoulding is affected by personal judgment.

However, some results were less reliable, such as the data for the SW-K soils recorded in Appendix B. While the COV of test results for intact and remoulded specimens (as summarized in Table B.2) is less than 2% after 365 days of curing, the corresponding figure at the very early stages is ca 10%. This suggests that the penetration test is less reliable for measuring the strengths of very weak soils. This may in part be attributable to unpredictable differences in the test conditions (e.g., cavity closure).

The undrained shear strength profiles of long-term cured SW-K soils treated with 5% lime exhibited significant oscillations in the strength profile of about 0.25D periodicity. This response may be the result of slip-plane generation, as predicted by the numerical modelling of deep steady penetration resistance of ball penetrometers in sensitive clays (Zhou and Randolph, 2009b).

5.4 Curing Technique

Two different curing techniques were employed to prevent water content loss during long term curing. The first technique was by flooding (F) the mould with water and the second was by sealing (S) the soils. Flooding progressively softens the upper layers over time. However, this effect depends on lime content. Figure 5-1 shows the results of penetration tests conducted on kaolin clay (K2) at $1.8W_{LL}$ treated with 1%, 3%, and 5% lime, using both techniques and cured for up to 365 days. Figure 5-1a shows the bearing pressure profiles of these soils and Figure 5-1b shows their undrained shear strengths. For the flooded soils (F), the bearing pressures at shallow depths is very low compared with the corresponding results for the sealed specimens (S). Thus, the flooded soils have lower undrained shear strengths, as shown in Figure 5-1b. For soils with 1% lime content, marked softening occurs to a depth of about half the thickness of the soil sample, but a thinner layer of soil is softened if the lime content is 5%. Evidently, flooding allows diffusion of lime from the soil into the overlying water. This is supported by the observation of the cured

specimens in which the diffused lime reacts with the carbon dioxide in the air to form a white crust of calcium bicarbonate on the water surface. Also pH measurements of the top softened layer of soil gave values of 11.0 or even less compared with pH values of 12.0 or more those of sealed specimens indicating a depletion of lime at least from top softened layer.

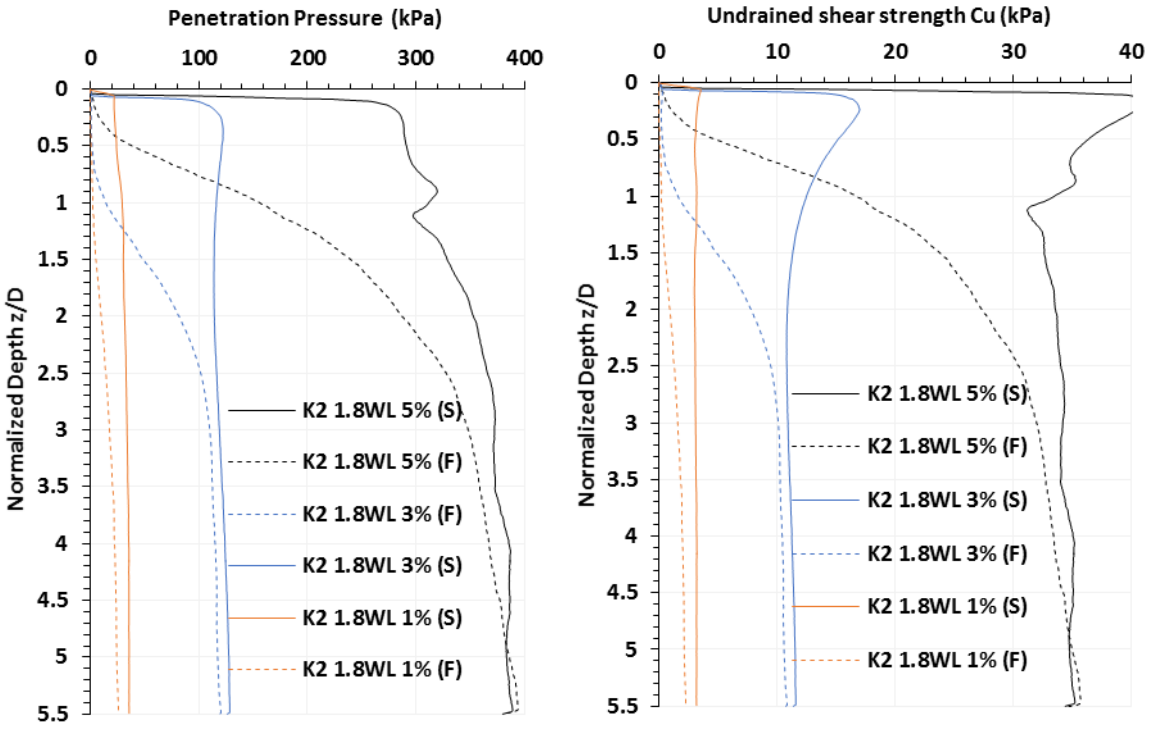

(a) Penetration pressure profile (b) Shear strength profile

Figure 5-1: Penetration test results for lime-admixed kaolin clay (K2) at 1.8W_{LL} and cured for 365 days: (a) bearing pressure, and, (b) undrained shear strength

The results shown in Table A.1 to Table A.9 indicates that the coefficients of variation of the sealed samples are significantly lower than those obtained using the flooding technique.

An illustration of the effects of curing technique on intact undrained shear strength is shown in Figure 5-2. In general, the flooding technique yields lower mean undrained shear strengths compared with the results obtained using the sealing technique, despite the (subjective) exclusion of those upper zones where softening is apparent. For soils with 1% lime content (Figure 5-2(a)), the softening is so extensive that the depth-averaged undrained shear strength at one year is less than the value obtained at 100 days. In addition, softened soil trapped beneath the disc can be dragged down with the penetrometer, resulting in a lower measured penetration resistance, as predicted by Hossain and Randolph (2009b).

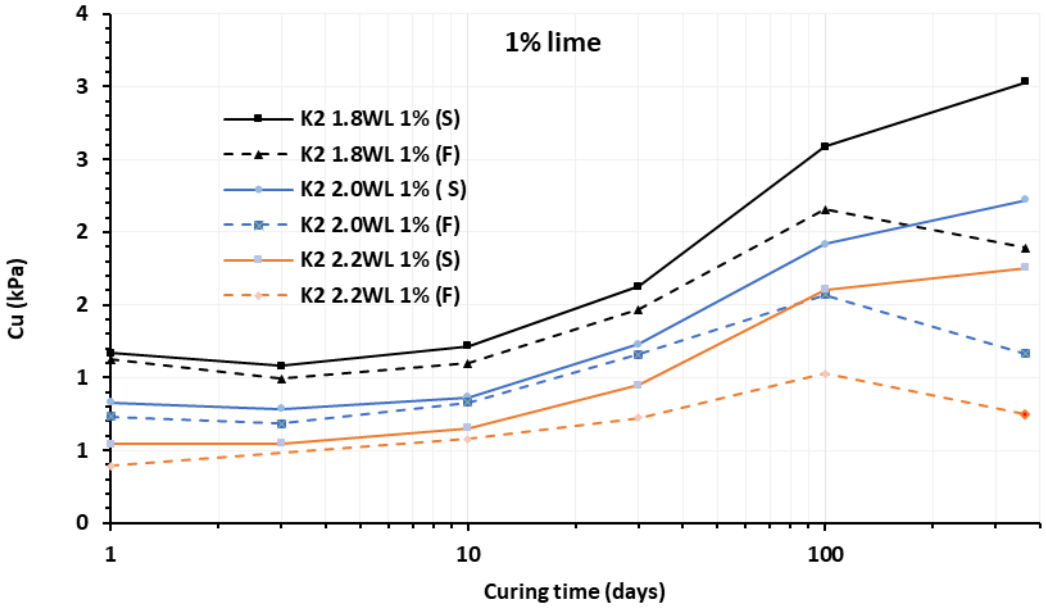

(a)

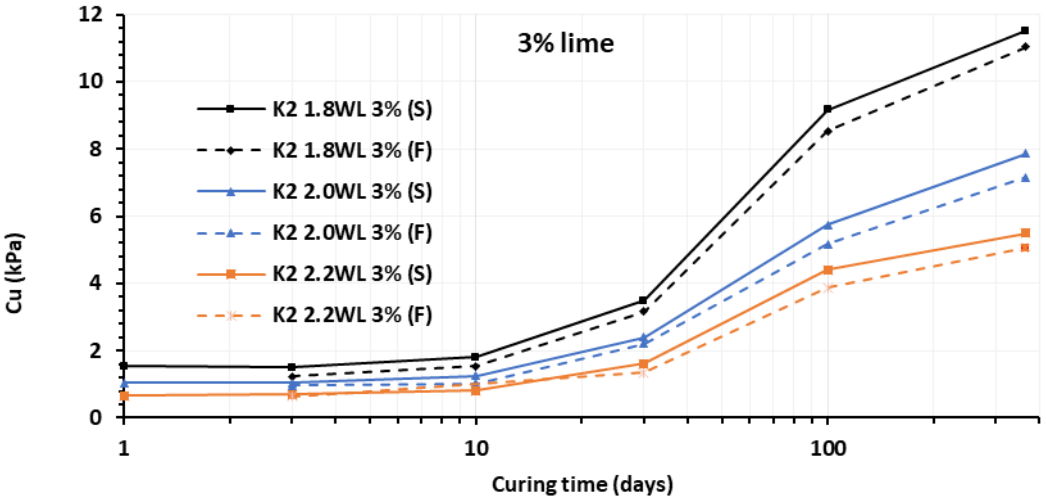

(b)

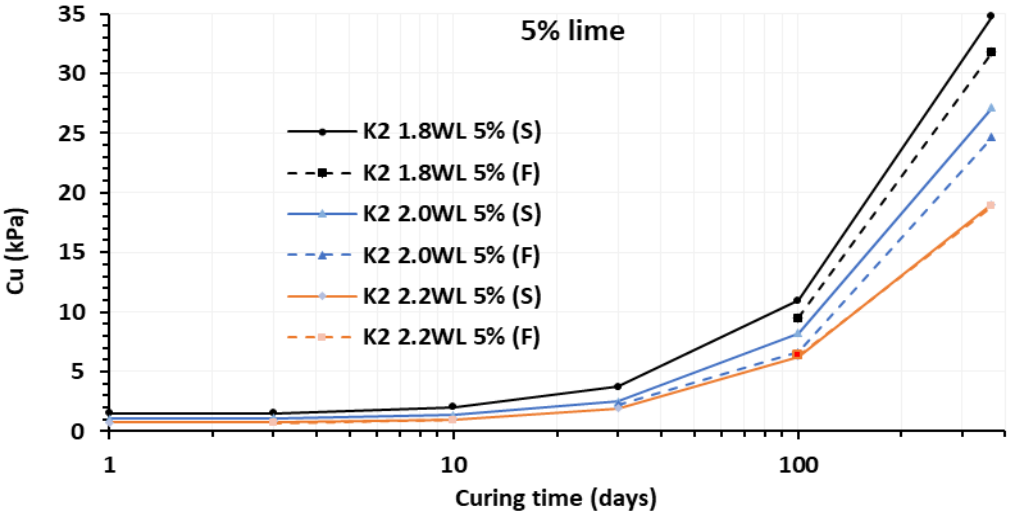

(c)

Figure 5-2: Effect of curing on the undrained shear strength of lime admixed kaolin clay (K2): (a) 1%, (b) 3%, and (c) 5% lime.

Figure 5-3 shows the effect of lime diffusion on the strength of remoulded admixed kaolin (K2) soil. No effect of flooding can be detected on the remoulded undrained shear strength up to 100 days of curing but after that time a noticeable reduction in strength occurs. Evidently beyond this time sufficient diffusion of lime occurs to reverse the ion exchange reactions and return the soil back to its original state (Diamond and Kinter, 1966). This reversal is absent at higher lime contents.

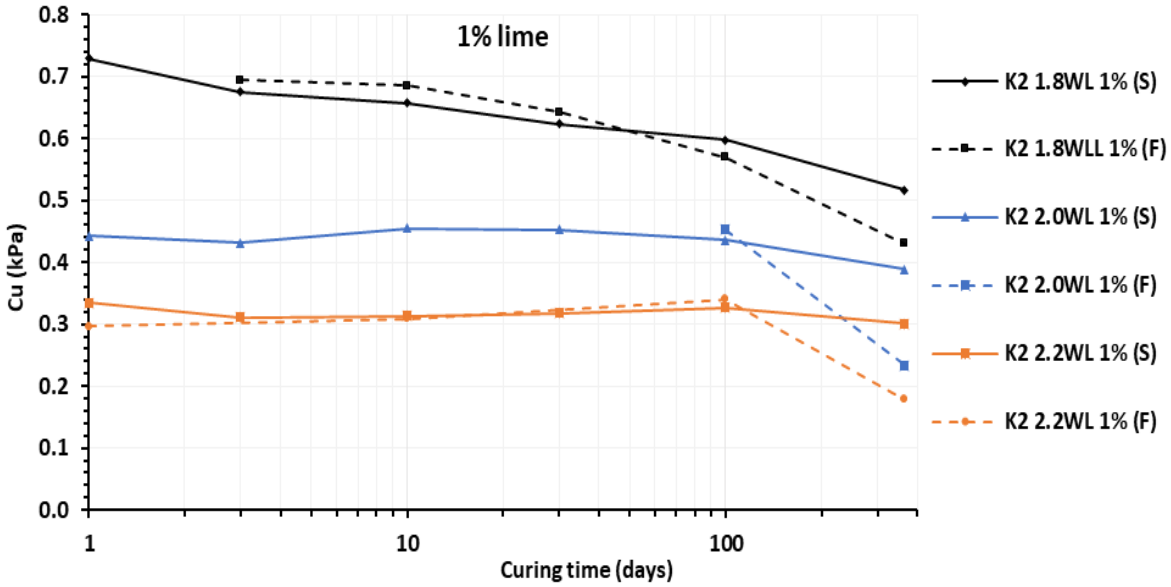

Figure 5-3: Effect of sample flooding on remoulded shear strength of 1% lime admixed kaolin (K2)

It appears that softening due to flooding depends not only on curing time but also on lime content. Figure 5-4 shows the strength profiles of flooded (F) lime-admixed kaolin samples at W=2.0 normalized by the corresponding shear strength Cu_{max} obtained from sealed (S) samples. The results show that the largest proportionate effect is on those soils with the lowest lime content and that the effect extends further into the soil.

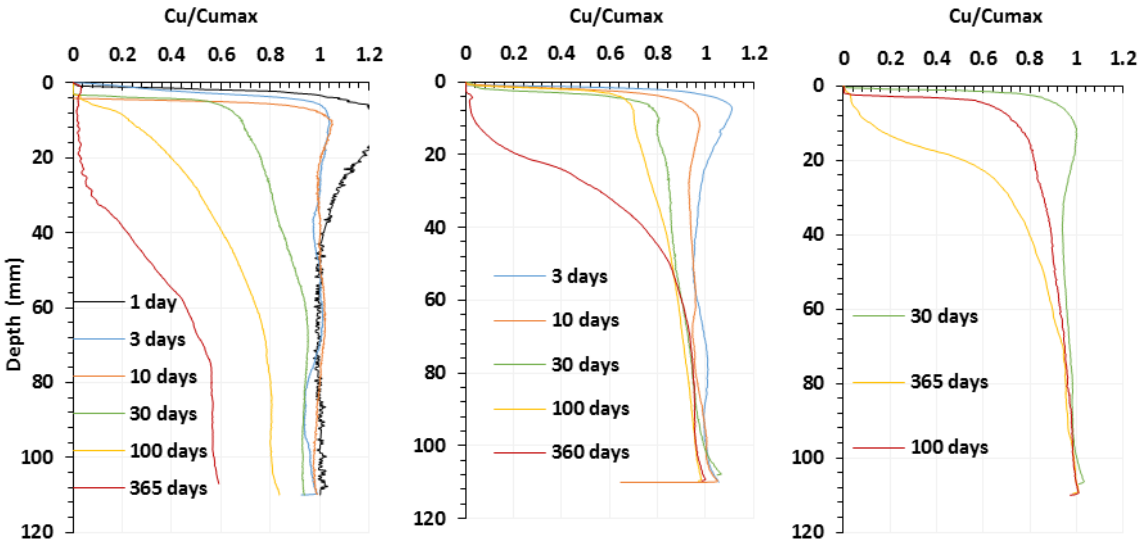

(a) 1% lime (b) 3% lime (c) 5% lime

Figure 5-4: Normalized strength profiles for lime admixed kaolin (K2). Flooded samples at $2.0w_{LL}$

5.5 Parametric Studies

The study encompasses a range of factors affecting the strength lime-admixed soil slurries, such as soil minerology, curing time, lime content, water content and curing temperature. All results were obtained using the sealing (S) curing technique unless otherwise stated.

5.5.1 Kaolin (K2) clay

The soil condition, water and lime contents, and temperature investigated for this soil type is summarized in Table 5-1 and Table 5-2.

Table 5-1: Scope of the parametric study

Curing period (days)	$W=w/W_{LL}$	Lime content %	Condition	Temp.
1 3 10 30 100 365	1.8 2.0 2.2	1 3 5	Intact Remoulded	Normal (20^{o}C)

Table 5-2: Summary of water content and lime content investigations.

$W=w/W_{LL}$	Lime content C (%)		
	1	3	5
1.8	●	●	●
2.0	●	●	●
2.2	●	●	●

Effect of curing time

The development of undrained shear strengths of these clays over time is shown in Figure 5-5. For all lime and water contents, shear strength increases with time. However, the strength gain increases with increasing lime content especially after long term curing. Figure 5-5 reveals the following trends: for 1% lime content, the ratio of 365-day strength to one-day strength is about three; for 3% lime content, the ratio is about eight while for 5% lime, it is about 15. The absolute values of the strengths at 365 days are very different too. For example, for $w_w=1.8W_{LL}$, the strengths for 1%, 3%, and 5% lime contents are 3.0, 11.5, and 35 kPa respectively. It can be seen that the strength at 365 days tends to continue to increase strongly for 5% lime but approaches a maximum for lower lime contents.

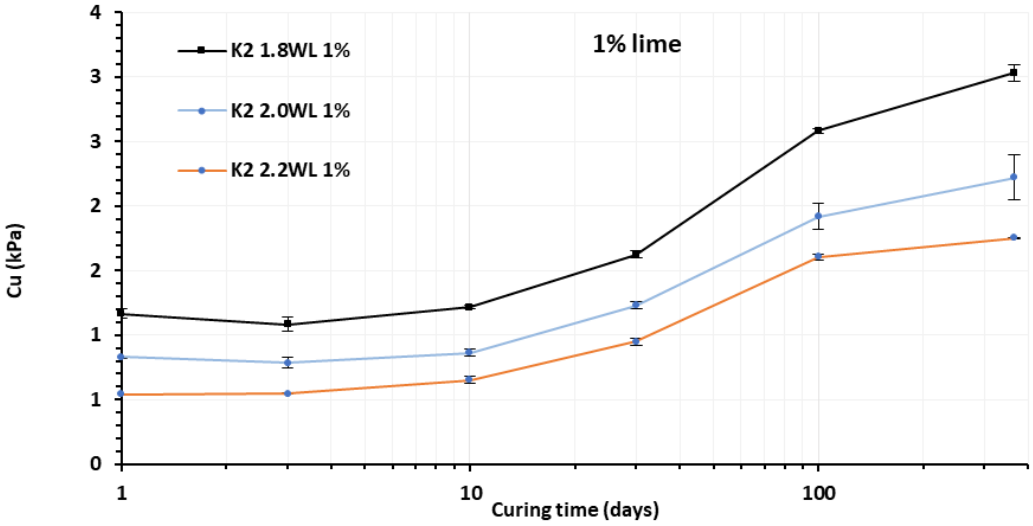

(a)

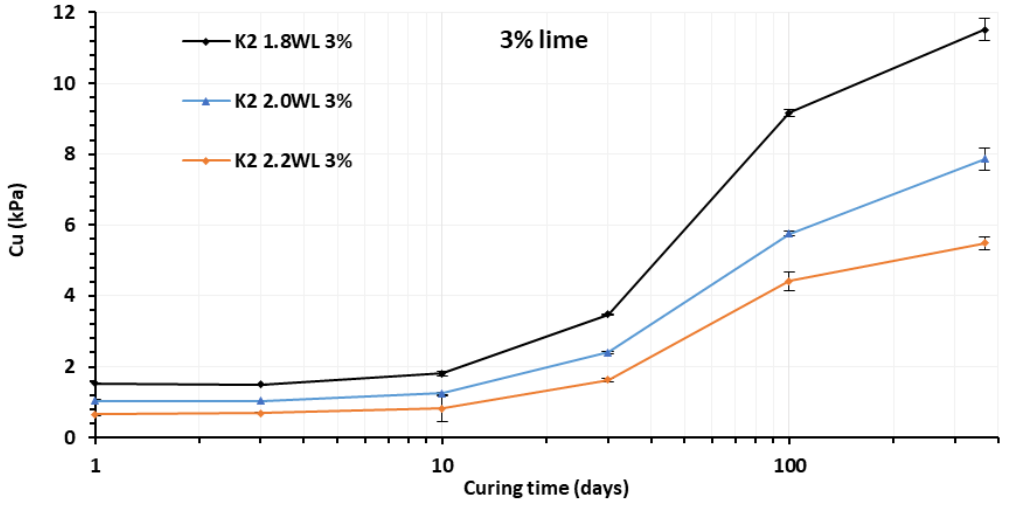

(b)

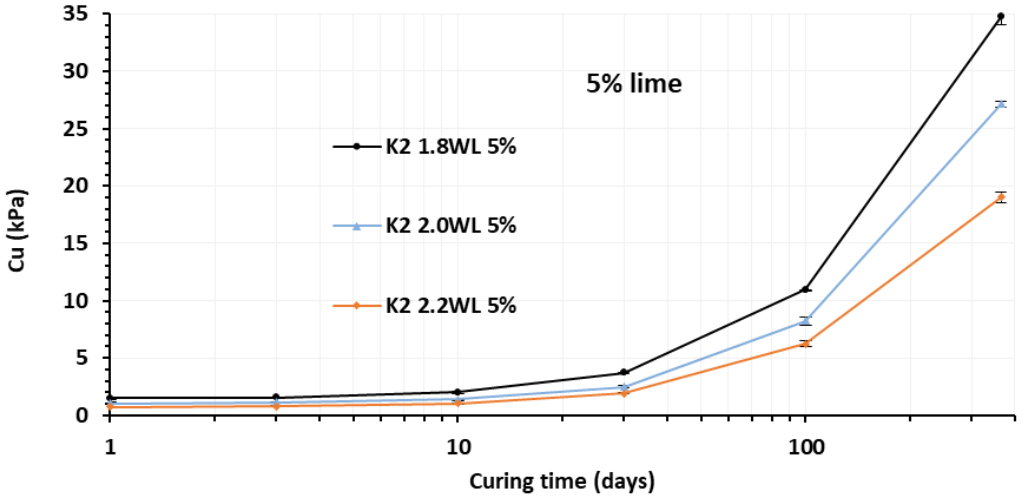

(c)

Figure 5-5: Undrained shear strength development of lime admixed kaolin (K2) clay: (a) 1%, (b) 3%, and (c) 5% lime contents.

These results are normalized with respect to their 30 days strengths in Figure 5-6. This emphasises the difference in long-term strength gain, as a function of lime content. This agrees with the observation that sufficient free calcium must be available to react with the clay minerals and to maintain a high alkaline environment.

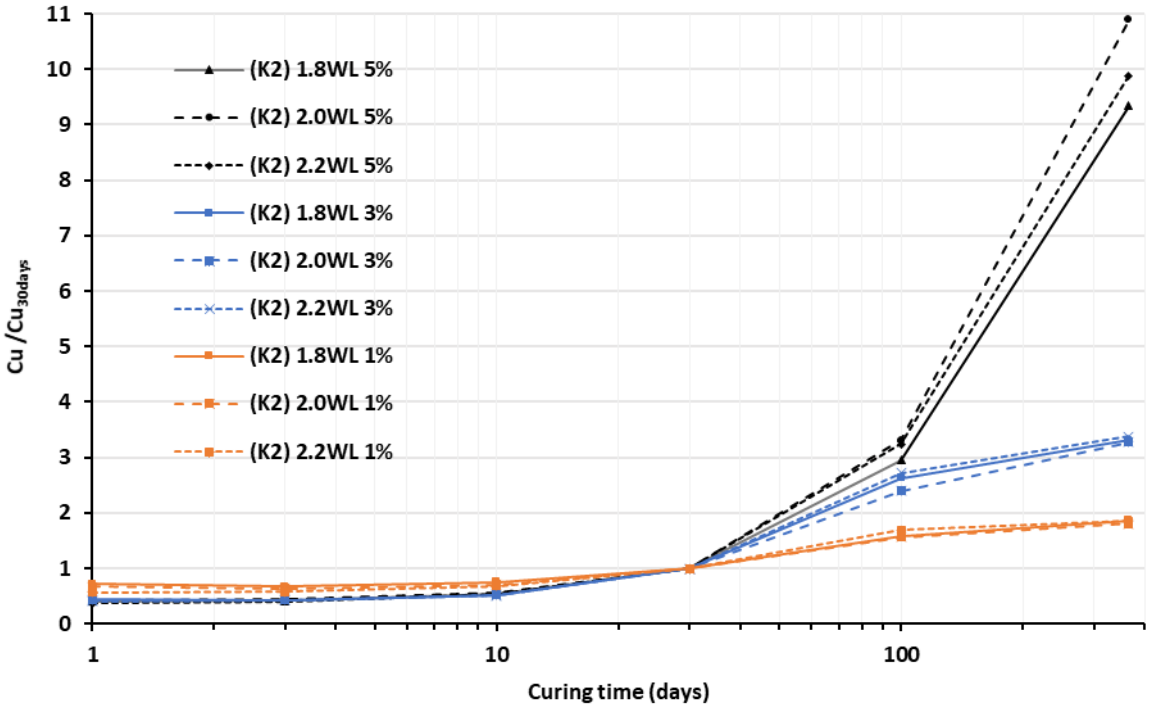

Figure 5-6: Normalized undrained shear strength of lime-admixed kaolin clay (K2)

Effect of lime content

As can be seen from the results shown in Figure 5-5, increasing the lime content significantly increases the undrained shear strength of kaolin. For kaolin slurries of W=1.8 after 365 days of curing, Cu increased to 3.1, 11.5, and 34.5 kPa for 1%, 3%, and 5% lime contents respectively. Normalizing the strengths with respect to the strength obtained using 1% lime (as shown in Figure 5-7) emphasises the point. The undrained shear strength of kaolin specimens treated with 5% lime after one year of curing is about 11-12 times the corresponding strengths for soils treated with 1% lime. For 3% lime content, the ratio after a year of curing is only 3-4.

A higher lime content also increases the rate of strength development with time. The one year strength of 1% lime treated soil exceeds the one-day strength by a factor of three: for a lime content of 5%, the factor is about 15.

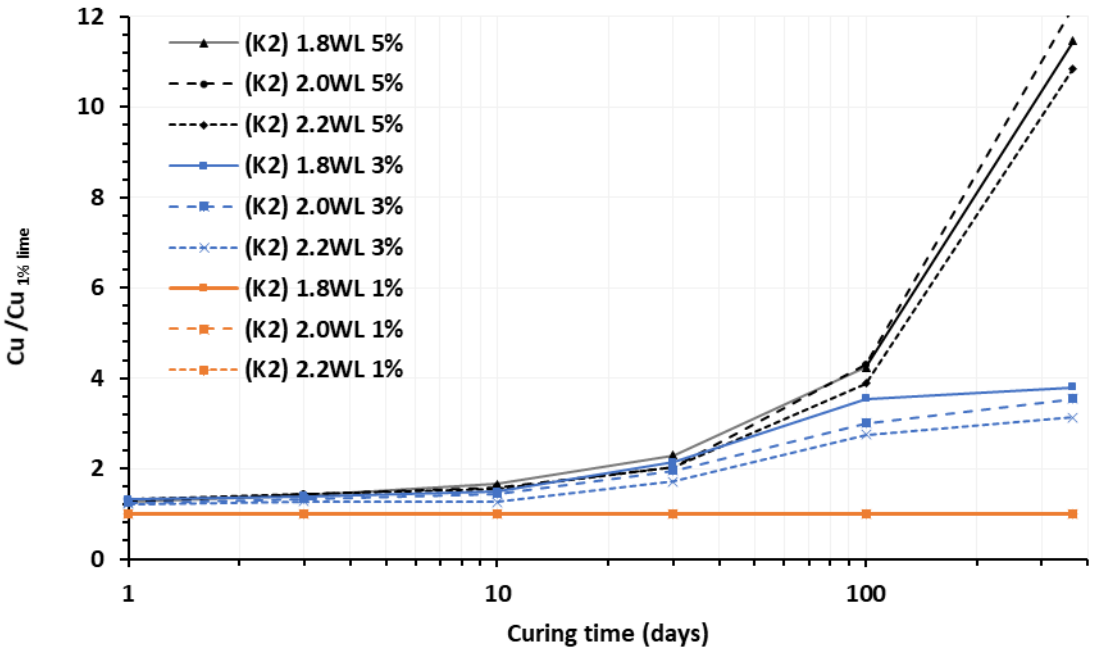

Figure 5-7: Undrained shear strength of lime-admixed kaolin clay (K2) normalized by the undrained shear strength of 1% lime-admixtures

The effect of water content

It is expected that soil strength must reduce with increased water content. However, normalizing strengths with respect to the strength of soils at $2.2W_{LL}$ water content (as shown in Figure 5-8) demonstrates the interesting result: the strength ratios of two soils of different water contents is largely independent of their lime content or curing period. Thus, for example the ratio of the strength of a soil with $w=1.8W_{LL}$ compared with a soil with a $w = 2.2W_{LL}$ is approximately two (2.0), regardless of the lime dosing rate, or the curing period. For a soil with $w = 2.0W_{LL}$, the ratio is approximately 1.5. These ratios do narrow slightly over time. Thus, the strength development of these lime-treated soils is relatively unaffected by changes in water content.

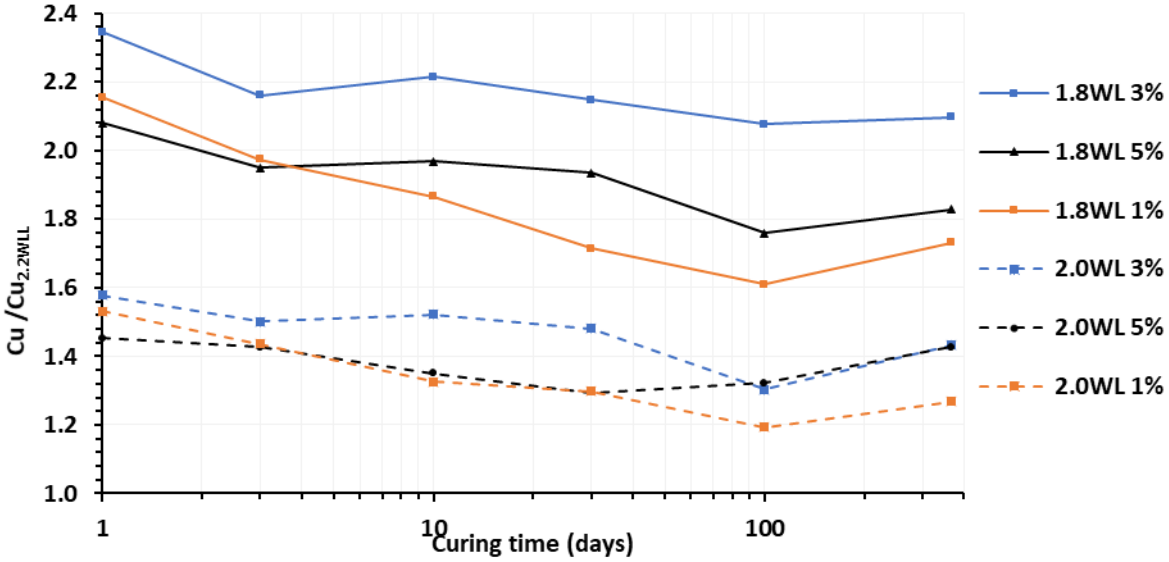

Figure 5-8: Undrained shear strengths of lime-admixed kaolin clay (K2) normalized with respect to the undrained shear strengths at $2.2W_{LL}$ water content

Remoulded shear strength

After curing, lime-admixed kaolin clay (K2) soils were remoulded by hand and their remoulded strengths were measured, Figure 5-9. A considerable drop in strength occurs due to remoulding, especially after long-term curing. For example, at $w=1.8W_{LL}$ and 5% lime content, after one year of curing, the undrained shear strength dropped from 34 kPa to 2.2 kPa, although this remains several orders of magnitude higher than the untreated soil. The major contribution to the cohesive improvement can be attributed to cementation bonding between particles during the pozzolanic reaction while the minor contribution arises from the ion exchange process. Although some (or all) of these gains may be lost if subsequent changes in pore water chemistry, due to diffusion or leaching of lime, reverses these reactions (Diamond and Kinter, 1966), mechanical restructuring has a lesser effect.

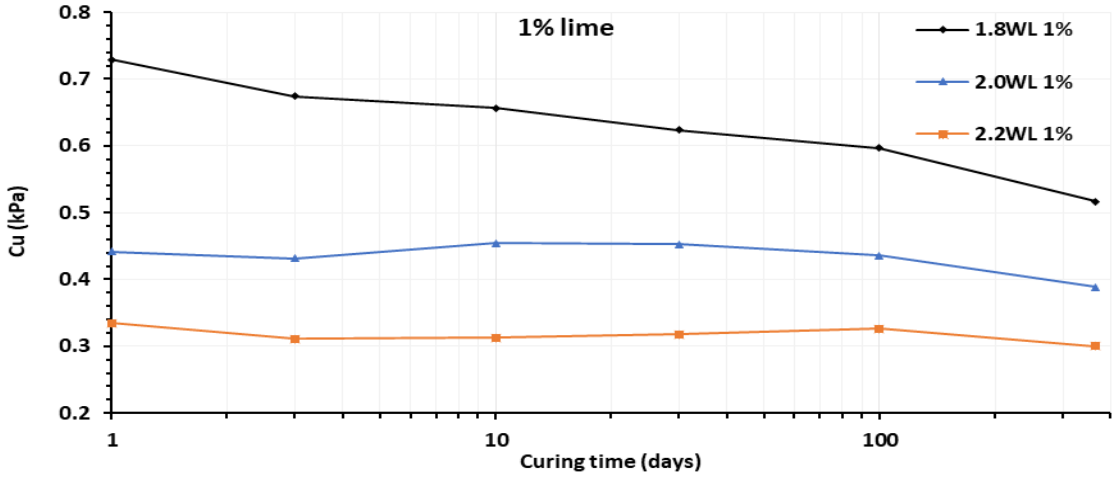

(a)

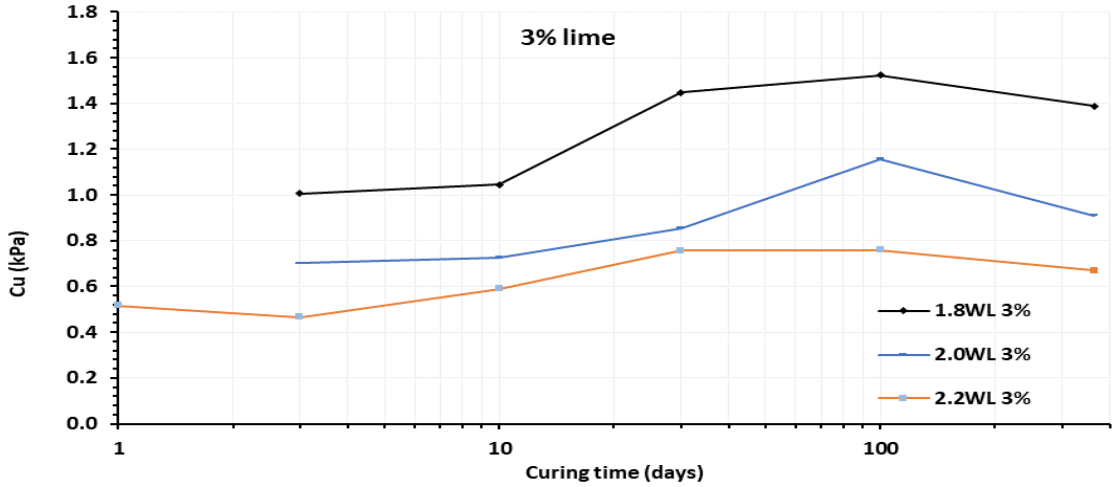

(b)

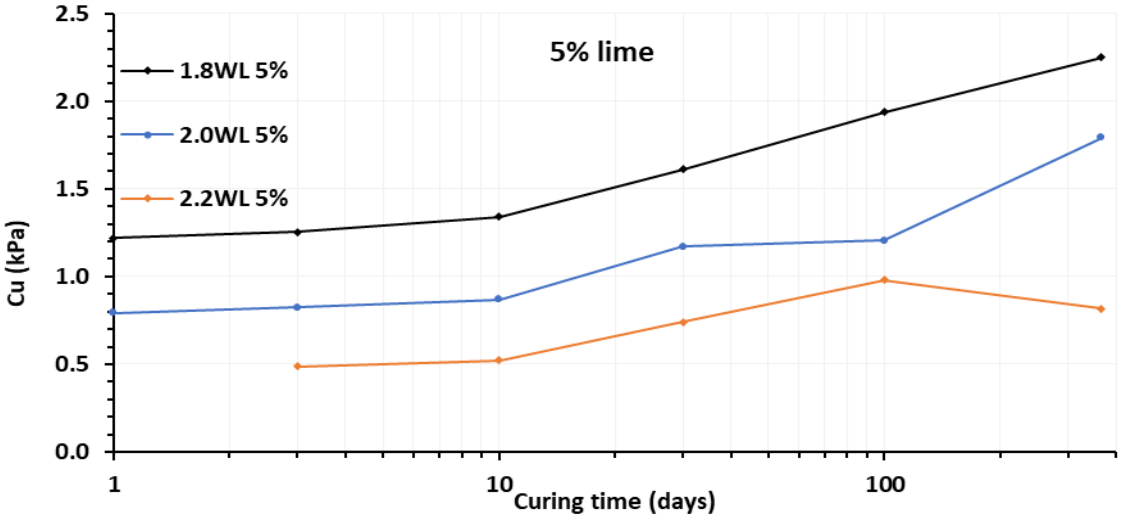

(c)

Figure 5-9: Remoulded undrained shear strength of lime-admixed kaolin: (a) 1%, (b) 3%, and (c) 5% lime contents.

Strength sensitivity due to remoulding

Figure 5-10 shows the development of strength sensitivity (S_t) in lime-admixed kaolin. Remarkably, soils with the same lime contents reach after one year the same sensitivities,

irrespective of water content. A similar observation for naturally structured clays has been noted by Sahdi et al. (2014).

The sensitivities after one year are 5.8, 8.4, and 15.4 for 1%, 3%, and 5% lime contents respectively. These are not very high sensitivities; a very high proportion of the strength is retained. This is quite unlike some natural quick clays, where collapse to a liquid state occurs.

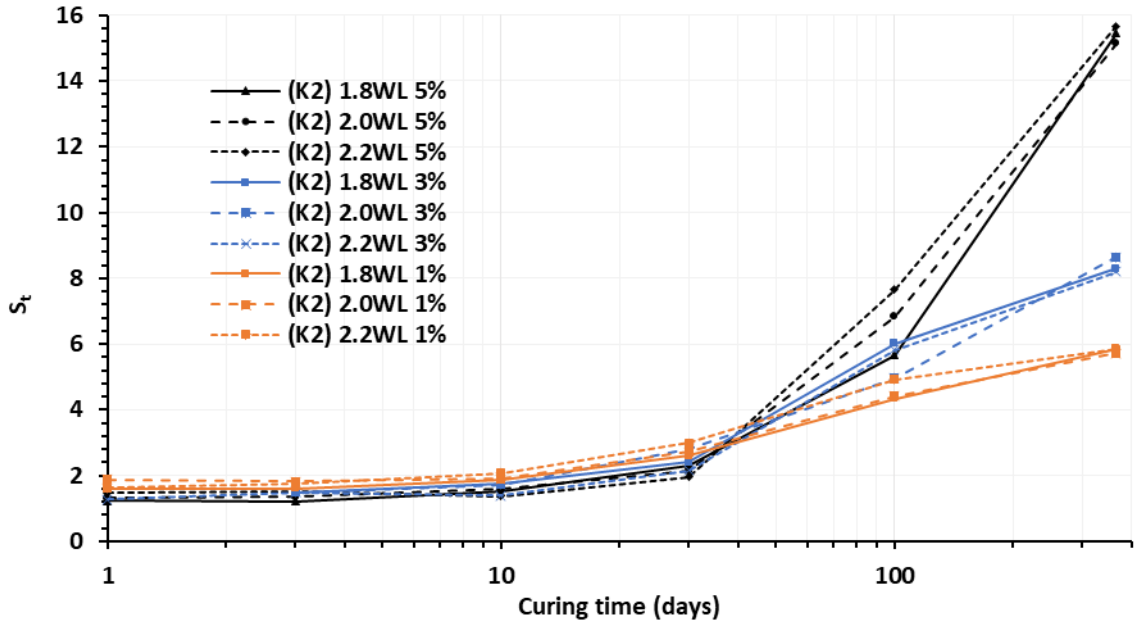

Figure 5-10: Strength sensitivity (S_t) of lime-admixed kaolin

Evolution of pH in kaolin

Figure 5-11 shows pH measurements for these lime treated kaolin soils. As expected, the higher the lime content, the higher was the initial pH value at the beginning of curing. Initial pH values are more strongly affected by lime content than water content. The initial pH values for soils treated with 3% and 5% lime are similar at about 12.8 compared to 12.5 for 1% lime. With increasing curing time, the pH decreases gradually due to the conversion of lime in the pozzolanic reaction process, as observed by (Al-Mukhtar et al., 2010). After ten days of curing, the rate of pH decrease tends to become constant with time. For 1% lime content, the pH dropped after one year to about 11.7, which is lower than the in the case of 1% lime which is lower than the nominal theoretical value of 12.0 which is necessary to sustain the pozzolanic reaction. For the 3% and 5% lime contents, the pH values approach 12.0, which suggests that the free lime is virtually depleted.

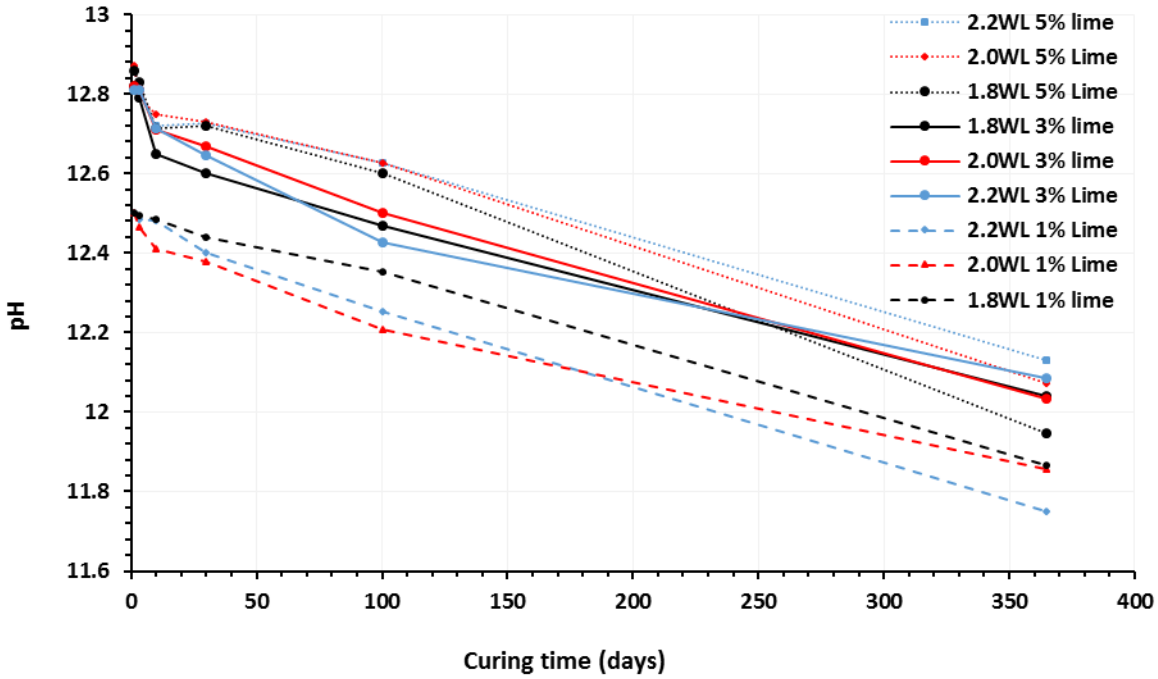

Figure 5-11: Evolution of pH in lime treated kaolin (K2)

Relationship between sensitivity and plasticity index

The plasticity indices of remoulded lime-admixed kaolin (K2) after 365 days of curing are listed in Table 5-3 below, and plotted in Figure 5-12. While both the liquid and plastic limits increase with increasing lime content, the plasticity index remains virtually unchanged.

Table 5-3: Index properties of lime-admixed kaolin after 365 days of curing

Lime C (%)	W_{LL}	W_{PL}	P.I.
0	67	34	33
1	76	38	38
3	86	52	35
5	98	61	37

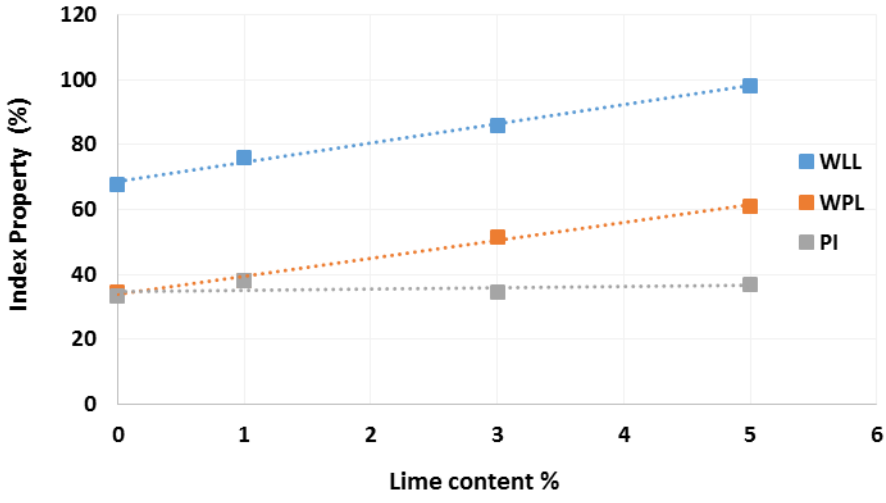

Figure 5-12: Plasticity indices of lime-admixed kaolin after 365 days of curing.

A correlation between sensitivity and liquidity index has been suggested by Wood (1990) for naturally structured soils (see Figure 2-28). For lime-admixed clays (after 365 days) the relationship is shown in Figure 5-13. However, this shows the opposite trend to that suggested by Wood (1990) and demonstrates the very different nature of chemically stabilized soils.

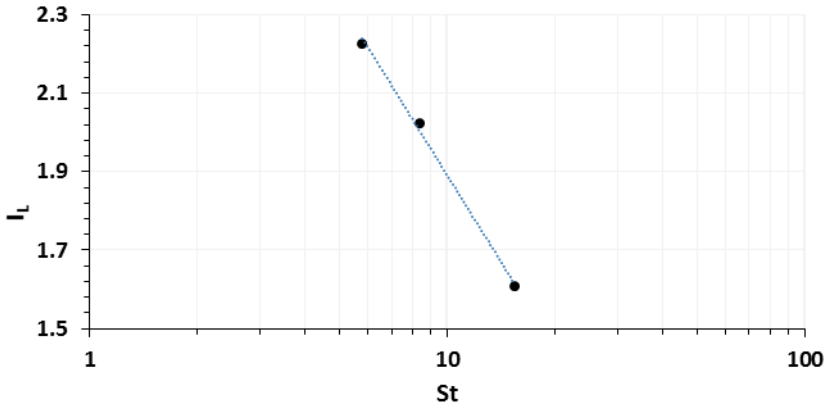

Figure 5-13: Correlation between liquidity index and the sensitivity of lime-admixed kaolin after 365 days

5.5.2 SW-K mix

The scope of the parametric study for this clay is summarised in Table 5-4. The lime-admixed slurries were prepared at the water and lime contents shown in Table 5-5.

Table 5-4: The scope of the parametric study

Curing period (days)	W=w/w_{LL}	Lime content C(%)	Condition	Temp.
1 3 10 30 100 365	1.8 2.2	3 5	Intact Remoulded	Normal (20°C)

Table 5-5: Water content and lime content combinations

W=w/w_{LL}	Lime content C (%)
1.8	**5**
1.8	**3**
2.2	**5**

Effect of lime content

The full results for the penetration tests conducted on this soil are given in Appendix B. Figure 5-14 shows how the undrained shear strength of these soils develops over time.

Interestingly, at one day, the undrained shear strength of the soil at a water content of $1.8W_{LL}$ water content slurries and 3% lime content is higher than that for a 5% lime content Adding more lime to this soil makes it more liquid. This may be attributed to the fact that the initial ion exchange process reduces the liquid limit of the soil and hence as more lime is added, the greater is the reduction in the liquid limit. This response of plastic soils to lime treatment has been noticed by other researchers (e.g., Bell (1996)). However, over time, the pozzolanic reaction dominates and higher strengths are obtained at higher lime contents. For W=1.8 after 365 days of curing, the undrained shear strength increases to 10.4 and 31.5 kPa for 3% and 5% lime contents, respectively. Remarkably, these values are very close to the Cu values obtained for kaolin at W=1.8 dosed with same lime contents. These values were 11.5 and 34.5 kPa for 3%, and 5% lime contents, respectively.

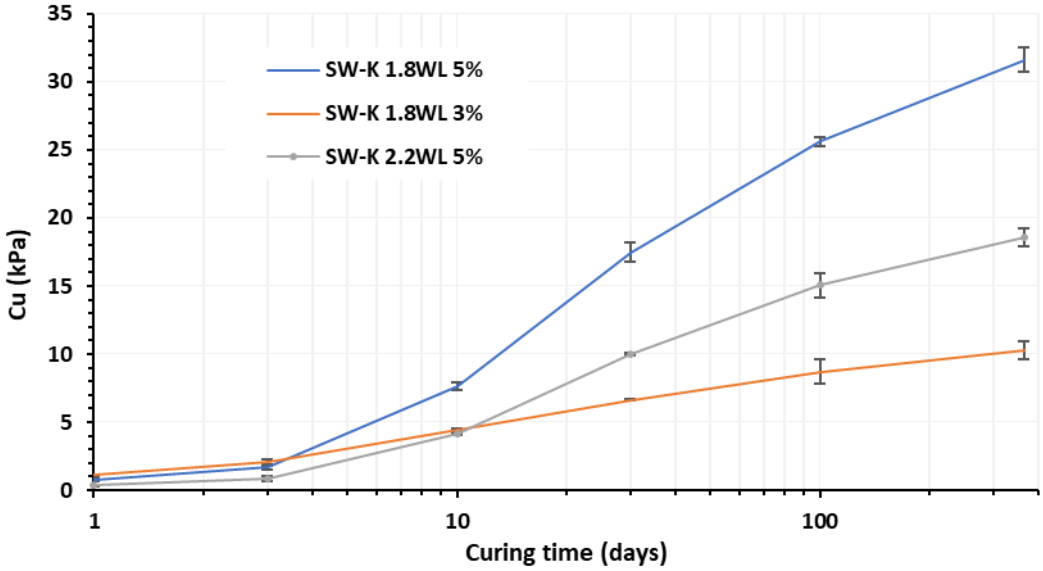

Figure 5-14: Undrained shear strength of lime-admixed SW-K soil

Effect of curing time

Normalizing the above results by their 30-day strengths (as shown in Figure 5-15) reveals that the trend of strength development is not strongly affected by initial water content, as also observed for kaolin soils (Figure 5.7) However, the short-term rate of increase in strength with time is higher for this soil than that of kaolin clay. For instance, the ratio $C_{u(365)}$ / $C_{u(30)}$ for this soil treated with 5% lime is only 1.8 while it was approximately ten (10) for kaolin. In other words, the time required for montmorillonitic soils to gain appreciable strength is much less that for kaolinitic soils. More than 50% of the strength gain in the montmorillonitic soil was achieved within the first 30 days of curing.

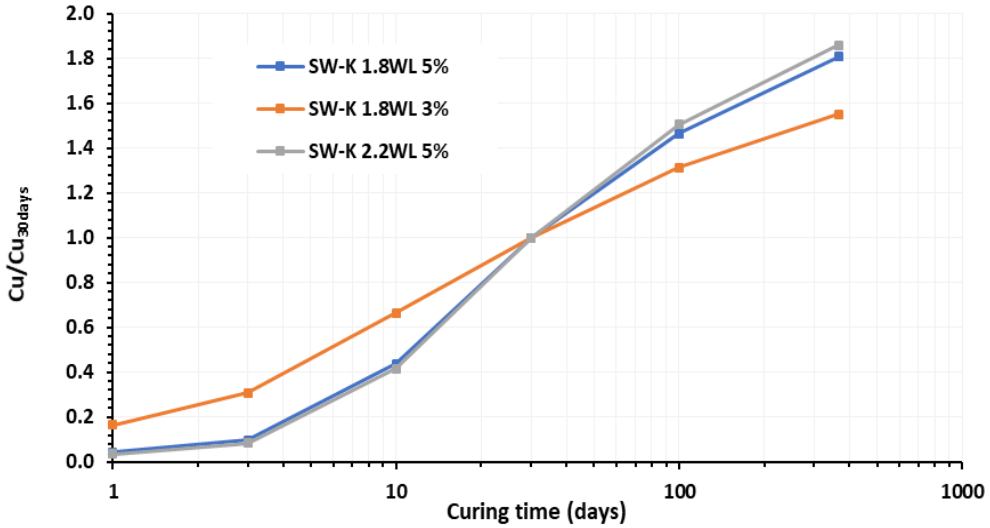

Figure 5-15: Normalized undrained shear strength of lime-admixed SW-K soil

Remoulded Strength

The results of penetration tests conducted on the same soil after hand remoulding are also summarized in Appendix B. The development of the remoulded undrained strength of these soils is shown in Figure 5-16. The soil increases in strength up to 100 days, but very little further strength gain occurs thereafter. At 100 days, the remoulded strength is 4.2 kPa for W=1.8 and 5% lime, compared to less than 0.5 kPa at one day. These values are evidently a fraction of the intact strength of 32 kPa after one year of curing,. Nevertheless, substantial strength remains (compared to the untreated soil). Again, up to about 30 days, the remoulded strength of the 3% lime content soil is higher than that for the 5% lime content soil, due to the decrease of the soil affinity to water (decreasing W_{LL}) with increasing lime content, as discused earlier. After 30 days of curing, the bonding is not easily broken by hand remoulding.

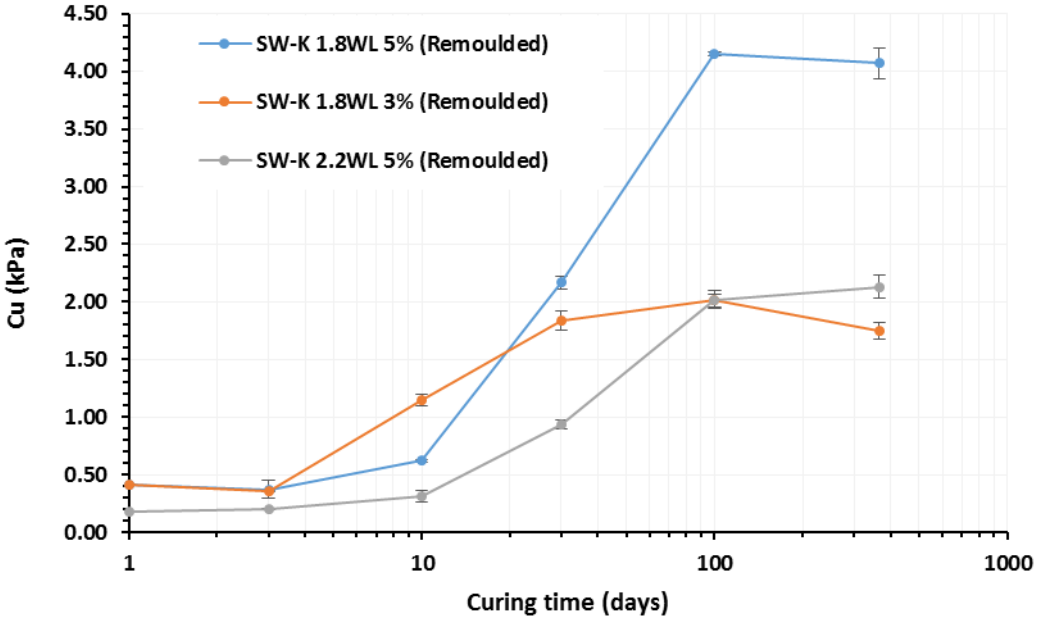

Figure 5-16: Remoulded undrained shear strength of SW-K soil

Strength sensitivity due to remoulding

Figure 5-17 shows the strength sensitivity S_t of these soils: these are typically in the range 8-10. As for the kaolin soils, the results show that strength is not strongly dependent on water content. However, the sensitivities are lower at $1.8W_{LL}$ than at $2.2W_{LL}$. The highly stable nature of the cementation bonding formed in these soils are not easily broken by 30 minutes of hand remoulding: the remoulded strengths are relatively high.

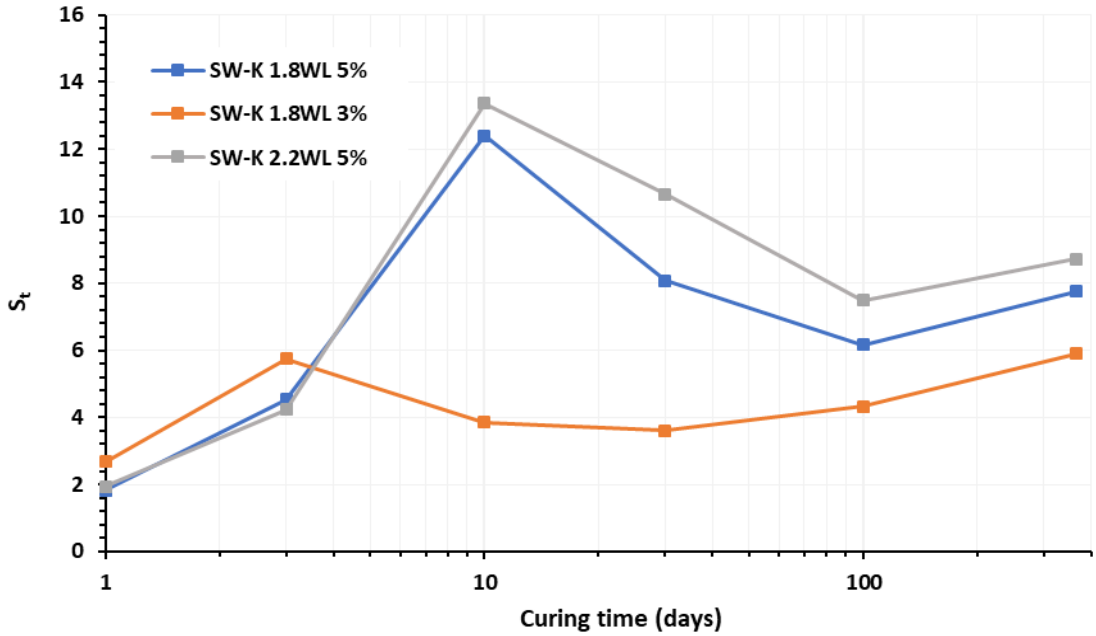

Figure 5-17: Strength sensitivity S_t of lime treated SW-K soil

pH development

Figure 5-18 shows the development of pH in these soils over time. The initial water content has only a minor effect on pH. Depending on the lime content, the consumption of lime causes a gradual decrease in pH. For 3% lime, pH begins to fall after 10 days as the lime is used up. For 5% lime, pH only begins to drop after 30 days. After a year of curing, the pH for 3% lime drops to about 11.6 indicating the depletion of all of the free lime. For 5% lime content, a pH value of 12 after one year suggests that the pozzolanic reaction may continue and further strength gain is possible.

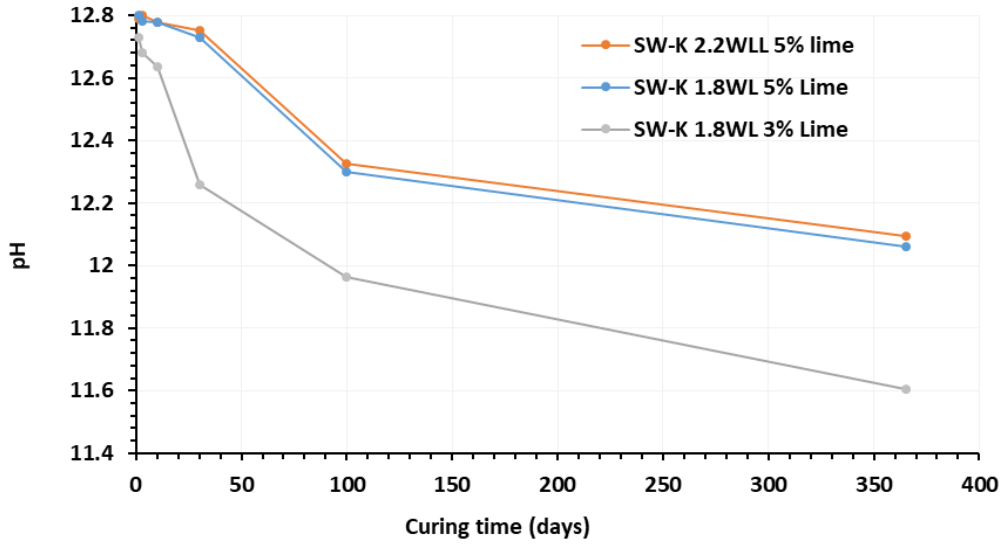

Figure 5-18: Evolution of pH in lime treated SW-k soil

5.5.3 CB montmorillonite

The scope of the parametric study on this soil is summarized in Table 5-6. The combinations of lime contents and water contents are listed in Table 5-7.

Table 5-6: Scope of the parametric study.

Curing period (days)	W=w/W_{LL}	Lime content C (%)	Condition	Temp.
1	1.8	3	Intact	Normal
3	2.2	5	Remoulded	(20°C)
10				
30				
100				
365				

Table 5-7: Water contents and lime contents

$W=w/W_{LL}$	Lime content C (%)
1.8	5
1.8	3
2.2	5
2.2	3

The full results of the penetration tests are given in Appendix C. The undrained shear strength profiles obtained from penetration tests of intact specimens are shown in Figure C.1 in Appendix C

Effect of lime content

The development of the intact undrained shear strength of these soils with curing time is shown in Figure 5-19. After 365 days of curing, slurries of W=1.8 admixed with 3% and 5% lime had strengths of 9 and 31 kPa respectively. The results indicate that in spite of the presence of calcium in the minerals of this soil, the ability of this montmorillonite to react with lime is very high. Higher strengths were obtained with increasing lime content. Again, the strengths at W=1.8 are very close to those obtained for kaolin and SW-K clays, despite the differences in their liquid limits.

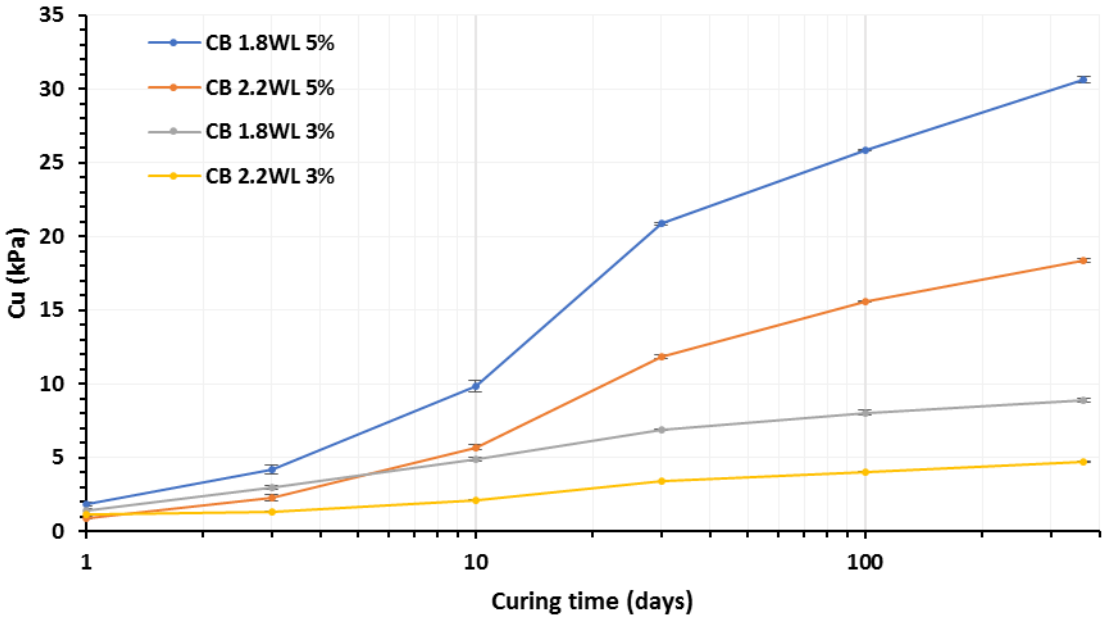

Figure 5-19: Undrained shear strength of lime-admixed CB bentonite soils

Effect of curing time

The results show a rapid early increase in the undrained shear strength with addition of lime. One month after curing, slurries of $1.8W_{LL}$ admixed with 5% lime, developed a strength of about 21 kPa, although the one-day strength was less than 2kPa. After 365 days of treatment, the strength increased up to 31kPa. This means that two thirds of the total strength gain was achieved within the first month of treatment, unlike kaolin where strength gain takes place over a much longer period of time.

Normalizing these strengths with the corresponding 30-day strengths, as shown in Figure 5-20, again reveals that the rate of strength gain follows a common trend. Despite some scatter in these results, two thirds of the maximum strength gains are achieved one month after mixing for all lime and water contents. Hence, curing samples of this soil for one month provides a good indication of the maximum expected strength. Looking more deeply into the results, it can be seen that the increase in strength for 5% lime is rather lower than for 3% lime. This may be attributed to the softening which occurs at higher lime contents at early times.

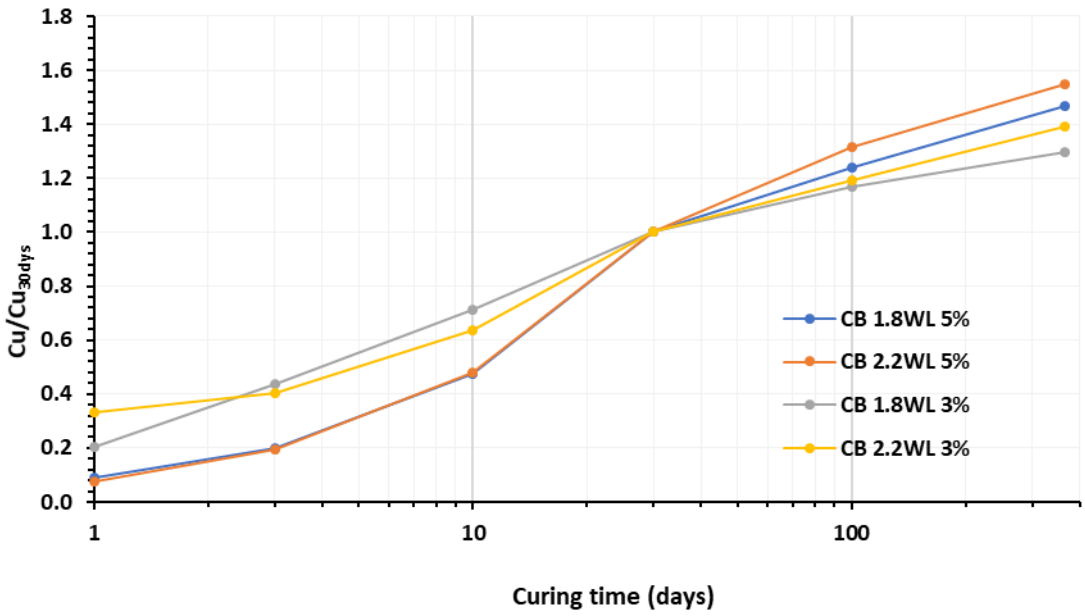

Figure 5-20:Undrained shear strength of CB montmorillonite normalized by their 30-day strengths

Remoulded undrained shear strength

The full results of penetration tests on these soils after hand remoulding are shown in Appendix C, summarized in Table C2. The development of remoulded undrained shear

strength with time is shown in Figure 5-21. Compared to the other soils investigated earlier, this soil suffers a higher drop in strength due to remoulding. For example, after 365 days of curing, the strength of the soil (w = 1.8W_{LL} , C = 5%) fell after remoulding from 31 kPa to 1.44 kPa. This is of course many times higher than the untreated soil strength.

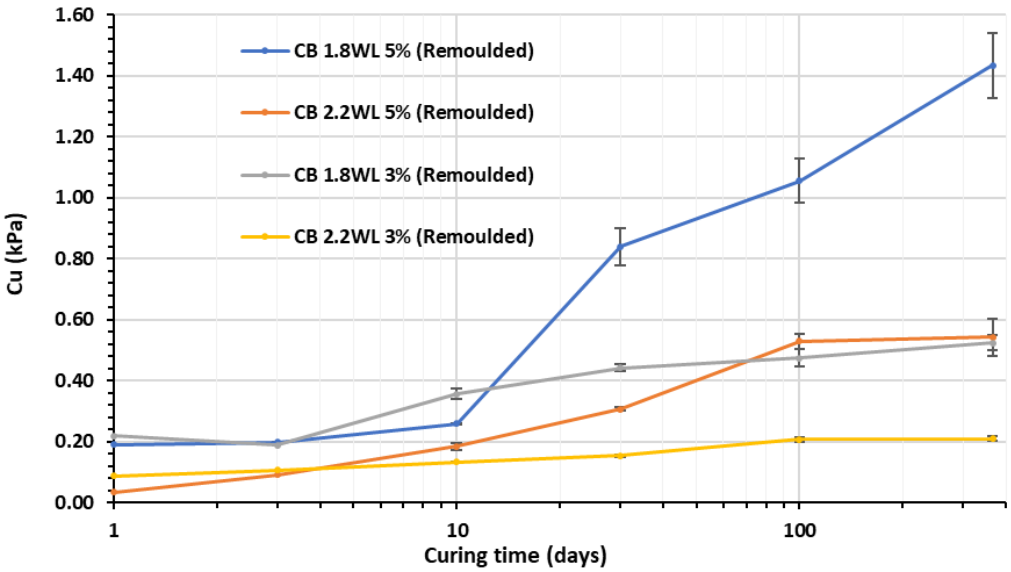

Figure 5-21: Remoulded undrained shear strength of lime-admixed CB bentonite

Strength sensitivity

The strength sensitivities of these soils due to remoulding are shown in Figure 5-22 below. Although these sensitivity values exhibit scatter, it is clear that high sensitivities in the range of 15-40 are achieved. Strain softening of this magnitude can make it difficult to establish peak undrained shear strengths using penetrometer test methods, particularly if the rate of strain softening is high. Close examination of the bearing resistance data suggests that some softening may have occurred.

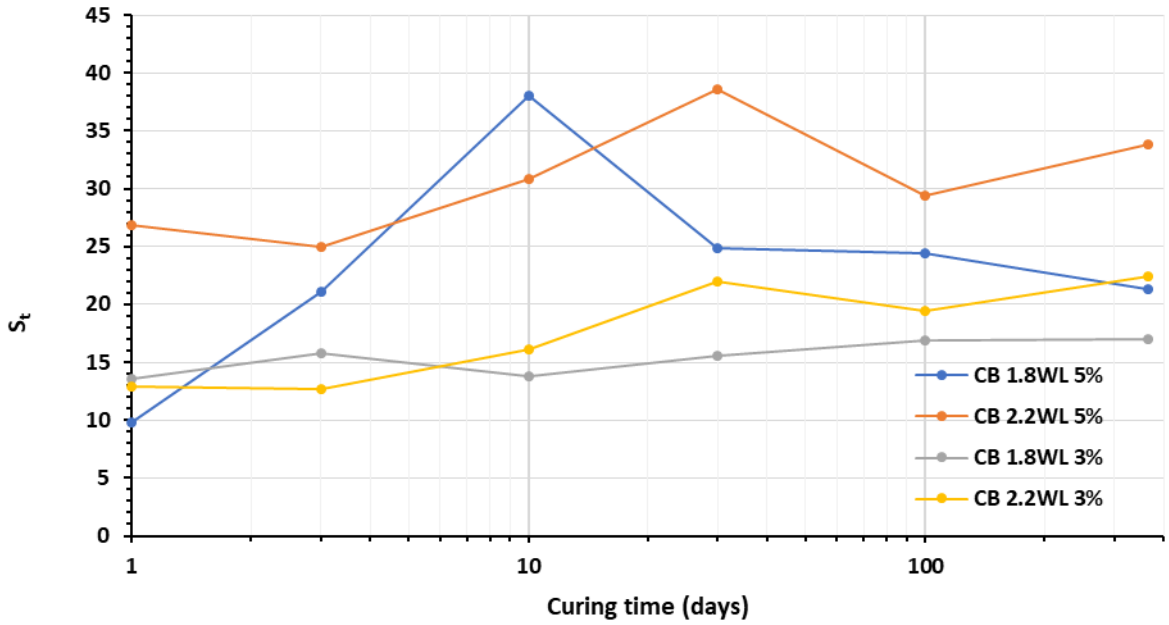

Figure 5-22: Strength sensitivity in lime treated CB montmorillonite

In addition, there are difficulties in the measurement of the undrained shear strength of these ultra-soft slurries. For example, for this soil at $2.2W_{LL}$ and 5% lime content, the remoulded one-day strength (Figure C2c) is of the order of 0.03kPa which cannot be measured accurately using the current apparatus. And, for such weak soils, back-flow of soil into the cavity is likely to occur during the penetration test, and this will be depth dependent. To overcome this latter problem, a bentonite slurry might be used to fill the cavity.

Evolution of pH in lime-admixed CB bentonite

Figure 5-23 shows the pH development in this clay over time. The decay in pH mostly occurs within 100 of curing when these soils develop most of their undrained strength. After that period, no further significant changes in pH occur as the free lime becomes depleted.

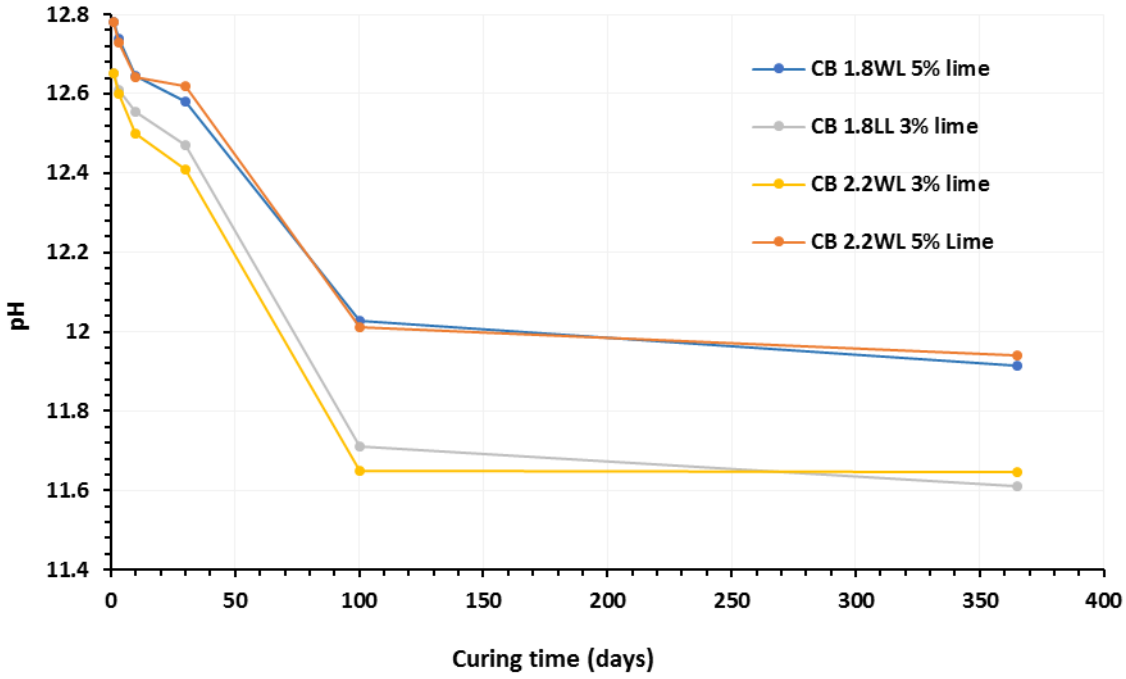

Figure 5-23: Evolution of pH in lime treated CB montmorillonite clay

5.5.4 Grangemouth soil

The scope of this parametric study is given in Table 5-8, and the combinations of water content and lime content in Table 5.9

Table 5-8: Scope of parametric study on Grangemouth soil.

Curing period (days)	$W=w/W_{LL}$	Lime content C (%)	Condition	Temp.
1 **3** **10** **30** **100** **365**	1.4 1.6	3 5	Intact Remoulded	Normal (20^oC)

Table 5-9: Combinations of water content and lime content

$W=w/W_{LL}$	Lime content C (%)
1.4	5
1.4	3
1.6	5
1.6	3

The full results of the penetration tests are given in Appendix D. Undrained shear strength profile data obtained from the tests of intact specimens are shown in Figures D1-D2, while the results are summarized in Tables D1-D2.

Effect of lime content

The development of undrained shear strength with curing time is shown in Figure 5-24. The most important finding about this soil type is that only (relatively) low strength gains could be achieved. The highest strength reached is no more than 4 kPa for a soil with $w = 1.4W_{LL}$ treated with 5% lime after 365 days of curing, while it was about 1.3kPa after one day. It was suspected that this might be due to the presence of organic matter in the soil, which gave the soil a dark colour. However, measurements of the organic matter, using two different techniques (as discussed in Chapter 3), showed that the organic content is only 7% which is less than the percentage loss of ignition for the kaolin soils. The reason for the weak effect of lime is the low clay mineral content, as revealed by the particle size distribution (Figure 3-4). Soils must contain enough pozzolana to react with the $Ca(OH)_2$ or otherwise adding more lime cannot yield additional strength (Janz and Johansson, 2002).

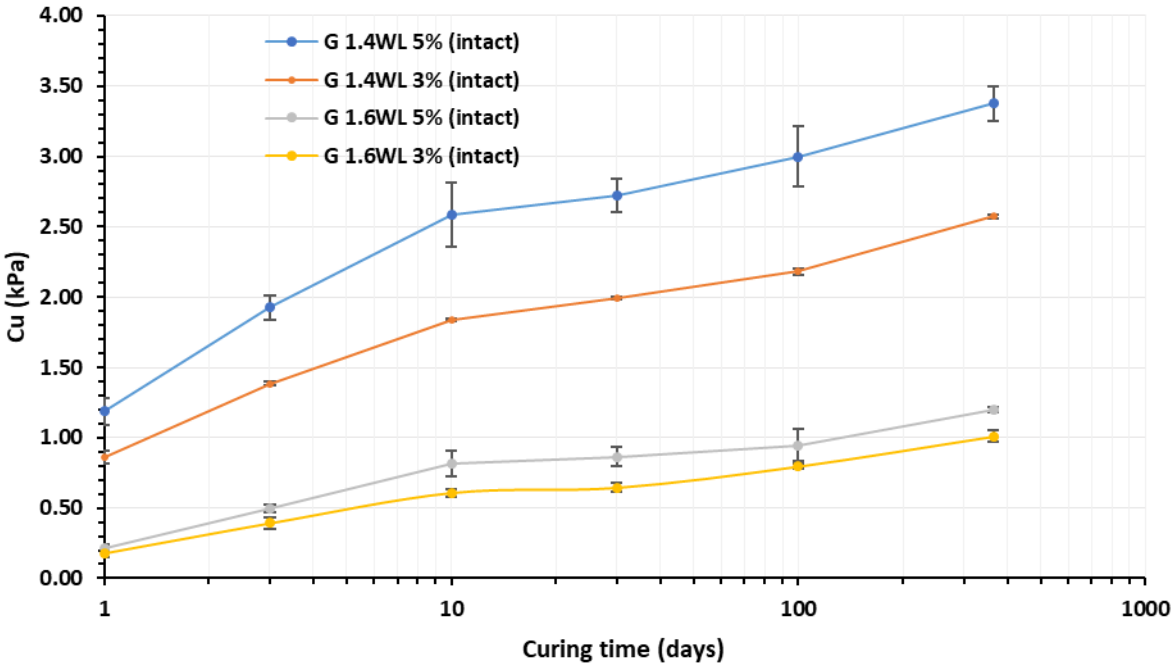

Figure 5-24: Undrained shear strength of lime-admixed Grangemouth soil

Effect of curing time

Normalizing this soil's strength with its 30-day strength yields the data shown in Figure 5-25. The normalized results reveal trends which differ from the other soils: the curves are group according to water content rather than lime content. This may be attributed to the reduced pozzolanic reaction in this soil: here the role of lime serves mainly to reduce the water content of the soil.

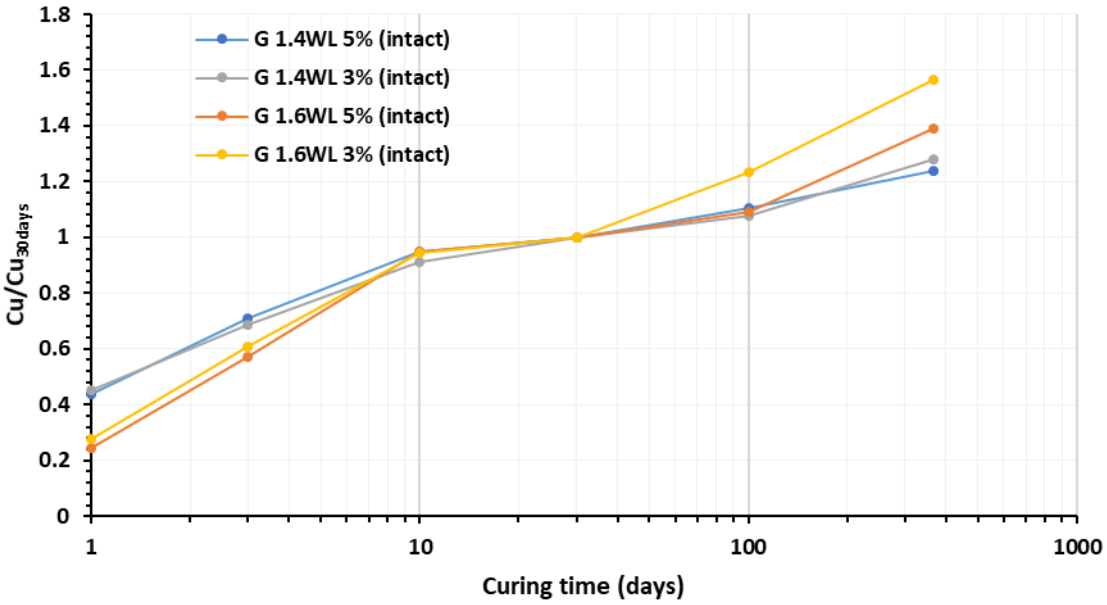

Figure 5-25: Normalised undrained shear strength of Grangemouth soil

Remoulded undrained shear strength

The penetration test results conducted after hand remoulding of these soils are shown in Figure D2, and the resulting undrained shear strengths and test statistics are listed in Table D2. The development of the remoulded undrained shear strengths of these soils is shown in Figure 5-26. No major drop in strength occurs as a result of remoulding. For example, the strength of clays at W=1.4 admixed with 5% lime and cured for 365 days dropped from 3.4 kPa to 0.6 kPa. The remarkable finding is that the remoulded undrained shear strength of all these soils fails to increase with curing time. This may be attributed to the limited development of pozzalonic structures, which can then be broken by remoulding.

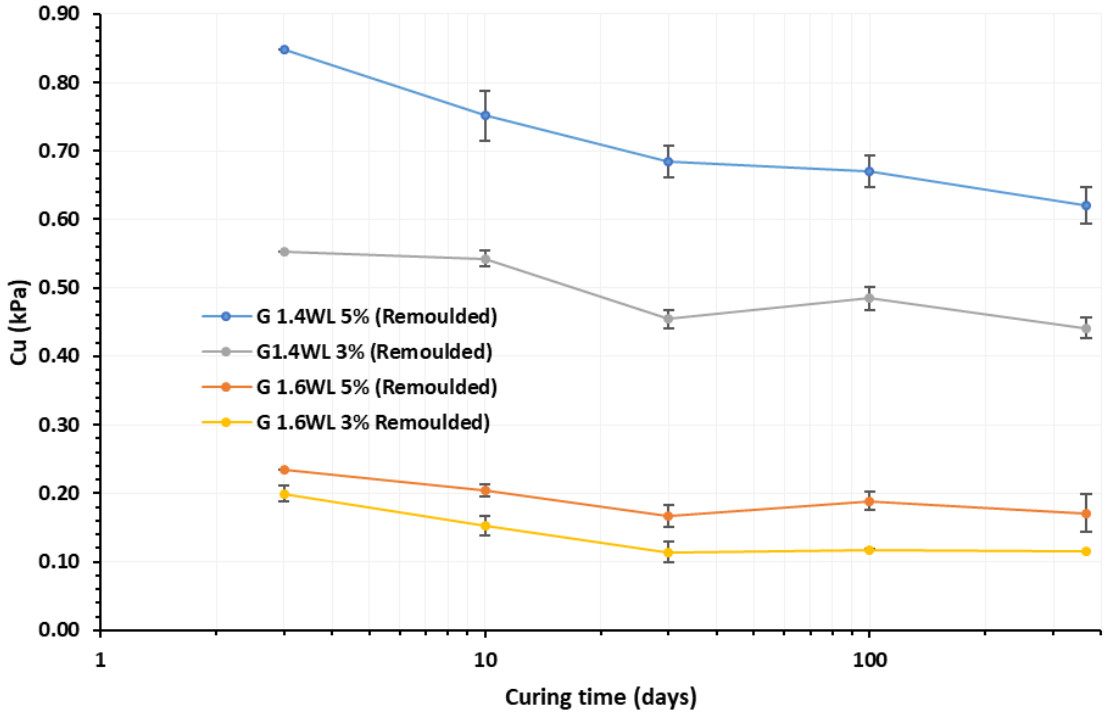

Figure 5-26: Remoulded undrained shear strength of Grangemouth soil

Strength sensitivity

The strength sensitivity is shown in Figure 5-27. Sensitivity values as high as 9 were recorded for these soils after one year reflecting the fact that while intact strength increases

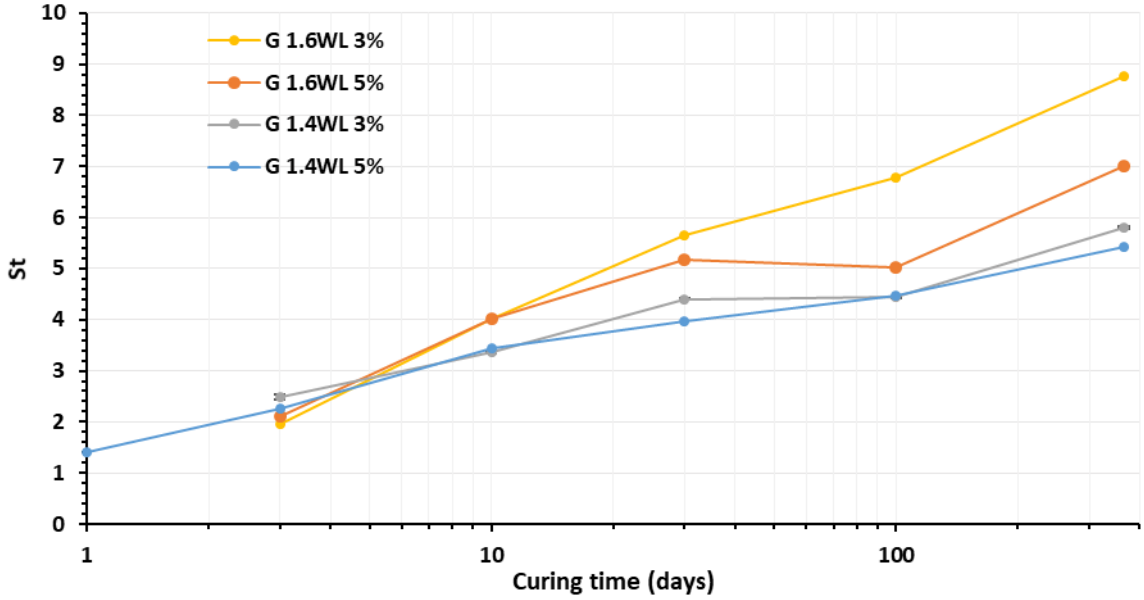

Figure 5-27: Strength sensitivity of Grangemouth soil

Evolution of pH in lime-admixed Grangemouth soil

Figure 5-28 shows the pH development in these soils over time. Although the pH drops steadily up to 100 days of curing, it does not fall below 12.0 in any of the cases tested. This indicates that there is a residual amount of free lime because there were insufficient clay minerals present to sustain the pozzolanic reaction. The excess pH is greatest for the 5% lime content, but this higher lime content still serves a purpose in yielding higher strengths.

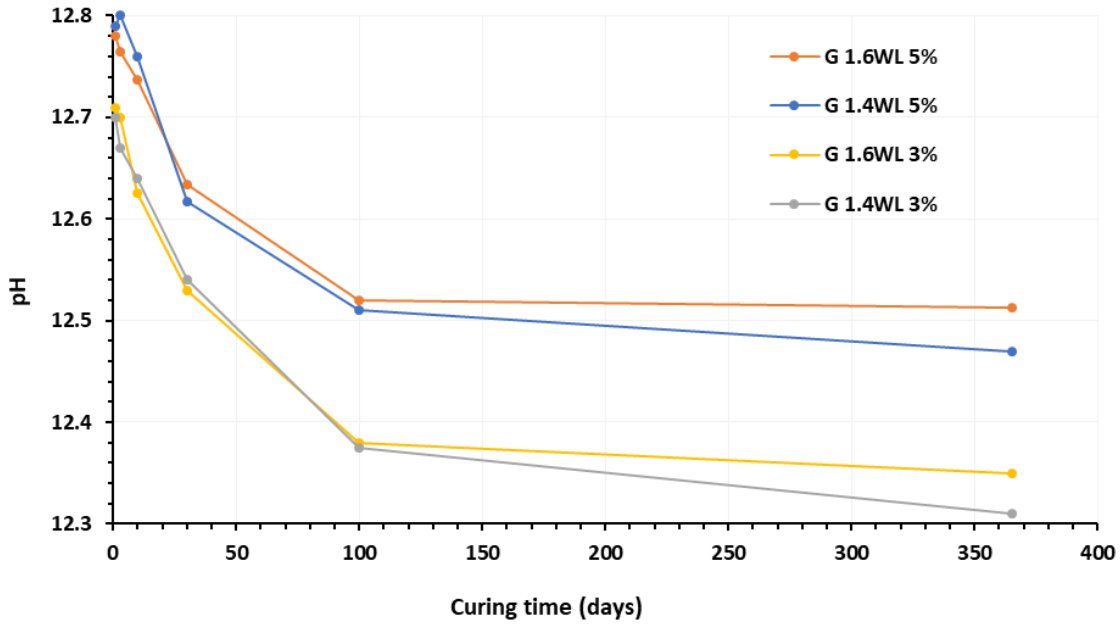

Figure 5-28: Evolution of pH in lime-treated Grangemouth soil

5.5.5 SW-S soil mix

The scope of this parametric study is outlined in Table 5.10, and the combinations of lime content and water contents are listed in Table 5-11.

Table 5-10: Scope of the parametric study.

Curing period (days)	$W=w/W_{LL}$	Lime content C (%)	Condition	Temp.
1 3 10 30 100 365	1.8 2.0	3 5	Intact Remoulded	Normal (20°C)

Table 5-11: Combinations of water contents and lime content

$W=w/W_{LL}$	Lime content C (%)
1.8	5
2.0	3
2.0	5

The full results of the penetration tests are given in Appendix E. Undrained shear strength profile data are given in Figures E1-E2, while the results are summarized in Tables E1-E2.

Effect of lime content

The immediate consequence of adding lime to this soil mix was to soften it: it appears that the ion exchange process with the sodium base montmorillonite minerals reduces the liquid limit of the soil mix and changes its consistency. This action causes separation of water from the mixture and results in the appearance of a water layer at the top of the soil. This certainly affects the subsequent development of strength, and gives rise to non-uniform strength profiles, as shown in Figure E.1 (for the case of W=1.8, with 5% lime cured for 365 days.). This also results in high values for the COV listed in Table E1. Nevertheless, the low COV values between the duplicated tests demonstrates that this is a repeatable phenomenon.

The development of undrained shear strength with time for this soil is shown in Figure 5-29. The main difference in this soil response compared to those reported earlier is the very high undrained shear strength which can be achieved after long-term curing, especially in the case of 5% lime content. For example, after 365 days of curing, this soil with W=1.8 and C=5% developed a strength of 114 kPa, although its one-day strength was only 0.3 kPa. This very high strength must reflect the high activity of SW montmorillonite minerals present in the soil mix. It might be conjectured that the presence of very fine sand particles in the soil mix may furnish a scaffold which enhances the strength, but this needs verification.

As usual, as can be seen from Figure 5-29, increased lime content increases the undrained shear strength. In the case of W = 2.0, the strength increases from 34kPa for 3% lime content to nearly 90kPa for 5% lime content, for soils cured for 365 days. This is despite the fact that at the early stages of curing (up to about 15 days), strength remains low. Increasing water content has only a small effect on strength. For example, at 365 days, strengths differ by about 20% between soils with water contents of 1.8 and 2.2 times the liquid limit.

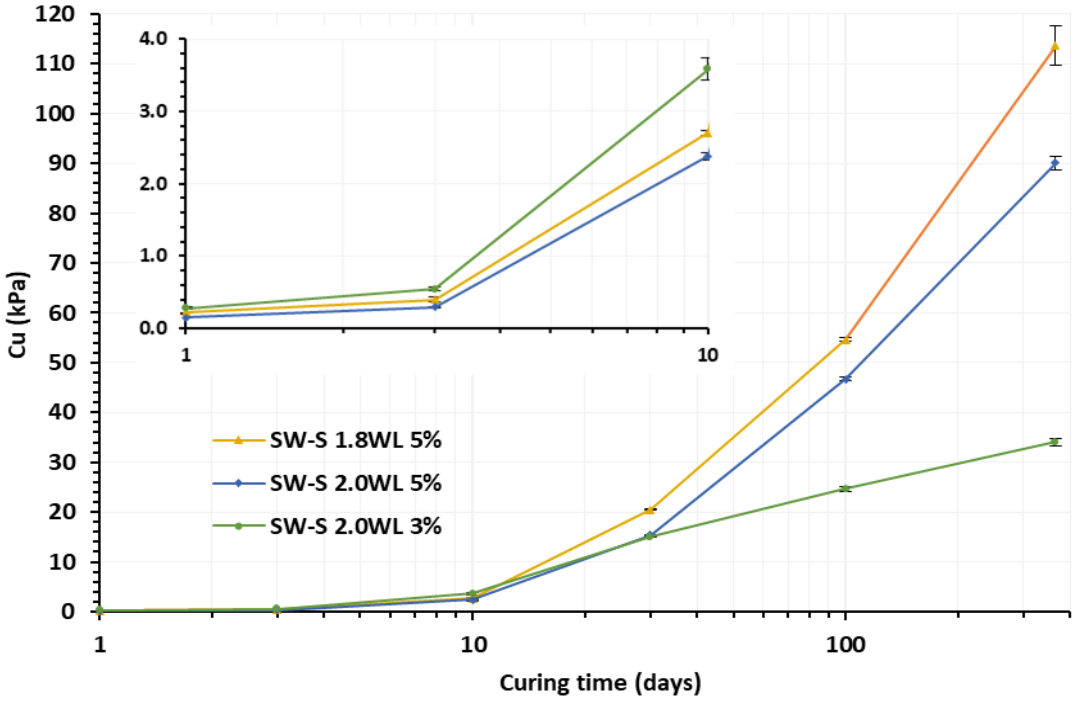

Figure 5-29: Undrained shear strength of the remoulded SW-S soil mix

Effect of curing time

Normalizing the strengths with respect to their corresponding 30-day strengths, as shown in Figure 5-30, reveals very similar trends, up to 30 days of curing. After this period, it is clear that the 3% lime content becomes depleted and relatively little further strength gain is achieved. On the other hand, the soils with 5% lime content sustain the pozzolanic reaction to one year (and beyond) and increase their strength five-fold.

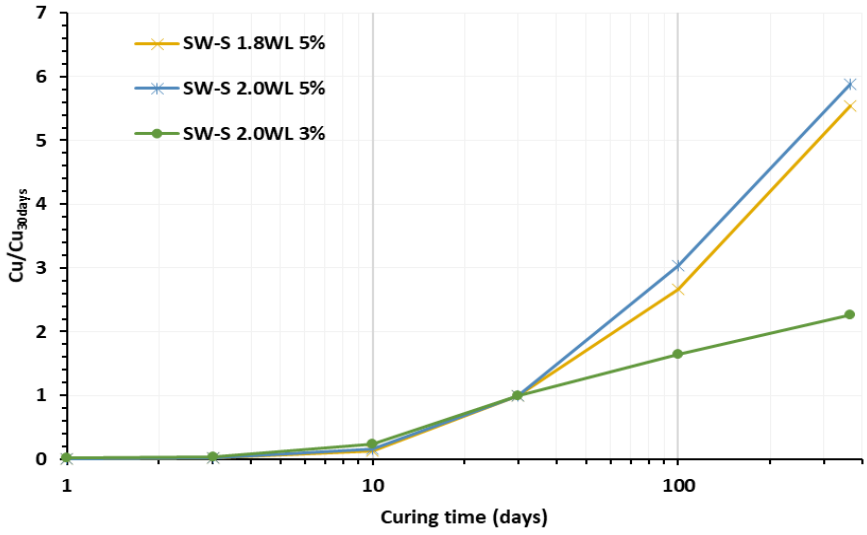

Figure 5-30: Normalized undrained shear strength of the lime-admixed SW-S soil mix

Remoulded undrained shear strength

The full results for the penetration tests on the remoulded are shown in Figure E.2 and summarized in Table E.2. The development of remoulded undrained shear strength with curing time is shown in Figure 5-31. Remoulding of this very strong soil at 365 days was very difficult. Hand remoulding took more than one hour and testifies to the "tough" nature of these soils. Higher remoulded shear strengths were recorded for soils with 5% lime contents than for those with 3% lime content, but this only reflected their higher intact strengths. Figure 5-31 shows that there is very little difference between the results of soils of different water content at the same lime content.

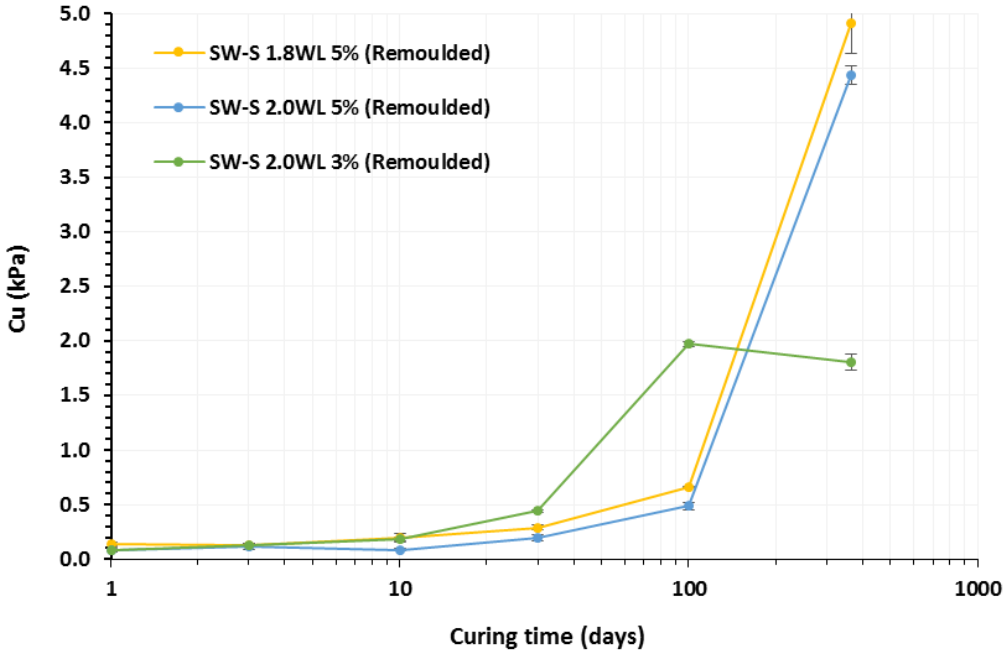

Figure 5-31: Undrained shear strength of the remoulded SW-S soil mix.

Strength Sensitivity

Figure 5-32 shows the strength sensitivity of the SW-S soil. For 5% lime content, the sensitivity continues to increase with increasing curing time up to about 100 days of curing, reaching the extreme value of 90. At this stage, the soil still retains substantial reserves of free lime. At 365 days, however, the increase in the intact strength is accompanied by building of relatively strong bonding that keeps the remoulded shear strength high and the sensitivity drops to about 20. Coincidentally perhaps, the sensitivity of these soils at 365 days were all found to be of about 20, irrespective of water content or lime content.

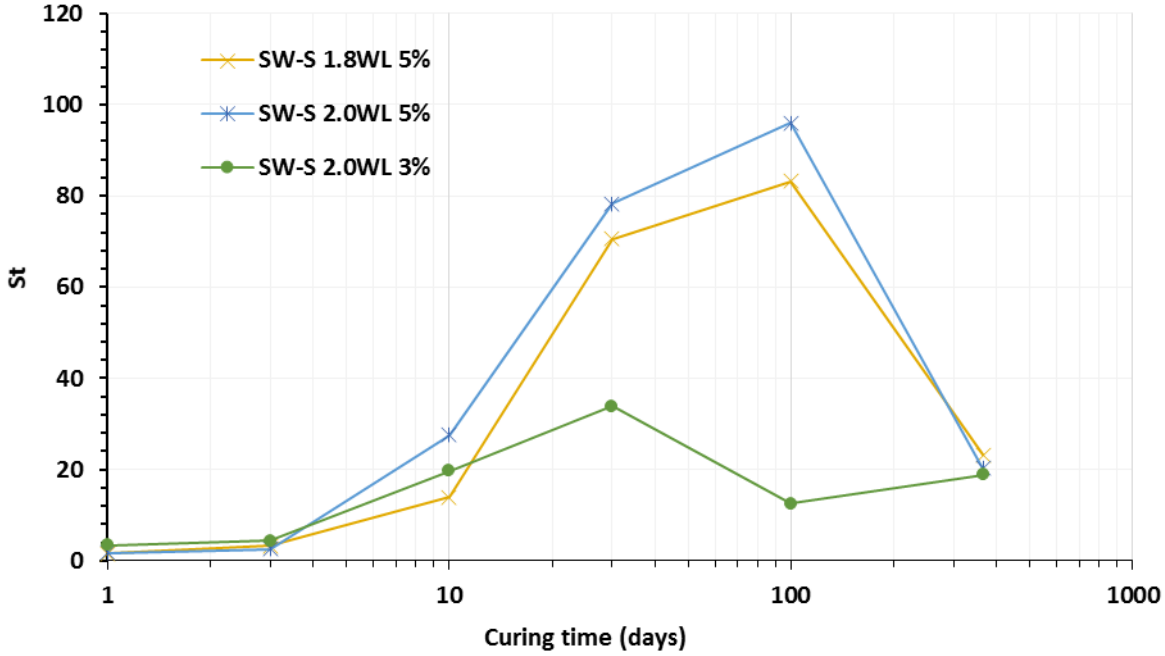

Figure 5-32: Strength sensitivity of the SW-S soil mix.

Evolution of pH in the admixed SW-S soil

Figure 5-33 shows the evolution of pH in this soil. Although the pH for different lime contents starts from the same value, the rates of decrease change 30 days after curing. For 3% lime content, the depletion of the free lime is evident at an early stage. For 5% lime content, pH falls steadily throughout and, up to one year, is still as high as 12.4. Thus further strength gain beyond one year is indicated, provided sufficient clay minerals are present.

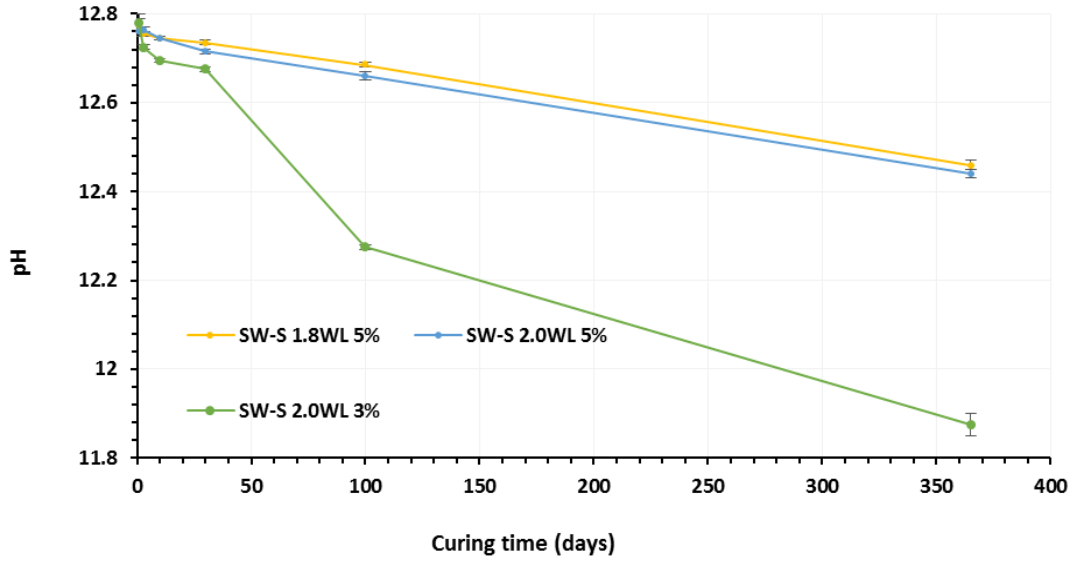

Figure 5-33: Evolution of pH in lime-treated SW-S soil

5.6 Effect of Curing Temperature

To investigate the effect of curing temperature, two soils were tested: the kaolin clay (K2) and the SW-K soil mix.

Kaolin (K2) clay slurries

The scope of this investigation is summarized in Table 5-12.

Table 5-12: Parametric study: effect of temperature on kaolin (K2) clay.

Curing period (days)	W=w/W_{LL}	Lime content C (%)	Condition	Temp.
1 3 10 30 100 365	1.8 2.2	1 5	Intact Remoulded	Normal (20°C) Hot curing (38°C) Cold curing (5°C)

For brevity, the complete results for cold and hot curing are given in Appendix F and Appendix G respectively.

Figure 5-34 compares the undrained shear strengths of cold-cured kaolin (K2) specimens with those cured at the normal curing temperature. The direct effect of cold curing is to slow the development of the strength by retarding the pozzolanic reaction (Janz and Johansson, 2002). For W=1.8 and 5% lime content (Figure 5-34(a)), the strength after 365 days of cold curing was 7.5 kPa while it was 35kPa for normal curing. Also, the higher the lime content, the more was the difference between the undrained shear strengths. For instance, after one year of curing, the ratio of strengths for cold-cured soils to those of normal-cured soils was 22% and 60% for 5% and 1% lime contents, respectively irrespective of water content.

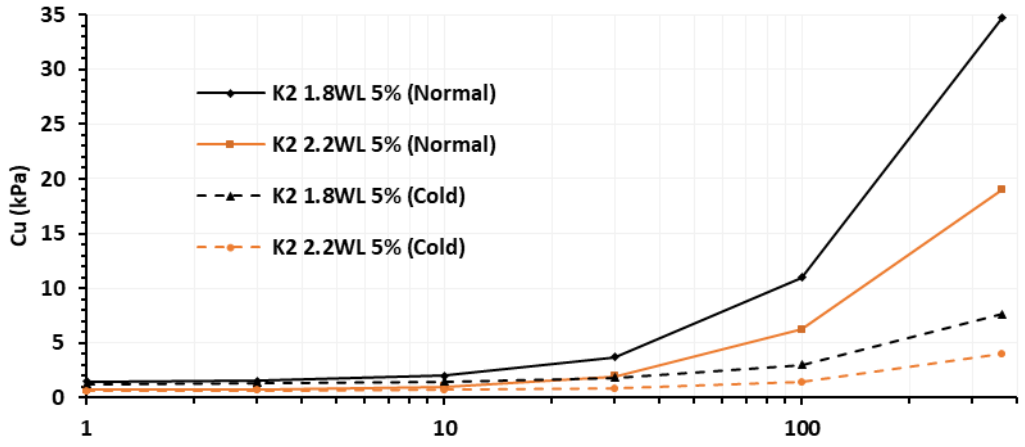

(a) 5% lime

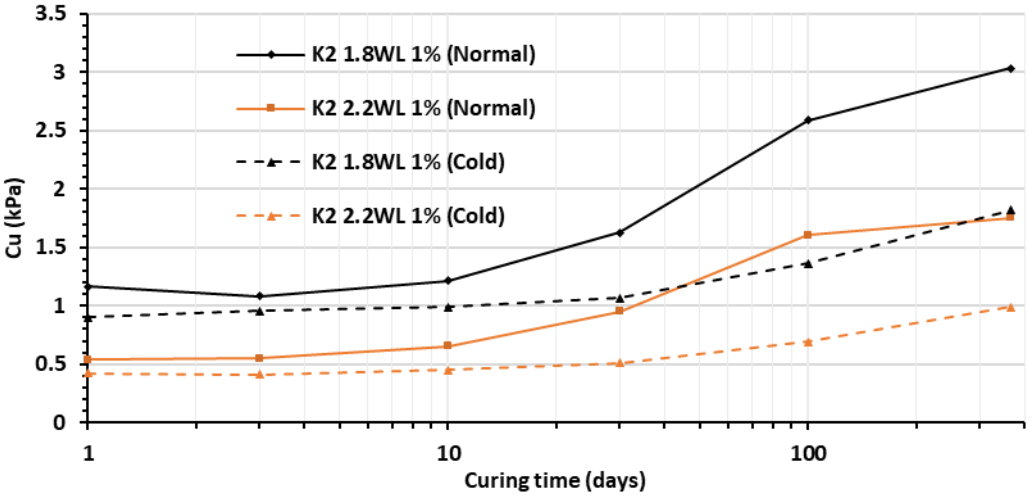

(a) 1% lime

Figure 5-34: Undrained shear strength of kaolin clay, under cold and normal curing conditions: (a) 5% and (b) 1% lime contents.

Increasing the curing temperature expedites the pozzolanic reaction and increases the strength in a shorter time. Figure 5-35 compares the undrained shear strength of kaolin (K2) clay cured under cold, normal, and hot conditions. For both lime contents, the strength increases faster with increasing curing temperatures. In Figure 5-35(b), for 1% lime, around 70% of the maximum (100 days) strength has been reached after 10 days of hot curing. After that, because of the depletion of free lime, the strength gain slows down compared to normal temperature curing. For 5% lime content (Figure 5-35(a)), a similar situation arises after 30 days of hot curing. Regardless of lime rates, the maximum (100 days) strengths obtained from hot curing are slightly higher than the maxima obtained from curing at normal temperatures. The 365 days of curing at normal temperatures is not enough to bring kaolin to its maximum undrained shear strength. Curing at higher temperature can be a useful tool to predict the ultimate strength that would be obtained if the soils were cured for longer periods.

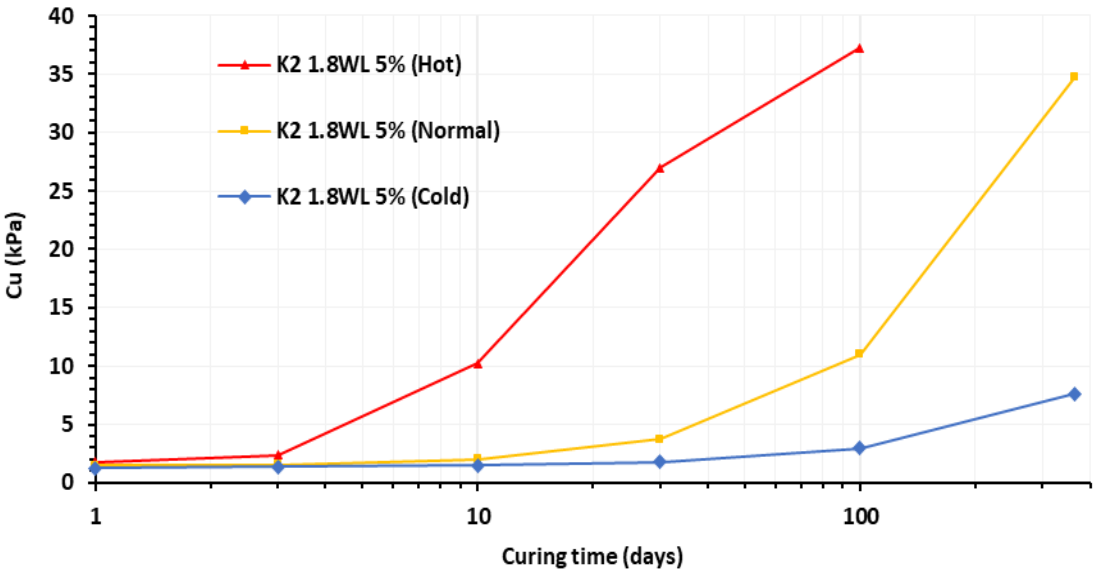

(a) 5% lime

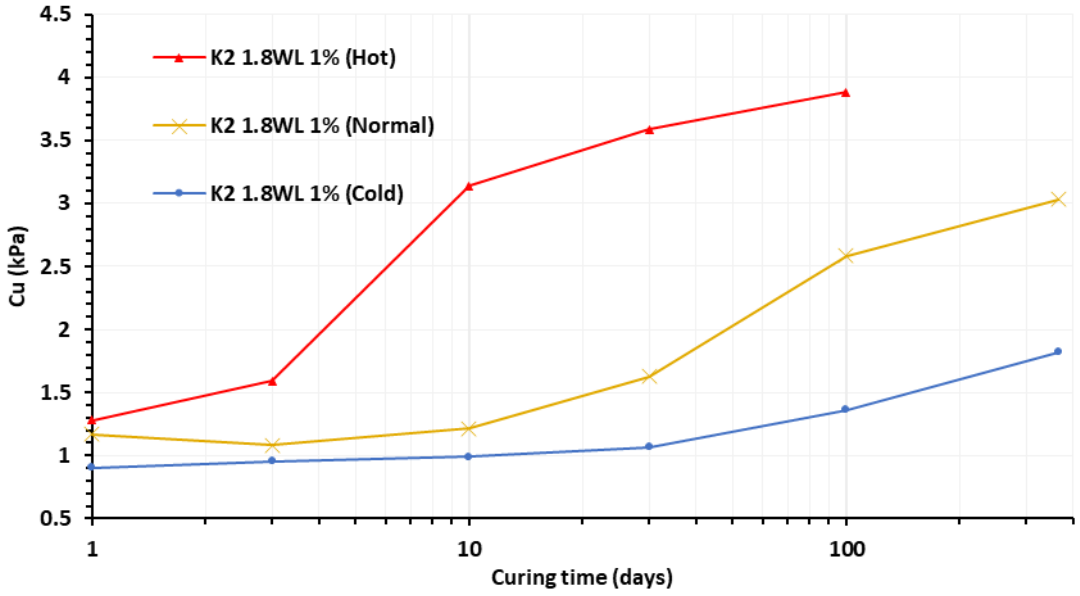

(b) 1% lime

Figure 5-35: Effect of curing temperature on the intact undrained shear strength of lime treated kaolin (K2): (a) 5% and (b) 1% lime contents.

Figure 5-36 compares the remoulded undrained shear strength of lime-treated kaolin (K2) slurries at W=1.8, cured at different temperatures. Increasing curing temperatures yielded higher remoulded undrained shear strengths, reflecting the differences in intact strength, but the effect of temperature is less pronounced on remoulded soils (than on intact soils).

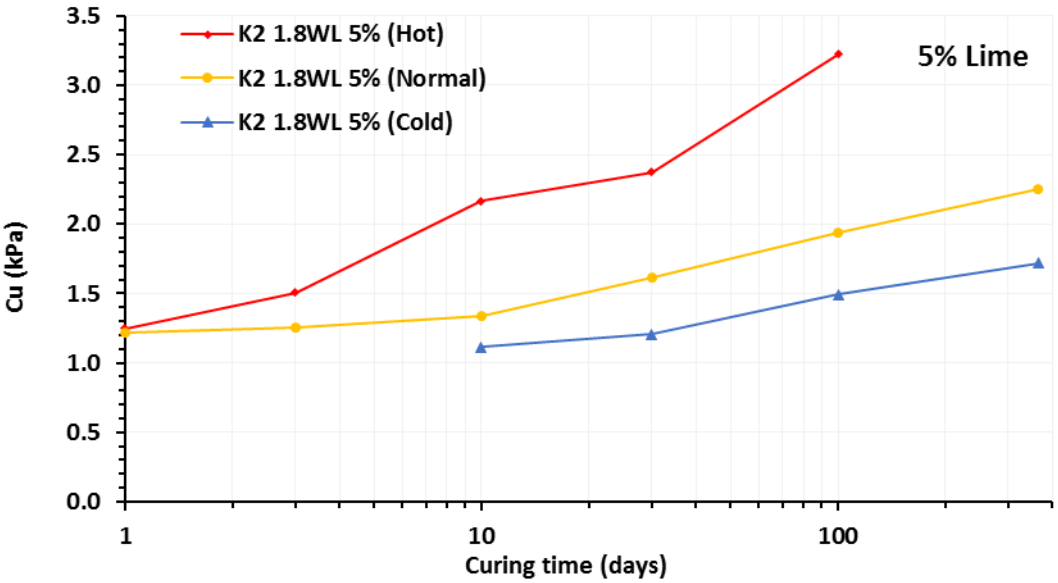

(a) 5% lime

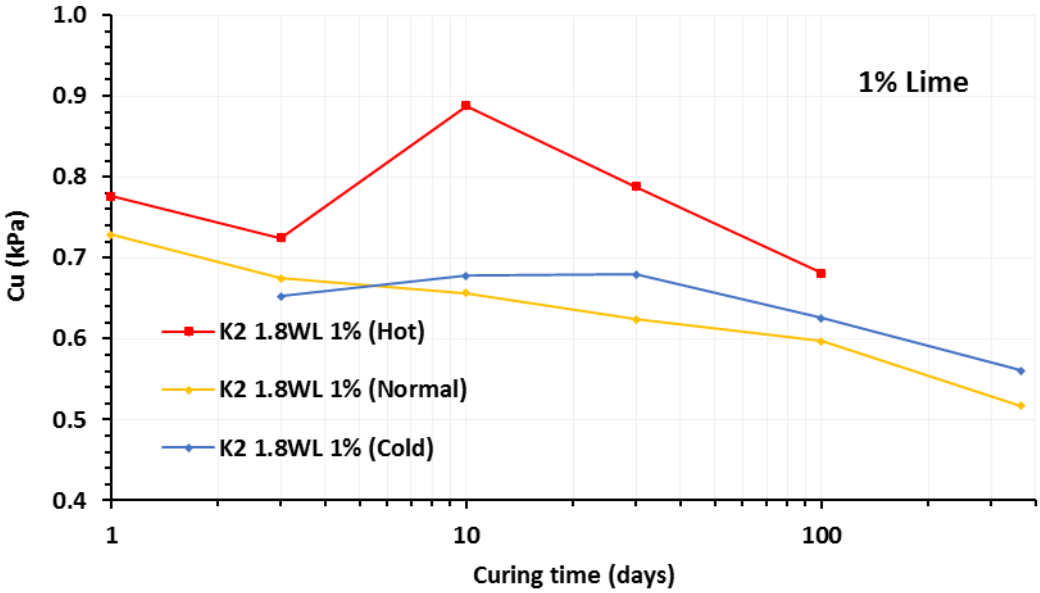

(b) 1% lime

Figure 5-36: Effect of curing temperature on the remoulded shear strength of lime-admixed kaolin

SW-K mix soil

The scope of the investigation of the effect of temperature on the lime-admixed SW-K soil is summarized in Table 5-13.

Table 5-13: Scope of parametric study on the SW-K soil mix

Curing period (days)	W=w/W_{LL}	Lime content C (%)	Condition	Temp.
1	1.8	3	Intact	Normal (20^{o}C)
3				
10		5	Remoulded	Hot curing (38^{o}C)
30				
100				Cold curing (5^{o}C)
365				

The complete results for cold and hot curing of this soil are given Appendix G. Figure 5-37 summarizes the development of the undrained shear strength of the SW-K soil mix at 1.8W_{LL} for lime contents of 3% and 5%, and cured at the three different temperatures. The results for the 5% lime content (shown in solid lines) indicates that increasing curing temperatures has a significant effect on the rate of increase of strength and the resulting ultimate undrained shear strength of the soil at the end of the curing period. However, the effect of temperature is not as high as for kaolin. After one year of curing, the undrained strength is about 22kPa and 32 kPa for cold and normal temperatures respectively. After 100 days of hot curing, the strength was about 35kpa. This response confirms that temperature increase increases the rate of strength gain with time.

For 3% lime-admixed soils, the difference between the results of the different curing temperatures decreases for longer curing periods. At 365 days of curing, there was no major difference between the results obtained from cold and normal curing. This response is different from that observed for kaolin in which the strength gain after one year of cold curing was 22-60% of that obtained after the same period of normal temperature curing. This difference can be attributed to the difference in the mineralogy of these two different soils: montmorillonite reacts faster with free lime, Similar observations have been made by (Diamond and Kinter, 1966) and (Al-Mukhtar et al., 2014).

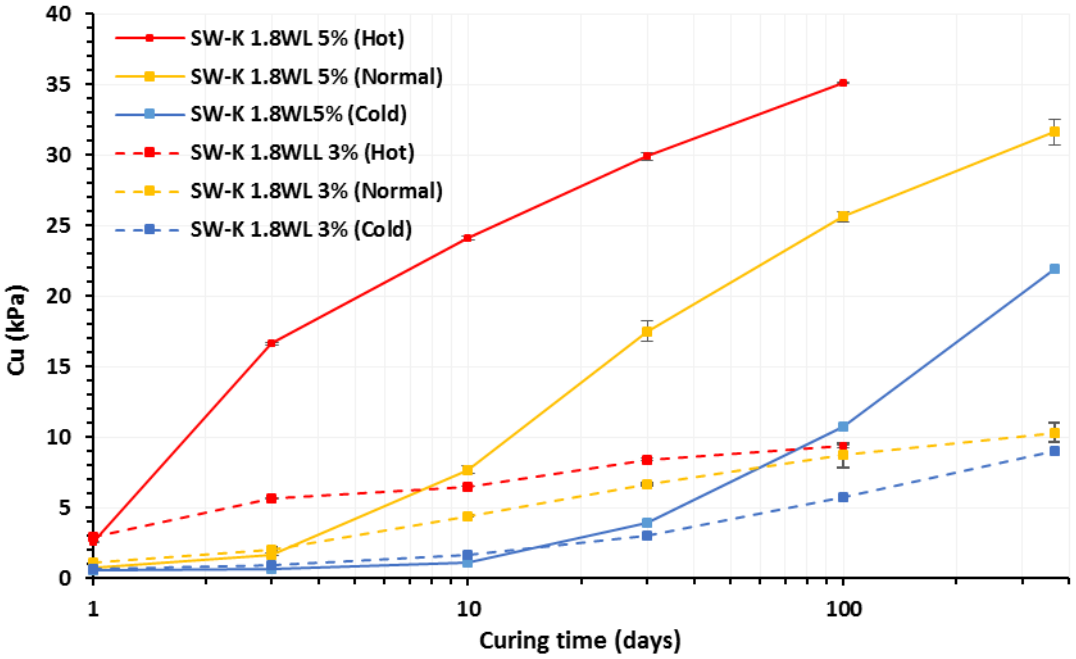

Figure 5-37: Undrained shear strength of intact lime treated SW-K mix soils.

A similar pattern can be seen in the undrained shear strength of the remoulded SW-K mix soil with curing temperatures as shown in Figure 5-38. However, some of the features of this plot are difficult to explain, such as the reduction (in some cases) of the undrained shear strengths after reaching a peak. Difficulties in controlling the degree of remoulding may be responsible.

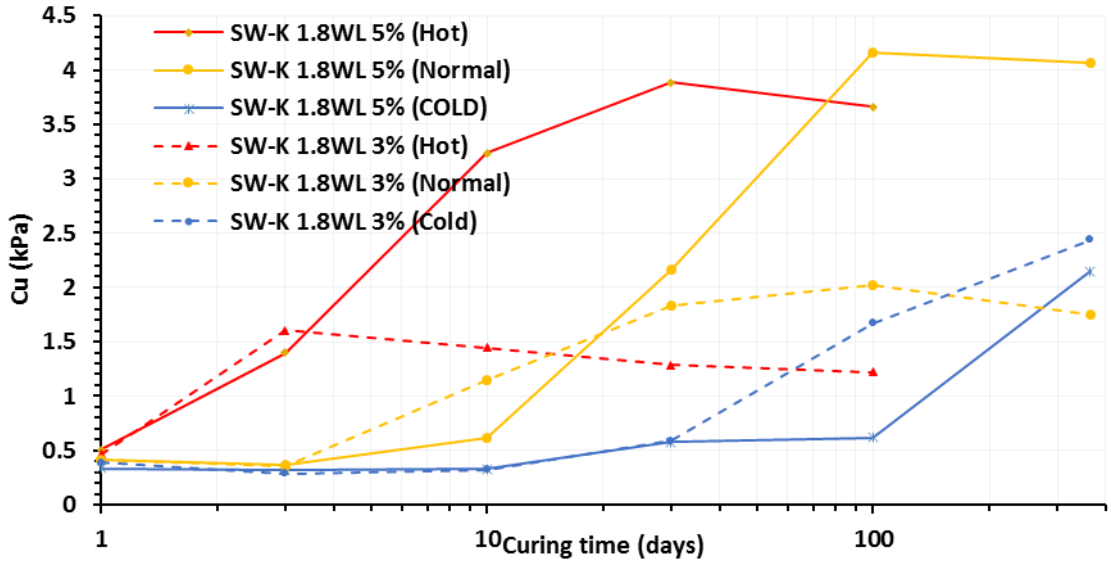

Figure 5-38: Undrained shear strength of remoulded lime-treated SW-K mix soils

5.7 Modelling Accelerated Curing

In this section, we explore the use of the Arrhenius model (Chapter 2) to model the accelerated aging of the lime-treated soils. We follow the procedure for equivalent time t_e determination suggested by (Marzano et al., 2008) for cement-treated soil, where:

$$t_e = t.\exp[-\frac{E_a}{R}(\frac{1}{T}-\frac{1}{T_o})] \quad \textbf{5.6}$$

which can be written as:

$$t_e = a_T.t \quad \textbf{5-6}$$

where:

$$a_T = \exp[-\frac{E_a}{R}(\frac{1}{T}-\frac{1}{T_o})] \quad \textbf{5-7}$$

in which a_T is a shift factor and t is the curing time. This equation and its parameters are discussed in detail in Chapter 2. Unlike (Marzano et al., 2008), the reference temperature T_o in this study is taken to be 5°C.

The data from test carried out at 20°C are shifted to the right of the 5°C results curve until the two sets of results are superposed, yielding a shift factor corresponding to 5°C. Again, shifting the data from the 38°C tests towards the left yields a shift factor corresponding to 38°C.

Figure 5-39 shows the undrained shear strengths of kaolin clay at water contents of $1.8W_{LL}$ and $2.2W_{LL}$ and cured at different temeprature. The shift factors for each lime content and curing temperature are shown in Table 5-14. As can be seen, the shift factors are lime content dependent. For kaolin clay, the higher the lime content, the lower is shift factor. The shift factors are independent of the water content of the soil, which is in agreement with the conclusions of (Marzano et al., 2008) for cement admixed soils.

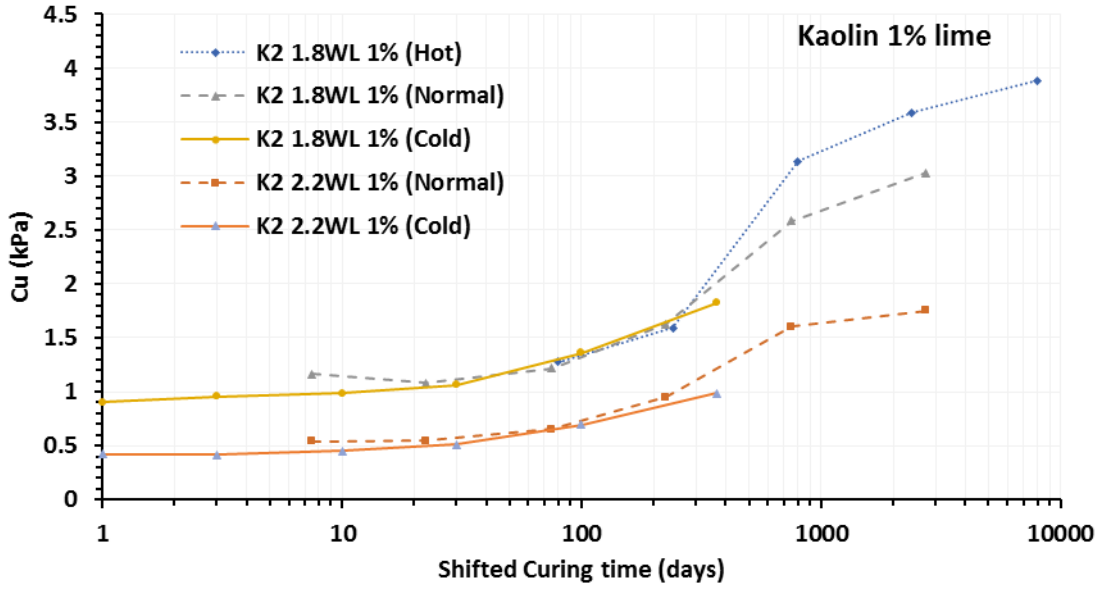

(a) 5% lime

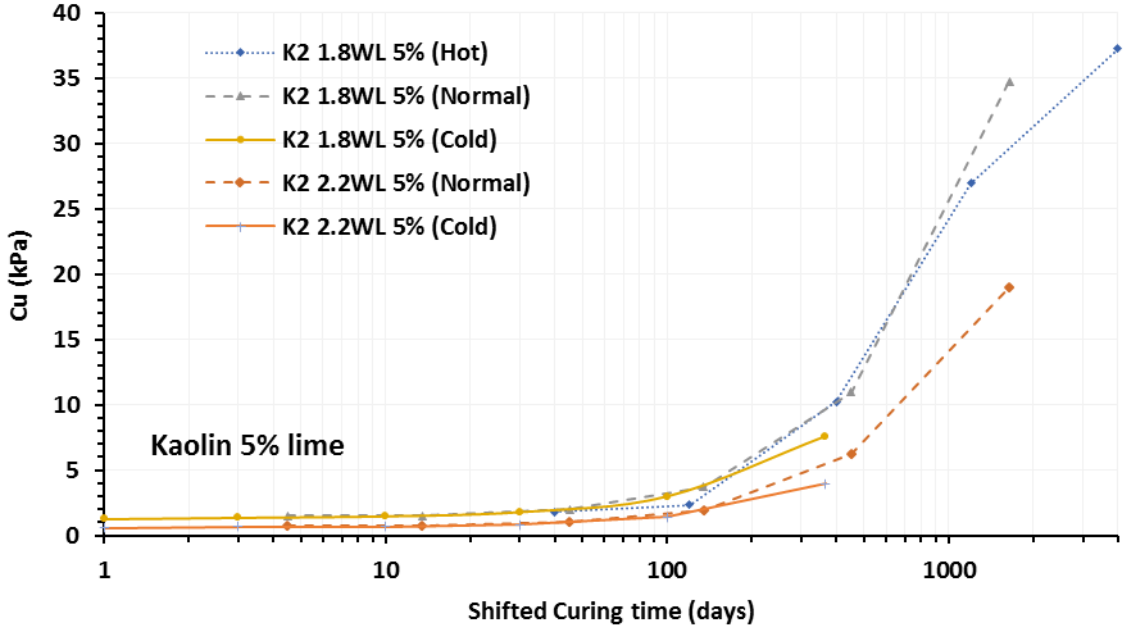

(b) 1% lime

Figure 5-39: Undrained shear strength of kaolin (K2) with shifted curing times, equivalent to 5°C

Figure 5-40 shows the undrained shear strengths of the SW-K soil mix at the water content of $1.8W_{LL}$ and lime contents of 3% and 5%. The shifting factors used for each lime content and curing tempratures are also shown in Table 5-14. The shift factors required for equivalent time curing are different from those used for kaolin clay which again agrees with the conclusions of (Al-Mukhtar et al., 2014) who report on the effect of mineralogical composition on the rate of lime consumption due to temperature change.

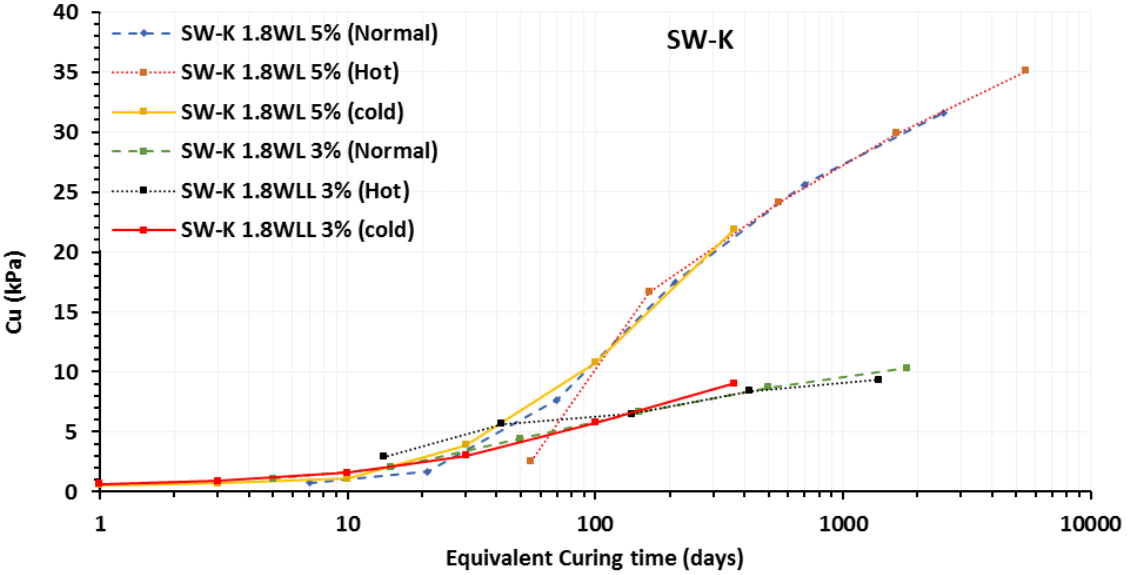

Figure 5-40: Undrained shear strength of the SW-K soil mix, with shifted curing time equivalent to 5C

Table 5-14: Shift factors for equivalent curing times

Soil type	Lime %	W	Shift factor a_t			Slope(E_a/R)	E_a(J/mol.)
			5°C(278°K)	20°C(293°K)	38°C(311°K)		
Kaolin (K2)	1	1.8	1	7.5	80	11391	94710
	5	1.8	1	4.5	40	9392	78090
	1	2.2	1	7.5		11391	94710
	5	2.2	1	4.5		9392	78090
SW-K	3	1.8	1	5	14	7266	60410
	5	1.8	1	7	55	10523	87490

Plotting the shift factors against $\frac{1}{T} - \frac{1}{T_o}$ as shown in Figure 5-41 produces straight lines whose slopes are proportional to the activation energy, E_a /R . The latter are listed in Table 5-14. From the slopes in Figure 5-41 and noting that the universal gas constant R=8.314 J/ mol. K, the activation energy E_a for each case can be determined.

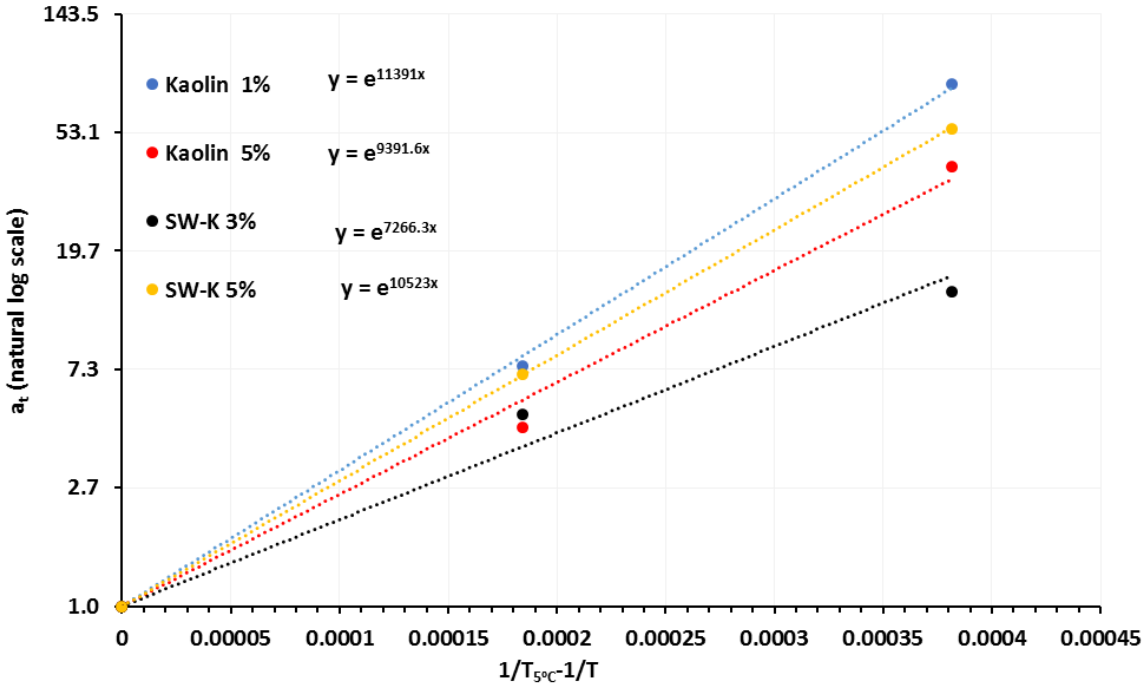

Figure 5-41: Natural logarithm of the shift factor against reciprocal of temperatures.

Once the activation energy E_a is determined, the shift factors for any temperature can be obtained, as depicted in Figure 5-42 for kaolin with a 5% lime content. For example, if the kaolin temperature in the field is 10°C, an accelerated test performed at 30°C would give a shift factor of 7. This means that a test carried out for 100 days at 30℃ would yield the same strength as a test in the field lasting 700 days. Using Figure 5-40, the expected undrained shear strength in that field condtion would be 20 kPa. This method can be a powerful tool for estimating long-term undrained shear strength of lime-treated soils in cold regions.

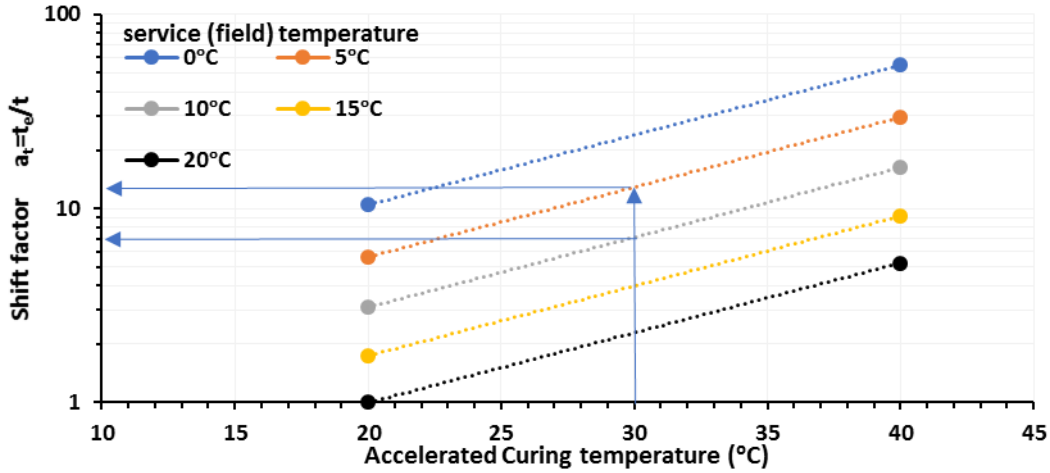

Figure 5-42: Shift factors for kaolin clay, with 5% lime content

5.8 Conclusions

From this experimental study, the following conclusions can be offered:

1. Curing lime-admixed soil in the presence of excess water can be counter-productive due to lime diffusion. Higher lime contents can offset these losses.
2. Lime contents as low as 1% can improve the mechanical properties of ultra-soft clays However, higher lime contents will produce much higher strengths provided that there are sufficient pozzolanic minerals present in the soil to sustain the pozzolanic reactions.
3. Although lime-treated soils have high sensitivity, they also show considerable ability of to absorb kneading energy and plastically deform before degrading. Moreover, the remoulded strengths of ultra-soft soils are much higher than their untreated counterparts. Reversion to the ultra-soft state does not occur.
4. The rate of strength gain varies widely from soil to soil. Figure 5-43 shows how strength gain develops in various soils, all admixed with 5% lime. The Grangemouth soil reaches nearly 40% of its (modest) 365-day strength after one day. Kaolin on the other hand steadily increases in strength over one year. CB bentonite rapidly increases in strength in the first three months.

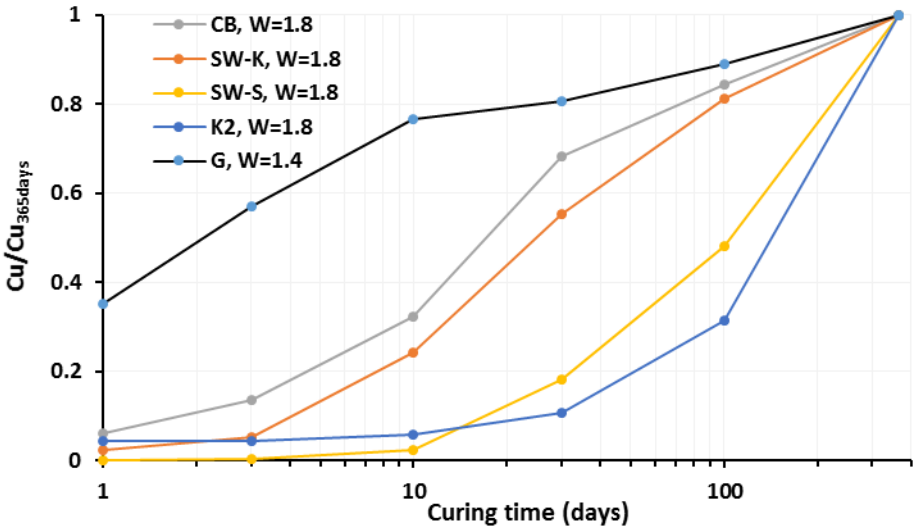

Figure 5-43: Strength gain rate of different soils admixed with 5% lime

5. Initially ultra-soft clays (i.e., excluding Grangemouth soil), reach remarkably similar undrained shear strengths after one year if the ratios of their initial water content to liquid limit (w/W_{LL}) are the same. Table 5-15 below shows these undrained shear strengths.

Table 5-15: Undrained shear strengths (kPa) of lime treated clays after one year

Lime C (%)	W =w /W_{LL}	C_u (kPa)		
		Kaolin (K2)	SW-K	CB
5	1.8	34.8	31.6	30.6
	2.2	19.0	18.6	18.7
3	1.8	11.5	10.3	8.9
	2.2	5.5		4.7

6. A natural soil (Grangemouth soil) containing a low proportion of clay was much less affected by lime. Evidently, sufficient clay minerals must be available for the pozzolanic reaction to proceed.
7. Except for the Grangemouth soil, lime content rather than water content has the most influence on undrained shear strength.
8. The rate of strength gain depends on curing temperature: the strength gain is fastest at elevated temperatures and vice-versa. The method suggested by (Marzano et al., 2008) for cement-treated soils based on the Arrhenius model provides a useful means of extrapolating the results of short-term curing at elevated temperatures to longer periods at cooler temperatures.
9. Soil pH measurements during curing provides useful evidence of lime depletion and may be used to determine optimal lime contents.

Chapter 6 COMPRESSIBILITY OF LIME-ADMIXED SOILS.

6.1 Introduction

One-dimensional compressibility tests can provide further information on the changes in the mechanical properties of lime-admixed soils. Although the effects of additives are well known, especially for clayey soils at low water contents close to their plastic limit, treatment of very soft materials like dredged slurries is more problematic because of their high-water content (Tremblay et al., 2001). Reported in this chapter are oedometer test results conducted on intact and remoulded lime-admixed soil specimens cured for 100 and 365 days. The main goal of the tests is to explore the effects of water content, lime content, and curing time on compressibility and "yield stress", i.e., the vertical effective stress which presages a distinct change in compressibility, as the soil structure is disrupted.

6.2 Oedometer Test Results

More than 150 oedometer tests were conducted to investigate the effect of lime content, water content and curing time. All tests were repeated at least once. Tests were also conducted on hand-remoulded specimens to assess the sensitivity of the lime-admixed soils. For sake of brevity, only mean values for each case are shown graphically.

Table 6-1 below lists the scope of the study.

Table 6-1: Scope of the parametric study.

Soil type	Lime content C (%)	W= w / W_{LL}	Curing period	Conditions	Comment
Kaolin	1 3 5	1.8 2.0 2.2	100 days 365 days	Cured at room Temperature	Intact and Remoulded
SW-K	3 5	1.8 2.2			
CB	3 5	1.8 2.2			
SW-S	3 5	1.8 2.0			
G	3 5	1.4 1.6			

Further details of the results obtained from each repeated test on intact and remoulded soil are summarized in Table 6-3 and Table 6-4 respectively. The vertical yield stress ($6'_{vy}$) was calculated using Casagrande method (Casagrande, 1936) although the method is somewhat subjective. Alternatives such as that using a bi-logarithmic scale (Butterfield, 1979; Hong et al., 2012; Sridharan et al., 1991) were found to yield no better results.

6.2.1 Repeatability of tests

In most cases, the oedometer tests were repeated on duplicate samples; sometimes more than once. As before, the arithmetic mean ($\bar{x}$) of the test results was assumed to be the population mean, and the standard deviations (S.D.) and coefficient of variation (COV) were computed on that basis. Thus, for a set of two tests, the standard deviation is equal to one half of the difference between the two test results. Calculations were made for the mean and median of the COV values obtained for each of the consolidation parameters. These data are shown in Table 6-2, from which we draw the following conclusions:

Table 6-2: COV analysis of the oedometer test results

	COV%			
	$6'_{vy}$	C_C	C_S	$б_{vr}$'
Mean	**8.8**	**2.1**	**0.01**	**13.2**
Median	**4.3**	**2.0**	**0.01**	**7.7**

For the vertical yield stress $6'_{vy}$ for intact specimens (Table 6-3), the median COV is 4.3% and the mean is 8.8%, which reveals that in some cases repeatability was poor. This can be attributed to the somewhat subjective nature of the method of calculation and the error magnification of the log scale. The same thing can be said about $б_{vr}$' for the remoulded specimens (Table 6-4) which will be discussed later. On the other hand, the COV for the compression indices Cc and the swell indices Cs are very satisfactory. This lends confidence to the experimental procedures adopted.

Table 6-3: Oedometer test results for intact lime-admixed soils cured for 100 and 365 days

Soil				Test No.									Statistics								
Type	W=w/W_{LL}	C (%)	Time (days)	1St test			2nd test			3rd test			C_c			C_s			σ'_{vy} (kPa)		
				C_c	C_s	σ'_{vy}	C_c	C_s	σ'_{vy}	C_c	C_s	σ'_{vy}	$\bar{x}$	S.D	COV	$\bar{x}$	S.D	COV	$\bar{x}$	S.D	COV
K2	1.8	5	365	1.2	0.2	110	1.3	0.2	100	1.3	0.2	105	1.3	0.07	5.2	0.16	0.01	6.02	105	4.1	3.9
K2	1.8	5	100	1.0	0.2	21	1.0	0.1	31				1.0	0.03	2.6	0.13	0.03	20.00	26	5.0	19.2
K2	2.0	5	365	1.4	0.2	85	1.3	0.1	75	1.3	0.2	65	1.3	0.03	2.5	0.15	0.01	8.50	75	8.2	10.9
K2	2.0	5	100	1.1	0.2	20	1.0	0.2	17				1.0	0.04	3.8	0.16	0.00	0.00	19	1.5	8.1
K2	2.2	5	365	1.4	0.2	55	1.4	0.2	50	1.4	0.2	53	1.4	0.02	1.7	0.16	0.01	5.10	53	2.1	3.9
K2	2.2	5	100	1.2	0.2	17	1.2	0.2	22				1.2	0.00	0.0	0.16	0.01	6.25	20	2.5	12.8
K2	1.8	3	365	1.0	0.2	25	1.0	0.2	25	1.0	0.2	35	1.0	0.02	2.4	0.17	0.00	2.83	28	4.7	16.6
K2	1.8	3	100	1.0	0.2	18	1.0	0.2	22				1.0	0.00	0.0	0.17	0.01	3.03	20	2.0	10.0
K2	2.0	3	365	1.0	0.2	15	1.1	0.2	16				1.0	0.03	2.4	0.16	0.01	6.25	16	0.5	3.2
K2	2.0	3	100	1.1	0.2	12	1.0	0.2	11				1.0	0.03	2.4	0.17	0.01	3.03	12	0.5	4.3
K2	2.2	3	365	1.1	0.2	12							1.1			0.16			12		
K2	2.2	3	100	1.2	0.2	11	1.1	0.2	12				1.1	0.02	2.2	0.17	0.01	5.88	12	0.5	4.3
K2	1.8	1	365	1.1	0.2	7	1.1	0.2	6	1.0	0.2	7	1.0	0.02	2.3	0.20	0.00	0.00	7	0.5	7.1
K2	1.8	1	100	1.1	0.2	8	1.1	0.2	8				1.1	0.03	2.3	0.20	0.01	2.56	8	0.0	0.0
K2	2.0	1	365	1.2	0.2	6	1.2	0.2	7	1.2	0.2	8	1.2	0.02	2.0	0.21	0.01	4.56	7	1.0	15.0
K2	2.0	1	100	1.2	0.2	6	1.2	0.2	6				1.2	0.01	0.4	0.18	0.02	8.57	6	0.0	0.0
K2	2.2	1	365	1.2	0.2	6	1.3	0.2	6	1.3	0.2	3	1.2	0.05	3.9	0.18	0.02	9.62	5	1.3	27.2
K2	2.2	1	100	1.3	0.2	5	1.3	0.2	5				1.3	0.03	2.0	0.18	0.00	2.86	5	0.0	0.0
CB	1.8	3	365	3.1	0.3	25	2.8	0.2	25	2.5	0.2	22	2.8	0.24	8.7	0.22	0.02	10.88	24	1.4	5.9
CB	1.8	3	100	2.9	0.2	14	2.4	0.2	14				2.7	0.25	9.4	0.20	0.00	0.00	14	0.0	0.0
CB	2.2	3	365	3.1	0.2	12	3.0	0.2	11				3.1	0.05	1.6	0.20	0.00	0.00	12	0.5	4.3
CB	2.2	3	100	2.8	0.2	11	2.9	0.2	11				2.9	0.05	1.8	0.20	0.00	0.00	11	0.0	0.0
CB	1.8	5	365	3.2	0.2	105	3.1	0.2	100	3.1	0.2	100	3.1	0.05	1.5	0.19	0.01	4.88	102	2.4	2.3
CB	1.8	5	100	2.9	0.2	70	3.0	0.2	68				3.0	0.05	1.7	0.19	0.01	5.26	69	1.0	1.4
CB	2.2	5	365	3.2	0.2	60	3.4	0.2	65	3.4	0.2	55	3.3	0.09	2.8	0.20	0.00	0.00	60	4.1	6.8
CB	2.2	5	100	3.4	0.2	40	3.4	0.2	45				3.4	0.00	0.0	0.20	0.00	0.00	43	2.5	5.9
SW-K	1.8	5	365	3.2	0.2	85	3.2	0.2	80	3.2	0.2	85	3.2	0.00	0.0	0.20	0.00	0.00	83	2.4	2.8
SW-K	1.8	5	100	3.3	0.2	70	3.2	0.2	65				3.3	0.05	1.5	0.20	0.00	0.00	68	2.5	3.7

Table 6-2: (continued) Oedometer test results for intact lime-admixed soils cured for 100 and 365 days.

Soil				Test No.									Statistics								
Type	W=w/W_{LL}	C (%)	Time (days)	1St test			2nd test			3rd test			C_c			C_s			σ'_{vy} (kPa)		
				C_c	C_s	σ'_{vy}	C_c	C_s	σ'_{vy}	C_c	C_s	σ'_{vy}	$\bar{x}$	S.D	COV	$\bar{x}$	S.D	COV	$\bar{x}$	S.D	COV
SW-K	2.2	5	365	3.4	0.3	55	3.2	0.3	57	3.3	0.3	40	3.3	0.08	2.5	0.25	0.00	0.00	51	7.6	15.0
SW-K	2.2	5	100	3.6	0.3	35	3.4	0.3	37				3.5	0.10	2.9	0.26	0.01	1.96	36	1.0	2.8
SW-K	1.8	3	365	3.0	0.3	25	2.8	0.3	22	2.7	0.3	20	2.8	0.12	4.4	0.28	0.02	8.32	22	2.1	9.2
SW-K	1.8	3	100	2.4	0.3	18							2.4			0.25			18		
SW-S	1.8	5	365	1.9	0.1	220	1.9	0.1	210				1.9	0.02	1.3	0.10	0.00	0.00	215	5.0	2.3
SW-S	1.8	5	100	1.8	0.1	100	1.9	0.1	110				1.9	0.05	2.7	0.10	0.00	0.00	105	5.0	4.8
SW-S	2.0	5	365	2.0	0.1	200							2.0			0.10			200		
SW-S	2.0	5	100	2.0	0.1	95	1.9	0.1					2.0	0.05	2.6	0.10	0.00	0.00	95	0.0	0.0
SW-S	2.0	3	100	1.7	0.1	51							1.7			0.10			51		
SW-S	2.0	3	365	1.7	0.1	55							1.7			0.10			55		
K1	1.8	5	365	1.3	0.1	110							1.3			0.14			110		
K1	1.8	1	365	1.0	0.2	7							1.0			0.20			7		
G	1.4	5	365	0.4	0.0	11	0.3	0.0	10				0.4	0.01	2.9	0.04	0.00	0.00	11	0.5	4.8
G	1.4	5	100	0.3	0.0	10	0.3	0.1	10				0.3	0.00	0.0	0.05	0.01	20.00	10	0.0	0.0
G	1.6	5	365	0.3	0.1	2	0.3	0.1	1				0.3	0.00	0.0	0.05	0.00	0.00	2	0.5	33.3
G	1.6	5	100	0.4	0.1	5	0.4	0.1	1				0.4	0.01	1.3	0.05	0.00	0.00	3	2.0	80.0
G	1.4	3	365	0.4	0.1	9							0.4			0.05			9		
G	1.4	3	100	0.4	0.1	8	0.3	0.0	10				0.4	0.00	1.4	0.05	0.01	10.00	9	1.0	11.1

Table 6-4: Oedometer test results for remoulded lime-admixed soils cured for 100 and 365 days

Soil				Tests						Statistics						Si
Type	W=w/W_{LL}	C (%)	Time (days)	1St test		2nd test		3rd test		Cc			$б'_{vr}$ (kPa)			
				Cc	$б'_{vr}$	Cc	$б'_{vr}$	Cc	$б'_{vr}$	$\bar{x}$	S.D	COV	$\bar{x}$	S.D	COV	
K2	1.8	5	365	0.8	6.0	0.8	7.5	0.7	5.0	0.8	0.03	4.4	6.2	1.0	16.7	17.0
K2	1.8	5	100	0.8	1.0					0.8			1.0			26.0
K2	2	5	365	0.9	3.0	0.8	5.0	0.9	1.0	0.9	0.03	3.8	3.0	1.6	54.4	25.0
K2	2	5	100	0.8	2.0	0.8	2.0			0.8	0.00	0.7	2.0	0.0	0.0	9.3
K2	2.2	5	365	1.0	2.5	0.9	2.5	0.9	2.0	0.9	0.05	4.9	2.3	0.2	10.1	22.6
K2	2.2	5	100	0.9	2.0	0.9	2.0			0.9	0.01	0.6	2.0	0.0	0.0	9.8
K2	1.8	3	365	0.8	1.5	0.8	1.7	0.8	1.7	0.8	0.01	1.2	1.6	0.1	5.8	17.3
K2	1.8	3	100	0.6	1.3	0.7	1.2			0.7	0.04	6.1	1.3	0.1	4.0	16.0
K2	2	3	365	0.9	3.1	0.8	1.0	0.9		0.9	0.02	2.2	2.1	1.1	51.2	7.6
K2	2	3	100	0.8	2.0	0.8	1.5			0.8	0.01	1.3	1.8	0.3	14.3	6.6
K2	2.2	3	365	0.8	0.9					0.8			0.9			13.3
K2	2.2	3	100	0.9	0.8	0.9	1.0			0.9	0.00	0.5	0.9	0.1	11.1	12.8
K2	1.8	1	365	0.7	0.8	0.7			1.3	0.7	0.00	0.7	1.1	0.3	23.8	6.3
K2	1.8	1	100	0.7	1.1					0.7			1.1			7.3
K2	2	1	365	0.8	0.6	0.8	1.4	0.8	1.4	0.8	0.01	1.6	1.1	0.4	33.3	6.0
K2	2	1	100	0.8	0.9	0.8	0.9			0.8	0.01	0.7	0.9	0.0	0.0	6.7
K2	2.2	1	365	0.9	0.9	0.9	0.9			0.9	0.01	1.1	0.9	0.0	0.0	5.4
K2	2.2	1	100	0.8	0.5	0.8	0.8			0.8	0.01	0.7	0.7	0.2	23.1	7.7
CB	1.8	3	365	1.7	3.5	1.7	0.6	1.7	1.5	1.7	0.01	0.8	1.9	1.2	64.9	12.9
CB	1.8	3	100	1.7	2.0	1.7	2.0			1.7	0.01	0.3	2.0	0.0	0.0	7.0
CB	2.2	3	365	2.0	1.0	1.9	0.9			1.9	0.01	0.5	1.0	0.1	5.3	12.1
CB	2.2	3	100	1.9	1.0	2.0	1.0			1.9	0.01	0.3	1.0	0.0	0.0	11.0
CB	1.8	5	365	1.6	4.0	1.8	2.5	1.6	3.0	1.7	0.09	5.4	3.2	0.6	19.7	32.1
CB	1.8	5	100	1.7	3.0	1.7	2.0			1.7	0.01	0.6	2.5	0.5	20.0	27.6
CB	2.2	5	365	2.1	1.5	2.1	2.5	2.1	0.9	2.1	0.00	0.0	1.6	0.7	40.4	36.7
CB	2.2	5	100	2.0	1.0	2.1	1.5			2.1	0.04	1.7	1.3	0.3	20.0	34.0
SW-K	1.8	5	365	2.0	6.0	2.0	5.0	2.0	3.0	2.0	0.02	1.2	4.7	1.2	26.7	17.9
SW-K	1.8	5	100	2.0	6.0	2.1	5.0			2.1	0.05	2.4	5.5	0.5	9.1	12.3
SW-K	2.2	5	365	2.2	3.5	2.2	3.5	2.2	3.0	2.2	0.02	1.1	3.3	0.2	7.1	15.2
SW-K	2.2	5	100	2.4	3.5	2.3	3.0			2.3	0.02	1.1	3.3	0.3	7.7	11.1
SW-K	1.8	3	365	1.6	3.0	1.7	2.5	1.7	3.0	1.7	0.04	2.4	2.8	0.2	8.3	7.9
SW-K	1.8	3	100	1.7	2.5					1.7			2.5			7.2
SW-S	1.8	5	365	1.1	2.5	1.1	2.0			1.1	0.01	0.9	2.3	0.3	11.1	95.6
SW-S	1.8	5	100	0.8	1.0	0.8	1.0			0.8	0.00	0.6	1.0	0.0	0.0	105
SW-S	2	5	365	1.0	1.0					1.0			1.0			200
SW-S	2	5	100	0.9	3.0	0.9	1.8			0.9	0.01	0.5	2.4	0.6	25.0	39.6
SW-S	2	3	100	1.0	3.0					1.0			3.0			17.0
SW-S	2	3	365	1.1	1.5					1.1			1.5			36.7
K1	1.8	5	365	0.7	1.8					0.7			1.8			61.1
K1	1.8	1	365	0.7	1.0					0.7			1.0			7.0
G	1.4	5	365	0.3	1.0	0.3	1.0			0.3	0.01	3.3	1.0	0.0	0.0	10.5
G	1.4	5	100	0.3	1.0	0.3	1.0			0.3	0.00	0.7	1.0	0.0	0.0	10.0
G	1.6	5	365	0.3	0.6	0.3	0.6			0.3	0.00	1.7	0.6	0.0	0.0	2.5
G	1.6	5	100	0.3	0.6	0.3	0.6			0.3	0.01	1.6	0.6	0.0	0.0	4.2
G	1.4	3	365	0.4	1.0					0.4			1.0			9.0
G	1.4	3	100	0.4	1.0	0.4	1.0			0.4	0.02	5.4	1.0	0.0	0.0	9.0

6.2.2 Kaolin (K2) clay

Figure 6-1 shows the results of the one-dimensional consolidation tests on intact lime-admixed kaolin (K2). The continuous lines represent the results of tests on soils cured for 365 days and the dotted lines are for tests of 100 days. The resulting yield stress ($6'_{vy}$) of each repeated test is summarized in Table 6-3. Figure 6-1 shows that the direct effect of the increase of the lime content is to increase the vertical yield stress of the kaolin. For example, at 1.8 times the liquid limit and 365 days curing time, the yield stresses are 8.0, 28, and 105 kPa for lime contents of 1%, 3%, and 5% respectively. On the other hand, increasing the water contents has an adverse effect on the resulting yield stress. For example, the yield stress for 5% lime content (Figure 6-1(a)) are 106, 75, and 52 kPa for water contents of 1.8, 2.0, and 2.2 (W_{LL}) respectively.

Aging tends to increase the yield stress. However, as shown in Figure 6-1(c) for low lime contents (1%), a decrease in yield stress is observed between 100 days and 365 days of curing. This parallels the observed decrease in undrained shear strength for these soils, which is believed to be a result of lime depletion.

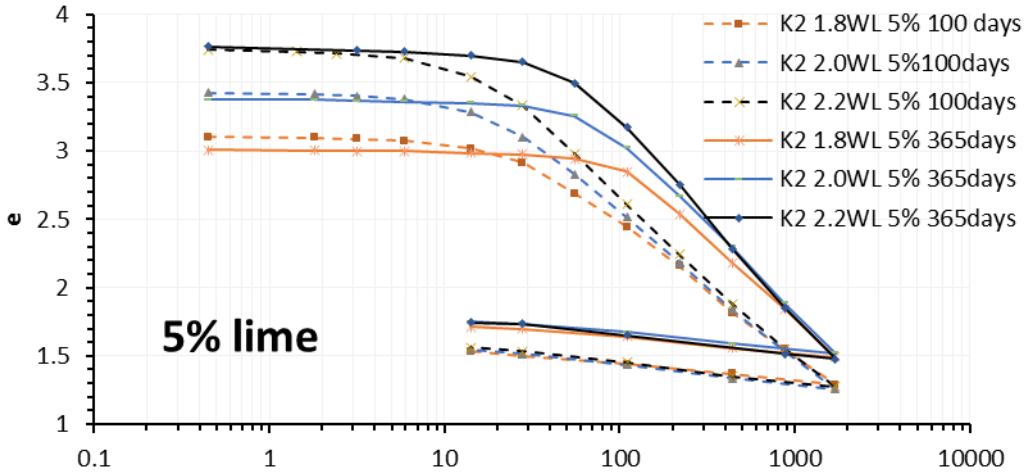

(a)

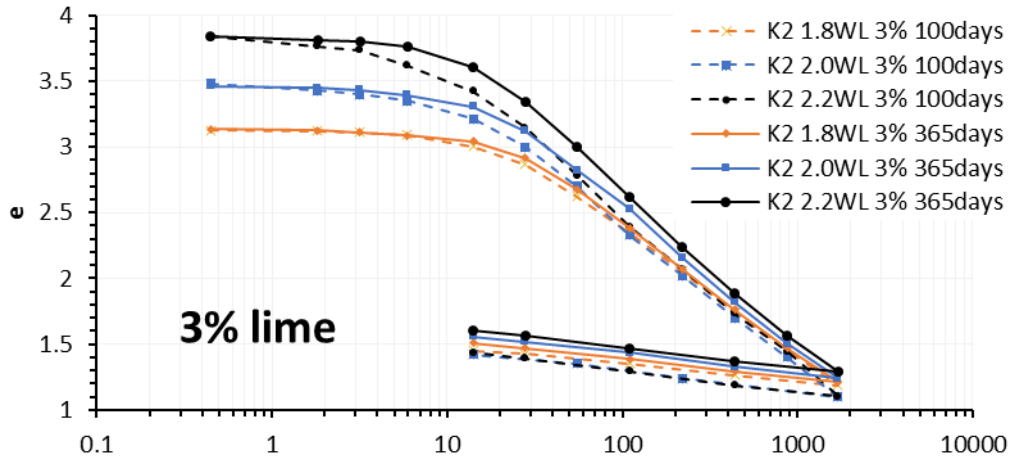

(b)

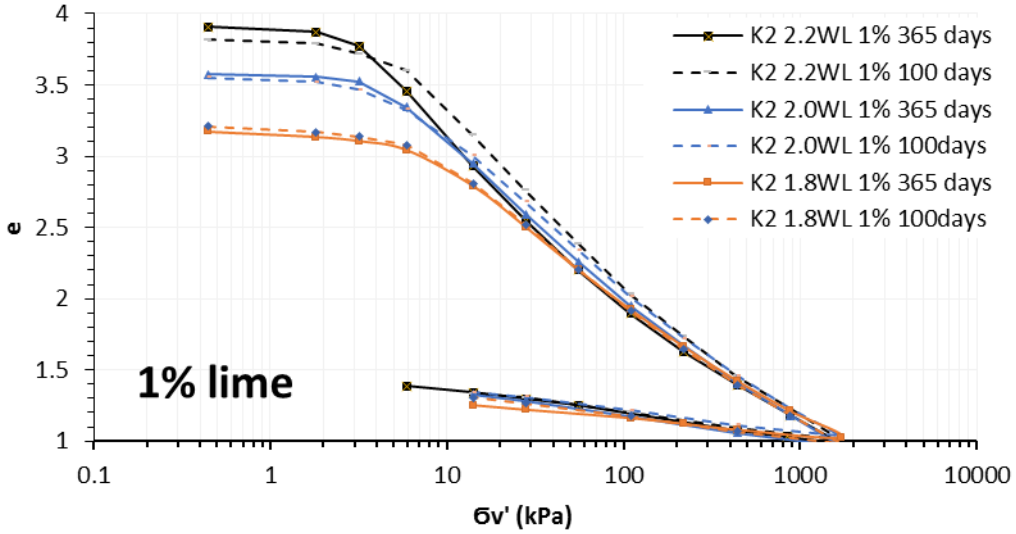

(c)

Figure 6-1: Oedometer test results for lime-admixed kaolin (K2) clay cured for 100 and 365 days.

Figure 6-2 summarizes the oedometer tests results for 365 days. The increase in yield stress with an increase in lime content is manifest by a shifting of the consolidation curve in the post yield state to the right. A similar behaviour has been observed for cement treated soils

(Gens and Nova, 1993) and lime-treated soils, at lower water contents (Tremblay et al., 2001). Consequently, higher vertical stresses are needed to bring about the same change in volumetric deformation at higher lime contents. It can be inferred that the soil structure is not destroyed immediately by primary yield but that substantial post-yield strain is required before convergence to one general post yield compression line occurs. This is observed at all water contents, as can be seen in Figure 6-2. The compression paths of the soils all follow a post-yield compression line that is unique for each lime content, regardless to the initial void ratio. This behaviour is similar to that observed by Lorenzo and Bergado (2004), Horpibulsuk et al. (2004a), and Rotta et al. (2003) for soils stabilized with Portland cement in which the compression index depends only on cement content, and not water content.

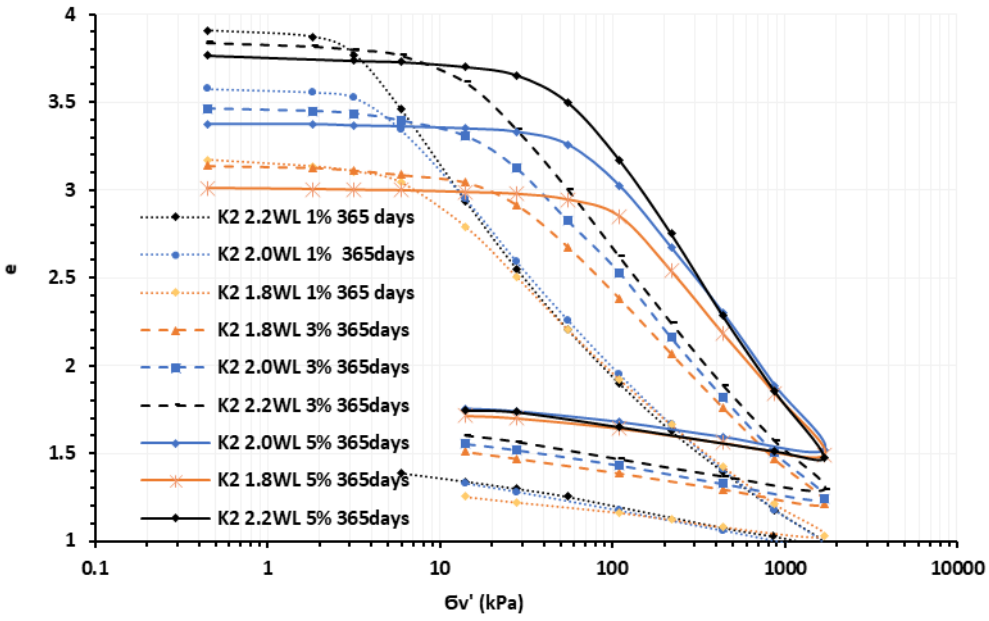

Figure 6-2: Oedometer tests results for kaolin (K2) clay cured for 365 days.

Figure 6-3 shows the results of oedometer tests on intact lime-admixed kaolin (K2) at different water contents cured for 100 and 365 days. In the pre-yield stages, the soils can be grouped according to their initial void ratios regardless of their curing period. The yield stresses of these soils in each group, differs according to their lime contents and curing time. In the post yield stages, soils follow three different sets of paths. The far right set is for the highest lime content (5%) cured for 365 days while the far left set is for soils of the least lime content (1%) irrespective their curing time. The medium set is for those of the modest lime content (3%) irrespective of their curing time and those of 5% lime at low curing time (100 days). These results suggest that the post peak behaviour of lime-admixed kaolin is controlled by the lime content and the curing time. This reflects the fact that pozzolanic reaction is a time and lime dependent process.

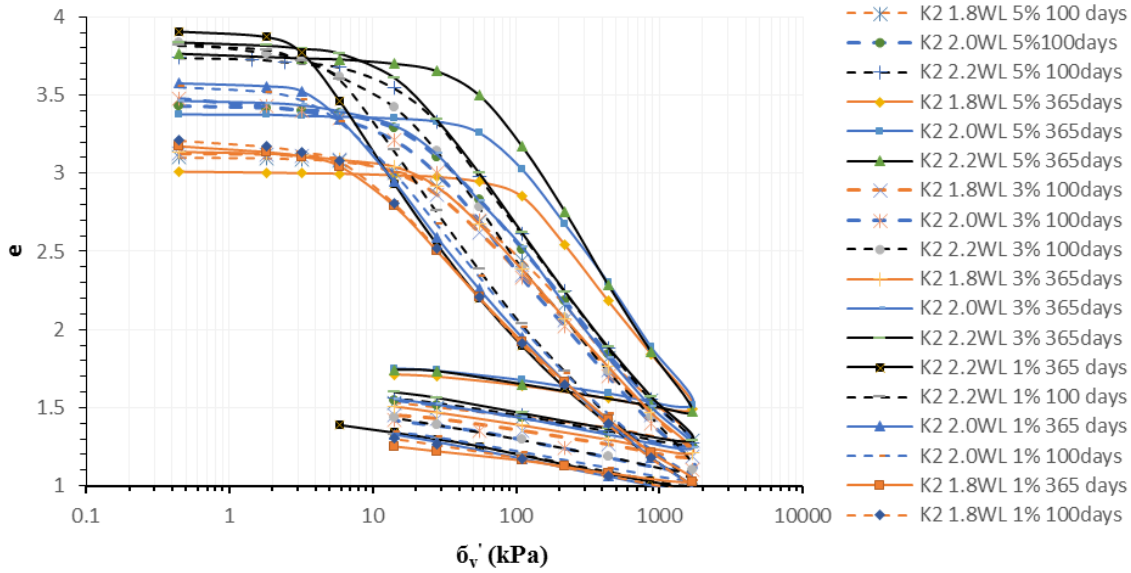

Figure 6-3: Oedometer tests results for intact lime-admixed kaolin (K2) clay cured for 100 and 365 days

Figure 6-4 compares the results of oedometer tests conducted on intact and remoulded lime-admixed kaolin (K2) cured for 365 days. Although the intact and remoulded soils start from the same void ratio, their paths diverge up to the yield stress, and then approach each other at higher stress levels, in much the same fashion as natural clays (Hong et al., 2012; Xiao and Lee, 2014). However, for 5% lime content, the convergence of the paths is not complete even at an applied vertical stress of 1600 kPa. Further strain may well be required to establish similar fabric and particle packing (Leroueil and Vaughan, 1990). Coincidence occurs for lime contents of 1% and 3%, at void ratios of 1.2 and 1.4 respectively. These void ratios correspond to water contents of 0.46 and 0.54, respectively, which are slightly different from their plastic limits (Chapter 5). This result is broadly consistent with the observations that coincidence occurs in natural clays at the plastic limit (Wood, 1990). It is also consistent with the finding that soil sensitivity of natural clays at the plastic limit is close to unity (Skemption and Northey, 1952).

These results indicate a direct relationship between the yield stress $6'_{vy}$ and the undrained shear strength of these sensitive soils, in which the yield point depends on the strength of soil structure.

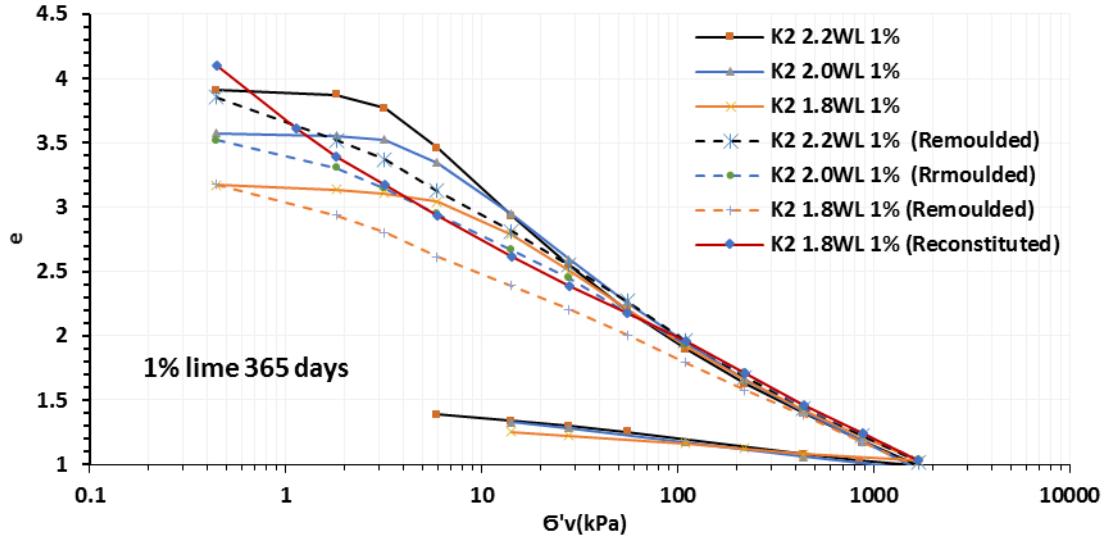

(a)

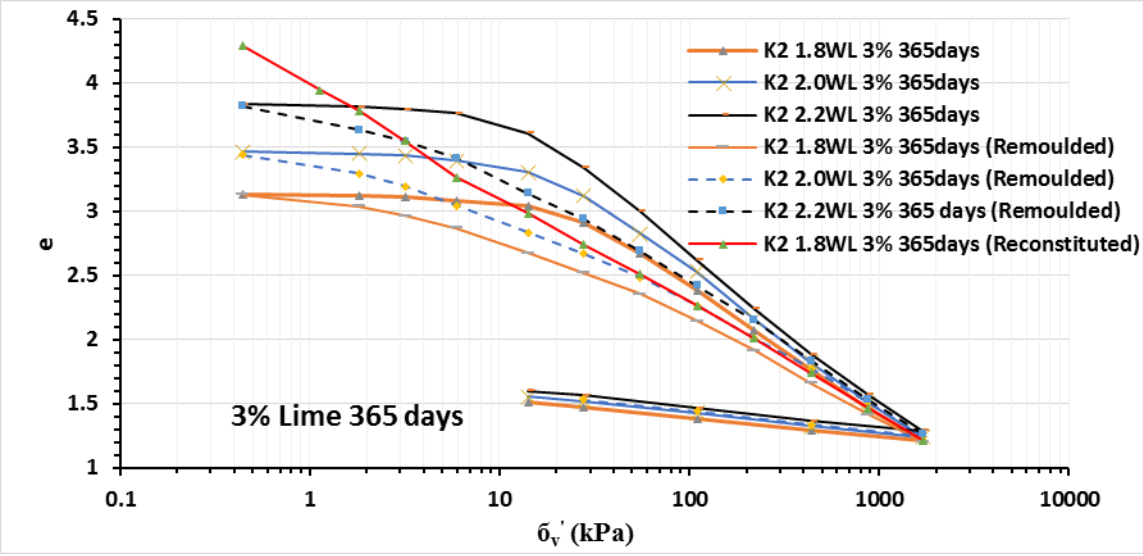

(b)

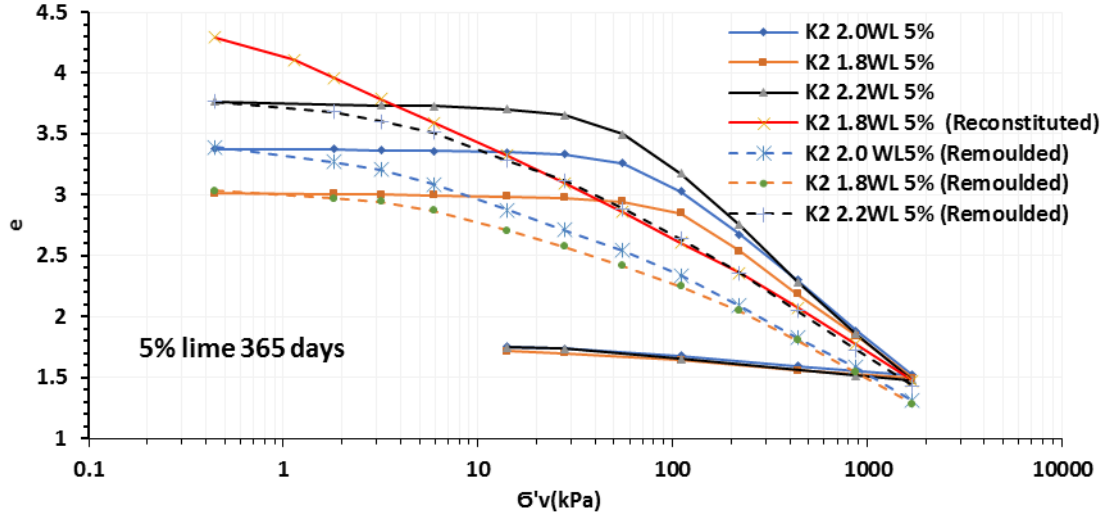

(c)

Figure 6-4: Oedometer test results for intact and remoulded lime-admixed kaolin (K2) cured for 365 days: (a) 1%, (b) 3%, and (c) 5% lime.

6.2.3 Kaolin (K1) clay

The results of the oedometer tests conducted on intact and remoulded specimens after curing for 365 days are shown in Figure 6-5. For this soil, identification of a yield stress, particularly for the lowest lime contents proved to be difficult. Moreover, there was a little evidence that coincidence between the compression curves of intact and remoulded soil would occur within the normal range of pressures. The reason for this anomalous response are not understood.

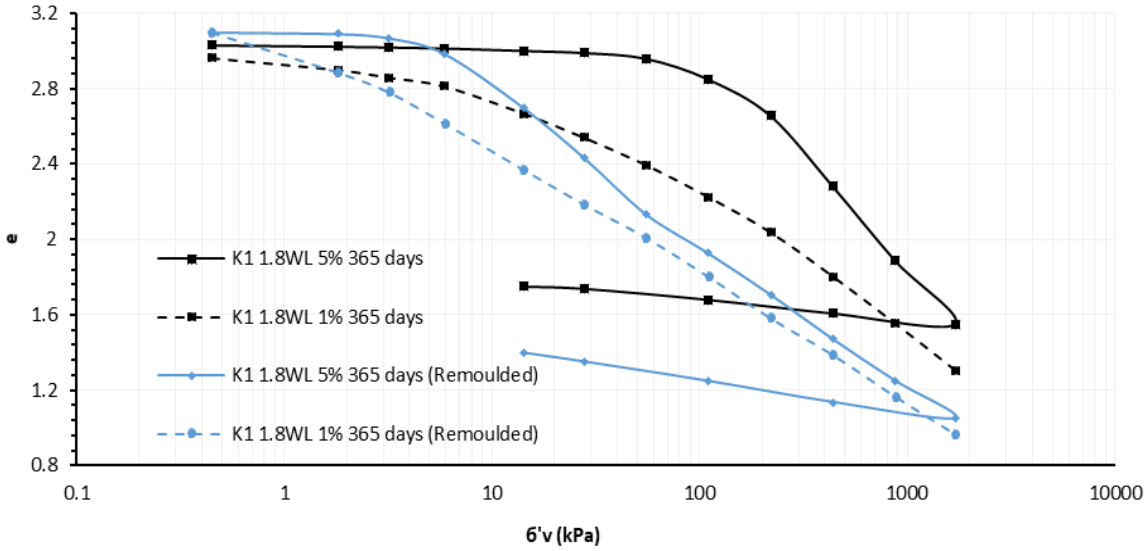

Figure 6-5: Oedometer test results on lime treated kaolin (K1) at 1.8WLL cured for 365 days

6.2.4 Calcium base bentonite (CB) clay

Figure 6-6 shows the results of oedometer tests on intact CB soil, dosed with 3% and 5% lime. The results of the repeated tests on intact specimens are summarized in Table 6-3. For this soil, the yield stress changes very little after 100 days of curing. This is analogous to the results obtained for the undrained shear strength (see section 5.5.3). Interestingly, the vertical yield stress for this soil (after 365 days) is very similar to that for kaolin clay (at the same w / W_{LL} ratio and lime content). For example, for 1.8W_{LL} and 5% lime content, the yield stresses for CB clay and kaolin (K2) clay are 102 and 105 kPa, respectively which are analogous to the undrained shear strengths of these soils (see Table 5-15). This again suggests a relationship between the undrained shear strength of these soils and the vertical yield stress from oedometer tests.

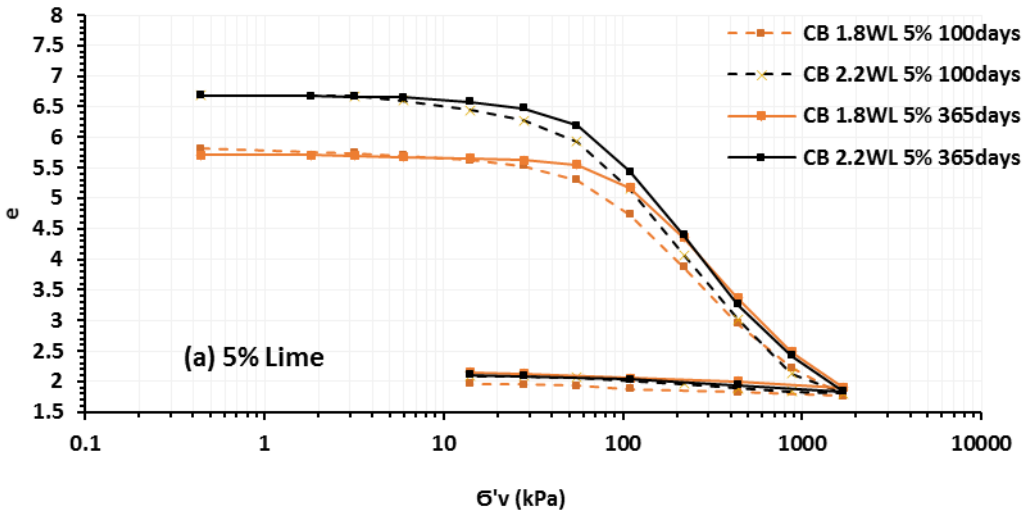

(a)

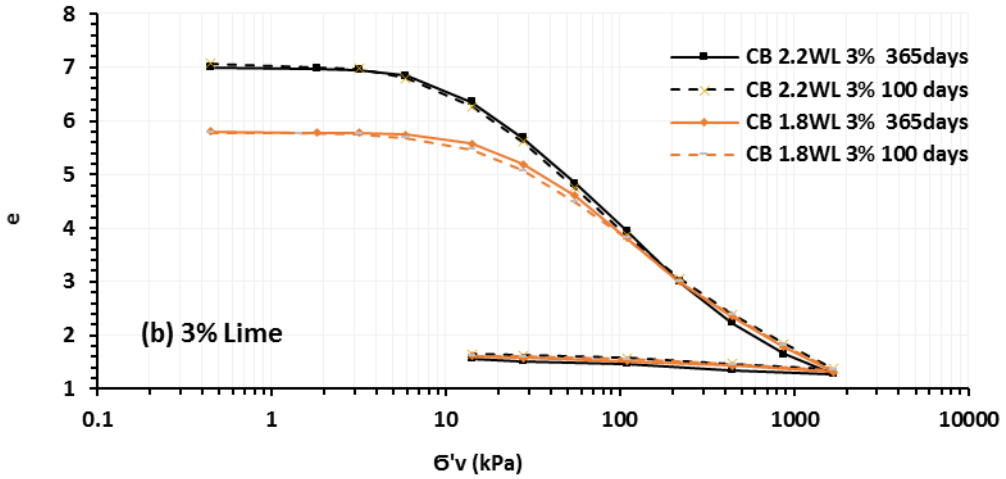

(b)

Figure 6-6: Oedometer test results for CB: (a): 5% lime and (b): 3% lime

Figure 6-7 compares the oedometer results for intact and remoulded CB clay after 365 days of curing. Coincidence between the curves is achieved at approximately 350 kPa for 3% lime, but over 2000 kPa for 5% lime. This may be attributed to the stronger and more durable bonding which is developed at higher lime contents.

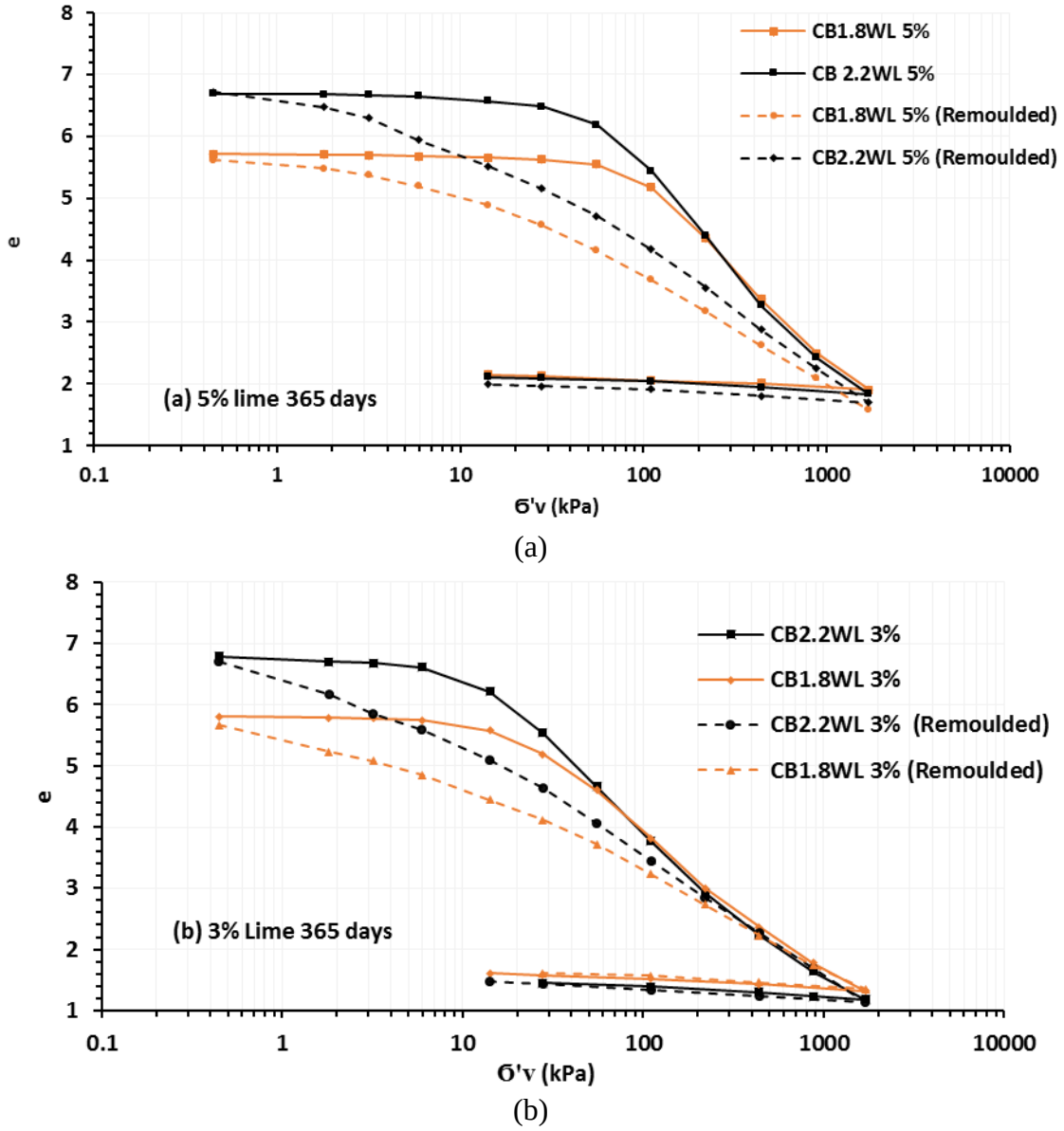

Figure 6-7: Oedometer results for intact and remoulded CB soil, at 365 days: (a): 5% lime and (b): 3% lime

Figure 6-8 summarizes the oedometer tests results for the intact CB soil after 365 days. This plot highlights the fact that the curves for the same lime content become coincident irrespective of the initial water contents. Rather higher consolidation stresses are required for the 5% lime content soils to coincide with the curves for 3% lime. The differences in the initial points of the curves (particularly for w =2.2W_{LL}) is attributed to the observed separation of water from the mix soon after admixing of the lime.

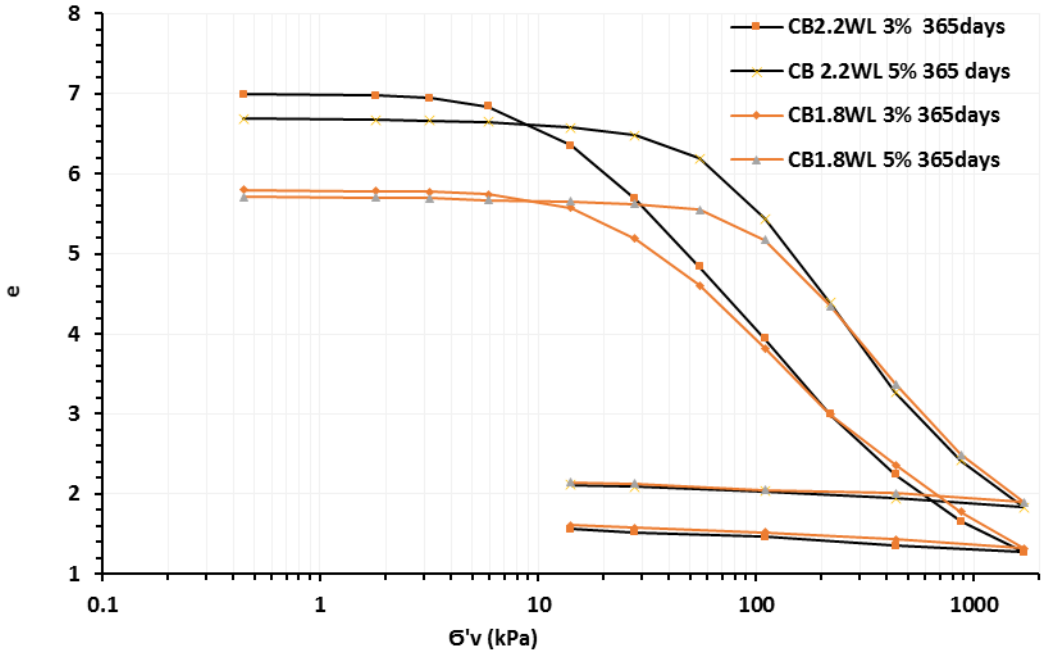

Figure 6-8: Oedometer results for intact lime-treated CB soil cured for 365 days

6.2.5 SW-K mix

Figure 6-9 shows the oedometer test results for intact SW-K admixtures specimens cured for 100 and 365 days. Again, irrespective of the initial water content, the paths followed by soils treated with same lime contents merge into one in the post-yield zone.

As summarized in Table 6-3, the yield stresses of intact specimens increase significantly with increasing curing time. For example, for soils with initial water contents of $1.8W_{LL}$ specimens, with 5% lime content, the vertical yield stresses are 68 kPa and 83 kPa after 100 and 365 days, respectively. This is different from that observed for CB soil, although both soils have the same liquid limits. Thus, the rate of the pozzolanic reaction cannot be characterized by liquid limit alone. However, there are similar features between the two soils: the paths are displaced to the right with increasing lime content.

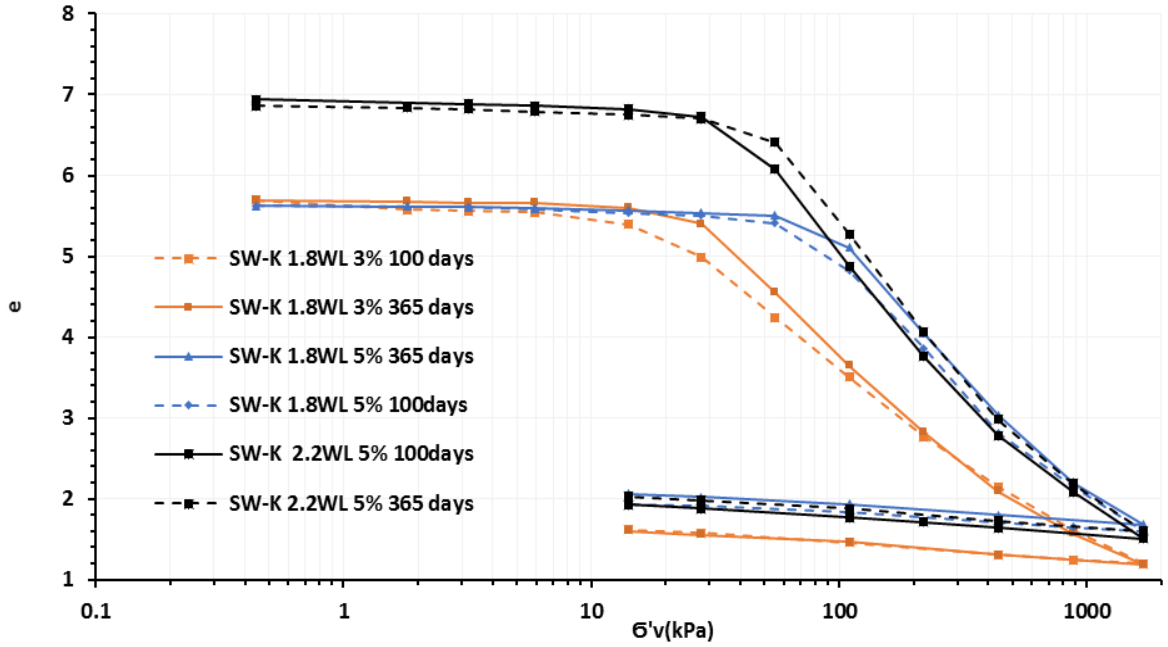

Figure 6-9: Oedometer test results for the lime-admixed SW-K mix.

Figure 6-10 shows that although most of the bonding is lost by remoulding, the curves for different lime contents do not coincide at high consolidation pressures. This figure shows that the vertical yield stress for 365-day samples are approximately the same as those for K2 and CB soils (at the same w / W_{LL} ratio and lime content). For example (at W=2.2 and 5% lime content), yield stress of 51, 53, and 60 kPa were found for SW-K, K2, and CB soils, respectively.

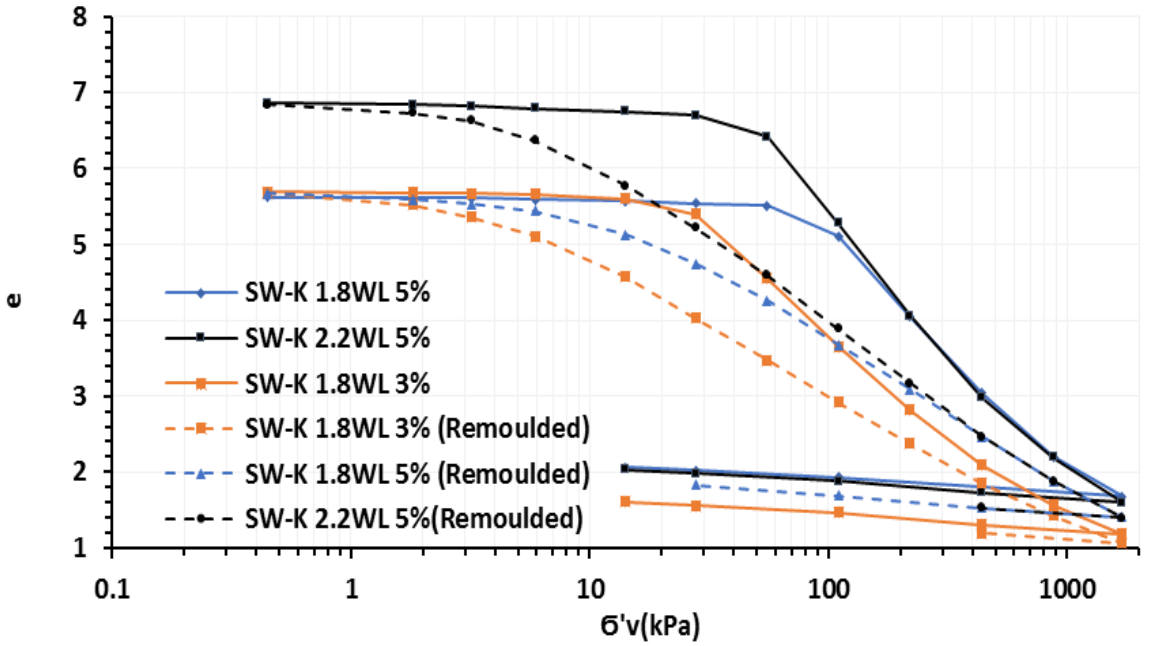

Figure 6-10: Oedometer results for intact and remoulded lime-admixed SW-K soils, cured for 365 days.

6.2.6 SW-S mix

Figure 6-11 shows the oedometer tests results for intact lime-admixed SW-S slurries specimens cured for 100 and 365 days. The results are summarized in Table 6-3. For 3% lime content, the yield stress hardly increases after 100 days, but for 5% lime content, the yield stress doubles (approximately) between 100 and 365 days. This underlines analogous observations during the penetration tests which demonstrate that sufficient lime must be available to sustain the pozzolanic reaction.

A small but significant decrease in initial void ratio can be observed between samples cured for 100 and 365 days. This can be attributed to the consumption of water by the pozzolanic reaction. This reduction of volume was apparent by visual inspection (particularly those with 5% lime content) although all the specimens were sealed in sealed containers as described elsewhere.

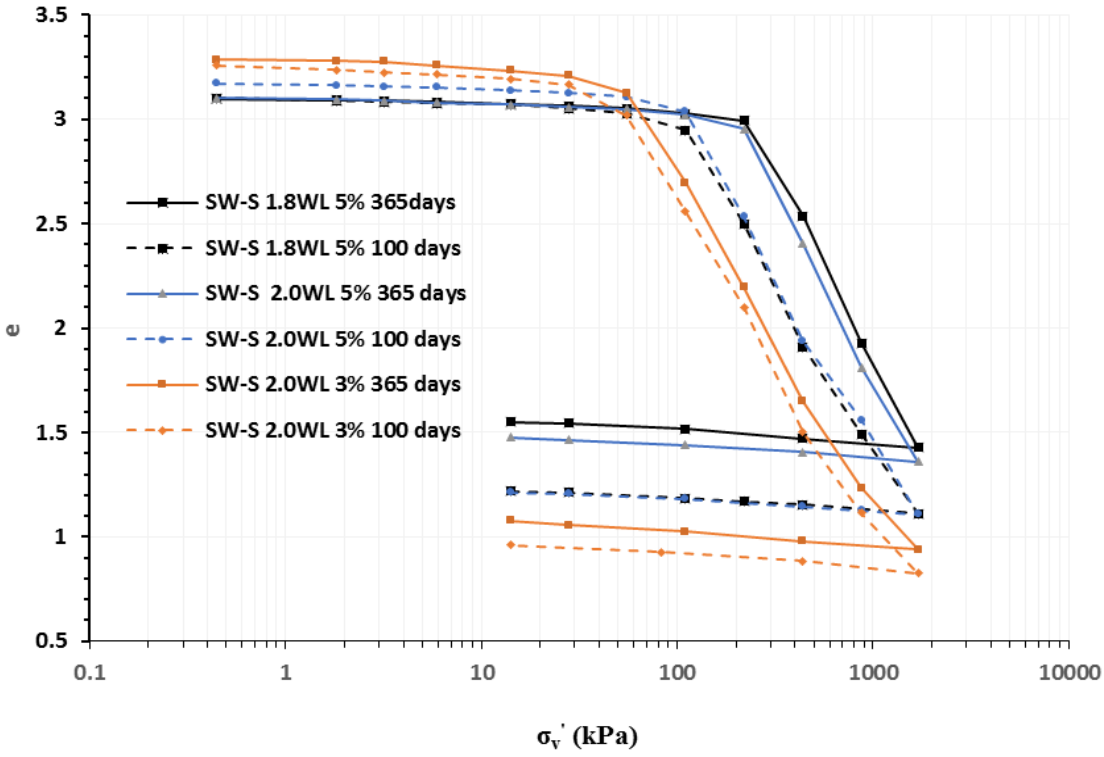

Figure 6-11: Oedometer tests results for lime-admixed SW-S soils.

A comparison between intact and remoulded samples after 365 curing days is shown in Figure 6-12. Qualitatively, the results display similar trends to those obtained for the other soils: remoulding destroys the soil structure which is manifest in the distinct yield stress in intact soil. However, over the (wide) range of consolidation pressure, there is a little difference between the compressibility of the intact and remoulded samples.

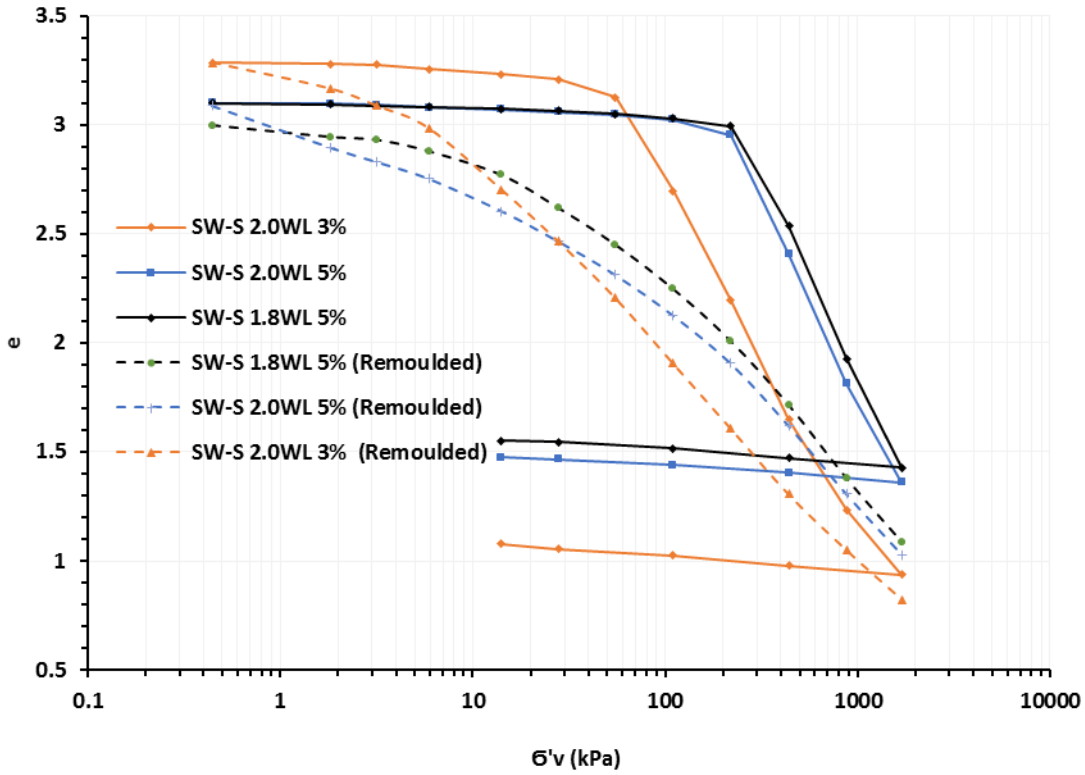

Figure 6-12: Effect of remoulding on oedometer test results for lime-admixed SW-S cured for 365 days.

6.2.7 Grangemouth soil

Figure 6-13(a) shows the oedometer test results for Grangemouth soil at 5% lime content: the results of repeated tests are summarized in Table 6-3. This soil behaves rather differently from the other soils: it is hard to identify a distinct yield stress, for example. Partial segregation of soil particles from the water was also observed, which makes the definition of water content (void ratio) problematic.

The curves, for different water contents and curing periods, differ little from each other and become coincident at very high consolidation pressure. Broadly similar trends are apparent in these soils treated with 3% lime (Figure 6-13b). The modest degree of cementation which takes place in this soil is manifest in the comparison between remoulded and intact soil (Figure 6-14): there is little difference between these consolidation curves.

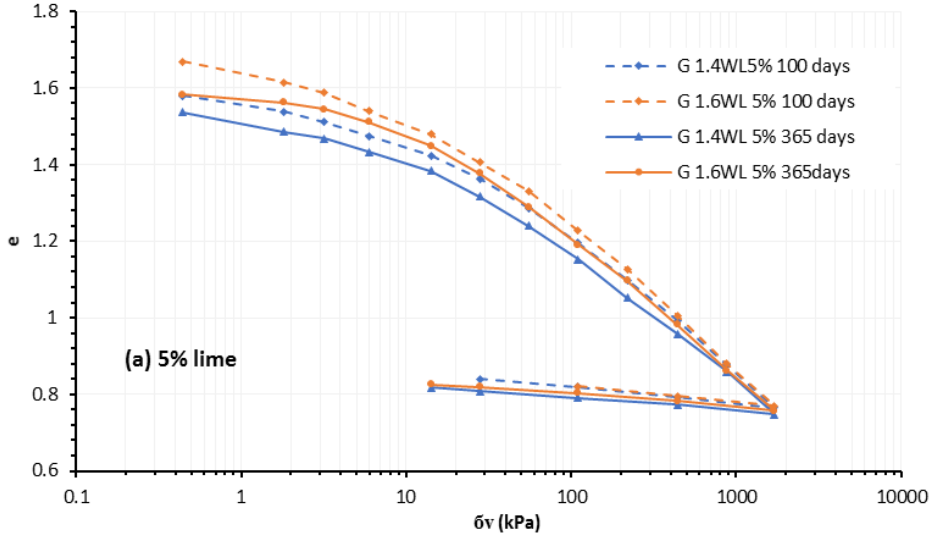

(a)

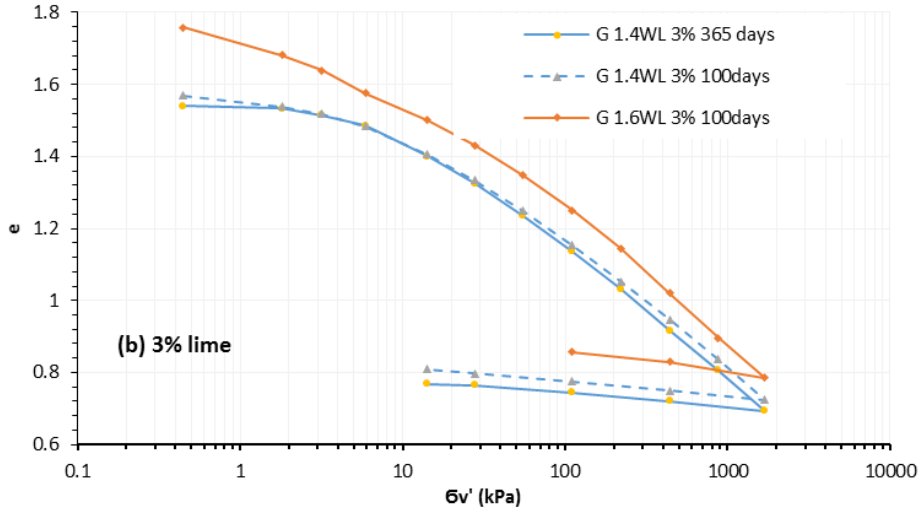

(b)

Figure 6-13: Oedometer test results for Grangemouth soil: (a) 5% lime content and (b) 3% lime content

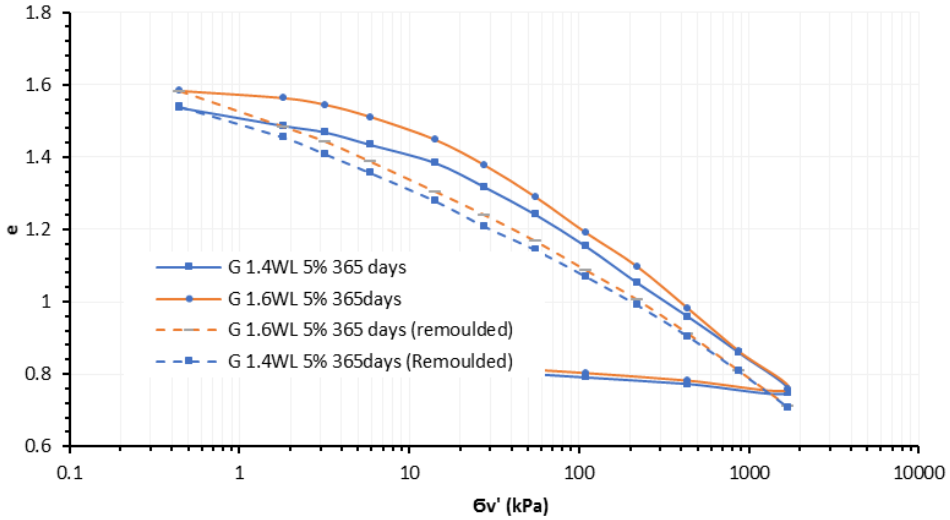

Figure 6-14: Oedometer test results for intact and remoulded (5% lime) Grangemouth soil, after 365 days

6.3 Discussion

The relationship between (oedometer) yield stress and undrained shear strength

The results show that clay admixtures with the same ratio of water content to liquid limit ($W=w / W_{LL}$) have similar yield stresses, as shown in Table 6-5. The results for coarse-grained soils (i.e., the SW-S soil mix or Grangemouth soil) can be quite different. This observation suggests that the correlation between undrained shear strength and yield stress σ_{vy}' for these sensitive soils depends on the strength of soil structure.

Table 6-5: Yield stresses σ_{vy}' (kPa) for lime-admixed clays (cured for 365 days).

Lime content C (%)	W= w / W_{LL}	Yield stress σ_{vy}' (kPa)		
		Kaolin (K2)	SW-K	CB
5	1.8	105	83	102
	2.2	53	51	60
3	1.8	28	22	24
	2.2	12		12

Figure 6-15 shows a scatter plot of vertical yield stress (from oedometer tests) and the corresponding undrained shear strength (obtained from penetration tests). The straight-line correlation between undrained shear strength and yield stress is

$$C_u = 0.45\ \sigma_{vy}' \qquad 6\text{-}1$$

The scatter may, in part, be attributed to the interpretation of vertical yield stress using the Casagrande method. It has been shown by Burland (1990) that for undisturbed natural sensitive clays that the ratio of undrained shear strength to the insitu vertical effective stress $S_u/\sigma_z' = \sim 0.3$, although for quick clays this ratio may be somewhat lower. Equation 6-1 gives a good match to Equation 2-17 suggested by Hassan and Ravaska (2009). Other correlations have been proposed between oedometer yield stress and undrained shear strength with other correlation factors ranges between 0.45~0.79 for artificially cemented soils (e.g. Federico et al. (2015) and Horpibulsuk et al. (2004b)).

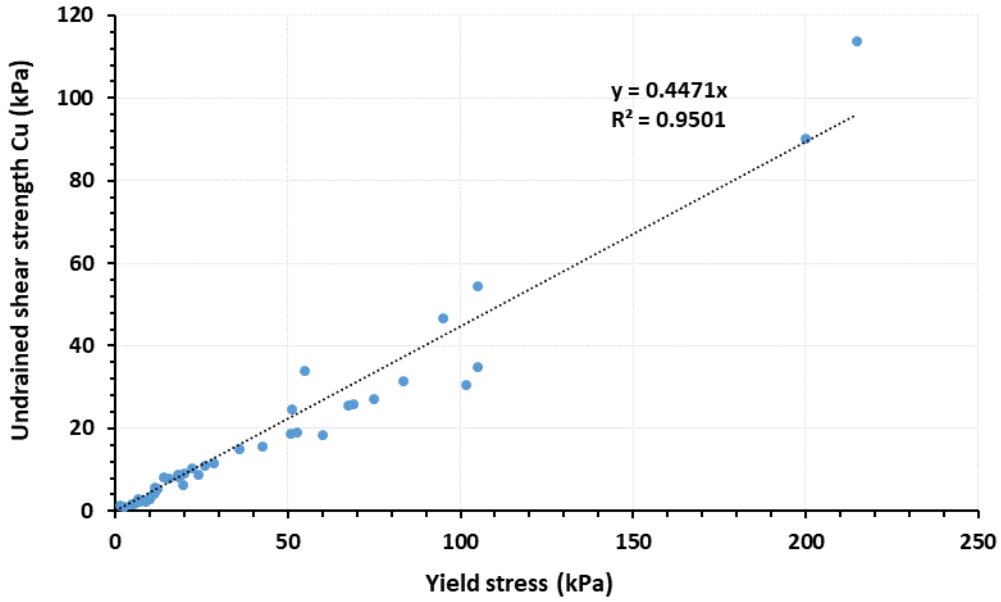

Figure 6-15: Correlation between undrained shear strength and oedometer yield stress.

Consolidation Indices

Figure 6-16 shows scatter plots which relate compression indices (C_c) and swell indices (C_s) with yield stress. Evidently, the C_c and C_s values are correlated with soil type, irrespective of yield stress. Soils with high liquid limits have the highest values of C_c and C_s and vice versa. Increasing lime content and curing time (as inferred by increasing yield stress) have little effect on these indices. Thus, different soils keep their identities in terms of C_c and C_s even after being admixed with lime that change the chemistry of the medium. The post yield consolidation curves, are shifted to the right by admixing soils with higher percentages of lime. Curves of different lime content (e.g., Figure 6-2) do not converge towards a unique path even at the highest stress level applied. Similar observations were made by Tremblay et al. (2001) for lime treated clays at lower water contents. They indicated that treated soils retain a memory of their fabric and the structure developed at much higher void ratios (Tremblay et al., 2001). Figure 6-16 which shows the extent of these changes demonstrates that the index values for each soil type remain distinct.

However with increasing lime content and curing time (and therefore $6'_{vy}$), there is a marginal increase in these soils' compression indices and a reduction in their swelling indices. This observation is consistent with the observations of Lorenzo and Bergado (2004) for cement-admixed soft plastic Bangkok clay who suggested that the increase in the compression index is caused by the excessive yielding of the soil at relatively higher magnitude of bonds. It is also consistent with the results obtained by Balasubramaniam et al. (1989) for lime treated plastic clay albeit for soils of much lower water contents.

However, these results are in contradiction with the results of Pakbaz and Farzi (2015) who found that the compression index C_c for lime-admixed mixtures of bentonite and sand decreased with increased additives.

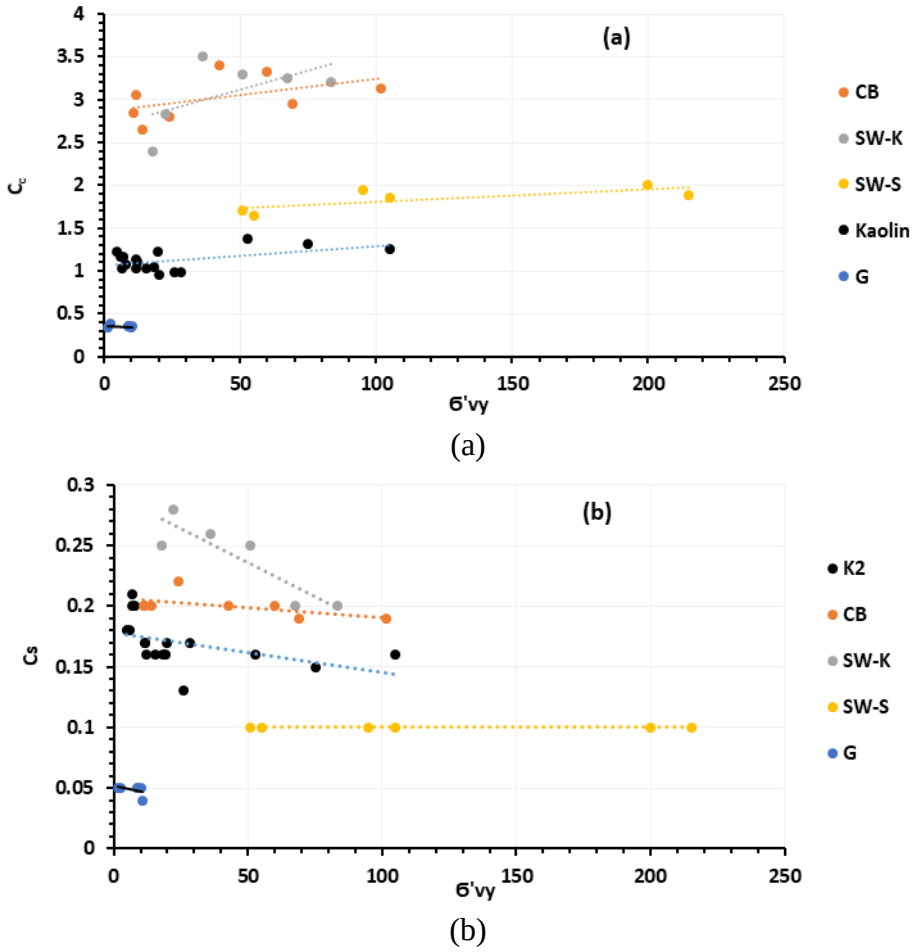

Figure 6-16: Scatter plots of: (a) compression indices Cc and (b) swell indices Cs.

Table 6-6 compares these Cc and Cs values for lime-admixed clays to some published values for undosed clays. For kaolin clay, the change in Cc due to lime treatment is more than that for montmorillonitic soils: Cc for kaolin becomes 1.3 due to lime treatment compared with approximately 0.35, while for CB and SW-K clays, C_c increases from about 2.2 to 3.0 due to lime treatment.

Table 6-6: Compression and swell indices for different soils before and after lime treatment

	Kaolin		CB		SW	
Index	**Before†**	**After**	**Before†**	**After**	**Before†**	**After**
Cc	0.25	1.2	2.0	3	2.2	3.1
Cs	0.06	0.16	0.4	0.2		0.24

†(Lambe and Whitman, 1979)

Soil sensitivity

In this section, we explore the possibility that there is a correlation between strength sensitivities S_t [i.e., the ratio of the peak to the residual undrained shear strength] and sensitivities obtained from oedometer tests. Two approaches are used to define the sensitivity from oedometer tests:

1. The initial sensitivity (S_i):

Referring to Figure 6-17, the initial sensitivity (S_i) can be defined as the ratio between the yield stress ($6'_{vy}$) for intact soils and the corresponding consolidation stress ($6'_{vr}$) at the same void ratio for remoulded soils (Xiao 2014):

$$S_i = \frac{6'_{vy}}{6'_{vr}} \qquad 6\text{-}2$$

Using the data obtained from the tests conducted on the intact and remoulded specimens, values of $6'_{vy}$ and $6'_{vr}$ were obtained for each test conducted as summarized in Table 6-3 and Table 6-4 respectively. The initial sensitivities S_i were then calculated based on the mean values of $6'_{vy}$ and $6'_{vr}$ as summarized in Table 6-4. For example, the initial sensitivity of kaolin, with 5% lime content, W = 1.8 and cured for 365 days is 17.

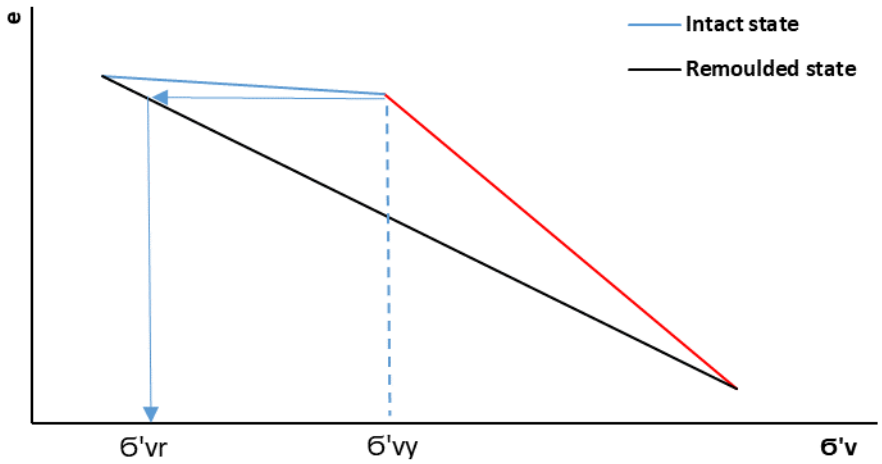

Figure 6-17: Parameters defining the initial sensitivity from oedometer test results.

2. The stress sensitivity (S_σ)

Using the methodology suggested by Cotecchia and Chandler (2000), shown in Figure 2-31 in terms of I_v versus $6'_v$, the oedometer test results of intact specimens were

reconstructed making use of the corresponding results in the reconstituted states. Referring to Figure 6-18, the stress sensitivity is calculated as the ratio of the vertical yield effective stress in the intact state to that at the same void ratio on the compression curve for the reconstituted state.

$$S_\sigma = \frac{6'_{vy}}{6^*_e} \qquad 6\text{-}3$$

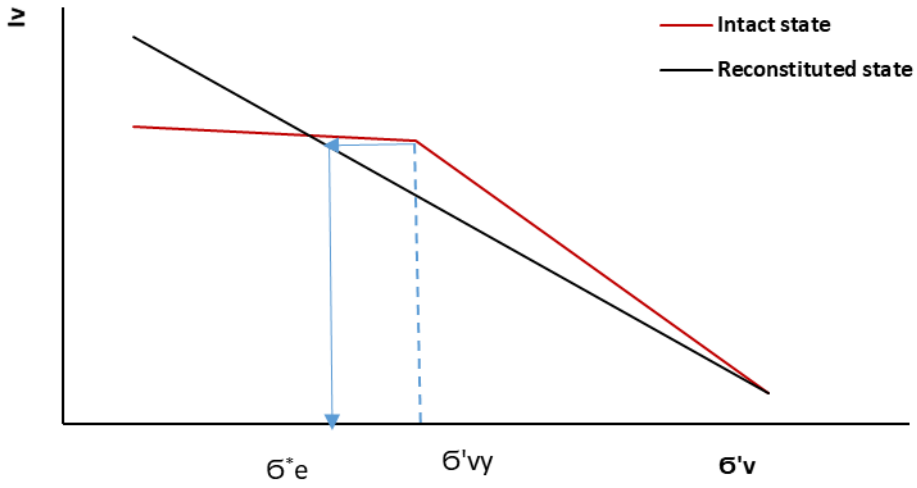

Figure 6-18: Parameters defining the stress sensitivity from oedometer test results.

For lime-admixed kaolin soil, cured for 365 days, samples were remoulded after adding distilled water to them to create reconstituted specimens. Oedometer compression tests were conducted on these soils, and the results are shown in Figure 6-4. Normalizing the oedometer test results using the void index I_v, as suggested by Burland (1990), the results for the intact kaolin K2 soils were re-plotted and are compared with the corresponding results obtained from the reconstituted soils in Figure 6-19.

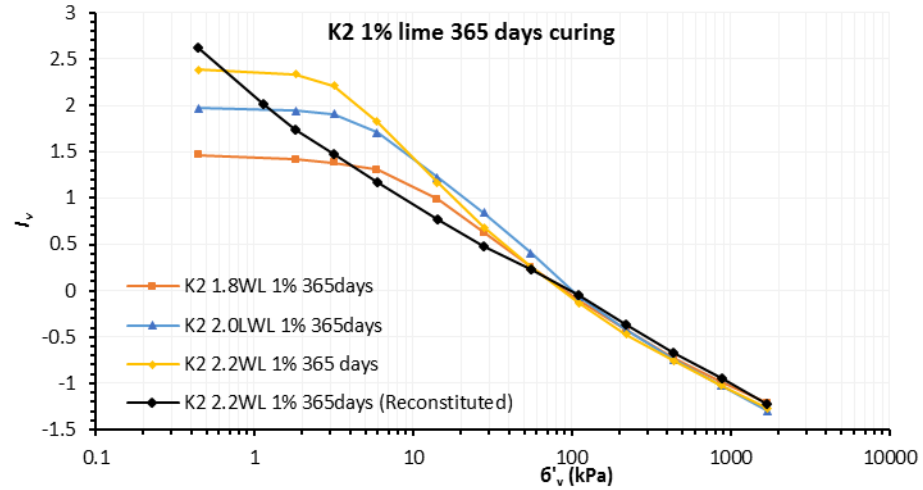

(a)

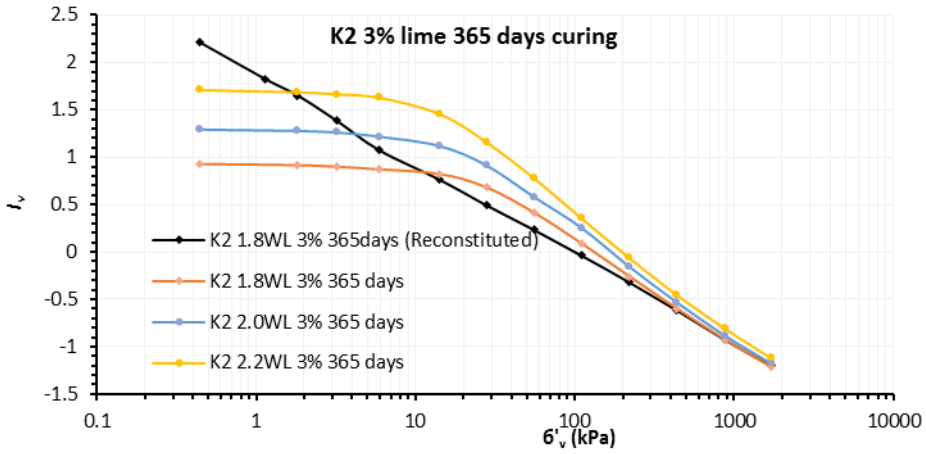

(b)

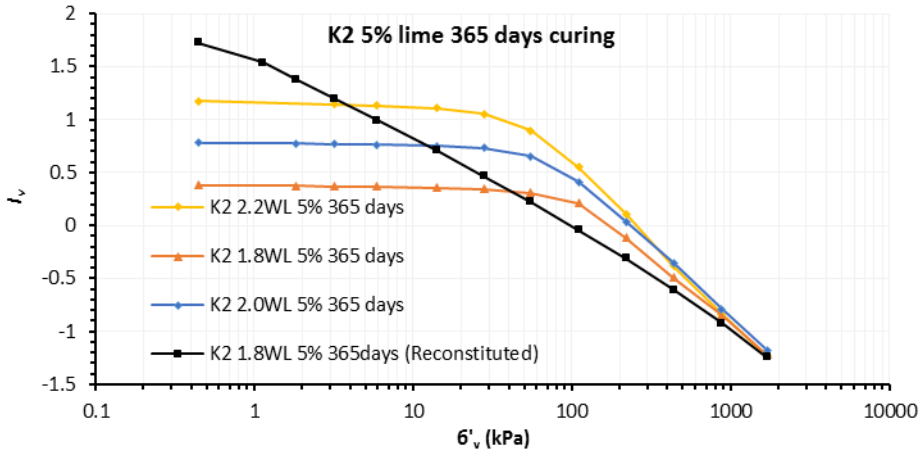

(c)

Figure 6-19: Oedometer test results for intact and reconstituted lime-admixed kaolin

The oedometer sensitivities calculated from each of these methods were compared with their corresponding strength sensitivities (using the S_t data from Chapter 5), and the results are shown in Figure 6-20. The data are widely scattered and poorly correlated, which suggests that neither the stress sensitivity framework of Cotecchia and Chandler (2000) nor the initial sensitivity approach (Xiao and Lee, 2014) work well in the context of artificially structured

soils. It can be concluded that for these soils, more reliable results for sensitivity can be obtained from strength tests.

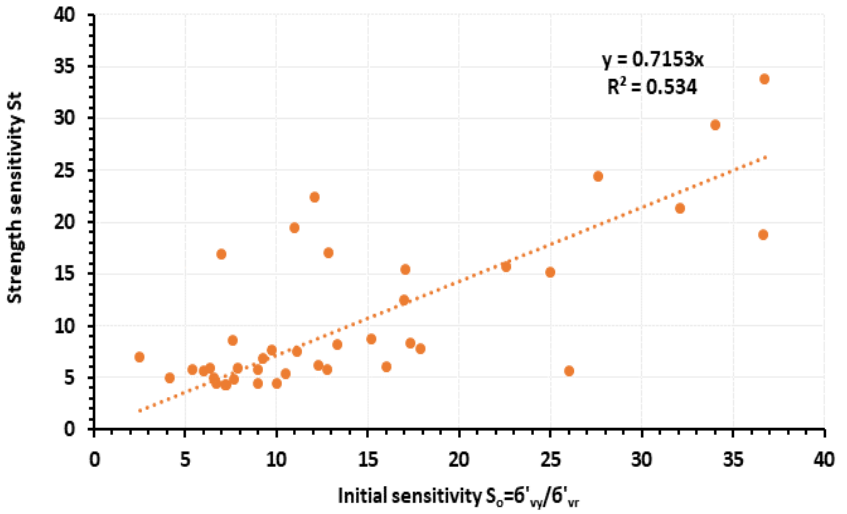

(a)

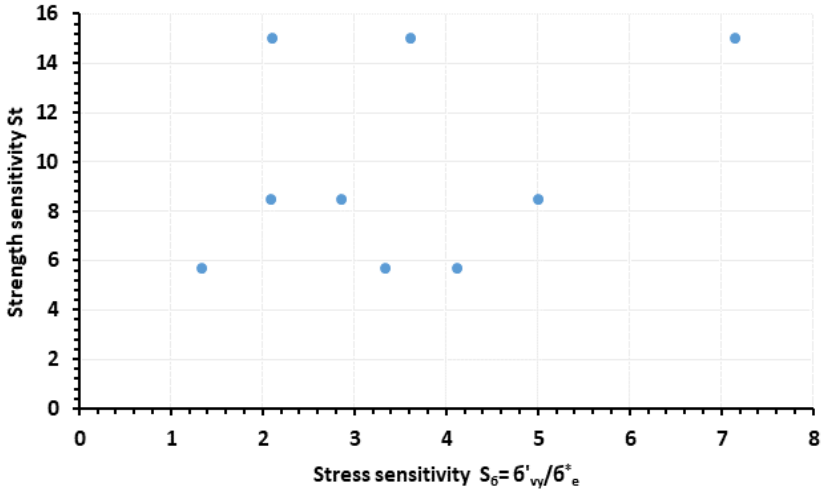

(b)

Figure 6-20: Scatter plots of oedometer "sensitivities" and sensitivity, for lime-admixed soils at 365 days: (a) using initial sensitivity Si and (b) using stress sensitivity S_σ.

6.4 Summary

1. The treatment of ultra-soft clays slurries with lime improves their compressibility characteristics by increasing the vertical yield stress and reducing their compressibilities.
2. Mechanical improvement depends on soil minerology and the availability of sufficient fines. Index values provide a useful indicator of additive effectiveness.
3. Initial water content is evidently an important factor: the lower the initial water content, the higher is the vertical yield stress after curing. However, clayey soils of different mineralogy but with the same ratio of water content to liquid limit have very similar yield stresses.
4. Increasing lime content and curing time causes an increase in yield stress. The consolidation path (post yield) is therefore shifted to the right.
5. The yield stress (from oedometer tests) is strongly correlated with undrained shear strength.
6. The post yield consolidation path of intact admixed soils is largely independent of the initial water content water content. This is consistent with the observations of Lorenzo and Bergado (2004) and Horpibulsuk et al. (2004a) for cement treated soils.
7. The consolidation paths of remoulded and intact soils tend to converge at high consolidation stress levels.
8. Methods for estimating sensitivity from oedometer test results are unsatisfactory.

Chapter 7 CONCLUSIONS

The undrained shear strength and one-dimensional compressibility of lime-admixed soil slurries was investigated experimentally in this project. An extensive campaign of penetration tests was conducted on different types of lime-admixed ultra-soft soils over a wide range of curing periods. The purpose of this study was to investigate the effect of parameters such as soil mineralogy, water content, lime content, curing time, and curing temperatures on the resulting undrained shear strength. The compressibility characteristics of these admixtures after long-term curing were also determined and correlated to their undrained shear strengths.

A numerical investigation, including small-strain FE and large-displacement FE modelling, was conducted to simulate the penetration of a rigid circular disc into soil. A focus of this study was the effect of the finite size of the test cells used in the experimental programme on bearing resistance. A closed-form expression for bearing capacity was employed to interpret the penetrometer test results.

7.1 Experimental Work

Penetration tests results

From the penetration test data, the principal conclusions drawn from this study may be summarized as follows:

- The undrained shear strength of lime-admixed soil increases over time: of the soils tested, CB bentonite exhibits the fastest early strength gain (typically two-thirds of its 365-day strength, at room temperature, is attained within 30 days). Comparatively, the strength gain in kaolin takes place at the slowest rate. These results are consistent with the difference in minerology of the soils tested. CB clay (as a typical montmorillonite) is highly reactive with lime compared to kaolin because of its higher cation exchange ability and softer mineralogical structure (Al-Mukhtar et al., 2014; Bell, 1996)
- After one year, the undrained shear strength of clay soils depends mainly on the ratio of initial water content to liquid limit (w / W_{LL}) and lime content. Different clays at the same (w / W_{LL}) ratio, admixed with same lime content, have approximately the

same undrained shear strength after one year of curing. This result is broadly consistent with the relationship (Wroth and Wood, 1978) between undrained shear strength, water content, and Atterberg limits, albeit that the range of water contents explored here range from 1.8-2.2W_{LL}

- For a given soil, regardless of lime content and curing period, the ratio of the initial water content to liquid limit is strongly correlated with undrained shear strength. For example, for kaolin, a reduction of (w / W_{LL}) from 2.2 to 1.8 results in a 100% increase in strength. When soil particles are in close proximity (low water content) it is easier for the pozzolanic reaction to build permanent bonds between them. This observation is similar to that of Horpibulsuk et al. (2003) and Zhang et al. (2013) who suggested that increases in water content reduces the number of contacts between the soil particles, which reduces the number of bonding sites.
- The pozzolanic chemical reaction requires the presence of sufficient active clay minerals to be effective: silty soils like Grangemouth soil (< 6% clay sizes) gain relatively little strength. Kaolin gains much less strength than SW Bentonex, etc. To be specific, strength gain depends on the availability of both silica (SiO_2) and alumina ($Al2O_3$), which is dissolved in the high alkaline environment to form the calcium aluminate silicate hydrate (CASH) bonding gel (Boardman et al., 2001; Janz and Johansson, 2002)
- Low (1%) lime content produces substantial strength gain in ultra-soft soils. However, as the lime is depleted over time, no further gain occurs. Higher lime contents accelerate the reaction and sustain it for much longer periods - longer than one year. This observation assumes that the reaction is not moderated or extinguished by depletion of the reactive soil minerals. Evidently, depletion of lime at early stages of the pozzolanic reaction leads to a decrease in the pH of the soil required for the pozzolanic reaction (Metelková et al., 2012) and no further increase in the strength is expected (Locat et al., 1996).
- Curing is accelerated at higher temperatures, and the Arrhenius model provides a satisfactory means of predicting the effect of temperature on strength gain. The results of strength measurements of lime admixed clays cured at different temperatures follow an Arrhenius type model, for all clay minerologies tested. This result is consistent with a pozzolanic chemical reaction, which is a temperature dependent process (Al-Mukhtar et al., 2014).
- Remoulding of admixed soils results in substantial loss of strength, but remoulded strengths remain comparable to the strength achieved several hours after admixing,

and a few orders of magnitude greater than the un-dosed soil. The work expended during remoulding is believed to fracture a significant proportion of the chemical bonds that have developed during the pozzolanic reaction.

- The sensitivity of an admixed soil is primarily linked to its lime content: greater lime content is associated with greater sensitivity. However, considerable work (energy) is required to remould these soils. In other words, these materials have none of the extreme brittleness of some natural "quick" clays.

One-dimensional compression tests

From the oedometer test results, the following conclusions were drawn:

- A distinct "yield stress" is apparent in tests on intact admixed soils. This yield stress increases with increasing lime content and curing time, in a similar manner to the undrained shear strength. These increases in yield stress shift the compression curves to the right. The continuous shifting of the normal compression curves at high stress level indicates that, even at high stresses, the treated soil retains a memory of the fabric and the structure developed at much higher void ratios (Tremblay et al., 2001). It also indicates that the amount of lime dictates the degree of bonding strength generated which is not totally "destructured" under high stress (Tremblay et al., 2001)
- For clay soils, the yield stress is a function of the ratio of water content and liquid limit, rather than water content alone. However, for soils with low clay contents, no such relation was found. This behaviour is analogous to that of the undrained shear strength developed in these soils.
- For lime-admixed soil slurries, the correlation $\boldsymbol{C_u} = 0.45\, 6'_{vy}$ is reasonably accurate irrespective of lime content and curing time. This relationship reflects the fact that the bonding strength plays a dominant role in the strength and the consolidation yield stress in these admixed soils (Horpibulsuk et al., 2004b)
- The post yield consolidation path of intact admixed soils is largely independent of the initial water content. Admixed soils with the same lime content coalesce into a single post yield consolidation path. These observations are consistent with the behaviour of cement admixed soils observed by other researchers (e.g. Horpibulsuk et al. (2004a) and (Lorenzo and Bergado, 2004)) in which each post-yield compression curve describes the limiting state of lime-admixed clay for particular lime content (Lorenzo and Bergado, 2004).

- The consolidation curves for remoulded soils are essentially linear on the conventional semi-logarithmic plot. Coincidence of the curves for intact and remoulded soils occurs only at high vertical effective stress.
- Soil sensitivities calculated based on the oedometer test results were unsatisfactory compared to the sensitivity calculated based on the intact and remoulded strengths.

Triaxial compression test results

- In the U-U triaxial tests, the deviator stress reached a peak at rather small axial strains (typically 3%) and then decreased with further strain, which is typical for lime admixed soils (ASTM 2004), albeit at much lower water contents. Positive excess pore pressures developed during shearing and reached values as high as 10 kPa and continued to increase even after the deviator stress had peaked.
- Skempton's pore pressure parameter A_f for these soils ranged between 0.1-0.4, which is in the range of lightly overconsolidated clays.
- The brittleness of the admixtures increased with increasing lime content and decreasing water content. The values of the brittleness index obtained from triaxial tests results increase with increasing lime contents.

Vane shear test results

- Good agreement was obtained between the undrained shear strength results obtained from vane shear and U-U triaxial compression tests, particularly for stronger soils.
- It was found that shaft resistance was significant and allowance for this factor was required.
- Even so, vane strength data remained (on average) 9% higher than triaxial measured strengths. Further tests are required to verify this observation.

pH measurements

According to the standard definitions (i.e., BS 1990) it was found by measuring pH that a lime content of 1% was sufficient for kaolin clay to meet the initial consumption of lime (ICL) threshold. However, 3% additive was required in most other cases. This observation is consistent with the differences in mineralogy: montmorillonitic soils have high cation exchange ability (which consumes more lime), while the exchange capacity of kaolinitic soils is far less (Diamond and Kinter, 1966; Eades and Grim, 1960)

pH values decrease during curing, as the additive is depleted. Thus, monitoring pH values provide a means of tracking the curing process.

Test techniques

- In the penetration tests, strain-rate effects were found to be less significant than expected, from published studies on natural soils. A penetration velocity of 250 mm/minute was found to be optimal (for a 20 mm penetrometer) for a wide range of parameters. For the smaller 10mm penetrometer, a higher penetrometer velocity (1000 mm/minute) was optimal.
- In these small-scale tests, diffusion of the additive into the surrounding water can soften a significant depth of the material. If a sample is flooded with water, then not only is a surface layer weakened but this material can be carried down into the underlying material during penetration testing, thus reducing the bearing resistance well below the softened zone.
- Softening, due to flooding, is time dependent and its effects become more apparent in samples cured for the longest periods: if samples are flooded, the entire sample depth (120 mm) may be softened to some degree, over the course of a year. For this reason, an alternative curing technique (sealing) should be employed, which maintains only a thin film of water over the sample.

7.2 Numerical Modelling

- Finite element analyses (and laboratory test data) confirmed that the penetration test results were not affected by the finite-size of the test chambers, provided that a disc diameter D of 30 mm or less was employed.
- Similarly, proximity effects, arising from the test chambers' rigid base, were found to be inconsequential unless the gap between the disk and the base become very small (i.e. $z'/D < 0.5$, where z' is the gap).
- Finite element simulations of disc penetration, using both small-strain and large displacement algorithms, were conducted in order to establish the relationship between (measured) bearing resistance and undrained shear strength. These analyses provided useful insight into the failure mechanisms, but sufficiently robust solutions could not be attained within the allotted period. Excessive distortion of the finite elements was suspected to be the root of the difficulty and warrants further investigation.

- From the best available published data, a closed-form expression was derived for the bearing capacity factor N_C , namely:

$$N_c = A - Be^{-M\left(\frac{Z}{D}\right)^N}$$

where the parameters A, B, M, N are taken to be: 11.0, 4.9, 1.06, 1.10, respectively. This equation was employed to infer undrained shear strength from the measured bearing pressures.

7.3 Novel Contributions

The principal novel element of the thesis is the exploration of the effect of slaked lime on the strength of clayey soils at very high water contents (slurries). This wide ranging study has provided insights into the effects of water content, lime content, soil mineralogy, duration, and temperature which have not been quantified before.

7.4 Recommendations for Further Study

The parametric study reported in the thesis on the factors affecting the undrained shear strength of lime-admixed soils might be extended in several ways: for example, tests on a wider range of soils, including natural soils with significant organic content might well reveal trends not captured by the present study. Although this study was prompted by offshore applications, the tests were conducted using pure water; further investigation is needed to establish whether the use of salt-water (at oceanic concentrations) would have affected the conclusions reported here.

The strain-softening behaviour of these soils is worthy of study in order to establish, in quantitative terms, their toughness. Data from ring-shear apparatus might then be employed in subsequent analysis, numerical modelling, and design.

Numerical modelling is an essential tool for interpreting penetration test data, and further work in this area (e.g. including appropriate strain-softening constitutive relationship, and explicit modelling of strain-rate and consolidation effects) would yield some benefits, albeit at the cost of significant effort.

Appendix A Kaolin clay (K2)

This section summarizes the results of penetration tests conducted on intact and remoulded specimens of lime treated kaolin (K2) clay cured under both sealed (S) and flooded (F) conditions.

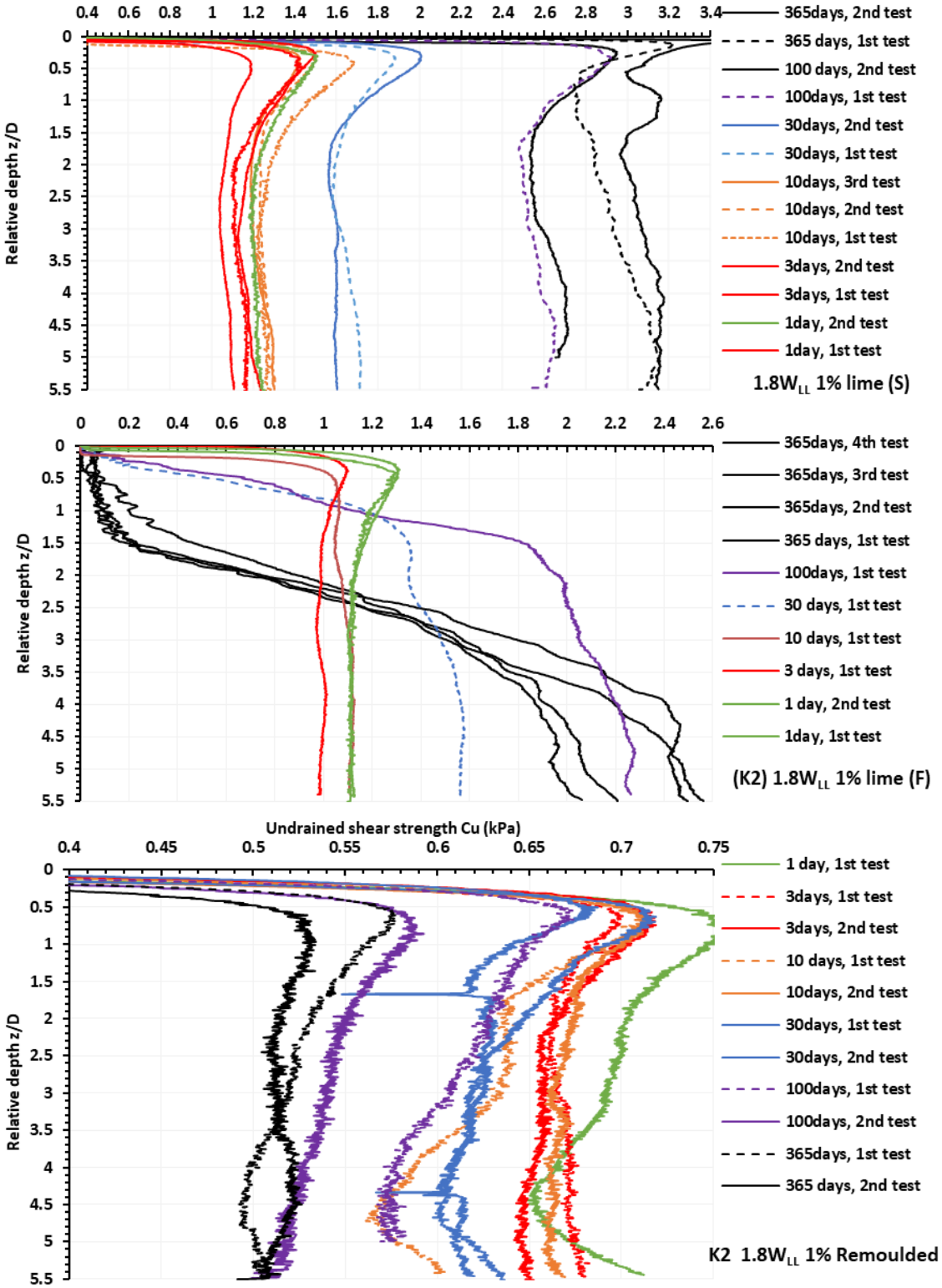

Figure A.1: Penetration test results for 1% lime admixed kaolin (K2) at 1.8WLL (a) Sealed (S), (b) flooded (F), and (c) after remoulding

Table A.1: Penetration test results for intact and remoulded kaolin (K2) at 1.8W_{LL} treated with 1% lime

Condition	Curing method	Curing Time (days)	Tests									Averaged Results		
			No.1			No.2			No.3			Cu (kPa)	ST.D.	C.O.V. %
			Cu (kPa)	ST.D.	C.O.V. %	Cu (kPa)	ST.D.	C.O.V. %	Cu (kPa)	ST.D.	C.O.V. %			
Intact condition	Sealed (S)	1	1.23	0.04	3.08	1.15	0.04	3.54				1.17	0.04	3.28
		3	1.18	0.04	3.49	1.07	0.02	2.05				1.08	0.06	5.14
		10	1.23	0.04	3.20	1.27	0.05	3.89	1.26	0.02	1.88	1.22	0.02	1.25
		30	1.65	0.05	2.80	1.60	0.03	1.89				1.63	0.03	1.63
		100	2.60	0.06	2.38	2.57	0.05	2.11				2.59	0.02	0.72
		365	3.10	0.06	2.04	2.97	0.12	4.17				3.03	0.06	2.10
	Flooded (F)	1	1.13	0.03	2.52	1.12	0.02	1.84				1.13	0.00	0.12
		3	0.99	0.01	1.25							0.99		
		10	1.10	0.03	2.36							1.10		
		30	1.47	0.11	7.24							1.47		
		100	2.16	0.10	4.66							2.16		
		365	1.74	0.36	20.61	2.03	0.51	24.90	1.90	0.54	28.53	1.89	0.12	6.19
Remoulded condition	Sealed (S)	1	0.73	0.02	2.92							0.73		
		3	0.66	0.01	2.12	0.67	0.01	0.84				0.67	0.01	1.07
		10	0.67	0.01	1.24	0.62	0.03	5.30				0.66	0.04	5.52
		30	0.63	0.02	3.66	0.62	0.01	1.51				0.62	0.01	1.21
		100	0.61	0.02	3.92	0.54	0.02	3.30				0.60	0.05	8.56
		365	0.52	0.02	3.59	0.52	0.01	1.18				0.52	0.00	0.07
	Flooded (F)	1												
		3	0.69	0.03	4.39							0.69		
		10	0.68	0.02	3.00							0.68		
		30	0.64	0.02	3.18							0.64		
		100	0.57	0.02	3.75							0.57		
		365	0.45	0.02	4.68	0.45	0.02	4.73	0.41	0.01	2.53	0.43		

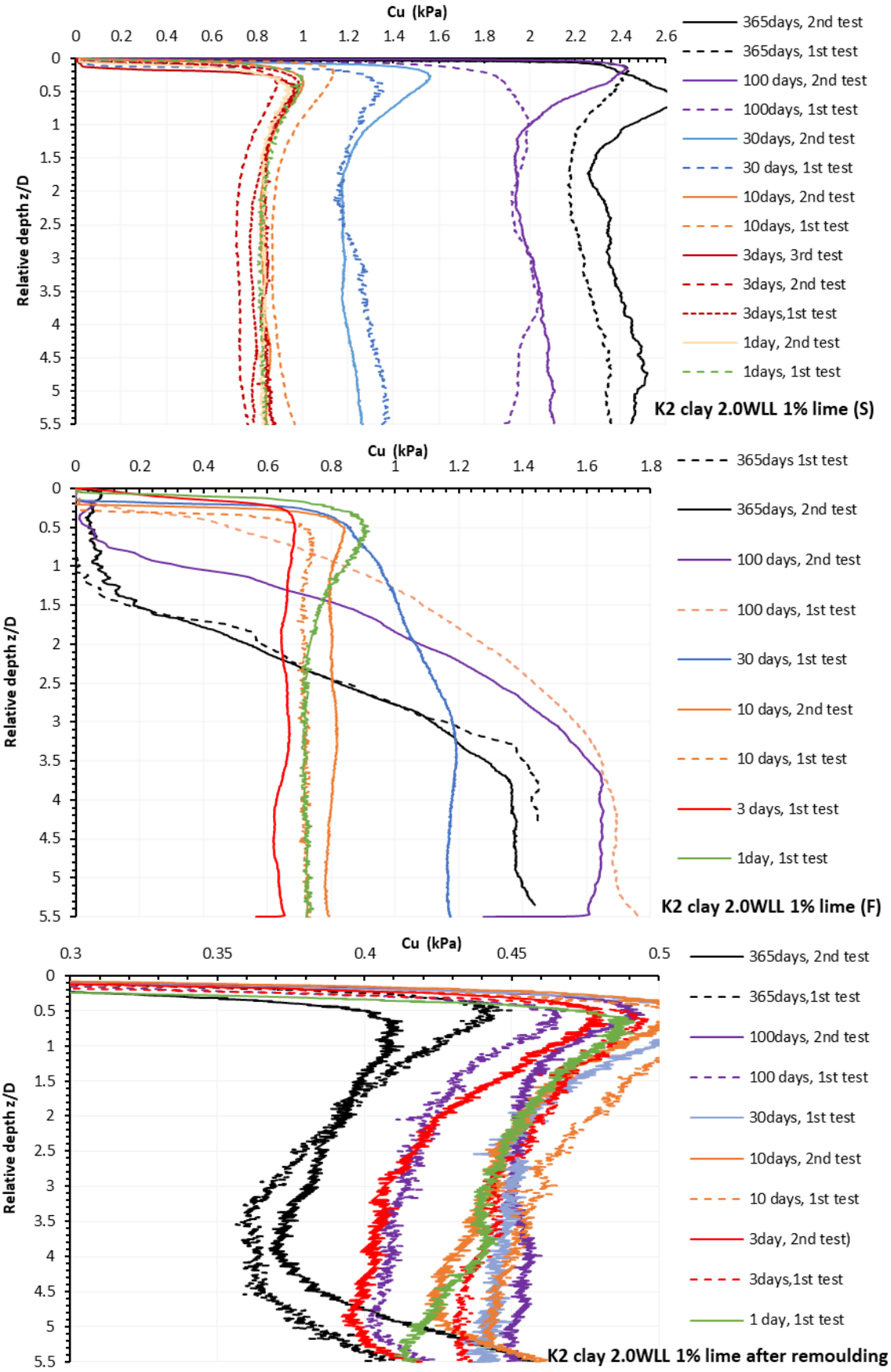

Figure A.2: Penetration test results for kaolin (K2) at 2.0W_{LL} treated with 1% lime: (a) sealed (S), (b) flooded (F), and (c) after remoulding

Table A.2: Penetration test results for intact and remoulded kaolin (K2) at 2.0W_{LL} with 1% lime

Condition	Curing method	Curing Time (days)	Tests									Averaged Results		
			No.1			No.2			No.3			Cu (kPa)	ST.D.	C.O.V. %
			Cu (kPa)	ST.D.	C.O.V. %	Cu (kPa)	ST.D.	C.O.V. %	Cu (kPa)	ST.D.	C.O.V. %			
Intact condition	Sealed (S)	1	0.83	0.01	1.14	0.83	0.02	2.39				0.83	0.00	0.10
		3	0.73	0.02	2.69	0.79	0.02	3.15	0.84	0.01	1.54	0.79	0.05	5.79
		10	0.84	0.02	1.87	0.89	0.03	3.30				0.86	0.03	3.41
		30	1.20	0.03	2.60	1.26	0.07	5.62				1.23	0.03	2.18
		100	2.02	0.06	3.04	1.82	0.03	1.87				1.92	0.10	5.29
		365	2.39	0.07	3.07	2.05	0.06	2.85				2.22	0.17	7.81
	Flooded (F)	1	0.73	0.03	3.74							0.73	0.00	0.00
		3	0.65	0.02	2.46	0.72	0.01	1.27				0.68	0.04	5.13
		10	0.80	0.01	1.33	0.86	0.02	2.43				0.83	0.03	3.71
		30	1.16	0.03	2.62							1.16	0.00	0.00
		100	1.60	0.12	7.62	1.53	0.16	10.25				1.57	0.04	2.34
		365	1.15	0.30	25.99	1.18	0.26	21.96				1.17	0.02	1.53
Remoulded condition	Sealed (S)	1	0.44	0.02	3.71							0.44		
		3	0.41	0.02	4.35	0.45	0.01	3.10				0.43	0.02	3.85
		10	0.45	0.02	4.11	0.46	0.02	3.86				0.45	0.01	1.72
		30	0.45	0.01	2.86							0.45		
		100	0.46	0.00	0.77	0.42	0.01	2.60				0.44	0.02	4.55
		365	0.39	0.02	5.04	0.38	0.02	4.55				0.39	0.01	1.53
	Flooded (F)	1												
		3												
		10												
		30												
		100	0.45	0.02	3.87							0.45		
		365	0.23	0.01	5.18							0.23		

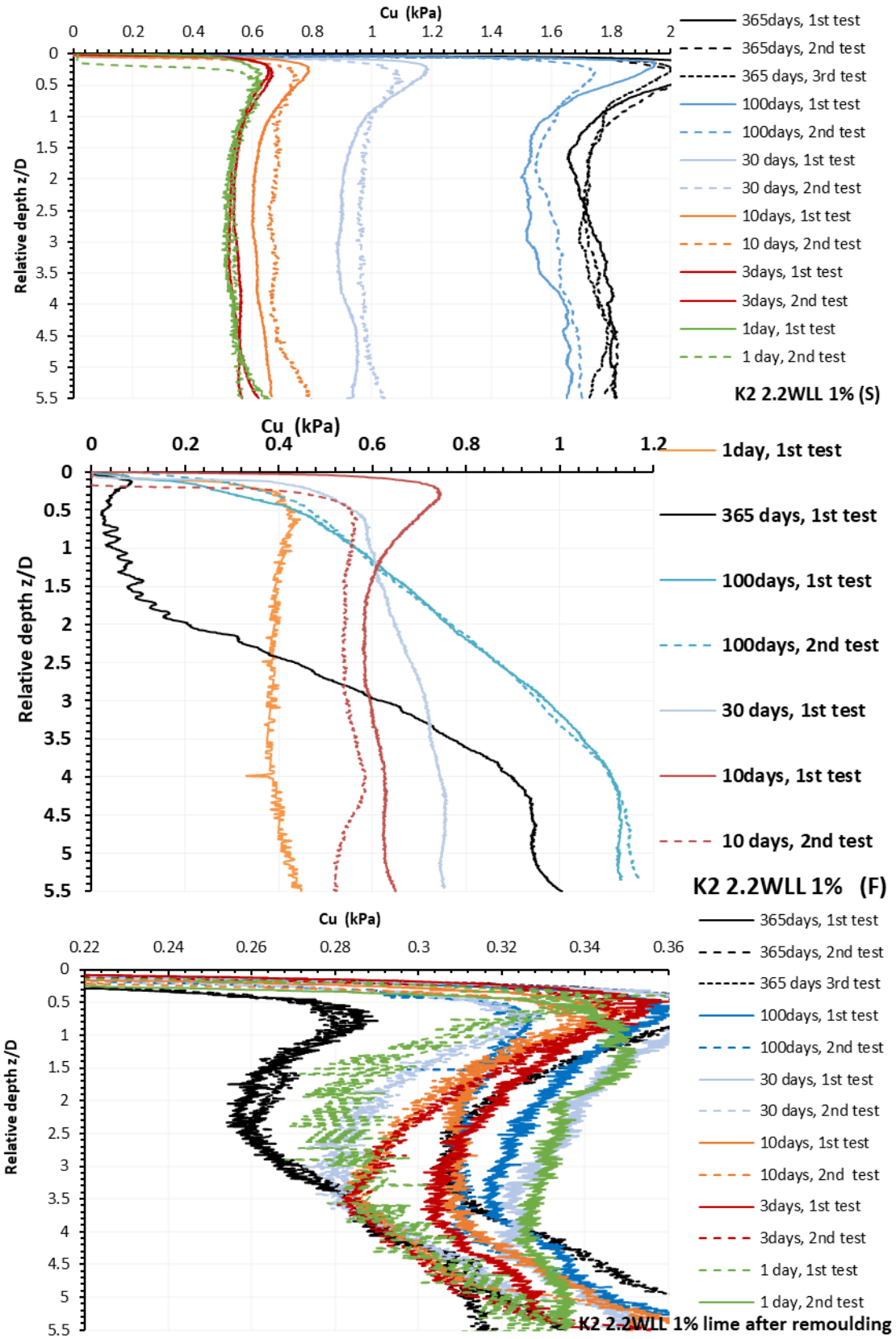

Figure A.3: Penetration tests results for kaolin clay (K2) at 2.2W_{LL} treated with 1% lime: (a) Sealed (S), (b) Flooded (F)

Table A.3: Penetration test results for kaolin clay at 2.2W_{LL} treated with 1% lime

Condition	Curing method	Curing Time (days)	Tests									Averaged Results		
			No.1			No.2			No.3					
			Cu (kPa)	ST.D.	C.O.V. %	Cu (kPa)	ST.D.	C.O.V. %	Cu (kPa)	ST.D.	C.O.V. %	Cu (kPa)	ST.D.	C.O.V. %
Intact condition	Sealed (S)	1	0.54	0.03	5.74	0.54	0.01	2.30				0.54	0.00	0.52
		3	0.55	0.01	1.58	0.54	0.02	4.24				0.55	0.00	0.76
		10	0.62	0.02	3.09	0.68	0.03	4.18				0.65	0.03	4.13
		30	0.98	0.02	1.97	0.92	0.03	2.73				0.95	0.03	3.10
		100	1.58	0.06	3.75	1.63	0.05	3.05				1.61	0.02	1.49
		365	1.76	0.05	2.94	1.76	0.04	2.14	1.74	0.03	1.62	1.75	0.01	0.42
	Flooded (F)	1	0.39	0.02	4.34							0.39		
		3												
		10	0.55	0.02	3.11	0.61	0.02	3.15				0.58	0.04	7.35
		30	0.72	0.03	4.30							0.72		
		100	1.03	0.12	11.29	1.03	0.12	11.85				1.03	0.00	0.08
		365	0.75	0.23	30.84							0.75		
Remoulded condition	Sealed (S)	1	0.33	0.01	2.16							0.33		
		3	0.32	0.01	3.24	0.30	0.02	5.37				0.31	0.01	2.91
		10	0.32	0.01	4.59	0.31	0.02	6.22				0.31	0.01	3.17
		30	0.34	0.01	3.16	0.30	0.02	6.65				0.32	0.02	7.83
		100	0.33	0.01	3.88	0.32	0.02	4.95				0.33	0.01	2.54
		365	0.28	0.02	8.32	0.28	0.02	7.03	0.33	0.03	8.19	0.30	0.03	9.37
	Flooded (F)	1	0.30	0.02	5.36							0.30		
		3												
		10	0.31	0.01	3.51							0.31		
		30												
		100	0.34	0.01	2.83							0.34		
		365	0.18	0.00	2.29							0.18		

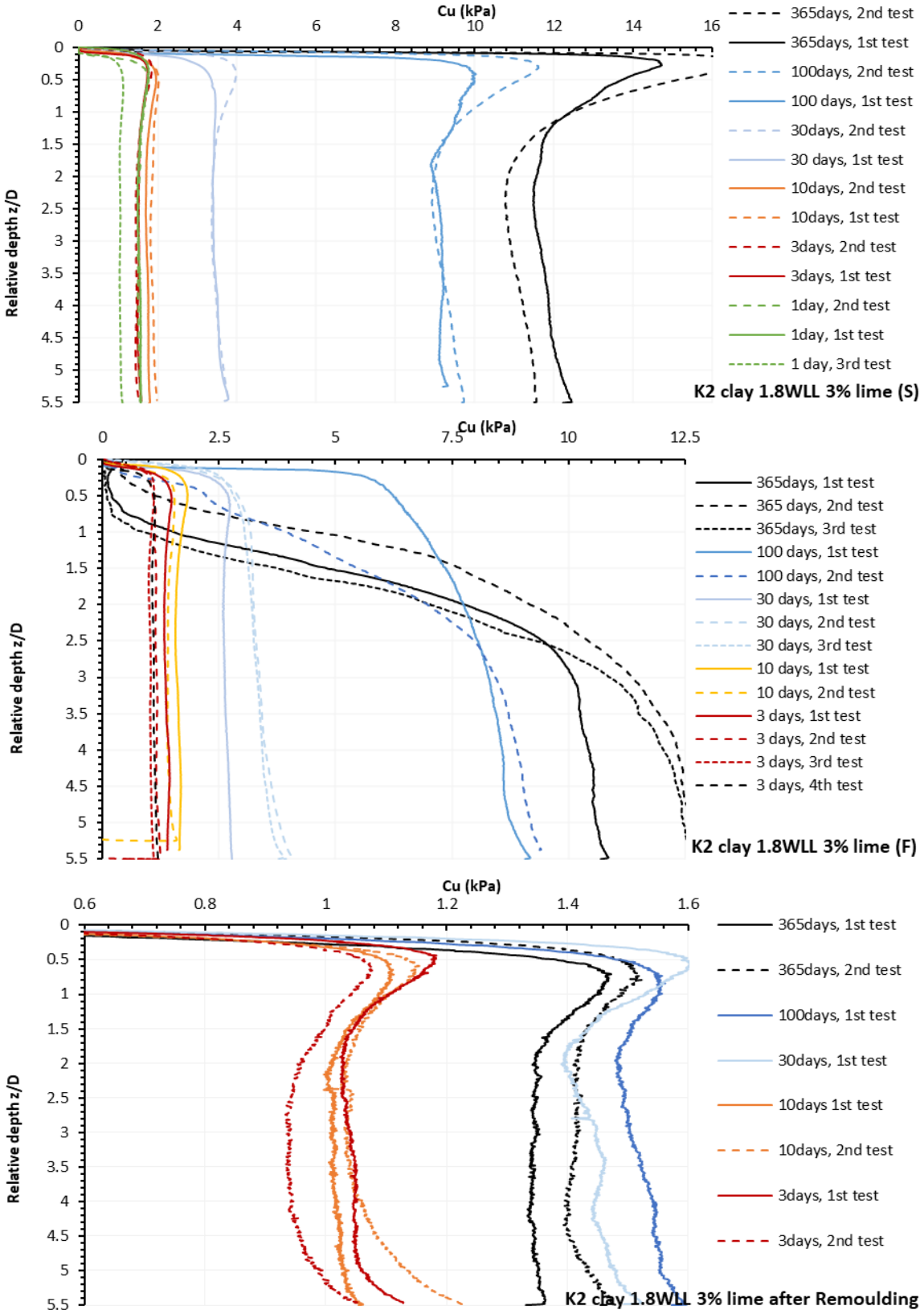

Figure A.4: Penetration test results for kaolin clay (K2) at 1.8W_{LL} treated with 3% lime: (a) Sealed (S), (b) flooded (F), and (c) after remoulding

Table A.4: Penetration test results for intact and remoulded kaolin clay (K2) at 1.8W_{LL} and 3% lime content

Condition	Curing method	Curing Time (days)	Tests									Averaged Results		
			No.1			No.2			No.3			Cu (kPa)	ST.D.	C.O.V. %
			Cu (kPa)	ST.D.	C.O.V. %	Cu (kPa)	ST.D.	C.O.V. %	Cu (kPa)	ST.D.	C.O.V. %			
Intact condition	Sealed (S)	1	1.54	0.11	7.32	1.53	0.03	1.98	1.54	0.03	2.11	1.53	0.01	0.37
		3	1.47	0.04	2.66	1.52	0.02	1.59				1.50	0.02	1.66
		10	1.74	0.03	1.81	1.88	0.04	2.19				1.81	0.07	3.66
		30	3.49	0.12	3.35	3.48	0.10	2.74				3.48	0.00	0.09
		100	9.27	0.26	2.76	9.05	0.20	2.16				9.16	0.11	1.20
		365	11.20	0.34	3.08	11.83	0.26	2.16				11.52	0.31	2.71
	Flooded (F)	1												
		3	1.38	0.04	2.76	1.16	0.03	2.44	1.16	0.15	12.88	1.23	0.10	8.25
		10	1.63	0.04	2.48	1.43	0.04	2.91				1.53	0.10	6.47
		30	2.66	0.06	2.10	3.45	0.23	6.62	3.36	0.19	5.64	3.16	0.35	11.23
		100	8.45	0.32	3.84	8.61	0.58	6.71				8.53	0.08	0.94
		365	10.11	0.67	6.60	11.77	1.00	8.48	11.23	1.51	13.41	11.04	0.69	6.26
Remoulded condition	Sealed (S)	1												
		3	0.96	0.03	3.13	1.05	0.02	1.95				1.01	0.04	4.17
		10	1.02	0.02	1.77	1.07	0.05	4.23				1.05	0.02	2.18
		30	1.45	0.03	2.07							1.45		
		100	1.52	0.81	53.10							1.52		
		365	1.36	0.02	1.71	1.42	0.02	1.49				1.39	0.03	2.44
	Flooded (F)	1												
		3	1.13	0.04	3.78							1.13		
		10	1.22	0.03	2.75	1.27	0.03	2.06				1.24	0.03	2.04
		30	1.39	0.04	2.55							1.39		
		100	1.34	0.02	1.27	1.65	0.03	2.04				1.50	0.16	10.38
		365	1.33	7.60	571.18	1.71	0.02	1.36	1.38	0.08	5.85	1.47	0.17	11.33

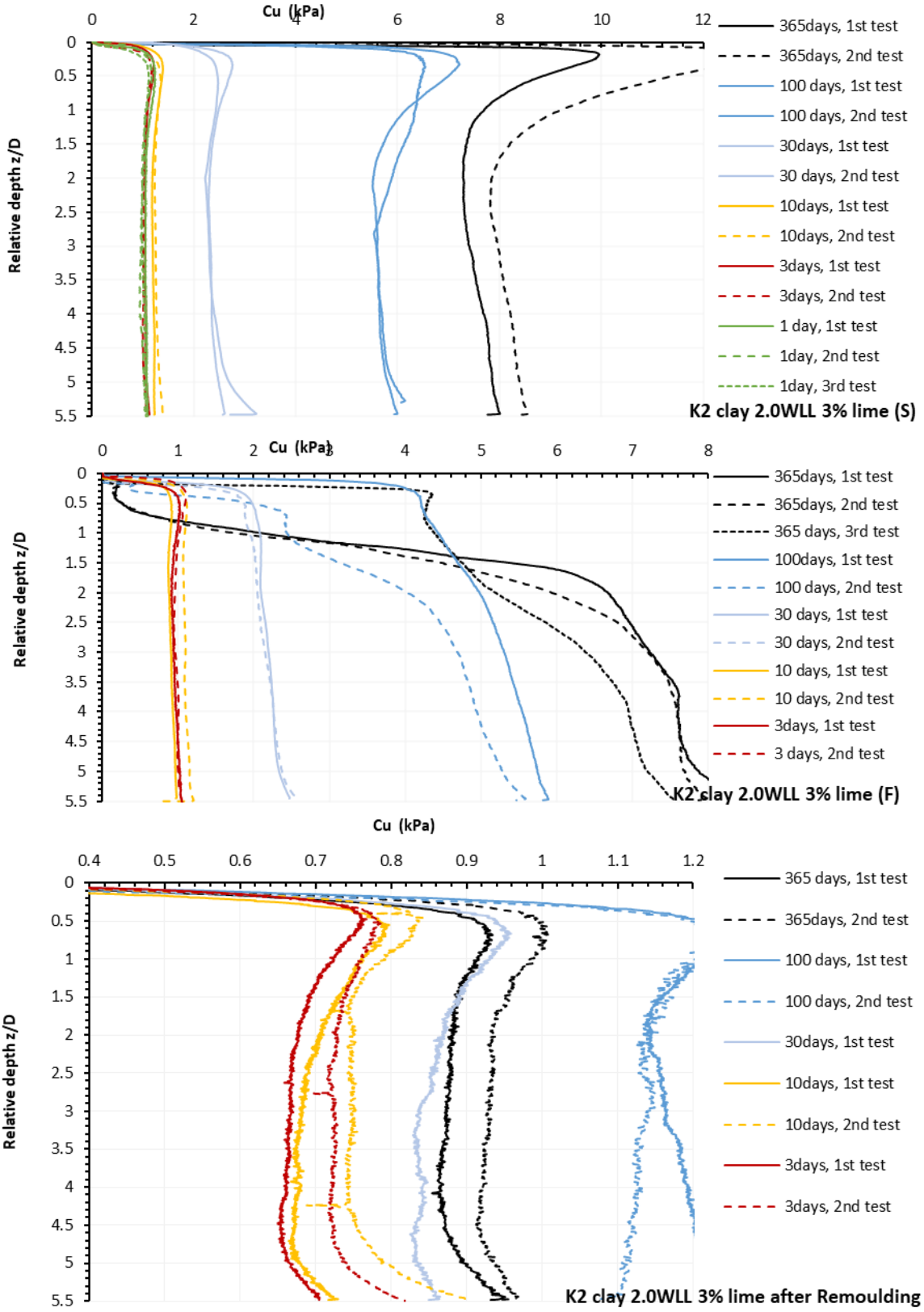

Figure A.5: Penetration test results for kaolin clay (K2) at 2.0W_{LL} treated with 3% lime: (a) sealed (S), (b) flooded (F), and (c) after remoulding

Table A.5: Penetration test results for intact and remoulded kaolin clay (K2) at 2.0W_{LL} and 3% lime content

Condition	Curing method	Curing Time (days)	Tests									Averaged Results		
			No.1			No.2			No.3			Cu (kPa)	ST.D.	C.O.V. %
			Cu (kPa)	ST.D.	C.O.V. %	Cu (kPa)	ST.D.	C.O.V. %	Cu (kPa)	ST.D.	C.O.V. %			
Intact condition	Sealed (S)	1	1.07	0.02	2.12	0.99	0.03	3.38	1.02	0.03	2.84	1.03	0.03	3.32
		3	1.06	0.02	1.77	1.02	0.02	1.96				1.04	0.02	1.65
		10	1.21	0.02	1.87	1.27	0.04	3.07				1.24	0.03	2.51
		30	2.38	0.08	3.21	2.43	0.21	8.75				2.40	0.02	1.01
		100	5.69	0.14	2.40	5.82	0.22	3.70				5.75	0.07	1.14
		365	7.56	0.22	2.95	8.18	0.28	3.37				7.87	0.31	3.92
	Flooded (F)	1												
		3	0.96	0.04	3.89	0.99	0.02	2.36				0.97	0.02	1.69
		10	0.92	0.03	3.67	1.11	0.03	2.91				1.01	0.09	9.35
		30	2.21	0.10	4.44	2.18	0.14	6.63				2.20	0.01	0.68
		100	5.46	0.24	4.46	4.87	0.36	7.34				5.17	0.30	5.73
		365	7.48	0.41	5.47	7.34	0.47	6.37	6.65	0.60	9.06	7.15	0.36	5.08
Remoulded condition	Sealed (S)	1												
		3	0.67	0.02	2.42	0.73	0.02	2.50				0.70	0.03	4.29
		10	0.69	0.02	3.52	0.76	0.03	4.01				0.73	0.03	4.56
		30	0.85	0.02	2.82							0.85		
		100	1.18	0.03	2.54	1.13	0.02	1.90				1.16	0.02	2.04
		365	0.88	0.02	2.02	0.94	0.02	1.70				0.91	0.03	2.90
	Flooded (F)	1												
		3												
		10												
		30												
		100	1.30	0.03	2.04							1.30		
		365	0.92	0.02	2.58	1.06	0.03	3.08				0.99	0.07	7.07

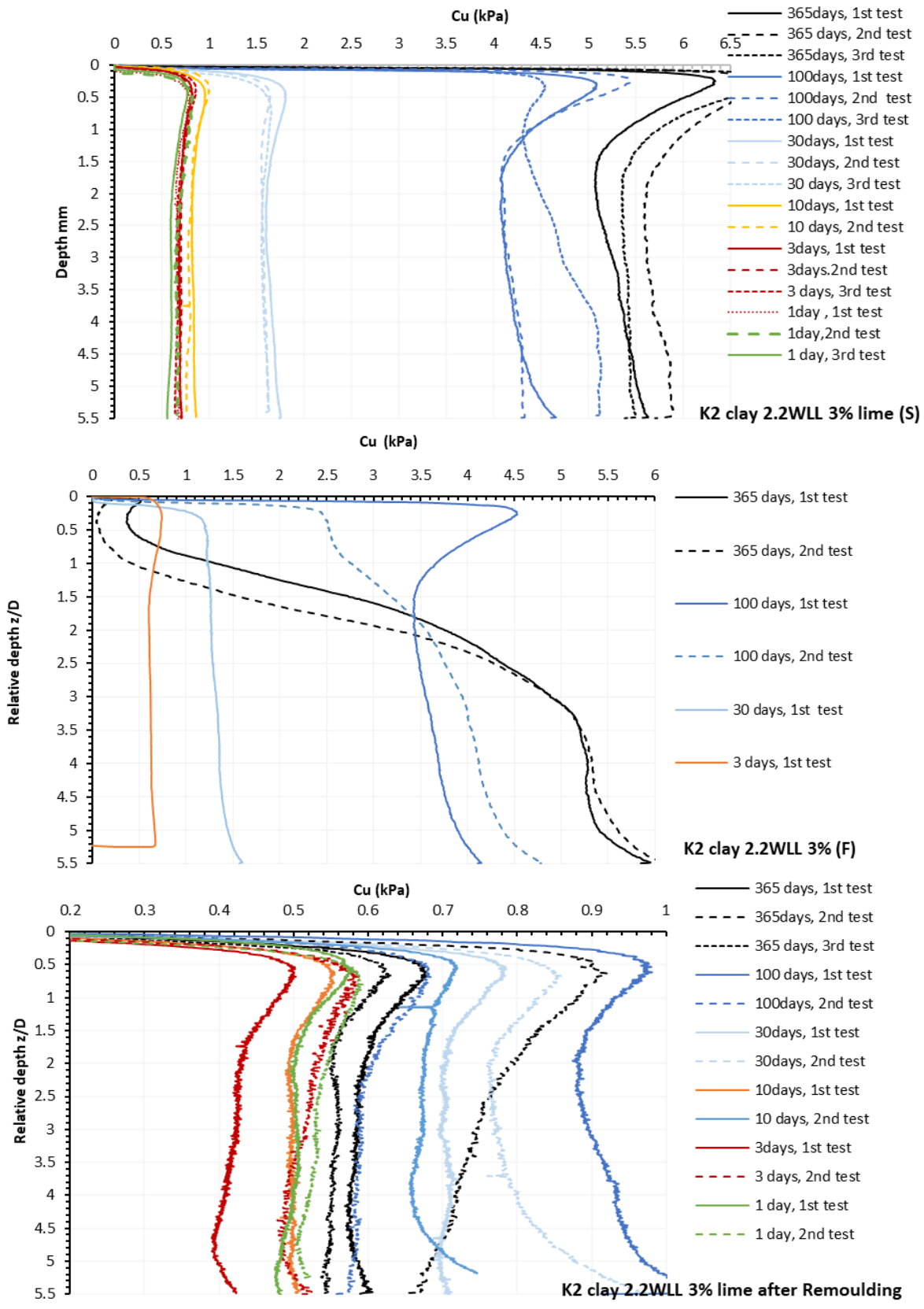

Figure A.6: Penetration test results for kaolin clay (K2) at 2.2W_{LL} treated with 1% lime: (a) sealed (S), (b) flooded (F), and (c) after remoulding

Table A-6: Penetration test results for intact and remoulded kaolin clay (K2) at 2.20W_{LL} with 3% lime

Condition	Curing method	Curing Time (days)	Tests									Averaged Results		
			No.1			No.2			No.3			Cu (kPa)	ST.D.	C.O.V. %
			Cu (kPa)	ST.D.	C.O.V. %	Cu (kPa)	ST.D.	C.O.V. %	Cu (kPa)	ST.D.	C.O.V. %			
Intact condition	Sealed (S)	1	0.68	0.02	2.40	0.68	0.03	4.79	0.61	0.03	4.84	0.65	0.03	5.23
		3	0.70	0.01	2.09	0.71	0.02	2.27	0.67	0.03	4.27	0.69	0.02	2.18
		10	0.84	0.02	1.86	0.80	0.03	3.51	1.59	0.02	1.54	0.82	0.36	44.31
		30	1.66	0.04	2.65	1.59	0.03	1.62				1.62	0.04	2.22
		100	4.23	0.14	3.30	4.21	0.09	2.03	4.79	0.29	6.10	4.41	0.27	6.15
		365	5.30	0.16	3.02	5.74	0.12	2.05	5.43	0.07	1.24	5.49	0.18	3.31
	Flooded (F)	1												
		3	0.63	0.02	2.89							0.63		
		10												
		30	1.34	0.08	5.89							1.34		
		100	3.64	0.18	4.99	4.08	0.27	6.70				3.86	0.22	5.70
		365	5.05	0.49	9.72	5.06	0.63	12.50				5.05	0.01	0.18
Remoulded condition	Sealed (S)	1	0.50	0.01	2.79	0.53	0.02	3.73				0.52	0.02	3.10
		3	0.42	0.02	4.68	0.51	0.02	4.61				0.47	0.05	9.97
		10	0.50	0.01	1.81	0.68	0.02	2.42				0.59	0.09	15.00
		30	0.71	0.01	1.65	0.81	0.05	6.15				0.76	0.05	6.59
		100	0.92	0.04	4.32	0.60	0.02	3.69				0.76	0.16	21.47
		365	0.59	0.02	2.77	0.75	0.05	7.26	0.56	0.01	1.93	0.67	0.08	12.62
	Flooded (F)	1												
		3												
		10												
		30												
		100	0.90	0.07	7.31	0.88	0.03	3.60	0.63	0.03	4.59	0.80	0.15	18.88
		365	0.75	0.02	2.96							0.75		

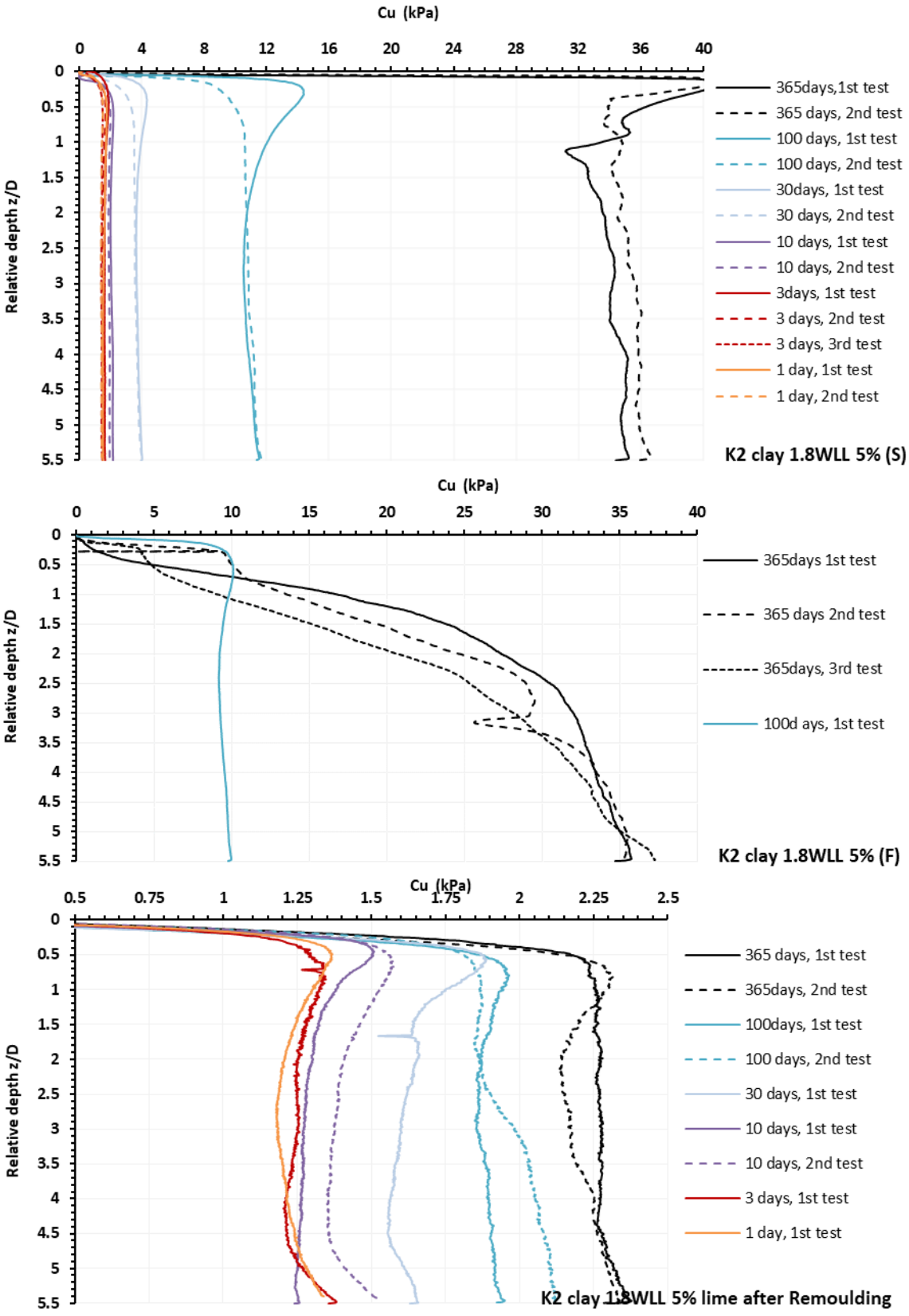

Figure A.7: Penetration test results for kaolin clay (K2) at 1.8WLL treated with 5% lime: (a) sealed (S), (b) flooded (F), and (c) after remoulding

Table A-7: Penetration test results for intact and remoulded kaolin clay (K2) at 1.8W_{LL} with 5% lime

Condition	Curing method	Curing Time (days)	Tests									Averaged Results		
			No.1			No.2			No.3			Cu (kPa)	ST.D.	C.O.V. %
			Cu (kPa)	ST.D.	C.O.V. %	Cu (kPa)	ST.D.	C.O.V. %	Cu (kPa)	ST.D.	C.O.V. %			
Intact condition	Sealed (S)	1	1.57	0.06	3.81	1.42	0.01	0.92				1.49	0.07	4.96
		3	1.64	0.02	1.53	1.51	0.03	1.68	1.44	0.02	1.10	1.53	0.08	5.32
		10	2.09	0.06	2.78	1.92	0.03	1.37				2.01	0.08	4.14
		30	3.78	0.11	2.78	3.67	0.12	3.41				3.72	0.06	1.49
		100	10.95	0.35	3.23	10.98	0.28	2.57				10.97	0.01	0.12
		365	34.09	0.93	2.73	35.43	0.62	1.74				34.76	0.67	1.93
	Flooded (F)	1												
		3												
		10												
		30												
		100	9.52	0.25	2.60							9.52		
		365	32.77	2.06	6.28	31.82	3.19	10.01	30.76	4.16	13.53	31.78	0.82	2.58
Remoulded condition	Sealed (S)	1	1.22	0.04	3.14							1.22		
		3	1.26	0.04	2.90							1.26		
		10	1.28	0.03	2.35	1.40	0.05	3.46				1.34	0.06	4.56
		30	1.61	0.04	2.60							1.61		
		100	1.89	0.02	1.25	1.99	0.10	4.88				1.94	0.05	2.43
		365	2.28	0.03	1.12	2.22	0.06	2.62				2.25	0.03	1.33
	Flooded (F)	1												
		3												
		10												
		30												
		100	1.79	0.09	4.88							1.79		
		365	2.30	0.06	2.64	2.53	0.07	2.22				2.42	0.11	4.63

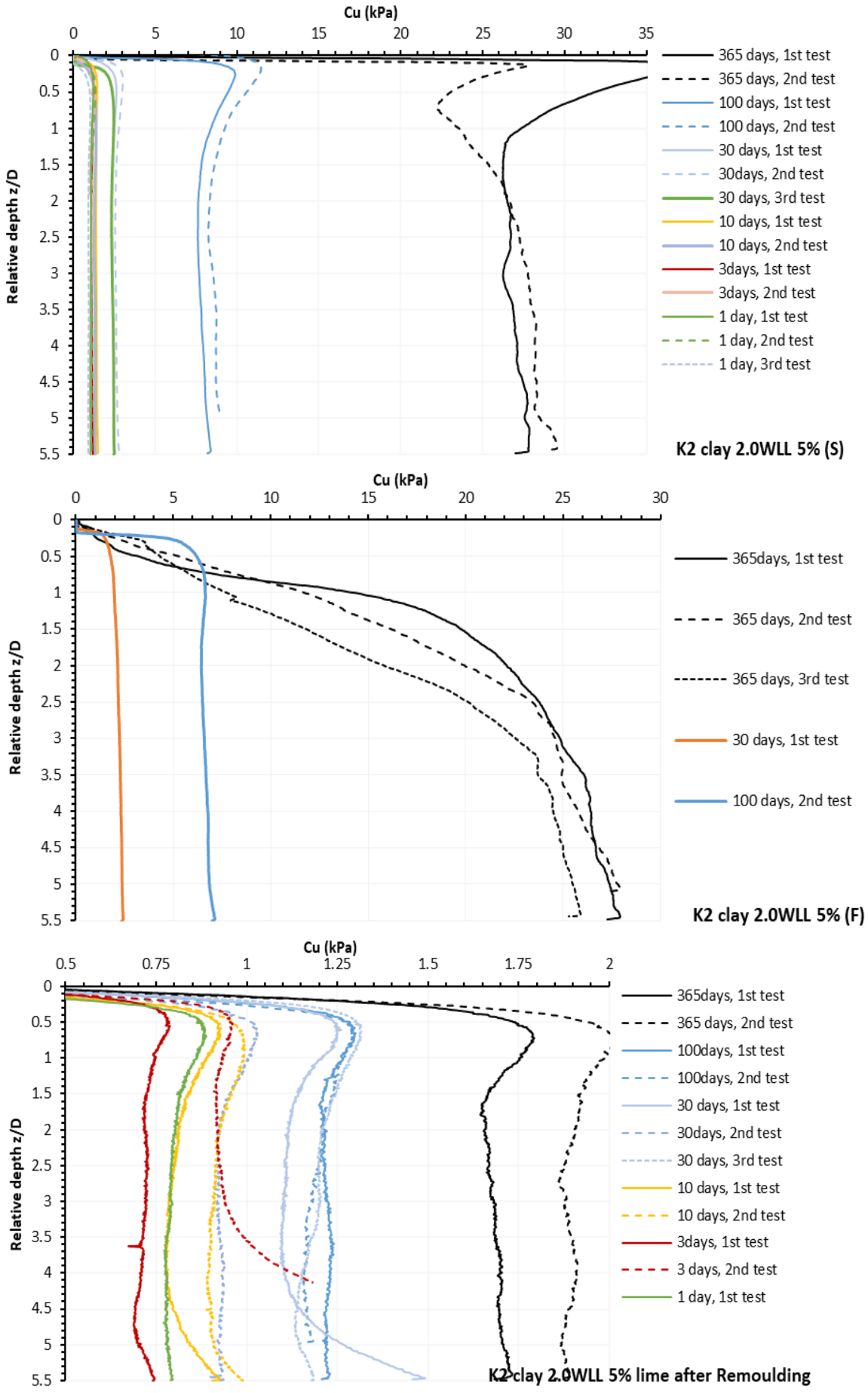

Figure A.8: Penetration test results for kaolin clay (K2) at 2.0W_{LL} treated with 5% lime: (a) sealed (S), (b) flooded (F), and (c) after remoulding

Table A.8: Penetration test results for intact and remoulded kaolin clay (K2) at 2.0WLL with 5% lime

Condition	Curing method	Curing Time (days)	Tests									Averaged Results		
			No.1			No.2			No.3			Cu (kPa)	ST.D.	C.O.V. %
			Cu (kPa)	ST.D.	C.O.V. %	Cu (kPa)	ST.D.	C.O.V. %	Cu (kPa)	ST.D.	C.O.V. %			
Intact condition	Sealed (S)	1	1.07	0.02	1.75	1.13	0.03	2.83	0.93	0.02	2.20	1.04	0.08	7.94
		3	1.15	0.02	1.40	1.09	0.04	3.62				1.12	0.03	2.69
		10	1.42	0.03	2.19	1.33	0.03	2.28				1.37	0.05	3.59
		30	2.42	0.05	2.01	2.63	0.06	2.33	2.42	0.05	2.15	2.49	0.10	4.09
		100	7.89	0.23	2.89	8.61	0.24	2.73				8.25	0.36	4.41
		365	26.90	0.52	1.93	27.36	1.39	5.09				27.13	0.23	0.85
	Flooded (F)	1												
		3												
		10												
		30	2.23	0.12	5.38							2.23		
		100	6.64	0.17	2.56							6.64		
		365	25.70	1.54	5.99	25.03	1.87	7.47	23.23	2.53	10.90	24.65	1.04	4.22
Remoulded condition	Sealed (S)	1	0.79	0.02	2.35							0.79		
		3	0.72	0.01	1.87	0.93	0.02	2.63				0.83	0.11	13.23
		10	0.82	0.04	4.46	0.92	0.03	2.93				0.87	0.05	6.08
		30	1.15	0.09	7.45	0.93	0.02	2.00	1.19	0.04	3.26	1.17	0.11	9.46
		100	1.22	0.01	0.85	1.19	0.03	2.56				1.21	0.02	1.29
		365	1.69	0.02	1.30	1.90	0.02	1.27				1.79	0.10	5.83
	Flooded (F)	1												
		3												
		10												
		30												
		100												
		365	2.44	0.06	2.27	1.83	0.06	3.45				2.13	0.31	14.36

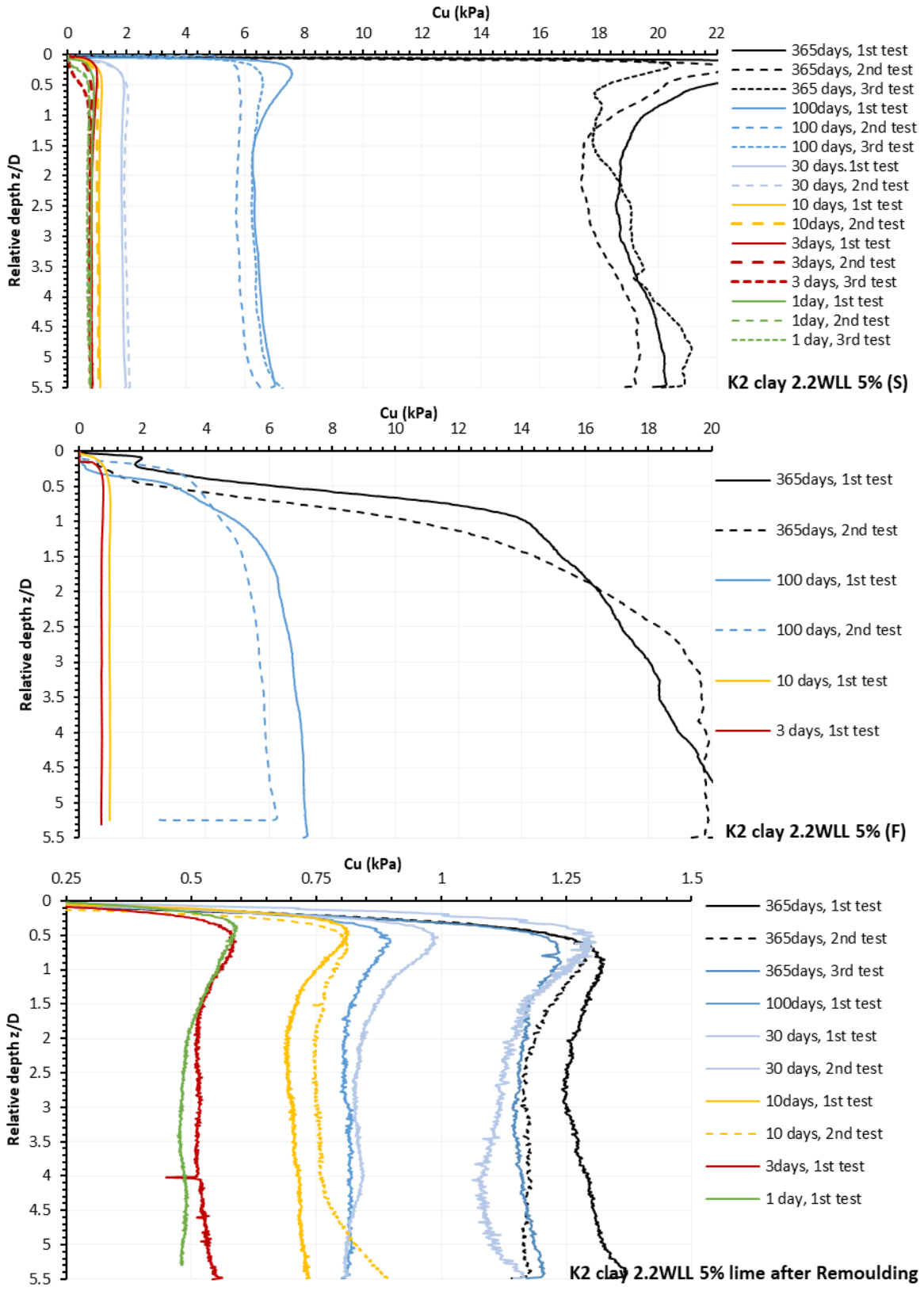

Figure A.9: Penetration tests results for 5% lime-admixed kaolin clay (K2) at 2.2W_{LL}: (a) sealed (S), (b) flooded (F), and (c) after remoulding

Table A.9: Penetration test results for intact and remoulded 5% lime-admixed kaolin clay (K2) at 2.20W_{LL}

Condition	Curing method	Curing Time (days)	Tests									Averaged Results		
			No.1			No.2			No.3			Cu (kPa)	ST.D.	C.O.V. %
			Cu (kPa)	ST.D.	C.O.V. %	Cu (kPa)	ST.D.	C.O.V. %	Cu (kPa)	ST.D.	C.O.V. %			
Intact condition	Sealed (S)	1	0.71	0.02	2.98	0.64	0.04	6.12	0.80	0.02	2.76	0.72	0.06	8.65
		3	0.82	0.02	3.00	0.78	0.01	1.87	0.75	0.01	1.61	0.78	0.03	3.99
		10	1.08	0.01	1.23	1.02	0.02	2.18				1.02	0.03	2.82
		30	1.86	0.04	2.01	1.99	0.06	2.88				1.92	0.06	3.23
		100	6.50	0.20	3.09	5.84	0.12	2.01	6.37	0.14	2.13	6.24	0.29	4.61
		365	19.30	0.58	3.02	18.34	0.74	4.04	19.41	1.06	5.48	19.02	0.48	2.52
	Flooded (F)	1												
		3	0.69	0.01	1.17							0.69		
		10	0.96	0.01	0.85							0.96		
		30												
		100	6.87	0.25	3.57	5.84	0.20	3.47				6.36	0.51	8.09
		365	18.75	1.23	6.54	19.30	0.84	4.34	18.53	0.27	1.44	18.86	0.33	1.72
Remoulded condition	Sealed (S)	1	0.49	0.02	3.17							0.49		
		3	0.52	0.01	2.37							0.52		
		10	0.71	0.01	1.92	0.77	0.03	4.50				0.74	0.03	4.39
		30	0.84	0.02	2.85	1.12	0.04	3.47				0.98	0.14	14.56
		100	0.82	0.01	1.20							0.82		
		365	1.29	0.03	2.39	1.18	0.03	2.24	1.17	0.02	1.61	1.21	0.05	4.37
	Flooded (F)	1												
		3												
		10												
		30												
		100	1.14	0.03	2.69							1.14		
		365	1.48	0.02	1.34	1.18	0.06	5.13	1.09	0.07	6.30	1.25	0.17	13.26

Appendix B SW-K mix

This appendix summarizes the results of penetration tests conducted on intact and remoulded samples of the SW-K soil prepared at $1.8W_{LL}$ and $2.2W_{LL}$.

Table B.1: Penetration test results for intact SW -K soil

W=W/W_{LL}	Lime%	Curing Time (days)	Tests												Averaged Results		
			No.1			No.2			No.3			No.4					
			Cu (kPa)	ST.D.	C.O.V. %	Cu (kPa)	ST.D.	C.O.V. %	Cu (kPa)	ST.D.	C.O.V. %	Cu (kPa)	ST.D.	C.O.V. %	Cu (kPa)	ST.D.	C.O.V. %
1.8	5	1	0.64	0.06	8.69	0.77	0.02	2.97	0.82	0.03	3.30	0.74	0.03	3.51	0.74	0.06	8.73
		3	1.57	0.09	3.42	1.77	0.05	3.07	1.82	0.05	2.71	1.55	0.04	2.83	1.68	0.12	7.28
		10	7.81	0.08	1.07	7.26	0.11	1.47	7.91	0.17	2.10				7.66	0.28	3.72
		30	16.5	0.26	1.57	18.0	0.21	1.18	18.0	0.33	1.85				17.5	0.72	4.14
		100	25.2	0.65	2.60	25.7	0.90	3.51	26.1	0.61	2.36				25.6	0.35	1.38
		365	30.6	0.84	2.76	31.5	0.68	2.14	32.8	0.63	1.93				31.6	0.90	2.86
1.8	3	1	1.21	0.02	1.90	1.05	0.02	2.35	1.05	0.03	2.42				1.10	0.07	6.79
		3	2.22	0.04	1.75	1.81	0.02	1.29	2.04	0.03	1.24	2.12	0.09	4.11	2.05	0.15	7.34
		10	4.33	0.08	1.96	4.39	0.14	3.25	4.54	0.07	1.62				4.42	0.09	2.00
		30	6.47	0.22	3.39	6.6	0.11	1.68	6.91	0.09	1.28				6.64	0.19	2.91
		100	8.72	0.15	1.72	8.7	0.23	2.61	8.73	0.23	2.64				8.72	0.01	0.08
		365	10.4	0.18	1.72	10.1	0.24	2.38	10.5	0.16	1.55				10.3	0.16	1.51
2.2	5	1	0.37	0.03	7.53	0.35	0.01	4.09	0.33	0.01	3.34	0.32	0.02	6.47	0.34	0.02	5.29
		3	0.75	0.03	4.34	0.75	0.02	2.69	0.71	0.01	1.67	1.14	0.03	2.61	0.83	0.18	20.98
		10	4.05	0.11	2.67	4.27	0.10	2.42	4.16	0.06	1.44				4.16	0.09	2.17
		30	10.1	0.08	0.74	9.93	0.13	1.28	9.96	0.08	0.77				10.0	0.08	0.84
		100	16.3	0.71	4.38	14.4	0.31	2.15	14.5	0.22	1.53				15.1	0.86	5.71
		365	19.6	0.70	3.57	18.3	0.21	1.17	18.1	0.25	1.38				18.6	0.67	3.60

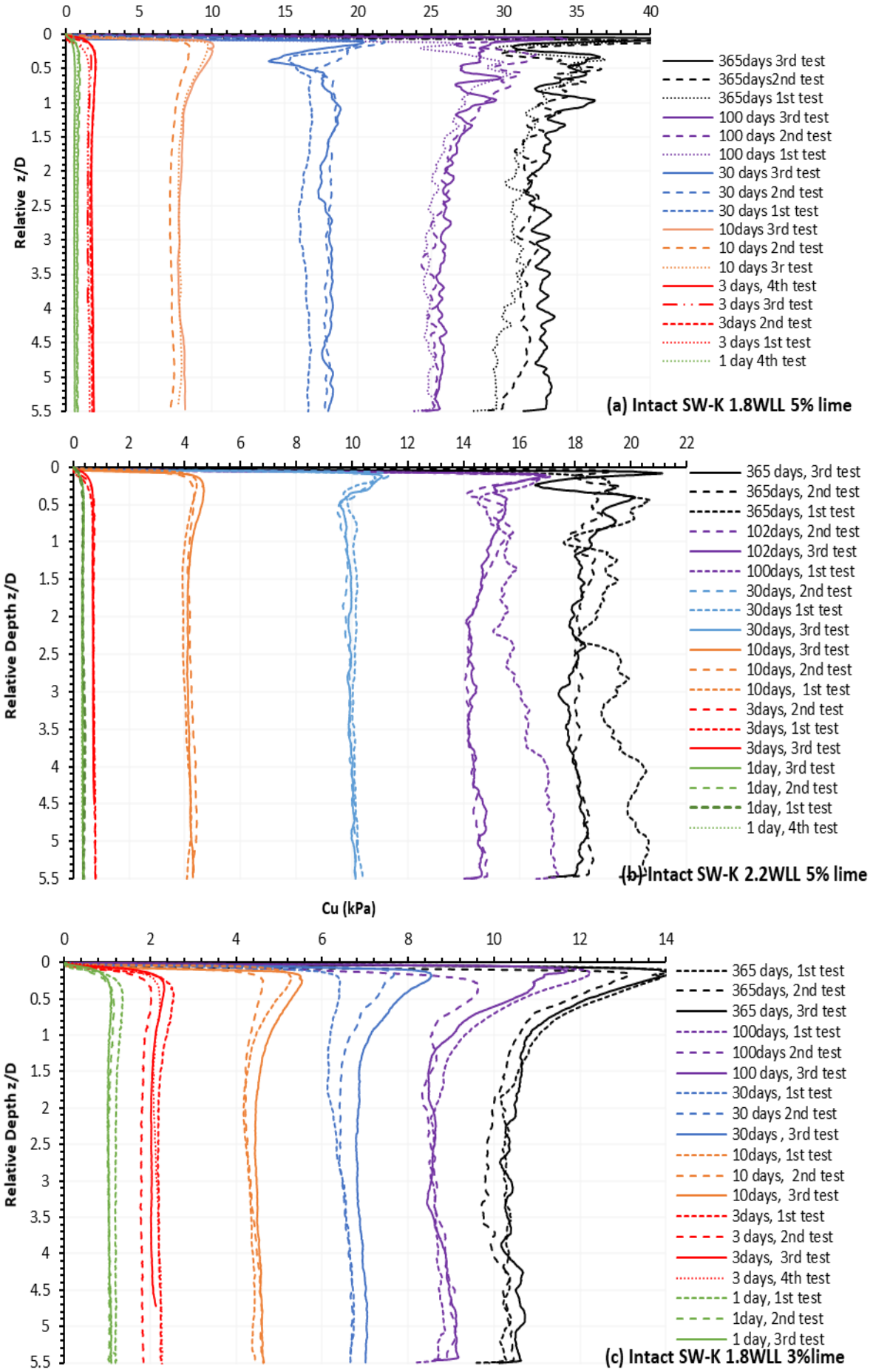

Figure B.1: Undrained shear strength profiles for intact SW-K soils : (a) at 1.8W_{LL} with 5% lime, (b) at 2.2W_{LL} with 5% lime, and (c) at 1.8W_{LL} with 3% lime.

Table B.2: Penetration test results for remoulded SW-K soil

W=W/W_{LL}	Lime%	Curing Time (days)	Tests									Averaged Results		
			No.1			No.2			No.3			Cu (kPa)	ST.D.	C.O.V. %
			Cu (kPa)	ST.D.	C.O.V. %	Cu (kPa)	ST.D.	C.O.V. %	Cu (kPa)	ST.D.	C.O.V. %			
1.8	5	1	0.42	0.02	3.62	0.40	0.02	3.57				0.41	0.01	1.68
		3	0.45	0.01	2.53	0.29	0.01	4.54				0.37	0.08	21.28
		10	0.62	0.02	2.81	0.63	0.02	2.51	0.61	0.01	1.91	0.62	0.01	1.89
		30	2.23	0.06	2.82	2.17	0.02	0.87	2.10	0.06	2.80	2.17	0.06	2.58
		100	4.13	0.12	3.01	4.17	0.10	2.44	4.16	0.10	2.50	4.15	0.02	0.46
		365	4.23	0.08	1.84	3.90	0.08	2.14	4.09	0.06	1.36	4.07	0.14	3.32
1.8	3	1	0.40	0.02	4.37	0.42	0.02	4.66				0.41	0.01	1.40
		3	0.36	0.02	4.28	0.36	0.03	8.16				0.36	0.00	0.45
		10	1.08	0.01	1.23	1.14	0.03	2.44	1.21	0.01	1.07	1.15	0.05	4.64
		30	1.72	0.03	1.81	1.92	0.02	1.16	1.88	0.03	1.59	1.84	0.09	4.67
		100	1.92	0.04	2.13	2.10	0.02	1.01	2.05	0.02	1.19	2.02	0.08	3.75
		365	1.65	0.03	1.58	1.83	0.02	1.16	1.76	0.03	1.73	1.75	0.07	4.18
2.2	5	1	0.17	0.03	5..57758	0.18	0.04	8.77				0.18	0.01	3.54
		3	0.19	0.01	4.09	0.20	0.03	13.78	0.20	0.04	19.98	0.20	0.01	3.76
		10	0.25	0.01	2.99	0.30	0.01	4.12	0.38	0.01	2.67	0.31	0.05	17.22
		30	0.91	0.02	2.09	0.99	0.01	1.16	0.91	0.03	2.98	0.94	0.04	4.09
		100	2.09	0.03	1.50	1.97	0.03	1.54	1.99	0.04	1.94	2.01	0.05	2.61
		365	2.23	0.03	1.40	2.17	0.03	1.60	2.00	0.04	1.76	2.13	0.10	4.54

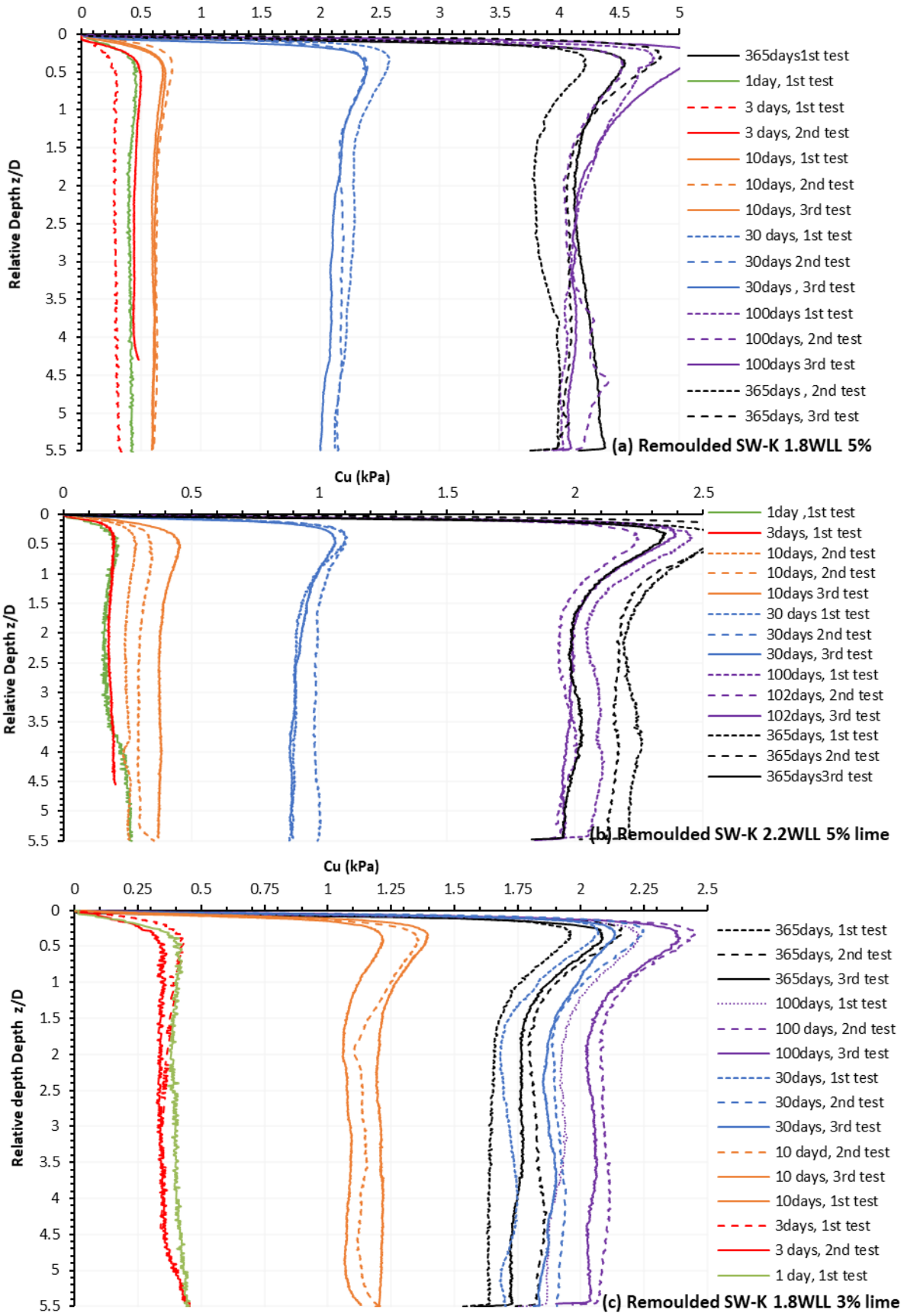

Figure B.2: Undrained shear strength profiles for remoulded SW-K soil: (a) at 1.8W_{LL} with 5% lime, (b) at 2.2W_{LL} with 5% lime, and (c) at 1.8W_{LL} with 3% lime

Appendix C CB Bentonite

This appendix summarizes the results of penetration tests conducted on intact and remoulded specimens of CB montmorillnite slurries prepared at $1.8W_{LL}$ and $2.2W_{LL}$.

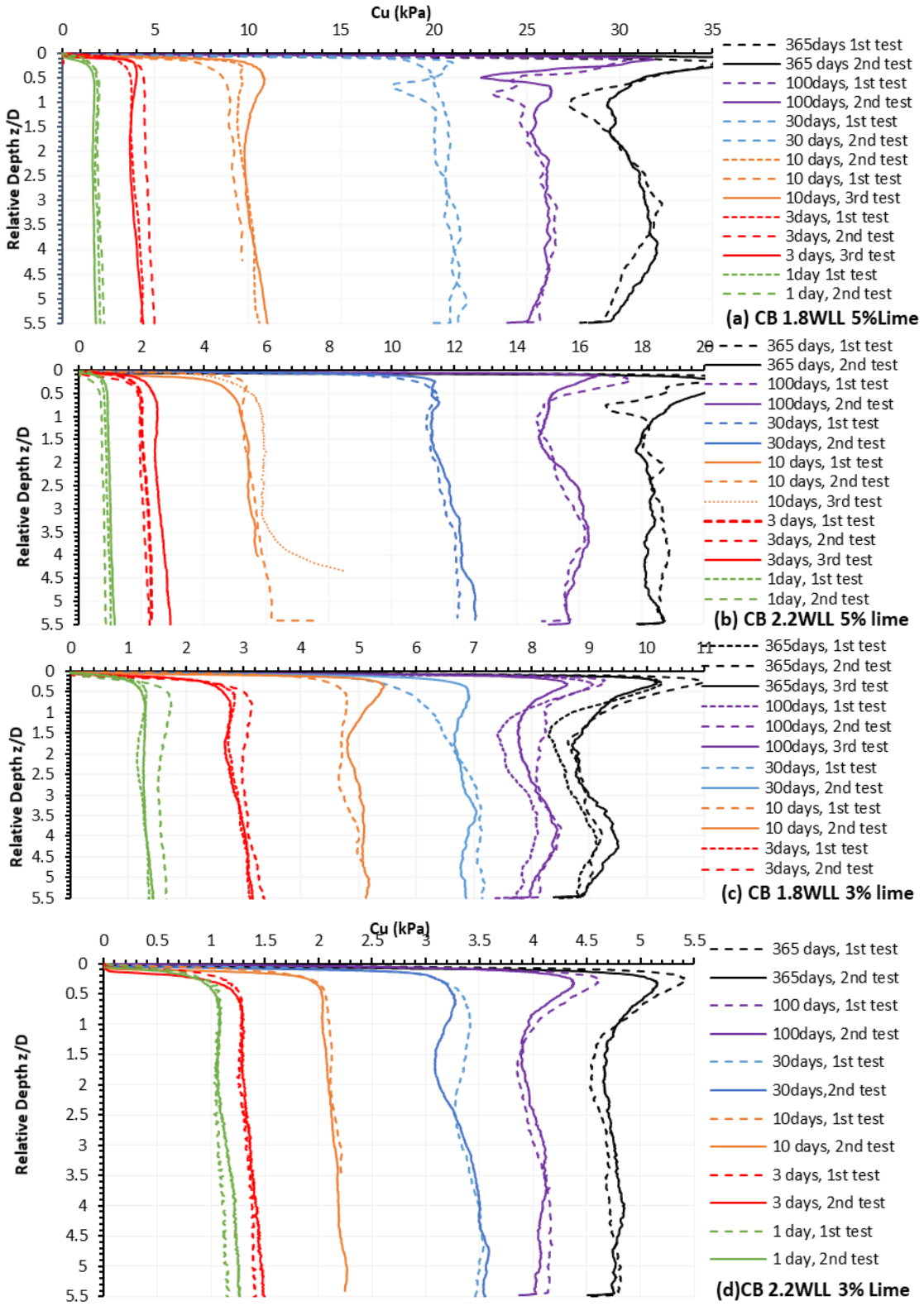

Figure C.1: Undrained shear strength profiles for intact CB soils: (a) at $1.8W_{LL}$ with 5% lime, (b) at $2.2W_{LL}$ with 5% lime, (c) at $1.8W_{LL}$ with 3% lime, and (d) at $2.2W_{LL}$ with 3% lime

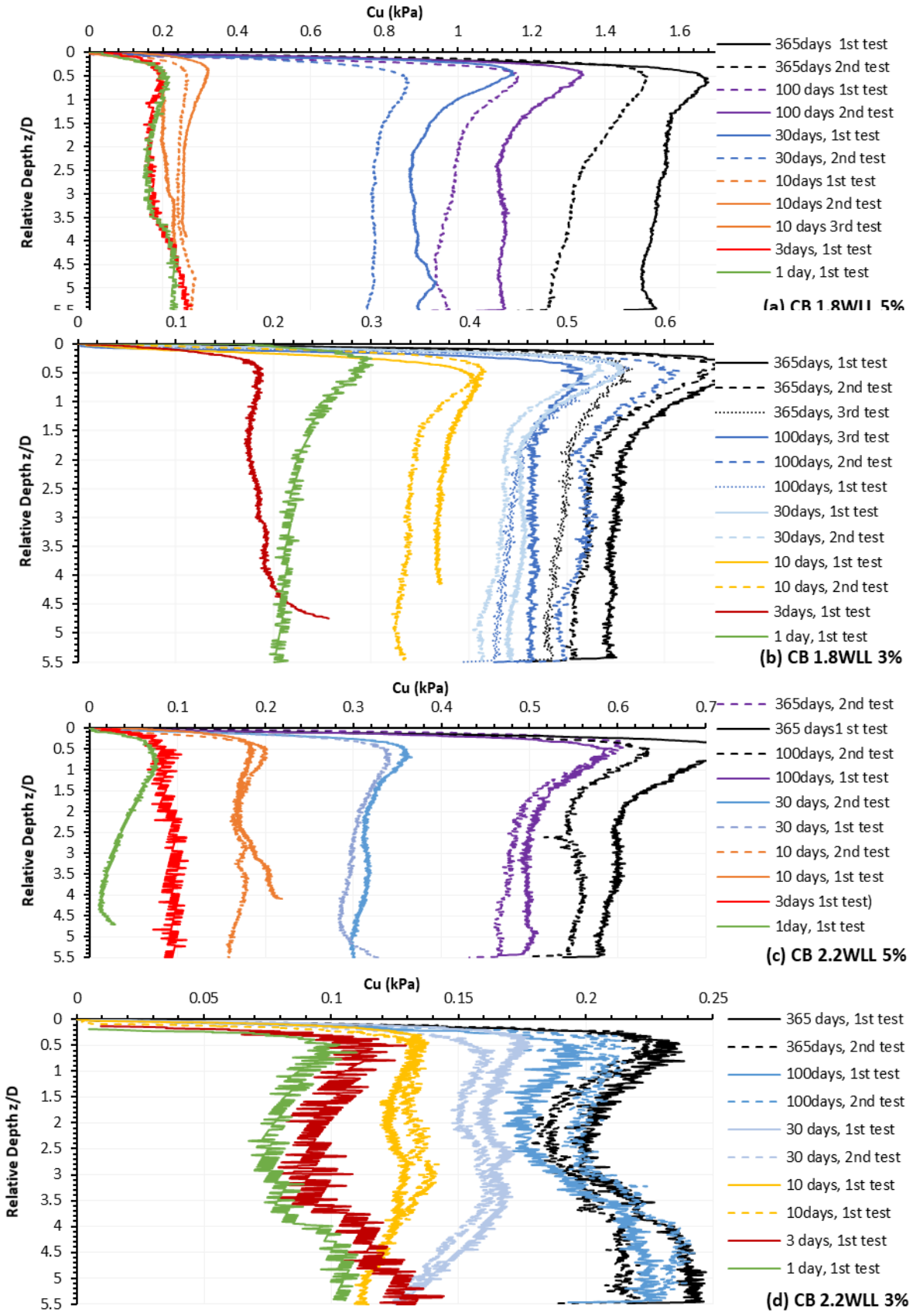

Figure C.2: Undrained shear strength profiles of remoulded CB soils: (a) at 1.8W_{LL} with 5% lime, (b) at 1.8W_{LL} with 3% lime, (c) at 2.2W_{LL} with 5% lime, and (d) at 2.2W_{LL} with 3% lime.

Table C.1: Penetration test results for intact CB soil

$W=W_w/W_{LL}$	Lime%	Curing Time (days)	Tests									Averaged Results		
			No.1			No.2			No.3			Cu (kPa)	ST.D.	C.O.V. %
			Cu (kPa)	ST.D.	C.O.V. %	Cu (kPa)	ST.D.	C.O.V. %	Cu (kPa)	ST.D.	C.O.V. %			
1.8	5	1	1.89	0.09	4.65	2.04	0.12	5.92	1.70	0.05	2.89	1.88	0.14	7.26
		3	4.02	0.23	5.83	4.65	0.17	3.61	3.93	0.24	6.17	4.20	0.32	7.65
		10	9.32	0.24	2.59	10.02	0.37	3.65	10.24	0.38	3.75	9.86	0.39	3.97
		30	20.93	0.33	1.55	20.76	0.53	2.54				20.84	0.09	0.41
		100	25.83	0.60	2.31	25.85	0.35	1.36				25.84	0.01	0.03
		365	30.39	1.23	4.06	30.80	0.84	2.73				30.60	0.20	0.66
1.8	3	1	1.26	0.07	5.57	1.59	0.05	3.32	1.31	0.05	3.98	1.39	0.15	10.44
		3	2.92	0.13	4.34	3.15	0.15	4.69	2.91	0.16	5.51	2.99	0.11	3.73
		10	4.80	0.13	2.64	5.01	0.11	2.19				4.91	0.11	2.19
		30	6.92	0.26	3.78	6.82	0.10	1.45				6.87	0.05	0.76
		100	7.80	0.22	2.84	8.23	0.13	1.58	8.08	0.22	2.78	8.03	0.18	2.21
		365	8.74	0.25	2.88	8.95	0.15	1.71	9.07	0.25	2.74	8.92	0.14	1.53
2.2	5	1	0.93	0.06	6.20	0.80	0.04	5.40	1.02	0.06	5.77	0.92	0.09	9.94
		3	2.20	0.11	5.01	2.08	0.11	5.10	2.64	0.16	6.14	2.31	0.24	10.42
		10	5.48	0.12	2.28	5.71	0.30	5.33	5.89	0.03	0.54	5.69	0.17	3.01
		30	11.74	0.36	3.04	12.00	0.46	3.85				11.87	0.13	1.09
		100	15.51	0.42	2.69	15.67	0.49	3.14				15.59	0.08	0.50
		365	18.52	0.24	1.29	18.22	0.18	1.01				18.37	0.15	0.83
2.2	3	1.00	1.09	0.04	3.46	1.16	0.07	6.27				1.12	0.03	3.11
		3.00	1.34	0.05	3.83	1.38	0.07	4.91				1.36	0.02	1.48
		10.00	2.17	0.07	3.05	2.15	0.07	3.22				2.16	0.01	0.43
		30.00	3.40	0.09	2.50	3.36	0.17	5.19				3.38	0.02	0.56
		100.00	4.04	0.11	2.84	4.03	0.07	1.84				4.03	0.00	0.12
		365.00	4.68	0.08	1.79	4.75	0.05	1.12				4.71	0.03	0.73

Table C.2: Penetration test results for remoulded CB soil

$W=W_w/W_{LL}$	Lime%	Curing Time (days)	Tests									Averaged Results		
			No.1			No.2			No.3			Cu (kPa)	ST.D.	C.O.V. %
			Cu (kPa)	ST.D.	C.O.V. %	Cu (kPa)	ST.D.	C.O.V. %	Cu (kPa)	ST.D.	C.O.V. %			
1.8	5	1	0.19	0.03	15.39							0.19	0.00	
		3	0.20	0.04	18.52							0.20	0.00	
		10	0.25	0.00	3.23	0.25	0.01	5.31	0.27	0.05	12.73	0.26	0.00	0.80
		30	0.90	0.03	3.11	0.78	0.02	2.56				0.84	0.06	7.28
		100	0.98	0.04	4.02	1.13	0.03	2.60				1.06	0.07	6.91
		365	1.54	0.03	2.13	1.33	0.07	5.05				1.43	0.11	7.50
1.8	3	1	0.12	0.04	6.77							0.22		
		3	0.19	0.02	7.98							0.19		
		10	0.37	0.01	2.16	0.34	0.01	3.15				0.36	0.02	4.98
		30	0.45	0.01	2.40	0.43	0.01	3.13				0.44	0.01	2.56
		100	0.44	0.02	3.85	0.51	0.02	3.25	0.47	0.01	1.30	0.48	0.03	6.05
		365	0.55	0.02	2.84	0.52	0.02	3.37	0.49	0.01	2.56	0.52	0.02	4.62
2.2	5	1	0.03	0.02	53.59							0.03		
		3	0.09	0.01	8.51							0.09		
		10	0.18	0.01	8.06	0.20	0.01	3.59	0.17	0.01	4.15	0.18	0.01	5.96
		30	0.30	0.01	4.22	0.31	0.01	3.32				0.31	0.01	1.98
		100	0.51	0.01	2.96	0.55	0.01	2.09				0.53	0.02	4.58
		365	0.60	0.02	3.70	0.48	0.02	4.06				0.54	0.06	10.98
2.2	3	1	0.09	0.01	14.00							0.09		
		3	0.11	0.02	13.52							0.11		
		10	0.13	0.00	2.65	0.13	0.01	3.20				0.13	0.00	0.41
		30	0.16	0.01	7.21	0.15	0.01	6.80				0.15	0.00	2.37
		100	0.20	0.02	9.96	0.22	0.02	7.32				0.21	0.01	3.85
		365	0.22	0.02	7.47	0.20	0.01	5.90				0.21	0.01	4.12

Appendix D Grangemouth soil

This appendix summarizes the results penetration tests conducted on intact and remoulded specimens of Grangemouth soil slurries prepared at $1.4W_{LL}$ and $1.6W_{LL}$.

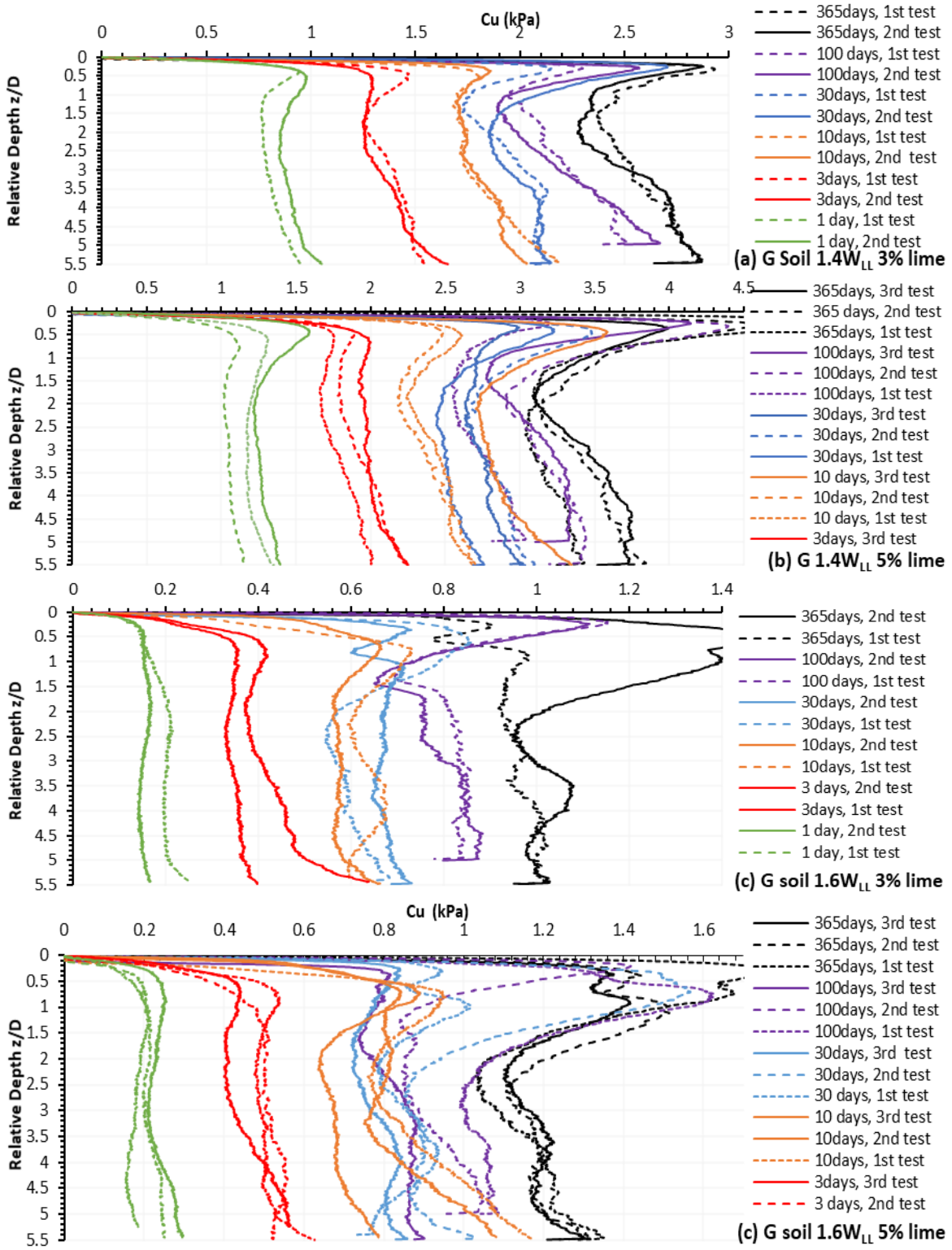

Figure D.1: Undrained shear strength profiles of intact Grangemouth soil: (a) at $1.4W_{LL}$ with 5% lime, (b) at $1.4W_{LL}$ with 3% lime, (c) at $1.6W_{LL}$ with 3% lime, and (d) at $1.6W_{LL}$ with 5% lime.

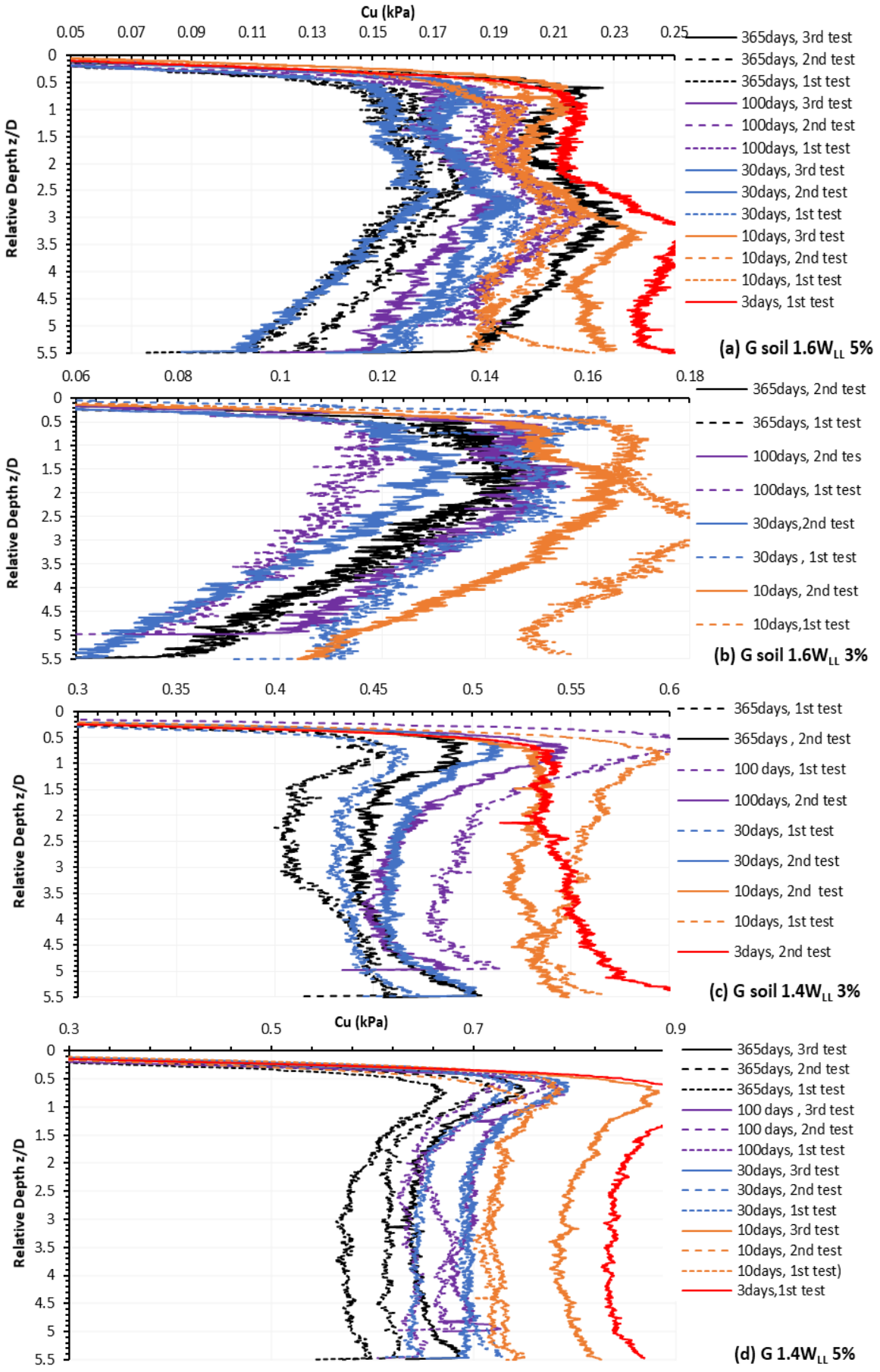

Figure D.2: Undrained shear strength profile of remoulded Grangemouth soil: (a) at 1.6W_{LL} with 5% lime, (b) at 1.6W_{LL} with 3% lime, (c) at 1.4W_{LL} with 3% lime, and (d) at 1.4W_{LL} with 5% lime.

Table D.1: Penetration test results for intact Grangemouth soil

$W=W_w/W_{LL}$	Lime%	Curing Time (days)	Tests									Averaged Results		
			No.1			No.2			No.3			Cu (kPa)	ST.D.	C.O.V. %
			Cu (kPa)	ST.D.	C.O.V. %	Cu (kPa)	ST.D.	C.O.V. %	Cu (kPa)	ST.D.	C.O.V. %			
1.40	3	1	0.82	0.05	6.33	0.90	0.05	5.18				0.86	0.04	5.03
		3	1.40	0.09	6.18	1.37	0.11	7.89				1.38	0.01	0.85
		10	1.85	0.15	8.01	1.82	0.10	5.27				1.84	0.01	0.61
		30	1.99	0.13	6.78	2.00	0.10	4.92				1.99	0.01	0.31
		100	2.21	0.15	6.83	2.16	0.21	9.58				2.18	0.03	1.17
		365	2.59	0.15	5.88	2.56	0.20	7.90				2.57	0.02	0.60
1.40	5	1	1.21	0.04	3.64	1.06	0.04	3.30	1.28	0.05	3.93	1.19	0.09	7.76
		3	1.81	0.12	6.40	1.96	0.14	7.23	2.01	0.08	3.95	1.93	0.09	4.51
		10	2.45	0.12	4.88	2.40	0.16	6.71	2.90	0.16	5.66	2.58	0.23	8.75
		30	2.56	0.09	3.42	2.84	0.13	4.40	2.76	0.09	3.42	2.72	0.12	4.40
		100	2.71	0.14	5.12	3.20	0.18	5.61	3.09	0.20	6.57	3.00	0.21	7.05
		365	3.20	0.12	3.71	3.45	0.20	5.67	3.47	0.23	6.57	3.37	0.12	3.65
1.60	3	1	0.20	0.01	5.65	0.15	0.01	5.37				0.18	0.02	13.25
		3	0.43	0.06	13.16	0.35	0.02	4.27				0.39	0.04	10.35
		10	0.64	0.03	5.15	0.58	0.02	3.49				0.61	0.03	4.67
		30	0.62	0.06	9.36	0.68	0.02	2.65				0.65	0.03	4.80
		100	0.81	0.05	5.77	0.78	0.06	7.68				0.80	0.01	1.81
		365	0.97	0.03	3.21	1.05	0.10	9.91				1.01	0.04	4.03
1.60	5	1	0.18	0.02	8.97	0.22	0.02	7.66	0.24	0.03	10.52	0.21	0.03	12.01
		3	0.52	0.02	4.04	0.51	0.03	5.27	0.46	0.06	12.22	0.50	0.03	5.24
		10	0.91	0.12	13.17	0.70	0.04	6.14	0.86	0.09	10.67	0.82	0.09	10.94
		30	0.86	0.06	7.18	0.95	0.13	13.88	0.78	0.04	5.32	0.86	0.07	7.91
		100	1.10	0.13	11.83	0.90	0.06	6.27	0.83	0.05	5.86	0.94	0.11	11.95
		365	1.18	0.10	8.76	1.22	0.10	8.56	1.20	0.06	5.43	1.20	0.02	1.47

Table D.2: Penetration test results for remoulded Grangemouth soil

$W=W_w/W_{LL}$	Lime%	Curing Time (days)	Tests									Averaged Results		
			No.1			No.2			No.3			Cu (kPa)	ST.D.	C.O.V. %
			Cu (kPa)	ST.D.	C.O.V. %	Cu (kPa)	ST.D.	C.O.V. %	Cu (kPa)	ST.D.	C.O.V. %			
1.40	3	1												
		3	0.55	0.02	3.31							0.55	0.00	0.00
		10	0.55	0.01	2.21	0.53	0.01	1.23				0.54	0.01	2.13
		30	0.44	0.01	2.19	0.47	0.01	2.66				0.45	0.01	2.96
		100	0.50	0.02	4.49	0.47	0.02	4.53				0.48	0.02	3.32
		365	0.43	0.02	4.12	0.46	0.02	3.35				0.44	0.02	3.41
1.40	5	1												
		3	0.85	0.02	2.25							0.85	0.00	0.00
		10	0.73	0.01	1.50	0.72	0.01	1.71	0.80	0.02	2.27	0.75	0.04	4.79
		30	0.65	0.02	2.67	0.70	0.02	2.16	0.70	0.01	1.96	0.68	0.02	3.35
		100	0.67	0.02	2.24	0.64	0.01	1.77	0.70	0.02	2.20	0.67	0.02	3.41
		365	0.59	0.02	3.44	0.62	0.01	2.30	0.65	0.02	2.63	0.62	0.03	4.32
1.60	3	1												
		3	0.20	0.03	15.75							0.20	0.00	0.00
		10	0.16	0.01	7.09	0.14	0.02	13.86				0.15	0.01	7.82
		30	0.13	0.02	13.09	0.10	0.02	23.57				0.11	0.01	12.70
		100	0.10	0.01	10.21	0.13	0.01	10.31				0.12	0.02	12.81
		365	0.12	0.02	18.40	0.11	0.02	19.67				0.12	0.00	0.97
1.60	5	1												
		3	0.23	0.01	5.97							0.23	0.00	0
		10	0.20	0.01	3.89	0.20	0.01	5.32	0.22	0.01	5.08	0.20	0.01	4.36
		30	0.18	0.01	6.64	0.15	0.02	12.24	0.18	0.01	5.77	0.17	0.02	9.26
		100	0.20	0.01	4.29	0.20	0.01	3.91	0.17	0.01	7.08	0.19	0.01	7.14
		365	0.15	0.02	12.17	0.16	0.02	9.70	0.21	0.01	5.56	0.17	0.03	15.74

Appendix E SW-S soil mix

This section summarizes the results of penetration tests conducted on intact and remoulded specimens of SW-S soil mix slurries prepared at $1.8W_{LL}$ and $2W_{LL}$

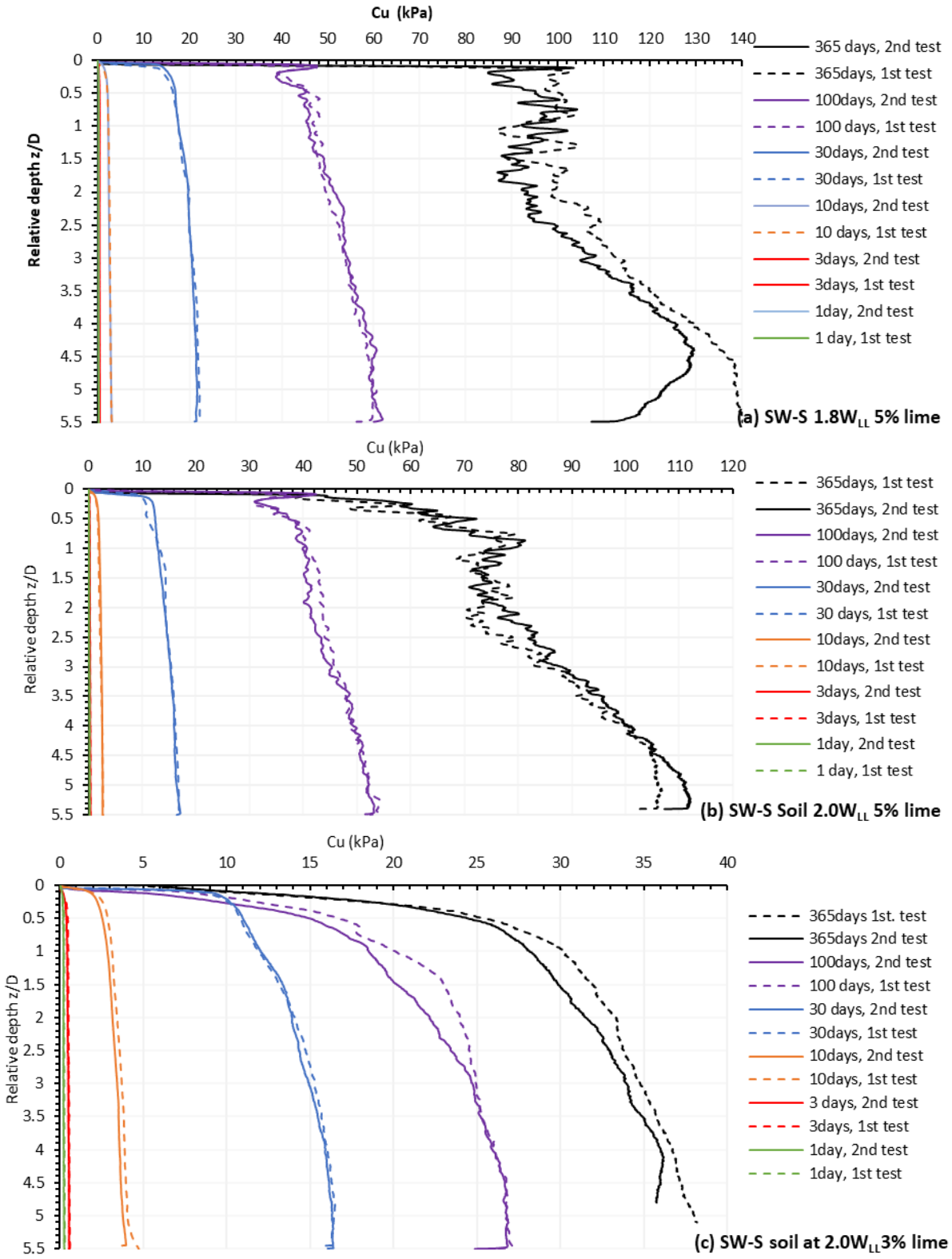

Figure E.1: Undrained shear strength profiles for intact SW-S soil: (a) at $1.8W_{LL}$ with 5% lime, (b) at $2.0W_{LL}$ with 5% lime, and (c) at $2.0W_{LL}$ with 3% lime.

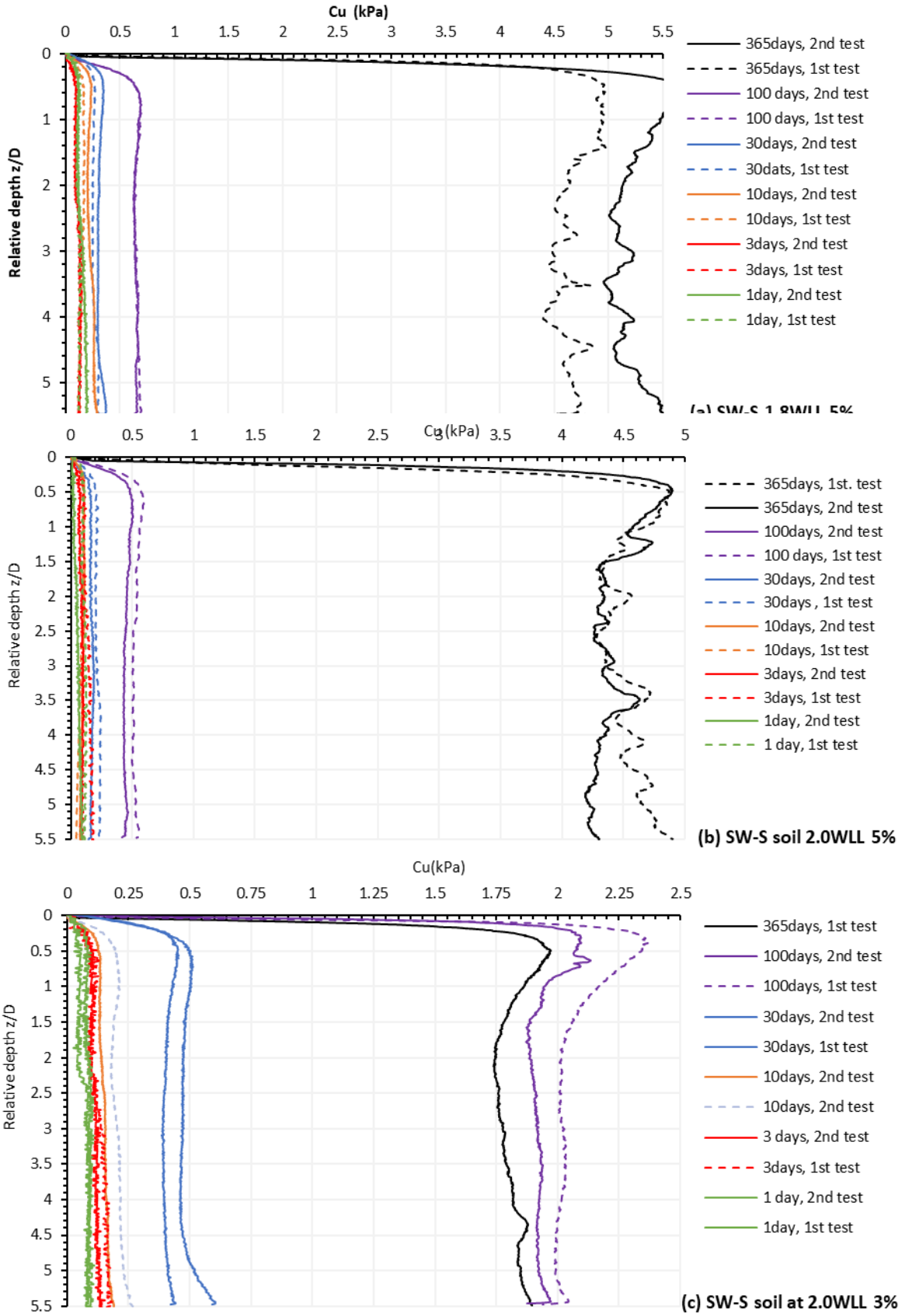

Figure E.2: Undrained shear strength profiles for remoulded SW-S soil: (a) at 1.8W_{LL} with 5% lime, (b) at 2.0W_{LL} with 5% lime, and (c) at 2.0W_{LL} with 3% lime.

Table E.1: Penetration test results for intact SW-S soil

$W'=W_w/W_{LL}$	Lime%	Curing Time (days)	Tests						Averaged Results		
			No.1			No.2			Cu (kPa)	ST.D.	C.O.V. %
			Cu (kPa)	ST.D.	C.O.V. %	Cu (kPa)	ST.D.	C.O.V. %			
1.8	5	1	0.23	0.02	8.96	0.23	0.02	9.04	0.23	0.00	1.22
		3	0.43	0.02	3.95	0.36	0.02	6.73	0.40	0.03	8.53
		10	2.74	0.16	6.02	2.67	0.22	8.40	2.71	0.03	1.22
		30	20.61	1.38	6.69	20.39	1.07	5.23	20.50	0.11	0.55
		100	54.21	4.19	7.73	54.98	4.43	8.06	54.59	0.38	0.70
		365	117.57	16.42	13.96	109.66	13.92	12.69	113.61	3.95	3.48
2.0	5	1	0.16	0.04	26.72	0.15	0.04	25.56	0.15	0.00	2.64
		3	0.30	0.04	12.41	0.30	0.03	11.30	0.30	0.00	0.32
		10	2.33	0.28	11.80	2.42	0.17	7.09	2.38	0.05	1.97
		30	15.47	1.01	6.53	15.20	1.12	7.34	15.34	0.14	0.88
		100	46.99	3.47	7.38	46.28	4.46	9.64	46.63	0.35	0.76
		365	91.42	13.50	14.77	88.74	13.23	14.91	90.08	1.34	1.49
2.0	3	1	0.29	0.04	11.98	0.26	0.04	17.27	0.28	0.02	5.84
		3	0.58	0.04	7.73	0.52	0.04	7.29	0.55	0.03	5.48
		10	3.74	0.33	8.87	3.43	0.28	8.26	3.58	0.15	4.20
		30	15.09	1.27	8.41	14.96	1.20	8.04	15.03	0.06	0.43
		100	25.02	1.60	6.39	24.22	2.48	10.23	24.62	0.40	1.64
		365	34.76	2.18	6.26	33.28	2.40	7.21	34.02	0.74	2.17

Table E.2: Penetration test results for remoulded SW-S soil

$W'=W_w/W_{LL}$	Lime%	Curing Time (days)	Tests						Averaged Results		
			No.1			No.2					
			Cu (kPa)	ST.D.	C.O.V. %	Cu (kPa)	ST.D.	C.O.V. %	Cu (kPa)	ST.D.	C.O.V. %
1.8	5	1	0.12	0.01	9.38	0.16	0.03	20.06	0.14	0.02	12.29
		3	0.13	0.02	14.81	0.12	0.02	14.76	0.12	0.00	2.26
		10	0.15	0.02	11.80	0.24	0.03	11.22	0.19	0.04	22.30
		30	0.27	0.02	7.97	0.31	0.02	6.35	0.29	0.02	7.79
		100	0.66	0.02	2.58	0.65	0.01	1.98	0.66	0.00	0.71
		365	4.64	0.14	3.01	5.18	0.14	2.71	4.91	0.27	5.55
2.0	5	1	0.11	0.01	10.27	0.06	0.02	31.16	0.09	0.03	30.74
		3	0.14	0.02	17.05	0.09	0.01	11.30	0.12	0.03	22.63
		10	0.08	0.02	24.66	0.10	0.01	12.32	0.09	0.01	11.10
		30	0.22	0.02	7.21	0.17	0.01	5.50	0.20	0.03	12.96
		100	0.52	0.02	3.51	0.45	0.02	3.59	0.49	0.04	7.82
		365	4.35	0.12	2.84	4.52	0.15	3.28	4.44	0.08	1.84
2.0	3	1	0.09	0.01	10.36	0.08	0.02	24.88	0.08	0.00	4.45
		3	0.14	0.03	18.88	0.11	0.01	11.67	0.13	0.01	10.02
		10	0.21	0.02	9.33	0.16	0.01	9.26	0.18	0.03	14.98
		30	0.48	0.03	6.08	0.40	0.01	2.86	0.44	0.04	9.00
		100	2.03	0.03	1.69	1.92	0.02	1.00	1.97	0.05	2.75
		365	1.80	0.04	2.38	1.94	0.07	5.38	1.80	0.07	3.88

Appendix F Cold curing

Table F.1: Penetration test results for intact kaolin (K2) soil, cured under cold conditions

$W'=W_w/W_{LL}$	Lime%	Curing Time (days)	Tests									Averaged Results		
			No.1			No.2			No.3					
			Cu (kPa)	ST.D.	C.O.V. %	Cu (kPa)	ST.D.	C.O.V. %	Cu (kPa)	ST.D.	C.O.V. %	Cu (kPa)	ST.D.	C.O.V. %
1.80	1	1	0.90	0.01	1.50							0.90	0.00	0.00
		3	0.97	0.01	1.24	0.97	0.04	4.11	0.93	0.02	1.83	0.96	0.02	1.92
		10	0.98	0.07	6.91	0.98	0.00	0.37	1.01	0.02	1.55	0.99	0.01	1.34
		30	1.11	0.03	2.42	1.04	0.02	1.45	1.04	0.01	0.69	1.07	0.03	2.98
		100	1.44	0.04	2.68	1.34	0.02	1.48	1.30	0.02	1.90	1.36	0.06	4.53
		365	1.98	0.05	2.70	1.81	0.04	2.28	1.68	0.04	2.67	1.82	0.12	6.84
2.2	1	1	0.41	0.02	3.88	0.43	0.02	3.50				0.42	0.01	2.64
		3	0.43	0.02	3.67	0.40	0.01	2.49				0.42	0.01	2.45
		10	0.46	0.01	1.78	0.42	0.01	1.69	0.47	0.02	5.22	0.45	0.02	4.78
		30	0.49	0.01	2.99	0.53	0.02	4.60	0.51	0.02	3.91	0.51	0.01	2.88
		100	0.69	0.03	4.34	0.65	0.02	2.79	0.74	0.02	3.25	0.69	0.04	5.37
		365	1.00	0.04	3.80	0.98	0.03	2.70				0.99	0.01	1.12
1.80	5	1	1.27	0.01	0.66	1.22	0.02	1.70				1.24	0.02	1.88
		3	1.36	0.02	1.37	1.27	0.02	1.66	1.41	0.02	1.49	1.35	0.06	4.35
		10	1.52	0.06	3.74	1.35	0.02	1.19	1.53	0.02	1.13	1.47	0.09	5.80
		30	1.83	0.05	2.76	1.67	0.01	0.51	1.88	0.03	1.36	1.79	0.09	5.06
		100	2.91	0.05	1.58	2.86	0.02	0.63	3.21	0.02	0.60	3.00	0.16	5.21
		365	7.44	0.10	1.29	7.56	0.07	0.86	7.83	0.08	1.02	7.61	0.16	2.16
2.20	5	1	0.59	0.02	2.78	0.59	0.03	5.27				0.59	0.00	0.38
		3	0.65	0.03	4.59	0.63	0.01	2.14	0.67	0.01	1.58	0.65	0.02	2.74
		10	0.70	0.02	3.57	0.69	0.02	2.94	0.65	0.02	2.76	0.68	0.02	3.12
		30	0.86	0.05	5.28	0.81	0.02	3.01	0.79	0.01	1.59	0.82	0.03	3.67
		100	1.41	0.07	5.12	1.37	0.05	3.78	1.45	0.06	4.03	1.41	0.04	2.51
		365	4.02	0.19	4.83	3.94	0.11	2.69				3.98	0.04	0.99

Table F.2: Penetration test results for remoulded kaolin (K2) soil, cured under cold conditions

$W'=W_w/W_{LL}$	Lime%		Curing Time (days)	Tests									Averaged Results		
				No.1			No.2			No.3			Cu (kPa)	ST.D.	C.O.V. %
				Cu (kPa)	ST.D.	C.O.V. %	Cu (kPa)	ST.D.	C.O.V. %	Cu (kPa)	ST.D.	C.O.V. %			
1.80	1		1												
			3	0.64	0.01	0.80	0.66	0.01	1.19				0.65	0.01	1.12
			10	0.69	0.03	3.83	0.67	0.02	2.95	0.67	0.02	2.54	0.68	0.01	1.75
			30	0.61	0.02	2.55	0.71	0.01	1.12	0.71	0.01	2.08	0.68	0.05	7.08
			100	0.63	0.01	2.09	0.62	0.03	4.28	0.63	0.02	3.87	0.63	0.01	1.03
			365	0.55	0.01	2.18	0.58	0.03	4.50	0.56	0.01	2.59	0.56	0.01	2.20
2.2	1		1	0.33	0.01	3.37							0.16		
			3	0.28	0.01	4.81							0.28		
			10	0.32	0.01	3.76	0.30	0.02	5.86	0.30	0.01	3.12	0.31	0.01	3.62
			30	0.30	0.01	4.52	0.31	0.01	4.55	0.33	0.01	3.56	0.31	0.01	3.75
			100	0.28	0.01	5.03	0.30	0.01	4.85	0.32	0.01	3.66	0.30	0.02	5.65
			365	0.28	0.02	8.71	0.30	0.02	5.98				0.29	0.01	4.56
1.80	5		1												
			3												
			10	1.14	0.06	5.68	1.02	0.02	2.12	1.18	0.02	2.04	1.11	0.07	6.10
			30	1.26	0.02	1.28	1.06	0.04	4.22	1.31	0.06	4.56	1.21	0.11	8.73
			100	1.60	0.03	1.65	1.34	0.03	2.23	1.53	0.05	3.34	1.49	0.11	7.29
			365	1.73	0.03	1.76	1.63	0.02	1.10	1.80	0.02	0.97	1.72	0.07	4.05
2.20	5		1	0.40	0.02	3.90									
			3	0.47	0.03	5.71							0.24		
			10	0.49	0.01	2.90	0.53	0.02	3.39	0.50	0.02	4.69	0.51		
			30	0.67	0.02	2.66	0.62	0.02	3.73	0.58	0.02	3.18	0.62	0.04	6.28
			100	0.91	0.03	3.17	0.67	0.02	2.47	0.75	0.01	1.54	0.78	0.10	12.94
			365	0.81	0.02	2.01	0.80	0.01	1.72				0.80	0.01	0.67

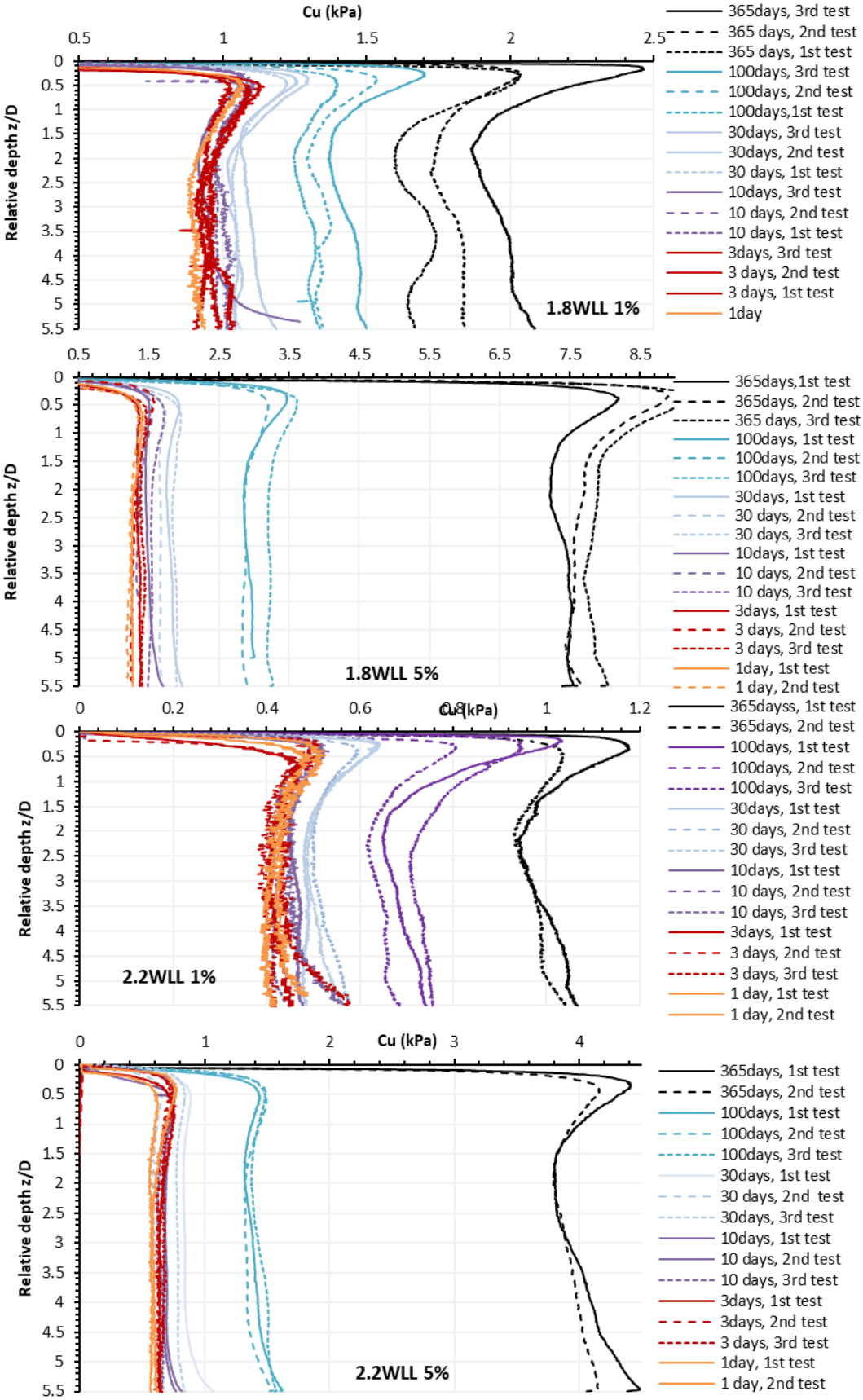

Figure F.1: Penetration test results for intact kaolin (K2) clay, cured under cold conditions

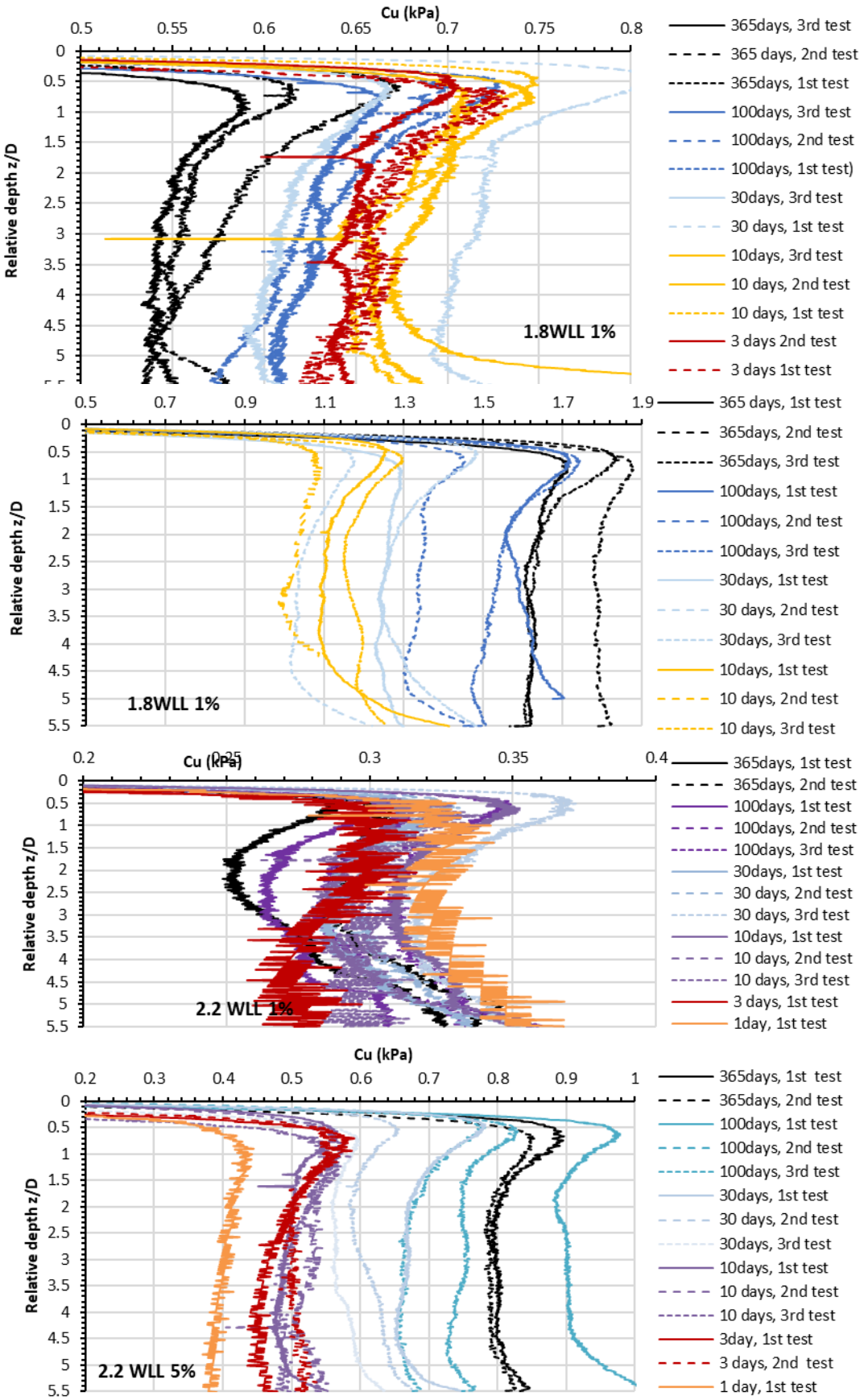

Figure F.2: Penetration test results for remoulded kaolin (K2) soil, cured under cold conditions

Table F.3: Penetration test results for intact & remoulded SW-K soil at 1.8W_{LL} cured under cold conditions

Condition	Curing method	Curing Time (days)	Tests									Averaged Results		
			No.1			No.2			No.3			Cu (kPa)	ST.D.	C.O.V. %
			Cu (kPa)	ST.D.	C.O.V. %	Cu (kPa)	ST.D.	C.O.V. %	Cu (kPa)	ST.D.	C.O.V. %			
Intact condition	3%	1	0.65	0.01	1.67	0.71	0.01	1.77				0.68	0.03	4.15
		3	0.93	0.01	0.86	0.85	0.01	1.04				0.89	0.04	4.72
		10	1.61	0.03	2.12	1.60	0.02	0.94				1.60	0.01	0.51
		30	2.93	0.06	1.97	3.08	0.06	2.10				3.00	0.07	2.45
		100	5.65	0.16	2.90	5.84	0.08	1.33				5.75	0.10	1.66
		365	9.07	0.32	3.51	9.01	0.22	2.46				9.04	0.03	0.34
	5%	1	0.50	0.02	3.88	0.66	0.01	1.75	0.54	0.01	1.38	0.57	0.07	11.73
		3	0.56	0.01	1.70	0.71	0.01	1.37	0.77	0.01	1.68	0.68	0.09	13.01
		10	1.00	0.02	2.30	0.99	0.03	3.08	1.32	0.01	0.89	1.10	0.15	13.70
		30	3.57	0.11	3.11	3.86	0.09	2.44	4.19	0.08	1.81	3.87	0.25	6.56
		100	10.82	0.11	1.03	10.78	0.04	0.40	10.65	0.09	0.87	10.75	0.07	0.67
		365	21.55	0.30	1.38	21.36	0.32	1.50	22.82	0.63	2.76	21.91	0.65	2.96
Remoulded condition	3%	1	0.41	0.01	2.78	0.37	0.01	2.53				0.39	0.02	6.20
		3	0.27	0.02	5.95	0.31	0.02	6.21				0.29	0.02	7.44
		10	0.32	0.01	3.99	0.32	0.02	4.90				0.32	0.00	0.00
		30	0.56	0.01	2.68	0.61	0.02	3.42				0.59	0.03	4.74
		100	1.65	0.02	1.23	1.69	0.01	0.87				1.67	0.02	1.37
		365	2.40	0.02	0.69	2.47	0.05	1.84				2.44	0.03	1.34
	5%	1	0.34	0.01	4.28	0.33	0.03	8.28	0.33	0.01	2.84	0.33	0.01	2.50
		3	0.34	0.02	5.06	0.30	0.03	9.40	0.32	0.02	5.90	0.32	0.01	4.14
		10	0.31	0.01	4.79	0.29	0.02	6.19	0.39	0.01	1.59	0.33	0.04	13.46
		30	0.46	0.00	0.92	0.70	0.06	8.86	0.57	0.01	2.53	0.58	0.10	16.95
		100	0.55	0.01	1.33	0.62	0.01	1.44	0.69	0.02	2.35	0.62	0.06	9.54
		365	2.02	0.01	0.63	2.06	0.01	0.69	2.37	0.02	0.77	2.15	0.16	7.31

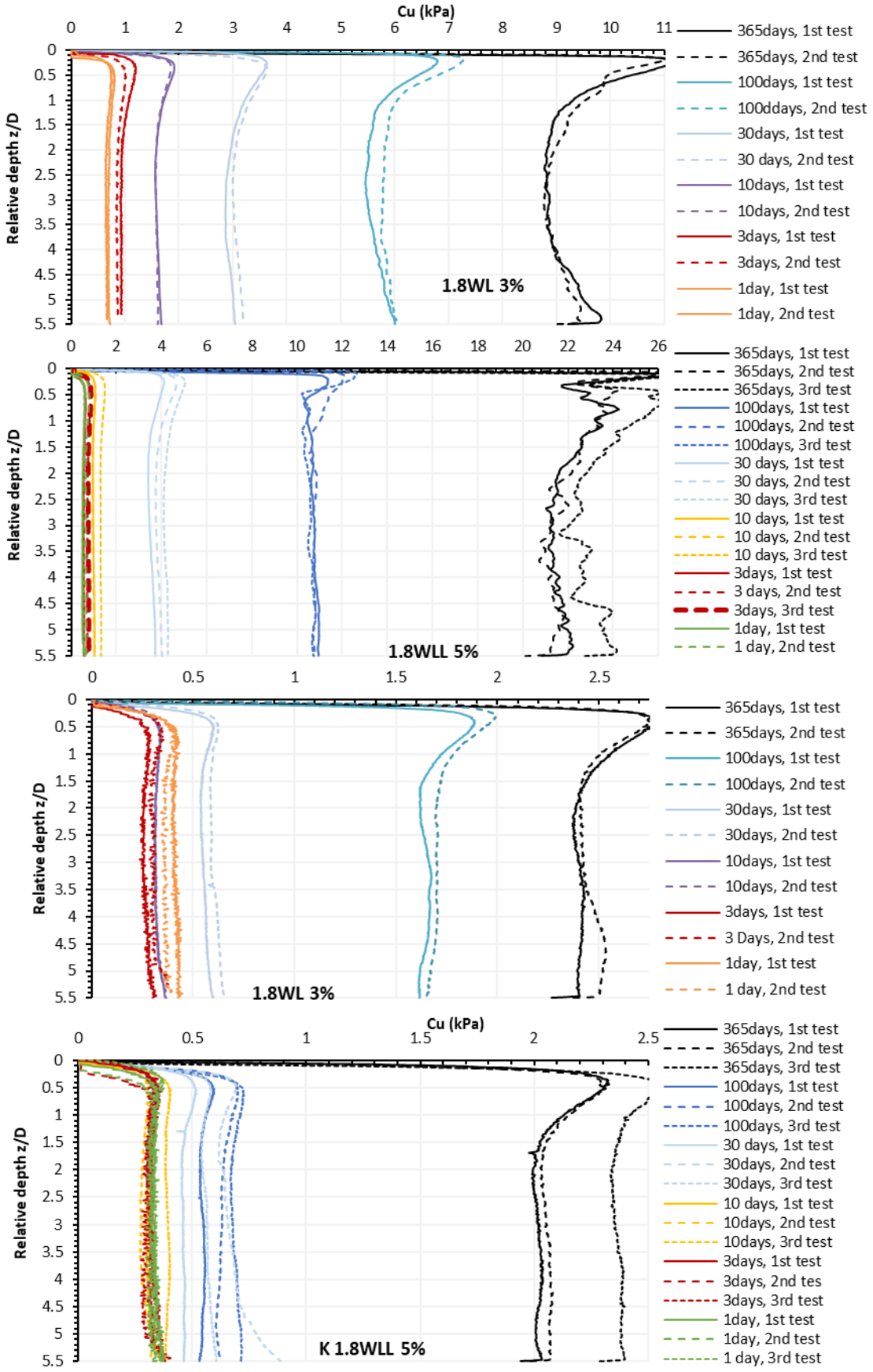

Figure F.3: Penetration test results for intact & remoulded SW-K soil at 1.8W_{LL}, cured under cold condition

Appendix G Hot curing

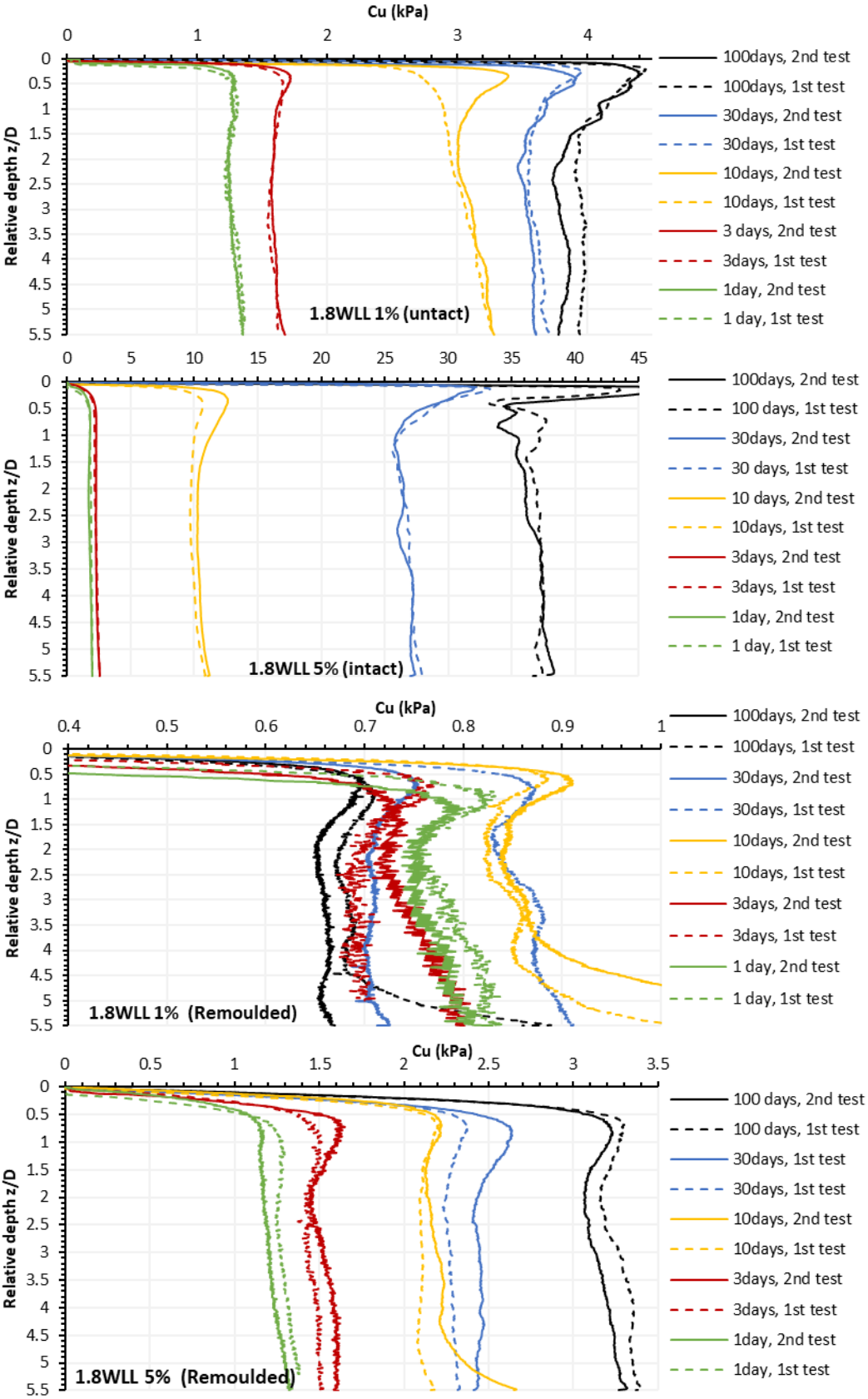

Figure G-1: Penetration test results for intact & remoulded kaolin clay at 1.8W_{LL} cured under hot conditions

Table G.1: Penetration test results for kaolin clay at 1.8W_{LL} cured under hot conditions

Condition	Lime%	Curing Time (days)	Tests						Averaged Results		
			No.1			No.2			Cu (kPa)	ST.D.	C.O.V. %
			Cu (kPa)	ST.D.	C.O.V. %	Cu (kPa)	ST.D.	C.O.V. %			
Intact condition	1	1	1.28	0.04	2.75	1.27	0.05	4.08	1.28	0.01	0.43
		3	1.60	0.02	1.54	1.58	0.03	1.69	1.59	0.01	0.45
		10	3.16	0.08	2.61	3.12	0.09	2.85	3.14	0.02	0.58
		30	3.56	0.04	1.09	3.62	0.05	1.40	3.59	0.03	0.84
		100	3.81	0.04	1.06	3.96	0.02	0.56	3.88	0.08	1.96
	5	1	1.81	0.09	4.88	1.82	0.07	3.82	1.82	0.00	0.21
		3	2.33	0.08	3.57	2.37	0.11	4.48	2.35	0.02	0.91
		10	10.46	0.25	2.42	10.02	0.33	3.28	10.24	0.22	2.14
		30	26.84	0.42	1.57	27.11	0.34	1.27	26.97	0.14	0.50
		100	37.24	0.62	1.67	37.26	0.18	0.49	37.25	0.01	0.02
Remoulded condition	1	1	0.76	0.02	2.72	0.79	0.03	3.21	0.78	0.01	1.88
		3	0.75	0.03	3.54	0.70	0.02	2.26	0.72	0.03	3.62
		10	0.92	0.11	11.84	0.86	0.04	4.63	0.89	0.03	3.25
		30	0.71	0.01	1.10	0.87	0.02	2.48	0.79	0.08	9.95
		100	0.66	0.01	1.17	0.70	0.04	6.00	0.68	0.02	2.86
	5	1	1.22	0.05	4.27	1.27	0.05	4.13	1.25	0.03	2.08
		3	1.54	0.05	3.55	1.47	0.03	2.18	1.51	0.04	2.45
		10	2.23	0.11	4.81	2.11	0.02	1.01	2.17	0.06	2.75
		30	2.46	0.05	1.85	2.28	0.02	1.08	2.37	0.09	3.71
		100	3.17	0.07	2.25	3.28	0.07	2.22	3.22	0.05	1.68

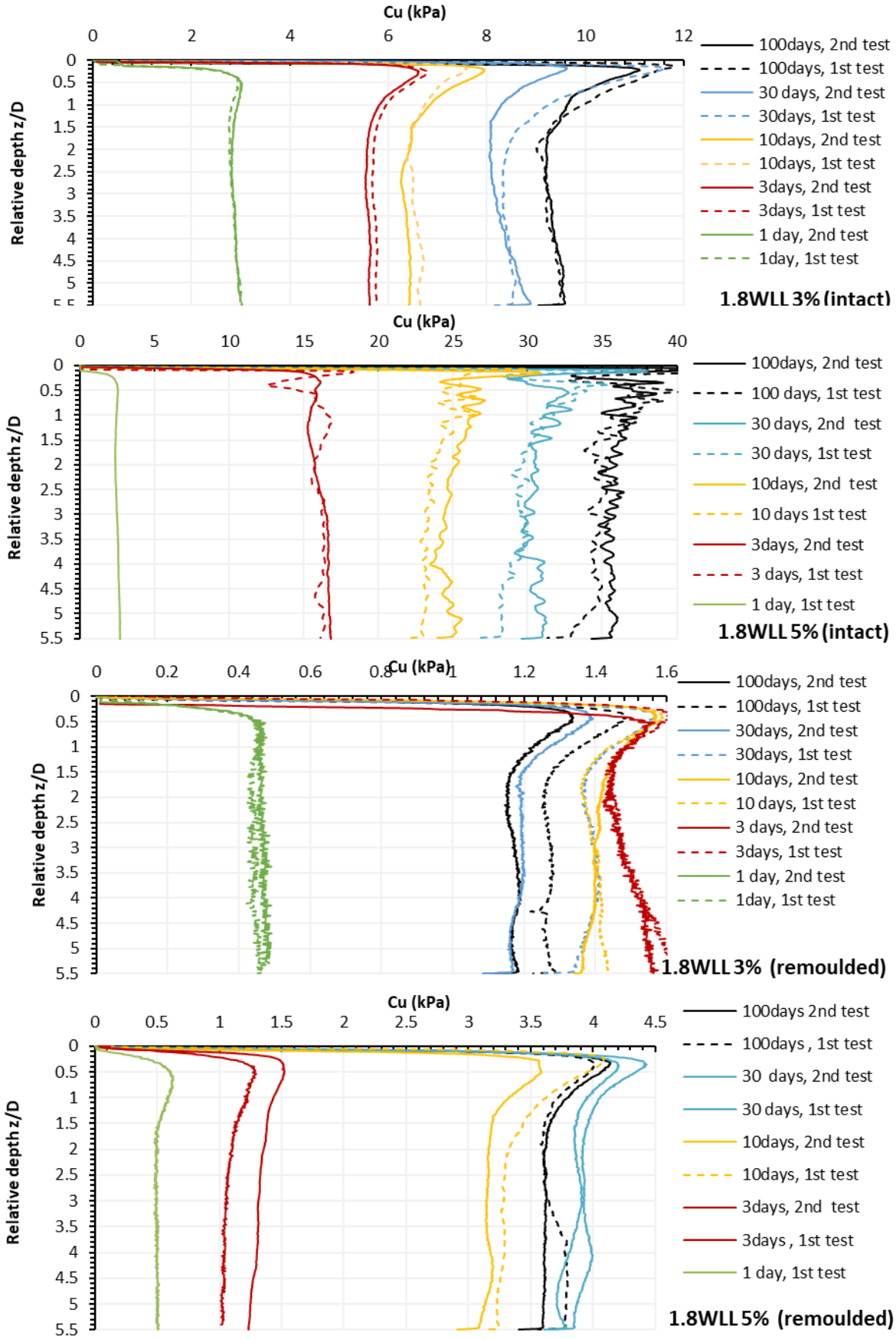

Figure G.2: Penetration test results for intact & remoulded SW-K soil at 1.8W_{LL} cured under hot conditions

Table G.2: Penetration test data for intact & remoulded SW-K soil at 1.8W_{LL} cured under hot conditions

Condition	Lime%	Curing Time (days)	Tests						Averaged Results		
			No.1			No.2			Cu (kPa)	ST.D.	C.O.V. %
			Cu (kPa)	ST.D.	C.O.V. %	Cu (kPa)	ST.D.	C.O.V. %			
Intact condition	3	1	2.89	0.06	1.94	2.89	0.07	2.54	2.89	0.00	0.12
		3	5.60	0.03	0.58	5.73	0.03	0.59	5.66	0.06	1.14
		10	6.38	0.06	0.97	6.57	0.09	1.42	6.47	0.10	1.48
		30	8.37	0.24	2.90	8.43	0.09	1.01	8.40	0.03	0.33
		100	9.37	0.13	1.43	9.32	0.13	1.45	9.34	0.02	0.25
	5	1	2.56	0.10	3.80				2.56		
		3	17.03	0.79	4.65	16.21	0.30	1.85	16.62	0.41	2.47
		10	24.82	0.61	2.47	23.43	0.56	2.37	24.12	0.69	2.87
		30	30.44	0.50	1.65	29.32	0.81	2.76	29.88	0.56	1.87
		100	35.56	0.32	0.91	34.66	0.74	2.14	35.11	0.45	1.28
Remoulded condition	3	1	0.49	0.01	2.14	0.44	0.01	2.14	0.47	0.02	4.59
		3	1.49	0.04	2.87	1.72	0.07	4.27	1.60	0.11	6.92
		10	1.40	0.03	1.82	1.48	0.05	3.28	1.44	0.04	2.79
		30	1.19	0.02	1.78	1.38	0.02	1.55	1.29	0.10	7.63
		100	1.17	0.01	1.26	1.27	0.02	1.45	1.22	0.05	3.99
	5	1	0.50	0.02	3.96				0.50		
		3	1.13	0.12	10.68	1.66	0.05	3.19	1.40	0.27	19.07
		10	3.16	0.04	1.29	3.31	0.09	2.66	3.24	0.07	2.31
		30	3.94	0.04	1.13	3.83	0.07	1.82	3.88	0.05	1.30
		100	3.62	0.04	1.00	3.70	0.08	2.11	3.66	0.04	1.03

REFERENCES

Abbo, A. J., and Sloan, S. W., 1995, A smooth hyperbolic approximation to the Mohr-Coulomb yield criterion: Computers & Structures, v. 54, no. 3, p. 427-441.

Al-Mukhtar, M., Lasledj, A., and Alcover, J.-F., 2010, Behaviour and mineralogy changes in lime-treated expansive soil at 20°C: Applied Clay Science, v. 50, no. 2, p. 191-198.

Al-Mukhtar, M., Lasledj, A., and Alcover, J. F., 2014, Lime consumption of different clayey soils: Applied Clay Science, v. 95, no. Supplement C, p. 133-145.

Andersen, L., and Clausen, J., 2009, Comments on "Flow rule effects in the Tresca model" by H.A. Taiebat and J.P. Carter [Computers and Geotechnics 35 (2008) 500–503]: Computers and Geotechnics, v. 36, no. 5, p. 911-913.

Ansari, Y., Pineda, J., Kouretzis, G., and Sheng, D., 2014, Experimental and numerical investigation of rate and softening effects on the undrained shear strength of Ballina clay: Australian Geomechanics Journal, v. 49, no. 4, p. 51-57.

ASTM, 2003, American Society of Testing Material, Standard Test Method for Making, Accelerated Curing, and Testing Concrete Compression Test Specimens, Volume C 684 – 99 (Reapproved 2003): West Conshohocken, PA. USA ASTM International.

-, 2004, American Society of Testing Material, Standard Test Methods for Unconfined Compressive Strength of Compacted Soil-Lime Mixtures: West Conshohocken, PA. USA ASTM International.

-, 2005, American Society of Testing Material, Standard Test Method for Laboratory Miniature Vane Shear Test for Saturated Fine-Grained Clayey Soil: West Conshohocken, PA, USA, ASTM International.

-, 2007, American Society of Testing Material, Standard Test Method for Unconsolidated-Undrained Triaxial Compression Test on Cohesive Soils. : West Conshohocken, PA. USA, ASTM International.

Atkinson, J. H., 1993, An introduction to the the mechanics of soils and foundations through critical state soil mechanics, London, UK, McGRAW-HILL BOOK COMPANY

Baghdadi, Z. A., 1982, Accelerated Strength Testing of Soil-Cement [Ph.D.: The University of Arizona.

Balasubramaniam, A. S., Bergado, D. T., Buessucesco, B. R., and Yang, W. C., 1989, Strength and deformation characteristics of lime-treated soft clays: Geotechnical Engineering, v. 20, p. 49-65.

Balasubramaniam, A. S., Lin, D. G., Sharma, S. S., Kamruzzaman, A. H. M., Uddin, K., and Bergado, D. T., 1999, Behavior of soft Bangkok clay treated with additives, 11th Asian Regional Conference on Soil Mechanics and Geotechnical Engineering: Seoul, Korea, p. 11-14.

Barnes, G. E., 2000, Soil Mechanics: Principles and Practice, Hampshire, UK, Palgrave MacMillan.

Bell, F. G., 1996, Lime stabilization of clay minerals and soils: Engineering Geology, v. 42, no. 4, p. 223-237.

-, 2007, Engineering Geology, Oxford, UK, Butterworth-Heinemann. Elsevier Ltd.

Benmebarek, S., Saifi, I., and Benmebarek, N., 2017, Depth factors for undrained bearing capacity of circular footing by numerical approach: Journal of Rock Mechanics and Geotechnical Engineering, v. 9, no. 4, p. 761-766.

Bergaya, F., Lagaly, G., and Vayer, M., 2006, Chapter 12.10 Cation and Anion Exchange, *in* Bergaya, F., Theng, B. K. G., and Lagaly, G., eds., Developments in Clay Science, Volume 1, Elsevier, p. 979-1001.

Bishop, A. W., 1967, Progressive failure-with special reference to the mechanism causing it, PYOC. Geotech. Conf., Volume 2: Oslo, p. 142-150.

Bishop, A. W., 1971, The Influence of Progressive Failure on the Choice of the Method of Stability Analysis: Géotechnique, v. 21, no. 2, p. 168-172.

Bishop, A. W., and Henkel, D. J., 1962, The measurement of soil properties in the triaxial test, London : .

Bjerrum, L., 1972, Embankments on Soft Ground, *in* Engineers, A. S. o. C., ed., Proceedings of the Specialty Conference on Performance of Earth and Earth-Supported Structures, Volume 2: Lafayette, Indiana, United States, p. 1-54.

Bo, M. W., Arulrajah, A., Sukmak, P., Horpibulsuk, S., and Leong, M., 2016, Mineralogy and Geotechnical Properties of Ultrasoft Soil from a Nearshore Mine Tailings Sedimentation Pond: Marine Georesources & Geotechnology, v. 34, no. 8, p. 782-791.

Boardman, D. I., Glendinning, S., and Rogers, C. D. F., 2001, Development of stabilisation and solidification in lime–clay mixes: Géotechnique, v. 51, no. 6, p. 533-543.

Bobei, D. C., and Locks, J., 2013, Characterization of Sensitive Soft Soils for the Waterview Connection Project, New Zealand, Proceedings of the 18th International Conference on Soil Mechanics and Geotechnical Engineering Paris.

Boukpeti, N., White, D. J., Randolph, M. F., and Low, H. E., 2009, Characterization of the Solid-Fluid Transition of Fine-Grained Sediments, ASME 2009 28th International Conference on Ocean, Offshore and Arctic Engineering: Honolulu, Hawaii, USA, ASME.

Brown, P. T., 1969, Numerical Analyses of Uniformly Loaded Circular Rafts on Deep Elastic Foundations: Géotechnique, v. 19, no. 3, p. 399-404.

BS, B. S. I., 1990a, British standards methods for soils for civil engineering purposes, Part 7. Shear strength tests(total stress): UK.

-, 1990b, Stabilized materials for civil engineering purposes, Part 2. Methods of test for cement-stabilized and lime stabilized materials, Volume 1924: London, UK, BSI.

Burland, J. B., 1990, On the compressibility and shear strength of natural clays: Géotechnique, v. 40, no. 3, p. 329-378.

Butterfield, R., 1979, A natural compression law for soils (an advance on e–log p′): Géotechnique, v. 29, no. 4, p. 469-480.

Casacrande, A., and Wilson, S. D., 1951, Effect of Rate of Loading on the Strength of Clays and Shales at Constant Water Content: Géotechnique, v. 2, no. 3, p. 251-263.

Casagrande, A., 1936, The determination of the preconsolidation load and its practical significance., Proceedings of the First International Conference on Soil Mechanics and Foundation Engineering, Volume 3: Cambridge, Mass., Harvard Printing Office, p. 60–64.

Cerato, A. B., and Lutenegger, A. J., 2004, Determining Intrinsic Compressibility of Fine-Grained Soils: Journal of Geotechnical and Geoenvironmental Engineering, v. 130, no. 8, p. 872-877.

Chandler, R. J., 1988, The in-situ measurement of the undrained shear strength of clays using the field vane, *in* Richards, A. F., ed., Vane shear strength testing in soils: Field & laboratory studies, Volume ASTM STP 1014: Philadelphia, U.S.A, American Society of Testing Material p. 13-44.

Charlton, T., and Rouainia, M., 2017, Geo-Risk 2017 : Impact of Spatial Variability, Probabilistic Site Characterization, and Geohazards . GSP 284 . 2017 Geo-Risk 2017: Denver, Colorado, American Society of Civil Engineers.

Chatterjee, S., Mana, D. S. K., Gourvenec, S., and Randolph, M. F., 2014, Large-Deformation Numerical Modeling of Short-Term Compression and Uplift Capacity of Offshore Shallow Foundations: Journal of Geotechnical and Geoenvironmental Engineering, v. 140, no. 3, p. 04013021.

CHATTERJEE, S., RANDOLPH, M. F., and WHITE, D. J., 2012, The effects of penetration rate and strain softening on the vertical penetration resistance of seabed pipelines: Géotechnique, v. 62, no. 7, p. 573-582.

Chen, H., and Wang, Q., 2006, The behaviour of organic matter in the process of soft soil stabilization using cement: Bulletin of Engineering Geology and the Environment, v. 65, no. 4, p. 445-448.
Chen, W.-F., 1975, Limit Analysis and Soil Plasticity, Amsterdam, Elsevier.
Cheng, L., and Cord-Ruwisch, R., 2012, In situ soil cementation with ureolytic bacteria by surface percolation: Ecological Engineering, v. 42, p. 64-72.
Cheng, L., Cord-Ruwisch, R., and Shahin, M. A., 2013, Cementation of sand soil by microbially induced calcite precipitation at various degrees of saturation: Canadian Geotechnical Journal, v. 50, no. 1, p. 81-90.
Chew, S. H., Kamruzzaman, A. H. M., and Lee, F. H., 2004, Physicochemical and Engineering Behavior of Cement Treated Clays: Journal of Geotechnical and Geoenvironmental Engineering, v. 130, no. 7, p. 696-706.
Chu, C., Wu, Z., Deng, Y., Chen, Y., and Wang, Q., 2017, Intrinsic compression behavior of remolded sand–clay mixture: Canadian Geotechnical Journal, v. 54, no. 7, p. 926-932.
Chung, S. F., and Randolph, M., 2004, Penetration resistance in soft clay for different shaped penetrometers, *in* Mayne, V. d. F., ed., Proceedings of the 2nd International Conference on Geotechnical and Geophysical Site Characterization, Volume 1: Rotterdam, Millpress Science, p. 671-677.
Chung, S. F., Randolph, M. F., and Schneider, J. A., 2006, Effect of penetration rate on penetrometer resistance in clay: Journal of Geotechnical and Geoenvironmental Engineering, v. 132, no. 9, p. 1188-1196.
Clausen, J., Damkilde, L., and Andersen, L., 2006, Efficient return algorithms for associated plasticity with multiple yield planes: International Journal for Numerical Methods in Engineering, v. 66, no. 6, p. 1036-1059.
Clayton, C. R. I., Hight, D. W., and Hopper, R. J., 1992, Progressive destructuring of Bothkennar clay. implications for sampling and reconsolidation procedures: Géotechnique, v. 42, no. 2, p. 219-239.
Clayton, C. R. I., Simons, N. E., and Matthews, M. C., 1995, Site investigation, Oxford, Blackwell Science.
Consoli, N. C., Prietto, P. D. M., and Ulbrich, L. A., 1998, Influence of Fiber and Cement Addition on Behavior of Sandy Soil: Journal of Geotechnical and Geoenvironmental Engineering, v. 124, no. 12, p. 1211-1214.
Cotecchia, F., and Chandler, R. J., 2000, A general framework for the mechanical behaviour of clays: Géotechnique, v. 50, no. 4, p. 431-447.
Das, B. M., 1984, Principles of Foundation Engineering, California, USA, Wadsworth Inc.
-, 1985, Advance Soil Mechanics, Singapore, McGraw-Hill Book Co.
-, 2002, Principles of geotechnical engineering, Pacific Grove, CA, Brooks Cole/Thompson Learning.
Dayal, U., and Allen, J. H., 1975, The Effect of Penetration Rate on the Strength of Remolded Clay and Sand Samples: Canadian Geotechnical Journal, v. 12, no. 3, p. 336-348.
DeAlencar, J. A., Chan, D. H., and Morgenstern., N. R., 1988, Progressive Failure in the Vane Test, *in* Richards, A. F., ed., Vane Shear Strength Testing in Soils: Field and Laboratory Studies: Philadelphia,PA. USA, ASTM International, p. 150-167.
DeJong, J. T., Yafrate, N. J., and DeGroot, D. J., 2011, Evaluation of Undrained Shear Strength Using Full-Flow Penetrometers: Journal of Geotechnical and Geoenvironmental Engineering, v. 137, no. 1, p. 14-26.
Diamond, S., and Kinter, E. B., 1966, Adsorption of calcium hydroxide by montmorillonite and kaolinite: Journal of Colloid and Interface Science, v. 22, no. 3, p. 240-249.
Eades, J. L., and Grim, R. E., 1960, Reactions of hydrated lime with pure clay minerals in soil stabilization, Highway Res. Bull: Washington, D.C., p. 51-63.

Eades, J. L., and Grim, R. E., 1966, A quick test to determine lime requirements for lime stabilization: Washington, D.C., Highway Res. Bull., p. 61-72.
Eason, G., and Shield, R. T., 1960, The plastic indentation of a semi-infinite solid by a perfectly rough circular punch: Zeitschrift für angewandte Mathematik und Physik ZAMP, v. 11, no. 1, p. 33-43.
Eckert, D., and Sims, J. T., 1995, Recommended soil pH and lime requirement test, *in* Sims, J. T., and Wolf, A., eds., Soil Testing in the Northeastern United States, Northeastern Regional Publication No. 493, p. 16–21.
Edwards, D. H., Zdravkovic, L., and Potts, D. M., 2005, Depth factors for undrained bearing capacity: Géotechnique, v. 55, no. 10, p. 755-758.
Ehrgott, J. Q., 1971, Calculation of stress and strain from triaxial test data on undrained soil specimens: U. S. Army Engineer Waterways Experiment Station.
Einav, I., and Randolph, M., 2006, Effect of strain rate on mobilised strength and thickness of curved shear bands: Géotechnique, v. 56, no. 7, p. 501-504.
Einav, I., and Randolph, M. F., 2005, Combining upper bound and strain path methods for evaluating penetration resistance: International Journal for Numerical Methods in Engineering, v. 63, no. 14, p. 1991-2016.
Fallah, S., Gavin, K., and Jalilvand, S., 2016, Numerical modelling of Cone Penetration Test in Clay using Coupled Eulerian Lagrangian Method, Civil Engineering Research in Ireland 2016: Ireland.
Fang, Z., and Harrison, J. P., 2001, A mechanical degradation index for rock: International Journal of Rock Mechanics and Mining Sciences, v. 38, no. 8, p. 1193-1199.
Federico, A., Vitone, C., and Murianni, A., 2015, On the mechanical behaviour of dredged submarine clayey sediments stabilized with lime or cement: Canadian Geotechnical Journal, v. 52, no. 12, p. 2030-2040.
Finnie, I. M. S., and Randolph, M. F., 1994, Punch-Through and Liquefaction Induced Failure of Shallow Foundations on Calcareous Sediments, Proceedings of the international conference on behaviour of offshore structures, Volume 1: Boston, MA, Pergamon, p. 217-230.
Ganesan, B., and Bolton, 2013, Characterisation of a high plasticity marine clay using a T-bar penetrometer: Underwater Technology, v. 31, p. 179-185.
Gens, A., and Nova, R., Conceptual bases for a constitutive model for bonded soils and weak rocks, *in* Proceedings Geotechnical Engineering of Hard Soils-Soft Rocks: Proceedings of an International Symposium, Athens, 1993, Athens, Greece, 1993, A.A. Balkema.
Gourvenec, S. M., and Mana, D. S. K., 2011, Undrained vertical bearing capacity factors for shallow foundations: Géotechnique Letters, v. 1, no. 4, p. 101-108.
Grabe, J., and Wu, L., 2016, Coupled Eulerian-Lagrangian simulation of the penetration and braking behaviour of ship anchors in clay: geotechnik, v. 39, no. 3, p. 168-174.
Graham, J., Crooks, J. H. A., and Bell, A. L., 1983, Time effects on the stress-strain behaviour of natural soft clays: Géotechnique, v. 33, no. 3, p. 327-340.
Gylland, A. S., Jostad, H. P., and Nordal, S., Failure geometry around a shear vane in sensitive clay, *in* Proceedings Nordic Geotechnical Meeting - NGM 2012, Copenhagen, Denmark, May 2012, Volume 1, Danish Geotechnical Society
Hamann, T., Qiu, G., and Grabe, J., 2015, Application of a Coupled Eulerian–Lagrangian approach on pile installation problems under partially drained conditions: Computers and Geotechnics, v. 63, p. 279-290.
Han, C., Wang, D., Gaudin, C., O'Loughlin, C. D., and Cassidy, M. J., 2016, Behaviour of vertically loaded plate anchors under sustained uplift: Géotechnique, v. 66, no. 8, p. 681-693.
Hasan, A. M., 2016, Small strain elastic behaviour of unsaturated soil investigated by bender/extender element testion [Ph.D.: University of Glasgow.

Hassan, M. M., and Ravaska, O., 2009, Strength and permeability characteristics of cement stabilized soft finnish clay, *in* Karstunen, M., and Leoni, M., eds., Geotechnics of Soft Soils – Focus on Ground Improvement: London, Taylor & Francis Group, p. 227-233.

Hawlader, B., Dutta, S., Fouzder, A., and Zakeri, A., 2015, Penetration of Steel Catenary Riser in Soft Clay Seabed: Finite-Element and Finite-Volume Methods: International Journal of Geomechanics, v. 15, no. 6, p. 04015008.

Head, K. H., 1988a, Manual of soil laboratory Testing. Volume 1: Soil Classification and Compaction Tests, UK, Pentech Press.

-, 1988b, Manual of Soil Laboratory Testing. Volume 2: Permeability, shear strength, and compressibility tests, London, Pentech Press.

-, 1988c, Manual of soil laboratory testing. Volume 3: Effective ttress tests, London, UK, Pentech press.

Heap, M. J., Kennedy, B. M., Pernin, N., Jacquemard, L., Baud, P., Farquharson, J. I., Scheu, B., Lavallée, Y., Gilg, H. A., Letham-Brake, M., Mayer, K., Jolly, A. D., Reuschlé, T., and Dingwell, D. B., 2015, Mechanical behaviour and failure modes in the Whakaari (White Island volcano) hydrothermal system, New Zealand: Journal of Volcanology and Geothermal Research, v. 295, p. 26-42.

Henkel, D. J., and Gilbert, G. D., 1952, The Effect Measured of the Rubber Membrane on the Triaxial Compression Strength of Clay Samples: Géotechnique, v. 3, no. 1, p. 20-29.

Hill, R., 1951, LXXXVIII. On the state of stress in a plastic-rigid body at the yield point: The London, Edinburgh, and Dublin Philosophical Magazine and Journal of Science, v. 42, no. 331, p. 868-875.

Hong, Z.-S., YIN, J., and CUI, Y.-J., 2010, Compression behaviour of reconstituted soils at high initial water contents: Géotechnique, v. 60, no. 9, p. 691-700.

Hong, Z.-S., Zeng, L.-L., Cui, Y.-J., Cai, Y.-Q., and Lin, C., 2012, Compression behaviour of natural and reconstituted clays: Géotechnique, v. 62, no. 4, p. 291-301.

Horpibulsuk, S., Bergado, D. T., and Lorenzo, G. A., 2004a, Compressibility of cement-admixed clays at high water content: Géotechnique, v. 54, no. 2, p. 151-154.

Horpibulsuk, S., and Liu, M. D., 2015, Structured Cam Clay Model with Cementation Effect: Geotechnical Engineering Journal of the SEAGS & AGSSEA, v. 46, no. 1, p. 86-94.

Horpibulsuk, S., Miura, N., and Bergado, D. T., 2004b, Undrained Shear Behavior of Cement Admixed Clay at High Water Content: Journal of Geotechnical and Geoenvironmental Engineering, v. 130, no. 10, p. 1096-1105.

Horpibulsuk, S., Miura, N., and Nagaraj, T. S., 2003, Assessment of strength development in cement-admixed high water content clays with Abrams' law as a basis: Géotechnique, v. 53, no. 4, p. 439-444.

Hossain, M., 2008, New mechanism-based design approaches for spudcan foundations in clay [PhD: The University of Western Australia.

Hossain, M. S., and Hu, Y., 2005, SOIL FAILURE MECHANISMS ASSOCIATED WITH SPUDCAN FOUNDATIONS ON CLAY Australian Geomechanics, v. 40, no. 3, p. 102-109.

Hossain, M. S., Hu, Y., Randolph, M. F., and White, D. J., 2005, Limiting cavity depth for spudcan foundations penetrating clay: Géotechnique, v. 55, no. 9, p. 679-690.

Hossain, M. S., and Randolph, M. F., 2009a, Effect of Strain Rate and Strain Softening on the Penetration Resistance of Spudcan Foundations on Clay: International Journal of Geomechanics, v. 9, no. 3, p. 122-132.

Hossain, M. S., and Randolph, M. F., 2009b, New Mechanism-Based Design Approach for Spudcan Foundations on Single Layer Clay: Journal of Geotechnical and Geoenvironmental Engineering, v. 135, no. 9, p. 1264-1274.

Hossain, M. S., and Randolph, M. F., 2010, Deep-penetrating spudcan foundations on layered clays: numerical analysis: Géotechnique, v. 60, no. 3, p. 171-184.

Hosterman, J. W., and Patterson, S. H., 1992, Bentonite and Fuller's earth resources of the United States. U.S. Geological Survey Professional Paper 1522: United States Government Printing Office.

Houlsby, G. T., and Martin, C. M., 2003, Undrained bearing capacity factors for conical footings on clay: Géotechnique, v. 53, no. 5, p. 513-520.

Houlsby, G. T., and Wroth, C. P., 1984, Calculation of Stresses on Shallow Penetrometers and Footings, *in* Denness, B., ed., Seabed Mechanics: Proceedings of a Symposium, sponsored jointly by the International Union of Theoretical and Applied Mechanics (IUTAM) and the International Union of Geodesy and Geophysics (IUGG), at the University of Newcastle upon Tyne, 5–9 September, 1983: Dordrecht, Springer Netherlands, p. 107-112.

Hu, P., Wang, D., Cassidy, M. J., and Stanier, S. A., 2014, Predicting the resistance profile of a spudcan penetrating sand overlying clay: Canadian Geotechnical Journal, v. 51, no. 10, p. 1151-1164.

Hu, Y., and Randolph, M., 1999, Plate-Penetrometer Penetration into NC Soil Using H-adaptive FE Method, *in* Pande, G. N., Pietruszczak, S., and Schweige, H. F., eds., Numerical Models in Geomechanics NUMOG VII: Netherlands p. 501-506.

Hu, Y., and Randolph, M. F., 1998, A practical numerical approach for large deformation problems in soil: International Journal for Numerical and Analytical Methods in Geomechanics, v. 22, no. 5, p. 327-350.

Hu, Y., Randolph, M. F., and Watson, P. G., 1999, Bearing Response of Skirted Foundation on Nonhomogeneous Soil: Journal of Geotechnical and Geoenvironmental Engineering, v. 125, no. 11, p. 924-935.

Hu, Y., Waston, P., and Randolph, M., 2001, Effect of interface friction on Nc value for plate-penetrometer, *in* Desai, C., Kundu, T., Harpalani, S., Contractor, D., and Kemeny, J., eds., Computer Methods and Advances in Geomechanics Volume 2: Tucson, Arizona, USA, CRC Press/Balkema, Rotterdam, p. 931-936.

Huang, J. T., and Airey, D. W., 1998, Properties of Artificially Cemented Carbonate Sand: Journal of Geotechnical and Geoenvironmental Engineering, v. 124, no. 6, p. 492-499.

Hui, P., Wang, D., Cassidy, M., and Yang, Q., Large Deformation Analysis of Spudcan Penetration into Sand Overlying Normally Consolidated Clay, *in* Proceedings Constitutive Modeling of Geomaterials, Berlin, Heidelberg, 2013// 2013, Springer Berlin Heidelberg, p. 723-733.

Jaeger, R., DeJong, J., Boulanger, R., and Randolph, M., 2010, Variable Penetration rate CPT in an intermediate soil, Proc., 2nd Int. symp. on cone peneteration testing Volume 2: Huntington Beach, CA, USA, Omnipress, Madison, WI.

Janz, M., and Johansson, s., 2002, The function of different binding agents in deep stabilization: Swedish Geotechnical Institute.

Kang, G.-o., Tsuchida, T., Kim, Y.-s., and Baek, W.-j., 2017, Influence of Humic Acid on the Strength Behavior of Cement-Treated Clay during Various Curing Stages: Journal of Materials in Civil Engineering, v. 29, no. 8, p. 04017057.

Kang, G., Tsuchida, T., and Athapaththu, A. M. R. G., 2015, Strength mobilization of cement-treated dredged clay during the early stages of curing: Soils and Foundations, v. 55, no. 2, p. 375-392.

Kayser, C., Larkin, T., and Singhal, N., 2011, Enhancement of the Shear Strength of Wastewater Residuals Using Industrial Waste By-Products: Journal of Environmental Engineering, v. 137, no. 11, p. 1002-1011.

Khoa, H. D. V., and Jostad, H. P., 2016, Application of Coupled Eulerian-Lagrangian Method to Large Deformation Analyses of Offshore Foundations and Suction Anchors.

Kim, K., Prezzi, M., Salgado, R., and Lee, W., 2008, Effect of Penetration Rate on Cone Penetration Resistance in Saturated Clayey Soils: Journal of Geotechnical and Geoenvironmental Engineering, v. 134, no. 8, p. 1142-1153.
Kim, Y. H., and Hossain, M. S., 2015, Dynamic installation of OMNI-Max anchors in clay: numerical analysis: Géotechnique, v. 65, no. 12, p. 1029-1037.
Kim, Y. H., Hossain, M. S., and Wang, D., 2015, Effect of strain rate and strain softening on embedment depth of a torpedo anchor in clay: Ocean Engineering, v. 108, p. 704-715.
Ko, J., Jeong, S., and Kim, J., 2017, Application of a Coupled Eulerian-Lagrangian Technique on Constructability Problems of Site on Very Soft Soil: Applied Sciences, v. 7, no. 10, p. 1080.
Kogure, K., Yamaguchi, H., and Ohira, Y., 1988, Comparison of strength and soil thrust characteristics among different soil shear tests: Journal of Terramechanics, v. 25, no. 3, p. 201-221.
Konkol, J., and Bałachowski, L., 2017, Numerical Modeling of Cone Penetration Test in Slightly Overconsolidated Clay with Arbitrary Lagrangian-Eulerian Formulation: Procedia Engineering, v. 175, p. 273-278.
Kristinof, R. E., and Marketos, G., 2016, Geotechnical characteristics of a high-porosity deep-sea clay sample retrieved from within a giant scour and its implications for local geological history: Quarterly Journal of Engineering Geology and Hydrogeology, v. 49, no. 2, p. 154-169.
Ladanyi, B., 1968, Study of Deep Penetration Tests in Sensitive Clays: NATIONAL RESEARCH COUNCIL OF CANADA.
Ladanyi, B., and Eden, w. J., 1969, Use of deep penetration test in sensative clay, *in* Canada, N. R. C. o., ed., Seventh international conference on soil mechanics and foundation engineering: Mexico, Division of building research. National Research Council of Canada, p. 225-230.
Lambe, T. W., and Whitman, R. V., 1979, Soil Mechanics, Singapore, John Wiley.
Le Runigo, B., Cuisinier, O., Cui, Y. J., Ferber, V., and Deneele, D., 2009, Impact of initial state on the fabric and permeability of a lime-treated silt under long-term leaching: Canadian Geotechnical Journal, v. 46, no. 11, p. 1243-1257.
Lee, I. K., White, W., and Ingles, O. G., 1983, Geotechnical engineering, Massachusetts, USA, Pitman Publishing Inc.
Lehane, B. M., O'Loughlin, C. D., Gaudin, C., and Randolph, M. F., 2009, Rate effects on penetrometer resistance in kaolin: Geotechnique, v. 59, no. 1, p. 41-52.
Lemaire, K., Deneele, D., Bonnet, S., and Legret, M., 2013, Effects of lime and cement treatment on the physicochemical, microstructural and mechanical characteristics of a plastic silt: Engineering Geology, v. 166, p. 255-261.
Leroueil, S., Tavenas, F., and Bihan, J.-P. L., 1983, Propriétés caractéristiques des argiles de l'est du Canada: Canadian Geotechnical Journal, v. 20, no. 4, p. 681-705.
Leroueil, S., Tavenas, F., and Locat, J., 1985, Discussion: Correlations between index tests and the properties of remoulded clays. Carrier III, W. D. and J. F. Beckman

Géotechnique, v. 35, no. 2, p. 223-229.
Leroueil, S., and Vaughan, P. R., 1990, The general and congruent effects of structure in natural soils and weak rocks: Géotechnique, v. 40, no. 3, p. 467-488.
Levin, E., 1955, INDENTATION PRESSURE OF A SMOOTH CIRCULAR PUNCH: Quarterly of Applied Mathematics, v. 13, no. 2, p. 133-137.
Li, Y. P., Yi, J. T., Lee, F. H., Goh, S. H., and Hu, J., 2018, Effect of Lattice Leg and Sleeve on the Transient Vertical Bearing Capacity of Deeply Penetrated Spudcans in Clay: Journal of Geotechnical and Geoenvironmental Engineering, v. 144, no. 5, p. 04018019.
Liu, E., Nie, Q., and Zhang, J., 2013, A new strength criterion for structured soils: Journal of Rock Mechanics and Geotechnical Engineering, v. 5, no. 2, p. 156-161.

Liu, J., Hu, Y., and Kong, X., 2005, Deep Penetration of Spudcan Foundation into Double Layered Soils: China Ocean Engineering, v. 19, no. 2, p. 309-324.
Liu, M. D., and Carter, J. P., 2000, Modelling the destructuring of soils during virgin compression: Géotechnique, v. 50, no. 4, p. 479-483.
Liu, M. D., Carter, J. P., and Desai, C. S., 2003, Modeling Compression Behavior of Structured Geomaterials: International Journal of Geomechanics, v. 3, no. 2, p. 191-204.
Locat, J., Bérubé, M.-A., and Choquette, M., 1990, Laboratory investigations on the lime stabilization of sensitive clays: shear strength development: Canadian Geotechnical Journal, v. 27, no. 3, p. 294-304.
Locat, J., and Demers, D., 1988, Viscosity, yield stress, remolded strength, and liquidity index relationships for sensitive clays: Canadian Geotechnical Journal, v. 25, no. 4, p. 799-806.
Locat, J., Tremblay, H., and Leroueil, S., 1996, Mechanical and hydraulic behaviour of a soft inorganic clay treated with lime: Canadian Geotechnical Journal, v. 33, no. 4, p. 654-669.
Loganathan, P., 1987, Soil Quality Considerations In The Selection Of Sites For Aquaculture, Food And Agriculture Organization of the United Nations, Volume http://www.fao.org/docrep/field/003/AC172E/AC172E00.htm.
Lorenzo, G. A., and Bergado, D. T., 2004, Fundamental Parameters of Cement-Admixed Clay—New Approach: Journal of Geotechnical and Geoenvironmental Engineering, v. 130, no. 10, p. 1042-1050.
Low, H. E., and Randolph, M. F., 2010, Strength Measurement for Near-Seabed Surface Soft Soil Using Manually Operated Miniature Full-Flow Penetrometer: Journal of Geotechnical and Geoenvironmental Engineering, v. 136, no. 11, p. 1565-1573.
Ma, J., Wang, D., and Randolph, M. F., 2014, A new contact algorithm in the material point method for geotechnical simulations: International Journal for Numerical and Analytical Methods in Geomechanics, v. 38, no. 11, p. 1197-1210.
Maher, M., and Ho, Y., 1993, Behavior of Fiber-Reinforced Cemented Sand Under Static and Cyclic Loads.
Mahmoodzadeh, F., Boylan, N., Randolph, M., and Cassidy, M., 2011, The Effect of Partial Drainage on Measurements by a Piezoball Penetrometer: Omae2011: Proceedings of the Asme 30th International Conference on Ocean, Offshore and Arctic Engineering, Vol 7, p. 1007-1016.
Mahmoodzadeh, H., and Randolph, M. F., 2014, Penetrometer Testing: Effect of Partial Consolidation on Subsequent Dissipation Response: Journal of Geotechnical and Geoenvironmental Engineering, v. 140, no. 6, p. 04014022.
Mana, D. S. K., Gourvenec, S., and Randolph, M. F., 2011, A numerical study of the vertical bearing capacity of skirted foundations, *in* Gourvenec, and White, eds., Frontiers in Offshore Geotechnics II, Volume 1: London, Taylor & Francis Group, p. 433-438.
Martin, C., and Randolph, M., 2001, Applications of the lower and upper bound theorems of plasticity to collapse of circular foundations: Proc. 10th Int. Conf. on Computer Methods and Advances in Geomechanics, Tucson, v. 2, p. 1417-1428.
Marzano, I. P., Al-Tabbaa, A., and Grisolia, M., Influence of curing temperature on the strength of cement-stabilised artificial clays, *in* Proceedings THE SECOND INTERNATIONAL WORKSHOP ON GEOTECHNICS OF SOFT SOILS, GLASGOW, SCOTLAND, 2009 2008, Volume 1, Taylor & Francis Group, London, p. 257-262.
Metelková, Z., Boháč, J., Přikryl, R., and Sedlářová, I., 2012, Maturation of loess treated with variable lime admixture: Pore space textural evolution and related phase changes: Applied Clay Science, v. 61, no. Supplement C, p. 37-43.
Mitchell, J. K., 1976, Fundamentals of Soil Behaviour., New York, J. Wiley.

Miura, N., Horpibulsuk, S., and Nagaraj, T. S., 2001, ENGINEERING BEHAVIOR OF CEMENT STABILIZED CLAY AT HIGH WATER CONTENT: SOILS AND FOUNDATIONS, v. 41, no. 5, p. 33-45.

Morin, P., and Dawe, C. R., 1987, Geotechnical properties of two deep-sea marine soils from the Labrador Sea: Canadian Geotechnical Journal, v. 24, no. 4, p. 536-548.

Nguyen, V. Q., and Merifield, R. S., 2012, Two- and three-dimensional undrained bearing capacity of embedded footings: Australian Geomechanics, v. 47, no. 2, p. 25-40.

Nova, R., Castellanza, R., and Tamagnini, C., 2003, A constitutive model for bonded geomaterials subject to mechanical and/or chemical degradation: International Journal for Numerical and Analytical Methods in Geomechanics, v. 27, no. 9, p. 705-732.

O'Malley, E. S., and Wright, S. G., 1987, REVIEW OF UNDRAINED SHEAR S1RENG1H TESTING ME1HODS USED BY THE TEXAS STATE DEPARTMENT OF HIGHWAYS AND PUBLIC TRANSPORTATION The University of Texas at Austin

Omar, T., and Sadrekarimi, A., 2014, Effects of Multiple Corrections on Triaxial Compression Testing of Sands: Journal of GeoEngineering, v. 9, no. 2, p. 75-83.

Osman, A. S., and Bolton, M. D., 2005, Simple plasticity-based prediction of the undrained settlement of shallow circular foundations on clay: Géotechnique, v. 55, no. 6, p. 435-447.

Osula, D. O. A., 1991, Lime modification of problem laterite: Engineering Geology, v. 30, no. 2, p. 141-154.

Osula, D. O. A., 1996, A comparative evaluation of cement and lime modification of laterite: Engineering Geology, v. 42, no. 1, p. 71-81.

Otani, J. U. N., Mukunoki, T., and Kikuchi, Y., 2002, VISUALIZATION FOR ENGINEERING PROPERTY OF IN-SITU LIGHT WEIGHT SOILS WITH AIR FOAMS: SOILS AND FOUNDATIONS, v. 42, no. 3, p. 93-105.

Ou, C.-Y., Chien, S.-C., Yang, C.-C., and Chen, C.-T., 2015, Mechanism of soil cementation by electroosmotic chemical treatment: Applied Clay Science, v. 104, p. 135-142.

Pakbaz, M. S., and Alipour, R., 2012, Influence of cement addition on the geotechnical properties of an Iranian clay: Applied Clay Science, v. 67-68, p. 1-4.

Pakbaz, M. S., and Farzi, M., 2015, Comparison of the effect of mixing methods (dry vs. wet) on mechanical and hydraulic properties of treated soil with cement or lime: Applied Clay Science, v. 105, no. Supplement C, p. 156-169.

Peck, G. M., 1966, Correspondence: Géotechnique, v. 16, no. 1, p. 76-77.

Pichler, T., Pucker, T., Hamann, T., Henke, S., and Qiu, G., 2012, High-Performance Abaqus Simulations in Soil Mechanics

Reloaded – Chances and Frontiers 3DS Simulia Community Conference: Providence, Rhode Island USA, Dassault Systemes.

Pinkert, S., and Klar, A., 2012, Discussion of "Evaluation of Undrained Shear Strength Using Full-Flow Penetrometers" by Jason T. DeJong, Nicholas J. Yafrate, and Don J. DeGroot: Journal of Geotechnical and Geoenvironmental Engineering, v. 138, no. 6, p. 763-765.

Pinkert, S., and Klar, A., Analytically and experimentally based resistance factors for" full-flow" penetrometers, *in* Proceedings 18th Int. Conf. on Soil Mechanics and Geotechnical Engineering, Paris, France, 2013, Volume 1: London, UK, International Society for Soil Mechanics and Geotechnical Engineering, p. 781–784.

Qiu, G., and Grabe, J., 2012, Numerical investigation of bearing capacity due to spudcan penetration in sand overlying clay: Canadian Geotechnical Journal, v. 49, no. 12, p. 1393-1407.

Qiu, G., and Henke, S., 2011, Controlled installation of spudcan foundations on loose sand overlying weak clay: Marine Structures, v. 24, no. 4, p. 528-550.

Qiu, G., Henke, S., and Grabe, J., 2011, Application of a Coupled Eulerian–Lagrangian approach on geomechanical problems involving large deformations: Computers and Geotechnics, v. 38, no. 1, p. 30-39.

Quang, N., Chun, J., Hino, T., and Negami, T., MECHANICAL PROPERTIES OF SOFT CLAYS LIGHTLY TREATED BY CEMENT/LIME, *in* Proceedings International Symposium on Sustainable Geosynthetics and Green Technology for Climate Change (SGCC) (Retirement Symposium for Prof. Dennes T. Bergado), Bangkok, Thailand, 20-21 June 2012 2012.

Raghunandan, M. E., Sharma, J. S., and Pradhan, B., 2014, A review on the effect of rubber membrane in triaxial tests: Arabian Journal of Geosciences, v. 8, no. 5, p. 3195-3206.

Randolph, M. F., and Andersen, K. H., 2006, Numerical Analysis of T-Bar Penetration in Soft Clay: International Journal of Geomechanics, v. 6, no. 6, p. 411-420.

Randolph, M. F., Wang, D., Zhou, H., Hossain, M. S., and Hu, Y., 2008, Large Deformation Finite Element Analysis for Offshore Applications. , The 12th International Conference of International Association for Computer Methods and Advances in Geomechanics (IACMAG) Goa, India.

Rao, S. N., and Rajasekaran, G., 1996, Reaction Products Formed in Lime-Stabilized Marine Clays: Journal of Geotechnical Engineering, v. 122, no. 5, p. 329-336.

Robinson, S., and Brown, M. J., 2013, Rate effects at varying strain levels in fine grained soils, Proc.of the 18th Int. Conf. on Soil Mechanics and Geotechnical Engineering, (ICSMGE 2013), Volume 1: Paris, FRANCE, International Society for Soil Mechanics and Geotechnical Engineering, p. 263-267.

Rotta, G. V., Consoli, N. C., Prietto, P. D. M., Coop, M. R., and Graham, J., 2003, Isotropic yielding in an artificially cemented soil cured under stress: Géotechnique, v. 53, no. 5, p. 493-501.

Roy, M., and Leblanc, A., 1988, Factors Affecting the Measurements and Interpretation of the Vane Strength in Soft Sensitive Clays, *in* Richards, A. F., ed., Vane Shear Strength Testing in Soils: Field and Laboratory Studies: Philadelphia,PA. USA, ASTM International, p. 117-128.

Sahdi, F., Gaudin, C., and White, D. J., 2014, Strength properties of ultra-soft kaolin: Canadian Geotechnical Journal, v. 51, no. 4, p. 420-431.

Sakr, M. A., Shahin, M. A., and Metwally, Y. M., 2008, Utilization of Lime for Stabilizing Soft Clay Soil of High Organic Content: Geotechnical and Geological Engineering, v. 27, no. 1, p. 105.

Salgado, R., Lyamin, A. V., Sloan, S. W., and Yu, H. S., 2004, Two- and three-dimensional bearing capacity of foundations in clay: Géotechnique, v. 54, no. 5, p. 297-306.

Sasanian, S., and Newson, T. A., 2014, Basic parameters governing the behaviour of cement-treated clays: Soils and Foundations, v. 54, no. 2, p. 209-224.

Satoh, T., Tsuchida, T., Mitsukuri, K., and Hong, Z., 2001, FIELD PLACING TEST OF LIGHTWEIGHT TREATED SOIL UNDER SEAWATER IN KUMAMOTO PORT: SOILS AND FOUNDATIONS, v. 41, no. 5, p. 145-154.

Schlue, B. F., Moerz, T., and Kreiter, S., 2010, Influence of Shear Rate on Undrained Vane Shear Strength of Organic Harbor Mud: Journal of Geotechnical and Geoenvironmental Engineering, v. 136, no. 10, p. 1437-1447.

Schneider, J. A., Lehane, B. M., and Schnaid, F., 2007, Velocity effects on Piezocone measurements in normally and over consolidated clays: International Journal of Physical Modelling in Geotechnics, v. 7, no. 2, p. 23-34.

Seng, S., and Tanaka, H., 2011, PROPERTIES OF CEMENT-TREATED SOILS DURING INITIAL CURING STAGES: SOILS AND FOUNDATIONS, v. 51, no. 5, p. 775-784.

Sheng, D., Cui, L., and Ansari, Y., 2013, Interpretation of Cone Factor in Undrained Soils via Full-Penetration Finite-Element Analysis: International Journal of Geomechanics, v. 13, no. 6, p. 745-753.

Shield, R. T., 1955, On the plastic flow of metals under conditions of axial symmetry: Proceedings of the Royal Society of London. Series A. Mathematical and Physical Sciences, v. 233, no. 1193, p. 267-287.

Silvestri, V., and Aubertin, M., 1988, Anisotropy and in-situ vane field vane tests tests, *in* Richards, A. F., ed., Vane shear strength testing in soils: field and laboratory studies.

studies, Volume Special Technical Publication 1014: Philadelphia, USA, American Society for Testing and Materials p. 88-103.

Silvestri, V., and Ewane, M., 2017, Mechanical Properties of an Artificially Cemented Clayey Material.

Simulia, 2014a, Abaqus6.14. Analysis user's guide: Analysis, Volume II.

-, 2014b, Abaqus online documentation, version 6.14: Abaqus theory guide, *in* Corp., D. S. e. S., ed.: Suresnes, France.

-, 2014c, Abaqus online documentation, version 6.14:Analysis user's ’S guide: Elements, Volume IV.

-, 2014d, EXAMPLE PROBLEMS GUIDE. VOLUME I: STATIC AND DYNAMIC ANALYSES, *in* Corp., D. S. e. S., ed., ABAQUS 6.14: Cedex, France.

Sissons, J. B., 1970, Geomorphology and foundation conditions around Grangemouth: Quarterly Journal of Engineering Geology and Hydrogeology, v. 3, no. 3, p. 183-191.

Skemption, A. W., and Northey, R. D., 1952, The Sensitivity of Clays: Géotechnique, v. 3, no. 1, p. 30-53.

Skempton, A. W., 1954, The Pore-Pressure Coefficients A and B: Géotechnique, v. 4, no. 4, p. 143-147.

Skempton, A. W., 1969, The consolidation of clays by gravitational compaction: Quarterly Journal of the Geological Society, v. 125, no. 1-4, p. 373-411.

Sloan, S. W., and Booker, J. R., 1986, Removal of singularities in tresca and mohr–coulomb yield functions: Communications in Applied Numerical Methods, v. 2, no. 2, p. 173-179.

Smith, G. N., 1990, Elements of Soil Mechanics, Oxford, UK, BSP Professional Books.

Sridharan, A., Abraham, B. M., and Jose, B. T., 1991, Improved technique for estimation of preconsolidation pressure: Géotechnique, v. 41, no. 2, p. 263-268.

Sridharan, A., and Allam, M. M., 1982, Volume Change Behavior of Desiccated Soils: Journal of the Geotechnical Engineering Division, v. 108, no. 8, p. 1057-1071.

Stewart, D. P., and Randolph, M. F., 1994, T-Bar Penetration Testing in Soft Clay: Journal of Geotechnical Engineering-Asce, v. 120, no. 12, p. 2230-2235.

Taiebat, H. A., and Carter, J. P., 2008, Flow rule effects in the Tresca model: Computers and Geotechnics, v. 35, no. 3, p. 500-503.

Tani, Z. a., and Craig, W. H., 1995, Bearing capacity of circular foundations on soft clay of strength increasing with depth: Soils and Foundations, v. 35, no. 4, p. 21-35.

Tapper, L., Martin, C. M., and Byrne, B. W., 2014, Undrained bearing capacity of circular footings on Tresca soil using adaptive finite element analysis, *in* Hicks, M. A., Brinkgreve, R. B. J., and Rohe, A., eds., 8th European Conf. on Numerical methods in Geotech. Eng., Volume 1: Delft, The Netherlands, CRC Press p. 669-704.

Tho, K. K., Leung, C. F., Chow, Y. K., and Swaddiwudhipong, S., 2012, Eulerian Finite-Element Technique for Analysis of Jack-Up Spudcan Penetration: International Journal of Geomechanics, v. 12, no. 1, p. 64-73.

Thompson, M. R., 1970, Design Coefficients for Lime-Soil Mixtures: Illinois Division of Highways, Res. and Dev., Research Project IHR-28 AASHTO Road Test.

Tian, Y., Cassidy, M. J., Randolph, M. F., Wang, D., and Gaudin, C., 2014, A simple implementation of RITSS and its application in large deformation analysis: Computers and Geotechnics, v. 56, p. 160-167.

Toll, D. G., 2010, Triax 5.1.7 user manual, *in* university, D., ed., Geotechnical System Research.

Tran, T. D., Cui, Y.-J., Tang, A. M., Audiguier, M., and Cojean, R., 2014, Effects of lime treatment on the microstructure and hydraulic conductivity of Héricourt clay: Journal of Rock Mechanics and Geotechnical Engineering, v. 6, no. 5, p. 399-404.

Tremblay, H., Leroueil, S., and Locat, J., 2001, Mechanical improvement and vertical yield stress prediction of clayey soils from eastern Canada treated with lime or cement: Canadian Geotechnical Journal, v. 38, no. 3, p. 567-579.

Veneman, P. L. M., and Edil, T. B., 1988, Micromorphological Aspects of the Vane Shear Test, *in* Richards, A. F., ed., Vane Shear Strength Testing in Soils: Field and Laboratory Studies: P.A. USA, ASTM International, p. 182-190.

Vichan, S., Rachan, R., and Horpibulsuk, S., 2013, Strength and microstructure development in Bangkok clay stabilized with calcium carbide residue and biomass ash: Scienceasia, v. 39, no. 2, p. 186-193.

Wang, D., White, D. J., and Randolph, M. F., 2010, Large-deformation finite element analysis of pipe penetration and large-amplitude lateral displacement: Canadian Geotechnical Journal, v. 47, no. 8, p. 842-856.

Wood, D. M., 1990, Soil Behaviour and Critical State Soil Mechanics, Cambridge, U.K., Cambridge University Press.

Wroth, C. P., and Wood, D. M., 1978, The correlation of index properties with some basic engineering properties of soils: Canadian Geotechnical Journal, v. 15, no. 2, p. 137-145.

Xiao, H.-W., and Lee, F.-H., 2014, An energy-based isotropic compression relation for cement-admixed soft clay: Géotechnique, v. 64, no. 5, p. 412-418.

Xiao, H., Lee, F. H., and Chin, K. G., 2014, Yielding of cement-treated marine clay: Soils and Foundations, v. 54, no. 3, p. 488-501.

Yafrate, N., DeJong, J., DeGroot, D., and Randolph, M., 2009, Evaluation of Remolded Shear Strength and Sensitivity of Soft Clay Using Full-Flow Penetrometers: Journal of Geotechnical and Geoenvironmental Engineering, v. 135, no. 9, p. 1179-1189.

Yafrate, N. J., and DeJong, J. T., 2007, Influence of Penetration Rate on Measured Resistance with Full Flow Penetrometers in Soft Clay, Advances in Measurement and Modeling of Soil Behavior, American Society of Civil Engineers.

Zeng, L.-L., Hong, Z.-S., and Cui, Y.-J., 2015, Determining the virgin compression lines of reconstituted clays at different initial water contents: Canadian Geotechnical Journal, v. 52, no. 9, p. 1408-1415.

Zhang, R. J., Santoso, A. M., Tan, T. S., and Phoon, K. K., 2013, Strength of High Water-Content Marine Clay Stabilized by Low Amount of Cement: Journal of Geotechnical and Geoenvironmental Engineering, v. 139, no. 12, p. 2170-2181.

Zhao, Y., and Liu, H., 2017, Toward a quick evaluation of the performance of gravity installed anchors in clay: Penetration and keying: Applied Ocean Research, v. 69, p. 148-159.

Zheng, J., Hossain, M. S., and Wang, D., 3D Large Deformation FE Analysis of Spudcan Foundations on Layered Clays Using CEL Approach, *in* Proceedings Constitutive Modeling of Geomaterials, Berlin, Heidelberg, 2013// 2013, Springer Berlin Heidelberg, p. 803-810.

Zheng, J., Hossain, M. S., and Wang, D., 2016, Prediction of spudcan penetration resistance profile in stiff-over-soft clays: Canadian Geotechnical Journal, v. 53, no. 12, p. 1978-1990.

Zhou, H., and Randolph, M. F., 2007, Computational Techniques and Shear Band Development for Cylindrical and Spherical Penetrometers in Strain-Softening Clay: International Journal of Geomechanics, v. 7, no. 4, p. 287-295.

Zhou, H., and Randolph, M. F., 2009a, Numerical investigations into cycling of full-flow penetrometers in soft clay: Geotechnique, v. 59, no. 10, p. 801-812.

-, 2009b, Resistance of full-flow penetrometers in rate-dependent and strain-softening clay: Geotechnique, v. 59, no. 2, p. 79-86.

Zhou, M., Hossain, M. S., Hu, Y., and Liu, H., 2016, Scale Issues and Interpretation of Ball Penetration in Stratified Deposits in Centrifuge Testing: Journal of Geotechnical and Geoenvironmental Engineering, v. 142, no. 5, p. 04015103.

Zukri, A., 2013, Pekan Soft Clay Treated With Hydrated Lime As A Method Of Soil Stabilizer: Malaysian Technical Universities Conference on Engineering & Technology 2012 (Mucet 2012), v. 53, p. 37-41.